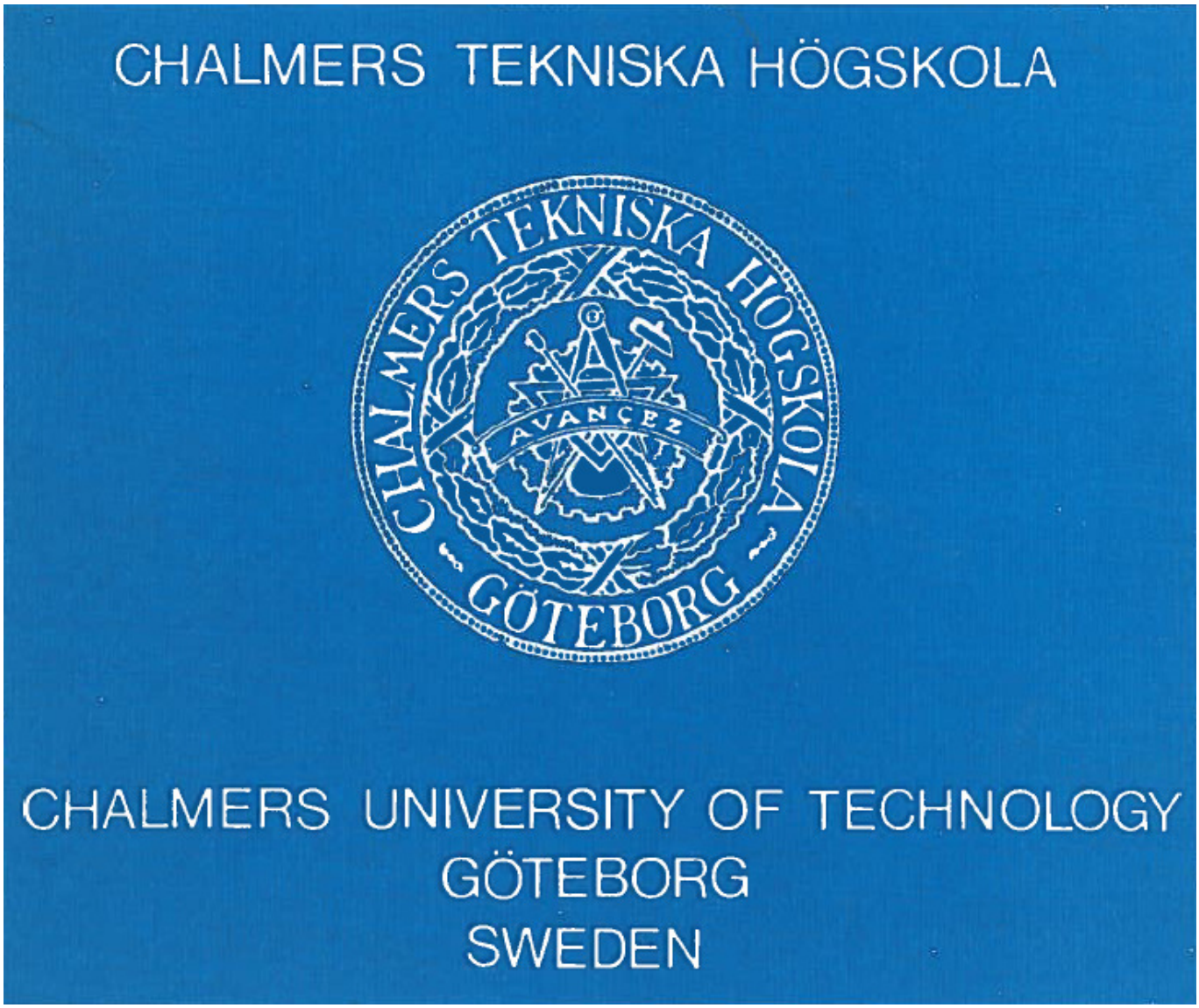

ON PROBABILITY IN GEOTECHNICS

RANDOM CALCULATION MODELS EXEMPLIFIED ON SLOPE STABILITY ANALYSIS AND GROUND-SUPERSTRUCTURE INTERACTION

VOLUME 1

CLAES ALÉN

DEPARTMENT OF GEOTECHNICAL ENGINEERING

1998

ON PROBABILITY IN GEOTECHNICS

Random calculation models exemplified on slope stability analysis and ground-superstructure interaction.

Claes Alén

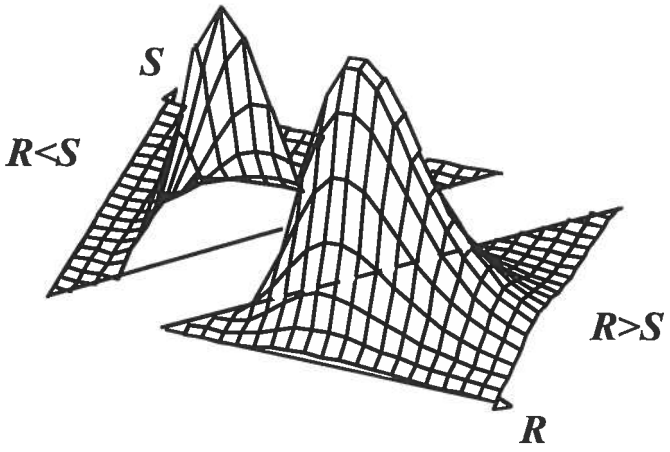

Submitted to the School of Civil Engineering,
Chalmers University of Technology
in partial fulfilment of the requirement
for the degree of Doctor of Philosophy

Department of Geotechnical Engineering
Chalmers University of Technology
S-412 96 Göteborg, Sweden

Göteborg 1998

Warum einfach wenn mann es
schön kompliziert machen kann?
Josse

ISBN 91-7197-637-X
ISSN 0346-718X

PREFACE

The thesis deals with the application of a probabilistic approach in geotechnical engineering. The study includes elements from three academic disciplines, geotechnics, mathematical statistics and structural mechanics.

The work was carried out at the Department of Geotechnical Engineering, Chalmers University of Technology, Göteborg under supervision of Prof. Göran Sällfors. His support and enthusiasm has been invaluable for the completion of this work.

The work has been financed by the Development Fund of the Swedish Construction Industry with additional support from the Swedish Council for Building Research and NCC AB.

Prof. emeritus Sven Hansbo, adj. Prof. Rolf Larsson and Docent Leif Jendeby have proof-read different parts of the manuscript from a geotechnical point of view. Prof. Holger Rootzén and Mattias Wallerstedt have given statistical guidance. Prof. Milton Harr, Purdue University, has contributed with discussions about application of probability in engineering.

Development of new ideas is always a result of many people's contributions. I want to thank my colleagues at NCC and at the Geotechnical Department at Chalmers for their contributions throughout the years. Everyone can not be mentioned here but let them br represented by two dear late colleagues. My first boss Sven-Erik Kvist who taught me the balance between simplicity and relevance in structural modelling. My deer friend Lennart 'Josse' Jonson, who was a sensible guide in the choice between professional ambition and participating in real life. He encouraged me to take the step into research.

The work has been carried out during a period of struggle for my family. I wish to express my genuine thanks to

- My ex-wife Inger, who has encouraged me in my work despite her own life in distress.
- My daughter Olivia, who has been forced to be more conscious of responsibility than is desirable for her age.
- My son Fabian, whose disrespectful but loving attitude has helped me to see the work from a healthy distance.

Finally I want to thank Simone. Her humour and observational nature has helped me to believe in a continuos rich life.

Göteborg, March 1998

Claes Alén

ON PROBABILITY IN GEOTECHNICS

Random calculation models exemplified on slope stability analysis and ground-superstructure interaction.

av

Claes Alén

AKADEMISK AVHANDLING

som för avläggande av
teknisk doktorsexamen
vid Chalmers tekniska högskola
försvaras vid offentlig disputation
onsdagen den 29 april 1998, kl. 10.15
sal HC1, Hörsalsvägen
Chalmers tekniska högskola
Göteborg.

Fakultetsopponent: Professor Steinar Nordal,
NTNU, Trondheim

Examinator: Professor Göran Sällfors

ON PROBABILITY IN GEOTECHNICS

Random calculation models exemplified on slope stability analysis and ground-superstructure interaction.

Claes Alén

Department of Geotechnical Engineering
Chalmers University of Technology
S-412 96 Göteborg, Sweden

ABSTRACT

The thesis deals with uncertainty in calculation modelling. Emphasis is put on the design state. Design is a chain of decisions under uncertainty. A probabilistic approach is used to describe the uncertainty and calculations as a way to reveal the uncertainty. Thus, a calculation method becomes an operative tool in a risk analysis, not merely a verification of a prescribed minimum level.

The work is a combination of elements from three different academic disciplines; geotechnics, structural mechanics and statistics. Different aspects from two fields of geotechnical modelling are discussed; slope stability as an example of ultimate limit state problems, and interaction ground /superstructure as an example of serviceability limit state problems.

For the mathematical solution different algorithms are used; mathematical analysis, point estimate method, Monte-Carlo simulation and reliability analysis.

Soil properties are described as random variables. Different uncertainties are accounted for; natural variations, systematic testing errors, random testing errors and errors due to limited testing. Pre-knowledge and test results are combined systematically using Bayesian statistics.

Three different levels of complexity of both slope stability analysis and ground/superstructure interaction are given. In both cases, structural models of the soil are given for the third level. For a slope a constant degree of mobilisation is not a prerequisite. Instead the deformation properties of the soil are considered. In the interaction analysis the soil is described as a continuous shear beam on elastic supports. The structural model of the soil can be calibrated against a more rigorous geotechnical model. To determine volumetric creep deformations in clay a simple creep model is presented, in which the soil deformations can be determined as a sum of elastic/plastic deformations and creep deformations.

Key words: design, geotechnics, probability, statistics, random, calculation, limit state, slope stability, interaction, creep.

ON PROBABILITY IN GEOTECHNICS

Claes Alén
Department of Geotechnical Engineering
Chalmers University of Technology
S-412 96 Göteborg, Sweden

ERRATA VOLUME 1

Page	Location[1]	Printed	Corrected
xxii	15a	$\tau_u \neq F \cdot \tau$	$\tau_{ult} \neq F \cdot \tau$
xxxi	3b	*K* stiffness of support	*S* stiffness of support
xxxiii	5a	(or often autocorrelation)	-
xxxiv	11a	flatness	peakedness
22	Fig 2.8	····· Gumbel	- - - - - Gumbel
40	(2.15)	$ß=\mu_M/\sigma_M$	$\beta=\mu_M/\sigma_M$
53	11b	section 2.5.3	section 2.4.3
83	8a	section 2.5.3	section 2.4.3
85	Foot note	Larsson	Larsson et al
92	5b	negatively curved plots	negatively skewed observations
98	Fig 3.28	$\Delta\sigma'=6kPa/m^2 z$	$\Delta\sigma'/\Delta z=6kPa/m$
99	Fig 3.30	$c'+\tan(\phi)$	$c'+\sigma'\cdot\tan(\phi)$
101	17a	section 2.3.3	section 2.2.3
106	Fig 4.1	Modified Cam Clay	[Modified] Cam Clay
117	(4.8)	$c=\tau_u=c'+(\sigma_{N,ult}-u)\cdot\tan(\phi)$	$c=\tau_{ult}=c'+(\sigma_{N,ult}-u)\cdot\tan(\phi)$
117	16a	$\tau_u \neq F \cdot \tau$	$\tau_{ult} \neq F \cdot \tau$
118	2a	…stresses…	…shear stresses…
123	1a-2a	…long time of slope stability…	…long time stability of a slope…
127	1a	Figure 4.1	Figure 4.9
131	Table 4.4	10^2	$10^{\ 2}$ (the digit 2 is a foot note)
131	Table 4.5	[kN/m³] (at 2 places)	[kN/m²]
138	(4.31)	$\ln(1+V^2)\cdot u_{x_j}$	$\sqrt{\ln(1+V_{x_j}^{\ 2})\cdot u_{x_j}}$
138	(4.31a)	$V\cdot u_{x_j}$	$V_{x_j}\cdot u_{x_j}$
139	Fig 4.17	$(-\beta\alpha_1,0)$	$(\beta\alpha_1,0)=(-\beta\lvert\alpha_1\rvert,0)$
147	Fig 4.24	$G_{b_i}\ldots G_{a_i}\ldots G_i$	$G_{b_i};M_{b_i}\ldots G_{a_i};M_{a_i}\ldots G_i;M_i$
155	Fig 4.30	(y-axis)	Stresses
		(x-axis)	'Toe' 'Crest'
162	1a-2a	limit of the support…….criterion[1].	-
162	Foot note	[1]The value….in this way too.	-
163	13a	2.2	section 2.1.2
167	(5.10)	$+s_0$	$[+s_0]$
171	3b-2b	simplified as	approximated as
171	(5.15)	=	≈
172	Foot note[1]	$\sigma(x,z,d)$	$\sigma(x,z)$
176	3a	page 17	page 172

[1] a = from above, b = from below

Page	Location	Printed	Corrected
179	(5.19c) lower version	$U_{c3}=\begin{cases}1{,}2\ldots.\\1-0{,}8\ldots.\end{cases}$	-
179	7a	5.19	5.19a
180	Foot note	figure X.X	figure P.3
183		EMBANCKO	EMBANKCO
183	Fig 5.11	····· Method A excl creep - - - Method B " "	- - - Method A excl creep ····· Method B " "
185	5a	page 23	page 179
185	16a	page 22	page 177
192	Table 5.3	H[m]	H[m] = thickness of soil layers
		M_1[kN/m²] M_1[kN/m²] M_1[kN/m²]	M_1[kN/m²] M_2[kN/m²] M_3[kN/m²]
192	Table 5.4	p_1 p_1	p_1 p_2
		Column '1' p_1 p_1 M_1 M_1 M_1	*Column '1'* p_1 p_2 M_1 M_2 M_3
193	Table 5.5	S_1[kN/m²] S_1[kN/m²] S_1[kN/m²]	S_1[kN/m²] S_2[kN/m²] S_3[kN/m²]
196	Table 5.7	Correlation 0,7	Correlation 0,5
198	Fig 5.23	····· f'_c - - - - $\sigma'_0+\Delta\sigma_0$ $=f(\sigma'_0+\Delta\sigma-f'_{c)}$	- - - - f'_c ····· $\sigma'_0+\Delta\sigma_0$ $=f(\sigma'_0+\Delta\sigma-p'_c)$
199	Table 5.8		B_p=0,3 m
199	Table 5.9	z_{N1} z_{N1} z_{N1}	z_{N1} z_{N2} z_{N3}
200	Fig 5.24	y-axis 'lognormal' scale	y-axis 'lognormal' scale, see appendix B
202	Table 5.10	$3\,10^3$ $32\,10^3$ $75\,10^3$	$3{\cdot}10^3$ $32{\cdot}10^3$ $75{\cdot}10^3$

REFERENCES

page 25 et al Harr (1986) →Harr (1987)

Alén & Lendeby →Alén & Jendeby

Cooper, M. R., (1996), The progressive development of a failure slip surface in over-consolidated clay at Selborne, UK, *Proc. 7th International Symposium on Landslides. Trondheim.*, Vol 2, Balkema, Rotterdam

Hansbo, S. (1957), A new approach to the determination of the shear strength of clay by the fall-cone test, *Proc. Swedish geotech. Inst., No 14*

Harr (1989), Probabilistic estimates for multivariate analyses, *Appl. Math. Modelling*, **Vol. 13**, May

He, J., (1993), *A geostatistical analysis of soil properties*, Report B, 1994:7. Department of Geotechnical Engineering. Chalmers University of Technology. Göteborg

He, J., (1994), *Three point estimate method schemes for skewed random variables*, Report B, 1993:8. Department of Geotechnical Engineering. Chalmers University of Technology. Göteborg

He, J. & Sällfors, G. (1994), An optimal point estimate method for uncertainty studies. *Appl. Math. Modelling*, **Vol. 18**,Sept.

Hintze, S., (1994), *Risk Analysis in foundation Engineering with Application to Piling in Loose Friction Soils in Urban Situations.* Doctoral thesis, Division of Soil and Rock Mechanics, Royal Institute of Technology, Stockholm

Matyas, E. L. & Santamarina, J. C., (1994), Negative skin friction and the neutral plane, *Can. Geotech. Jour.* **Vol 31,** No 4, Aug.

Svanø, G. & Emdal, A., (1988), KRYKON VER. 02, A FEM Program for One-dimensional consolidation analysis including creep effects, Report STF69 F88009, SINTEF, Trondheim

Yu, H. S:, Salgado, R., Sloan, S. W. & Kim, J. K. (1998), Limit analysis versus Limit Equilibrium, *Jour. of Geotech. Geoenvirom Eng.* **Vol 124**, No 1, Jan.

CONTENTS

5 Interaction Ground/Superstructure

APPENDICES

SUMMARY

"The problems of soil mechanics may be divided into two principal groups - the stability problems and the elasticity problems. The stability problems deal with the conditions for the equilibrium of ideal soils immediately preceding ultimate failure by plastic flow."

"Elasticity problems deal with the deformations of the soil due to its own weight or due to external forces such as the weight of the building. All settlement problems belong in this category." (Terzaghi, 1943)

Σ.1 General

In this thesis different aspects of geotechnical modelling are discussed. It is a combination of elements from three different academic disciplines:

- Geotechnics
- Structural mechanics
- Statistics

The work is based upon examples from two fields of geotechnical modelling:

- Slope stability, i.e. an example of stability problems
- Interaction ground/superstructure, i.e. an example of elasticity problems

All sorts of technical calculations involve a certain amount of uncertainty. In this thesis a probabilistic approach is used as a way to quantify uncertainty.

New calculation methods should, to be operative in design, show a balance between:

- Realistic description of reality
- Simplicity
- Improvement of the state-of-the-art
- Recognition.
- Adaptation to codes
- Possibility of further improvements

Hence improved accuracy and precision of a method is not necessarily an improvement in engineering practice. In design the level of refinement has to be valued in the light of the purpose of the method. In the author's experience three different levels of complexity is a useful separation of methods with different accuracy and precision.

Σ.2 Calculation models

During the last decades it has become mandatory to verify structures in two different limit states, the ultimate limit state and the serviceability limit state. Different calculation models can be used for the verification of the two different limit states.

Safety margin

In the evaluation of safety, the concept factor of safety, $F = R/S$, has traditionally been used in both geotechnical and structural engineering. A complication, when engineers from the two disciplines have to co-operate is that the geotechnical engineer often considers uncertainty as a resistance problem, while the structural engineer is more concerned with the uncertainty of the actions. Hence it is not indisputable whether an improvement should be regarded as an increase of the resistance or a decrease of the action. The alternative safety concept, the safety margin $M = R - S$, does not have this draw-back. In this thesis a dimensionless safety margin is presented as an alternative:

$$m = \frac{R - S}{R} \qquad \text{(i)}$$

with the convenient range [0-100%]. There is a unique relation between this dimensionless safety margin and the factor of safety, $m = 1 - (1/F)$. This means that the safety margin, in the same way as the factor of safety but unlike the conventionally defined safety margin, can be used as a relative measure of safety, e.g. to determine the critical slip surface in a slope stability analysis.

Probabilistic interpretation of deterministic modelling

In traditional, deterministic modelling the action and the resistance are represented by fixed and known values. Such an interpretation

implies that the safety margin actually has a sufficiently large, positive value.

In a probabilistic approach both the resistance and the action can take a wide range of values. This can be interpreted as that the action and the resistance have fixed but unknown values. The same is then valid for the safety margin. A sufficiently low probability of failure is obtained if the safety margin is at least not negative for a physically possible but unlikely combination of the resistance and the action.

Random models to describe uncertainty

To describe the unlikeness mentioned in the previous section, variables in the calculation are given as random variables, i.e. variables in which the probability of different outcomes is given by probability distributions. A number of distributions can be used for this purpose, for example:

- normal distribution
- lognormal distribution
- Extreme value distributions
- β-distributions
- Exponential distribution

The choice of distribution for a particular random variable is far from trivial from a statistical point of view. This is valid especially for calculations in the ultimate limit state in which very low values of the probability of failure are foreseen. Hence the tails of the distributions govern the design. An ordinary geotechnical testing then represents too small samples for the evaluation of an underlying distribution. In principle the type of distribution should be chosen from the physical characteristics of a variable. However, in the applications in this thesis the probability of failure represents a formal probability, at least in the ultimate limit state. In such cases the choice of distribution can often be seen as a code issue, i.e. the probability demanded and the choice of distribution is an inseparable pair. In applications of this latter type the lognormal distribution can serve as a comprehensive distribution, at least in a

probabilistic analysis of the main characteristics of a problem. The normal distribution, which is defined for negative values, has to be used with caution as the negative values often represent physically impossible situations.

Algorithms

The physical model in a probabilistic analysis does not have to differ from the model used in a deterministic analysis. However, for the mathematical solution one has to use special algorithms:

- Mathematical analysis
- PEM
- Monte-Carlo simulation
- Reliability analysis

The algorithms presented above serve as useful tools in the solution of probabilistic analyses. The mathematical analysis is a straight forward method, however, restricted to not too complex problems. In *PEM*, the point estimate method, the input variables are given as two-point estimations, see Figure Σ.i. It is a simple method, which is easy to apply in a traditional deterministic model. The results are restricted to approximate values of the mean value and the variance of unknown variables. The practical application is limited to problems with a small number of random variables.

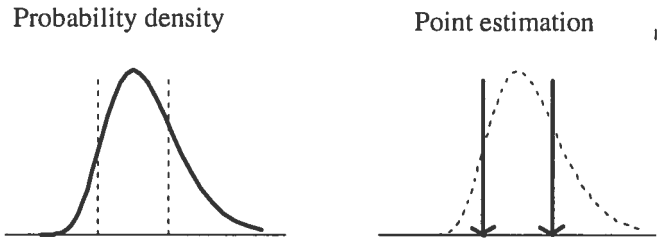

Figure Σ.*i* Principle of point estimate method - PEM

In a Monte-Carlo simulation values of input variables are simulated from a given distribution of the variable, see Figure Σ.ii. The simulation results in the complete distribution of any unknown, resulting variable. The accuracy is governed by the number of iterations. Only practical reasons limit the accuracy of the results. To obtain the tails of a distribution a very large number of iterations is required.

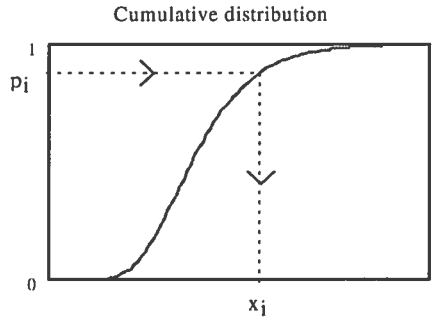

Figure Σ.ii Iteration step of a basic variable in Monte-Carlo simulation

In reliability analysis, the probability of failure can be represented by the reliability index β, see Figure Σ.iii.

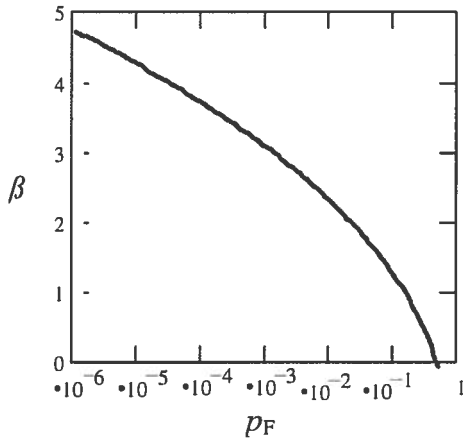

Figure Σ.iii Relation between reliability index β and formal probability of failure p_F.

Figure Σ.iii is based upon the original definition of β as a function of the parameters of the safety margin:

$$\beta = \frac{\mu_M}{\sigma_M} \qquad (\Sigma.ii)$$

To obtain a formulation, which is invariant of the mathematical formulation of the safety margin the reliability index can be defined as a geometrical property related to the failure surface, the reliability index $\beta_{H\text{-}L}$. The basic random variables X of a problem then have to be transformed into a set of independent standard normal variables U, cf. Figure Σ.iv.

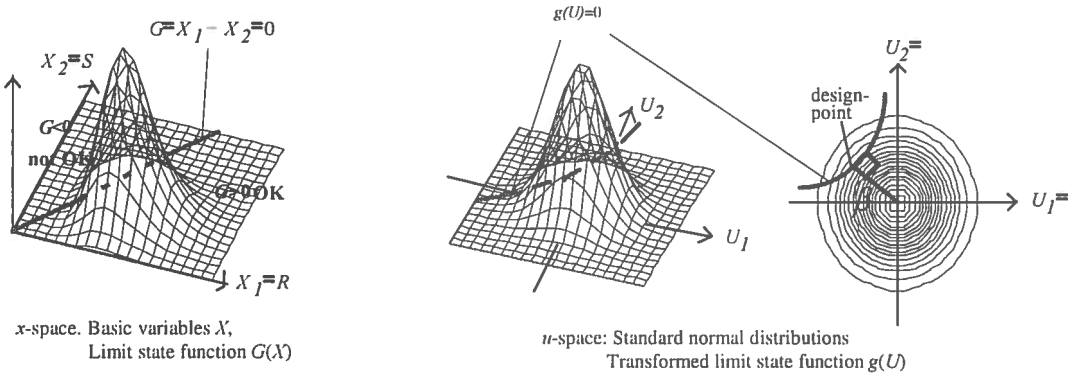

Figure Σ.iv Transformation of basic variables from x-space to u-space. The reliability index $\beta_{H\text{-}L}$.

Reliability analysis is used to calculate very small probabilities, preferably probabilities of failure. In this way the reliability analysis and the Monte Carlo simulation complement each other

Σ.3 Soil properties

When describing soil properties as random variables different uncertainties have to be accounted for

- Natural variation in the soil
- Systematic errors in the test method
- Random errors due to the test method
- Errors due to limited number of tests

Geostatistics

Geotechnical testing gives test values for soil properties in single points, while geotechnical problems usually are governed by the average values of soil properties of a volume. In geostatistics soil properties are modelled as random fields, i.e. an infinite number of random variables, each applied in a single point of a soil volume. The main purpose of geostatistics is to describe the dependence between these variables. Figure Σ.v shows observations of the shear strength versus depth together with two different alternative of a trend model of the shear strentgth. Deviations from the trend are in geostatistics considered as random variables. Plots of the correlation between such pairs of random variables, as a function of the distances between them, are called correlogram.

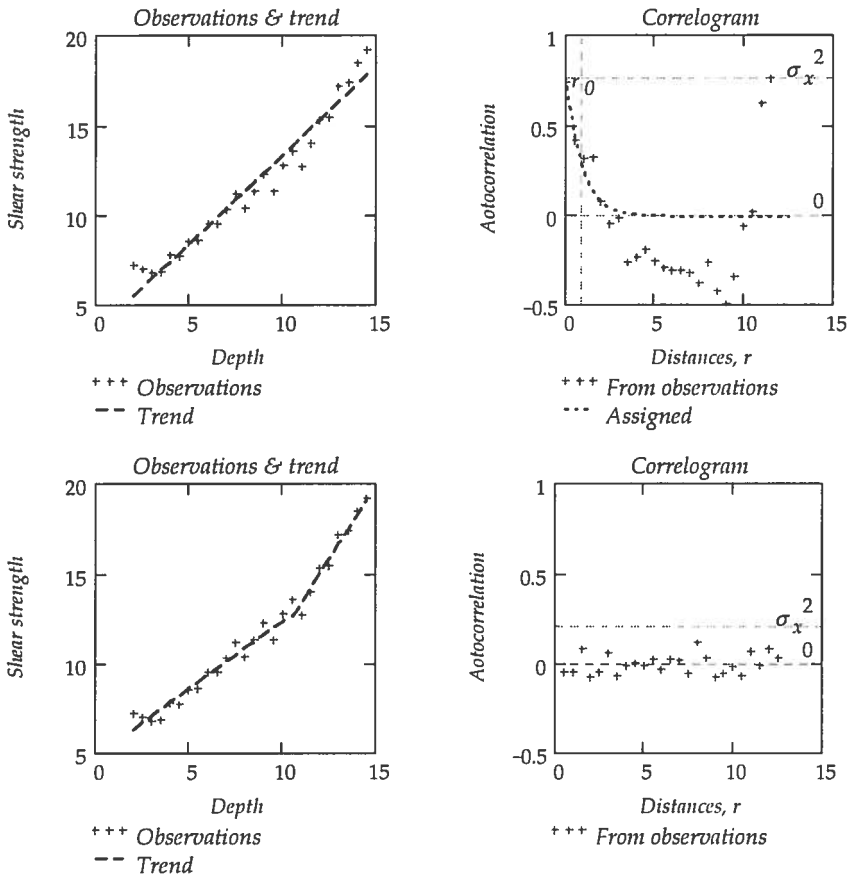

Figure Σ.v Influence on a statistical analysis from alternative models of reality.

Figure Σ.v draws the attention to an important issue in probabilistic modelling. The correlograms in the figure give completely different results for two, from a deterministic point of view, similar models of the shear strength. Hence, in random modelling the variations and the applied model form an unseparable pair. If both the test method and the model are perfect no variations exist. An interpretation of this is that variations in a probabilistic analysis are a measure of lack of knowledge.

Bayesian statistics

In traditional geotechnical design, pre-knowledge and test results are combined. In a statistical analysis this can be done systematically by Bayesian statistics. As an example, a prior distribution of an unknown mean value of a basic variable can be updated based upon added information, e.g. test results, see equation Σ.iii.

$$\begin{pmatrix}\text{Posterior prob.}\\ \text{of the true mean}\\ \text{given the sample}\end{pmatrix} = \begin{pmatrix}\text{Norma -}\\ \text{lising}\\ \text{constant}\end{pmatrix} \cdot \begin{pmatrix}\text{Sample likelihood}\\ \text{given}\\ \text{the true mean}\end{pmatrix} \begin{pmatrix}\text{Prior prob.}\\ \text{of the true}\\ \text{mean}\end{pmatrix} \qquad (\Sigma.\text{iii})$$

Thus with the added information the uncertainty of the unknown parameter is reduced.

Assume a situation in which pre-knowledge shall be valued as equivalent to the results of a test series. The pre-knowledge of the property can then be interpreted as an equivalent sample $\mathbf{x}_1$ of m tests such that:

$$\mu' = \bar{x}_1 \text{ and } m = \frac{\sigma^2}{\sigma'^2} \qquad (\Sigma.\text{iv})$$

if the standard deviation is known and

$$\ln \mu' = \overline{\ln x_1} \text{ and } m = \frac{V^2}{V'^2} \qquad (\Sigma.\text{v})$$

if the coefficient of variation is known. The parameter σ or V here denotes uncertainty of the basic variable, i.e. including measurement errors, while σ' or V' denote the uncertainty of the mean value of the basic variable. The result of such an up-dating process is given in Table Σ.ι.

	Prior information		**Up-dating no.1**		**Up-dating no. 2**	
	μ [kPa]	V [%]	μ [kPa]	V [%]	μ [kPa]	V [%]
Prior	-	-	15,6	19	14,1	12
Likelihood	-	-	13,9	6	13,8	5
Posterior	-	-	14,1	6	14,0	4
Baysian	15,6	22	14,1	12	14,0	11

Table Σ.i Baysian up-dating of the undrained shear strength. (=table 3.1 for z=10)

Pore pressure

It is a well-known fact that many failures in geotechnical design originate in mistakes in the assessment of the pore pressure. Hence, a procedure of a probabilistic description is of interest. An investigation of ground-water data from 39 observation series from the south of Sweden, shows that the application of a 'best' choice of distribution is far from trivial, see Figure Σ.vi. As could be expected,

variations in the topography of the landscape play a more important role than the choice of probability distribution.

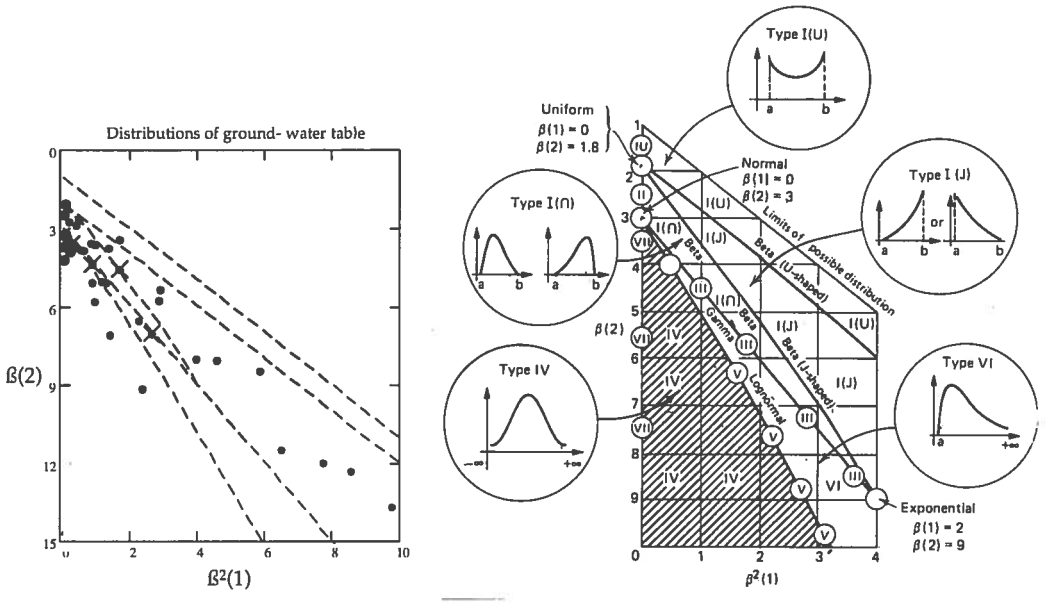

Figure Σ.vi Distributions of groundwater observations. Annual maxima.

Shear strength

The drained shear strength is normally given as a function of two effective stress parameters, the cohesion intercept c' and the friction angle ϕ. The difficult problem to asses the correlation between these two variables can be eliminated from the analysis by treating the shear strength, in a stress range of interest, as a random variable. The shear strength can in many practical cases be modelled in a wide stress range with only $\tan\phi$ as a random variable. This requires the use of the concept of attraction, i.e. cohesion seen as pre-stress instead of as adhesion.

If one wants to describe the undrained shear strength with effective stress parameters it s necessary to know the pore pressure in a failure zone is known. The magnitude of shear induced pore pressure is a complex problem. Hence in practical cases one is often forced to determine the shear strength as an 'index' value from field or laboratory tests. Hence the uncertainty of the test method has to be incorporated into a probabilistic description.

Σ.4 Slope stability - Ultimate limit state design

A pragmatic way to describe different situations of drainage conditions in a slope is to separate slope stability analysis into:

- Drained analysis
- Undrained analysis
- Combined analysis

Shear strength

To determine the in-situ stress state in a slope is difficult. Despite this, great efforts are made in slope stability analysis to relate the shear strength to this 'unkown' stress state:

$$c = c' + (\sigma - u) \cdot \tan(\phi) \qquad (\Sigma.vi)$$

In this thesis an alternative proposal is presented, i.e. to define the shear strength as the shear stress at failure:

$$c = \tau_{ult} = c' + (\sigma_{N,ult} - u) \cdot \tan(\phi) \qquad (\Sigma.vii)$$

in which $\tau_u \neq F \cdot \tau$. Besides the logical advantage with the definition, the amount of calculation work is reduced considerably in a slope stability analysis. This latter advantage is the main purpose of the definition in this thesis.

'Stable' slopes

An often raised issue is how to interpret in a probabilistic way the fact that a natural slope has proved to be stable during a long time. In this thesis the idea is presented that the observed fact of stability can be regarded as an ultimate control, hence the probability distribution for the safety margin can be truncated. This means that a slope with a long history has a larger safety than a new slope if the slopes in all other respects are equivalent.

Application

In the beginning of this section it was stated that a useful separation of calculation models is in three levels of complexity. Such a separation for slope stability analysis is summarised in the following.

Level 1- 'Design chart'

The level 1 method presented in this thesis is a probabilistic interpretation of the well-known 'design chart' method given by the equation:

$$F = \frac{N \cdot \overline{c_u}}{P_a} \qquad (\Sigma.viii)$$

with the safety margin $m = \ln(F)$. As an example, the distribution of the safety margin is given in Figure Σ.vii. The scale of the y-axis is in a normal probabilistic scale, i.e. a normal distribution gives a straight line. The simplicity of the procedure makes it a good complement to a more careful, deterministic analysis as well as a starting point for a comprehensive probabilistic analysis.

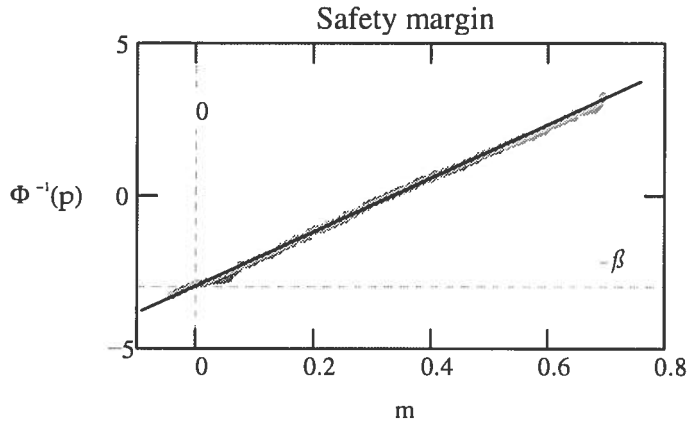

Figure Σ.vii Level 1. Undrained analysis. Reliability analysis and Monte Carlo simulation of the safety margin m=ln(F).

Level 2 - Bishop's simplified method

Bishop's simplified method is a well-known and often used model for slope stability analysis. In this thesis the method is combined with the shear strength presented in the section 'shear strength' and adapted to combined analysis. A result obtained from the analysis is that different types of analyses result in different critical slip circles, see Figure Σ.viii. The distribution of the safety margin for the 'most' critical slip circle is shown in Figure Σ.ix.

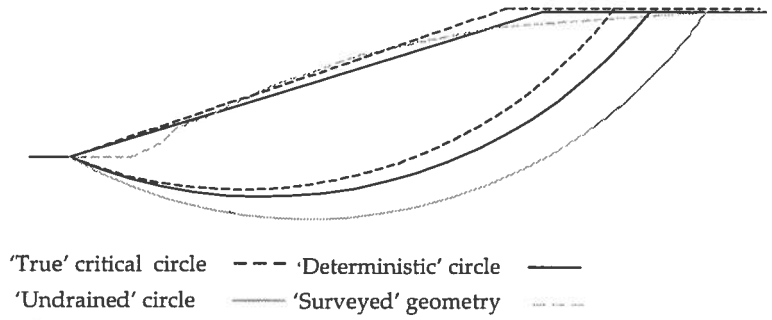

Figure Σ.viii 'Critical' slip circles

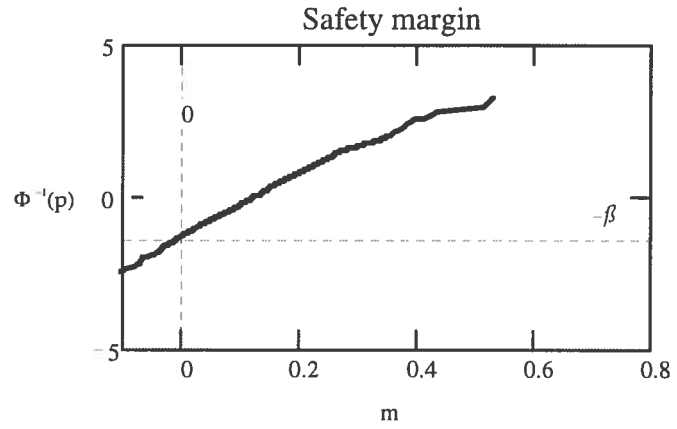

Figure Σ.ix Level 2. Combined analysis. Monte Carlo simulation of the safety margin. Alt. 'true critical circle'

Level 3 - A shear beam model

A proposal for a discrete element model for slope stability analyses is outlined. A slope is in the method modelled as a frame work of shear beams, see Figure Σ.x.

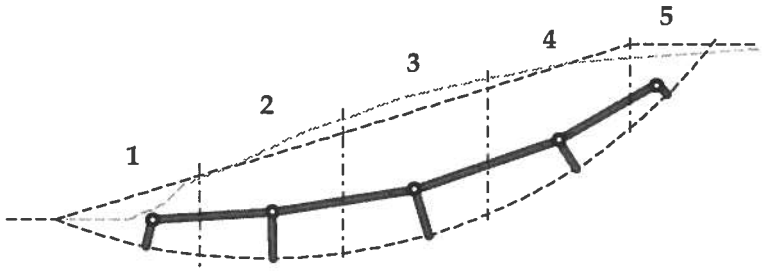

Figure Σ.x Geometry of the shear beam model.

The method does not include any assumption of a constant degree of mobilisation along a slip surface. Instead the deformation properties of the soil are considered. Figure Σ.xi shows the distribu-

tion of normal stresses at the slip surface for two different assumptions of stiffness distribution.

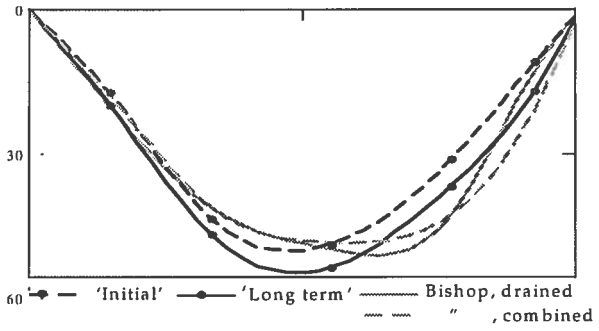

Figure Σ.xi Normal effective stress distribution.

The result of a probabilistic analysis is shown in Figure Σ.xii. The figure is an analysis of the same slip circle as the result in Figure Σ.ix.

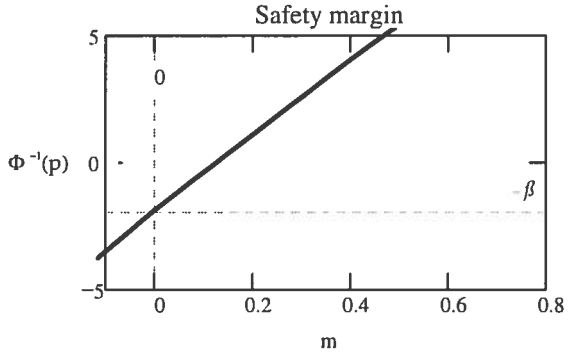

Figure Σ.xii Level 3. Shear beam model. Combined analysis. PEM-calculation of the safety margin. Alt. 'true critical circle'

Σ.5 Interaction ground/superstructure

Interaction between the ground and the superstructure is an issue of combining geotechnical and structural engineering. This thesis presents a number of means aimed at this purpose.

Spread foundations

As a tool of rapid assessments of stresses and strains in the soil Boussinesque's solution for an elastic half sphere is given an approximate formulation with high accuracy. Based upon this the vertical stress for a uniformly distributed surcharge p on an area B times L becomes:

$$\sigma_v(x,y,z)=\frac{p}{\pi^2}\cdot\left[\left[\frac{2z(B+2x)}{4z^2+(B+2x)^2}+\operatorname{atan}\left(\frac{B+2x}{2z}\right)\right]+\left[\frac{2z(B-2x)}{4z^2+(B-2x)^2}+\operatorname{atan}\left(\frac{B-2x}{2z}\right)\right]\right]\cdot\left[\left[\frac{2z(L+2y)}{4z^2+(L+2y)^2}+\operatorname{atan}\left(\frac{L+2y}{2z}\right)\right]+\left[\frac{2z(L-2y)}{4z^2+(L-2y)^2}+\operatorname{atan}\left(\frac{L-2y}{2z}\right)\right]\right] \qquad (\Sigma.ix)$$

Closed formulas for the settlements of the ground surface can be obtained by integration. As an example , the settlements of a line load can be approximated as:

$$s(x)\approx\frac{p}{\pi\cdot M}\cdot\begin{cases}\left[\left(\frac{50\cdot H}{40x+H}\right)^{2/3}-1\right] & ;\quad x>B/4\\ \left[\left(\frac{50\cdot H}{10\cdot B+H}\right)^{2/3}-1\right] & ;\quad x<B/4\end{cases} \qquad (\Sigma.x)$$

Piled foundation

Piled foundation adds an extra complexity as two elements with very different stiffness, the pile element and the soil have to interact. A useful tool is the concept 'the neutral plane', which can be estimated as:

$$z_{Nf}\approx 0{,}7\cdot(1-\eta)\cdot L \qquad (\Sigma.xi)$$

for constant shaft friction and as:

$$z_{Ng}=0{,}85\cdot\sqrt{1-\eta}\cdot L \qquad (\Sigma.xii)$$

for increasing shaft friction, where in both formulas η is the degree of mobilisation for the shaft friction.

A creep model

To determine volumetric creep deformations in clay a simple rheological model is given, see Figure Σ.xiii. Based upon the model the total deformations can be determined as a sum of elastic/plastic deformations and creep deformations by the equation:

$$s(t) = U_{\sigma}(t) \cdot \frac{P}{S} + s_{\sigma}(t) \qquad (\Sigma.\text{xiii})$$

The elastic/platic deformations are delayed compared to classical theory, Figure Σ.xiv.

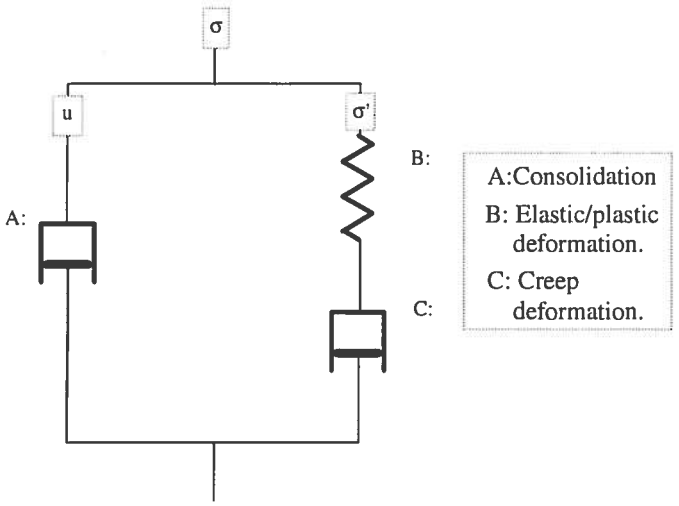

Figure Σ.xiii Rheological creep model

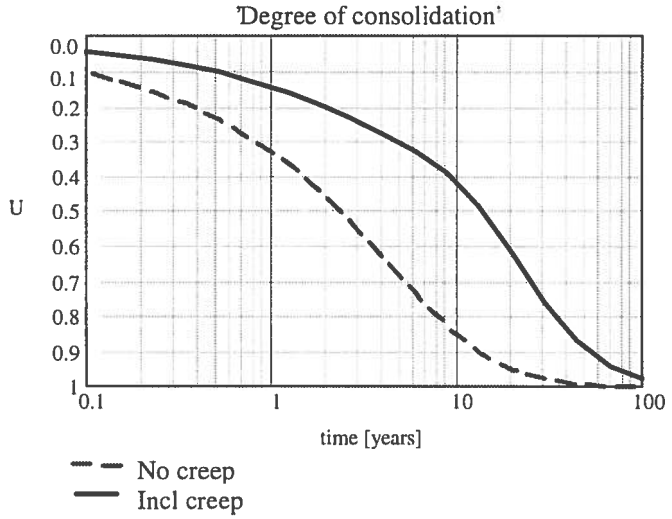

Figure Σ.xiv Influence of the dissipation of excess pore pressure due to creep.

An example of an application of the creep model outlined above is presented in Figure Σ.xv. The results are compared with results from a finite element method developed in Trondheim.

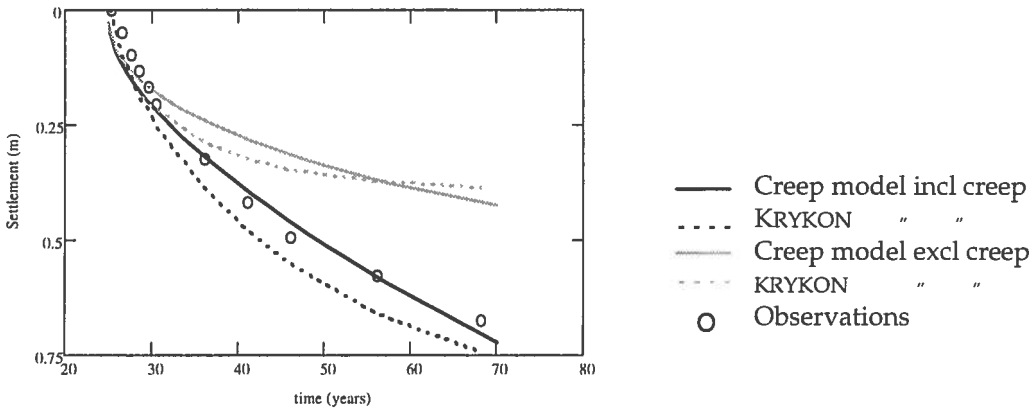

Figure Σ.xv Oslo railroad customs building. Calculated and observed settlements. From (Alén, 1998b) and (Svanø et al., 1991).

Application

Similarly as for slope stability applications are presented for three different levels of refinement. Figure Σ.xvi shows the cross-section of the analysed superstructure.

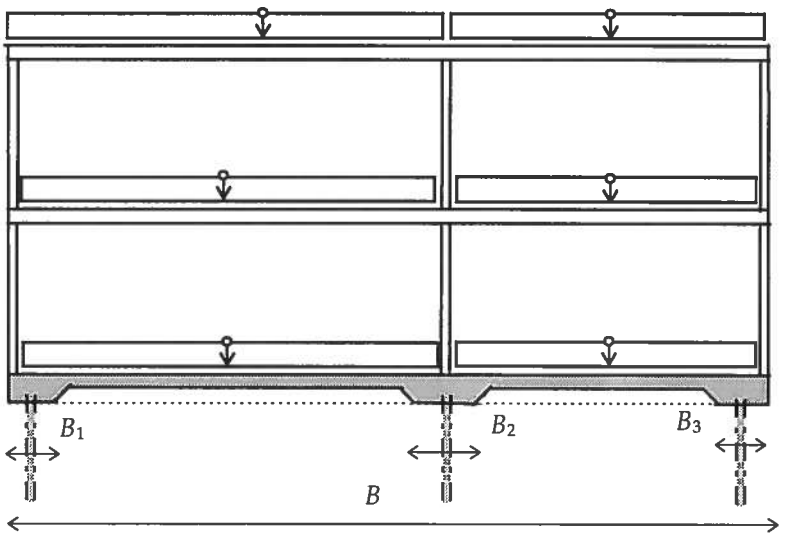

Figure Σ.xvi Cross-section of superstructure

Level 1 is based upon assumptions of rigid superstructure or fixed supports alternatively, Figure Σ.xvii.

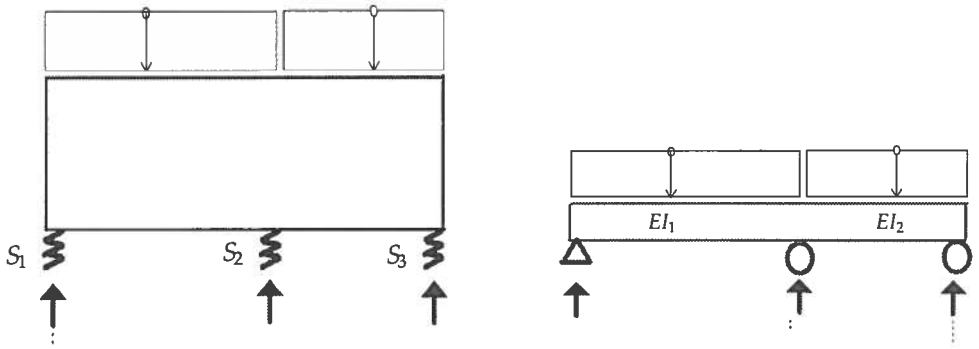

Figure Σ.xvii Level-1. Interaction model:
Rigid superstructure/Flexible supports and
Fixed supports/Flexible superstructure respectively.

Level 2 is an analysis of an elastic superstructure and spring supports, Figure Σ.xviii.

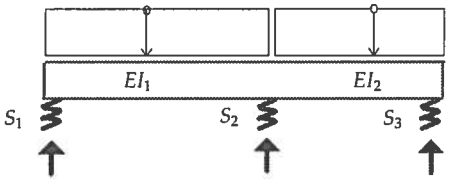

Figure Σ.xviii Level-2. Interaction model:
Flexible superstructure/Flexible supports.

In level 3 interaction in the ground between the supports is considered.

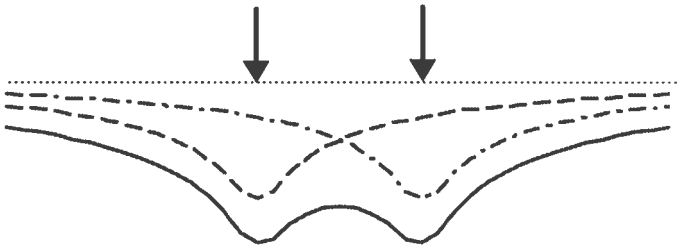

Figure Σ.xix Interaction in the ground between supports

A soil beam model represents the soil in the interaction analysis, Figure Σ.xx. The soil beam is a continuous shear beam on elastic supports. The idea behind the model is to calibrate the properties of the beam against a more rigorous geotechnical model.

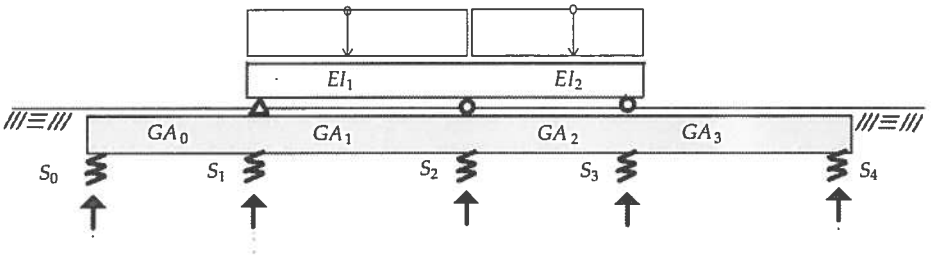

Figure Σ.xx Level-3. Soil beam model. Interaction between supports. Flexible superstructure/Flexible supports.

Figure Σ.xxi shows settlements obtained with the soil beam model.

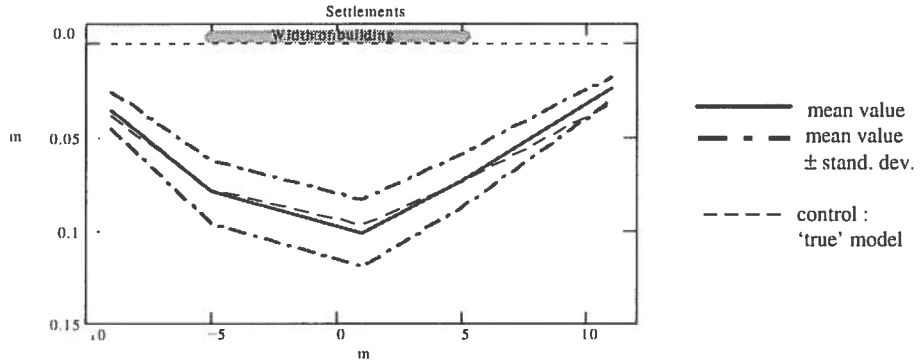

Figure Σ.xxi Soil beam model. Settlements.

Reactions and a bending section moment in the superstructure is summarised in Table Σ.ii. The table shows clearly the difficulties to determine appropriate section forces in a superstructure.

	R_1 [kN]		R_2 [kN]		R_3 [kN]		M [kNm]	
	μ	*V%*	μ	*V%*	μ	*V%*	μ	*V%*
Level 1	*Rigid superstructure*							
,	49	22	130	15	22	35	-70	17
Level 1	*Fixed supports*							
	73	20	66	19	61	18	80	28
Level - 2	*Flexible superstructure*							
	65	20	88	17	47	21	28	60
Level - 3,	*Soil beam model*							
	65	20	86	15	48	19	32	38

Table Σ.ii Example of interaction models Reaction and section forces.

NOTATIONS

This thesis includes concepts from three different disciplines, geotechnics, structural mechanics and mathematical statistics. Each discipline includes a number of concepts for which more or less standardised ways of notation exist. However, none of the disciplines have a complete standard set of notations. In geotechnics and structural mechanics different notations are used for the same concept and the same notation may be used for completely different concepts. As a result of this, notations used in this thesis may seem strange to some readers familiar with only one of the disciplines, even though they are very natural and standardised in another discipline. Below a list of notations, which are used in this thesis, is given. The list follows as closely as possible the notations used in the European design standards, the Eurocodes (e.g. ENV 1991-1 or ENV 1997-1). In modern codes, in structural mechanics, different notations for material properties as compared to stresses and strains have been introduced. This approach is adopted in this thesis. For example, lowercase Latin letters are used for strength parameters, while lowercase Greek letters are used for stresses.

Geotechnics and Structural mechanics

Latin uppercase letters

A	section area
E	modulus of elasticity
E	horizontal forces between slices in slope stability analyses
F	global safety factor
F_c	global safety factor, undrained conditions or total stress analysis
$F_{c,\phi}$	global safety factor, drained conditions or effective stress analysis
F_{comb}	global safety factor, combined analysis
G	permanent action (load)
G	shear modulus
I	moment of inertia
K	stiffness of support
M	compression modulus
M	moment, section force in a structure

M	safety margin
N	normal force
N	Section force in structure
P	action (load)
Q	variable action (load)
R	bearing capacity (resistance)
S	action effect (solicitation)
T	shear force between slices in slope stability analysis
W	vertical load on slices in slope stability analysis

Latin lowercase letters

a	attraction, cohesion given as 'prestressing'
c	shear strength
c'	cohesion intercept, cohesion given as 'adhesion'
c_u	undrained shear strength
$c_{c,\phi}$	drained shear strength incl. cohesion and friction
c_ϕ	" " " " friction
c_{comb}	combined shear strength, the minimum of the drained and the undrained shear strength
d	index for design value
f	degree of mobilisation
k	index for characteristic value
m	dimensionless safety margin
p'_c	preconsolidation pressure
u	pore pressure
y	deformation

Greek letters

α	angle
γ	partial factor or unit weight
ε	strain
θ	inclination of slope, (β used as a statistic parameter)
ϕ	angle of friction (also for effective stresses)
ϕ	diameter
σ	(compression)stress
σ'	effective stress

τ	shear stress

Statistics

Latin uppercase letters

$C[.,.]$	operator for calculation of autocovariance (or often autocorrelation)
$Cov[.,.]$	operator for calculation of covariance
$D[.]$	operator for calculation of standard deviation
$E[.]$	linear operator for calculation of expected (mean) value
$F(.)$	cumulative distribution
$G(.)$	limit state function
$Gu(\mu;\sigma)$	Gumbel distribution with mean value μ and standard deviation σ
$LN(\mu;\sigma)$	lognormal distribution with mean value μ and standard deviation σ
$LN_V(\mu;V)$	lognormal distribution with mean value μ and coefficient of variation V
$N(\mu;\sigma)$	normal distribution with mean value μ and standard deviation σ
PEM	*'p*oint *e*stimate *m*ethod'
$PD(\mu;\sigma)$	probability distribution with mean value μ and standard deviation σ
$\mathcal{R}$	Reliability
$R[.,.]$	operator for calculation of autocorrelation
V	coefficient of variation
$Var[.]$	operator for calculation of variance
$\mathbf{X}$	vector of random variables
X,Y,Z	random variables
$\hat{X},\hat{Y},\hat{Z}$	estimates of random variables

Latin lowercase letters

f	density(frequency) of probability
inf	lower bound (of an interval)
p	probability
$p(a\|b)$	conditional probability, $p(a)$ if b is given
r	estimate of coefficient of correlation

r	separating distance (in geostatistics)
s^2	estimate of variance (from a sample)
sup	upper bound (of an interval)
$\bar{x}$	mean value of a sample
x,y,z	samples of random variables
x,y,z	single values of random variables

Greek letters

α	sensitivity factor
β	reliability index
$\beta(1)$	skewness of a random (stochastic) variable
$\beta(2)$	kurtosis (flatness) of a random (stochastic) variable
$\varphi(.)$	density function for standard normal distribution, $N(0;1)$
μ	mean value of population
$\rho(X;Y)$	coefficient of correlation of two random variables X and Y
σ	standard deviation of a population
σ^2	variance of a population
Φ (.)	standard normal distribution[=N(0;1)]
$\gamma[.,.]$	operator for calculation of semivariance

Mathematical conventions

Equations in the thesis are mainly written with the software 'Microsoft Equation 2.1'. Hence, default conventions in this equation editor are used to simplify the typing. However, some of the appendices are prints of 'Mathcad' files, in which cases the notations differ slightly from other parts of the thesis. For example, Mathcad uses three different types of equal signs:

:= Definition symbol

= Equals sign in numerical applications

= Equal sign in symbolic applications

The two different expressions

$$if(x, a, b)$$

a	if x
b	otherwise

are equal with the meaning - a if x is true and b if x is false.

$A^{\langle n \rangle}$ denotes the n^{th} column of the matrix A

Multiplication point has to be used to separate e.g. the function $r(x-a)$ and the product $r \cdot (x-a)$. This convention is used frequently throughout the thesis to avoid misunderstandings.

Comma is used, when possible, as a decimal separator. This has not been possible, due to soft-ware reasons, in calculations and plots from 'Mathcad' files.

READER'S MANUAL

Structure of the thesis

The structure of this thesis may not follow a traditional academic concept in engineering. It is an attempt to synthesise ideas of calculation modelling from three different disciplines, geotechnics, structural mechanics and mathematical statistics. The basic principle is to describe a phenomenon in three stages:

- On a general level
- From a geotechnical point of view
- By examples

The thesis is divided into two volumes. A consecutive description of the subject area is given in volume 1, supplemented with a number of more specific appendices in volume 2. The main idea is that it should be possible to read the two volumes separately, although the areas covered are strongly interrelated.

Volume 1 contains four main chapters:

- Chapter 2 - Calculation models
- Chapter 3 - Modelling of soil properties
- Chapter 4 - Slope stability
- Chapter 5 - Interaction ground/superstructure

Chapter 2 forms the background to the three other chapters, while these three chapters are mostly independent of each other.

The order of the appendices in volume 2 follows the same order as the topics are covered in volume 1.

Overview

Chapter 2 - Calculations models contain, as a background, a general description of traditional, deterministic models. Random models are introduced on a principle level. A number of algorithms are discussed.

Uncertainty in the determination of soil properties is the main subject of Chapter 3 - Modelling of soil properties. How to deal with the problem with a probabilistic approach is discussed both principally and by examples.

Chapter 4 - Slope stability exemplifies the application of ultimate limit state analysis. The description is based upon three different levels of refinement of calculations.

The important interrelation between structural and geotechnical engineering is described in Chapter 5 - Interaction ground/superstructure. The main emphasis in the chapter is on serviceability limit state analysis.

The appendices in volume 2 give a description of certain topics covered in volume 1. The purpose is to collect detailed summaries, derivations of formulas etc., in order to give a logical and uninterrupted description in volume 1.

SOURCES OF INFORMATION

This thesis is based upon two main sources of information

- The author's professional experience during twenty years as a structural engineer
- Traditional academic literature survey

Professional design is mainly a team work. Persons with different backgrounds and experiences form a project team, with the purpose of making an optimal design. Participating in a number of such project teams means developing a personal design philosophy, which is the result of influences from many different persons and situations. This type of experience forms the base on which this thesis builds. As this is a process over several years it is difficult, if not impossible, to afterwards separate the different influences. Thus, without minimising the importance of these sources, it has not always been possible to give strict academic references. This remark mainly concerns Chapter 1 and Chapter 2.

A literature review is a quick and efficient way of obtaining knowledge of a subject. Consequently the literature review plays an important role in research. Different ideas gathered in such studies are referenced in this thesis. However, it is to a large extent an assembly of certain concepts which, taken separately in the different disciplines, belong to the basic, although not always, trivial concepts. Consequently, the effort has been to give an objective description of different models, procedures, methods, concepts etc., but the interpretation and way of applying them in design must be regarded as the author's own invention. In such cases, reference has not always been given to cited references. Nevertheless, even in this case some references play a more important role than others. Therefore, a number of the references could be named as main references, i.e. they have played an important role as a background for this thesis even in parts where it has not been possible to cite them directly. These are:

Ang & Tang (1975), Benjamin & Cornell (1970), Blom (1984 a & b), Ditlevsen (1984), Hansbo (1994)[1], Harr (1987), Hult (1968), Janbu

[1] Or more correctly, earlier set books used in undergraduate courses.

(1989), Mathcad (1995), Samuelsson & Wiberg (1988 & 1990), Thoft-Christensen & Baker (1980)

EXCLUSIONS

The contents of this thesis are by necessity limited. The ambition has been to describe topics from three disciplines, which together work as a unity. Thus, the purpose is to give an interrelatied survey of the subject and not a profound description of the separate parts. However, even with this limited objective, a number of approaches are excluded from the thesis, with the only purpose to reduce the extent of the project.:

- The thesis contains nothing specific about modelling of actions, with the exception of soil density and pore pressure. However, in Chapter 5, interaction ground/superstructure, effects of actions are considered.
- Examples of geotechnical applications are concentrated on soft clays.
- Finite element models are only covered on a very basic level.
- Geometrical models in three dimensions are excluded.

1 INTRODUCTION

1.1 Background

Today much effort in construction industry is put on how to predict the future. This can include giving a scenario of a ten-years perspective, an economic budget for the next year or a detailed planning of a building project. The purpose of these different tasks can be said to obtain good basic data for decision-making in order to minimise the risk for something unexpected to happen. The different activities can be said to be a part of a more or less systematised risk analysis.

In design technical calculations are important tools for verifying the function of a structure. However, the complexity of real problems have forced the analysis to be simplified. The calculations are in most cases done on the 'safe' side. This means that traditional calculations are normally not accurate enough to be used in a risk analysis. The easy access to computers today, means that more complex models can be treated. Different alternatives and 'what if' can be used. It is desirable is to develop this possibility in order to be able to determine probabilities or quantifying risks.

1.2 Geotechnics

1.2.1 General

The use of probabilistic methods in science has a long tradition. Normally , application of statistical analysis is based upon an extensive amount of observed data. In geotechnical applications the test results are limited. In statistical terms they form very small samples. To be able to apply probabilistic analysis in day-to day geotechnical practice, the idea of mathematical statistics has to be unorthodox. Application of such a concept can be structured into five different areas:

- Properties of soils - Natural variations - Soil models
- Tests - Accuracy and precision - Test methods
- Calculations - Model uncertainty -Calculation models
- Decision - Objective - Risk/Chance
- Control - Quality of performance - Monitoring

Each of these parts are important for the function of the system. However, they can be regarded as independent of each other, in the sense that methods can be developed separately in each area.

This thesis is dealing with the first three points, with emphasis on the third, calculations. The ambition is to apply different probabilistic methods to geotechnical problems. It deals with models of different accuracy and precision. For practical purposes, engineering simplicity are preferred rather than scientific refinement. However, results should be an improvement compared to present practice.

Two different types of problems are studied more in depth:

- Slope stability
- Interaction ground/superstructure

Those two types of problems are central in geotechnical engineering. They involve together a main part of relevant questions and complement each other in covering the subject.

1.2.2 Slope stability.

Analyses are mainly governed by shear strength, pore pressure, and actions. Action is here used as a generalisation of the traditional concept load, ENV 1991-1 (1994). The main issue is whether a slope, from a stability point of view, can be regarded as safe or not. The analysis is an example of design in ultimate limit state. Design criteria, with demand on low values of probability of failure, requires consideration of the extreme values, 'the tails', of random distributions. It also covers a field in which today's design practice includes rather 'high' risks.

1.2.3 Interaction ground/superstructure

Deformation are normally governing the design. Bearing capacity is then of minor concern. A failure will not lead to collapse but merely to damages and economic loss. Thus , the analysis is mainly done in the serviceability limit state. The risks varies between projects. They can range from minor cracks in partitions to a long time production shut-down at insufficient foundations of the manufacturing machinery. Maintenance costs have to balanced against construction costs. The problem is an optimisation problem. From a statistical point of view this means that the intermediate parts of statistical distributions have to be considered.

Interaction between the ground and the superstructure covers an area, which is frequently neglected in design. Structural codes demand interaction to be taken into consideration, see e.g. ENV 1997-1 (1994)). Despite this, very little is usually done in practice. To some extent this is due to complex calculation methods. A maybe more important reason might be lack of communication between structural and geotechnical engineers. In a successful interaction design, the structural engineer's knowledge of the frame has to be coupled to the geotechnical engineer's knowledge of the soil. By talking different design languages there is a risk that obtained information will be lost in the design process.

1.3 Calculations in the design process

Engineering can be divided into two different disciplines, engineering art and engineering science. It is difficult to give a clear distinction between these two parts, but if the art discipline is characterised by words as fantasy and intuition, key-words for the science part might be knowledge and understanding. Design is a creative task, which for its success demands a good balance between the two.

The process of design is a chain of decisions under uncertainty. A probabilistic approach is a method of describing such an uncertainty, and the calculation becomes a way to reveal the uncertainty. Thus, a calculation method should be seen as an operative tool in a constructive process and not merely as a verification of a prescribed minimum level.

1.4 Operative methods

As said previously, this thesis is concentrating on applications of calculation models in the geotechnical field. It is a synthesise of elements from three disciplines

- Geotechnical engineering
- Structural engineering
- Mathematical science

The coarse of action is to describe and develop what can be called operative calculations methods, i.e. here understood as methods that take all relevant factors into account and give a realistic result of their influence. The methods can be seen as a tool-box for a craftsman. The main limitation should be the professional skill of the crafts-man and not the quality of the tools. Thus, the calculation method should not be the obstacle, they must make room for the intuition of the designer to be put into design practice

Two elements that can characterise a calculation are its accuracy and precision. These two do not necessary go together, see Figure 1.1

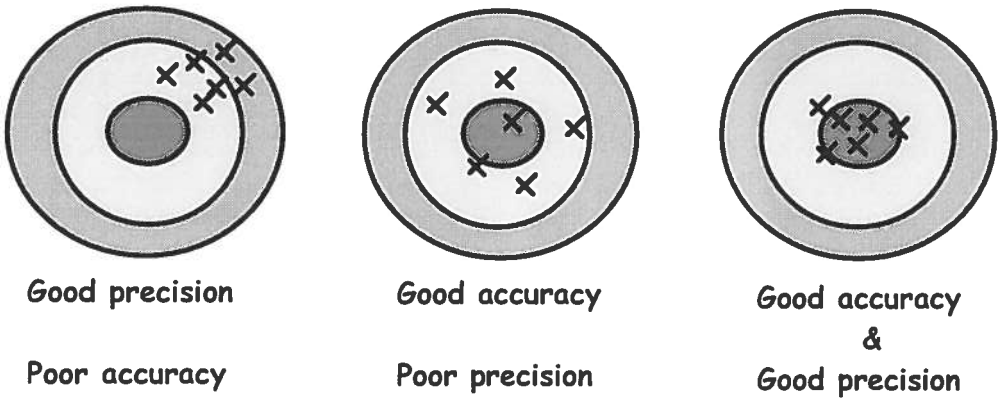

Figure 1.1 Precision and accuracy

A both accurate and precise calculation model is not necessarily better than a less precise one. It has to be seen in the light of its purpose. Often the former model demands more effort to carry out. In such cases, there must be a balance between the effort and the results. A precise, but not accurate model can fulfil it's purpose if it is a model on the safe side. However, it is a blunt instrument as it is

normally impossible to quantify how safe it is[1]. Thus, such a model leave no room for improvement of a design. An accurate, but not precise model can serve this purpose. It is possible to see the results of alterations. However, to be useful in practice, one must be able to quantify the uncertainty involved in the model. In this thesis, this is the purpose of the probabilistic approach.

Both accuracy and precision at the same time is of course excellent qualities. However, they should not be the only objectives in the developing of new calculation techniques. A good model means a sufficient balance between the following elements:

- Realistic description of reality. One can not expect an exact description of reality. However, there must be an amount of realism in the results. In recent years there has been a development into complex, deterministic models. The result of such refined methods are completely dependent upon the relevance of the input data. There must be a balance between the quality of the input data and the mathematical model.

- Simplicity. To be able to use a method one must understand the principles behind it. This does not mean that the mathematical calculations in themselves have to be trivial. Programming of complex mathematics can be left to specialists.

- Improvement of the state-of-the-art. A typical calculation in geotechnical engineering involves uncertain knowledge about unique projects. A natural ambition, with a new method, is to obtain a better base for decision making compared to today's practice.

- Recognition. In the field of geotechnics a large amount of emperi exists, tried in daily practice. Such knowledge must be inherited by new methods.

- Adaptation to codes. A calculation model can be ever so excellent. If it does not fulfil the requirement of society, its benefit will be reduced.

- Possibility of further improvements. A new model, regardless of its qualities, should never to be treated as the final one.

[1] If the 'error' is known the model is both precise and accurate.

2 CALCULATION MODELS

2.1 Traditional/deterministic models

2.1.1 General

Technical calculations are normally a central part in the design of buildings and other civil engineering projects. The purpose is to obtain basic data for decision-making in a project as a whole or for part of it. The results of the calculation are in this respect only one part of the complete basic data. In order to satisfy the demand of the builder and the society the conceptualisation and the corresponding calculations should give a relevant description of the actual behaviour of the structure. However, the knowledge is not sufficient to result in an exact description of the behaviour of the structure under all possible loading conditions. Even in those cases when the knowledge is very comprehensive, a simplified calculation is often used due to purely practical reasons. The calculation model is in this respect an approximate description of the true behaviour of the structure.

Calculation models develop in an everlasting process. New assumptions are added to existing methods. The idea is in general to improve the accuracy and the precision of the results. However, there is a danger in carrying this process too far. A model, which from the beginning is simple and easy to use, can be developed and become very complex and difficult to understand without resulting in any substantial improvement of the results. In such cases it might be better to incorporate the improved knowledge in a new formulation of the concept.

Ever since the days of Pythagoras, the number 'three' has been used to structure human thinking. This applies to philosophy, religion, politics etc. but also to such a down-to-earth subject as geotechnical engineering. A slope, for example, is divided into an active, an intermediate and a passive zone. Similarly, the complexity and accuracy of calculation models can often be classified hierarchically in three levels. This applies to the modelling of the physical reality, for example, one can use an elastic model (level 1), an elastic/plastic model (level 2) or a non-linear model (level 3). In the same way, the uncertainty of basic data and/or calculation results can be described by a fixed number (level 1), an interval (level 2) or as a continuous

distribution (level 3). The level of approximation chosen in a practical case is normally a balance between the demand of realism and precision versus how much effort one is willing to invest in the calculations.

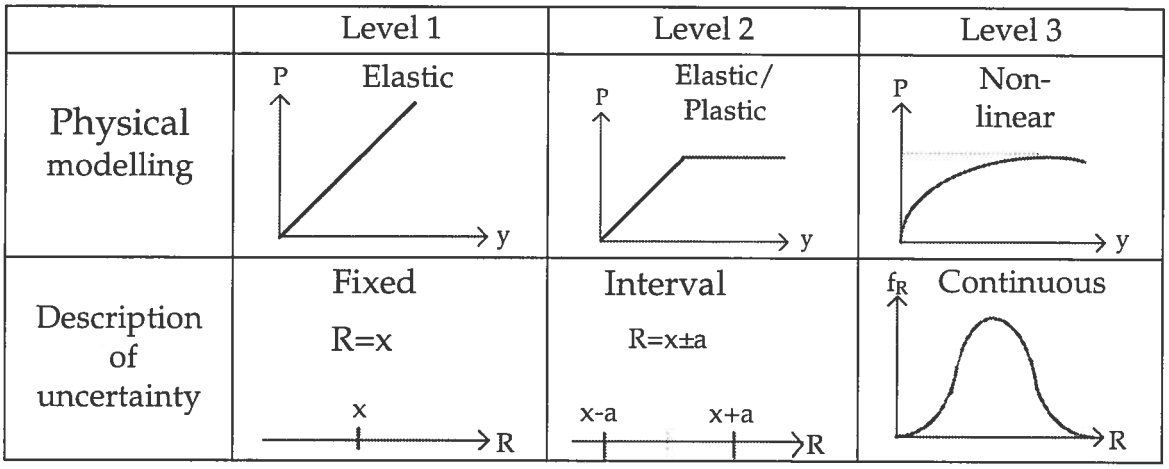

Figure 2.1 Different levels of refinement of models for calculation.

2.1.2 Principles of Calculation

Statically determined/undetermined structures

The geotechnical calculation models used and discussed in this thesis deal with bearing capacity and deformation problems for structures and soils. A useful separation of such problems can be obtained by separating them into statically determined and statically undetermined problems. Statically determined problems are those for which a number of equilibrium equations are sufficient to determine the internal forces. Thus the internal forces in the structure or the soil are independent of the deformations. For statically undetermined problems on the other hand, an unlimited number of solutions exist, which all satisfy the equilibrium equations. The correct solution is the solution which leads to deformations which are compatible with the deformation properties. This may lead to quite complex analyses. However, it is not always necessary to find the correct solution. Often a lower bound and/or an upper bound solution will be sufficient.

Limit analysis

In recent decades it has become mandatory in the design to verify structures in two different limit states, ultimate limit state and serviceability limit state. These two states give different types of de-

sign criteria for determining the calculation model. Verifying ultimate limit state corresponds to verifying an inequality, e.g. the bearing capacity (R) must be larger than the action effect (S), thus the criteria is $R \geq S$. As it is not necessary to know exactly when the equality is valid, simplifying assumptions of the calculation model can be introduced as long as these assumptions do not lead to an overestimation of the capacity or an underestimation of the action effect. The analysis is said to be on the safe side. In the serviceability limit state it is desirable to describe the expected behaviour. In this case, design on the safe side will often lead to uneconomic solutions. In principle this means that the calculation models used in the serviceability limit state in such a case should be more sophisticated than those used in the ultimate limit state. However, a design on the unsafe side will normally not result in a catastrophe. Thus, from a practical point of view, simplified models can also in this case often be used.

The behaviour of a structure can often be illustrated by a load/deformation-curve. In Figure 2.2, a typical curve is given. In the figure, the limits for ultimate limit state and serviceability limit state are indicated.

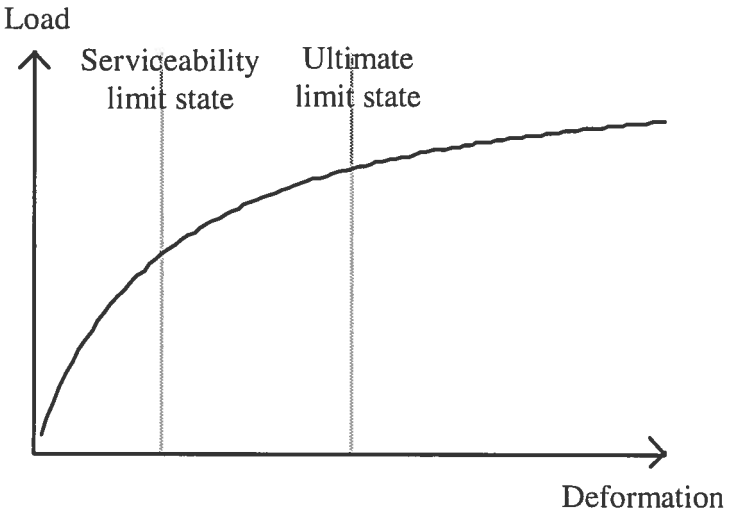

Figure 2.2 Serviceability limit state and ultimate limit state defined on a basis of a load/deformation curve.

In engineering practice, load/deformation curves are often assumed to be linear or bilinear, see Figure 2.3. In serviceability limit state, deformations can in most cases be assumed to be elastic. If, in ultimate limit state, the plastic part of the curve is long enough, the failure will be ductile. This means that there is a possibility of re-

distribution of forces between different parts of a structure. The bearing capacity can then be calculated with limit analysis, see e.g. Calladine, (1969) or Heyman, (1964). The limit actions will be that set of actions and action effects which transform the structure into a mechanism. When dealing with limit analysis the calculations usually concern the complete structure or large parts of it. When dealing with local stresses and corresponding strengths, one often refers to theory of plasticity.

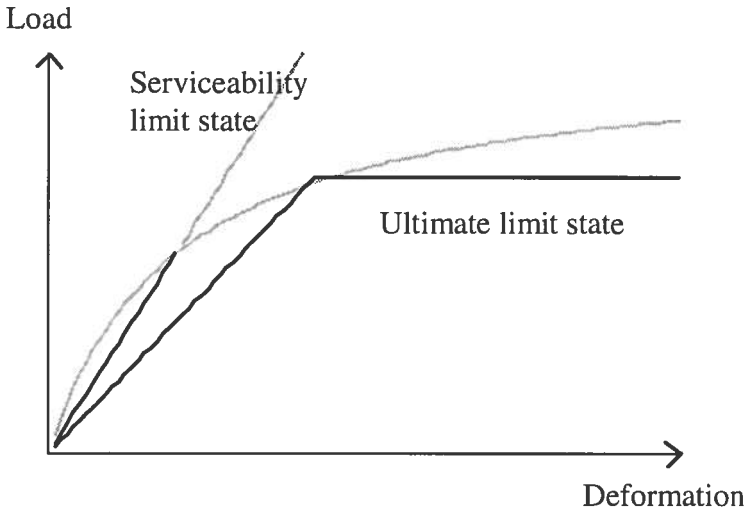

Figure 2.3 Load/deformation curves.
Serviceability limit state - Linear elastic.
Ultimate limit state - Elastic/plastic.

In applications of limit analysis two main theorems are used

- the lower bound theorem
- the upper bound theorem

The lower bound theorem is based on an equilibrium approach. If a set of actions and action effects satisfy equilibrium, and those action effects do not violate the bearing capacity in any part of the structure, the external actions are also on the safe side. The solution given by this theorem is a lower bound solution. Calculations based upon theory of elasticity fulfil the equilibrium criterion. Thus theory of elasticity is a special case of the lower bound theorem. In this case even deformations can be calculated. This is not the normal case in a limit analysis. The upper bound theorem is based upon a kinematical approach. A failure mechanism is assumed. For an incremental displacement, corresponding sets of actions and action effects are calculated. This set of actions forms an upper bound solution. As

the solution is an upper bound solution, it is essential to choose a mechanism close to the correct one. Only one failure mechanism exists, which does not violate the strength rule in any part of the structures. For that mechanism, the lower and upper bound theorem give the same solution, the theoretically correct solution. This solution is independent of the initial stresses. Thus, an important advantage with the limit analysis is the way it deals with the problem of initial stresses. Elastic solutions are often assumed to be initially stress-free, even if actual structures normally have residual stresses of significant magnitude. In limit analysis, the initial stresses can be ignored if it is the strength of a structure that is of major concern.

Both the lower and the upper bound theorem demand and assume a deformation capacity for which redistribution of action effects can take place. This means that a ductile failure must be governing the problem. In Figure 2.4, two often used stress/strain relations are illustrated.

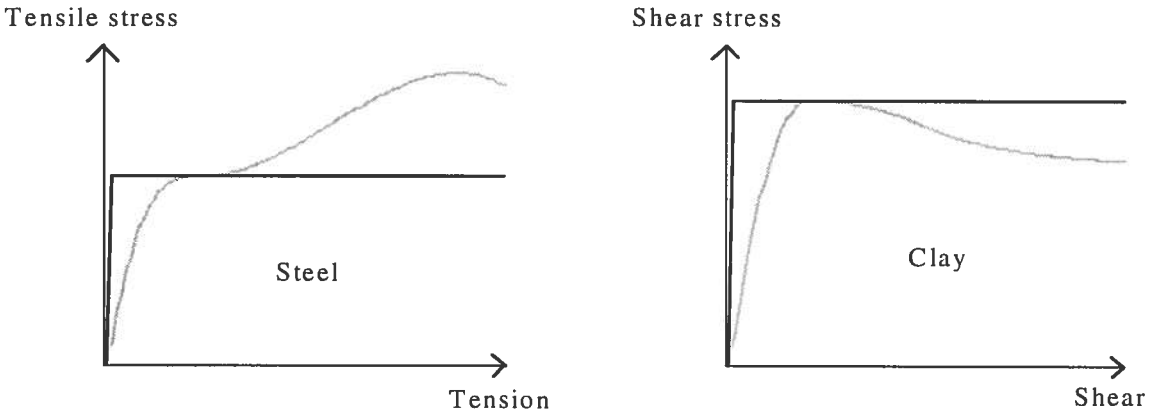

Figure 2.4 Typical stress-strain diagram for steel and clay respectively and corresponding approximations normally used in calculations based upon theory of plasticity.

The left figure illustrates a tension stress/strain relation for steel, together with a typical approximation used in the theory of plasticity. The right figure shows a similar shear stress/strain relation for clay at short term loading and the corresponding typical approximation. It can be seen from the figure that the approximation for steel is conservative. Overestimation of the strength at small deformations is well balanced against a conservative assumption close to collapse. For clay the conditions are more complicated. In principle, no possibility of redistribution of stresses exists unless

only the residual strength of the clay is taken into account. However, this is rarely done in practice. The concept of the lower and upper bound theorem is very useful when the problem is to judge whether a calculation model is on the safe side or not. This is further discussed in Chapter 4, Slope stability.

2.2 Safety Concepts

2.2.1 Factor of safety

Traditionally, the concept of a factor of safety has been used to describe the safety level both in geotechnical and structural engineering practice. In general terms the factor of safety can be defined as the ratio between the bearing capacity, R, and the action effect, S:

$$F = \frac{R}{S} \tag{2.1}$$

However, there does not exist any unique definition of the factor of safety. In geotechnical engineering practice, the factor of safety is mostly defined as the ratio between the average shear strength and the average shear stress. This can be seen as a concept in which the safety is put on the bearing capacity. In structural engineering it has been more natural to see the factor of safety as an enlargement of the action effect. For a prescribed minimum value of the factor of safety we get the two different criteria for design:

$$\frac{R/F}{S} \geq 1 \qquad \text{and} \tag{2.2}$$

$$\frac{R}{F \cdot S} \geq 1 \qquad \text{respectively} \tag{2.2a}$$

In these basic cases both inequalities lead to the relation:

$$\frac{R}{S} \geq F \tag{2.2b}$$

In other more complex circumstances it is not always trivial to define the criteria for design. A common and natural way is to apply the factor of safety only on the variable part of the load:

$$\frac{R}{F \cdot Q + G} \geq 1 \tag{2.3}$$

which gives

$$\frac{R-G}{Q} \geq F \tag{2.3a}$$

This is another value than

$$\frac{R}{Q+G} \geq F \tag{2.2c}$$

Similarly, when a structure is strengthened, the factor of safety is put only on the added part of the bearing capacity:

$$\left(R_0 + \frac{\Delta R}{F}\right) \Big/ S \geq 1 \tag{2.4}$$

resulting in

$$\Delta R \geq F \cdot (S - R_0) \tag{2.4a}$$

to be compared with

$$\Delta R \geq F \cdot S - R_0 \tag{2.2d}$$

2.2.2 Reliability index

In many new codes the ambition is to prescribe an acceptable risk. Risk can in this case be taken from a general risk concept, i.e. risk is a function of both the consequences of a failure, as well as the probability for this to happen. To describe the probability of failure, the uncertainty in the input data as well as the uncertainty of the calculation model must be considered. This could basically be done in two different ways, a stochastic/probabilistic analysis or a deterministic analysis. In a probabilistic calculation the variables are assumed to take values according to given random distributions. The probability of failure can then be calculated. The probability calculated in this way should normally be regarded as a formal probability, mainly because the calculated probabilities are often of such a small magnitude that they can not be related to experience. For example, it is difficult to mentally appreciate the meaning of a probability of 10^{-6}. The ambition is to obtain a description of the risk measurement, which facilitates the comparison of, for example, different foundation alternatives. A frequency interpretation in a clas-

sical sense is only meaningful in those rare cases when the amount of input data is large compared to the calculated probability. To underline the formal nature of the probability of failure, this probability is often given as an alternative risk concept, the reliability index β. For each value of probability a corresponding value of β is given, see example in Table 2.1. The values correspond to the formal function $p = \Phi(-\beta)$, thus the probability of failure is related to the standard normal distribution, see section 2.3.2. A more detailed description of the reliability index β is given in section 2.4.4.

Probability of failure (p)	0,5	10^{-1}	10^{-2}	10^{-3}	10^{-4}	10^{-5}	10^{-6}
Reliability index ß	0	1,3	2,3	3,1	3,7	4,2	4,7

Table 2.1 Relationship between formal probability of failure and reliability index β

2.2.3 Safety margin / Partial factors

Analyses, based upon a probabilistic concept, are in daily practice often replaced by a format in which partial factors are used. This format can be seen as a quasi probabilistic one. By separating the global factor of safety in an action part and a bearing capacity part, called partial factors, the design criteria according to the inequality 2.2. can be rewritten as

$$\frac{R}{S} \geq F = \gamma_R \cdot \gamma_S \qquad (2.5)$$

which again can be rewritten as

$$\frac{R}{\gamma_R} - \gamma_s \cdot S \geq 0 \qquad (2.5a)$$

The difference between the bearing capacity and the action effect is often called the safety margin, M=R-S. Thus

$$M = \frac{R}{\gamma_R} - \gamma_s \cdot S \geq 0 \qquad (2.6)$$

is the simplest way to describe the design criteria in the partial factor format.

By introducing more than two partial factors, more complex relations can easily be written, e.g.

$$M = \frac{R}{\gamma_R} - (\gamma_Q \cdot Q + \gamma_G \cdot G) \geq 0 \qquad (2.6a)$$

To determine a design value, the actual value to be used as input to the design criteria, is in the partial factor format a process in two steps. First typical values of the variables are determined. Those are formally named characteristic values, e.g. R_k and S_k respectively. These values can be seen as a given fractile of the variable when regarded as a random variable. Secondly, design values of the variables are obtained from the characteristic values by multiplying or dividing them with a partial factor. If the partial factors ≥ unity, 'safe' design values are obtained by multiplying action variables and dividing resisting variables, i.e. $R_d = R_k / \gamma_R$ and $S_d = \gamma_S \cdot S_k$. Combined with limit state design, i.e. separating design into ultimate limit state and serviceability limit state, this format has successfully been used in structural engineering since the 1970s. Formally, traditional design with a global factor of safety, (F), can be seen as a simplified procedure with all partial factors except one taken as unity. However, philosophically the two methods are quite different. In the traditional, deterministic method the action and the resistance are represented by fixed and known values. This means that the resistance *is* R, the action effect *is* S, which gives, when the action is multiplied by a global factor of safety, F, a safety margin :

$$M = R - S \geq F \cdot S - S = (F - 1) \cdot S \qquad (2.7)$$

or , when the resistance is divided by a global factor of safety, F

$$M = R - S \geq R - R / F = (1 - 1 / F) \cdot R \qquad (2.8)$$

Thus $F > 1$ implies $M > 0$.

By prescribing the factor of safety sufficiently larger than unity, a sufficiently large safety margin is obtained.

In the partial factor format, a probabilistic approach means that both R and S can take a wide range of values. This could be interpreted as the action and the resistance having fixed but unknown values.

The same is then valid for M also. The design values should represent one possible but unlikely combination, i.e. the resistance *is* $R_d = R_k/\gamma$ and the action *is* $S_d = \gamma_S \cdot S_k$. The unlikeness is quantified by the values of the partial factors. As M at least is not negative at the same time, as R and S have the rare combination R_d and S_d, the probability of failure is consequently low. This interpretation of the partial factor format means that the value of a partial factor should be chosen in such a way that a physically impossible design value is not obtained.

In Figure 2.5 the principal difference in describing a resistance variable in a probabilistic calculation compared to the partial factor format is illustrated. In structural engineering the 5-percentile is normally used as characteristic value. In Figure 2.5 the mean value is used instead, which is the normal case in geotechnical engineering both according to the European geotechnical code, EC7, (ENV 1997-1) and the Swedish structural code (BKR94:1). The characteristic value will then basically be the same as the deterministic value traditionally used[1].

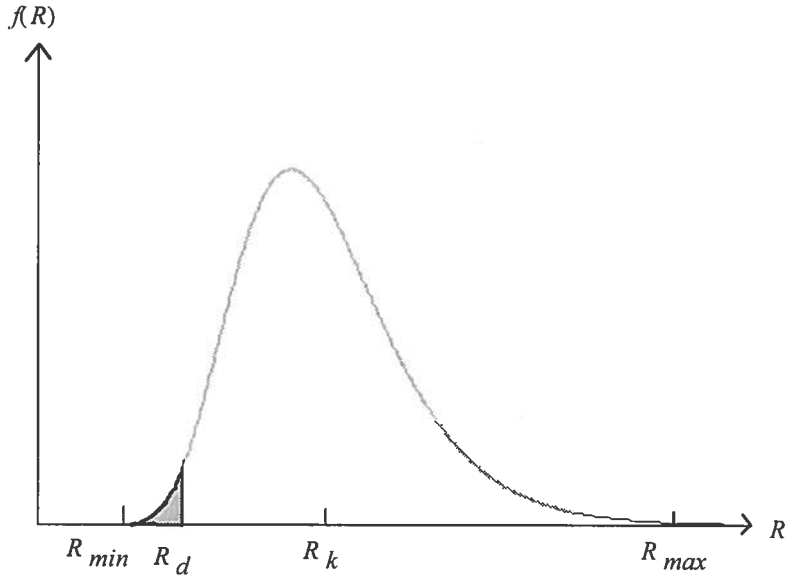

Figure 2.5 Principal description of the resistance in the partial factor format and a probabilistic concept respectively.
Partial factor format - The resistance = fixed values, R_k and R_d.
Probabilistic concept - The resistance = a random variable
Dotted area in the figure corresponds to the probability for the resistance to be less than the design value used in the partial format

[1] This is an interpretation, which can be discussed, cf. Chapter 3, section 3.5.1 'General'.

2.3 Random models

2.3.1 General

In the previous sections 2.1.2 and 2.2 different principles of mathematical descriptions of a physical property or relation have been described. These models described are approximations with different degrees of precision. A further complication is that the input data rarely is well defined. The results of the analysis are thus characterised by an uncertainty which depends on both uncertainty in the input data and uncertainty related to the calculation model. At its best, it can be concluded whether the results are on the safe side or not. A better approach would be if the uncertainty could be quantified.

A traditional calculation model consists of an equation or an algorithm where the values of the input data are determined in each case. As a result a unique solution of the problem is obtained. Such a solution can be called deterministic. If the designer feels uncertain about the accuracy, some of the values can be changed. By repeating this procedure a sufficiently large number of times an image of the range of the solution will be obtained. However, if there are many uncertain parameters the procedure will be far too cumbersome and unrealistic. If in calculations, in the sense 'most likely'/'best case'/'worst case', three values of each parameter are used, the number of calculations will be 3^N, where N is the number of variables. Apart from the extensive calculation work the same number of calculation results must be handled.

A more convenient way to deal with the problem above is to describe the uncertainty for the input variables as well as, if possible, for the calculation model. In its simplest form this can be done by applying two values for each variable, one value for the magnitude of the variable and one which reflects the scatter. This is, in a systematic way, done in mathematical statistics. Instead of dealing with common deterministic variables, random variables are used. These can take a range of values with different degrees of probability. Size and scatter are given by a number of parameters, e.g. the mean value and the standard deviation. By describing the pattern for the variation of the probability, a probability distribution is obtained. Graphically it can be illustrated as a 'bell shaped' density function, see Figure 2.6.

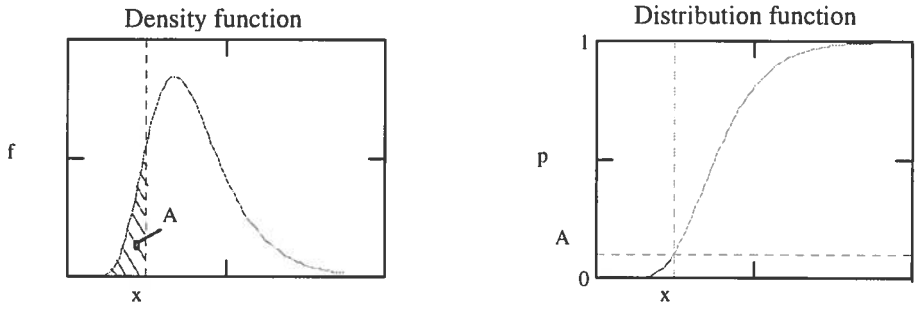

Figure 2.6 Example of a random variable illustrated by a density function or a distribution function

In classical statistics, in which the different outcomes can be given a frequency interpretation, the density function is named a frequency function. For a given value, the integral of the density function yields the probability for the random variable to be less than, or equal to, the given value. Such an integral is named a cumulative distribution function or only a distribution function.

Describing properties by random variables offers a possibility to consider uncertainties in the input data as well as in the calculation model in a consistent way. The difference compared to a deterministic model lies mainly in how the input parameters are given. The underlying physical model is the same. The uncertainty in the model can be taken into account by model factors given as random variables. The disadvantage with a probabilistic calculation model compared to a deterministic one is that the analysis becomes more complex. In order to maintain the level of complexity used in the deterministic calculation, it is often necessary to introduce a more simple physical description of the system. The question is whether to make the calculations "approximately right or exactly wrong"[1], i.e. with good accuracy or good precision.

2.3.2 Distributions

There exist a large number of different statistical distributions which are suitable for describing geotechnical problems. Which one to prefer depends on the nature of the property and to some extent on the problem at hand. Below, a summary of some continuous distributions often used in geotechnical modelling is given.

[1] Freely after a maxim with origin unknown to the author.

Normal distribution

This distribution is probably the most well known. It is often used due to its simplicity and its availability, even in many cases when it poorly describes a physical property. One of the most important theorems in mathematical statistics is the central limit theorem. It states that the normal distribution, under rather general conditions, is a good approximation for variables which are the sum of other variables[1], see e.g. (Benjamin and Cornell, 1970). An important case is the description of a parameter of a distribution if the parameter in itself can be seen as a mean value, i.e. a weighted sum, of other properties. As illustrated by its name, the central limit theorem, this same approximation is best for the central parts of the distribution. However, the normal distribution is an open distribution, i.e. there is no upper or lower bound for the distribution. Thus it is defined even for negative values. If for example the bearing capacity is given as a normal distribution, this assumption implies that bearing capacity can be negative, if only with a small probability. However, this small probability is not in any case negligible in ultimate limit state, where one has to deal with such small probabilities of failure. Another name, often used for the normal distribution, is the Gaussian distribution. A special case of the normal distribution is the standard normal distribution, i.e. the normal distribution with a mean value equal to zero and a standard deviation equal to unity. Any normal distribution can be transformed into the standard normal distribution by the transformation:

$$y = \frac{x - \mu}{\sigma} \tag{2.9}$$

This is a common transformation in statistics named location-scale transformation (Rootzén, 1995). The mean value, μ, serves as a location parameter and the standard deviation, σ, serves as a scale parameter. It implies, vaguely, that a variable is normed from its physical importance by the location parameter and by its statistical uncertainty by the scale parameter.

[1] A sum of independent normal distributions is also a normal distribution

Lognormal distribution

A property is lognormally distributed if the logarithm of the property is normal distributed. From the central limit theorem then follows that the lognormal distribution is a good approximation for products or ratios of random variables. As the logarithm of a negative value is not defined, a lognormal distribution can not take negative values. This is one reason the lognormal distribution is commonly used as a convenient way to describe resistance variables. (ISO 2394, 1986). Precaution should be taken not to apply the distribution too widely for other physical properties. The non-negative characteristic can also be fulfilled by using another distribution, the permeability of a soil can for example be modelled as an exponential distribution (Harr, 1997).

By taking the logarithm of a variable, calculations of lognormal distributions can be transformed into calculations of normal distributions, which in most cases is more convenient. A disadvantage with the distribution is that a location scale transformation will change the properties of the distribution unless the coefficient of variation is kept unchanged by the transformation.

Extreme Value distributions

In technical calculations it is often only the maximum or the minimum values of a physical property which is of interest, for example the wind load on a building under its entire life cycle. The wind force at a certain location varies quite randomly. The maximum value of a wind force in a year is dependent on the distribution of the wind force in time. This maximum value will be different from year to year, while even the maximum value can be described as a random variable. Such distributions of maximum (or minimum) extreme values of an underlying distribution form a class of distributions called extreme value distributions. If the extreme values represent, for example, the yearly maxima as described above, it is said to describe a 'partial maxima model'. If instead the extreme values are defined by all values in a time series, which exceed a given value, the model is called a 'peak over threshold model' (Rootzén, 1995). The two different principles are illustrated in Figure 2.7. The principles of maximum values are easily applied on minimum values by the use of the identity $\min\{x_i\} = \max\{-x_i\}$, (see e.g. Madsen et al., 1986)

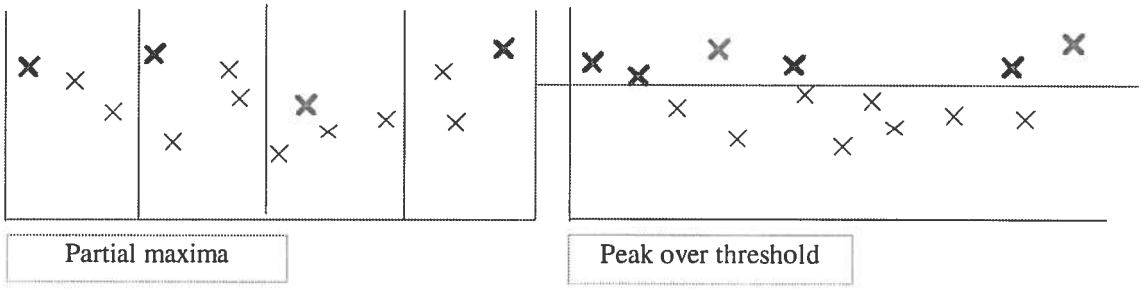

Figure 2.7 Principles of describing extreme values.

The Gumbel (or type I) distribution is a special case in the class of extreme value distributions, which is often used to describe the maximum of extreme values of loads, ENV 1991-1, 1994. The 'shape' of the distribution is 'unchanged' by a location and scale transformation (cf. appendix B).

Comparison between normal, lognormal and Gumbel distribution

In Figure 2.8 plots of a normal distribution, a lognormal distribution and a Gumbel distribution are shown. The scale of the y-axis for the plots of the cumulative distributions is chosen such that a lognormal distribution gives a straight line, i.e. as the inverse of a lognormal distribution, see appendix B. Each of the distributions shown in the figure can be defined by two parameters, e.g. the mean value and the standard deviation. In the figure the distributions are compared for the mean value equal to unity and three different values of the standard deviation; 0,05; 0,20 and 0,35. For the lowest value the normal distribution and the lognormal distribution are close to each other, while for the highest value the lognormal and the Gumbel distribution become almost identical[1].

[1] This is not valid for negative values as the lognormal distribution is undefined for $x \leq 0$

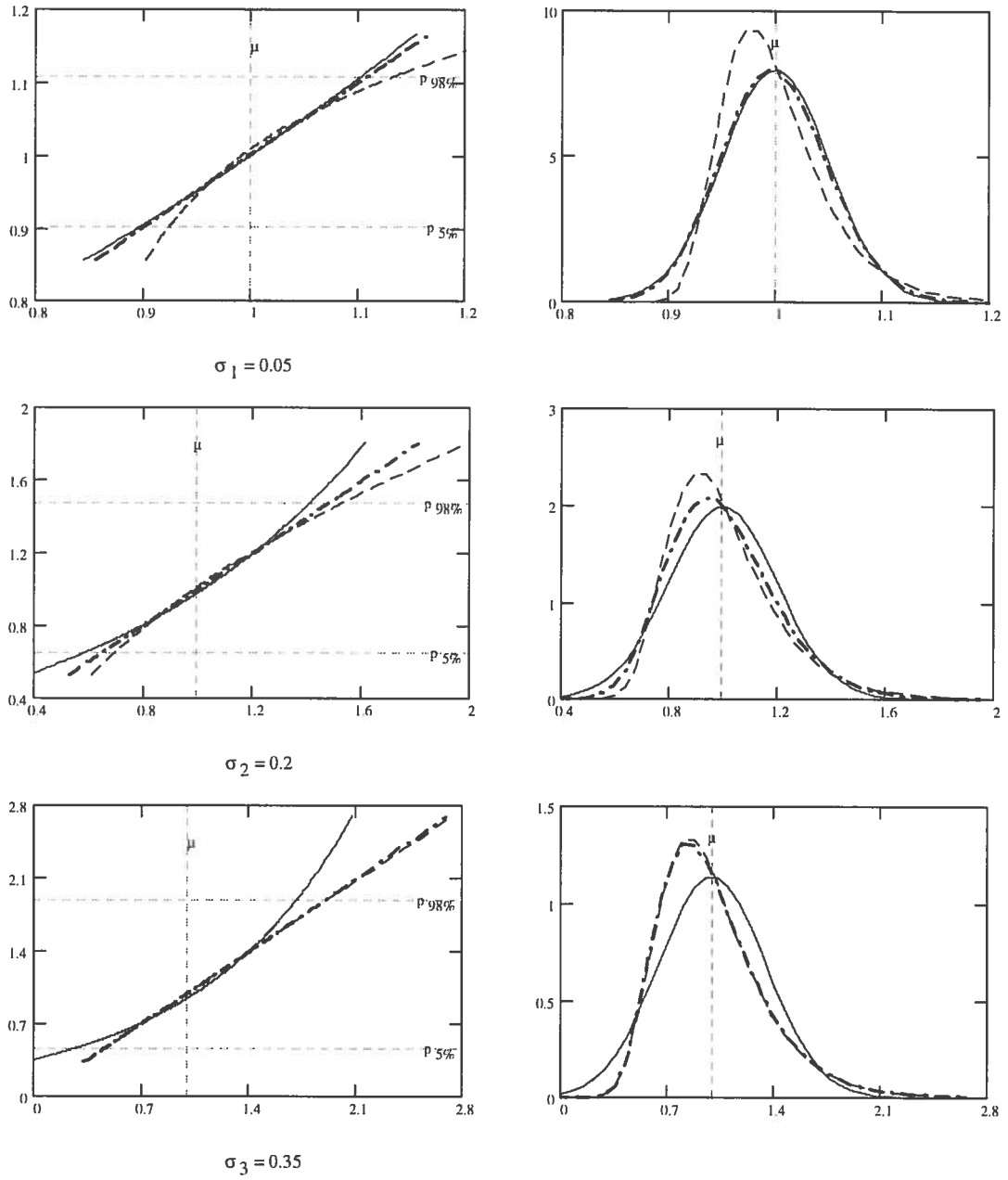

Figure 2.8 Comparison of the normal distribution, the lognormal distribution and the Gumbel distribution
——— normal — - — · lognormal ····· Gumbel
Left graphs show cumulative distributions.
Right graphs show the corresponding density functions.
(μ=1, σ=0,05; 0,20 and =0,35 respectively)

Permanent, structural loads, which have a small coefficient of variation[1], are often modelled as a normal distribution in engineering practice. Variable loads, which normally have a high coefficient of variation, are often modelled as Gumbel distributions, cf. pre-

[1] Definition see appendix A

vious section. An interesting conclusion, which might be drawn from what is said above and from Figure 2.8, is that the lognormal distribution can serve as a useful distribution describing both permanent and variable structural loads in engineering practice.[1]

β-*distribution*

An interesting distribution from a practical point of view is the ß-distribution. It can be defined by four parameters, the mean value, the standard deviation, the minimum value and the maximum value (Harr, 1987). The distribution gives maximum entropy for these four parameters. The entropy concept is here used as a measurement of the amount of 'disorder'. The distribution can, with the conditions given above, be seen as a distribution with a maximum disorder, i.e. a distribution on the 'safe side'. Another, more common, way to define the distribution is to replace the minimum- and maximum values with values of the skewness and kurtosis (peakedness) of the distribution. The density function for a β-distribution can have very different shapes, see Figure 2.9.

It should be noted that the distributions named type VI in Figure 2.9, which are unbounded in their upper part, are no β-distributions[2]. A disadvantage with the β-distribution, when calculating small probabilities, is that the tails are principally governed by the assumption of the minimum and maximum values[3]. As one seldom have in-depth knowledge of these values, they are normally outside the range of any measured value, the calculated probabilities are somewhat arbitrary. It should be pointed out that the name β-distribution has nothing to do with the reliability index *ß*.

[1]This should not be interpreted such that the lognormal distribution is comprehensive distribution, which can replace other distributions in detailed analysis. Only that it might work as a simple engineering tool for rapid assessments.

[2] Nor are the distributions in the shadowed area any β-distributions.

[3] Or the values of the skewness and the kurtosis.

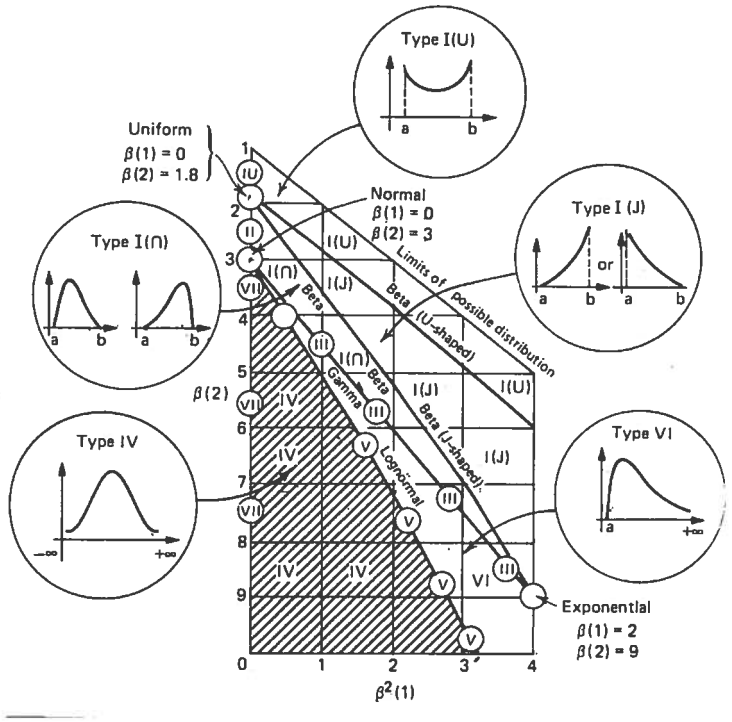

Figure 2.9 Scheme for different types distributions. The scheme, which was compiled by Pearsson and Hartley, is taken from (Harr, 1987).

Exponential distribution

The reliability of a system is the probability that it will fulfil given requirements, i.e. the opposite to failure. Thus the reliability that a system survives longer than a time, t, is given as, $\mathcal{R}(t) = 1 - F(t)$, where $F(t)$ is the distribution for the failure time. The failure rate at time, t [1], can be found as the conditional probability for the change of failure time given that the system is reliable at time t (see e.g Lapin 1983):

$$h(t) = \frac{dF}{dt} \cdot \frac{1}{\mathcal{R}(t)} = \frac{f(t)}{\mathcal{R}(t)} \qquad (2.10)$$

The failure rate changes typically with time as given in Figure 2.10.

[1] Also called the hazard function.

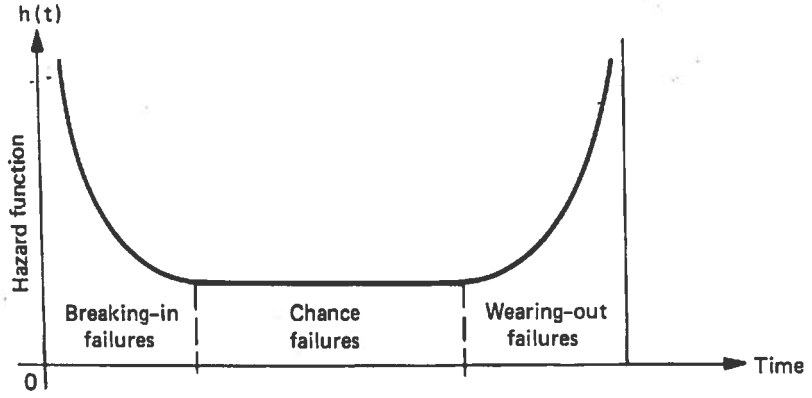

Figure 2.10 Failure rate with time. From Harr (1986)

In geotechnical engineering, during the serviceability state, failure can often be seen as a chance occurrence, i.e. a constant failure rate. Introducing the failure rate, λ, and recalling $\mathcal{R}(t)$ = 1- $F(t)$, i.e. $d\mathcal{R}(t)/dt = -f(t)$ it follows from equation 2.10 that (see e.g. Harr, 1986):

$$f(t) = \lambda \cdot \exp(-t \cdot \lambda) \tag{2.11}$$

$$F(t) = 1 - \cdot \exp(-t \cdot \lambda) \tag{2.11a}$$

$$\mathcal{R}(t) = \exp(-t \cdot \lambda) \tag{2.11b}$$

The distribution for the life time (and reliability), given by equation 2.11, is the exponential distribution. The appearance of the graphs of the density probability and the cumulative probability are shown in Figure 2.11. As could be seen from equation 2.11 the distribution is defined by a single parameter, e.g. the failure rate (or mean value[1]). This could serve as an intuitive support for the fact that the exponential distribution is the distribution of maximum entropy when only one parameter is known, cf. page 23 (Harr, 1986). Apart from life time analyses it is therefore a distribution to describe variables, which are known only as to their magnitude. An example of such knowledge in geotechnical engineering might be the permeability (Harr, 1997). However, in most cases the information given is not that restricted. For example, one knows by experience that a resistance variable has a coefficient of variation considerably smaller than, say 50%. The exponential distribution, which has a coefficient

[1] $\mu = 1/\lambda$

of variation equal to 100%, is then a conservative choice for modelling of the variable.

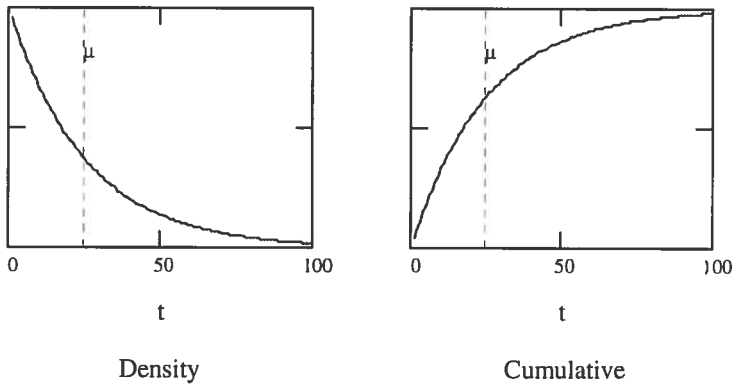

Figure 2.11 Exponential distribution

Choice of distributions

When choosing a statistical distribution for describing a physical property, one normally must rely on existing knowledge of the physical nature of the property. The number of samples tested is normally so small in a geotechnical investigation that one should expect to obtain very little information about the shape of the distribution. Hence, it is normally not possible to determine the type of distribution solely from the result of a geotechnical investigation. This is clearly illustrated in Figure 2.12 and Figure 2.13. The figures show the result of two simulations of samples of twenty units. Translated into geotechnical testing, this would mean an extensive testing. In each simulation a sample is taken from each of three given distributions, a normal distribution, a lognormal distribution and a Gumbel distribution. All distributions are with known mean value and standard deviation, $\mu = 1$, $\sigma = 0{,}2$, see Figure 2.8. The simulations used are examples of Monte Carlo simulations described later, see 2.4.3. For each simulation, the sample is based upon the same probability series of twenty random numbers. It can be concluded from the figures that the difference between the two different simulations is much greater than the differences between the three distributions in any of the simulations.

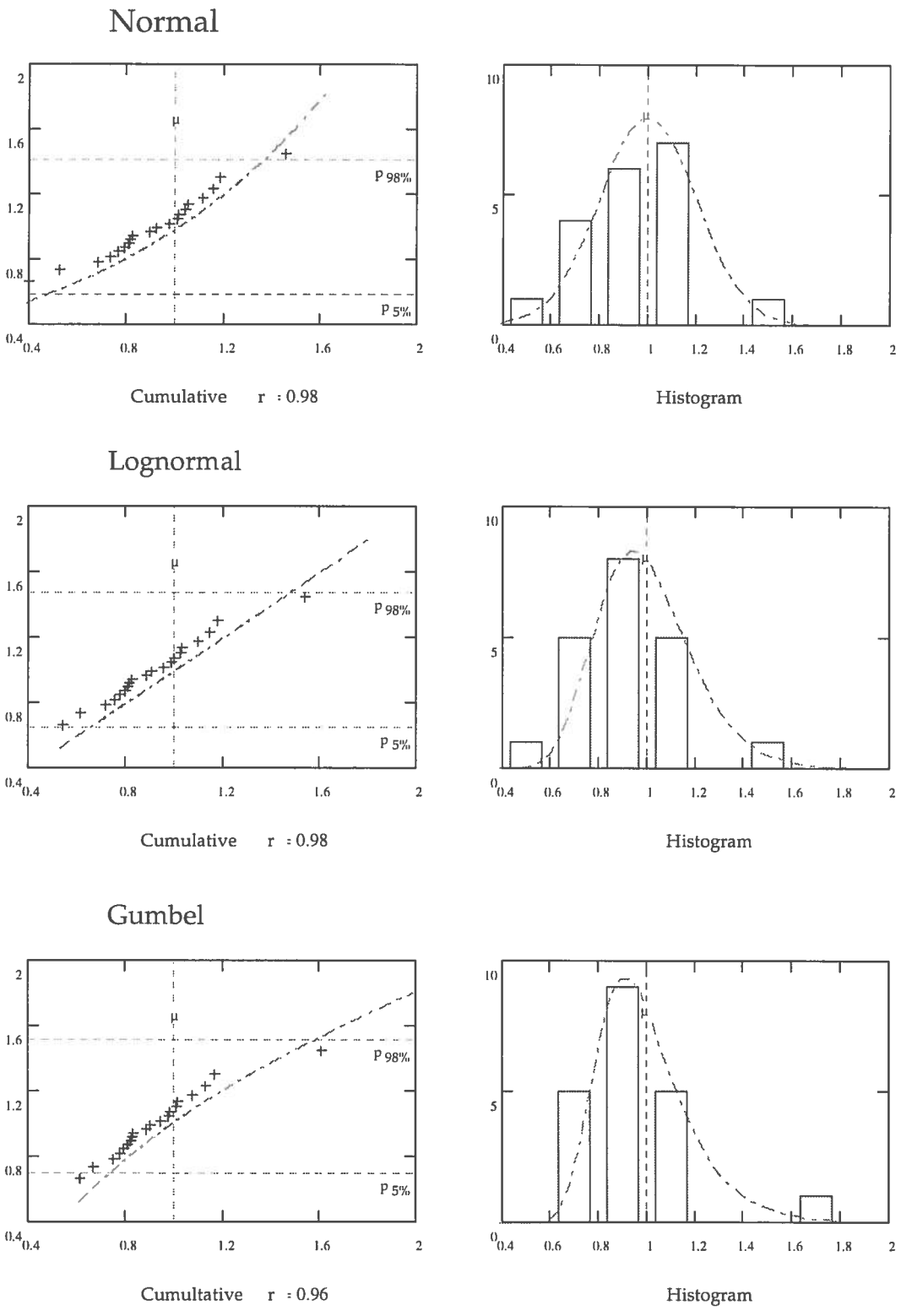

Figure 2.12 Simulation A of a sample from a normal, a lognormal and Gumbel distribution. Sample size = 20. Parameters of population in each case, $\mu = 1$; $\sigma = 0{,}20$

– – – – – – true distribution + + + + + sample

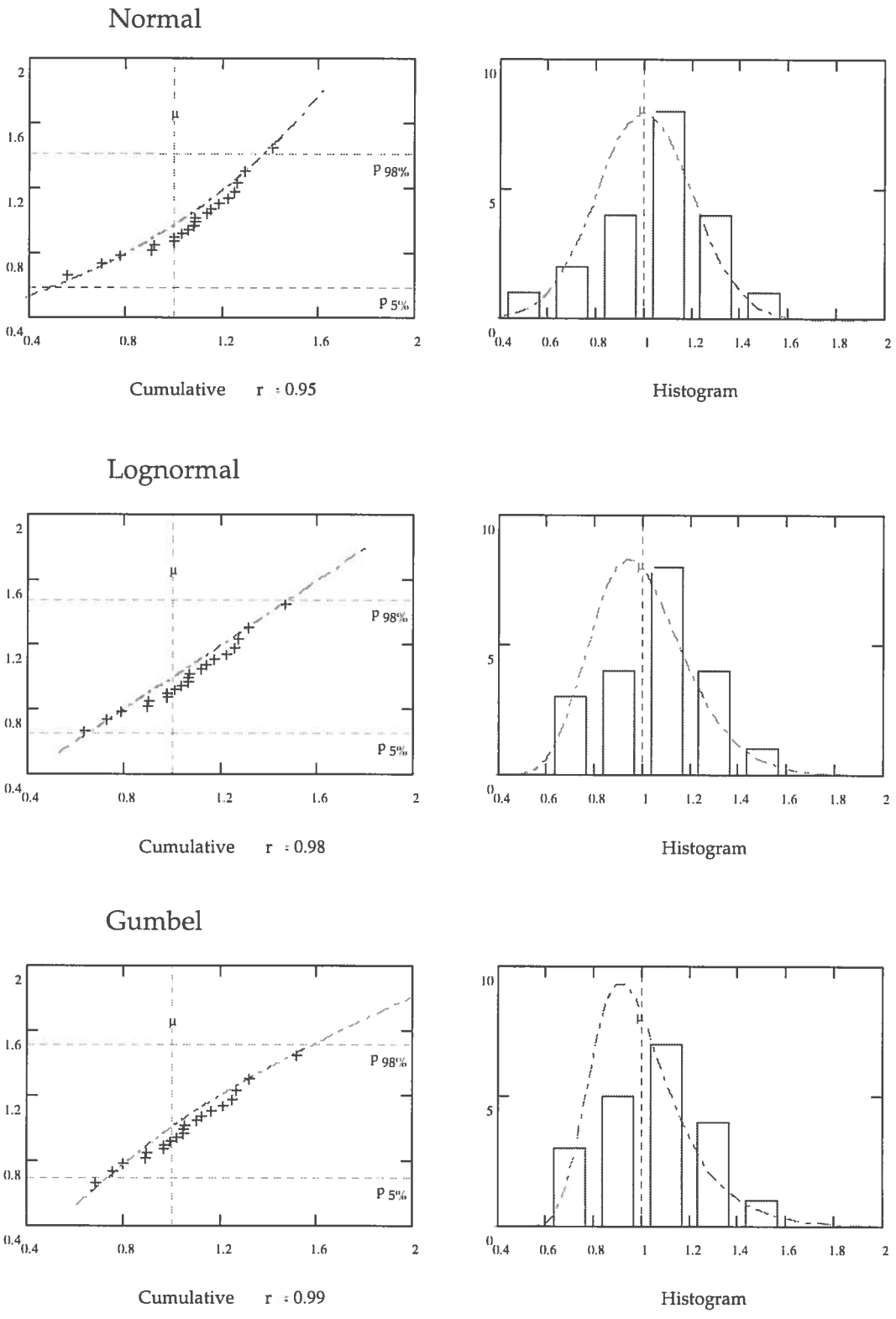

Figure 2.13 Simulation B of a sample from a normal, a lognormal and Gumbel distribution. Sample size = 20. Parameters of population in each case, $\mu = 1$; $\sigma = 0{,}20$

— · — · — · — true distribution + + + + + sample

A statement, which to some extent is contradictory to the idea that a distribution should be chosen from physical properties, is that the choice of distribution is a true code issue and not up to the individual engineer (Ditlevsen, 1993). The idea behind this is that the formal probability demanded and the choice of distributions are an unseparable pair, based upon empirical knowledge and often originating from calibration of existing structures. This implies that, when developing a probabilistic model, one has to take the complete model into account and not only a separate part.[1]

A common reason for a particular choice of distributions is a wish to obtain simple calculations. This is a strong reason, which must not be neglected. In this respect it is worth noticing that nowadays many computer programs, reaching from spread sheet programs to specialised statistical programs, contain functions for analysis with probability distributions. For example, all calculations and corresponding graphs in this section are undertaken with the software Mathcad, which is a comprehensive program for mathematical analysis (Mathcad, 1995).

2.3.3 Dependence / Correlation

Two different random variables often do not vary independently of each other. As a measurement of this dependence the concept of correlation is often used. It could be described as a measure of linear co-variation between two variables, see Figure 2.14

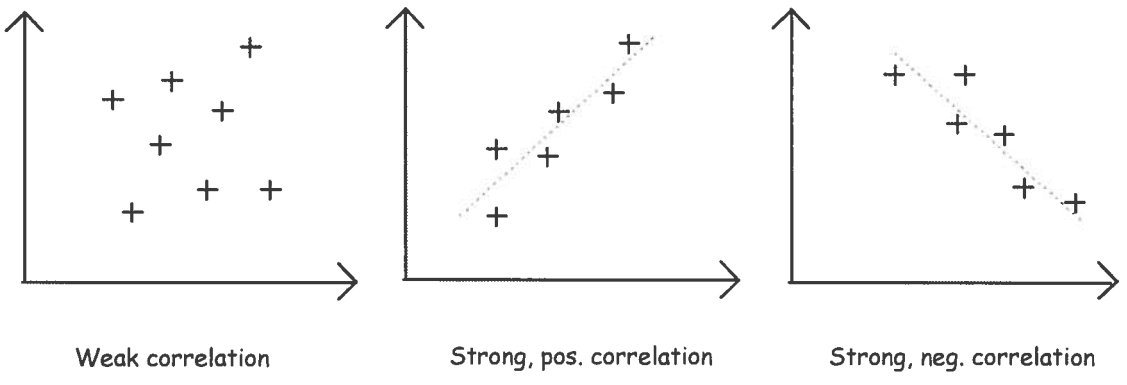

Figure 2.14 Principle graphs illustrating correlation (/ linear co-variation)

[1] This argument should not be restricted to the use of probabilistic thinking, but might be used in many other situations of engineering practice.

The correlation is a measure of the statistical dependence, if any, between two variables but does not constitute proof that the causal dependence really exists.[1] Nor does it say anything about cause and effect. For example, a phenomenon B can be caused by a phenomenon A, alternatively A can be caused by B or, as a third alternative, both A and B can be caused by a third phenomenon C. In all these three cases there might exist a statistical correlation between A and B. An example, from geotechnical engineering, of the third case, is the cause of the soil strength (A) and the soil stiffness (B), which are both caused by the pre soil pressure (C). The magnitude of correlation between two variables is expressed as the covariance, $Cov[X,Y]$ or, in a dimensionless form, as the coefficient of correlation, ρ (for exact definition, see appendix A).

Mutual dependency between more than two variables can be expressed with the covariance matrix, which for a number of variables, $X_1, X_2, \ldots, X_n$ will be defined as:

$$\mathbf{C}_x = \begin{bmatrix} Var[X_1] & Cov[X_1,X_2] & \cdots & Cov[X_1,X_n] \\ Cov[X_1,X_2] & Var[X_2] & & \vdots \\ \vdots & & \ddots & \\ Cov[X_1,X_n] & \cdots & & Var[X_n] \end{bmatrix} \tag{2.12}$$

or, in a dimensionless form, the correlation matrix:

$$\rho = \begin{bmatrix} 1 & \rho_{x_1x_2} & \cdots & \rho_{x_1x_n} \\ \rho_{x_1x_2} & 1 & & \vdots \\ \vdots & & \ddots & \\ \rho_{x_1xn} & \cdots & & 1 \end{bmatrix} \tag{2.12a}$$

If the covariance matrix, or the correlation matrix, is a diagonal matrix, obviously the variables are uncorrelated. According to the spectral theorem for symmetric matrices[2], such a set of uncorrelated variables, $Y_1, Y_2 \ldots Y_n$, can be obtained by the transformation (see e.g. Thoft-Cristensen, 1980, or Harr, 1986):

$$\mathbf{Y} = \mathbf{A}^T \cdot \mathbf{X} \tag{2.13}$$

[1] Frequently observed correlation is frequently taken as a proof of dependency.
[2] See e.g. Beta, (1990)

where **A** is an orthogonal matrix with column vectors equal to the pairwise orthogonal and normed eigenvectors of $\mathbf{C}_x$. **Y** is the column vector $(Y_1, Y_2, \ldots Yn)^T$ and **X** is the column vector $(X_1, X_2, \ldots X_n)^T$. Furthermore,

$$\mathbf{C}_y = \mathbf{A}^T \cdot \mathbf{C}_x \cdot \mathbf{A} = \mathrm{diag}(\lambda_1, \lambda_2, \cdots, \lambda_n) \qquad (2.14)$$

where $\lambda_1, \lambda_2, \cdots, \lambda_n$ are the eigenvalues of $\mathbf{C}_x$. From the above it can be seen that a set of subjectively assessed coefficients of correlation can lead to an impossible situation, namely negative eigenvalues of the covariance matrix, which implies negative variances of the independent variables. Such an example is caused by the fact that the coefficients of correlation are not independent of each other, cf. the example above with soil strength, soil stiffness and pre soil pressure.

In appendix C the procedure described above is exemplified in a special, but important, case - two correlated variables. It is also shown how the procedure can be utilised in simulation of two correlated variables, cf. Monte Carlo simulation described later in section 2.4.3.

2.4 Algorithms

The purpose of solving problems, with the help of statistical methods, is to be able to calculate the probability for different outcomes, especially the probability of exceeding the ultimate limit state or the serviceability limit state. For many simple cases rules exist for mathematical operations with functions of random variables, see appendix A. However, in most cases different types of approximate methods for calculating probabilities of interest have to be used. Which method should be used, depends on what type of problem is at hand and the precision or accuracy required. In serviceability limit state design the calculated probabilities are rather large, normally larger than 1%. Such probabilities can be taken as real probabilities, that is the outcome can to a certain degree be given a frequency interpretation. The problem is in this case governed by the intermediate parts of the distributions. In ultimate limit state design it is considerably smaller probabilities which are of interest, 10^{-4} to 10^{-6}. Probabilities in this range have to be seen as formal. It is difficult mentally, to give them a realistic interpretation.

They are governed by the tails of the distributions, which can be seen as extrapolations of observed values, a circumstance which even more underlines the formal nature of the probability of failure.

In this section, a summary of some different methods suitable for the calculation of probabilities in engineering practice is presented.

2.4.1 Mathematical analysis

Random models normally deal with functions of random variables. In general no explicit formulas exist for determining the type or the parameters of the distributions involved. Thus, one is normally restricted to using different numerical and/or approximate methods. However, for simple, but important, cases explicit solutions can be obtained. These can be divided into four different groups:

- Exact solutions which give the unknown parameters of a distribution
- Exact solutions which give both the type and the parameters of an unknown distribution
- Approximate solutions which give the unknown parameters of a distribution
- Approximate solutions which give both the type and the parameters of an unknown distribution

The expected value for the sum of two variables is equal to the sum of the expected values of the two variables. The same principle is valid for the variances of two independent variables. These are two examples from the first group. A sum of two independent normal distributions is also a normal distribution, which is an example from the second group.

An approximate way to determine expected values and variances is to use Gaussian approximation for a function of random variables, e.g. $E[g(x)] = g(E[X])$[1]. This forms an application from the third group[2].

---

[1] The formula is derived as a truncated Taylor expansion around the expected value, $f(x) = f(\mu) + f'(\mu) \cdot (x - \mu)$

[2] For more examples, see appendices A and D.

The statement that a normal distribution often is a good approximation for a sum of random variables is an example from the last group, see page 19.

The examples above can be found in basic text books of statistics, see e.g. (Blom, 1984). In appendix A other examples of formulas, which can be useful in this context, are given. The appendix is not intended to be complete, but it constitutes a comprehensive summary, which is not easily found in the literature.

2.4.2 Point Estimate Method (PEM)

The Point estimation method, (see e.g. Harr, 1987) can be seen as a systematised version of a 'what if'-calculation. The method was developed by Rosenblueth (1975). The name is somewhat unfortunate as the term 'point estimation' normally has a different meaning in statistics, where it is used to denote estimation of a parameter to have a specific value, to be compared with the term 'interval estimation', an estimation of a parameter to lie in a interval. In PEM each random variable is defined by two numbers, see Figure 2.15. The mean value of these two numbers gives the magnitude of the variable, and the difference is a measure of the uncertainty.

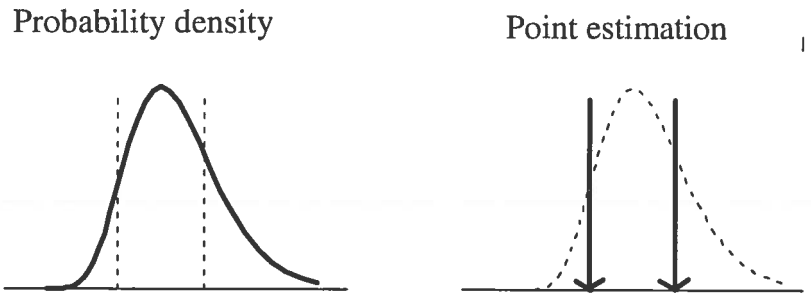

Figure 2.15 Principle of describing a random variable in PEM

In the original form of PEM, the calculations were made for any combinations of input data. For N numbers of variables this will lead to 2^N numbers of calculations. The major advantage with the point estimation method is its simplicity. Each calculation is nothing but a standard deterministic calculation. It can be performed even in those cases when the calculation is done by an algorithm in which interim values have to be read from for example a graph. The same applies to calculations using a computer program for which the source code of the executable files is not available. A PEM-calcula-

tion gives as the result the mean value and the standard deviation of an unknown random variable. This resulting variable could for example be a traditional global factor of safety or a safety margin. The method gives no information about the type or the shape of the distribution. When calculating the probability of failure the type of distribution has to be assumed in some other way. A consequence of this is that different mathematical formulations of the failure criteria, e.g. as a factor of safety or a safety margin, have to be combined with different assumptions of the type of resulting distribution, if the same probability of failure shall be obtained. According to this and to what was stated on page 19, a normal distribution should not be assumed routinely.

The result of a PEM-calculation is correct for sums of uncorrelated or correlated variables[1]. It also gives the correct values for products of uncorrelated variables. For a division by uncorrelated variables the method returns a better approximation than a Taylor approximation[2]. The error given by the PEM-approximation is on 'the safe side' and less than half the error obtained by a Taylor approximation. There is an uncertainty about the accuracy of the PEM-method for more complex functions. The more linear the function is, the more accurate the method probably is. For this reason a safety margin is to be preferred before a factor of safety.

In recent years alterations of the method have been presented, mostly with the purpose to bring down the number of calculations, which can be limited to 2·N, see e.g. Harr (1989) and He and Sällfors (1994). He has also presented a version in which the skewness of the input data can be accounted for (He, 1993). The disadvantage with the latter versions is that the mathematical simplicity of the method has to a certain extent been lost. With the same mathematical complexity, calculations can normally be done with reliability calculations described later in section 2.4.4.

2.4.3 Monte Carlo simulation

Monte Carlo simulation has many similarities with the Point Estimate Method. In the same way as for the PEM, a number of traditional, deterministic calculations are performed for different sets of

[1] For this and the following statements, see appendix D.
[2] Of first degree.

values for the input parameters. However, the number of calculations is considerably higher in the Monte Carlo method compared to the PEM method.[1] For a calculated probability of failure p, as a rule of thumb, the necessary number of calculations can be set to $100/p$, for a satisfactory precision (Bjerager, 1989). Input data of the different variables are simulated randomly from the assumed distributions. Each calculation gives one outcome for any unknown variable. The principle of simulation is illustrated in Figure 2.16. In an iteration i, a random probability p_i results in the variable value x_{ji} of a variable X_j. In each iteration, values x_{1i}, $x_{2i,...}$ $x_{ji,...}$ x_{ni} are simulated for all independent variables X_1, $X_{2,...}$ $X_{j,...}$ X_n. A corresponding value for an unknown variable Y, which is a function of the variables X, can then be calculated as $y_i=f(x_{1i}, x_{2i,...} x_{ji,...} x_{ni})$. A large number of iterations will result in a large number of values y_1, y_2 , ..., y_i ,... , with the correct distribution. In this way even the distributions of the variables can be obtained. At a sufficiently large number of simulations the results of the calculation will converge to the mathematically correct answer. The large number of simulations demands a computerised algorithm for the calculation.[2]

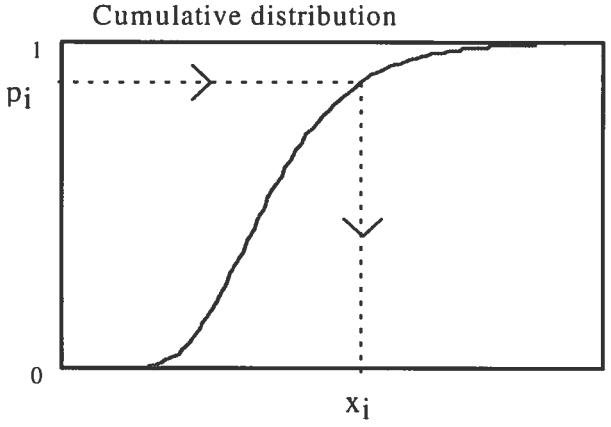

Figure 2.16 The principle of Monte Carlo simulation. Iteration i of a variable X

Even for the Monte Carlo simulation new versions, which reduce the number of simulations, have been developed. For example randomly drawn input data by the procedure Latin Hypercube can be characterised as sampling without replacement, while traditional

[1] That is for a small number of variables, cf. section 2.4.2.

[2] Besides with mathematical and statistical software, this could often be achieved with simple spread sheet programs.

Monte Carlo simulation is sampling with replacement (@t Risk, 1994). In a Latin Hypercube simulation of n iterations the y-axis, see Figure 2.16, is divided into n equal intervals and a random number are drawn from each interval. In this way, values are forced to be drawn from the tails of a distribution. In traditional Monte Carlo simulation, random numbers are drawn randomly from the full extent of the y-axis, 0-1. The former procedure is mainly favourable when the tails of a distribution are of major interest. Compared to traditional Monte Carlo simulation, the number of necessary simulations can in this way be reduced, down to about 35 % according to @t Risk (1994). When comparing the Monte Carlo method and PEM, one has to remember that the former also gives the distribution of an unknown property. In many cases, it is not more difficult to estimate the type of distribution for the result than for the input data. In such cases it is not meaningful to make a large number of calculations. For example, if only the mean value and the standard deviation of a variable are of interest, the number of iterations can be reduced quite substantially. In Figure 2.17 and Figure 2.18 the results of two Monte Carlo simulations of a normal and a lognormal distribution respectively are presented. The first twenty iterations of each simulation are the same as those shown in Figure 2.12 and Figure 2.13. The figures show, apart from the mean value μ and the standard deviation σ, the coefficient of skewness β_1 and the difference between the coefficient of kurtosis (peakedness) β_2 and 3. [1] In the figures are also marked the true values of the parameters of the assumed distributions, which are $\mu=1$; $\sigma=0,2$ and for the normal distribution $\beta_{N1}=0$ and $\beta_{N2}-3=0$ respectively, while the values for the lognormal distribution are $\beta_{L1}=0,6$ and $\beta_{L2}-3=0,67$ respectively, see appendix A.

[1] The coefficient of kurtosis for a normal distribution is equal to 3.

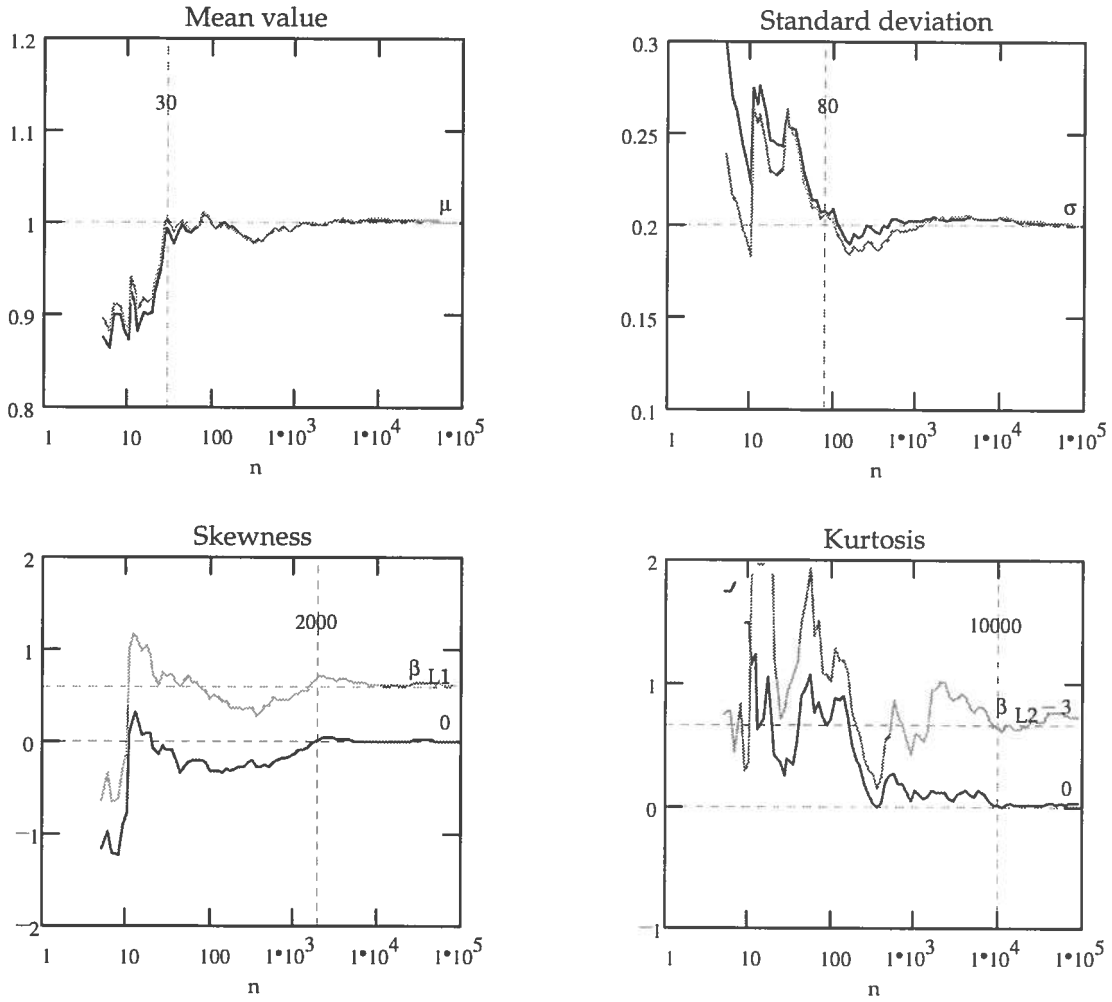

Figure 2.17 Monte Carlo simulation , A (cf. Figure 2.12), of a distribution *PD*(1;0,2)
——— normal, ——— lognormal distribution.
Number of iterations = 100 000
β_{L1} = coefficient of skewness, lognormal distribution,
β_{L2} = " " kurtosis, " "

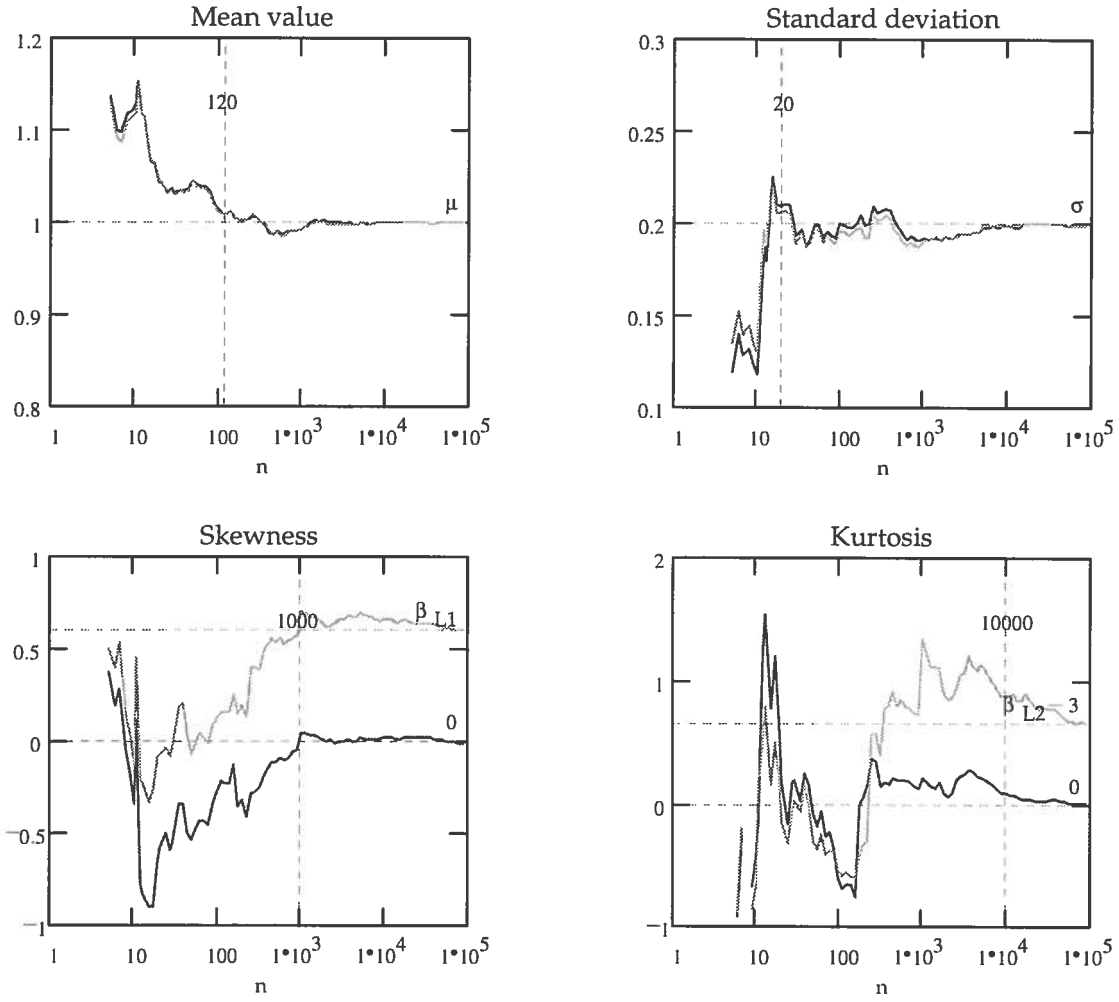

Figure 2.18 Monte Carlo simulation, B (cf. Figure 2.13), of a distribution *PD*(1;0,2)
——— normal, ——— lognormal distribution.
Number of iterations = 100 000
β_{L1} = coefficient of skewness, lognormal distribution,
β_{L2} = " " kurtosis, " "

In the simulations, shown in Figure 2.17 and Figure 2.18, the mean values and the standard deviation are stabilised after less than 150 iterations. Rather good values are obtained after about 20 iterations. However, if one has to determine the type of the distribution, considerably more iterations are demanded. In Figure 2.19 the results of the simulations after 100 and 1000 iterations respectively compared to the scheme presented in Figure 2.9 are shown. The coefficient of kurtosis is plotted along the vertical axis and the coefficient of skewness squared is plotted along the horizontal axis. The solid line in the figure describes the properties of a lognormal distribution, with the right ring defining the lognormal distribution at hand. The

filled, left ring defines the location for a normal distribution. For both simulations A and B the type of distribution can be regarded as undefined after 100 iterations, while there is a fairly good agreement with the type of distributions and the simulations after 1000 iterations[1].

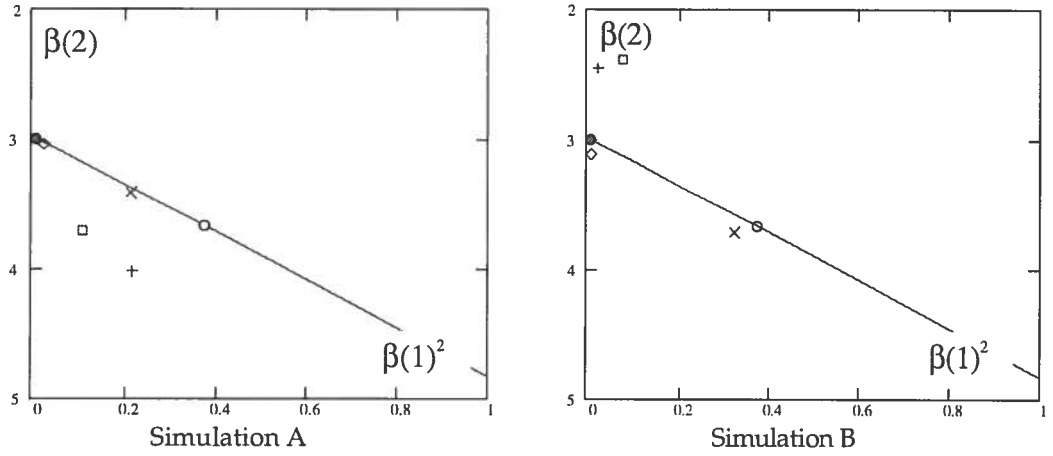

Figure 2.19 Determination of type of distribution by Monte - Carlo simulation.
Simulations of
lognormal + and normal □ distribution after 100 iterations
" × " " ◇ " " 1000 "
——— lognormal distributions o lognormal distribution at hand
● normal distribution

2.4.4 Reliability analyses - reliability index ß

General

When calculating small, formal probabilities of failure, the above mentioned methods are not suitable. The PEM-method due to its lack of sufficient accuracy and the Monte Carlo simulation due to the large number of calculations required in order to get any accuracy of the tails. For the analyses of 'small probabilities' the concept of a reliability index ß has been introduced. The simplest and original definition of the reliability index ß is based upon a safety margin defined as the difference between the resistance and the action effect, or in more general terms, the difference between the capacity and the demand.

[1] Simulation A coincides close to a lognormal distribution with V= 15% and simulation B to a lognormal distribution with V= 19%.

The original definition of the reliability index was:

$$ß=\mu_M/\sigma_M \tag{2.15}$$

i.e. the ratio of the mean value and the standard deviation of the safety margin (Benjamin and Cornell, 1970). If, and only if, the safety margin is normally distributed, the probability of failure can be calculated as:

$$p_F = \Phi(-ß) \tag{2.16}$$

A number of closely related procedures, which all make use of the reliability index $ß$ as a measurement of reliability, have been developed (see e.g Thoft-Christensen & Baker, 1982, Madsen et al., 1986, Bjerager, 1989 or Ditlevsen & Madsen, 1990). All these procedures are often referred to, in Sweden, as the $ß$-method (Olsson, 1986). Normally, the safety margin has a more complex definition than the above. A safety margin, $G(\mathbf{X})$, can then be described, where $\mathbf{X}$ is a vector of basic variables, $X_1....X_n$, which governs the problem at hand. The function $G(.)$ is called the limit state function. It is normally formulated such that $G(\mathbf{X}) < 0$ describes failure while $G(\mathbf{X}) > 0$ is a safe state. The probability of failure can then be written as $p = p(\mathbf{X}|G(\mathbf{X}) \leq 0)$ and the reliability index $ß=\mu_G/\sigma_G$.

Reliability index $ß_{H\text{-}L}$

The drawback with the simple definition of $ß$ as stated in the previous section, is that it is not invariant of the formulation of the limit state function $G(.)$. This is conceptually the same problem as the difficulties of choosing an appropriate distribution for the result of a PEM calculation, see section 2.4.2. The limit state function can be written in an indefinite number of ways (Ditlevsen & Madsen 1990). Two trivial, but different ways, to describe the reliability are $R/S>1$ and $R\text{-}S>0$, which correspond to $M = lnR\text{-}lnS$ and $M = R\text{-}S$ respectively. These two different formulations do not give the same value of $ß$. To overcome this weakness in the definition of $ß$, i.e. by equation 2.15, an alternative formulation has been suggested. Presented by Hasofer & Lind (1974), it is often referred to as the reliability index by Hasofer-Lind, $ß_{HL}$. Below, a short summary of the procedure to determine the reliability index is given. For a more detailed description, see e.g. (Thoft-Christensen & Baker, 1982). An

example of the procedure will come in section 4.6.2. The basic variables, i.e. the base vector **X**, defines a basic variable space. This space is divided into a safe and an unsafe region by the failure surface, $G(\mathbf{X}) = 0$. The procedure means that the base vector **X** is transformed into a vector **U** of independent, standard normal distributions $\Phi(u_i)$., (cf. section 2.3.3 and section 2.3.2). Hereby the n-dimensional vector space $(X_1.....X_n)$ is transformed to the m-dimensional vector space $(U_1...U_m)$. This means that the two vector spaces do not need to have the same dimension (Bjerager, 1989). The transformation maps the failure surface $G(\mathbf{X})=0$ to a corresponding failure surface $g(\mathbf{U})=0$, such that $p=p(\mathbf{U} \mid g(\mathbf{U}) \leq 0)$. The reliability index β is then defined as the shortest distance between the origin and the failure surface in the u-space. The corresponding point of the failure surface is often called the design point. It marks the most probable failure point. The name can lead to misunderstandings as the actual design may not only be based upon probability of failure. The procedure means that β is defined in relation to the failure surface and not to a certain formulation of the limit state function, $G(.)$. For this reason the reliability index, β_{HL}, is sometimes also called the geometrical reliability index, which is a more descriptive name (Ditlevsen & Madsen, 1990). In Figure 2.20 the procedure is shown for a simple case $G(X_1,X_2) = G(R,S)=R-S(= M)$, with $R = LN(\mu_R;\sigma_R)$ and $S=N(\mu_S;\sigma_S)$.

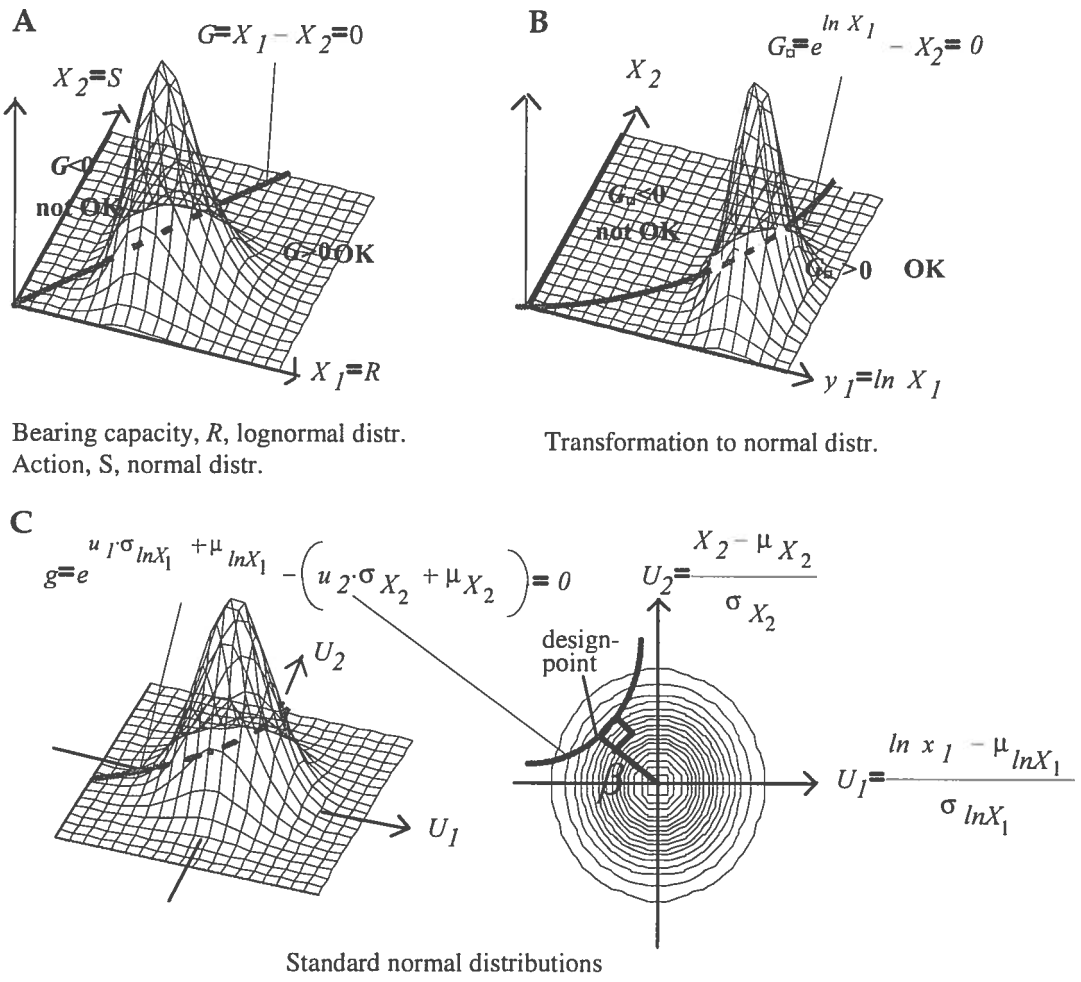

Figure 2.20 Illustration of the ß-method. Transformation of the safety margin and the limit state function from the vector space x to the normalised vector space u.

The figure shows the joint density for different combinations of the basic variables, in this case R and S. The procedure implies that the distributions of the basic variables are transformed into equivalent distributions, i.e. the set of standard normal distributions. Instead, the physical significance and the statistical uncertainty of the different variables are transformed into the limit function by the reformulation $G(\mathbf{X})$ to $g(\mathbf{U})$, cf. page 19. From the figure it can be seen that this means that the failure surface, which is linear in the x-space, is no longer linear in the u-space. When calculating the probability of failure, the failure surface $g(\mathbf{U})=0$ is replaced by its tangent plane in the design point. The probability of failure is then calculated as the part of the total probability, which is cut off by this

tangent plane. The relationship between the probability of failure and the reliability index is then equal to the earlier mentioned special case, $p=\Phi(-\beta)$. If $g(\mathbf{U})=0$ is a hyper plane, the calculation of the probability of failure is exact (based upon given assumptions). In this special case the different definitions of the reliability index will give the same results. The transformation of the resistance, R, given as a lognormal distribution, see Figure 2.20, is a special case of the transformation (see e.g. Bjerager, 1989, or Ditlevsen & Madsen, 1990):

$$\Phi(u_i) = F_{X_i}(x_i) \quad \rightarrow \quad u_i = \Phi^{-1}\left[F_{X_i}(x_i)\right] \tag{2.17}$$

The version of reliability analysis outlined above is normally referred to as *FORM* (*F*irst *O*rder *R*eliability *M*ethod). If the failure surface is instead taken to be a parabolic surface, the analysis is called *SORM* (*S*econd *O*rder *R*eliability *M*ethod) (Bjerager, 1989).

The coordinates for the design point in the u-space are often denoted $\alpha_1\beta$, $\alpha_2\beta$,... $\alpha_n\beta$. For the example in Figure 2.20, with $X_1=R$ and $X_2=S$, i.e. $\alpha_R\beta$ and $\alpha_S\beta$, the corresponding values in the x-space will be:

$$R_d = \exp(\mu_{\ln R} + \alpha_R \beta \cdot \sigma_{\ln R}) \tag{2.18}$$

or for 'smal' values of the coefficient of variation, cf. appendix A:

$$R_d = \mu_R \cdot \exp(\alpha_R \beta \cdot V_R) \tag{2.18a}$$

and:

$$S_d = \mu_S + \alpha_S \beta \cdot \sigma_S \tag{2.19}$$

The values α_1, α_2,... α_n, which are called sensitivity factors, are measurements of the influence of the different basic variables on the problem at hand. They represent a very important result of a reliability analysis, for a thorough understanding of a complex problem. The design point defines the most probable combination of basic variables for a given reliability index β. Thus, if this combination is taken as a sufficiently unlikely combination, cf. section 2.2.3, the equations 2.18 and 2.19 can be used to calibrate appropriate values for the partial factors, see also appendix A.

In the example given by Figure 2.20 it is assumed that the basic variables are independent of each other. A number of different transformations have been proposed in the literature to take account of the dependency between the variables in a general case, (see e.g. Bjerager, 1989, and Ditlevsen & Madsen, 1990). When the dependency is given by the covariance matrix, a set of independent variables can be obtained by the linear transformation given by equation 2.13. However, it has to be noted that the distributions of these unknowns, defined by the transformation, might be far from any standard type of distribution, despite the fact that the basic variables are known[1]. In appendix C is outlined a simplified procedure for two correlated variables. It is shown that the coefficient of correlation is fairly little affected by the transformation of lognormal or Gumbel distributions into standard normal distributions according to equation 2.17. Hence, a pair of uncorrelated variables can be obtained by applying equation 2.13 to the transformed distributions instead of the basic variables.

System analysis - general reliability index ß

The determination of the reliability index and the probability of failure as given in the previous section are valid for a single component, e.g. a beam in a building or a given slip circle in a slope stability analysis. This is the same level of analysis, which normally is applied in engineering practice using deterministic analysis. In this respect, there is no reason to raise the ambition because a probabilistic analysis is undertaken. However, from the point of view of principle it can be of interest to extend the procedure into systems of components.

The two simplest forms of systems are series systems and parallel systems (see e.g. Thoft-Christensen & Baker, 1980, or Harr, 1986). In a series system, failure is reached as soon as a single component fails, e.g. a link in a chain. Statically determined structures behave as a series system as the structure collapse if a single structural member collapses. System failure in a parallel system demands failure of all components, e.g. all piles in a pile group.[2] Structures with a high

[1] The type of distribution is normally changed by a linear combination, cf. section 2.4.1.

[2] If the pile group is arranged so that redistribution of loads can take place from one pile to another.

degree of statical indeterminacy, will not fail due to a single element failure as long as redistribution of loads can take place. Thus such systems can with preference be seen as parallel systems. The series system and the parallel system are two extremes of a redundant system, i.e. a system in which one or more of the elements are redundant in order to make the system stable. Assume as special case of a redundant system defined as the number of components, r, of the total number of components, n, which must function for the system to work, i.e. a so called r-out-of-n system(Harr 1986). For a parallel system then $r=1$ and for a series system $r=n$.

Systems can be interpreted in a more abstract way than as a description of the relation between different 'physical elements' of a structure. Different failure modes for a structure, for example, can be seen as different components of a system. System failure occurs when one failure mode is reached, i.e. one component fails. This means that the failure modes define a series system. More complex systems can be modelled as a combination of series and parallel systems. For example, if the different failure modes are modelled as parallel systems, the total system will be a series system of a parallel subsystem (Thoft- Christensen & Baker, 1980).

Relationships between the safety margin for a system and the relationship for its different components can be established. The following relation is valid for series systems (Bjerager, 1989):

$$G(\mathbf{X})_{series} = \min\{G(\mathbf{X})_i\} \tag{2.20}$$

and for parallel systems

$$G(\mathbf{X})_{par} = \max\{G(\mathbf{X})_i\} \tag{2.21}$$

Thus, when calculating the probability of failure of a system, one has to take into account not only the structure of the components, but also the characteristics of the single components. For parallel systems it is of vital importance whether the failure of a component is brittle or ductile. The correlation between the different components is another factor which plays an important role in system analysis.

The reliability of a system[1], $\mathcal{R}$, , i.e.

$$\mathcal{R} = p(G(\mathbf{X}) > 0) \tag{2.22}$$

In the same way the probability of failure, F, can be defined as:

$$F = p(G(\mathbf{X}) < 0) \tag{2.23}$$

For a series system of n uncorrelated components one obtains the reliability as:

$$\mathcal{R} = \prod_n \mathcal{R}_i \tag{2.24}$$

where $\mathcal{R}_i$ is the reliability of the i^{th} component. Obviously, F=1-$\mathcal{R}$, (c.f. page 24), which gives:

$$F = 1 - \mathcal{R} = 1 - \prod_n \mathcal{R}_i = 1 - \prod_n (1\text{-}F_i) \tag{2.24a}$$

If it is assumed that the probabilities of failure are small, i.e. $F_i \cdot F_j \approx 0$, the equation can be approximated as (Harr, 1986):

$$F \approx \sum_n F_i \tag{2.24b}$$

For a parallel system on n uncorrelated, brittle components the probability of failure can be calculated as:

$$F = \prod_n F_i \tag{2.25}$$

If all components of a redundant system, r of n, cf. page 45, are equally reliable, equation 2.24 and equation 2.25 can be combined as (Harr, 1986):

$$\mathcal{R} = \sum_{k=r}^{n} \binom{n}{k} \cdot \mathcal{R}_\bullet^k \cdot (1 - \mathcal{R}_\bullet)^{n-k} \tag{2.26}$$

where $\mathcal{R}_i$=$\mathcal{R}_j$=...=$\mathcal{R}_\bullet$

[1]i.e. is the probability of 'success'

A parallel system with ductile, uncorrelated components is rather easily analysed, as the strength of the system, R, can be calculated as:

$$R = \sum_n R_i \tag{2.27}$$

Thus the problem is reduced to determine the sum of uncorrelated, random variables, cf. page 19.

Calculation of systems with correlated components is more complex in general. As a principal illustration of the influence of correlation, the solutions for two special cases are given below:

- Series systems, with equally correlated components
- Parallel systems, with ductile, equally correlated components

It is assumed that the strength of all components is normally distributed, $N(\mu_i,\sigma_i)$. Further it is assumed that the loads are deterministic and the reliability of any component is given by the same reliability index β_e. The solutions, which were first given by Grigoriu & Tukstra, are taken from (Thoft-Christensen & Baker, 1986). For the series system the probability of failure can be calculated as:

$$F(\rho) = 1 - \int_{-\infty}^{\infty} \left[\Phi\left(\frac{\beta_e + \sqrt{\rho}\cdot x}{\sqrt{1-\rho}}\right) \right]^n \cdot \varphi(x)dx \tag{2.28}$$

A system reliablity index β_S can then be calculated as:

$$\beta_S = -\Phi^{-1}(F(\rho)) \tag{2.29}$$

For the parallel system the corresponding system reliability index is:

$$\beta_S = \beta_e \cdot \sqrt{\frac{n}{1+\rho\cdot(n-1)}} \tag{2.30}$$

The probability of failure then becomes:

$$F(\rho) = \Phi(-\beta_S) \tag{2.31}$$

The results of a calculation of the system reliability are shown in Figure 2.21. As can be seen in the figure, for a parallel system the system reliability is larger than the component reliability but decreases with correlation. For a series system the relation is the opposite, the system reliability is smaller than the component reliability, but increases with correlation. This principle result is important in application of probabilistic analysis. In geotechnical engineering the soil can normally be considered as a parallel system, as redistribution of stresses can take place in the soil mass. The influence of local weak points diminishes with volume. Thus a large volume increases the reliability. In structural engineering, separate elements can be seen as serial systems. The probability of encountering a weak point is increased with volume, i.e. the reliability decreases with volume.

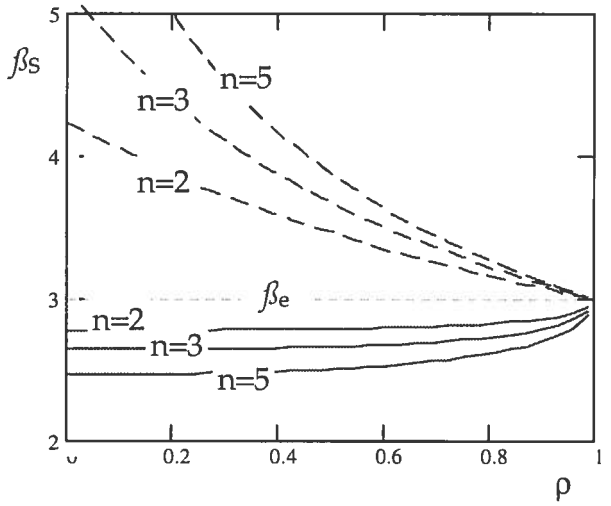

Figure 2.21 Reliability index, β_S, as a function of the coefficient of correlation, ρ
-------- parallel system ——— series system
Component reliability index $\beta_e = 3$

When calculating the probability of failure corresponding to a given β_{HL}, see page 42, it was assumed that the limit state function $G(.)$ as well as the, to the u-space transformed, function, $g(.)$, is linear or can be approximated as a linear function, i.e. the tangent plane in the design point. However, this assumption might be too crude. For example, in system analysis as described previously in this section, each failure mode describes a local minimum. Obviously, in such a case it cannot be justified to describe the failure surface as one hyper-plane. Another example, perhaps not so often encountered in engineering practice, is when the radius of curvature of the failure surface at the design point is small. A generalisation of the defini-

tion of the reliability index can then be used (Ditlevsen & Madsen, 1990). The definition is based upon the same relation between the probability of failure and the reliability index as in FORM, i.e. $p_F = \Phi(-ß)$. However, instead of defining p as a function of $ß$, the relation is inverted. Thus, the generalised reliability index $ß$ can be seen as the value, which satisfies the equality[1]:

$$\beta = -\Phi^{-1}(p_F) \tag{2.32}$$

This is in fact the way the system reliability was determined in equation 2.29.

Summary

The procedures for calculating the reliability with the reliability index $ß$ are especially effective when one deals with very small probabilities of failure. The calculations can be done with available commercial computer programs, e.g. PROBAN and Strurel (Ditlevsen & Madsen, 1990). For not too complicated problems the algorithms needed can be performed with the help of generalised mathematical software programs.

2.4.5 Conclusion

In random calculation models the probability of different outcomes of a calculation must be determined. In the general case it is desirable to give the complete distributions of all outcomes. However, in most cases it is sufficient to determine the probability for an undesirable outcome, e.g. the probability of failure. Normally, exact calculation methods do not exist. Instead an approximate method has to be adopted.

[1] The proper definition given in (Ditlevsen & Madsen, 1990) is mathematically more complex.

Four different concepts of calculating the probability of failure has been discussed in this chapter. They can be summarised as:

Mathematical analysis - A straightforward method: However, available methods restrict the application to not too complex problems.

Point estimate method, PEM - Simple method, which gives the first two moments of a distribution.

Monte Carlo simulation - A method, which gives the complete distribution of any unknown variable[1]. The accuracy of the method is governed by the number of iterations. Only practical reasons limit the accuracy of the results. To obtain the tails of a distribution, a large number of iterations are required.

Reliability analysis with reliability index ß - The method is used to calculate very small probabilities, preferably probabilities of failure. In this way the reliability analysis and the Monte Carlo simulation complement each other.

In Figure 2.22 a comparison of the three latter methods is shown. The figure shows the result of a calculation of the bearing capacity of a friction pile determined as:

$$R = \int_0^L \alpha(z) \cdot C_u(z) \cdot \Theta(z) dz \qquad (2.33)$$

with the random variables $\alpha(z)$, being the ratio between the shaft friction and the undrained shear strength, $c_u(z)$ the undrained shear strength and $\Theta(z)$, the circumference of the pile. L is the pile length. The figure is taken from the preparation work for the Swedish national application document to EC7 (Alén et al., 1993a).

[1] If this unknown variable can be modelled as a function (or algorithm) of known variables.

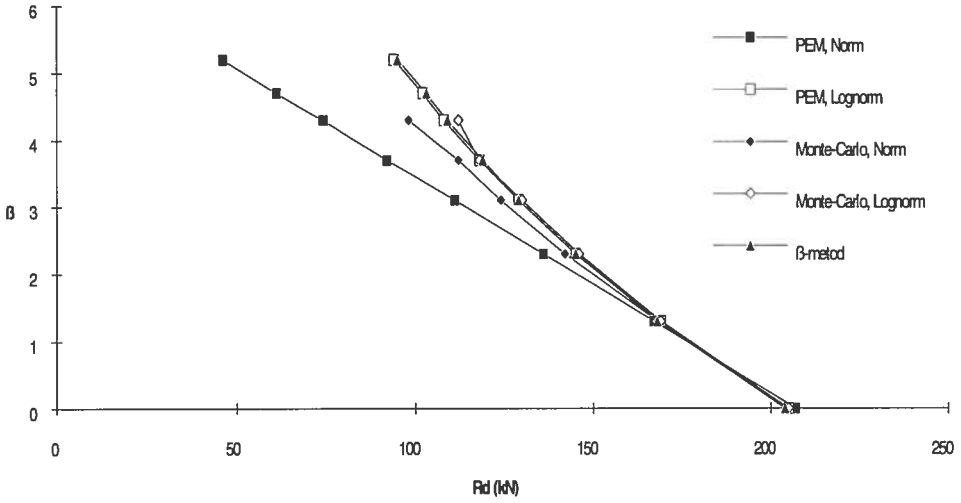

Figure 2.22 Comparison between PEM, Monte Carlo simulation and analysis with reliability index *ß*. The example shows a calculation of the bearing capacity for a friction pile From (Alén et al., 1993a).

The results in Figure 2.22 are based upon the following assumptions. In the interpretation of the PEM-calculation the bearing capacity is assumed to be either normal distributed or lognormal distributed. In the Monte Carlo simulation the input variables are assumed to be either normal distributed or lognormal distributed. The reliability analysis is performed with the assumption of lognormal distributed variables. The results of the PEM-calculation (lognormal assumption), the Monte Carlo calculation (lognormal assumption) and the reliability analysis are in extremely good agreement. The PEM-calculation and the Monte Carlo calculation with assumptions of normal distributions show less good agreement. This is merely a consequence of the fact that it normally is difficult to determine the types of the output distributions even if the input distributions are known. For the Monte Carlo calculation no *ß*-value larger than 4,3 was determined[1].

[1] For the calculation of the value 4,3, the computation time was about 3,5 hours on a PC 486/ 66 MHz.

3 MODELLING OF SOIL PROPERTIES

3.1 General

3.1.1 Uncertainties

The properties of a soil are normally determined by field- and/or laboratory testing. The uncertainty in the testing has to be considered in the interpretation of the test results. To describe variations in a systematic way, the uncertainties can be divided into different categories (Christian et al., 1992).

- *Natural variation in a soil profile.* This incorporates random variations in the soil compared to an applied model.
- *Systematic errors in the testing method - Bias.* This is a question of the precision of a test method. Normally the testing method or the model should be calibrated in such a way that no systematic errors are at hand.
- *Random errors in the testing method.* Such errors are due to low accuracy of the method. They also include differences in the test results arising from a lack of skill or accuracy of the persons performing the tests.
- *Errors due to the limited number of tests.* The test results might not be representative. This type of error is dominating in geotechnical testing, as even a comprehensive testing can be seen as a small sample from a statistical point of view, cf. the results of simulations in Chapter 2 (section 2.5.3)

The first two types of uncertainties can be described as physical uncertainties, while the two latter can be called statistical uncertainties.

Systematic differences between the results from a test method and the true values can barely be dealt with in a specific project only. By systematic comparison of test results and actual behaviour in many projects one can try to find the average value of differences. The interpretation of the test method should be calibrated in such a way that this average value becomes zero. The remaining differences will then be random. Random errors in the testing method will not affect the actual behaviour of a structure. If such errors could be separated

from the others it will mean that the uncertainty one has to deal with in a practical design case can be reduced.

3.1.2 Reality versus model

In Figure 3.1 the principle relation between an observed behaviour and a presumed model is shown. The difference between the real behaviour and the model is in the figure named variation. This implies that one cannot speak about variation in the soil without considering the assumed model at the same time. If both the test method and the model are perfect, no variations will exist. This could be interpreted as that the variations are not any variation in the physical reality but an attempt to quantify the lack of knowledge. Another way of expressing this is that the properties at a specific point are deterministic but unknown. It is not meaningful to assume that they will vary randomly, except with time[1]. On the other hand, the ability to describe or determine the properties can vary quite substantially.

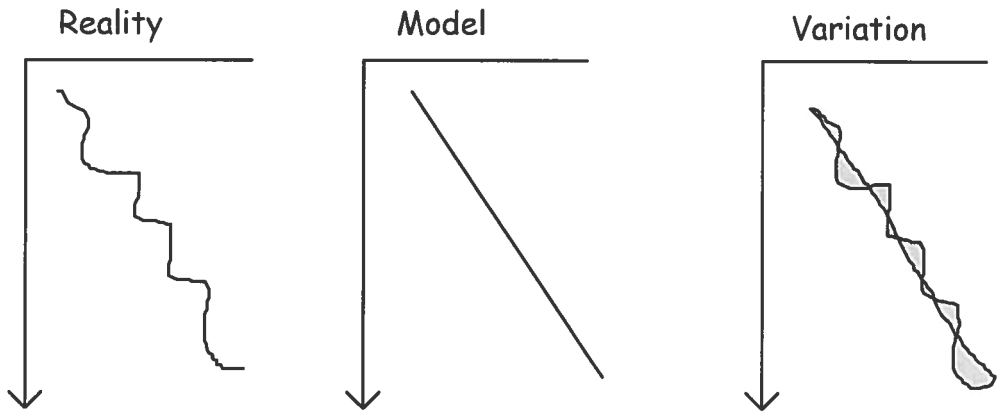

Figure 3.1 Schematic description of variation as a function of reality and model.

The importance of relating variations to a presumed model can be illustrated with an example from dynamic testing of driven piles. In Figure 3.2 three examples of the mobilised bearing capacity of a pile as a function of the driving energy are shown. The three different plots represent three different soils respectively with, from left to right, normal natural variations, large natural variations and small natural variations. Usually the evaluated bearing capacity will be

[1] This is a pragmatic standpoint from an engineering point of view. Philosophically (or even scientifically) the true nature of randomness is a much more complex issue.

higher, the more driving energy is induced in the pile. This principle relation is shown in the left plot of the figure in which the filled boxes show observations of a 'normal' natural behaviour and the solid line represents a model with good accuracy. If, during a dynamic test series in a soil with a large scatter, the driving energy is varied in order to obtain a certain required bearing capacity, the situation in the middle plot of the figure might arise. The illusion of a very small scatter of the bearing capacity seems to be at hand, despite the fact that there is a huge discrepancy between the reality and the model. Finally, the right plot shows a situation with full coordination between the model and the reality[1]. If in this case the scatter of the bearing capacity is determined without considering the driving energy, the results will be completely misleading.

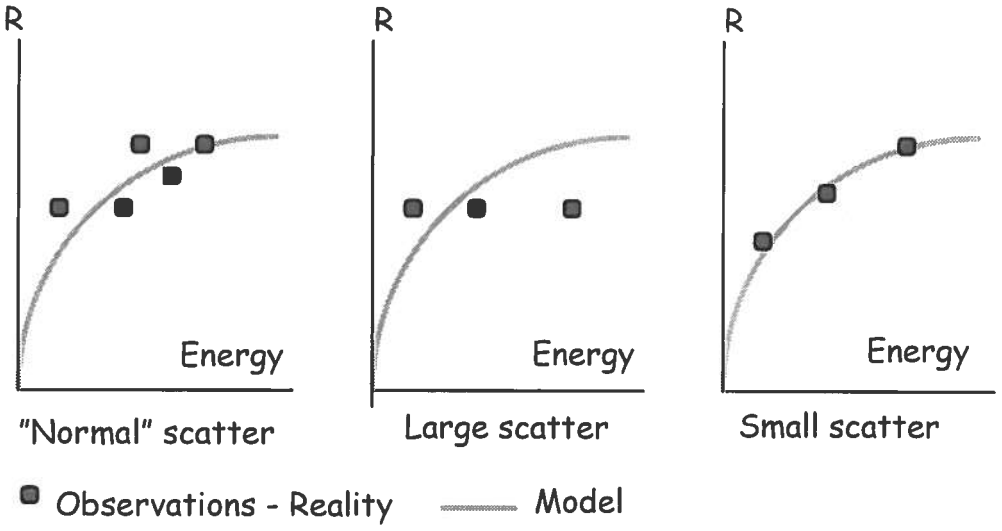

Figure 3.2 Principle for evaluation of the scatter of test results in dynamic pile testing.

3.1.3 'Micro'/'macro'-level

Introduction

In many cases the real behaviour of a material is based upon properties, which physically can be described as stringently only on a micro level, e.g. a molecule level. However, this type of knowledge might be unnecessary in the actual case. In the former cases it can be simpler and more convenient to formulate the problem on a comprehensive macro level. An illustrating example of this principle is

[1] In this case the model is both accurate and precise.

the stress concept introduced by Cauchy (Strifors, 1991). The concept implies that the inter molecule forces are averaged over an actual area. The stress concept and the closely related strain concept have such a central and well-known application in engineering problem, that one often thinks about them as real physical properties and not merely as approximations of a complex reality. Thus, in engineering practice, one normally is not interested in the actual behaviour of a material but only in the properties on a suitable level, i.e. only the average behaviour has to be correct. This can be described with a probabilistic approach. The variables in a simple physical model are associated with probability distributions. By integration over actual areas or volumes, one will obtain the average properties, which can be compared to the results measured in field- or laboratory tests.

The principle discussed above, i.e. that the relations at a macro level of interest are described by a probabilistic interpretation from an underlying micro level, may be possible to use in many applications in geotechnical engineering. Below, as an example, the derivation of a water retention curve is given.

Example - Water retention curve

In Figure 3.3 is shown a model intended to describe the capillarity in a soil profile. It can be used to simulate a water retention curve, i.e. a curve, which defines the relationship between negative pore pressure, matrix suction, and the degree of water saturation in an unsaturated soil profile (see e.g. Tremblay, 1995, or Öberg, 1997).

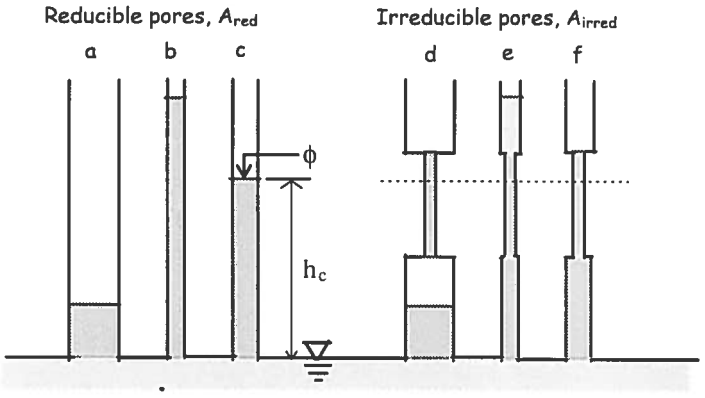

Figure 3.3 Capillary rise model

The model in Figure 3.3 is very simple. In a horizontal section of a soil profile a distribution of vertical capillary channels exists. The

water in some of these channels is connected to the underlying ground water table. The pore pressure, at a certain level, in such a channel is therefore determined by the level compared to the water table. The capillary rise, h_c, is proportional to the inverse of the pore diameter, ϕ (see e.g. Therzaghi & Peck, 1948):

$$h_c = \frac{4 \cdot T \cdot \cos\alpha}{\gamma_w \cdot \phi} = \frac{k}{\phi} \tag{3.1}$$

In equation 3.1, the product $T \cdot \cos\alpha$ denotes the vertical component of the surface tension of water and γ_w the unit weight of the pore water, while k is a constant, with dimension [length^2], defined by the equation. If a channel at a certain level has a capillary rise which is lower than the actual level, the channel is disconnected from the ground water table[1]. By integration over an assumed distribution of pore diameters a related value of pore pressure and water saturation can be calculated for each level h_c, see equations 3.2-3.6 below. The degree of water saturation has a lower bound, as some of the pores are filled with irreducible water. Thus the total area can be divided into a reducible part[2] and an irreducible part[3], cf. Figure 3.3. If the density function for the assumed distribution of pore diameters is $f(x)$, the saturated area[4] becomes:

$$A(\phi) = \int_{\phi_{min}}^{\phi} f(x) \cdot \pi \cdot \frac{x^2}{4} dx \tag{3.2}$$

If the irreducible part of the total pore area is assumed to be α, the saturated area of 'disconnected', irreducible water[5] is:

$$A_{irred}(\phi) = \alpha \cdot \int_{\phi}^{\phi_{max}} f(x) \cdot \pi \cdot \frac{x^2}{4} dx \tag{3.3}$$

Then, the degree of saturation can be obtained as the ratio between the saturated area and the total area:

---

[1] a & d in the figure
[2] a-c " " "
[3] d-f " " "
[4] b,c,e&f " " "
[5] d " " "

$$S(\phi) = \frac{A(\phi) + A_{irred}(\phi)}{A_{total}} = \frac{A(\phi) + A_{irred}(\phi)}{A(\phi_{max})} \tag{3.4}$$

The total (negative) pore 'force' can be obtained from equation 3.1:

$$P(\phi) = \int_{\phi_{min}}^{\phi} f(x) \cdot \frac{k}{\phi} \cdot \pi \cdot \frac{x^2}{4} dx \tag{3.5}$$

Finally, the (negative) pore pressure is:

$$p(\phi) = P(\phi)/A(\phi) \tag{3.6}$$

The equations above are based upon the simplifying assumption that the distribution of irreducible pores is equal to the distribution of the total pore area. The negative pore pressure in those pores which are determined by meniscus forces (see e.g. Tremblay, 1995) is usually not determined in 'conventional' field or laboratory tests, i.e. here defined as testing, which involves pressure readings in a water phase (Öberg Högsta, 1997). Consequently, that part of the negative pore pressure is also neglected in the equations above. By plotting pairs of values of water saturation and pore pressure, the water retention curve can be displayed. In Figure 3.4, the results of such a simulation of two soil samples are compared with the results from laboratory tests. In the figure are also shown the assumed distributions of an 'effective pore diameter' defined as ϕ/k, i.e. the inverse of the capillary rise, (cf. equation 3.1).

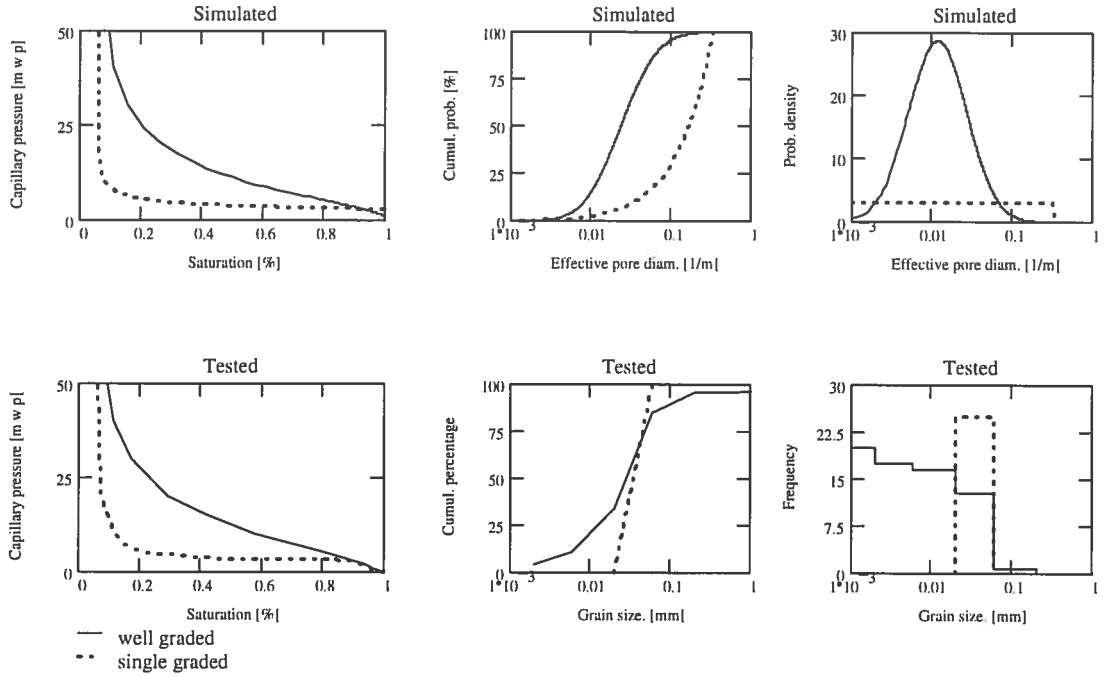

Figure 3.4 Simulation of the water retention curve for well graded (a) and single graded (b) friction material compared to results from laboratory testing. Note the log-scale in four of the plots.

The data of the two soil samples and the laboratory test results shown in Figure 3.4 are taken from (Andersson & Wiklert, 1972). The two soil samples are also presented in (Öberg, 1997). The well graded soil represents a natural silt from the north of Sweden, while the single graded soil is a sieved fraction from different natural sources. The pore diameters of the well graded silt are simulated with a lognormal distribution with mean value 0,033 m^{-1} and coefficient of variation 100%, while the single graded sample is simulated with a uniform distribution in the interval 0,0017 m^{-1} - 0,33 m^{-1}. If k is assumed to be of the magnitude $2 \cdot 10^{-5}$ m^2 (cf. Terzaghi & Peck, 1948), this corresponds to 'actual' pore diameters, which for the well-graded silt gives a mean value of 0,7 µm and for the single fraction diameters between 0,03 µm and 7 µm. It might look as if the areas covered by the density and frequency curves differ from each other, i.e. diverted from unity. However, this is an optical illusion caused by the logarithmic scale of the horizontal axis.

Perhaps the procedure described above will be a way to obtain the relationship between a distribution for effective pore diameters and

the corresponding distribution of grains[1]. This first example indicates that a well-graded soil corresponds to a poorly graded 'pore material' and vice versa.

3.1.4 Control / truncation

Test results can be used as a control of an assumed situation. Control is here used in the sense that it is presupposed that the assumption has to be reconsidered if it is not fulfilled. Such a case can for example be that a structure is redesigned if a soil property does not fulfil a minimum condition. Thus values which will be rejected by the control condition do not have to be implemented in the analysis. If the property at hand is modelled as a random variable, the variable in such a case can be truncated. In Figure 3.5 the principle situation is outlined. A variable X is assumed to be defined in the range $[x_{inf}; x_{sup}]$. For the untruncated variable this corresponds to nominal probabilities in the range $[p_{inf}; p_{sup}]=[F(x_{inf}); F(x_{sup})]$. Figure 3.5 gives the linear relation between the truncated distribution F_{tr} and the nominal value F of the untruncated distribution as:

$$F_{tr}(x) = \frac{F(x) - F(x_{inf})}{F(x_{sup}) - F(x_{inf})} \tag{3.7}$$

The corresponding density function is:

$$f_{tr}(x) = \frac{dF_{tr}(x)}{dx} = \frac{f(x)}{F(x_{sup}) - F(x_{inf})} \tag{3.8}$$

while the inverse distribution F_{tr}^{-1} becomes:

$$F_{tr}^{-1}(p) = F^{-1}(p_{nom}) = F^{-1}(p_{inf} + p \cdot (p_{sup} - p_{inf})) \tag{3.9}$$

[1] Whether such a relationship is of any further benefit is beyond the scope of the applications presented later in this thesis. It is here purely used as an illustration of the versatility of a probabilistic approach. For the purpose of shear strength analysis, Öberg (1997) has presented a very simple method for the estimation of the water retention curve.

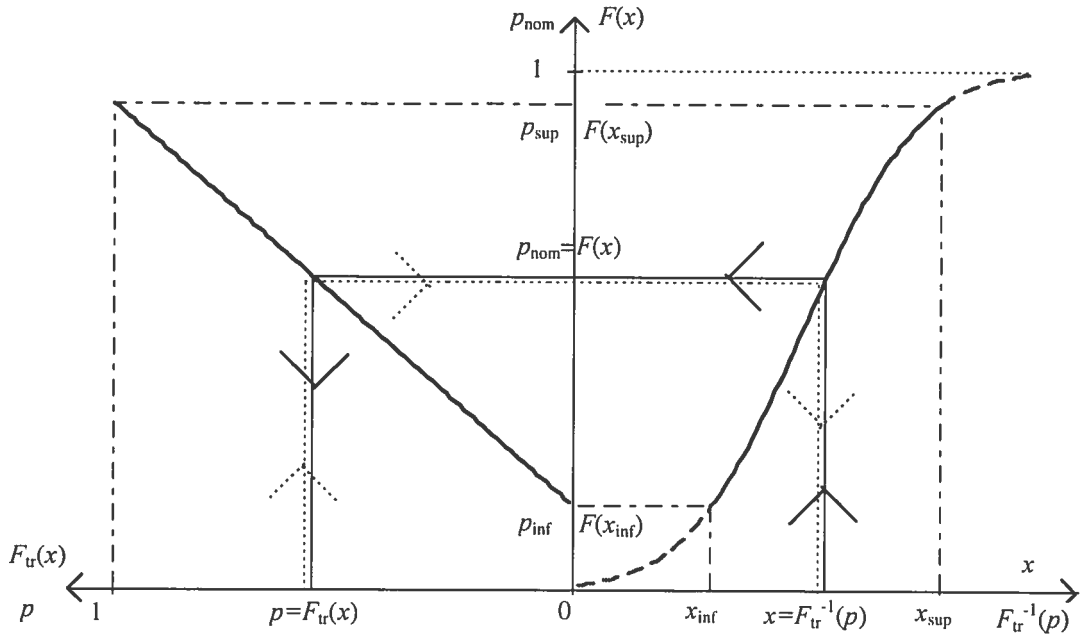

Figure 3.5 Truncation of a distribution. $F_{tr}(x)\,;x\in\{x_{inf};x_{sup}\}$ is truncated distribution. $F(x)$ is corresponding untruncated distribution.

3.2 Properties of a volume

3.2.1 General

In design, a soil property is often represented by the average value in a certain volume[1]. For natural variations of the soil property it is then desirable to determine the dependence between the properties at different points as a function of the distance between the points. The average value in a volume of a physical property must not be mixed up with the mean value of a random variable, describing the same property at a single point. The average value, described as a random variable, always has a smaller variation than the single-point variable, a phenomenon sometimes referred to as variance reduction, cf. appendix A (A.2.3 Linear combination). The probability of encountering a weak point increases with the volume considered. Thus, if a local weakness can induce a failure, the mean value, which governs the design, has to be decreased compared with the single point mean. This is the same phenomenon as was discussed in Chapter 2, page 48, when comparing parallel systems and serial systems, cf. Figure 2.21. The characteristics of the average value in a

[1] The 'volume' might also be a surface or distance depending on the calculation model.

volume are insignificant in this case. This means that the positive effect of variance reduction can only be accounted for in those cases when it is the average value of a volume, and not a local one, that governs a problem. Christian et al. (1992) give the following simple relationship for the reduction of the variance

$$\frac{Var\left[x_{average}\right]}{Var[x]} \approx \frac{2 \cdot r_0}{L} \tag{3.10}$$

In the formula, r_0 is the autocorrelation distance, which is defined later in this chapter, see page 64, and L is a characteristic distance representing the actual volume, e.g. the length of a foundation structure or a slip surface.

3.2.2 Geostatistics

Introduction

Geostatistics deals with methods which describe the properties of a soil volume based upon a limited number of samples. The soil is modelled as a random field, which is a stochastic process defined by three co-ordinates in space[1], see e.g. (Vanmarcke, 1977). This means that the properties of the soil in a specific point is described as a random variable[2]. The total volume is determined by an indefinite number of variables, which are strongly dependent on each other. The main purpose of the geostatistics is to describe this dependence or intercorrelation between variables. Below, a summary of the basic ideas of geostatistics, applied on a geotechnical investigation, is given. It is based upon descriptions of the subject reported in (Christian et al., 1992), (Davis, 1986), (DeGroot & Baecher, 1993) and (Kulhawy, 1992). In appendix E, definitions and derivations of formulas are assembled.

[1] And eventually a fourth co-ordinate for time.
[2] And at a specific time.

Application to a geotechnical investigation

Assume that a geotechnical property, Q, can be described with a function, e.g. a trend with depth, $t(z)$,. Deviation from this trend is denoted $x(z)$, which in turn can be described as a sum of natural variations in the soil $c(z)$ and random deviations due to the test procedure $\varepsilon(z)$. This gives:

$$Q(z) = t(z) + x(z) \text{ with } x(z) = c(z) + \varepsilon(z) \qquad (3.11)$$

$t(z)$ is here the traditional, deterministic model of $Q(z)$, while $x(z)$ is the variation, the uncertainty of the model, see Figure 3.6. The situation is illustrated in which the deterministic model is given as a linear trend.

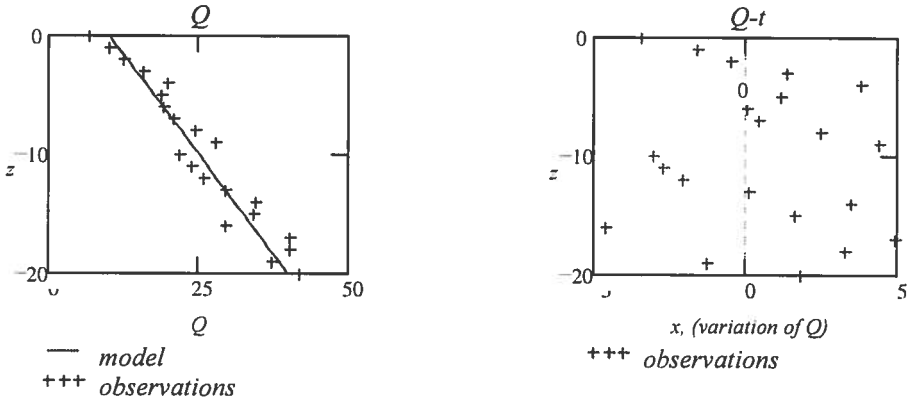

Figure 3.6 Observations of a geotechnical property versus a model of the property.

Assume that the model $Q(z)$ is correct, i.e. there are no systematic deviations between the model and the reality. This means that the mean value of $c(z)$ is zero. If also the test method is correct, the mean value of $\varepsilon(z)$ is zero. Thus the mean value of $x(z)$ is zero, which means that $x(z)$ often is treated as a stationary, random process[1]. There is no reason to believe that errors in the test method are dependent on minor variations in the soil. The functions $c(z)$ and $\varepsilon(z)$ are thus independent of each other. If the variations are large, i.e. the tests are performed on, in reality, different types of soils, the in-

[1] This is not the definition of a stationary random. For such a process the statistical dependence is only governed by the 'distance' ,between the variables and not absolute locations (or directions). For a strict definition, see e.g. (Thoft-Christensen & Baker, 1982). See also 'discussion' later in this section.

dependence may not be valid. However, in that case the idea of describing variations with random variables might not be meaningful.

Assume that there exist a number of tests for the property Q (and x) as above. The test values of x can be seen as a sample of x. It is of interest to establish the dependence between values measured at different depths. A value at a defined level z_i can be seen as an outcome of the random variable $x(z_i)$. Thus the dependence, or at least the correlation, can be determined from the covariance between all the variables $x(z_i)$. In geostatistics it is normally assumed to exist statistical stationarity. Hence the relation between the variables is dependent only on the distance, r, between two variables and not on the absolute location, i.e. the correlation between $x(z_i)$ and $x(z_i+r)$ is a function of r but not z_i. It is measured as the autocovariance, $C_x(r)$ or 'normed' by dividing with the standard deviation of $x(z_i)$ and $x(z_i+r)$, the autocorrelation coefficient.

Autocovariance and autocorrelation distance

The autocovariance is a measurement of the covariation between values from different levels, i.e. how good can a value be predicted if values some distance away are known. It is often assumed to be of the form[1]:

$$C_x(r) = \sigma_c^2 \cdot e^{-\frac{r}{r_0}} \tag{3.12}$$

which is an exponential, decreasing function. The autocorrelation distance r_0, is defined by the equationen:

$$C_x(r_0) = \sigma_c^2 \cdot e^{-1} = 0{,}37 \cdot \sigma_c^2 \tag{3.13}$$

It serves as a measure of how fast $C_x(r)$ decreases.

The reason for giving the autocovariance as a function of σ_c^2 is as follows:

> If, as assumed above, the mean value of x is equal to zero, the autocovariance is, see appendix E:
>
> $$C_x(r) = E[x(z) \cdot x(z+r)] \tag{3.14}$$

It can be estimated as[2]:

$$\hat{C}_x(r) = \frac{1}{n-1}\sum_i x(z_i)\cdot x(z_i + r) \qquad (3.15)$$

r=0 and equation 3.14 gives:

$$C_x(0) = \sigma_x^2 \qquad (3.12a)$$

while equation 3.15 gives:

$$\hat{C}_x(0) = \frac{1}{n-1}\sum_i x(z_i)^2 \qquad (3.15a)$$

As x=c+ε and c and ε are independent, the following applies:

$$\sigma_x^2 = \sigma_c^2 + \sigma_\varepsilon^2 \qquad (3.16)$$

Here σ_c^2 is the part of the variance which occurs from natural variations while σ_ε^2 is the variance caused by measurement errors and hence is independent or r. If there are no measurement errors the autocovariance is

$$C_x(0) = \sigma_x^2 = \sigma_c^2 \qquad (3.12b)$$

Measurement errors do not affect the autocovariance for r>0, as these errors are independent of r. The autocorrelation function should therefore be described with a decreasing function with the limit

$$\lim_{r\to 0} C_x(r) = \sigma_c^2 \qquad (3.17)$$

The function given by equation 3.12 fulfils these requirements. It should be observed that the function has a jump $\left(\sigma_x^2 - \sigma_c^2\right)$ at r=0 as

[1] Other assumptions do exist, see examples in appendix F.

[2] The value of the denominator, n-1, is not indisputable. Different 'existing' alternatives coincide for small values of r. Hence, in the application at hand in which one is interested of the behaviour for such small distances, the different definitions are of secondary importance.

$$C_x(0) = \sigma_x^2 \qquad (3.12c)$$

The jump is equal to the variance of measurement errors, σ_ε^2.

Whether the measured values $x(z_i)$ are dependent on each other or caused by random errors can be viewed from a plot of $C_x(r)$. Such a plot, the autocovariance versus the separating distance, is called a correlogram. In Figure 3.7 a correlogram is given for two cases:

- Natural variations and measurement errors. Natural variance at each level ('at a point') is 70% of total, i.e. $\sigma_c^2 = 0{,}7 \cdot \sigma_x^2$
- Only measurement errors, i.e. $\sigma_c^2 = 0$

From Figure 3.7 two things of interest can be found, the variance of measurement errors, $\sigma_x^2 - \sigma_c^2$, and the autocorrelation distance, r_0. To determine the random errors of measurement is of course of great importance, as these do not affect a real structure. The autocorrelation distance is of interest because a short autocorrelation distance levels out the accumulated variances along a distance compared to the variance at a point, cf. section 3.2.1.

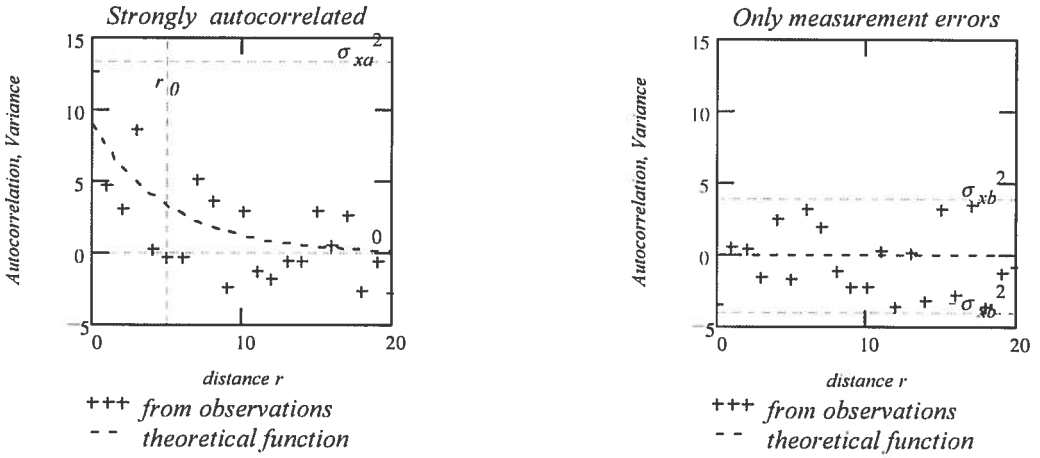

Figure 3.7 Schematic illustration of correlograms for a sample of strongly autocorrelated observations and a sample of uncorrelated observations.

The values plotted in Figure 3.7 show the random scatter of a sample. Thus it is not a trivial thing to plot the theoretical autocorrelation function. In Figure 3.8 three different interpretations of the autocorrelation are shown. Two differently simulated samples, of which the left one is the same as that shown previously in Figure

3.7, are from the same underlying population. The three different interpretations are based upon the assumption that the variances of natural variations are 100%, 70% or 40% respectively of the total variance.

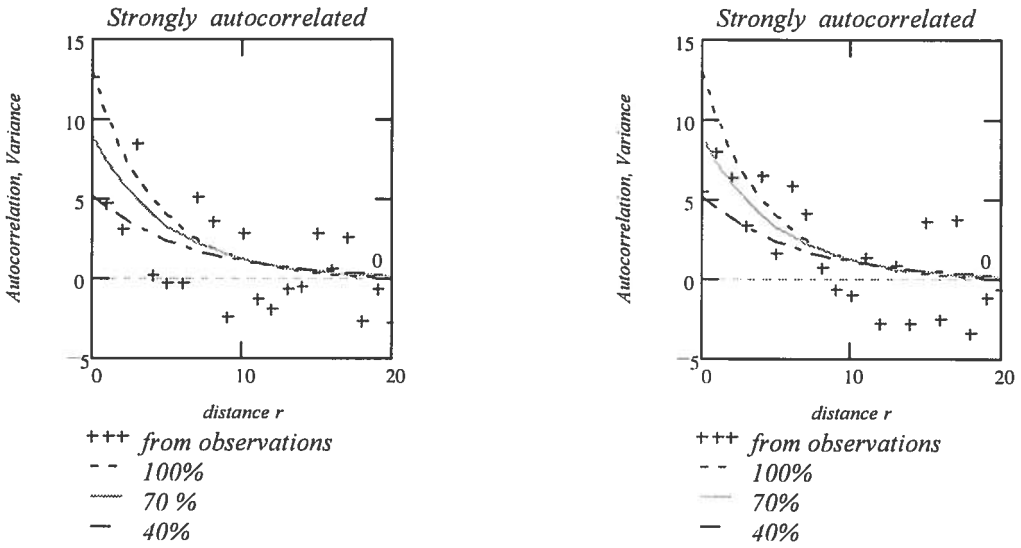

Figure 3.8 Different interpretations of the autocorrelation from a sample of observations. Each figure shows a simulation of sample from the same population.

The double purpose of a correlogram, the determination of both measurement errors and the variance reduction, has a levelling effect. Large interpreted measurement errors, σ_c^2, give a small variance reduction, (due to a large r_0) and vice versa, cf. equation 3.10, which in this case can be rewritten as:

$$\sigma^2_{design} \approx \frac{2}{L} \cdot r_0 \cdot \sigma_c^2 \qquad (3.10a)$$

where σ^2_{design} is the variance, which should govern the design. The autocorrelation distance for the three different interpretations in Figure 3.8 is chosen such that the design variance is equal for all the three different interpretations. The aforementioned levelling effect has been shown by Christian et al. (1992). Alén and Jendeby (1993) have shown that the design value of the variance for the bearing capacity of a friction pile is only marginally effected by different interpretations of the autocorrelation.

Semi-variance

Instead of using the autocovariance, the covariation between properties from different levels can be determined by the so-called semi-variance, $\gamma_x(r)$, see appendix E. Between the semi-variance, the variance and the autocovariance the following relation is valid:

$$\gamma_x(r) = Var(x) - C_x(r) \tag{3.18}$$

if x is a stationary random process.

The plot of the semi variance versus the separating distance is called a variogram.

Examples of application - Nödinge

The method for determining random measurement errors and the autocorrelation distance, described in the previous section, has been applied to the test results from a test site at Nödinge. The site contains deep deposits of soft, homogeneous clay (Mangushev, 1994). Field vane tests and piston samples have been performed in eight different bore-holes. The distance between the bore-holes varied between 1-54 m, see Figure 3.9.

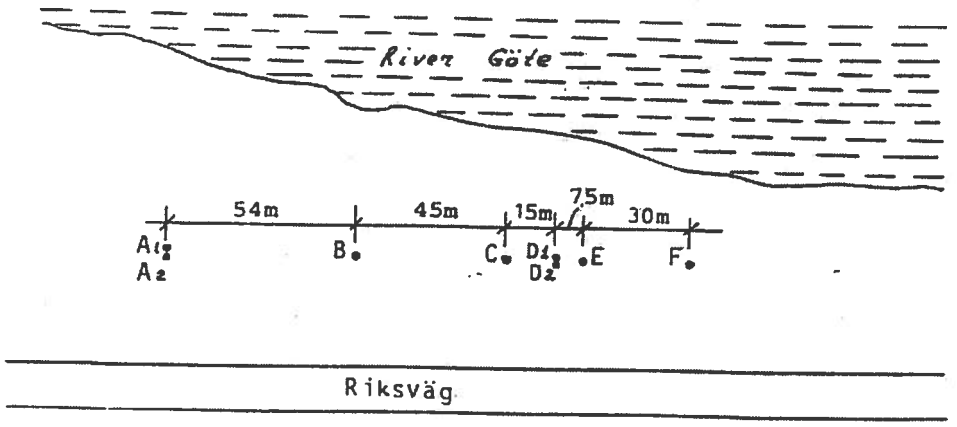

Figure 3.9 Bore hole situation at the Nödinge site. (From Mangushev, 1994)

The purpose of the varying horizontal distances used was to obtain observations of different separating distances for the determination of the horizontal autocorrelation distance. Field vane tests were per-

formed at depth intervals of 0,5 m, which is closer than normal, in order to be able to determine short vertical autocorrelation distances. In five of the bore holes oedometer tests were performed at each metre. The tests were done with constant rate of strain (Sällfors, 1975). The extent of the investigation was more extensive than normal.

Geostatical parameters, autocovariance and semi-variance have been evaluated for the following geotechnical properties:

- Reduced, undrained shear strength determined by field vane test and fall cone, both vertically and horizontally.
- Pre-consolidation pressure, vertically.

The calculations are presented in detail in (Alén, 1998a). An extract of the geostatistical analyses of the shear strength, three examples, is given in appendix F. In Figure 3.10 the result of one calculation to determine the vertical autocorrelation is shown. The clay has been described with a single trend line. In this case there is no tendency for the autocorrelation to go to zero for large separating distances. This should not be interpreted as if there is a great autocorrelation distance. The result is an effect of the fact that the model, the trend, can be seen as incorrect as there is a change of the clay from a glacial to a post glacial layer at approximately 8-10 m depth. Thus the chosen model, a single trend, causes a systematic error, which varies with depth. The mean value of x is not zero, and hence the prerequisites for the theory are not fulfilled, cf. page 63. In a statistical language, the model is said to be biased.

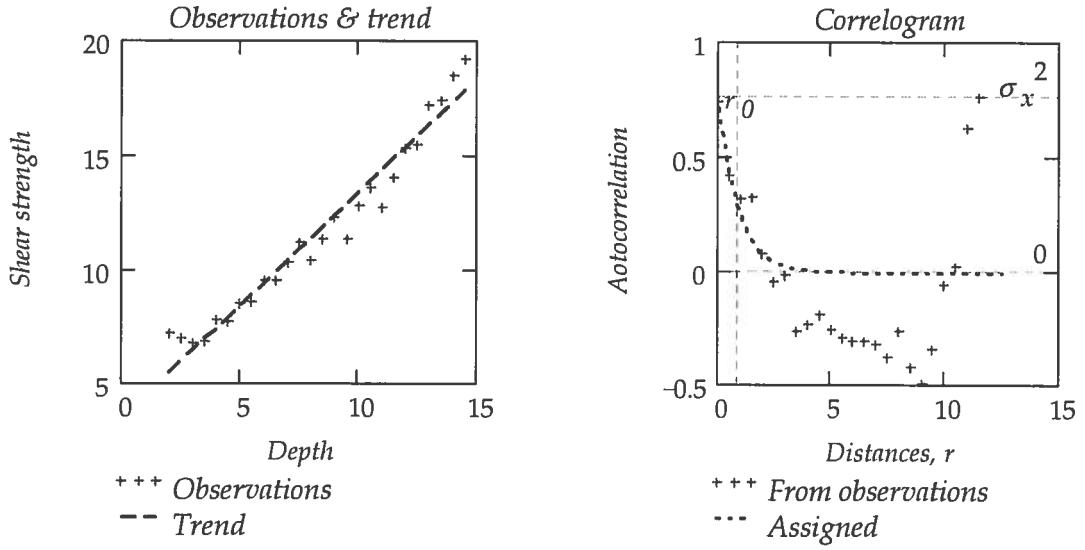

Figure 3.10 Determination of vertical autocorrelation for the undrained shear strength. Linear shear strength model. Data from one bore hole. Example 1 in appendix F.

In Figure 3.11 the result of an alternative calculation is shown. In this case a bi-linear relationship has been used to describe the increase in undrained shear strength with increasing depth.

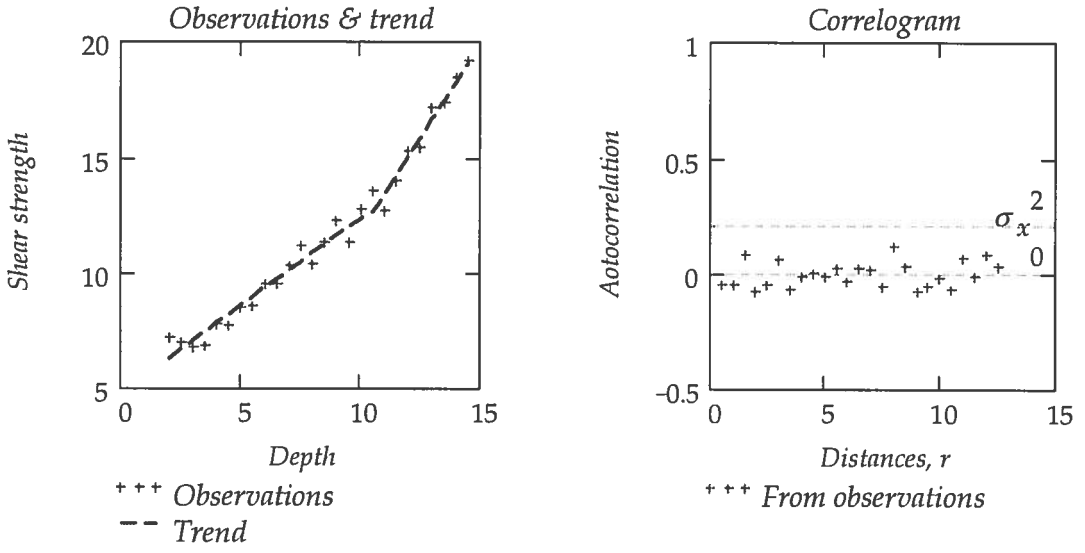

Figure 3.11 Determination of vertical autocorrelation for the undrained shear strength. Bi-linear shear strength model. Example 2 in appendix F.

The correlogram Figure 3.11 shows a noise scatter and a considerably smaller variation. The autocorrelation distance can from a practical point be regarded as zero. The results of a third example are shown in Figure 3.12. In this case it is the horizontal

autocorrelation which has been investigated. It differs from the previous examples as the applied soil model is based upon data from all the eight bore holes, see Figure 3.9. In the two former examples, the calculations were based upon an applied trend model for a separate bore hole. Consequently, the significance of that particular hole was not considered, i.e. the uncertainty of the mean was not taken into account. This is done in this latter case, with all test results examined. Thus, the applied trend model can be regarded as a 'mean value' of the trends for the eight different bore holes. The results form a similar pattern to those presented in Figure 3.11. However, the variations are larger. This is natural as the results in this case, as discussed, also includes the variation of the mean.

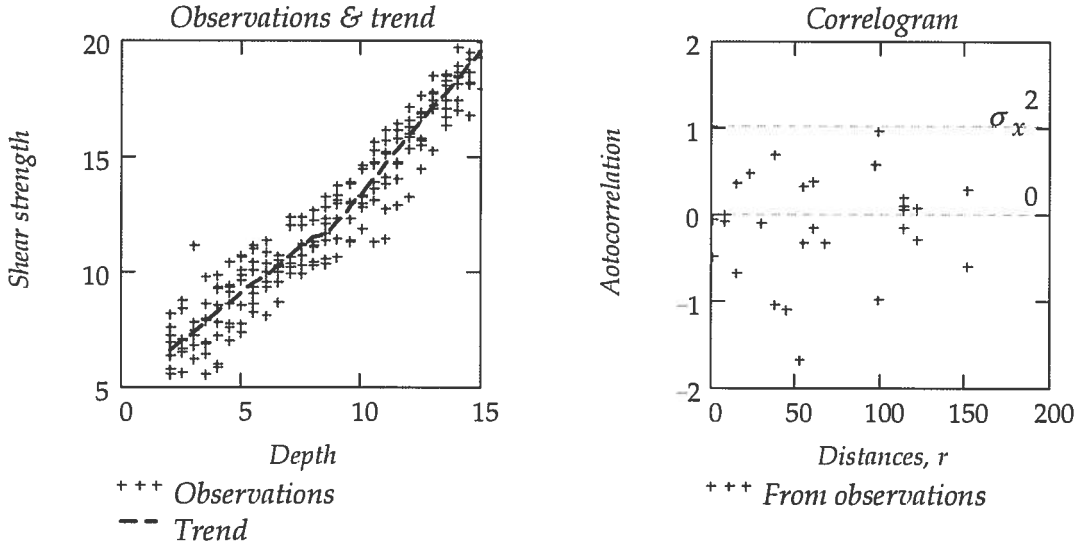

Figure 3.12 Determination of horizontal autocorrelation for the undrained shear strength. Bi-linear shear strength model in vertical direction. Example 3 in appendix F.

The results of the geostatistical analyses demonstrate a close dependence between the soil model assumed and the parameters obtained. An incorrect model, i.e. with systematic errors, shows a distinct dependence between separating distance and autocorrelation. This will only show up as long as the systematic error changes sign depending on the location of the tested samples. A systematic error, which has the same error throughout the complete profile, will not show up with this method. The autocorrelation distances interpreted are negligible, i.e. the distances are less than the difference between different test points. This could be interpreted as that the scatter between the model and the observed values depends on ran-

dom errors in the test method. Thus, from a practical point of view, no distinction between natural variations and measurement errors can be established[1]. The variations in a single bore hole can be regarded as measurement errors and thus neglected in a design situation. However, there remains a variation in the test results obtained from different bore holes, i.e. the uncertainty in the mean value, due to a limited number of tests, which has to be considered in a design situation.

Discussion

It has been shown how one, with the help of geostatistics, can try to separate natural variations from random errors in testing. In appendix F, the procedure is presented using examples from a test site at Nödinge. The basic assumption is that there exists a positive relationship between the soil properties at different points, which decreases with the distance between the points. This relation is normally called autocorrelation. The assumption can in normal geotechnical terms be expressed as that the soil has to be homogeneous, which implies that, at larger distances, there only exists a random distribution of natural variations. If one applies geostatical methods to a non-homogeneous profile, one will obtain an autocorrelation, which is strongly dependent on separating distances. The level of the autocorrelation might then be more dependent on the extension of the volume tested[2]. This was shown by an autocorrelation distance, which did not decrease to zero at large distances, see Figure 3.10. Furthermore, it is assumed that it is only the relative distances between test points and not the absolute co-ordinates of the points which govern the relationship. This latter assumption can be discussed[3]. It implies that one assumes that the distance relations between soil samples taken from different depths are equal, despite the fact that they can differ by thousands of years between the times of the sedimentation of different layers.

---

[1] Sällfors (1975) has shown variations of the natural water content in clay samples of 100 mm height taken from different depths. They indicate that there exist small-scale natural variations of the clay, but these can be neglected in practical deign.

[2] Vertically and/or horizontally.

[3] If the assumptions do not hold, the deviations from the trend do not form a stationary process, cf. page 64.

3.3 Bayesian statistics

3.3.1 Introduction

Testing of material properties in geotechnical projects is normally quite restricted in extent. This means that the result of testing has to be considered as a sample. The results are not to be considered as representative of the complete soil profile. In classical statistics this is described by means of confidence intervals for the interpreted parameters, i.e. interval estimations of unknown parameters. To obtain sufficiently narrow intervals the tested samples have to be rather large. In geotechnical engineering this would mean a more extensive testing than is usual.

Geotechnical investigations are normally strongly influenced by expectations of the results, i.e. pre-knowledge is considered. Pre-knowledge and objective test results can systematically be brought together by means of Bayesian statistics. The principles of this part of mathematical statistics are outlined below. The summary is mainly based upon descriptions given by Benjamin & Cornell (1970) and Ang & Tang (1975).

3.3.2 Principles

Assume that the true state of the sample space for a random variable is given by the values of a parameter θ, see Figure 3.13.

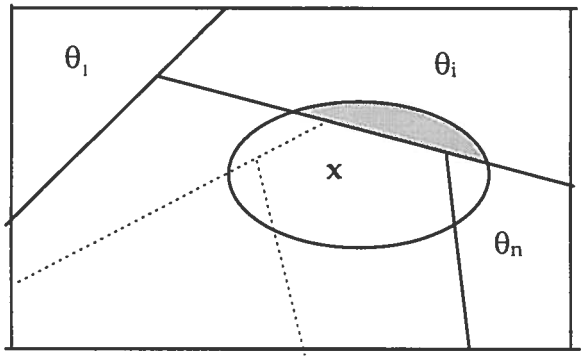

Figure 3.13 A sample **x** of a random variable **X** given by a parameter θ.

The probability of the shaded area in the figure is the probability that the true state is θ_i, given the sample **x**, i.e. a so called conditional probability. e

The conditional probability can be calculated as, see e.g. Beta (1990):

$$p(\theta_i|\mathbf{x}) = \frac{p(\theta_i \cap \mathbf{x})}{p(\mathbf{x})} = \frac{p(\mathbf{x}|\theta_i)\cdot p(\theta_i)}{\sum_n p(\mathbf{x}|\theta_i)\cdot p(\theta_i)} \tag{3.19}$$

This equation is known as Bayes' theorem. It was first discovered by Thomas Bayes in the eighteenth century (Harr, 1987). It serves as the base for Bayesian statistics, in which à priori distribution of an unknown parameter, e.g. the mean value of a basic variable, is updated based upon added information, e.g. test results. Thus with the added information the uncertainty of the unknown parameter is reduced. The denominator in equation 3.19 gives the total probability of obtaining the sample. In the equation it makes the conditional probability, $p(\theta_i|\mathbf{x})$, into a true probability, i.e. $\sum_n p(\theta_i|\mathbf{x}) = 1$. Thus it works as a normalising constant. Bayes' theorem can be given in words as, (cf. Benjamin & Cornell 1970):

$$\begin{pmatrix} \textit{Posterior prob.} \\ \textit{of the true state } \theta \\ \textit{given the sample} \end{pmatrix} = \begin{pmatrix} \textit{Norma -} \\ \textit{lising} \\ \textit{constant} \end{pmatrix} \cdot \begin{pmatrix} \textit{Sample likelihood} \\ \textit{given} \\ \textit{the true state } \theta \end{pmatrix} \begin{pmatrix} \textit{Prior prob.} \\ \textit{of the true} \\ \textit{state } \theta \end{pmatrix} \tag{3.19a}$$

Let the variable X belong to a continuous distribution with the density function $f_x(x,\theta)$. Here θ is a parameter of the distribution[1], e.g the mean value μ or the standard deviation σ. The sample likelihood, $L(\theta)$, i.e. the probability of getting a sample $\mathbf{x} = (x_1, x_2, \cdots, x_i, \cdots, x_n)$, is then determined as (see e.g. Blom 1984b):

$$\begin{aligned} L(\theta) &= L(\theta|x_1, x_2, \cdots, x_i, \cdots, x_n) = p(x|\theta) = \\ &= f_x(x_1|\theta)\cdot f_x(x_2|\theta)\cdot\ldots\cdot f_x(x_i|\theta)\cdot\ldots\cdot f_x(x_n|\theta) = \prod_n f_x(x_i|\theta) \end{aligned} \tag{3.20}$$

[1] θ can in the general case be a vector, i.e. a 'multi-dimensional' parameter.

The function $L(\theta)$ is called the likelihood function[1]. Bayes' theorem can now be rewritten for continuous distributions of θ as:

$$f_\theta''(\theta) = k \cdot L(\theta) \cdot f_\theta'(\theta) \tag{3.19b}$$

with the normalising constant $k = 1 \Big/ \int_{-\infty}^{\infty} L(\theta) \cdot f_\theta'(\theta) d\theta$. The posterior density function for the parameter θ is denoted by " while the prior density function is denoted by '.

The procedure of Bayesian updating of a random variable X means that a parameter[2] for the distribution is also given as a random variable. By added information the uncertainty of this latter variable is reduced, i.e. the uncertainty of the posterior distribution is less than the uncertainty for the prior distribution. However, regardless of how much additional information is given, some uncertainty, in principle, will always remain. This uncertainty can be incorporated into the Bayesian prediction of the variable X by the Bayesian distribution (Bejamin & Cornell, 1970):

$$\hat{f}_x(x) = \int_{-\infty}^{\infty} f_x(x|\theta) \cdot f_\theta(\theta) d\theta \tag{3.21}$$

where $f_x(x|\theta)$ is the 'true' underlying model of the variable, while $f_\theta(\theta)$ can be either the posterior or the prior distribution. It has to be noticed that the unknown parameter by the integration does not appear in the Bayesian distribution. On the other hand, the integration also implies that the uncertainty of the parameter, given by $f_\theta(\theta)$, is included in $\hat{f}_x(x)$. Thus this latter distribution can be expected to be wider than the true distribution $f_x(x)$. The mathematics of Bayesian statistics are simplified if the prior and the posterior distributions are of the same type. This is the case for a number of combinations of basic and prior distributions. Such pairs of distributions are called conjugate distributions.

---

[1] In the maximum-likelihood method the value of θ, which maximises the likelihood function, is used as a point estimator of the parameter (see e.g. Blom, 1984b)

[2] Or several parameters.

In appendix G, various aspects of Bayesian statistics for two simple but important cases of conjugate distributions are discussed:

- Normal distributions, known standard deviation
- Lognormal distributions, known coefficient of variation

The results are discussed below. Other cases of conjugate distributions are given and discussed in e.g. (Benjamin & Cornell, 1970) and (Ang & Tang, 1975). Benjamin & Cornell give, for example, a comprehensive summary of the case when both μ and σ are unknown. Ang & Tang tabulate a number of conjugate pairs.

3.3.3 Discussion

Known variation - standard deviation or coefficient of variation

In appendix G results of Bayesian statistics for two common situations in geotechnical design are derived; the magnitude of a geotechnical property is unknown, but the variation of the same property, based upon pre-knowledge, is considered as known. Two different cases are described, the standard deviation, σ, is known and the coefficient of variation, V, is known.

It is concluded that the mean value of a property can be up-dated by information given by a sample $\mathbf{x}_2$ of n tests. The pre-knowledge of the property can then be interpreted as an equivalent sample $\mathbf{x}_1$ of m tests such that:

$$\bar{x}_1 = \mu' \text{ and } m = \frac{\sigma^2}{\sigma'^2} \tag{3.22}$$

if the standard deviation is known and

$$\overline{\ln x_1} = \ln \mu' \text{ and } m = \frac{V^2}{V'^2} \tag{3.23}$$

if the coefficient of variation is known.

In the same way, the uncertainty of the mean value, i.e. the posterior distribution, can be described as:

$$\mu'' = \frac{m \cdot \overline{x_1} + n \cdot \overline{x_2}}{m+n} \text{ and } \sigma'' = \sigma / \sqrt{m+n} \tag{3.24}$$

or

$$\mu'' = \exp\left(\frac{m \cdot \overline{\ln x_1} + n \cdot \overline{\ln x_2}}{m+n} \right) \text{ and } V'' = V / \sqrt{m+n} \tag{3.25}$$

respectively. Finally, the uncertainty of the basic variable is given by the Bayesian distribution such that:

$$\mu_x = \mu'' \tag{3.26}$$

and

$$\sigma_x = \sigma \cdot \sqrt{\frac{m+n+1}{m+n}} \text{ or } V_x = V \cdot \sqrt{\frac{m+n+1}{m+n}} \tag{3.27}$$

depending on whether the standard deviation or the coefficient of variation is known.

In the derivations of the formulas above it was assumed that both the basic variable and the mean value of the basic variable could be modelled as normal distributions in the case of known standard deviation, while the distributions were modelled as lognormal distributions when the coefficient of variation was known. However, the purpose of the updating process can be seen as a way of obtaining relevant parameters of a geotechnical property for application in practical design. For a given limited sample, it is the characteristics of the central parts of the distributions which are invoked by the updating process. Hence, the choice of a normal or lognormal distribution is of minor importance. This is illustrated in Figure 3.14 in which the 5-percentile of a random variable is shown. The variable has a simple linear form, $X=a+b \cdot z$ with the mean value $10+z$, which for example could be a model of the undrained shear strength, increasing with depth. By simulating values from assumed distributions, the parameters of the corresponding Bayesian distribution are recalculated by equations 3.26 and 3.27.

The input data for the cases shown in Figure 3.14 can be summarised as:

- Standard deviation 3,5. Lognormal distribution.
  Case A m=5; n=0, Case A+B m=5; n=5
- Standard deviation 3,5. Normal distribution.
  Case A m=5; n=0, Case A+B m=5; n=5
- Coefficient of variation 20%. Lognormal distribution.
  Case A m=5; n=0, Case A+B m=5; n=5
- Coefficient of variation 20%. Normal distribution.
  Case A m=5; n=0, Case A+B m=5; n=5

As can be seen in Figure 3.14 there is no significant difference in the results whether the underlying distribution is lognormal or normal. In the derivation of equations 3.23-3.27, it was further assumed that the known coefficient of variation had to be of moderate magnitude, $V<25\%\text{-}30\%$, to permit Gaussian approximation of the lognormal distribution. However, even this restriction might be loosened in an updating process. Figure 3.15 shows the results of simulations with deliberately high values of the scatter of the random variable, $\sigma=5,5$, and $V=55\%$ for the cases constant standard deviation and constant coefficient of variation, respectively.

From the results shown in Figure 3.15 it seems that the given formulas should be applicable even in this case in a practical up-dating situation. However, as discussed earlier in section 2.4.2, there are other reasons for a normal distribution being an unsuitable choice for the random variable in this latter case. Hence, the Bayesian approach does not appear to be the limiting factor in the choice of distribution even if one wants to keep the mathematics on a simple level.

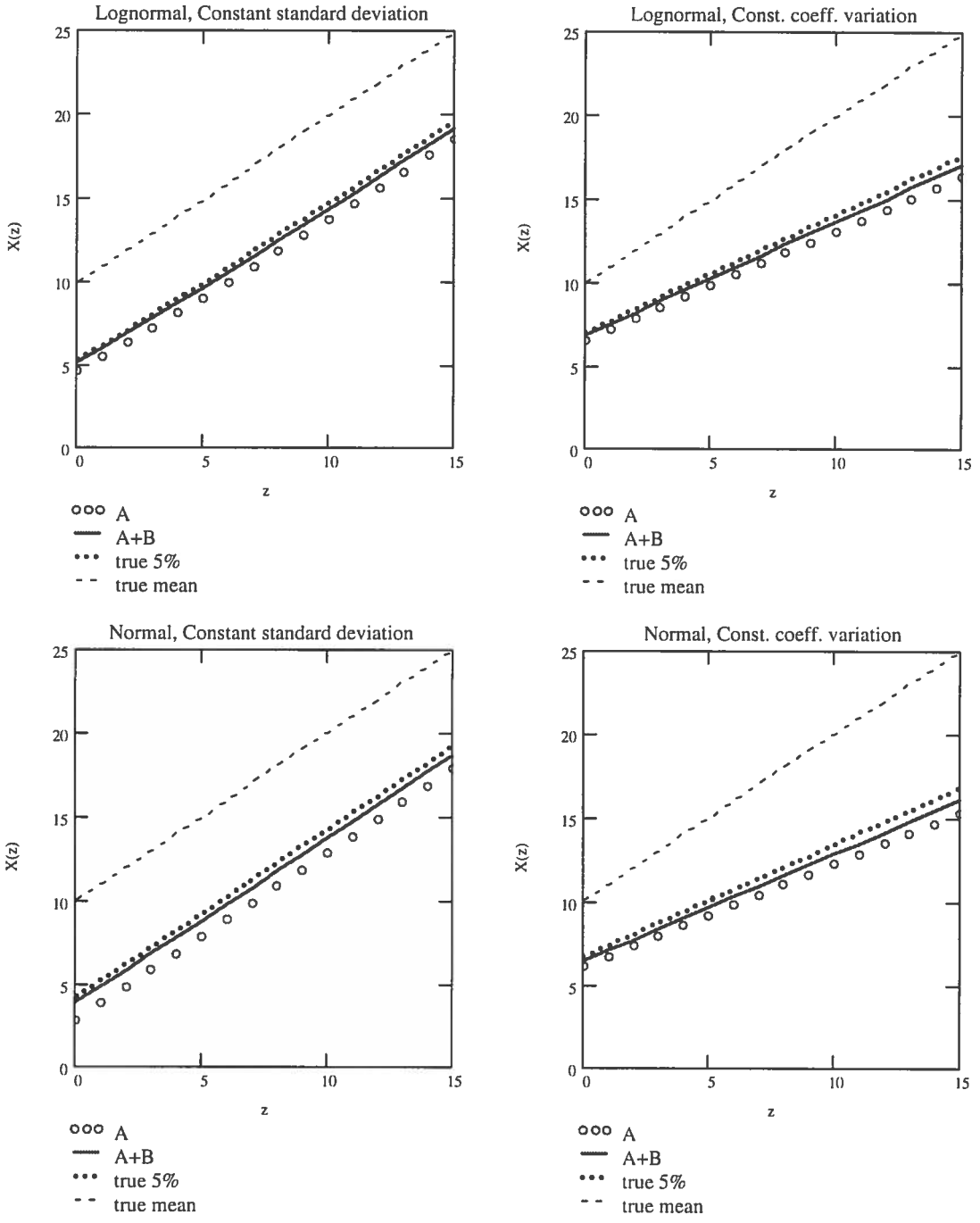

Figure 3.14 Simulation of the 5-percentile for a Bayesian distribution of a random variable. Left figures, σ=3,5. Right figures V=20%
Case A: 5 values. Case A+B: 5+5 values

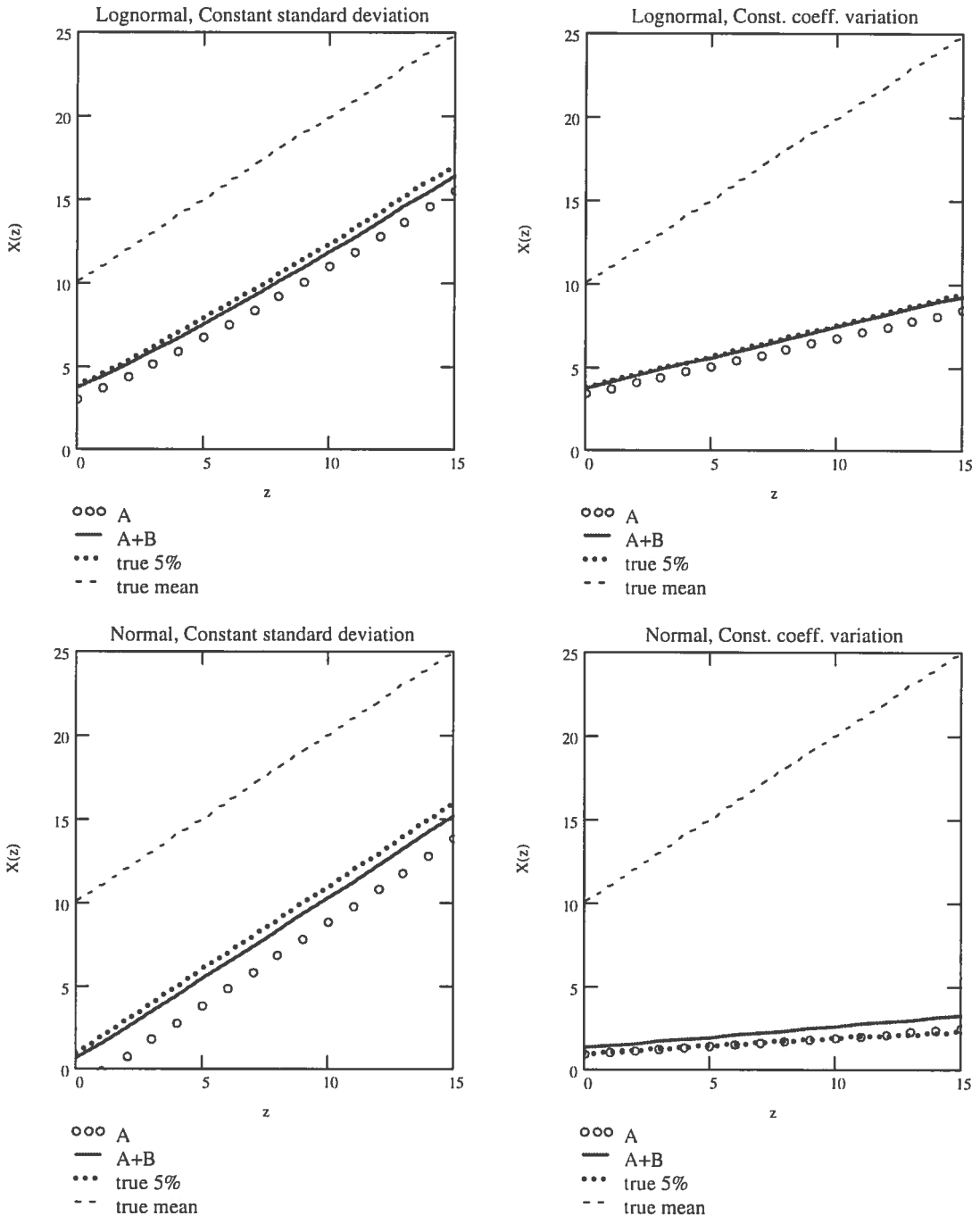

Figure 3.15 Simulation of the 5-percentile for a Bayesian distribution of a random variable. Left figures, σ=5,5. Right figures V=55%
Case A: 5 values. Case A+B: 5+5 values

Interpretation of variation

In section 3.1.1 four different sorts of uncertainty of geotechnical properties were discussed.

- Natural variations
- Systematic errors
- Testing errors
- Errors due to limited number of tests

In Bayesian statistics one has to handle two different sorts of uncertainty:

- Uncertainty of the basic variable
- Uncertainty of parameters of the basic variable

Finally, in section 3.2.2, Geostatistics, the variance was divided into natural variations σ_c^2 and testing errors σ_ε^2.

How do these different schemes fit together? As mentioned earlier, see section 3.1.1, there is no reason to incorporate systematic errors into an analysis. The pragmatic statement that the variance can be seen as a measure of lack of knowledge, see section 3.1.2, implies that systematic errors have to be known, otherwise they can not be identified as systematic. Thus, by definition, systematic errors can always be calibrated out of the analytical model. In section 3.2.2 systematic errors were revealed by an odd looking correlogram, see Figure 3.10, but were eliminated by a careful description of the soil model.

Natural variations and testing errors, given as variances, make up the variance of the basic variable. They are incorporated in any observation of a geotechnical property. Thus, they form a part of the uncertainty of the basic variable given by equation 3.27. The difference between the variances of the Bayesian distribution and the basic variable is due to the uncertainty of the mean value, i.e. an effect of the limited number of tests. In those cases, when the model can be given with both high precision and accuracy, there exist no 'natural' variations, see e.g. Figure 3.11 and Figure 3.12. At the same time, the testing errors do not affect a real design. Hence, the only

uncertainty one has to consider in such a case is the uncertainty due to the limited number of tests, i.e. in Bayesian statistics the uncertainty given by the prior or the posterior distribution.

The prior information can be given as an equivalent number of tests, given by the ratio σ^2/σ'^2. The numerator is the uncertainty of the basic variable. That is the variations of the basic variable, including test errors, compared to an assumed model. These can be seen as the small-scale variations observed in a test sample, see e.g. Figure 3.11. This type of uncertainty is principally unaffected by the amount of tests[1], but can be reduced in a design situation compared to the point variance, cf. equation 3.10a. They form an integrated part of the modelling of the soil. The uncertainty of the denominator is the uncertainty of the mean value, i.e. the uncertainty of the 'magnitude' of the model before testing. It can be regarded as an effect of large-scale fluctuations of the soil properties, superimposing the variations of a single test. Incorporating sample information reduces this uncertainty rapidly, see e.g. equation 3.24. In this way the testing can be seen as a calibration of the model.

For an 'infinite' number of tests, the uncertainty of the mean value is eliminated. Consequently the variance of the basic variable and the Bayesian distribution become equal.

Two non-existing but illustrating extreme cases of Bayesian updating can be worth noticing:

- The uncertainty of the basic variable is negligible, ≈ 0. This makes prior information irrelevant, $m \approx 0$, but a single test value, x, eliminates any uncertainty, $\mu_x \approx x$ and $\sigma_x \approx 0$.

- The uncertainty of the mean value is neglible, ≈ 0. Test results will not add any information as $m \approx \infty$, which makes $\mu_x \approx \mu'$ and $\sigma_x \approx \sigma$.

Known mean value. Unknown variation.

This case is from a mathematical point of view more complex than the case with known variation discussed previously in this section.

[1] The knowledge of such uncertainty might be increased at very extensive testing.

However, the mentioned complexity is no reason to avoid the analysis of such a case. The mathematical models can be found in the literature. For example, as mentioned earlier, Benjamin & Cornell (1970) describe the general case 'unknown mean value and unknown variation'. On the other hand, from a geotechnical point of view it can be discussed whether it is worthwhile to put too much effort into a highly sophisticated analysis. As indicated by the simulation examples in section 2.5.3, one can not expect to estimate the variance with a high degree of accuracy in a single project. Thus the variance has to be obtained as a weighted parameter from different projects. At the same time, the variance is the difference between the applied model and reality, cf. section 3.1.2. For this reason it is not a straightforward task to compare variances obtained in different projects and perhaps by different persons. Furthermore, the variance originates from several divergent sources, cf. the discussion previously in this section. Obviously, the application in a design problem of even a 'known' variance might be an intricate assignment.

From what is said above, it might be concluded that the precision of a correct mathematical analysis might be illusory. From a practical point of view, a simple procedure, in which the standard deviation or the coefficient of variation alternatively is seen as the unknown variable and not a parameter of the unknown variable, can be just as sufficient. The expected value of the variation can then be obtained as a weighted mean value from different projects, c.f. e.g. equation 3.24. Compared to a complete Bayesian analysis, the uncertainty of the variation, e.g. the standard deviation of the standard deviation, is not determined - a fact which, in the light of what is said above, can be seen as acceptable. It is here understood that the variance is estimated from rather large test projects, to make the uncertainty of the mean value negligible.

3.3.4 Example

Introduction

Various examples of the Bayesian approach can be found in the literature. Olsson (1986) discusses Bayesian statistics in connection with sheet pile calculations. Hintze (1994) has shown an example of how it can be used to update an valuation of expected settlements for a pile foundation.

An example, with application of Bayesian statistics as discussed above in the previous sections, will be given. It is based on data from the same test site, which were analysed with geostatistical methods in section 3.2.2 and appendix F.

Assume a design situation in which one has to design shaft bearing piles. In such a case it is in principle the average shear strength along the pile, and not any single point shear strength, which forms the basic variable in the Bayesian analysis. The undrained shear strength at the test site at Nödinge shows a very typical behaviour of increasing strength with depth, see Figure 3.10 - Figure 3.12. Presume that the shear strength can be given as a linear model with depth, which, for the sake of simplicity, can be modelled as a single trend line.[1]:

$$c_u = a + b \cdot z \tag{3.28}$$

The average shear strength can then be written as:

$$c_{u,average} = a + b \cdot L/2 \tag{3.29}$$

if L is the pile length and z is given from the pile head. To be correct one then has to know the pile length before the design in order to choose the correct basic variable. As more versatile approach is to treat the trend line as a random object, as it puts the focus entirely on the shear strength and not on the geometry of the structure to design.[2]

[1] On page 69 a single trend line was rejected, as it caused a biased model of the shear strength. However, this was in the context that one wanted to analyse the variances between the observations and the model. In this case when it is the average behaviour, which is of interest, the simple model will serve its purpose. There is nothing that prevents one to use a bi-linear trend line in this case either, but the analysis will not gain much benefit from it.

[2] This is entirely a formal remark. As both approaches are based upon linear combinations of the parameters a and b for the trend line, they give the same result.

In the example the testing is assumed to have taken place on two different occasions. Hence, the up-dating of the shear strength in the example will be given as a two-step procedure

- First judgmental information is combined with samples from three bore-holes, A_1, B and D_1, see Figure 3.9
- The results of the first up-dating process are supplemented with test results from five additional bore-holes, A_2, C, D_2, E and F.

Prior information

The undrained shear strength can be given by the empirical relation[1]:

$$c_u = 0{,}3 \cdot \sqrt{w_L} \cdot p'_c \qquad (3.30)$$

where w_L is the liquid limit and p'_c is the preconsolidation pressure. Assume from local experience that OCR=1,25, w_L=0,75 and in-situ-stresses $\sigma'_0 = \sigma_0 - u = 15 \cdot z - 12 \cdot (z - 1{,}5)$ [kPa], incorporating knowledge of a strong artesian pore pressure. Taking this as the best information of the mean value for the prior distribution results in:

$$\mu' = 5{,}85 + 0{,}97 \cdot z \text{ [kPa]} \qquad (3.31)$$

Assume the uncertainty of this empirical relation is given as the standard deviation of μ′, in this case σ′=3 kPa. The uncertainty of the basic variable, i.e. the linear trend, is the uncertainty which can be expected in the determination of the regression line from the test results from one bore-hole. Thus it is considerably reduced compared to the at-a-point variance of the shear strength. The results of the calculations presented in section 3.2.2 ended in the conclusion that these variations in a single bore-hole could be neglected in the design situation. However, test results from different bore-holes are diverging. These variations have to be interpreted as either natural variations in a horizontal direction or as if the test errors from bore-hole to bore-hole are larger than the errors in a single hole. Given any of the interpretations they can be regarded as uncertainty of the mean at a particular test site in

---

1 $c_{u,unred} = 0{,}45 \cdot w_L \cdot p'_c$ (*Hansbo*, 1957)

$c_{u,red} = f(w_L) \cdot c_{u,unred}$ (*Larsson*, 1984) *with* $f(w_L) = (0{,}43/w_L)^{0{,}45} \approx \sqrt{0{,}45/w_L}$

contrary to uncertainty of the prior distribution, which rather has to be seen as related to experience from a local region. In this case it is assumed that σ=1,5 kPa. Based on the equations in section 3.3.3 the assumptions can be systemised. This means that the prior information can be regarded as equal to m=0,25 number of tests[1] and that the best prediction of the shear strength, prior to testing, is the Bayesian distribution with the mean value given by equation 3.31 and the standard deviation 3,35 kPa.[2]

Up-dating no. 1

Given the results from three test holes, the judgemental information can be up-dated as a combination of the prior distribution and the likelihood of getting the samples. In Figure 3.16 the input data needed are summarised. As can be seen in the figure, the assumed shear strength seems to be rather optimistic. The right part of the figure shows the prior distribution and the likelihood function forming the right hand side of Bayes' theorem, see equation 3.19a.

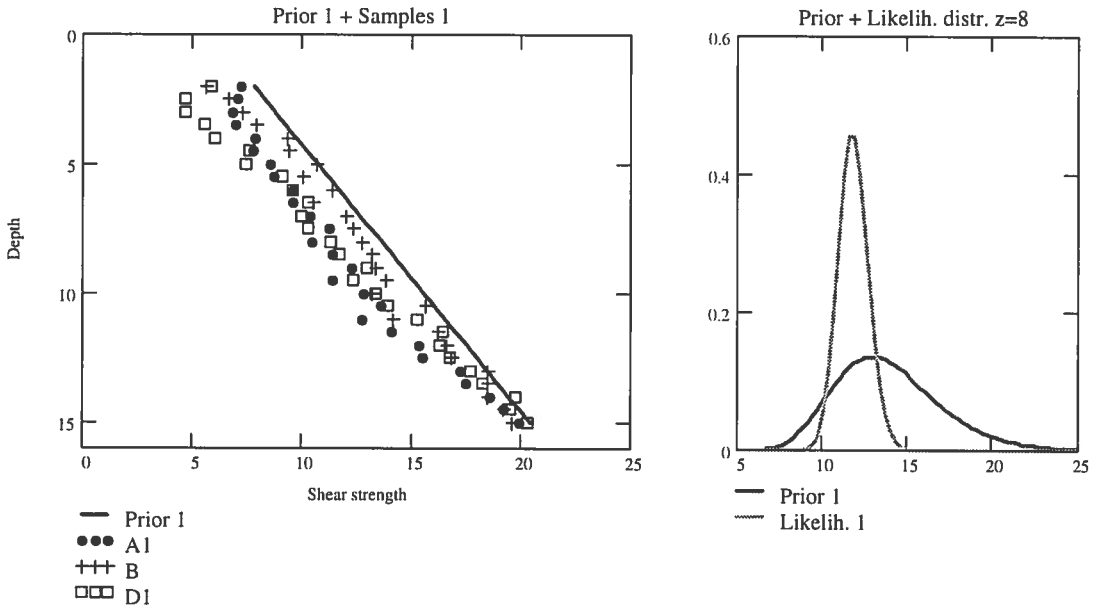

Figure 3.16 Input data for up-dating process no. 1.
Left part. Mean value of prior distribution and test values
Right part. Prior and likelihood distributions for z=8.

There exists a considerable difference between the prior distribution and the likelihood distribution. Hence, the up-dating process will

[1] By equation 3.22

[2] Equation 3.27 with m=0,25 and n=0.

invoke considerably more information in the posterior distribution than in the prior distribution. The posterior (or Bayesian) mean can now be calculated from equation 3.24:

$$\mu_1'' = \frac{m \cdot \mu' + \sum_{i=1}^{3} a_i + b_i \cdot z}{m+3} = 3{,}47 + 1{,}07 \cdot z \ \text{[kPa]} \qquad (3.32)$$

where a_i and b_i are the parameters of the regression lines from the three different test holes, A_1, B and D_1. The standard deviation of the up-dated Bayesian distribution is:

$$\sigma_{Cu} = 1{,}5 \cdot \sqrt{\frac{m+3+1}{m+3}} = 1{,}72 \quad [kPa] \qquad (3.33)$$

In Figure 3.19 the result of the updated distributions is illustrated. Despite the fact that the mean value has decreased, the left tail of the Bayesian distribution has moved 'upwards' due to the decreased variance. Hence, a probabilistic approach gives room for larger design values of the shear strength .

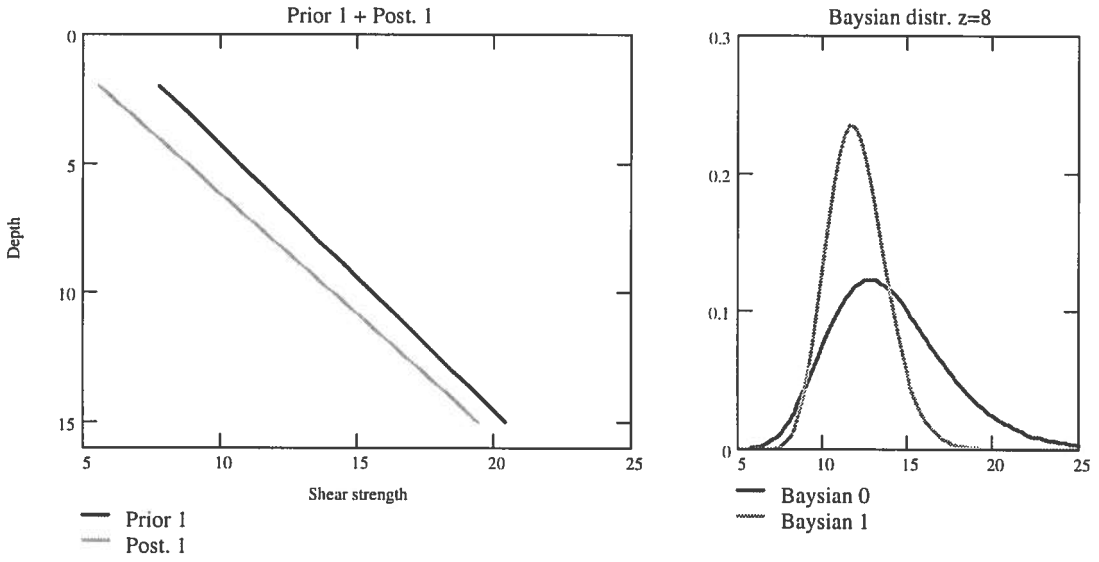

Figure 3.17 Result of up-dating process no. 1.
Left part. Mean values of prior and posterior distributions
Right part. Bayesian distributions before and after up-dating. z=8
Note: The mean of prior and posterior distributions are equivalent to the mean of the Bayesian distributions before or after updating.

Up-dating no. 2

Given additional information from the last five bore-holes, the shear strength can be up-dated again. However, from the input data, given in Figure 3.18, it can be seen that the prior distribution and the likelihood function are very similar in shape. Thus, the expected result of the up-dating process will result in a very small change of the mean value and as a reduction of the standard deviation, see results in Table 3.1.

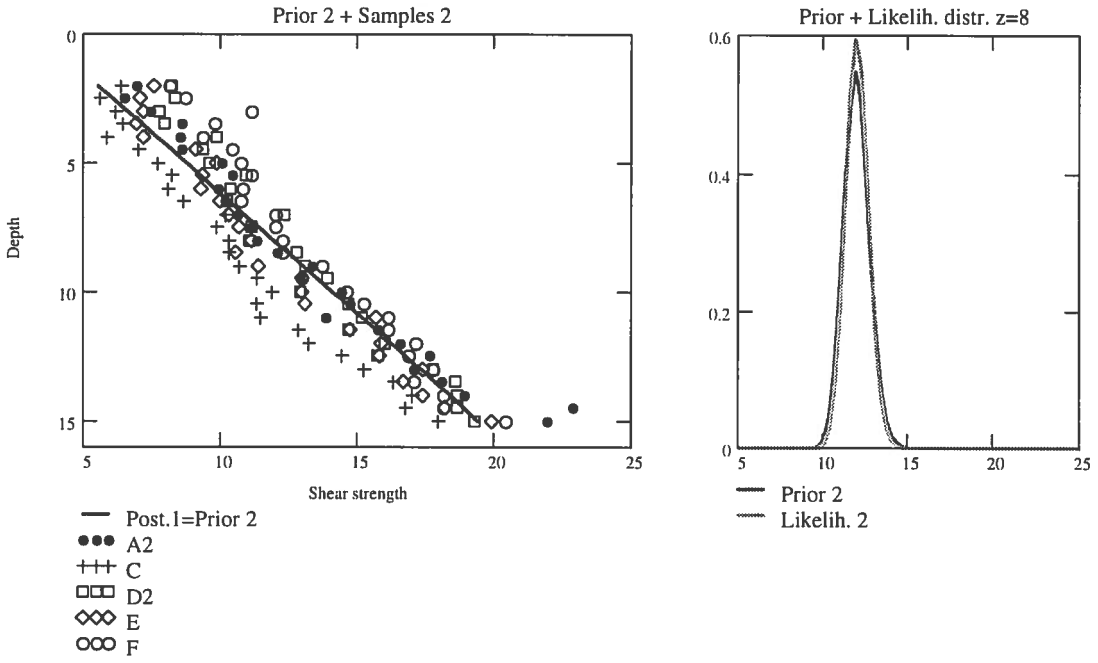

Figure 3.18 Input data for up-dating process no. 2.
Left part. Mean value of prior distribution and test values.
Right part. Prior and likelihood distributions for z=8

The posterior (or Bayesian) mean can now be calculated from the up-dated prior, i.e. $\mu_2' = \mu_1''$ and from the added information of the five remaining bore-holes:

$$\mu_2'' = \frac{(m+3)\cdot\mu_2' + \sum_{i=1}^{5} a_i + b_i \cdot z}{m+3+5} = 4{,}09 + 0{,}99 \cdot z \ \text{[kPa]} \quad (3.34)$$

where a_i and b_i are the parameters of the regression lines from the last five holes.

The standard deviation of the up-dated Bayesian distribution is:

$$\sigma_{Cu} = 1{,}5 \cdot \sqrt{\frac{m+8+1}{m+8}} = 1{,}59 \quad [kPa] \tag{3.35}$$

In Figure 3.19 the result of the updated distributions is illustrated.

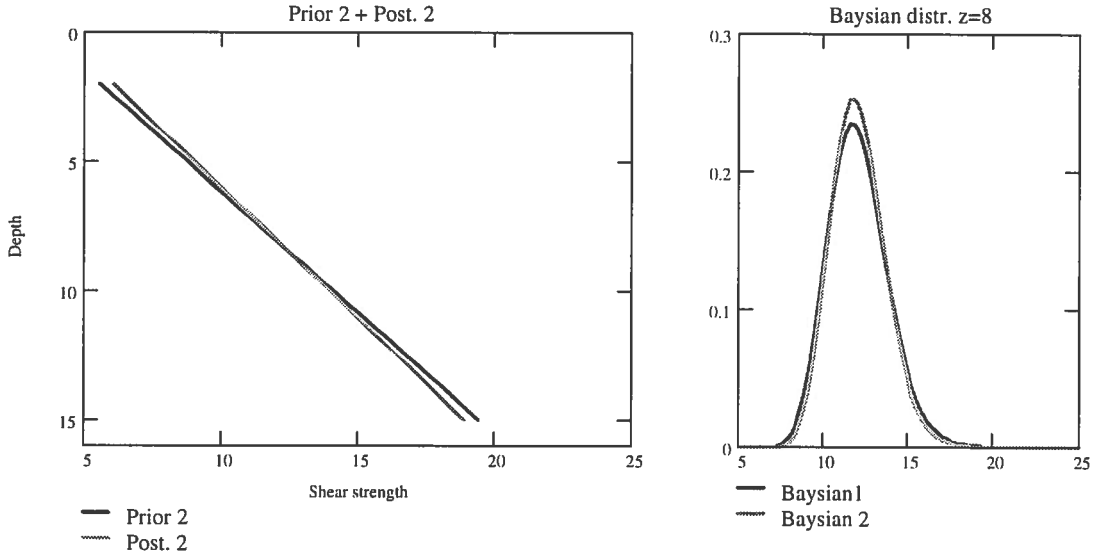

Figure 3.19 Result of up-dating process no. 2.
Left part. Mean values of prior and posterior distributions.
Right part. Bayesian distributions before and after up-dating. z=8
Note: The mean of prior and posterior distributions are equivalent to the mean of the Bayesian distributions before or after updating.

Summary

The results of the calculations are summarised in Table 3.1

	Prior information		**Up-dating no. 1**		**Up-dating no. 2**	
	μ [kPa]	σ [kPa]	μ [kPa]	σ [kPa)	μ [kPa]	σ [kPa]
Prior	-	-	5,85+0,97z	3,0	3,43+1,07z	0,83
Likelihood	-	-	3,23+1,07z	0,87	4,52+0,93z	0,67
Posterior	-	-	3,43+1,07z	0,83	4,09+0,99z	0,52
Bayesian	5,85+0,97z	3,35	3,43+1,07z	1,72	4,09+0,99z	1,59

Table 3.1 Bayesian up-dating of the undrained shear strength.

It can be noted that none of the distributions have the same standard deviation as the known standard deviation of the basic variable, σ=1,5kPa. However, it will appear as the standard deviation for the Bayesian distribution for an unlimited number of tests. The likelihood functions are calculated according to the formulas

given in appendix G. They are not requisite to obtain the other results but are here given as an illustration. The density curves shown in the figures are lognormal distributions.

3.4 Various soil properties

3.4.1 Density of soil

Density is normally treated as an action. It could be regarded as a sum of the weight of a number of small particles. This should mean that a normal distribution is a suitable description of the density. Normally, it is high values of a load which govern a problem, i.e. the right hand tail of a distribution. However, the shear strength of soil is to a large extent dependent on the stresses in the soil. Thus, the soil density forms both action and bearing capacity. This makes soil density a special property. When modelled as a probability distribution, both tails of the distribution might govern the problem. If a low value of the density is crucial, there is a risk that, when modelling with a normal distribution, nominal negative values will affect the result substantially. The corresponding problem exists when partial coefficients are used, as it is essential whether the density is multiplied by a load factor or divided by a strength factor. An intricate problem has arisen in application of the partial factor format as defined by Euro codes (ENV 1991-1 and ENV 1997-1). In these the action (load) factors are given by large nominal values. This is due to the structural tradition to incorporate uncertainties of both the loads and the calculation model in the values of the actions, cf. Chapter 2.2.1, 'Factor of safety'. This entails in some cases that, when the partial factors are applied to characteristic unit weights of soil and water, design values are obtained that must be regarded as physically impossible[1], cf. the discussion on how to interpret the partial factor format in section 2.2.3' Safety margin/Partial factors'.

3.4.2 Pore pressure

General

The value of the pore pressure is the most essential factor in effective stress analysis. As high pore pressure implies a reduced shear

[1] An obvious way to solve such a problem is of course to separate the partial factor into one action factor, applied to the actions, and one model factor, applied to the action effects.

strength, it seems reasonable to treat the pore pressure as a part of the shear strength. However, the pore pressure is in nature more to be regarded as a load. There is no essential difference in the variation of the pore pressure in a year compared to the variation of an external water level or the variation of the snow load or the wind load. From a mathematical point of view the pore pressure should be treated as an action. A suitable distribution for the pore pressure from this point of view is an extreme value distribution, e.g. a Gumbel distribution.

Example

Svensson och Sällfors (1982) have published observations of annual maxima and minima of the ground-water table at 39 places in the south of Sweden. The observation series ranges from 8-28 years. By inspections of plots on normal distribution paper of the test series, cf. appendix B, the observation series can be separated into three different types:

- Plots with positive curvature - 29 series
- Linear plots - 9 series.
- Plots with negative curvature - 3 series.

Typical plots are given in Figure 3.20. The upper left figure shows observations from one location, tube 13002, which give a linear plot. The lower left figure shows observations from a location, tube 4009, which give a negative curved plot. Finally, the right figures are examples from two locations, tube 13004 and tube 64002, which form the largest group, positive curved plots.

An alternative way to characterise the different plots in statistical terms includes:

- Series with negative skewness - positively curved plots.
- Symmetric series - linear plots.
- Series with positive skewness - negatively curved plots.

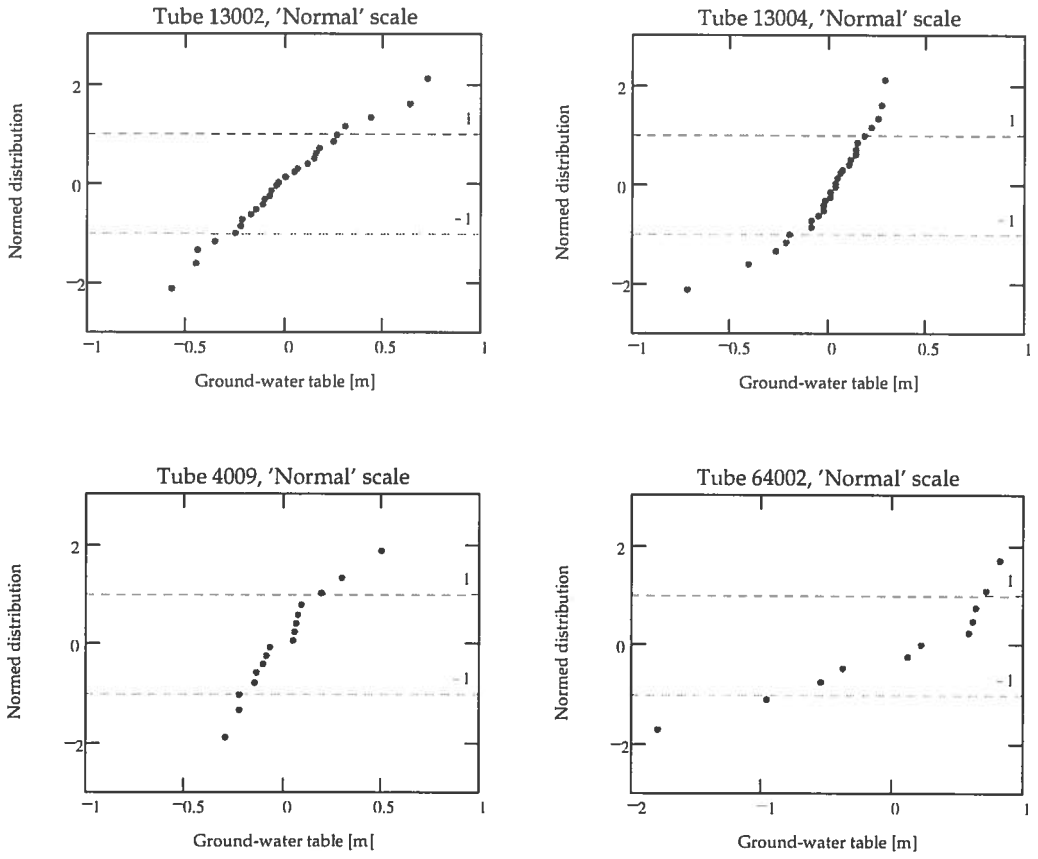

Figure 3.20 Observations of ground-water table. Annual maxima.
Probability scale on y-axis, $\Phi^{-1}(p)$. Tube=observation point.

An overview of all the test series is given in Figure 3.21. The figure shows a plot of the skewness and the peakedness of the observations, which is of the same type as Figure 2.9. The different types of observations are separated in the figure. Grey points show negatively curved plots, the rings are the symmetric series, while the positively skewed observations are shown as black points. The examples given in Figure 3.20 are marked with crosses. As can be seen from the figure it is difficult to draw any general conclusion about the type of distributions.

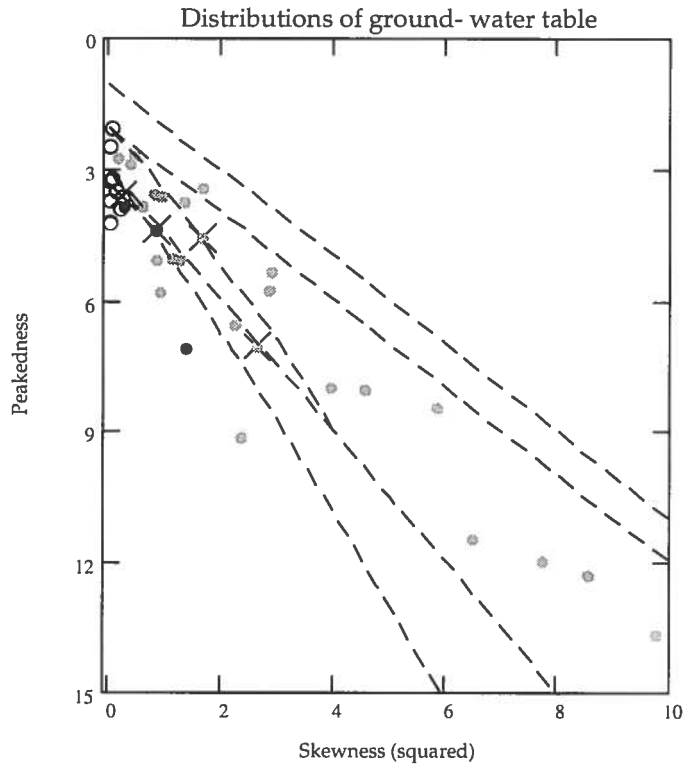

Figure 3.21 Observations of ground-water table. Annual maxima. Estimates of types of distributions.

To test the hypothesis that a Gumbel distribution would be a better choice of distribution than a normal distribution, plots were also made on a Gumbel paper, see Figure 3.22. In general, agreement was not better. However, from both types of plots, the majority of observation series show a tendency towards a restrained increase, i.e. test series with negative skewness. Physically, this might be explained as if the topography of the landscape works as a spill-way. Hence, the extreme value model, peak over threshold, see section 2.3.2, 'Extreme value distributions', might be a suitable way to model the maximum of the ground-water table for those test series. The values 0,15 m and 0,5 m respectively, marked in Figure 3.22 can serve as thresholds[1].

[1] In this particular case only annual maxima data are available. Hence the application is very 'rough'. In a correct 'peak over threshold' all values over the threshold should be considered.

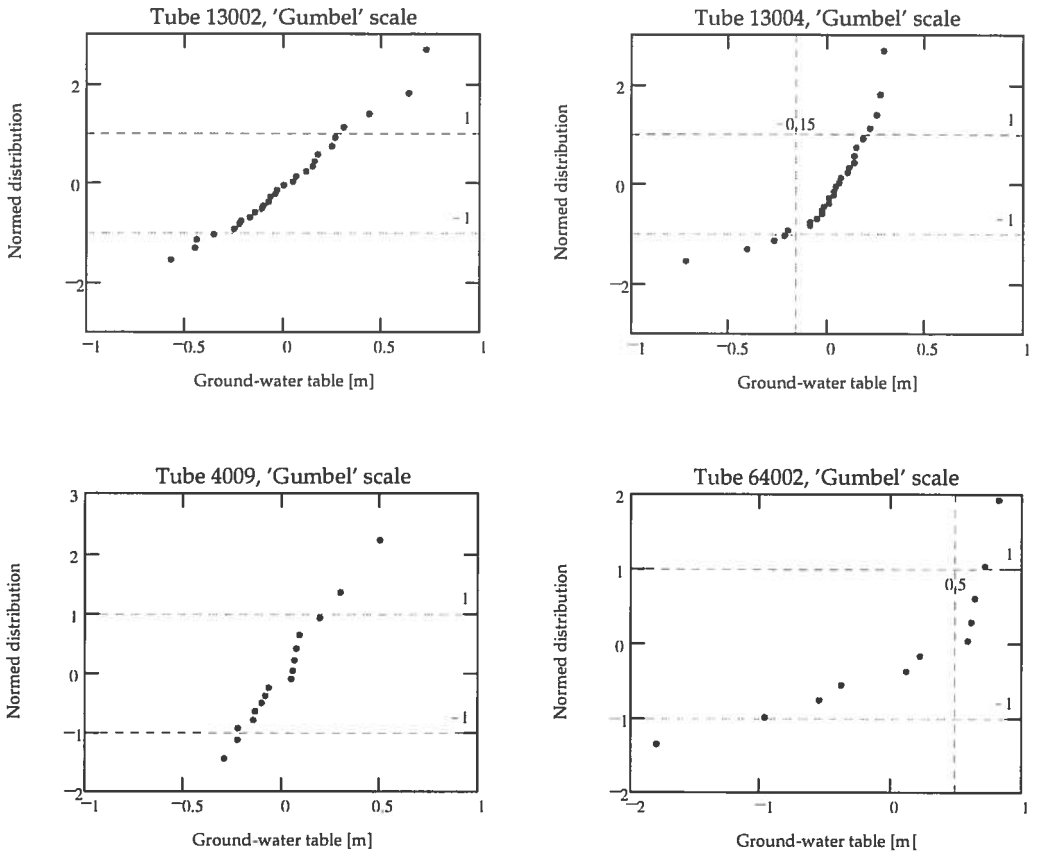

Figure 3.22 Observations of ground-water table. Annual maxima. Probability scale on y-axis, $F^{-1}_{Gu,normed}(p)$.

To examine the influence on a design value of the pore pressure, the '100-years' water table was evaluated 'graphically'[1] from the plots given previously. The results are given in Figure 3.23 - Figure 3.26. For the symmetric series and the series with positive skewness an assumption of a Gumbel distribution resulted in a somewhat higher water table, about 0,25 m. The two test series with negative skewness were evaluated for the two different assumptions, a linear regression for all observations and a truncation by a 'threshold'. As could be expected by the outlook of the plots, the two different assumptions give very different results. For the series with the highest skewness, Figure 3.26, an analysis without respect to the threshold will be completely misleading. Apart from the fact that the design value is reduced by the threshold model, the choice of distribution also becomes less important.

[1] The intersection between a linear regression of the observations and the 'normed' value of the given distribution corresponding to p=99%, the horizontal line in the figures .

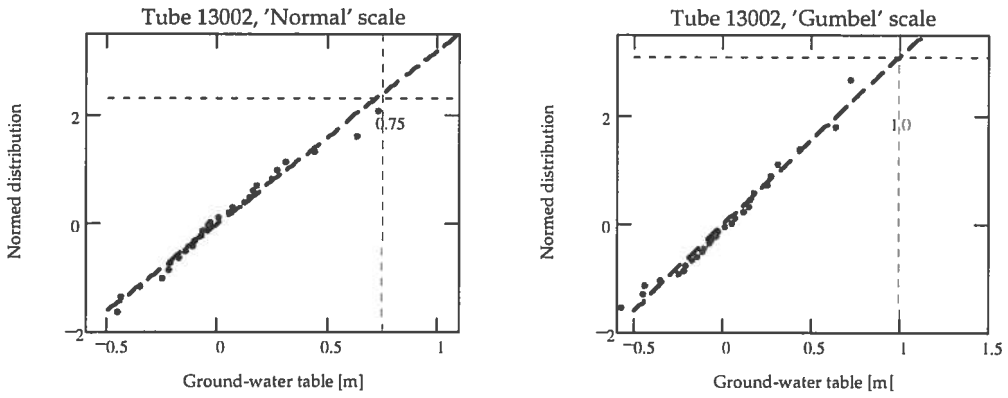

Figure 3.23 Evaluation of the '100-years' ground water table. Symmetric observations. Probability scale on y-axis.

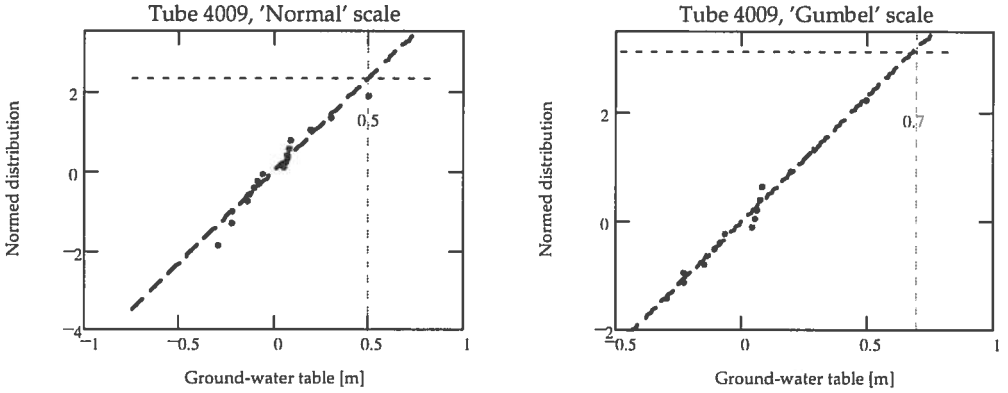

Figure 3.24 Evaluation of the '100-years' ground water table. Positively skewed observations. Probability scale on y-axis.

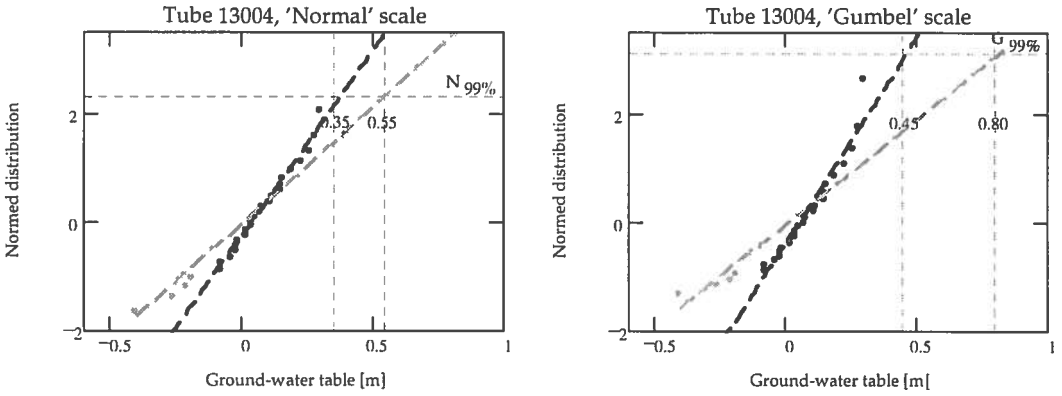

Figure 3.25 Evaluation of the '100-years' ground water table. Negatively skewed observations. Probability scale on y-axis.*
– – – – linear regression for all observations > 0,15 m
– – – – " " " " " .

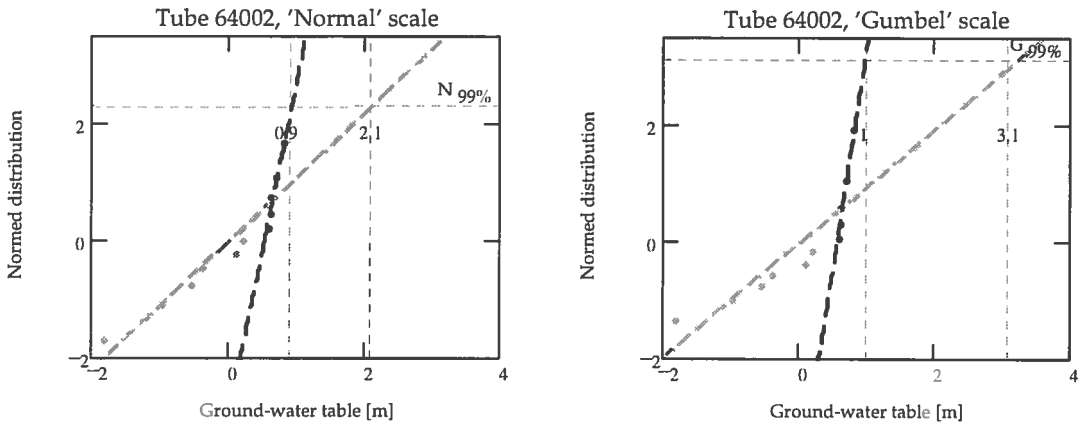

Figure 3.26 Evaluation of the '100-years' ground water table. Negatively skewed observations. Probability scale on y-axis.
– – – – linear regression for all observations > 0,5 m
– – – – " " " " "

Svenson & Sällfors (1982) have made an evaluation of the 'best' choice of distribution for extreme values of the ground water table. Their analysis included some of the observations discussed above. They arrived at that time to the conclusion that a normal distribution showed the best fit to their observed data. This is contradictory to the plot in Figure 3.21. One has to point out that only five of the 39 test series shown in the figure were included in the investigation by Svensson & Sällfors. Further, the test series were short, about 20 years, why it is doubtful whether it is possible to draw any definitive conclusions about the type of distribution.

It has to be remarked that the examples of application, from a statistical point of view, are 'crude'. In principle, a normal distribution or a Gumbel distribution, which have no lower bound, should not be applied in threshold model. A simple alternative would have been an exponential distribution, which has a 'distinc't lower bound, see Figure 2.11. Furhter, the 'curved shape' of the observations from some the ground-water holes had probably be better described with a generalised extreme value distribution, These are defined by an extra parameter compared with the special case, the Gumbel distribution (Rootzén, 1995). However, such an analysis goes beyond the scope in this thesis.

3.4.3 Shear strength

Drained shear stress

In drained analysis the description of the shear strength is normally given by some failure criterion based upon soil parameters. For practical purposes the Mohr-Coloumb criterion is mostly sufficient:

$$c = c' + \sigma' \cdot \tan(\phi) \tag{3.36}$$

The soil parameters, the cohesion intercept c' and the angle of internal friction ϕ, interpreted from for example triaxial tests, are in principle negatively correlated, see Figure 3.27. Thus if the shear strength is described as a function of random variables by equation 3.36, besides the cohesion, c', and the friction, $\tan(\phi)$, the correlation between these two parameters has to be established.

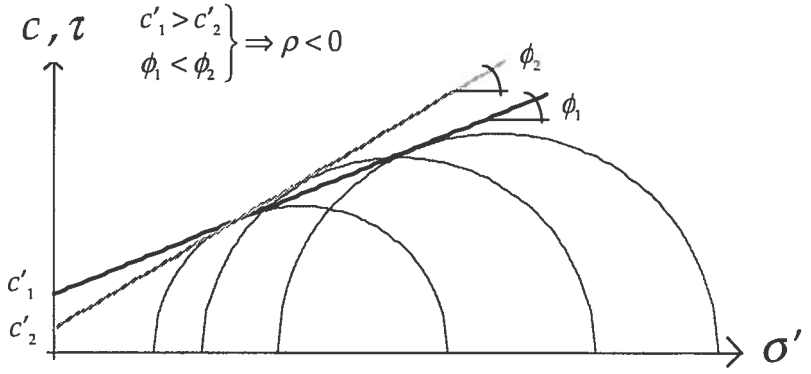

Figure 3.27 Interpretation of c' and ϕ from triaxial tests.

The situation illustrated in Figure 3.27 implies a rather large task in a probabilistic approach. However, from a practical point of view, the two soil parameters can be regarded just as fictive tools to describe the shear strength at a certain stress level of interest[1], i.e. in a certain stress range. Thus, any combination of c', $\tan(\phi)$ and the correlation between them that results in an appropriate shear strength is sufficient. In Figure 3.28 two examples of different sets of parameters, which both result in an almost identical drained shear strength, are given. The dashed line in the left plot shows the mean

[1] The common discussion in geotechnics, whether the cohesion intercept is a real or fictitious property of the soil, then also becomes insignificant.

value, while the outer graphs in the same plot show the mean value plus/minus one standard deviation.

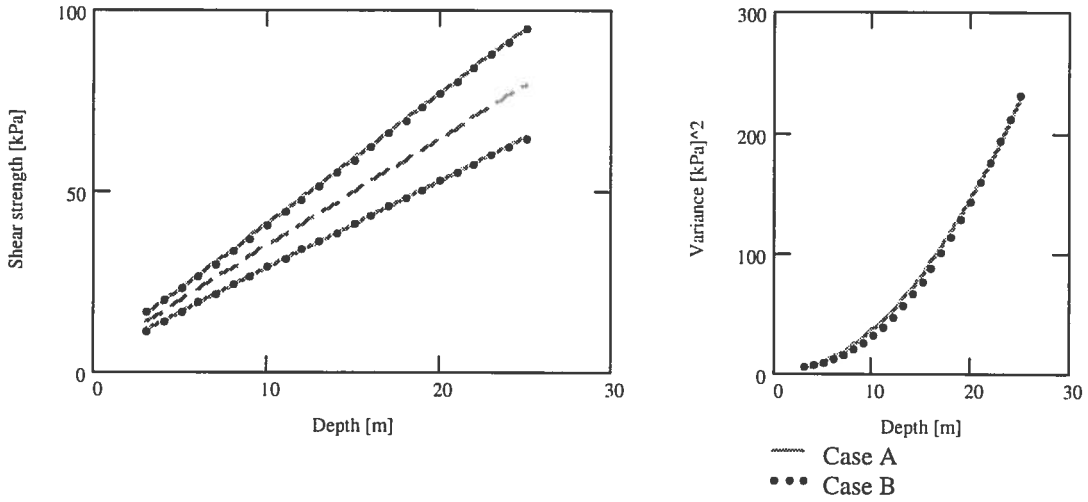

Figure 3.28 Drained shear strength given by equation 3.36.
$\mu_{c'}$=5kPa; μ_{tan}=0,5; $\Delta\sigma'$=6kPa/m^2·z; Case A: $\sigma_{c'}$=1kPa; σ_{tan}=0,10; ρ=0
Case B: $\sigma_{c'}$=3kPa; σ_{tan}=0,11; ρ=-0,5

Thus it is the line, given by equation 3.36, which is the uncertain object and not the two individual soil parameters. An interesting approach in this context is to describe the cohesion by the attraction parameter, *a* (see e.g. Janbu, 1989)[1], i.e the cohesion seen as pre-stressing and not as adhesion between the clay aggregates. Equation 3.36 then becomes:

$$c = (a + \sigma') \cdot \tan(\phi) \qquad (3.36a)$$

The formulation entails the shear strength to be described in a realistic way as a function of only one random variable, $\tan(\phi)$. The example shown in Figure 3.28 is compared to such a case in Figure 3.29.

[1] This is a very interesting approach inmany respects, but these are beyond the scope of this thesis.

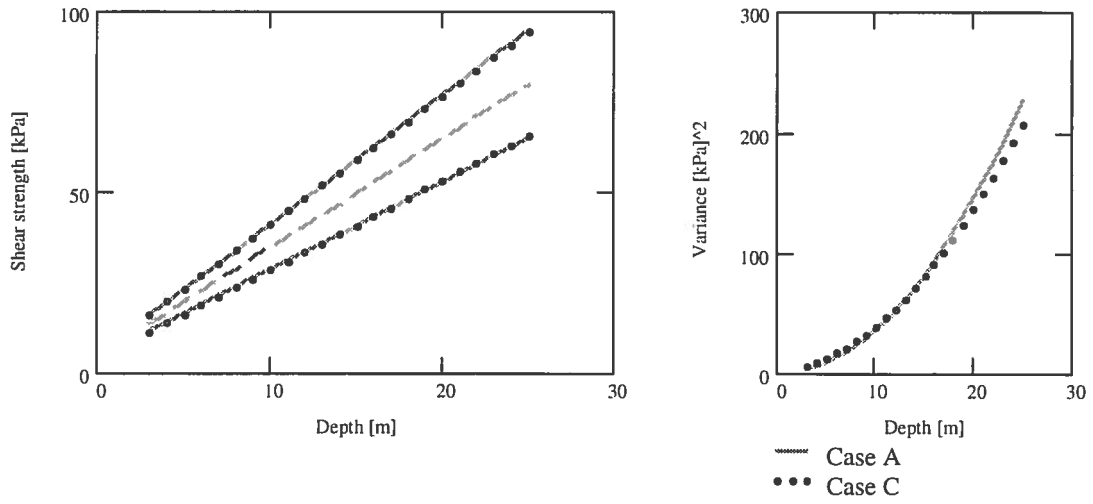

Figure 3.29 Drained shear strength with depth. Case A, see Figure 3.28. Case C is given by equation 3.36a: a=10kPa (fixed); σ_{tan}=0,09.

Undrained shear stress

While effective stresses are used for drained analysis, undrained analysis is mostly combined with total stresses. However, the physical failure mechanism in the soil ought to be the same, independent of the analysis method. This means, in principle, that the undrained shear strength ought to be possible to be described in the same way as the drained shear strength, i.e by equation 3.36, which can be rewritten as:

$$c = c' + (\sigma - u) \cdot \tan(\phi) \qquad (3.36b)$$

In Figure 3.30 the two different methods of analysis are summarised:

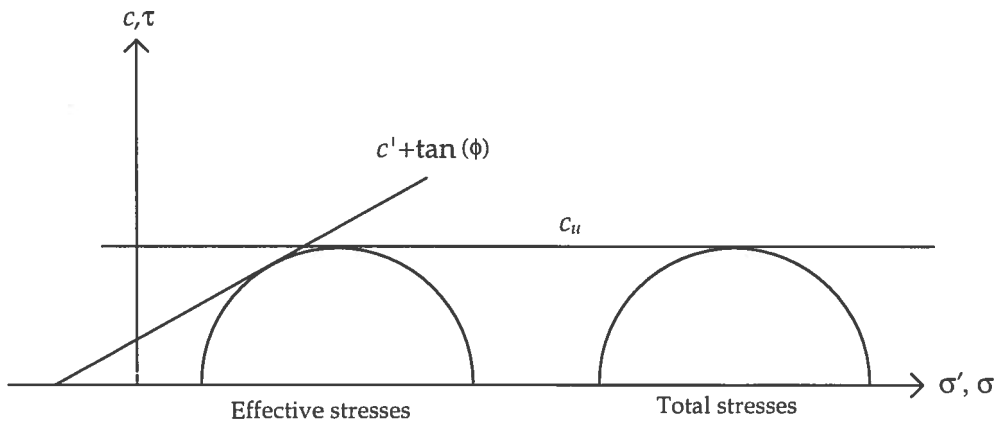

Figure 3.30 Comparison of the shear strength as a function of effective stresses or total stresses.

The left hand circle in the figure is Mohr´s stress circle for effective stresses while the right hand circle is Mohr´s stress circle for total stresses. From the figure the pore pressure at failure can be deducted, i.e. the horizontal distance between the two circles, which, with the assumption $\sin(\phi) = 0{,}5$, becomes:

$$u = \frac{c'}{\tan(\phi)} + \frac{3 \cdot \sigma_3 - \sigma_1}{2} \tag{3.37}$$

However, this pore pressure can not be taken as a critical pore pressure to be measured in the soil. The pore pressure in a failure zone is to a high degree induced by shearing, i.e. the shear deformation causes a volumetric change and thus a corresponding rapid change of the local pore pressure. If the soil contracts at failure[1], the pore pressure will increase rapidly close to the failure surface. Thus equation 3.37 gives the sum of the initial pore pressure, u_0, governed by the overall ground water situation and the local, shear induced pore pressure, Δu. The latter part of the pore pressure will, in accordance with equation 3.37, be:

$$\Delta u = \frac{c'}{\tan(\phi)} + \frac{3 \cdot \sigma'_3 - \sigma'_1}{2} \tag{3.38}$$

The principal effective stresses in equation 3.38 are the stresses in the soil, before any increase of the shear strains preceding the failure, i.e. for a stress circle between the two circles shown in Figure 3.30. The magnitude of the second term in equation 3.38 is difficult to determine as it is formed as the difference of two uncertain terms of the same magnitude. Thus, the equation should merely be seen as an illustration of the failure mechanism. In practice, the pore pressure caused by the shear strain is complicated to determine. Thus, the undrained shear strength mostly has to be seen as a compound value of the three parameters c' (or a), $\tan(\phi)$ and Δu, of which the first two are strength parameters, while the last one to a large extent is governed by deformation properties. Hence, in undrained analysis the shear strength is normally determined as a nominal value[2] from field or laboratory tests, e.g. by field vane or fall cone respectively. This means that the shear strength is deter-

[1] Even a dilatant soil contracts at failure if the shear stresses decrease.
[2] Often increasing with depth.

mined as the actual shear stress at failure in the test sample. In a similar manner as the drained shear strength could be described as a 'random object', the failure line defined by equation 3.36, the undrained shear strength can be given as a 'random object', i.e. a function, which describes the shear strength versus depth. For example, in section 3.2.2 the undrained shear strength was given by a bi-linear model, see page 69. In a later example, section 3.3.4, the same shear strength was modelled as a single trend line.

3.5 Simplified application in deterministic analysis

3.5.1 General

The interpretation of test results has as its main aim to determine suitable values for practical design. If the design is done with probabilistic methods, one tries to determine reasonable values of actual parameters of the distributions at hand. However, in normal practice the design is done with deterministic methods, e.g. the partial factor format. This demands that one can give characteristic values of the properties concerned, see section 2.3.3.

In the preparation of the European geotechnical code, EC 7 (ENV 1997-1, 1994), much of the discussion has concerned how to define the characteristic value. The final result of this discussion has been a vague description, "cautious estimate". In the Swedish national application document it has been specified how this shall be done in the form of an estimated value, see (Alén et al., 1993a &1993b, or Alén, 1995). The aim is to assess an interval, containing the mean value. In the determination of the interval, the scatter of the test results, the number of tests and any systematical errors in the test method have to be considered. Pre-knowledge might also be accounted for. If a low respectively a high value is governing a problem, the lower bound respectively the upper bound of the interval is equal to the characteristic value. As a summary, in a probabilistic language, the characteristic value has to be seen as the population mean instead of the sample mean. In a more extensive investigation it is possible to estimate the mean value purely from the test results, but normally the scatter of results forces one to consider the uncertainty of the tests. If the uncertainty of the characteristic value is low, i.e. the expected interval is very narrow, the interval can be replaced with its middle value.

3.5.2 Application

In the documentation of the proposed principles in the Swedish national document, an example is given as an illustration, see appendix H. The example refers to evaluation of the undrained shear strength for the test field in Nödinge, which has been analysed with geostatistical methods in section 3.2.2/appendix F and Bayesian statistics in section 3.3.4. The different types of uncertainty, discussed in section 3.1.1, are treated as follow:

- *Natural variation* - The geostatistical analysis, see appendix F, shows that the autocorrelation distance is very small with a detailed description of the increase of shear strength by depth. Thus the variation can be neglected in practical design. Only the uncertainty in the mean value has to be considered. This can be done by assuming regression lines for the shear strength for each bore hole and treating these lines as uncertain objects[1], instead of the single values from each test level.

- *Systematic errors in testing*. Field vane tests are normally considered as reliable if properly performed. However, the observed values have to be adjusted (cf. prENV 1997-3). Reduction in this case has been made with respect to the liquid limit according to recommendation by SGI (Larsson et al., 1984)[2].

- *Random errors in testing* - The procedure by treating the regression lines as uncertain objects (and not the single test values) eliminates, or at least reduces, this type of errors considerably.

- *Few sample testing* - Test results from 8 bore holes exist. The discrepancy between these have been considered by a simple formula for the characteristic value:

$$c_{u,char} = \bar{c}_u \left(1 - \frac{V}{\sqrt{n}}\right) \tag{3.39}$$

[1] The slope and the intercept of the regression lines are regarded as random variables.

[2] The reduction is based upon back calculations of failures of slopes, why the reduction incorporates any errors that arise from the calculation model. Thus, the reduction might be too large in an analysis in which the model uncertainty is accounted for explicitly.

In the formula, $\bar{c}_u$ is the mean value of the test results. V is a prescribed value of the coefficient of variation (15%) and n the number of tests (bore holes). The equation is a compromise between a complete statistical analysis and a pragmatic approach. It expresses the idea that the mean value can be obtained from a small sample/a specific project, while the scatter, at its best, can be interpreted from large samples/experience from many projects, i.e. pre-knowledge. The given characteristic value corresponds approximately to the lower bound of a 70% confidence interval for the mean value, if the coefficient of variation is known.

4 SLOPE STABILITY

4.1 Introduction

In traditional slope stability analyses, a soil body of a slope is analysed for a sliding motion along a slip surface. The most common assumption is a rotation for a slip circle, but other composite slip surfaces as well as translational motions can be considered. Long slip surfaces are often assumed to be plane and the motion a translation along the slope. The analysis is normally divided into two different calculation principles:

- Drained analysis
- Undrained analysis

The first principle is correct in those cases with full consolidation, while the latter describes a situation when no consolidation takes place before failure. This means that the two different principles describe two extreme cases. It is natural to treat undrained analysis as a short term case using a total stress concept and drained analysis as a long term case using effective stresses, cf. section 3.4.3. Nevertheless, the two principles are commonly used for situations between those two extremes. The results and interpretations of an analysis in such a case has to be considered as purely empirical. However, as the normal situation is complex a correct interpretation is not obvious. For example, in many cases a back analysis of a failure indicates an undrained failure, despite the fact that there is no evidence of any immediately preceding triggering mechanism. In such cases, it seems likely that a drained failure, in some part of a slope, releases the rest of the slope, i.e. the shear deformations induce excessive pore-pressure in nearby parts and thus there is a risk of undrained failure. As a more stringent way to describe this situation, a concept referred to as

- Combined analysis

has been suggested, among others, by Sällfors & Larsson (1984). This is, as the name indicates, a combination of the two principles mentioned above. In the analysis the slip surface is subdivided into a number of parts and the lowest value of the undrained or the drained shear strength is used for each part of the slip surface. Thus,

the analysis is a mixture of full and no consolidation. The combined analysis is in principle an effective stress analysis, although the undrained shear strength is given as a nominal value, since the shear induced pore pressure, cf. section 3.4.3 'Undrained shear stress', is unknown, or at least difficult to prescribe, at the slip surface. Though a concept which involves partial drainage had been principally more correct, the combined analysis is a simple and practical way to describe a situation with diverging drainage and consolidation situations in different parts of a slope.

An alternative way to interpret the concept combined analysis is to compare it with the critical state concept (see e.g. Wood, 1990). In Figure 4.1 the flow rule given by the Cam clay model[1] is compared with a compound flow rule given by Mohr Coulomb, the undrained shear strength and the preconsolidation pressure in the principal planes, (Larsson & Sällfors, 1981). The Cam clay rule, which is an ellipse in the [*p*;*q*] plane, is in Figure 4.1 transformed to the $\left[(\sigma_1' + \sigma_3')/2;(\sigma_1' - \sigma_3')/2\right]$ plane. The [*p*;*q*] plot then becomes a [*p*+*q*/6; *q*/2] plot[2], if $\sigma_2' = \sigma_3'$.

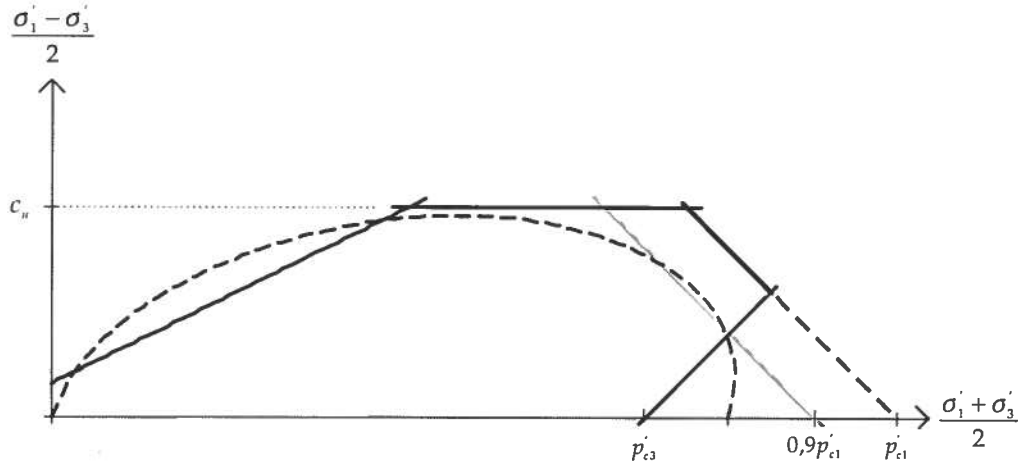

Figure 4.1 Comparison between two different flow rules.
- - - Modified Cam Clay —— Larsson & Sällfors, 1981

[1] Former Modified Cam Clay

[2]

$$q = \sigma_1' - \sigma_3';\quad \sigma_1' = q + \sigma_3';\quad p = \frac{\sigma_1' + \sigma_2' + \sigma_3'}{3} = \frac{q + 3\cdot\sigma_3'}{3};\quad \sigma_3' = p - \frac{q}{3},\quad \sigma_1' = q + p - \frac{q}{3} = p + \frac{2\cdot q}{3};$$

$$\frac{\sigma_1' + \sigma_3'}{2} = \frac{\left[p + \frac{2\cdot q}{3}\right] + \left(p - \frac{q}{3}\right)}{2} = p + \frac{q}{6};\qquad \frac{\sigma_1' - \sigma_3'}{2} = \frac{\left(p + \frac{2\cdot q}{3}\right) - \left(p - \frac{q}{3}\right)}{2} = \frac{q}{2}$$

Figure 4.1 is based upon the assumption that the relation between the preconsolidation pressures in the principal planes is $p'_{c2} = p'_{c3} = 0{,}7p'_{c1}$. The undrained shear strength is assumed to be $0{,}25 \cdot p'_{c1}$, cf. section 3.3.4. There is an overall good agreement between the two flow rules, which strengthens the concept of combined analysis as a convenient way to describe the strength of a clay slope. However, one should not apply the concept without consideration. The concept of combined analysis should be restricted to slopes where it is likely that an undrained failure can occur in parts of the slope, i.e. that some triggering factor can cause an sufficiently large increased pore pressure. If no such triggering factor is at hand the concept might be too conservative.

4.2 Concept of safety

4.2.1 Factor of safety

There is a strong tradition to use the global factor of safety, cf. 2.2.1, to establish the safety of a slope. The factor of safety is then normally defined as the ratio between the shear strength and the shear stress:

$$F = \frac{c}{\tau} \tag{4.1}$$

Another analogue concept is the degree of mobilisation defined as the ratio between the shear stress and the shear strength:

$$f = \frac{\tau}{c} = \frac{1}{F} \tag{4.2}$$

4.2.2 Safety margin

General

Both the shear strength and the shear stress vary along a potential slip surface. Accordingly, the factor of safety and the degree of mobilisation vary along the slip surface too. To obtain a unique definition for a given slip surface both the strength and the stress are normally interpreted as average values along the slip surface. Remedial work to increase the safety of a slope gives rise to a problem with the definition of the factor of safety given in the previous section. It is difficult to decide whether the reinforcement

shall be treated as an increase of the shear strength or a decrease of the shear stress[1]. Obviously the value of the factor of safety[2] depends on the interpretation. A way to overcome this problem is to use the safety margin instead, cf. section 2.2.3. The safety margin is, unlike the factor of safety, invariant for different 'natural' formulations of the slope stability. Natural formulations are here restricted to the case when the safety margin is described as a sum of resisting and driving forces or moment alternatively, i.e. is in principle[3]:

$$M = c - \tau \tag{4.3}$$

As discussed in section 2.2.3, the safety margin is the natural safety concept when using partial factors. Reliability analyses are based upon a safety margin G(x), see section 2.4.4. The formulation of the Morgenstern & Price method[4] presented by Li & Lumb (1987), see coming discussion in section 4.4.2 and section 4.6.1, uses the concept of a safety margin. The reason for this is that the safety margin has a more linear formulation, which makes it more convenient in reliability analyses. For the same reason a safety margin is to be preferred in calculation with the point estimate method, see section 2.4.2. Hence there are two main reasons for replacing the traditional factor of safety with the safety margin:

- To use the (global) factor of safety in conjunction with partial factors is, if not impossible, at least very confusing.
- In a probabilistic approach, the safety margin is for computational reasons to be preferred.

[1] Or a combination of both.

[2] Or the degree of mobilisation.

[3] As discussed previously in section 2.4.4, reliability index $\beta_{H\text{-}L}$ there exist an infinite number of ways to describe M so that the condition M>0 corresponds to a safe state and $M< 0$ implies failure, e. g. $\{M^3 \geq 0\} \equiv \{M \geq 0\}$, which all, based upon the same physical assumptions, give the same value of the reliability index, β_{HL}.

[4] Morgenstern & Price (1965)

A dimensionless safety margin

A disadvantage with using the concept of safety margin exists in traditional slope stability calculations. The factor of safety is used to establish the critical slip surface. This is not as easy with the help of the safety margin, which is strongly dependent on the volume involved. A way to overcome this difficulty is to use a dimensionless safety margin. In appendix J a suggestion of such a dimensionless safety margin m is presented:

$$m = \frac{R-S}{R} = \left[\frac{c-\tau}{c}\right] = 1 - f = 1 - 1/F \qquad (4.4)$$

In Figure 4.2 the relationship between the global factor of safety and the dimensionless safety margin is illustrated. In the figure it can be seen that there is a one-to-one relation with the factor of safety [1]. Thus the empirical knowledge from using the factor of safety can be inherited by the proposed safety margin. It can, in the same way as the factor of safety, be used to find the critical slip surface. It might be remarked that the slip surface with the smallest safety margin or the smallest factor of safety must not be the same as the slip surface with the largest probability of failure (Li & Lumb, 1987). The safety margin, given by equation 4.4, takes values between 0% - 100%, which is a convenient property of a safety margin. If R and S (or c and τ) are given by characteristic values, the safety margin can be called the characteristic safety margin, m_k. For a safe state it has to have a value sufficiently larger than zero, similarly as the factor of safety has to be sufficiently larger than unity. If the safety margin is given by the design values of R and S, which is convenient in partial factor design, all values larger or equal to zero denote a safe state.

[1] Or the degree of mobilisation.

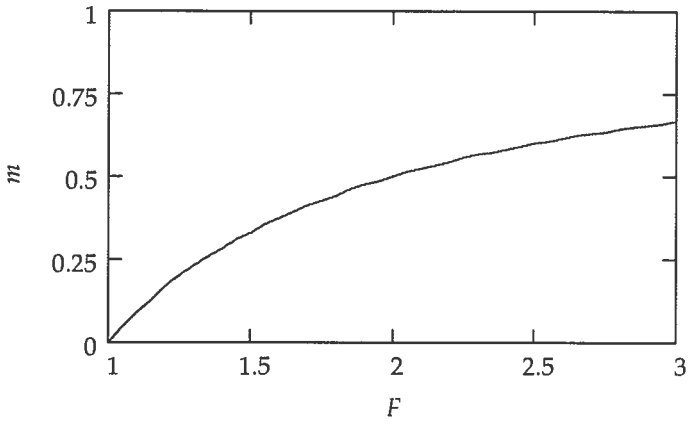

Figure 4.2 Relation between dimensionless safety margin, m and the factor of safety, F.

In a probabilistic calculation the safety margin is a random variable, defined by the two random variables R and S. The purpose of the denominator is to use it as a scaling factor. Hence in a probabilistic approach, when R and S are random variables, the denominator does not need to be a random variable. In the formulation:

$$m = \frac{R - S}{R_{fixed}} \tag{4.5}$$

m is a linear combination of R and S. In this latter case the range, for a safe state, is altered to $0 - R_{sup}/R_{fixed}$. The fixed value of the denominator can with advantage be chosen as the mean value of R.

4.3 Calculation methods

4.3.1 General

Calculation methods in slope stability analysis can be divided into two main classes.

- Methods in which deformations are not (explicitly) considered
- Methods in which deformations are calculated.

The first class can be divided into two sub classes

- Limit equilibrium methods
- Limit analysis

These two latter classes are from a geotechnical point of view very similar. They are both based upon calculations of the safety for assumed slip surfaces and, in principle, only the circumstances at failure are considered. Limit equilibrium methods are by far the most commonly used in daily practice. They are often referred to as traditional methods. Solely based upon equilibrium equations, they should, from a structural mechanical point of view, be restricted to statically determined slip surfaces. As the drained shear strength is dependent on the stress field in the soil, limit equilibrium methods would then only be possible to use in undrained analysis. However, since a long time they have been used also in drained analysis. The problem with statical indeterminacy is in those cases solved by two assumptions.

- A force field is established by intuitive assumptions of the locations and the directions of the forces in the soil.
- The degree of mobilisation of the shear strength is constant along the slip surface.

In limit analyses the statical indeterminacy is also solved by assumptions of the slope behaviour. The assumption of a constant degree of mobilisation is valid for those methods too, but instead of solving the problem with equilibrium equations, internal and external work are set equal for an assumed failure pattern. The assumption of an internal force field is in this case replaced by assumptions about the degree of mobilisation along internal failure surfaces.

Methods in which the deformations are calculated are normally finite element analyses based upon elastic or elastic/plastic behaviour of the soil. With such methods there is a possibility to describe the behaviour of the entire slope in detail, both before and at failure. However, to obtain realistic results the knowledge of input parameters has to be very detailed. Normally there is a poor balance between the refined calculation methods and the accuracy in available soil data. For complex geometry and slopes of compounded material with very different properties, numerical problems often occur at the solution. Finite element methods are yet not so developed and accessible that they are used frequently in practical design. However, the development of finite element programs is very rapid, so their use will probably increase in the future

4.3.2 Drained analysis / Effective stresses

The shear strength is governed by internal friction and cohesion. External actions and the density of the soil determine the stresses and thereby also the internal friction. Thus the shear strength is partly governed by the actions. To be able to calculate the safety of the slope, the force field in the slope has to be known. The traditional method to use is the method of slices. The method was used for the first time for the analysis of a slide in the harbour of Göteborg in 1916 (Pettersson & Hultin, 1955). An assumed sliding body is divided into a number of vertical slices. By applying equilibrium equations for the system of slices, the shear forces for the assumed slip surface can be calculated. The problem is statically indetermined, i.e. there exist an infinite number of sets of interslice forces which fulfil the equilibrium conditions. If the deformation properties of the slices are known, the problem can be analysed with structural mechanical methods, by searching the set of forces which result in corresponding deformations. In traditional slope analysis another way has been chosen. A sufficient number of constraints of the internal forces are asessed, which define the location and the directions of internal forces. The degree of mobilisation is assumed to be constant along the shearing surface. This is in principle an unjustified assumption, but has been shown to give good results, especially for slopes with a regular geometry and homogeneous soil conditions (Janbu, 1989). It corresponds in structural mechanics to a given stiffness distribution throughout the soil. However, it is not trivial to explicitly give the stiffness distribution, which corresponds to a constant degree of mobilisation. Different existing slice methods differ mainly in the way the interslice forces are defined. In no method are the deformation properties accounted for. If both force and moment equilibrium exist for each slice the method is called rigorous, while if only force or moment equilibrium exists for all the slices, the method is named simplified. It is not self-evident that a rigorous method is more accurate than a simplified method. It is only valid if the assumptions of the interslice forces are more realistic for the rigorous method compared to the simplified one (Michalowski, 1995).

As mentioned in the previous paragraph there exist a number of different slice methods. Traditionally they are characterised in two different ways:

A. By the physical approximations. As the problem is statically undetermined, additional assumptions have to be made to obtain an unambiguous solution. Those assumptions concern:

- Location of the resultant of weight of the slices
- Location of the interslice forces
- Inclination of the interslice forces
- Degree of mobilisation for the different slices
- Location of the reaction at the base of the slices

B By the mathematical procedure in which the problem defined by A is solved.

The mathematical procedures are to a high degree characterised by the means, which existed at the time of the presentation of a particular method. Pettersson and Hultin used a graphical solution. Many later methods are characterised by the possibility to solve the problem by slide rule calculations. This has, especially for the rigorous methods, meant that they have had to be solved by an iterative procedure. With today's easy access to computers there is no reason to restrict the solution procedure to the original one proposed by different authors.

4.3.3 Undrained analysis / Total stresses

This situation is in principle very simple to calculate, at least for circular slip surfaces. The undrained shear strength is assumed to be independent of changes of the stresses[1] and the degree of mobilisation is constant. A presumed slip surface will then be statically determinate for rotation. The degree of mobilisation can be calculated by a moment equilibrium equation. For complex geometry and layered soil, the slope can be divided into an arbitrary number of parts. The influence of each part can be calculated separately and the total result summarised. The slope can be divided in different

[1] At least in a short time perspective.

ways, when calculating the influence of action effects and shear resistance respectively. However, normally the same diversion in vertical slices as for drained analysis is chosen, see 4.3.2. This is a necessity if the undrained analysis shall be used as a part of a combined analysis.

4.3.4 In-situ stress state

It is often discussed whether limit equilibrium methods can be used to determine the in-situ stresses in a slope. The analysis with a limit equilibrium method is in principle a pure failure state analysis. For example, 'locked-in' stresses in the slope are insignificant for the solution obtained. One will receive the same result for a natural slope created by river erosion, with high 'locked-in' horizontal stresses as for an embankment with the same geometry and strength properties. This is due to the fact that the analysis is based upon the assumption of an equal degree of mobilisation of the shear strength. In Figure 4.3, triaxial test results for a Norwegian clay is shown. From the figure it can be concluded that the friction is fully mobilised at very small strains, less than 1,5%. This means that the assumption of a constant degree of mobilisation, lower than 100%, implies equal and small strains, which seems to be an unlikely situation, at least as a general case. As an example, for a fill in the passive zone, resulting in a lower degree of mobilisation, the strains in the active zone have to decrease. Hence the result of the analysis is the average stress state along the slip surface, while the distribution of the stresses along the slip surface is not accounted for. Regardless of this statement, comparison between analysis results and field observations show that the limit equilibrium method often, but far from always, can predict the in-situ stresses. For examples, see Ranka (1994) or Cooper (1996).

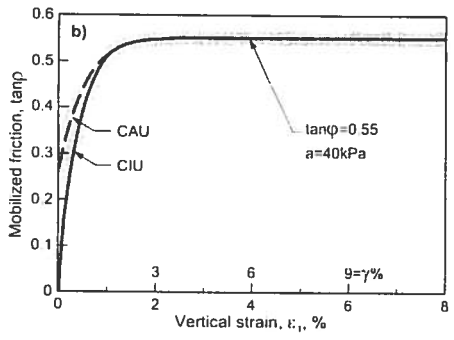

Figure 4.3 Triaxial test results. Mobilised friction as a function of strain. (From Janbu, 1996.)

4.3.5 Progressive failure

A typical stress path from a consolidated, undrained, active triaxial test is given in Figure 4.4.

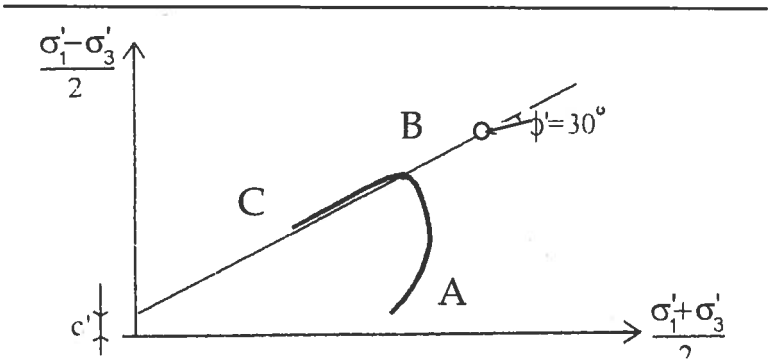

Figure 4.4 Stress paths in a consolidated, undrained triaxial. (From Rankka, 1994.)

In Figure 4.4 three points are marked on the stress path. The corresponding process is graphed in Figure 4.5, which shows the shear stress as a function of the shear. The same points as in Figure 4.4 are marked in this figure too. Between points B and C the deviator stresses follow Mohr-Coloumb's failure criterion. This means that the shear stress decreases between point B and point C. Between points C_0 and C_∞ the test sample will show a continuing compressive strain due to creep, cf. coming discussion of volumetric creep in section 5.4. and appendix P

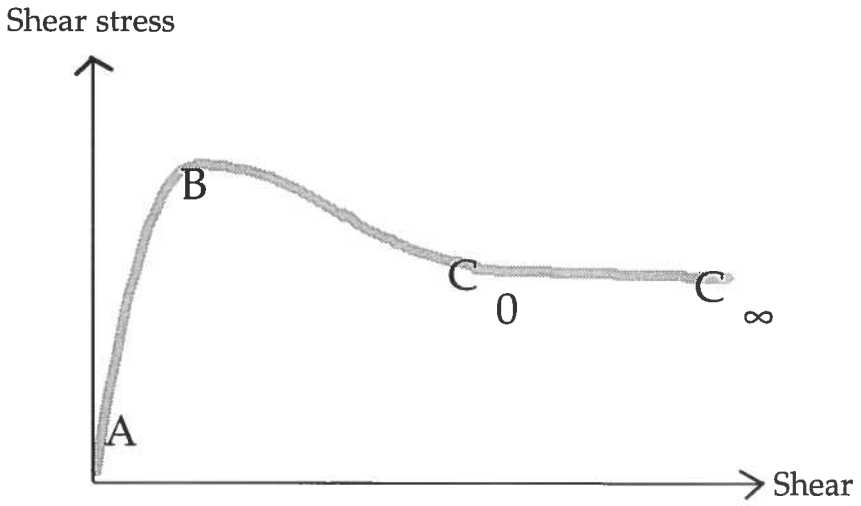

Figure 4.5 The shear stress as a function of the shear.
Interpretation of the triaxial test result in Figure 4.4.

A similar relation as in Figure 4.5 can exist for slope stability failure, which means that the shear strength decreases at continuing shear after it has reached a maximum value. In slope stability calculations normally the peak value of the shear strength is assumed. To obtain correct calculation results the peak strength has to be reached simultaneously in all parts of the slip surface. If this is an unjustified assumption, e.g. for long slip surfaces[1], the traditional way to deal with the shear strength is an assumption on the unsafe side, cf. figure 2.4 in section 2.1.2. The failure is then called a progressive failure. What is said above mainly concerns undrained failure for clay and, to some degree friction material in a dense state. For effective stress analysis in clay the mobilised friction principally follows the Mohr-Coulumb criterion, see Figure 4.4. From the figure can be seen that there is no decrease in the frictional strength, measured as tan(ϕ), for increasing strain, cf. (Janbu, 1996). Thus, as the overall equilibrium has to be maintained, the decrease in shear strength and accordingly shear stresses at failure will be compensated by a redistribution of the stresses.

4.3.6 The shear strength of the soil in slope stability analyses.

In practical application the Mohr-Coloumb criterion is normally assumedd, cf. section 3.4.3:

$$c = c' + (\sigma - u) \cdot \tan(\phi) \tag{4.6}$$

In traditional application the actual stresses, i.e. total stresses and pore pressure, are applied in equation 4.6. In limit equilibrium analysis, this means that the shear stress along a potential slip surface will be:

$$\tau = \frac{c' + (\sigma_N - u) \cdot \tan(\phi)}{F} \tag{4.7}$$

A complication in this approach is that the factor of safety, F, is the unknown variable sought. Hence, F has to be solved by an iterative procedure. If instead the shear strength is defined as the shear stress at failure, which for example is in accordance with the interpretation of the undrained shear strength from testing, cf. section 3.4.3

[1] Long slip surfaces here means slip surfaces which cover a substantially larger area compared to any factor triggering a failure.

'undrained shear stress', this means that the shear stress and the shear strength can be calculated separately. The principle equation corresponding to equation 4.7 becomes in this case:

$$c = \tau_u = c' + (\sigma_{N,ult} - u) \cdot \tan(\phi) \qquad (4.8)$$

in which index *ult* denotes the failure state. Then an iteration procedure as in equation 4.7 is not needed. The calculation will be the same as the first iteration in a traditional analysis with the assumption F=1[1]. In appendix K an example with this approach is shown. The factor of safety is somewhat smaller than a traditionally calculated one. The difference will be in the range 0-10%, with the smallest value for factors of safety close to 1.0. The probability of a factor of safety less than unity will be the same in the two approaches[2]. Thus, the alternative without iteration is more suitable for a probability calculation as it demands less calculation work. It has to be remarked that for the shear stresses given by equation 4.7 and equation 4.8 the inequality $\tau_u \neq F \cdot \tau$ is valid.

4.3.7 Safe or unsafe calculations

Slope stability analyses with limit equilibrium methods are mainly a limit analysis by the upper bound theorem, see *section 2.2*. An overall failure mechanism is assumed. Unlike normal limit analyses, which are solved by energy methods, the factor of safety is calculated with equilibrium equations. However, as the slip surface is statically determined, by given assumptions, the two different calculation principles will render the same results. Thus, as long as the correct critical slip surface is not calculated, the result is an upper bound solution. Yet, in application on a given slip surface, the calculation follows in principle the lower bound theorem. Simplified assumptions about the interslice forces are made and equilibrium equations are put forward. Such an analysis should result in a lower bound solution. However, the complete conditions for a proper lower bound solution are not always fulfilled. The different slices are not in equilibrium from all points of view in simplified methods. The stresses may exceed the strength in some part of the slope. For example tension stresses are often obtained in the upper part of a slope. The shear strength may also be exceeded between some of the

[1] Or a safety margin m=0.

[2] Or the probability of a safety margin less than zero.

slices. The assumption of the shear strength as a peak value makes redistribution of stresses impossible. A conclusion is that it is not a trivial task to determine whether a result of a limit equilibrium method is on the safe side or not. However, comparisons between the results of limit equilibrium methods and limit analysis show that the results normally fall in a narrow band (Michalowski, 1995, and Yu et al., 1998). Furthermore it is also possible to use the principles of the lower and upper bound theorem to judge whether a particular assumption is conservative or not. To ignore the shear stresses between the slices, which is a frequent assumption, is for example an assumption on the safe side according to the lower bound theorem.

4.4 Random models

Application by random models on slope stability analysis can be made by methods of different degrees of accuracy. From the principles discussed in section 2.1.1, a separation of methods can be made in three levels of different complexity.

- Level 1 - The slope stability given by a simple formula.
- Level 2 - The slope stability given by limit equilibrium methods or limit analysis
- Level 3 - The deformation of the soil is considered

4.4.1 Level 1 - The slope stability given by a single formula.

Solutions of systematised slope stability calculations were given by Taylor (1937), results which were presented and further developed by Janbu (1954). The results are published in the form of stability charts. For undrained analysis the factor of safety is given by the formula:

$$F = \frac{N(\theta,d) \cdot c_u}{\gamma \cdot H} \tag{4.9}$$

where N is a dimensionless stability number which depends on θ, the inclination of the slope, and d, the depth of the slip surface given in a dimensionless form. H is the height of the slope, c_u the average undrained shear strength and γ the density of the soil.

Sah et al. (1994) presented a simple formulation of drained analysis based upon calculations with maximum-likelihood estimation for a number of slopes:

$$F = 2.27 \cdot \frac{c \cdot \cos ec(\theta)}{\gamma \cdot H} + 1.54 \cdot (1 - r_u) \cdot \cot(\theta) \cdot \tan(\phi) \quad (4.10)$$

where c is the cohesion, r_u the pore pressure ratio while the other symbols remain the same as in equation 4.9.

For combined analysis a simple formula was calibrated for a maximum slope height of a sub water slope in the Göta river (Alén & Sällfors, 1994):

$$H_{max} = \frac{(\pi / 2 - \theta)^2}{0.65 \cdot \sqrt{F_{comb}} - 0.5} + \frac{1.8}{F_{comb}^{1.5}} \quad (4.11)$$

The formulas above are examples of approaches which are well suited for random modelling. The uncertainty in the calculation model can be treated by a correction factor given as a random variable. The simplified model is balanced by the simplicity in which the uncertainty of the input data and the calculation model can be given.

For formulas like those mentioned above, a calculation by any of the methods presented in section 2.4, the Point Estimate method, Monte Carlo simulation or reliability analysis, can be made. In addition, the probability of failure for equation 4.9 can also be solved analytically, see coming description in section 4.5.1.

4.4.2 Level 2 - The slope stability by traditional limit equilibrium methods or limit analyses

As mentioned in section 4.3.1, most stability calculations are made at this level. In application of random models there is no reason to use more sophisticated methods than in a corresponding deterministic analysis. Li & Lumb (1987) presented an analytical and thus differentiable formulation of Morgenstern & Price´s method. Li (1992) extended this to a unified scheme to solve rigorous slice methods. The scheme means that the safety margin[1] can be described with an unambiguous analytical formulation. Besides this,

[1] Or the degree of mobilisation or the factor of safety.

such a formulation speeds up the traditional calculations and it has the great advantage that existing methods for the determination of the probability of failure can be used. These methods normally demand that the limit state function can be given as an analytical formulation (see section 2.4.4,). Irrespective of what is stated above, the shortcomings of any slice method will remain from the deterministic practice, e.g. the difficulty in finding the critical slip surface and judging the accuracy of the method applied. In section 4.6 a simplified procedure and results of this type of analysis are presented.

Limit analysis by the upper bound theorem can be used as an alternative to limit equilibrium methods in the same manner as in deterministic calculations, see section 4.3.1. From a random calculation point of view, they do not offer any difficulties, nor, however, any substantial advantages compared to limit equilibrium methods. Hence, the judgement, which sort of method to use, remains from the deterministic design situation.

4.4.3 Level 3 - The deformation of the soil is considered

Limit equilibrium methods have their drawbacks. The deformation properties of the soil are not considered. The assumption of an equal degree of mobilisation throughout the potential slip surface means that the actual stress state, in principle, is unknown. For combined analysis for example, see section 4.1, the choice between drained and undrained shear strength, in different parts of the slope, is then somewhat arbitrary. Another disadvantage is that progressive failure is not addressed. For this type of analysis primarily finite element methods exist. Such types of calculations are used to give a comprehensive description of the behaviour of the slope at different stages up to failure. However, slope stability analysis is typically an ultimate limit analysis. The behaviour before failure is from this point of view of minor concern. Accordingly a finite element analysis might be an unnecessarily ambitious tool for the purpose. Furthermore, finite element calculations normally demand a sophisticated description of input data, which rarely is available in normal practice. Moreover, a random finite element analysis will necessarily be very complex. To simplify the problem a discrete element model can be used. In this context such a model can be described as a simplified finite element model with a limited number

of simple elements. The purpose is not to fully describe the behaviour of the soil in the slope from all respects. The elements should instead be regarded as fictitious elements, which in a relevant way describes important aspects of the soil behaviour in the failure state. Chang (1992) presented a model in which he describes a slope as a system of masses and springs. Another alternative is to use traditional beam elements. In this way existing and well established methods from structural mechanics can be used. Such a model in which the slope is modelled as a system of shear beams is presented in (Alén, 1996b). In Figure 4.6, the modelling of the slope is illustrated.

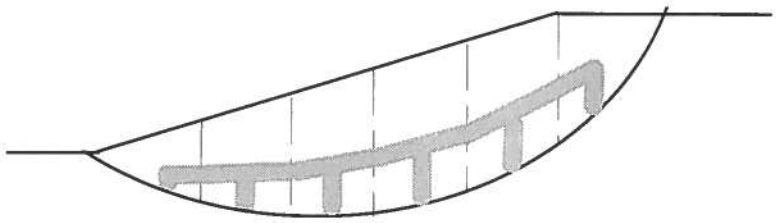

Figure 4.6 A proposal for a slope model of linked shear beams.

By dividing the slope in 'slices' a calculation is obtained, which connects to traditional methods. By the proposed model, progressive failure can be taken into account. Depending on the constraints in the joints, different levels of complexity in the force field can be simulated. The soil properties are given by fictitious properties of the beams. In the random analysis, methods developed for structural mechanics can be used. In section 4.6.2 such a model is illustrated.

4.4.4 Improvement of slope stability

The result of a stability analysis might lead to a situation in which the calculated stability of a slope is considered insufficient. However, despite the low calculated safety, a natural slope can have proved to be stable for a very long time. If such a slope is compared with for example an embankment with the same geometry and the same estimated soil properties, i.e. the same calculated safety, it seems natural to regard the natural slope as more safe compared to the embankment. The question is then how to incorporate this

knowledge in the analysis. In section 3.1.4 it was discussed how control can be incorporated into a probabilistic analysis by truncation of probabilistic distributions. The observed fact that a slope has been stable for a long time can be regarded as an ultimate control of the slope. A pragmatic way to distinguish the two situations described above is to apply truncated distributions in the calculation of the safety margin for the natural slope. In the case described above, i.e. the calculated safety is insufficient, the result can be a decision to improve the stability of the slope. With the approach of truncations proposed above, the improved natural slope will have a larger reliability index than the corresponding embankment, or in more general terms: A slope with a long history has a larger safety than a new slope if the slopes in all other respects are equivalent. It does not exclude the possibility that the 'old' slope can be on the edge of instability, i.e. a minor disturbance can trigger a failure.

In Table 4.1 the results of a stability analysis of a 'proved stable' slope are given. The table shows the reliability index for an improved slope. The results are based upon the assumption that the safety margin for the unimproved slope is a distribution $PD(m_0;0{,}15)$ and for the improved slope $PD(m_1;0{,}18)$, i.e. an improvement with a distribution $PD(m_1 - m_0;0{,}1)$. Table 4.2 shows the corresponding results for an 'unproved stable' slope, i.e. a slope with a safety margin after improvement $N(m_1;0{,}18)$. In appendix L the theoretical considerations of the calculations are described.

$m_0\downarrow\backslash m_1\rightarrow$	0	0,1	0,2	0,3
0	0,9	1,6	2,4	3,1
0,1	---	1,1	1,8	2,5
0,2	---	---	1,4	2,0
0,3	---	---	---	1,8

Table 4.1 Reliability index β for a 'proved stable' slope after improvement. σ_{m0}=0,15; σ_{m1}=0,18

m_1	0	0,1	0,2	0,3
β	0	0,6	1,1	1,7

Table 4.2 Reliability index β for an 'unproved stable' slope after improvement. σ_{m0}=0,15; σ_{m1}=0,18

A Monte Carlo simulation of the safety margin for the two cases described above is shown in Figure 4.7.

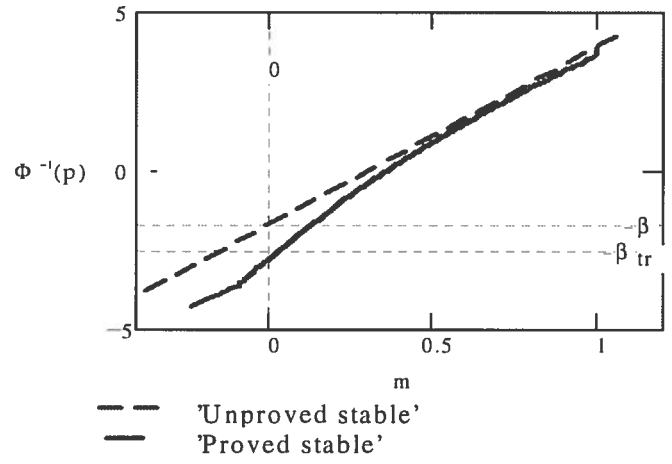

Figure 4.7 Simulation of safety margin of improved slope. $m_1 = 0{,}3 ; m_0 = 0{,}1$

The proposed procedure makes it possible to interpret long time of slope stability systematically in slope stability analysis. An inspection of the special case, a slope with low safety , m=0, shows that the formal probability of failure[1] for a 'proved stable' slope will decrease from 50% to 20% compared with an 'unproved stable' slope, even without any improvement. For the other extreme case of no improvement, i.e. m_0=m_1=0,3, the differences between the formal probabilities of failure are much smaller, 5% and 4% between the slopes, respectively.

4.5 Application of a level 1 method

4.5.1 Theory

The traditional way to describe the safety level in a slope is with the global factor of safety, F. If this concept is used in a probabilistic approach, the probability of failure is then obtained as the probability of F being less than unity, p(F<1).

The factor of safety for undrained analysis and circular slip surfaces can be expressed as in equation 4.9:

$$F = \frac{N \cdot \overline{c_u}}{\gamma \cdot H} = \frac{N \cdot \overline{c_u}}{P_d} \qquad (4.9a)$$

The notation $\overline{c_u}$ for the undrained shear strength is here used to underline that it is the average undrained shear strength along the slip

[1] $p = \Phi(-\beta)$, see section 2.4.4

circle which has to be applied in the formula. P_d is a general notation for the denominator. In the case with external water pressure at the toe of the slope, the formula can be expressed as[1]:

$$F = \frac{N \cdot \overline{c_u}}{\gamma \cdot H - \gamma_w \cdot D_w} \tag{4.9b}$$

Here γ_w is the density of the water and D_w is the water depth. If the factors in equation 4.9 are treated as independent, lognormal random variables, ln(*F*) becomes a sum of normal random variables:

$$\ln(F) = \ln(N) + \ln(c_u) - \ln(P_d) \tag{4.12}$$

With the notation N(μ;σ) for the normal distribution, equation 4.12 becomes:

$$\ln(F) = N(\mu_{\ln F}; \sigma_{\ln F}) \tag{4.12a}$$

with $\mu_{\ln F} = \mu_{\ln N} + \mu_{\ln c_u} - \mu_{\ln P_d}$ and $\sigma_{\ln(F)} = \sqrt{\sigma^2_{\ln(N_0)} + \sigma^2_{\ln(c_u)} + \sigma^2_{\ln(P_d)}}$.

If the coefficient of variations for the right hand side variables is small, say less than 25-30%, the formulation of the parameters can be simplified to, cf. appendix A

$\mu_{\ln F} \approx \ln(\mu_N) + \ln(\mu_{c_u}) - \ln(\mu_{P_d})$ and $\sigma_{\ln F} \approx \sqrt{V^2_{N_0} + V^2_{c_u} + V^2_{P_d}}$,.

The probability of slope failure is then easily obtained as $p(\ln(F) < 0) \equiv p(F < 1)$, which means that ln(*F*) can be used as the safety margin. This formulation of the safety margin is closely related to the proposed formulation of a dimensionless safety margin given in section 4.2.2. The latter safety margin can be obtained as a Taylor approximation of m=ln(F) around the value F=1.[2]

[1]The principle formulation of the denominator is often adjusted by division with a factor μ_w , cf. appendix O.

[2] $\frac{d\ln(F)}{dF} = \frac{1}{F} \Rightarrow \ln(F) \approx \ln(1) + \frac{1}{F} \cdot (F-1) = 1 - \frac{1}{F}$, which corresponds to the definition of m proposed, see equation 4.4.

The reliability index β can easily be obtained as the safety margin for the normal distribution $m=\ln(F)$, see equation 2.15:

$$\beta = \frac{\mu_{\ln F}}{\sigma_{\ln F}} \tag{4.13}$$

An example of application of the outlined procedure is given in the following section.

4.5.2 Example

Site description

A number of information sites were to be constructed at the approaches to Göteborg, in connection with the World Championships in Athletics, Göteborg 1995. One of them, on the motor-way from Stockholm, was to be constructed 10 km east of Göteborg on the outskirts of a suburban town, Partille. The information site was to be situated at the bank of Säveån, a small secondary river to the Göta River. The banks of the river are known to be very slide active. Traditional limit equilibrium analyses indicated a non-sufficient stability according to the national code from the Swedish Road Administration. Probability analyses were undertaken in order to obtain an exemption from the strict rules of the national code.

Results from probabilistic analyses - Information site at Partille

The information site covers an area of approximately 300 m by 120 m. The geometry of the slope varies rather much over the area, why quite an extensive analysis was necessary. Deterministic and probabilistic analyses were undertaken in eight different sections of the site. The results of the deterministic, undrained analysis, for one of the sections named 600, are shown in the left part of Figure 4.8. In the figure each row in the matrix gives results for slip circles with the same starting point at the crest. For each row, the slip circle with the lowest factor of safety is plotted in the figure. The corresponding value of the factor of safety is shaded in the matrix. In the right part of Figure 4.8, the results of the probabilistic analysis are given. The matrix gives the reliability index for the same slip circles as in the deterministic analysis. The circles drawn and the shaded results are chosen by the same principle as in the deterministic analysis, that is the critical slip circle for each different starting point. A comparison

between the results shows that it is not the same slip circles that are critical in the two different types of analysis.

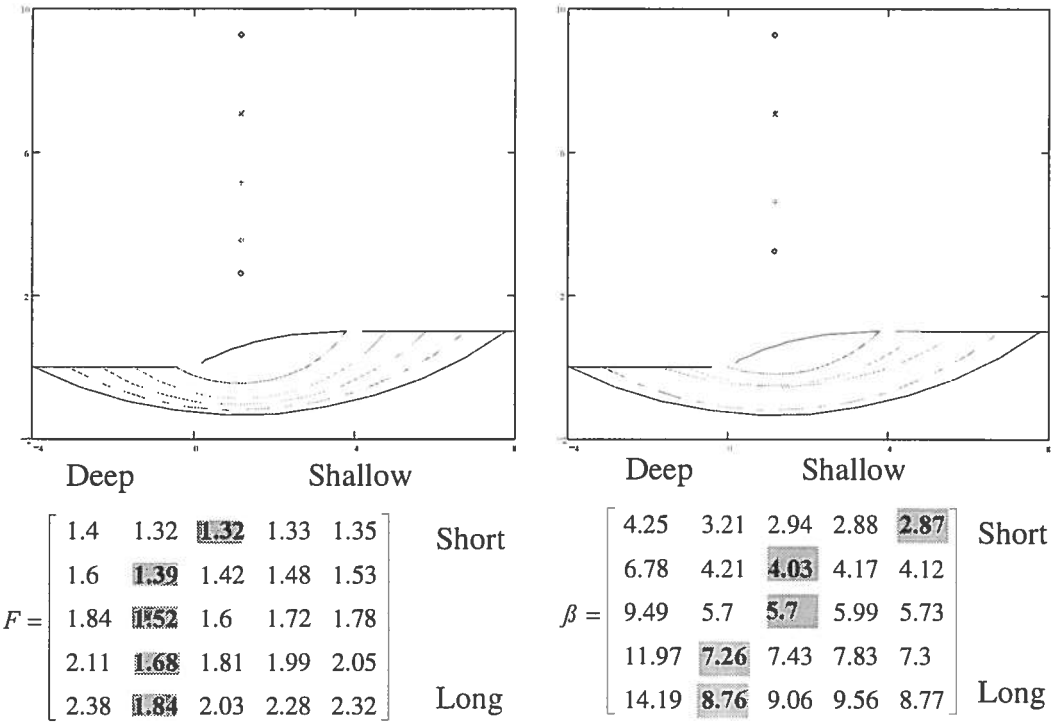

Figure 4.8 Results of undrained analysis, section 600. From (Alén, 1996a)

As can be seen from the results given in Figure 4.8, it is the short slip circles, just reaching the crest, that are critical. The factors of safety are approximately equal regardless of the depth of the slip circles, indicating that there is a fairly large zone, which has about the same degree of mobilisation, while the reliability index increases slightly with depth. The critical slip circle with β=2,9 is a toe circle. As an example of the analysis, a detailed description of the calculations is shown below. The calculations shown are somewhat modified compared to the original analyses presented earlier by the author (Alén, 1996a).

Deterministic analysis

The probabilistic procedure outlined in section 4.5.1 is based upon analyses of slopes with regular geometry. Thus the real surveyed geometry of a section has to be approximated. In appendix M a procedure in which an arbitrary geometry can be approximated to a simple slope geometry, defined as a linear slope with a prescribed horizontal level for both the toe and a the crest level. The procedure results in a slope with the same mass and mass centre as the original

one. In Figure 4.1, the approximation obtained in section 600 is shown.

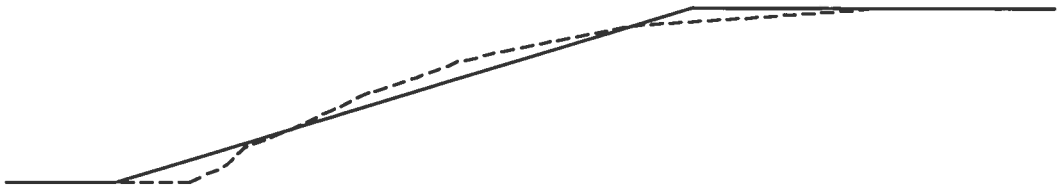

Figure 4.9 Section 600. Analysed geometry compared with 'surveyed'[1] geometry.

The stability number N, in equation 4.9, as well as the location of the critical slip circle, is usually obtained from design charts. To simplify the computational calculations, explicit approximations of the analysis behind the design charts can be derived. In appendix M, such approximations for a slip circle as in Figure 4.10 are given[2], resulting in explicit equations with the following general form:

$$\begin{aligned} x_c &= f_1(b)\cdot H \\ y &= f_2(d,b)\cdot H \\ N &= f_3(y_c,d,b) \end{aligned} \qquad (4.14a\text{-}c)$$

with the relative depth $d = D/H$ and the slope inclination $b = B/H$. The minimum depth $d_{\min}$ can be derived from the equation:

$$R = \sqrt{x_c^2 + y_c^2} = y_c + d_{\min}\cdot H \qquad (4.15)$$

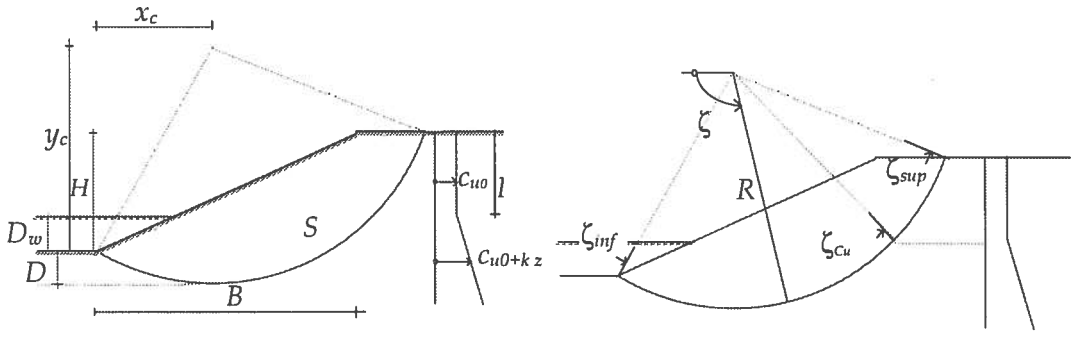

Figure 4.10 Notations used in the analysis of section 600.

[1] The geometry is interpreted from a topographic map.
[2] The approximations in appendix M are restricted to slip circles which pass below or through the toe.

The average shear strength can be written as:

$$\bar{c}_u = \frac{1}{S} \cdot \int_{\varsigma_{inf}}^{\varsigma_{sup}} c_u(\varsigma) R d\varsigma \qquad (4.16)$$

However, in cases where the increase of the shear strength is assumed to be given by the absolute level, the integral given by equation 4.16 can often be simplified to:

$$\bar{c}_u \approx \bar{c}_{u,toe} + k \cdot d \cdot H/\sqrt{2} \qquad (4.17)$$

where $\bar{c}_{u,toe}$ is the estimated average shear strength for a toe circle with depth $d \approx 0$. For the slope at hand, a comparison between an exact integration by equation 4.16 and the approximate formulation by equation 4.17 is given, for different assumed depths of the slip circle, in Figure 4.11.

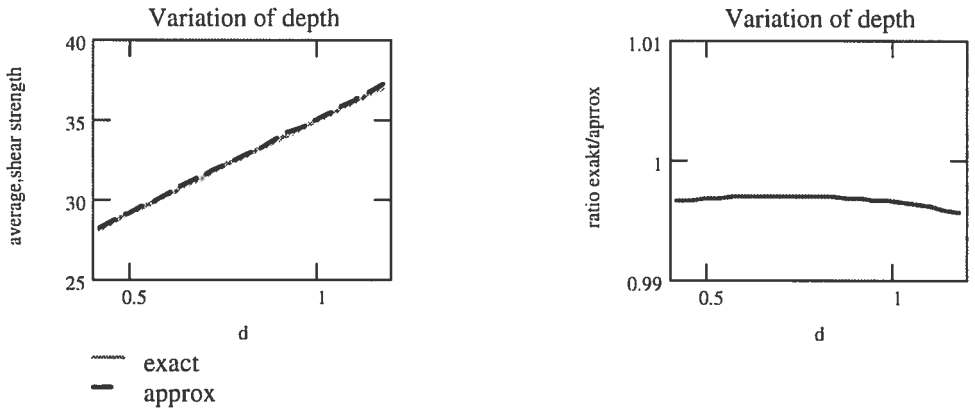

Figure 4.11 Comparison between exact and approximate calculation of average shear strength.

The left plot of Figure 4.11 shows the increase of the average shear strength with the depth of the slip circle. The right plot shows the ratio between the two different formulations. As can be seen from the figure, the approximate formulation is extemely accurate in this case. In Table 4.3, the results of a deterministic calculation and the corresponding input data are given. The results are given as the factor of safety F and the two different concepts of safety margin $m=\ln F$ and $m=1-1/F=1-f$. The table is based upon a relative depth $d_{min}=0{,}42$ obtained from equation 4.15.

Result			Geometry				Soil parameters			
F	m [lnF]	m [1-f]	H [m]	B [m]	D_w [m]	D_{cu} [m]	$c_{u0}k$ [kPa]	k [kPa/m]	γ [kN/m³]	γ_w [kN/m³]
1,39	0,33	0,28	10	31,7	1	6	20	1,65	16	10

Table 4.3 Result of deterministic analysis and corresponding input data.

Reliability analysis

The stability number N, the average shear strength c_u and the unbalanced stresses at the toe plane P_d are regarded as random variables in the reliability analysis. The input data used in the deterministic analysis are taken as mean values. Additionally one has to estimate the corresponding coefficient of variations. The stability number is a function of the slope inclination b, for a given depth d, see Figure 4.12.

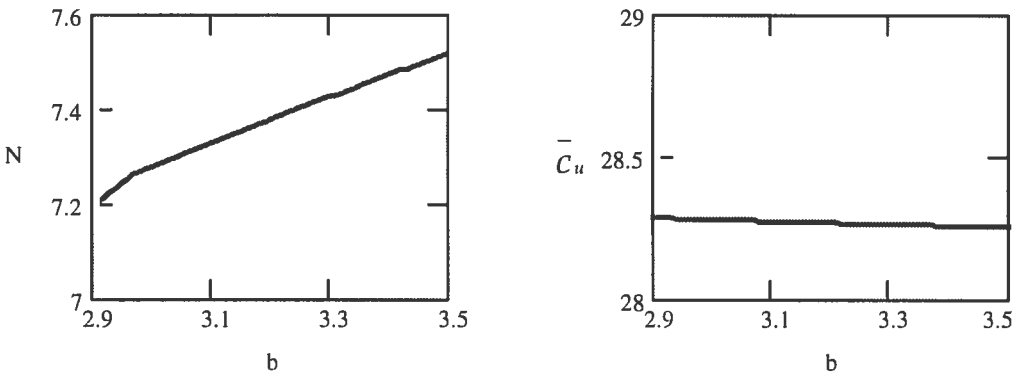

Figure 4.12 section 600. Variation of the stability number N and the average shear strength c_u with the slope inclination b.

From Figure 4.12 it can be seen that he variation of N is close to linear. Thus the coefficient of variation for the stability number can be obtained as:

$$V_N = \frac{N(b+\sigma_b) - N(b-\sigma_b)}{2 \cdot \mu_N} \tag{4.18}$$

In Figure 4.12. the average shear strength as a function of the inclination is also given. The figure shows that the shear strength is practically independent of the inclination.

Figure 4.13 shows the influence on the average shear strength of variations in the slope height. The figure also shows the variation of the average shear strength compared with the variation of the shear

strength c_{u0} in the top layers. There is a slight variation of the shear strength with the assumed slope height. However, the variation is much weaker than the variation with the 'initial' shear strength of the top layers. The grey areas in the right plot in Figure 4.13 illustrates the covariation with height variations, H=8-12m, i.e. equal to the variations in the left plot. In the light of the uncertainty generally associated with the estimation of the variation of c_u , see section 3.3.3 'Interpretation of variation', the influence of variations of the height is small. Hence, in a practical application the average shear strength can be considered independent of H.

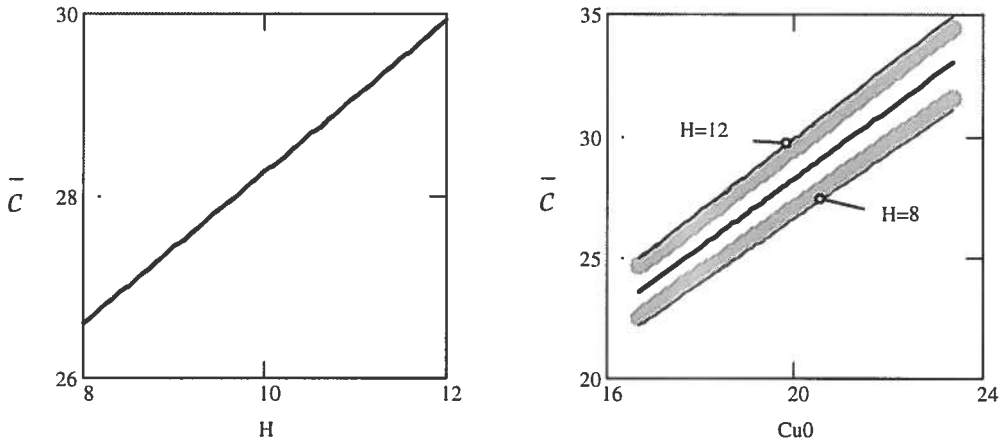

Figure 4.13 Variation of the average shear strength c_u with the slope height H and the 'constant' shear strength in the top layers, respectively.

The denominator of equation 4.9b can be seen as a sum of two independent random variables, γH and $\gamma_w D_w$, of which the first variable itself is a product of two other random variables, while the last one is a product of a constant value, γ_w, and a random variable D_w . The mean value of γH can, with Gaussian approximation, be written as, see appendix A:

$$\mu_{\gamma H} \approx \mu_{\gamma} \cdot \mu_{H} \tag{4.19}$$

and the coefficient of variation as:

$$V_{\gamma H} \approx \sqrt{V_{\gamma}^{2} + V_{H}^{2}} \tag{4.20}$$

Hence the coefficient of variation of P_d becomes:

$$V_{Pd} = \frac{\sqrt{\sigma_{\gamma H}^{\ 2} + \sigma_{\gamma D_w}^{\ 2}}}{\mu_{Pd}} \approx \frac{\sqrt{\left(V_{\gamma H} \cdot \mu_\gamma \cdot \mu_H\right)^2 + \gamma_w \cdot \sigma_{D_w}^{\ 2}}}{\mu_\gamma \cdot \mu_H - \gamma_w \cdot \mu_{D_w}} \qquad (4.21)$$

The safety margin $m=\ln(F)$ can now be calculated according to equation 4.12a and the reliability index β by equation 4.13. Input data are given in Table 4.4, and values derived from the basic data are given in Table 4.5.

	Geometry				Soil parameters			
	H [m]	B [m]	D_w [m]	D_{cu} [m]	c_{u0} [kPa]	k [kPa/m]	γ [kN/m³]	γ_w [kN/m³]
Fixed	-	-	-	6 [1]	-	1,65 [1]	-	10[2]
μ	10	31,7	1	-	20	-	16	
σ	0,5	3	0,5	-	2,5	-	0,5	
V%	5	10	50	-	12,5	-	3	

Table 4.4 Input data for reliability analysis

	N	$\bar{c}$ [kPa]	γH [kN/m³]	P_d [kN/m³]
μ	7,4	28,3	160	150
σ	0,17	2,5	9,4	10,7
V%	2,3	9	5,9	7

Table 4.5 Derived data for reliability analysis

As the so derived safety margin is assumed to be a lognormal distribution, the traditional factor of safety, which obviously is a random variable, can be approximated as, see appendix A:

$$\mu_F \approx \exp(\mu_m) \quad \text{and} \quad \sigma_F \approx \sigma_m \cdot \mu_F \qquad (4.22)$$

As an alternative, the reliability index, based upon the factor of safety, is often derived as[3]:

$$\beta_F = \frac{\mu_F - 1}{\sigma_F} \qquad (4.23)$$

[1] To regard k and D_{cu} as fixed results with a constant standard deviation of the average shear strength, cf. appendix H.

[2] The variation is negligible.

[3] For a discussion of this definition, see summary later in this section.

The results of the reliability analysis are given in Table 4.6

	μ	σ	ß
m	0,33	0,12	2,77
F	1,39	0,16	2,36

Table 4.6 Result of reliability analysis

As can be seen from Table 4.6, the reliability indices, in the two different approaches, differ. This will be discussed below in the 'Summary'. To give the reliability index ß with two decimals is beyond the significance of the analysis, but it is done here to make comparison of the precision with alternative calculations possible.

PEM-method

A PEM-analysis can be performed with the data given in Table 4.5. The table incorporates data for three random variables, i.e. eight numbers of PEM-calculations for the possible combinations of input data μ±σ. The mean value for *m* is obtained as the mean value of the eight calculations

$$\mu_m = E\left[m_{\mu\pm\sigma}\right] \tag{4.24}$$

while the standard deviation is derived with the principle formula:

$$\sigma_m^{\,2} = E\left[m_{\mu\pm\sigma}^{\,2}\right] - E\left[m_{\mu\pm\sigma}\right]^2 \tag{4.25}$$

The index $\mu\pm\sigma$ denotes all possible combinations. The factor of safety can be calculated similarly. The results of the PEM-calculations are given in Table 4.7.

	μ	σ	ß
m	0,33	0,12	2,81
F	1,40	0,16	2,44

Table 4.7 Result of PEM-calculation

Monte Carlo simulation

A Monte Carlo simulation can be undertaken with the same input data as in the previous section. However, the large amount of iterations in a Monte Carlo simulation demands in practice a computer program for the calculations. Hence the calculation can just as well

be based upon the basic data given in Table 4.4. The result of such Monte Carlo simulations, with 1000 iterations each, is given in table Table 4.8.

	μ	σ	ß
m	0,33	0,11	2,92
F	1,41	0,16	2,50

Table 4.8 Result of Monte Carlo simulation

Summary

An inspection of the results in Table 4.6 - Table 4.8 shows that there is very little difference between the results obtained by the different algorithms used. On the other hand, there seems to be a discrepancy between the results obtained from the calculation of a safety margin and the result based upon the factor of safety. However, this is due to the way the reliability index $ß_F$ is defined in equation 4.23. An alternative definition, in agreement with the reliability index $ß_{H\text{-}L}$, see section 2.4.4 , will give another value as shown below. The definitions of the reliability index according to equation 4.13 and equation 4.23 are both based upon the assumption that the corresponding property is normal distributed. The justification for such an assumption can be inspected from the results of the Monte Carlo simulation shown in Figure 4.14 and Figure 4.15.

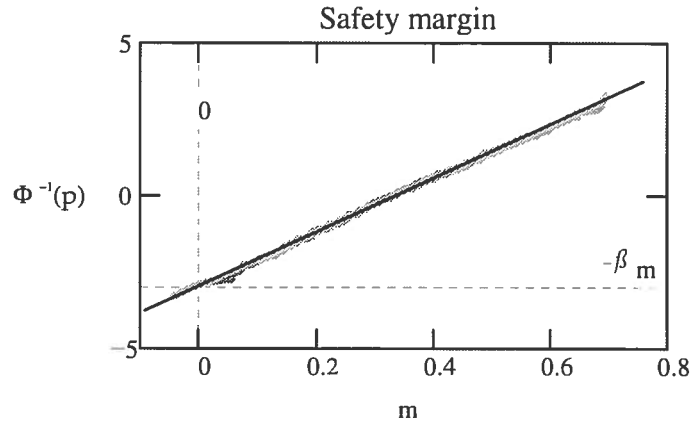

Figure 4.14 Monte Carlo simulation of the safety margin m=ln(F)

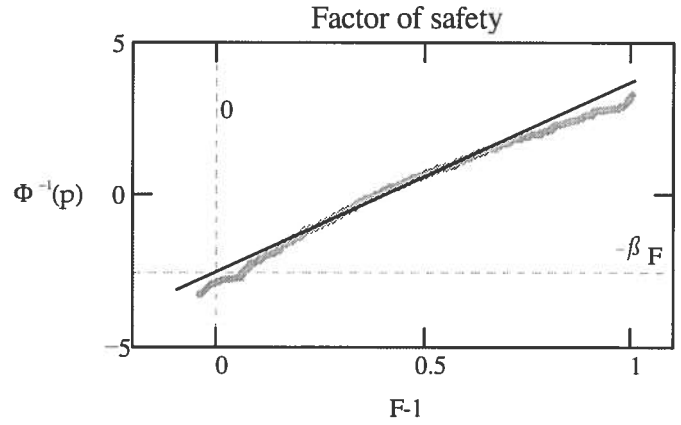

Figure 4.15 Monte Carlo simulation of the factor of safety F

Figure 4.14 and Figure 4.15 are plotted on normal 'probability paper', see appendix B. The plot $\{\Phi^{-1}(p)\cdot\sigma+\mu;\Phi^{-1}(p)\}$, which is the black line, is a linear plot of a normal distribution. As can be seen in the figures, the assumption of a normal distribution is highly justified for the safety margin ln(F) but not for F-1. For the probability of failure p_F and m=0, one obtains the point:

$$\{m=0;-\beta\}=\{\Phi^{-1}(p_F)\cdot\sigma+\mu;\Phi^{-1}(p_F)\} \tag{4.26}$$

which is the intersection of the dotted lines in the figures. The right part of the equation is obtained by equation 2.32:

$$\beta=-\Phi^{-1}(p_F) \tag{4.27}$$

An assumption of the factor of safety to be lognormal implies that:

$$p_F=p(F<1)\approx\Phi\left(\frac{\ln(1)-\ln(\mu_F)}{V_F}\right) \tag{4.28}$$

Equation 4.28 and the results of the PEM-calculation $\mu_F=1{,}4$ and $\sigma_F=0{,}16$ give $p_F=1{,}62\cdot10^{-3}$. Equation 4.27 then results in β=2,94, which is close to the values derived for the safety margin approach, equation 4.13, but larger than values obtained from equation 4.23. Hence, all the three algorithms give similar results if one interprets the results in an appropriate manner.

4.6 Application of a level 2 - method.

4.6.1 Background

Limit equilibrium methods can be seen as good deterministic models for slope stability analyses. However, they are not easily used in a probabilistic analysis. Li's unified scheme, see section 4.4.2, means that reliability analyses, with recognised methods, can be used in slope stability analyses, even if the formulas presented are not trivial. Commercial slope stability programs can, from an operator's view, be seen somewhat as a 'black box'. Even if one has a good knowledge of the principles of the calculation, it is hard to control all the details. From what is said above it can be concluded that there is a need of a great deal of programming work before Li´s method can be used in a computer software of slope analysis suitable for day-to-day practice. As an alternative, the results of an approach with Bishop's simplified method (Bishop, 1955) is presented below.

Another alternative is to use the PEM-method, see section 2.4.2. An advantage of using PEM, in this case, would be that the deterministic solution scheme does not need to be reformulated. This implies that even 'black box' programs can be used for the probabilistic analysis. However, considerably fewer parameters can be considered as random variables, if one wants to restrict the amount of calculation work.

4.6.2 Example

Introduction

In section 4.5.2 a slope was analysed with a probabilistic approach, based upon a 'design chart' method. However, the analysis was restricted to the critical slip circle for undrained analysis. For the slope at hand, a combined analysis is expected to govern the stability, why this type of analysis has to be incorporated into the probabilistic scheme. Similarly as was stated for the level-1 analysis, the reliability analysis is simplified if it can be formulated explicitly. In appendix N, a detailed description of Bishop's simplified method is given. The description combines the method with the shear strength concept discussed in section 4.3.6

Input data

A combined analysis for the same slope as the example presented in section 4.5.2 can be performed as described below[1]. The random variables from the undrained analysis have to be supplemented with input data which govern the combined shear strength. The input variables required are shown in Figure 4.16.

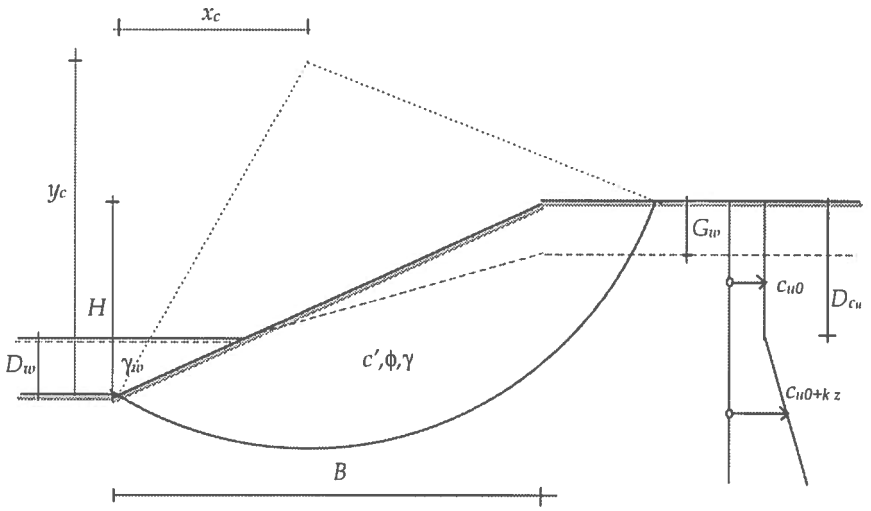

Figure 4.16 Input variables for the reliability analysis.

In the same way as the example in section 4.5.2, the geometry can be transformed to a section with simple geometry, see appendix M. If the cohesion intercept c' is replaced with the corresponding attraction *a*, the number of random variables can be reduced with one variable, cf. section 3.4.3, drained shear strength.. The input data used in a reliability analysis are summarised in Table 4.9. In accordance with the level 1 analysis γ_w, D_{Cu} and k are treated as fixed variables. The choice to give the location of the critical slip circle as three alternatives of fixed variables is discussed below in the section 'Location of critical slip circle'.

[1] To shorten the description, the analysis is restricted to toe circles, which for the slope at hand are expected to govern the stability.

	Geometry				Soil parameters		
	x_c [m]	y_c [m]	D_{Cu} [m]		γ_w [kN/m³]	k [kPa/m]	a [kPa]
Fixed (3 alt.)	15,9 13 11,5	28,2 30 29	6		10	1,65	3,5
	H [m]	B [m]	D_w [m]	G_w [m]	γ [kN/m³]	c_{u0} [kPa]	tanϕ
μ	10	31,7	1	2	16	20	0,58
σ	0,5	3	0,5	0,5	0,5	2,5	0,03
Type of distr.	*N*	*N*	*N*	*N*	*LN*	*LN*	*LN*

Table 4.9 Input data for the reliability analysis.

Reliability analysis

To determine the reliability index ß, the algorithm outlined in section 2.4.4 reliability index $ß_{H\text{-}L}$ can be used. For the limit state function $G(\mathbf{X})$, the formulation of the safety margin by equation N.14c, appendix N ,can be used:

$$m = \frac{m_R \cdot \bar{c}(0) - m_S \cdot \gamma \cdot H}{\mu_{m_R} \cdot \mu_c} \tag{4.29}$$

where $m_R = f_1(x_c, y_c, H)$ is a measure of the geometric resistance and $m_S = f_2(x_c, y_c, H, B, D_w, \gamma, \gamma_w)$ is a measure of the geometric driving. The average shear strength for the stress state at failure, i.e. m=0, is a function $\bar{c}(0) = f_3(x_c, y_c, H, B, D_w, G_w, D_{Cu}, \gamma, \gamma_w, c_{u0}, k, a, \tan\phi)$. Finally, the product $\mu_{m_R} \cdot \mu_c$ in the denominator serves just as a scaling factor, cf. appendix J. Thus the safety margin becomes the limit state function:

$$m = G(x_c, y_c, H, B, D_w, G_w, D_{Cu}, \gamma, \gamma_w, c_{u0}, k, a, \tan\phi) \tag{4.29a}$$

A normal random variable X_i is transformed to the u-space by the transformation:

$$X_i = \mu_{X_i} + \sigma_{X_i} \cdot u_{X_i} \tag{4.30}$$

A lognormal random variable X_j is transformed as:

$$X_j = \exp\left[\ln(\mu_{X_j}) - \frac{1}{2}\cdot\ln(1+V_{X_j}{}^2) + \ln(1+V^2)\cdot u_{X_j}\right] \quad (4.31)$$

or approximately for small values of V (<25-30%):

$$X_j \approx \exp\left[\ln(\mu_{X_j}) + V\cdot u_{X_j}\right] \quad (4.31a)$$

Hence, the limit state function in the u-space can be written as:

$$\begin{aligned} m &= G(x_c, y_c, H, \ldots, k, a, \tan\phi) \approx \\ &\approx G(x_c, y_c, \mu_H + \sigma_H\cdot u_H, \ldots, k, a, \exp(\mu_{\tan\phi} + V_{\tan\phi}\cdot u_{\tan\phi}) = \\ &= g(u_H, \ldots, u_{\tan\phi}) \end{aligned} \quad (4.29b)$$

as the fixed variables become constants in the reliability analysis and hence do not need to be transformed to the u-space. For the determination of the reliability index $ß_{H\text{-}L}$, which is given by the shortest distance between the failure surface, g=0, and origo[1], an iterative optimisation method presented by Thoft-Christensen and Baker, (1982) can be used.

- The design point is given by the sensitivity factors α_i and the reliability index $ß$, see Figure 4.17:

$$g(ß\cdot\alpha_H, ß\cdot\alpha_B, \ldots, ß\cdot\alpha_{\tan\phi}) = g(ß\cdot\alpha) = 0 \quad (4.32)$$

- The sensitivity factors are obtained by iteration, which for a step j+1 becomes:

$$\alpha_{i,j+1} = \frac{-\dfrac{\partial g(ß_j\cdot\alpha_j)}{\partial u_i}}{\left[\sum_{i=1}^{n}\left(\dfrac{\partial g(ß_j\cdot\alpha_j)}{\partial u_i}\right)^2\right]} \quad (4.33)$$

- The reliability index $ß_{j+1}$ is the root to the equation:

$$g(ß\cdot\alpha_{j+1}) = 0 \quad (4.32a)$$

[1] See figure 2.20

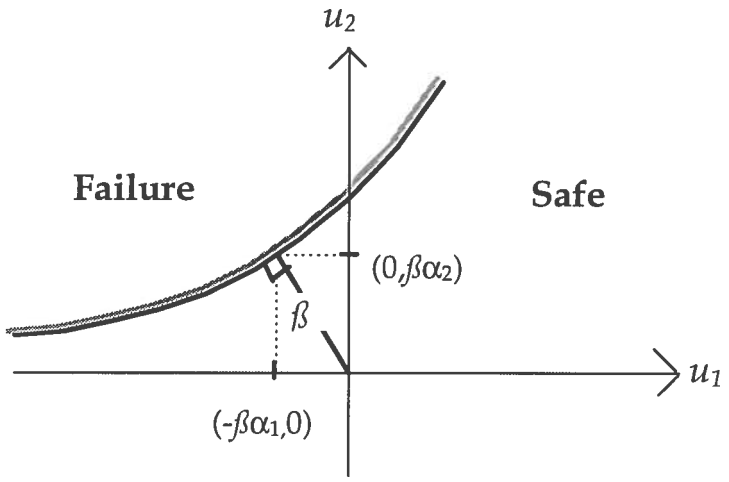

Figure 4.17 Relation between sensitivity factors α and reliability index $ß$.

The sensitivity factor for a variable is a measure of the influence of the uncertainty of that variable. From Figure 4.17 it can be seen that if a low value of a variable, u_1, i.e. a 'resistance' variable, governs the design the sensitivity factor becomes negative, while for a high value of a variable, u_2, i.e. an 'action' variable, the sensitivity factor becomes positive[1]. Further, from the definition of the sensitivity factors by equation 4.32 it follows that:

$$ß = \left[\sum_{i=1}^{n}(ß\cdot\alpha_i)^2\right]^{\frac{1}{2}} = ß\cdot\left[\sum_{i=1}^{n}(\alpha_i)^2\right]^{\frac{1}{2}} \qquad (4.34)$$

or

$$\sum_{i=1}^{n}(\alpha_i)^2 = 1 \qquad (4.34a)$$

This means that a sensitivity factor squared serves as a relative influence on the analysis of a particular variable.

Location of critical slip circle

In the example of undrained analysis, presented in section 4.5.2, the coordinates of the critical slip circle centre were given by explicit formulas. However, the same slip circle will not normally govern the combined analysis. The procedure, outlined in the previous section, to determine the reliability index is in principle an optimising

[1] In ENV 1991-1, (1994) the sensitivity factors are defined with the opposite sign.

algorithm. Hence, one could expect that the location of the critical slip circle could be obtained by giving the coordinates for the rotation centre as random variables. Unfortunately, if one does not know the correct location, it means that one, by assigning values to the coordinates as random variables, incorrectly adopts a subjective importance of a particular critical circle. Hence, the solving algorithm will not converge to the correct slip circle. Furthermore, if one tries to avoid the problem by adopting diffuse random variables for the coordinates, the solving algorithm does not converge at all, due to numerical problems.

Despite what is said above, the technique of giving the location centre as random variables can be used in the following way. The solution of the reliability analysis will result in values of the sensitivity factors. The sign of these factors will reveal in which way one has to adjust the values of an initial guess. A consequence of this is that, if the initial guess is 'correct', the values of the sensitivity factors for the rotation centre will be close to zero.

Results of reliability analysis

Reliability analyses were undertaken for three different alternatives:

- Combined analysis for the critical slip circle that governs the undrained analysis.
- Combined analysis for the critical slip circle that governs the deterministic, combined analysis.
- Combined analysis for the critical slip circle that governs the reliability analysis, i.e. the 'true' critical circle based upon given assumptions.

The first two alternatives are analysed for comparison with the last alternative. In principle, it is only the latter alternative which is of interest in a reliability analysis.

In Table 4.10 the results of the reliability analysis for the alternative 'undrained slip circle' are shown. The value of the safety margin m is a result of a deterministic analysis, i.e. a calculation using equation 4.29 and mean values of the variables[1].

x_c=	15,9	y_c=	28,2	m=	14%	β=	1,8
	H	B	Dw	G_w	γ	c_{u0}	$tan\phi$
α	0,47	-0,30	-0.07	-0,10	0,25	-0,77	-0,12
'α^2'	22%	9%	0,5%	1%	6%	60%	1,5%
μ	10	31,7	1	2	16	20	0,58
'design point'	10,4	30,1	0,9	1,9	16,2	16,8	0,57

Table 4.10 Results of reliability analysis. Alt. 'undrained circle'.

As the safety margin is given with an explicit formula, the location of the critical slip circle, in a deterministic analysis, is rather easy to determine. In principle, a numerical optimising algorithm can be used. However, as the variation of the safety margin close to the correct location is very smooth, numerical convergence problems can occur. An alternative method, frequently used, is shown in Figure 4.18. The safety margin is plotted as a function of the rotation centre. Hence, the critical rotation centre can be determined by inspection. The figure shows the result of a deterministic, combined analysis.

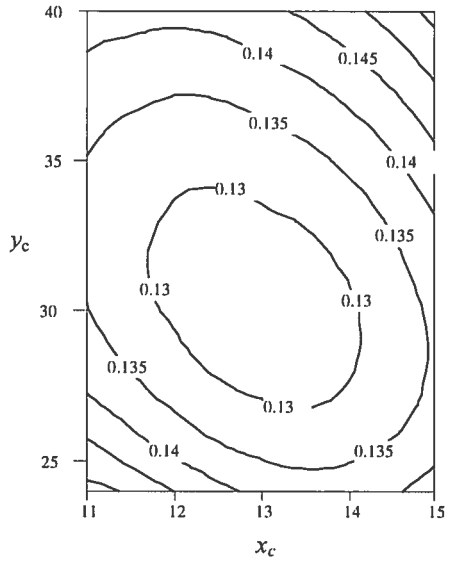

Figure 4.18 Deterministic dimensionless safety margin as a function of the coordinates for the slip circle centre.

[1] This is equal to the definition of the safety margin given by equation 4.4.

The result of a reliability analysis, with a critical slop circle determined from Figure 4.18, is shown in Table 4.11.

x_c=	13	y_c=	30	m=	13%	β=	1,4
	H	B	Dw	G_w	γ	c_{u0}	$tan\phi$
α	0,47	-0,5	-0.06	-0,14	0,16	-0,68	-0,15
'α^2'	22%	25%	0,5%	2%	2,5%	46%	2%
μ	10	31,7	1	2	16	20	0,58
'design point'	10,3	29,6	0,95	1,9	16,1	17,7	0,57

Table 4.11 Results of reliability analyses. Alt. 'deterministic combined circle'.

The principles discussed above for the location of the critical slip circle are also valid for the reliability analysis. The numerical problems in a numerical optimising procedure become more pronounced in this case, due to the complex calculation algorithm. The alternative, with a plot as in Figure 4.18, can be used but for the reliability index instead of the safety margin. Figure 4.19 shows such a plot. It is based upon considerably fewer calculated values than the plot in Figure 4.18 [1], hence the irregular shape of the contours. In this case the number of calculations demanded can be reduced by assigning random variables to the co-ordinates, see page 140.

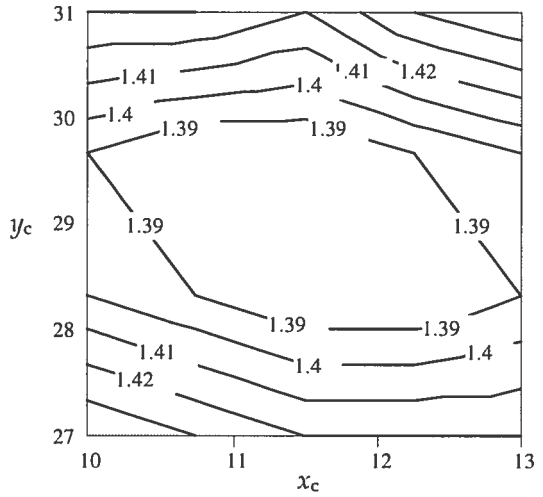

Figure 4.19 Reliability index β as a function of the centre of the slip circle.

[1] Twenty values compared with 320 in Figure 4.18.

The result of the reliability analysis for the last case, the 'true' critical circle is shown in Table 4.12.

x_c=	11,5	y_c=	29	m=	13%	ß=	1,4
	H	B	Dw	G_w	γ	c_{u0}	$tan\phi$
α	0,46	-0,59	-0.05	-0,16	0,11	-0,61	-0,17
'α^2'	21%	35%	0,5%	2,5%	1%	37%	3%
μ	10	31,7	1	2	16	20	0,58
'design point'	10,3	29,3	1,0	1,9	16,1	18,1	0,57

Table 4.12 Result of reliability analysis. Alt. 'true critical circle'.

Monte Carlo simulation

The reliability analysis presented in the previous section was based upon a safety margin in accordance with equation 4.5, $m = (R-S)/\mu_R$. This is a slight modification of the proposed basic safety margin in equation 4.4, which is written as $m = (R-S)/R$. The analysis in section 4.5.2 was based upon another concept, $m = \ln(F)$. Finally, in the literature the safety margin m=F-1 is commonly used. To investigate the influence of these different definitions of a safety margin, Monte Carlo simulation was performed for the four alternatives:

- A: $m = (R-S)/\mu_R$
- B: $m = (R-S)/R$
- C: $m = \ln(F)$
- D. $=F-1$

In the same way as in the reliability analysis, simulations were performed for three different slip circles. The results of the simulations are shown in Figure 4.20- Figure 4.22. The plots are of the same type as in Figure 4.14 and Figure 4.15. The values of ß, marked in the figures, are the values for the corresponding slip circles determined in the reliability analysis.

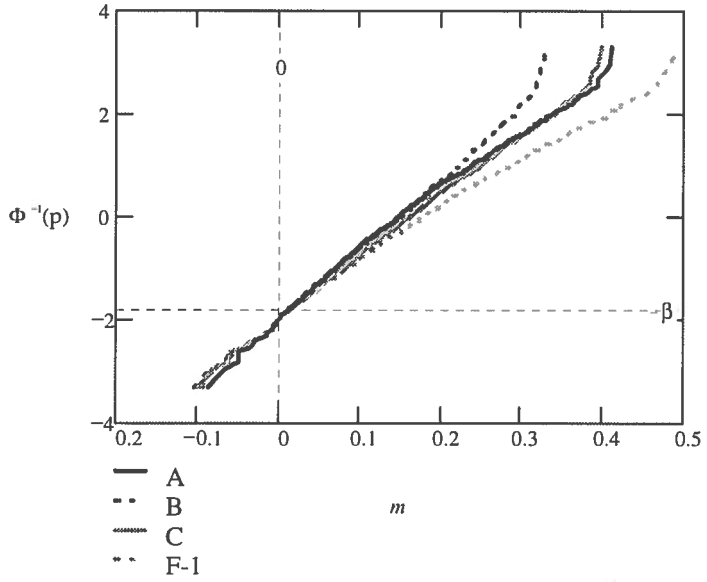

Figure 4.20 Monte Carlo simulation of the safety margin. Alt. 'undrained circle'.

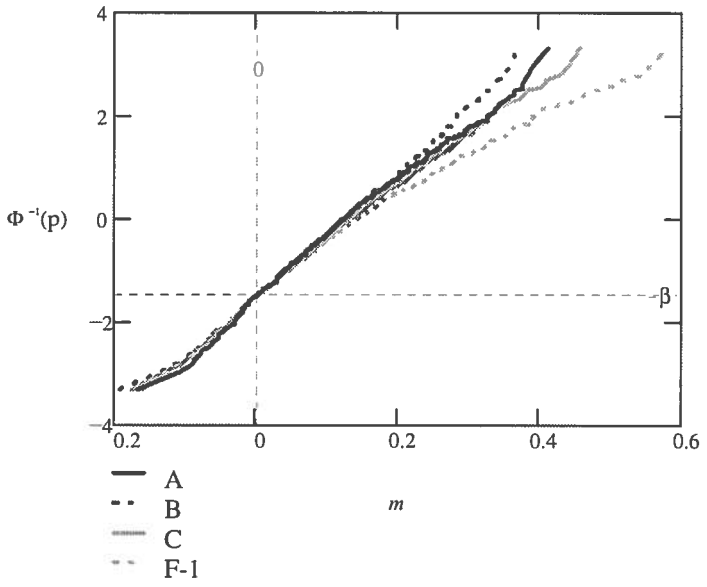

Figure 4.21 Monte Carlo simulation of the safety margin. Alt. 'deterministic combined circle'.

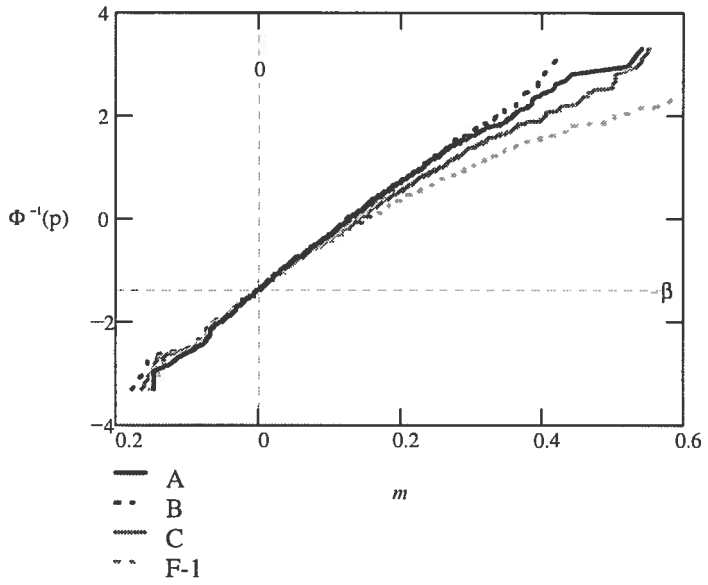

Figure 4.22 Monte Carlo simulation of the safety margin. Alt. 'true critical circle'

Summary

The safety of a slope was determined for a combined analysis. Two types of probabilistic approach were used, reliability analysis and Monte Carlo simulation. Seven parameters were modelled as random variables. Three different slip circles were investigated, see Figure 4.23. A comparison with the result given in section 4.5.2 shows that combined analysis governs the stability. The safety is overestimated if only the slip circle, which governs undrained analysis, is considered. The critical slip circle becomes different for deterministic and reliability analysis. However, the difference between the results of the analysis is small for these latter two circles. The influence of the uncertainty of the undrained shear strength is considerable for all three types of circles, but is naturally more pronounced for the 'undrained circle'. For the critical circles of combined analysis, the influence of the inclination of the slope, given as the length of the slope B, is quite substantial. For the other variables there are small differences between the influences of the variables on the three different types of circles analysed.

The Monte Carlo simulation is in good agreement with the result of the reliability analysis. The different formulations of the safety margin are of less importance for values close to zero, i.e. close to failure. The divergence between the different formulations for

higher values of the safety margin is of secondary importance in a stability analysis.

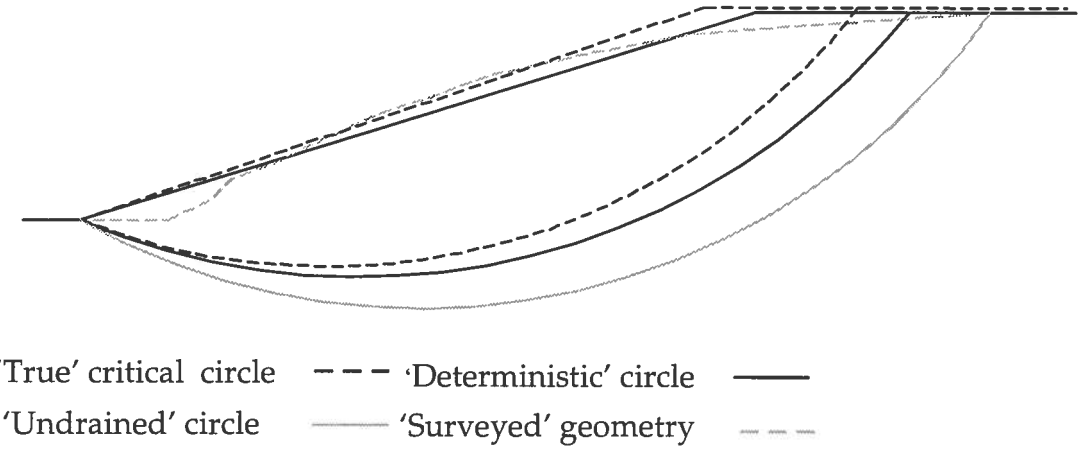

Figure 4.23 Geometry of slope and 'critical' slip circles

The number of parameters treated as random variables, in this case seven, means that a calculation with the PEM-method would have required 128 calculations. Thus the PEM-method is unsuitable for this type of analysis, unless it is not incorporated systematically in a software program.

4.7 Application of a level 3 - method

4.7.1 A Shear Beam Model

General description

A slope is modelled as a frame work of shear beams, see Figure 4.24. The concept is an extension of the traditional slice methods. By its structural mechanic nature it forms a link between traditional limit equilibrium methods and finite element methods. The beam elements are described with their section area, together with an appropriate shear and compression modulus respectively. It is the reactions at the supports which are of main interest. These are determined by the stiffness distribution between the different frame elements. As the absolute values of the deformations are of minor concern, it is only necessary to give relative and not absolute properties of the different beams. The assignment of the stiffness of the elements replaces the idea of a constant degree of mobilisation in a traditional analysis. Different degrees of complexity in the force distribution can be simulated by constraints in the nodes and at the

supports. This corresponds to different assumptions regarding the interslice forces in ordinary slice methods. In principle[1], any rigorous limit equilibrium method can be formulated as a shear beam model. For example, a described line of thrust, as in Janbu's GPS method (see e.g. Janbu 1996), can be defined by prescribing the position of the nodes between the slices and assuming hinges in these nodes. The limitation to rigorous methods depends on the fact that equilibrium is a prerequisite for any structural frame analysis. A distinct feature of the proposed method is that the traditional assumption of a constant degree of mobilisation of the shear strength is abandoned. This gives an opportunity to take progressive failure into account.

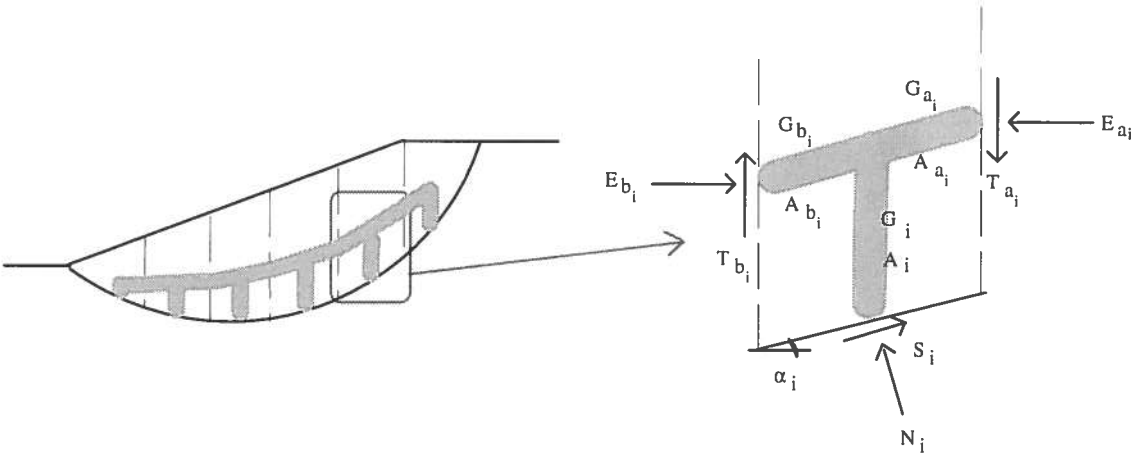

Figure 4.24 A slope modelled as a frame-work of shear beams

For a specified slip surface, the shear beam model will, as a result, give the internal and external forces for a structure in equilibrium. If these forces do not exceed the corresponding strength in any point, the solution is on the safe side. This follows from the lower bound theorem, see section 2.1.2 'limit analysis.' The statement has to be somewhat modified in those cases when the shear strength is characterised with a residual strength less than the peak strength[2].

[1] The set of stiffness of the elements, which corresponds to a constant degree of mobilisation, is not easily obtained.

[2] This is valid for any limit equilibrium method.

Safety concept

In a structure one can normally distinguish between a collapse of the system and a collapse of a single element. In a slope stability analysis it is only the system collapse which is of interest. A total failure corresponds to the situation when all supporting elements have collapsed. A safety concept should work as a measurement of the likeliness for this to occur. The global factor of safety and the safety margin are such concepts.

For a slip surface, modelled as a polygon of n different segments, both the resistance, **R**, and the action, **S**, can be seen as a vector sum of local vectors, $\mathbf{R}_i$ and $\mathbf{S}_i$:

$$\mathbf{R}=\mathbf{R}_1+\mathbf{R}_2+...+\mathbf{R}_i+...+\mathbf{R}_n$$

$$\mathbf{S}=\mathbf{S}_1+\mathbf{S}_2+...+\mathbf{S}_i+...+\mathbf{S}_n \qquad (4.35)$$

In traditional analyses, with the assumption of a constant degree of mobilisation throughout the slope, **R** and **S** are colinear. Thus a safety margin can be defined as, cf. equation 4.4:

$$m=\frac{|\mathbf{R}|-|\mathbf{S}|}{|\mathbf{R}|} \qquad (4.36)$$

If the degree of mobilisation is not constant, **R** and **S** are not collinear , see Figure 4.25. The definition of m is then not evident.

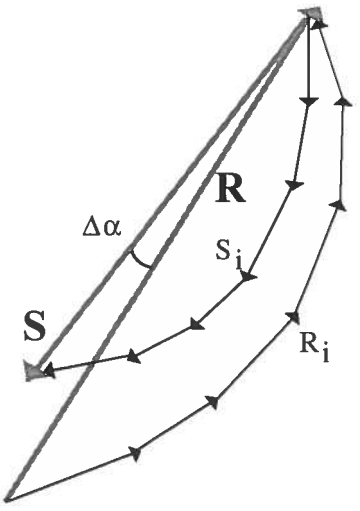

Figure 4.25 Principal shear resistance, **R**, and shear force, **S**, for an arbitrarily shaped slip surface.

One way to define a safety margin is to use the projection of **R** on **S.** The definition, in accordance with equation 4.36, then becomes:

$$m = \frac{|\mathbf{R}| \cdot \cos(\Delta\alpha) - |\mathbf{S}|}{|\mathbf{R}| \cdot \cos(\Delta\alpha)} \tag{4.36a}$$

where $\Delta\alpha$ is the angle between **R** and **S**. If local safety margins, $m_i = (|\mathbf{R}_i| - |\mathbf{S}_i|)/|\mathbf{R}_i|$, are defined, equation 4.36a can be rewritten as:

$$m = \frac{|\mathbf{R}| \cdot \cos(\Delta\alpha) - |\mathbf{S}|}{|\mathbf{R}| \cdot \cos(\Delta\alpha)} = \frac{\sum_n |\mathbf{R}_i| \cdot \cos(\Delta\alpha_i) - \sum_n |\mathbf{S}_i| \cdot \cos(\Delta\alpha_i)}{\sum_n |\mathbf{R}_i| \cdot \cos(\Delta\alpha_i)}$$

$$= \frac{\sum_n m_i \cdot |\mathbf{R}_i| \cdot \cos(\Delta\alpha_i)}{\sum_n |\mathbf{R}_i| \cdot \cos(\Delta\alpha_i)} \tag{4.36b}$$

where $\mathbf{S_i}$ and $\mathbf{R_i}$ are the local shear force and the shear resistance respectively for a slice *i*. $\Delta\alpha_i$ is the angle between those local vectors and the resulting shear force. The global safety margin can, according to this formulation, be seen as a weighted mean value of local values.

Progressive failure

The principal relationship between the shear stresses and the shear strength can be illustrated as in Figure 4.26. The figure illustrates an assumption that the shear stresses are elastic up to a peak value. In a traditional, deterministic analysis this peak value is reached simultaneously for all parts of the slip surface. Thus, the behaviour to the right of the peak value is of no interest in the analysis. However, if the deformation of the soil is considered in an ultimate limit state analysis, values of the shear strength below the peak value have to be taken into account for large deformations.

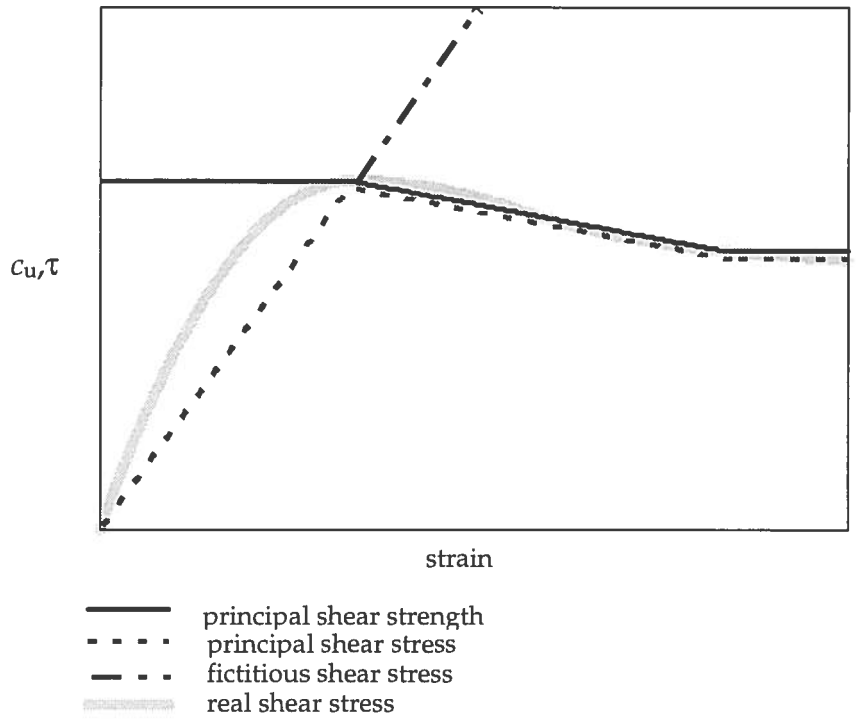

Figure 4.26 Principal relationship between the shear strength and the shear stresses as a function of the shear deformation

One way to consider shear strength below the peak value , in the shear beam model, is to make an iterative calculation. Figure 4.27 illustrates the procedure for the first two iterations.

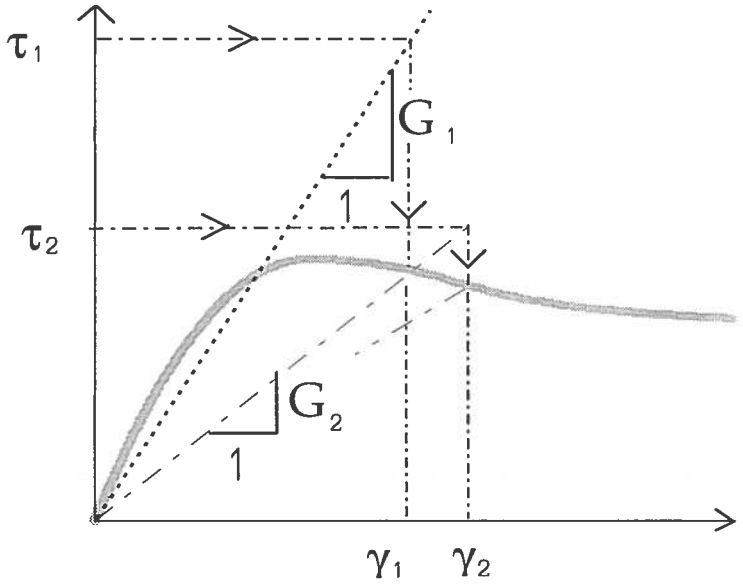

Figure 4.27 Iteration procedure for the shear modulus in a progressive failure analysis

For an iteration i, elastic shear strains are calculated for a secant shear modulus, G_i. This means that the strains, beyond the peak

value, follow the dotted line in the figure. A secant value of the shear modulus, G_{i+1}, which can be derived from the calculated strains, is used as input in the next iteration step i+1 or summarised as:

$$\begin{aligned} &\text{Iteration } i: && G_i \Rightarrow [\tau_i;\gamma_i] \Rightarrow G_{i+1} \\ &\text{Iteration } i+1: && G_{i+1} \Rightarrow [\tau_{i+1};\gamma_{i+1}] \Rightarrow G_{i+2} \end{aligned} \qquad (4.37)$$

As an alternative, a simple, though rough way to consider progressive failure is to permit, in equation 4.36b, local safety margins < 0. [1] That is $\tau_1 > c_u$ as in Figure 4.27. The idea is that redistribution of shear forces, between different slices, can and will take place, even though the redistribution in itself is not determined. The assumption that redistribution of forces can take place is supported by the results from triaxial testing of clay. In Figure 4.3, section 4.3.4, the frictional strength, tanϕ, as a function of the strain was given. The figure showed that the friction strength is reached for small strains and is unaltered in a large range of the strains. Hence the ratio between shear stresses and normal stresses is constant for increasing deformations. This requires a redistribution of forces for a loading or unloading situation of a slope. Another conclusion, which can be drawn from Figure 4.3, is that the issue of progressive failure is mainly a matter for undrained analysis, or the undrained parts of a slope in a combined analysis.

4.7.2 Example- A shear beam model

Introduction

In section 4.5.2 a slope was analysed with a 'design chart'-method. In section 4.6.2 the analysis was extended to a combined analysis and different potential slip surfaces. In this section the same slope is analysed with a shear beam model. The analysis is restricted to the potential slip circle resulting from the reliability analysis in section 4.6.2, i.e. in principle the most likely slip circle.

[1] For progressive failure this is a calculation on the unsafe side, but to a lesser degree than in a calculation with a constant degree of mobilisation.

The shear beam model

A detailed description of the shear beam model used is given in appendix O. The geometry of the shear beam model used in the example is given in Figure 4.28. The analysis is based upon the transformed geometry of the slope, cf. Figure 4.9. The reason for this is the same as in the previous analyses, i.e. to make it possible to give a random description of the geometry by the two basic variables H and B. However, apart from this, there is no reason to base a shear beam model upon such a simplified geometry. Nor must the analysis be restricted to potential circular slip surfaces.

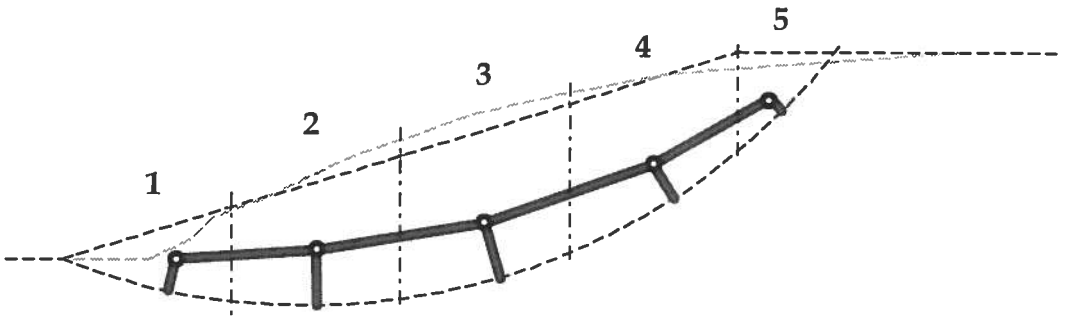

Figure 4.28 Geometry of the shear beam model in section 600.

The shear beam model inspired by the limit equilibrium method GPS (see e.g. Janbu, 1996). Hence a 'line of thrust' is prescribed. This is achieved by applying hinges in the nodes along the line of thrust. The deformation properties are prescribed with a compression stiffness for each of the longitudinal compression struts and a shear stiffness for each of the shear legs. The structure is made stable by assuming the shear struts as fixed at the shear surface.

Deterministic analysis

As a prestage to a probabilistic analysis, a corresponding deterministic analysis of the slope is performed, with the assessed mean values as input for the basic variables. Input data for the analysis are presented in Table 4.13. The notations used are the same as in section Example 4.6.2, see Figure 4.16.

Geometry						
x_c [m]	y_c [m]	H [m]	D_w [m]	G_w [m]	B [m]	D_{Cu} [m]
11,5	29	10	1	2	31,7	6
Soil parameters						
γ [kN/m³]	γ_w [kN/m³]	c_{u0} [kPa]	k [kPa/m]	a [kPa]	tanϕ	
31,7	10	20	1,65	3,5	0,57	

Table 4.13 Input data for the deterministic analysis

A distinct feature of the shear beam model is that different alternatives of stiffness distribution throughout the slope can be accounted for. In appendix O, a slope is analysed for two different types of stiffness distribution:

- A stiffness distribution based upon the geometry of the slope
- A stiffness distribution based upon a hypothesis of long time shear creep in the slope.

These two types can be seen as two extreme alternatives. In the first alternative, 'initial' deformation properties, based upon the slope geometry combined with a constant shear modulus G and a compression modulus M, are applied. The second alternative describes a long term situation, assuming shear creep in the slope. Hence, 'secant values' for the shear stiffness are used. The deterministic analysis of the section at hand is undertaken for two similar assumptions of shear stiffness distribution, see Figure 4.29.

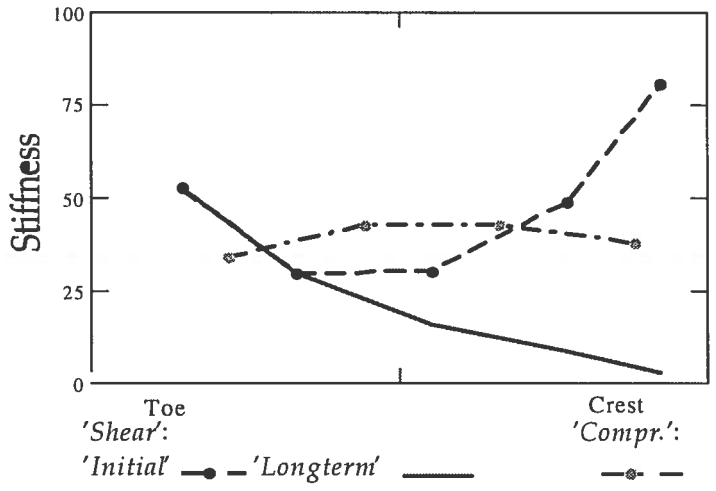

Figure 4.29 Distribution of shear stiffness and compression stiffness from toe to crest.

Figure 4.29 also shows the compression stiffness used, which is equal in the two analyses. For the first alternative the analysis is restricted to a combined analysis. In Table 4.3 the results of the analysis are presented. The column m shows the total safety margin for a combined analysis, calculated according to equation 4.36. The columns m_1 - m_2 show the local safety margins for each 'slice', cf. Figure 4.28. The first assumption of an 'initial' shear stiffness distribution corresponds to a totally unrealistic shear stress distribution. The active zone is highly overstressed, while the passive zone is almost inactive. The second alternative, the 'long time creep situation', results in a slope with a degree of mobilisation, which is rather equal throughout the slope. In the interpretation of the in-situ stress state, the results of the drained analysis are probably the most correct.[1]

		m	m_1	m_2	m_3	m_4	m_5
Alt A	combined	0,02	0,96	0,71	0,36	-0,5	-3,3
Alt.B	combined	0,15	0,23	0,21	0,07	0,16	0,08
	drained	-	0,23	0,21	0,20	0,17	0,08
	undrained	-	0,65	0,25	0,07	0,16	0,46

Table 4.14 Section 600. Safety margins. Result of deterministic analysis.

Figure 4.30 shows the normal effective stress distribution obtained as a result of the two different assumptions of shear stiffness distribution. For comparison, the stress distribution, which corresponds to the analysis with Bishop's simplified method, see section 4.6.2, is also given. In the second alternative of shear stiffness distribution, the normal stresses are increased. This is due to a redistribution of the equilibrium stresses from shear stresses to normal stresses.

[1] For the long term situation both a combined failure and an undrained failure can normally be assumed to be preceded by a triggering factor, which changes the stress state, cf. section 4.1.

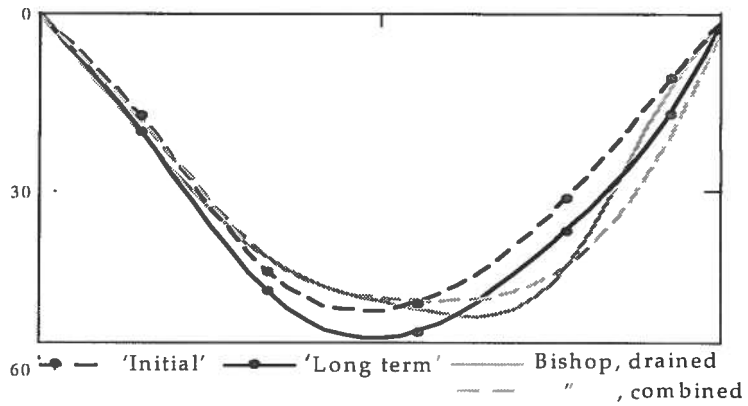

Figure 4.30 Normal effective stress distribution.

Probabilistic analysis

The shear beam model, outlined above, should be seen as a prototype model. In principle, the safety margin according to equation 4.36 can be given a formulation as, cf. equation 4.29a:

$$m = G(x_c, y_c, H, B, D_w, G_w, D_{Cu}, \gamma, \gamma_w, c_{u0}, k, a, \tan\phi) \qquad (4.38)$$

However, for a detailed formulation, equation 4.38 becomes more complex, compared with the formulation of the safety margin for Bishop's simplified method. To be able to perform a reliability analysis as in section 4.6.2, efforts must be made to obtain effective numerical algorithms for the solution. The same applies with regard to a Monte-Carlo simulation. As an example of a less time consuming analysis, a limited PEM calculation is presented below.

In section 4.6.2 it was stated that a PEM-calculation for the slope with 7 basic, random variables would demand 128 calculations. However, an inspection of the results in Table 4.12 gives at hand that, for the 7 variables, only the variation of three variables had any major influence. Prescribing the other four variables as deterministic reduces the number of calculations demanded considerably from 128 to only 8. Hence, a PEM-analysis is made with only the three variables, H, B and c_{u0}, as random variables. To incorporate the uncertainty of the other four variables into the analysis, the deterministic values of these are calibrated against results of reliability analyses with Bishop´s method. In Table 4.12 the results of a reliability analysis are given. Assigning deterministic values of the four least important variables as the arithmetic mean of the mean value and the design value results in very similar results, see Table 4.15.

The three lowest rows show an extract of Table 4.12. For comparison, the results are shown with an insignificant number of digits.

x_c=	11,5	y_c=	29	m=	13%	β=	1,38
	H	B	Dw	G_w	γ	c_{u0}	$tan\phi$
Fixed	-	-	0,98	1,95	16,04	-	0,574
α	0,48	-0,61	-	-	-	-0,63	-
'α^2'	23%	37%	-	-	-	40%	-
μ	10	31,7	-	-	-	20	-
'design point'	10,3	29,2	-	-	-	17,9	-
'Table 4.12'				m=	13%	β=	1,38
	H	B	Dw	G_w	γ	c_{u0}	$tan\phi$
'design point'	10,3	29,3	0,97	1,89	16,08	18,01	0,57

Table 4.15 Result of an alternative reliability analysis with Bishop´s simplified method.

Fixed variables							
D_{Cu} [m]	D_w [m]	G_w [m]	γ_w [kN/m³]	γ [kN/m³]	k [kPa/m]	a [kPa]	tanϕ
6	0,98	1,95	10	16,04	1,65	3,48	0,574
Random variables							
H_- [m]	H_+ [m]	B_- [m]	B_+ [m]	c_{u0}- [kPa]	c_{u0}+ [kPa]		
9,5	10,5	28,7	34,7	17,5	22,5		

Table 4.16 Input data for PEM- analysis

As can be seen from Table 4.16, the differences between the two analyses are small. Hence, it seems appropriate to undertake a PEM-analysis with the number of random variables limited to three variables.

Two different forms of PEM-analysis are performed, an analysis of the slope with the shear beam model and, as a comparison, an analysis with Bishop´s simplified method. The shear beam model is restricted to the 'long term' shear stiffness distribution.

In Table 4.17 the results of calculation of both the global safety margin and local safety margins for each 'slice' are given.

	m	m_1	m_2	m_3	m_4	m_5	m_{bish}
μ	0,13	0,26	0,21	0,08	0,09	-0,22	0,12
σ	0,07	0,12	0,08	0,11	0,05	0,28	0,08
	ß=1,9						ß=1,5

Table 4.17 Safety margin and corresponding reliability index from PEM-analysis

As can be seen in Table 4.16, the reliability index is improved for the shear beam model compared with Bishop's model. This is due to both an increase of the mean value and a reduction of the variance. It can also be noticed that the safety margin for slice 5 is negative and differs significantly from the deterministic analysis, see Table 4.14. It can be interpreted as that it is not a trivial thing to prescribe a 'correct' shear stiffness distribution. Results of the shear strength and the stress analysis are given in Table 4.18 - Table 4.20. The variation of both the stresses and the shear strength is small compared with the variation of the safety margins. This is natural as the safety margin is the difference between two values of the same magnitude, in principle c-τ. An inspection of the local values for slice 3 and slice 5 shows a considerably smaller variation for slice 3 than slice 5. This is not surprising as it is a well-known fact that the stress state in the upper active zone is difficult to model. The large variation of the pore pressure for slice 5 might just be a result of a crude modelling of the pore pressure situation in the slope.

	c_{comb}	σ_N	u	σ'_N	τ
μ	20	73	39	34	18
V[%]	8	10	10	11	13

Table 4.18 Average shear strength and stresses.

	c_{comb}	σ_N	u	σ'_N	τ
μ	28	115	61	54	26
V[%]	9	10	9	10	11

Table 4.19 Shear strength and stresses for 'slice' 3.

	c_{comb}	σ_N	u	σ'_N	τ
μ	9	20	8	12	11
V[%]	28	25	60	36	11

Table 4.20 Shear strength and stresses for 'slice' 5.

5 INTERACTION GROUND/SUPERSTRUCTURE

5.1 Background

There are two main reasons for considering the interaction between the ground and the superstructure:

- For a good functioning of the superstructure, it is important to control both the absolute settlements and the differential settlements.
- The action effects in a statically undetermined structure are strongly governed by the settlements of the supports. Beigler, (1976) showed that the calculated internal bending moments in a frame can vary and even change sign, depending on whether interaction between the ground and the superstructure is considered or not.

On the other hand, collapse of foundations is rare. Thus interaction is mainly an action/deformation problem. In practical design two different professions are concerned with the problem, the geotechnical and the structural engineer. A successful design is therefore dependent upon the co-operation between these two professions. From this point of view it is important that calculation methods and the nomenclature are co-ordinated.

5.2 Principles of Calculation

5.2.1 Calculation levels

In a statically determined structure, the reactions at the supports are independent of the deformations at the supports. Hence, the geotechnical analysis and the structural analysis can be separated. This means that interaction analysis, in principle, is only a task for statically undetermined superstructures. Also in this area, the calculation methods can be separated into three different levels, cf. section 2.1 and section 4.4-4.7. Below a division of methods, based upon the author's experience of methods commonlyare used in engineering practice, is given:

1. Rigid supports/elastic superstructure or rigid superstructure/elastic supports.

2. Elastic supports and elastic superstructure.

3. Non-linear elastic/plastic supports and/or non-linear elastic/plastic superstructure.

Level 1 - Rigid supports/elastic superstructure or rigid superstructure/elastic supports

This level incorporates two extreme cases. A superstructure with elastic properties and rigid supports is traditionally the most common model for the design of foundations. Obviously, this model is in many cases not relevant. If the foundation of the superstructure is very stiff, e.g. load-bearing basement walls, the other extreme case, a rigid superstructure on spring supports, might be a more realistic model. From a calculation point of view, the two different principles are simple. The interaction part of the calculation becomes trivial. In the first case, the deformation properties of the soil can be ignored and in the second case the deformation properties of the superstructure can be ignored.

Level 2 - Elastic supports and elastic superstructure

Elastic superstructure is a commonly used model in structural engineering. If the supports are assumed to be elastic too, a far more realistic model of the combined behaviour of the system can be obtained. A common approximation in this case is that the elastic supports are assumed to work independently of each other. In reality there exists a strong link between neighbouring supports through the soil. An advantage with this approach is that existing programs in structural mechanics, based on theory of elasticity, can be used. One application of this type of model is when the foundation structure can be treated as continuous beams. The system ground/superstructure is in this case often treated as a beam on a bed of independent, elastic springs, a so-called Winkler bed.

Level 3 - Non-linear elastic/plastic supports and/or non-linear elastic/plastic superstructure

The calculation of the interaction between the ground and the superstructure is a complex problem. For this reason it is often

assumed that an appropriate treatment demands a highly sophisticated calculation model. Thus, for example, non-linear finite element programs may be used. Unfortunately, existing programs for calculation of ground/superstructure interaction are often biased towards either geotechnics or structural mechanics. For example, in FEM-programs with a sophisticated soil model, the superstructure often has to be modelled as a rigid body. Another problem is that materials with very different deformation properties often result in numerical difficulties. Interaction between the supports through the superstructure can usually not be treated in such a case. The same is valid for programs intended for structural frame analysis. Non-linear behaviour of the supports might be modelled by parallel springs with plastic couplings. However, interaction between the supports through the ground can not be described. In some existing models, e.g. for calculation of piled raft foundations, where the soil is described as an elastic/plastic body, the superstructure is described as a simple beam or grillage model.

In Figure 5.1 the three different levels of calculation models are illustrated in principle. For the first level the supports are treated as rigid/plastic, i.e. the first extreme case described under level 1. For such a support, the bearing capacity gives an upper limit for the support reaction. The second level describes an elastic/plastic support: Even in this case the bearing capacity defines an upper limit. However, as the settlements of the supports are calculated, it is possible to introduce a criterion of deformation which governs the design. In the last case the relation between the support reactions and the deformations is given by a continuous, non-linear function. In this case the upper limit of the support reaction has to be defined explicitly, e.g. by a deformation criterion[1].

[1] The value of the bearing capacity used in levels 1 and 2 is normally obtained in this way too.

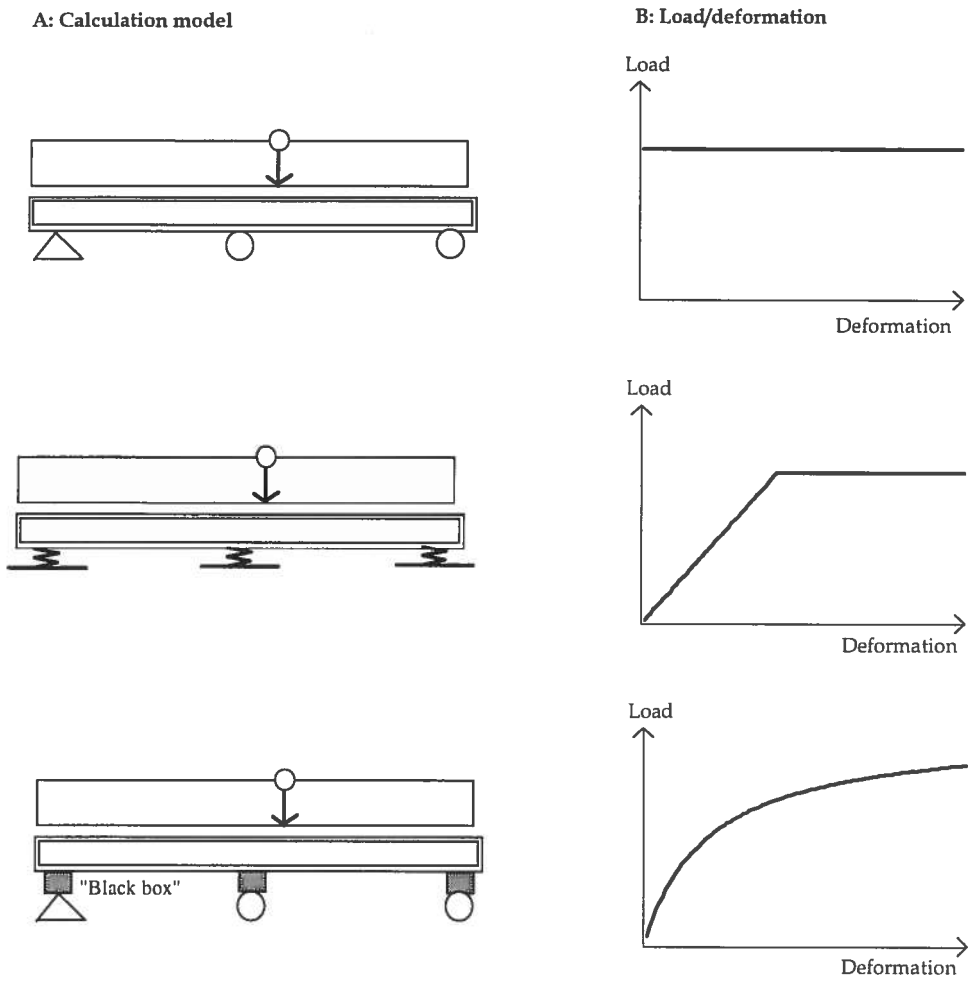

Figure 5.1 Interaction ground/superstructure. Principles of calculation models and corresponding load/deformation relations for the supports.
Level 1 - Rigid/plastic supports
Level 2 Elastic/plastic supports
Level 3 Non-linear elastic/plastic supports.

limit of the support reaction has to be defined explicitly, e.g. by a deformation criterion[1].

5.2.2 Ultimate limit state/ Serviceability limit state.

Modern design practice is to split up the design of structures into two cases; ultimate limit state and serviceability limit state, see e.g. ENV 1991-1. (1994) When considering the interaction problem, the elegance of this design practice is evident. Limit state design can easily be adopted in the ultimate limit state. This design method has

[1] The value of the bearing capacity used in levels 1 and 2 is normally obtained in this way too.

been described previously in general terms in section 2.1.2 'Limit and in connection with slope stability analysis in section 4.3.7.. In the latter section it is demonstrated that it is not a trivial task to combine limit state design and a traditional approach of slope stability analysis. However, since limit state design is developed in structural mechanics it is more easily adopted in a ground/superstructure interaction problem. Hence, the ultimate limit state design often becomes simple. In section 5.2.1 different levels of calculation models were discussed. The principal application of such different levels of ultimate limit state design is shown in Figure 5.1. The two design principles of level 1-methods (section 5.2.1) are both examples of the application of the lower bound theorem, see *2.2*. In both cases simplifying assumptions are made, after which internal forces and reactions are calculated with equilibrium equations. Thus, if the two prerequisites are fulfilled, that is redistribution of internal forces can take place and the strength is not overridden in any part of the structure, the result is on the safe side.

Design in the serviceability limit state is mainly restricted to a problem of calculating the correct deformation. However, this is not simple in interaction problems. If good precision is to be obtained one must choose calculation methods of level 2 or level 3 in section 5.2.1[1]

5.3 Foundation methods

5.3.1 General

When interaction between the superstructure and the ground is considered in the design process, it is more important to solve the problem as a whole, instead of giving very detailed descriptions of the different parts. It is desirable to have basic principles upon which the design can be based. In the forthcoming sections two types of foundation methods, spread foundations and piled foundations, are described in this way. The aim is not to replace detailed descriptions found elsewhere. Nevertheless, the benefit with a comprehensive but simplified design is often superior to a more detailed but split one.

[1] Eventually three-dimensional analysis too.

For both types of foundation, examples of derived formulas for the distribution of stresses and settlements are given. Some of the formulas can give an impression of being complicated. However, they are all developed to give closed form solutions. Thus, they are differentiable and therefore suitable for reliability analysis. Furthermore, they are very fast to compute. For example, this means that a Monte Carlo-simulation, with many repetitive calculations, becomes very rapid.

5.3.2 Spread foundations

Spread foundations can be regarded as a collective name for foundations with pads, strips and rafts (ENV 1997-1, 1994). The calculation of settlements for a spread foundation is in principle a simple task. The action effects of the superstructure should be applied at the foundation level. The vertical stress distribution, $\sigma_v(x,z)$, has to be determined for all points in the soil profile. Settlements can then be calculated as:

$$s(x) = \int_0^H \frac{\sigma(x,z)}{M} dz \tag{5.1}$$

where x is a horizontal coordinate and z is a vertical coordinate. M is here a general term for a compression modulus, for which the integral yields a correct settlement distribution at the foundation level. Whether this modulus is best applied as a constrained modulus or a modulus of elasticity has to be considered for the problem at hand. In Alén (1997) closed forms are derived for both stress distributions and settlements for spread foundations. The formulas are approximations based on Boussinesque's solution for a load applied on an elastic half sphere (see e.g. Terzaghi, 1943). For a pad or raft, with width B and length L, and a surcharge p, the vertical stress distribution can be written as the product:

$$\sigma_v(x,y,z)=\frac{p}{\pi^2}\cdot\left[\left[\frac{2z(B+2x)}{4z^2+(B+2x)^2}+\operatorname{atan}\left(\frac{B+2x}{2z}\right)\right]+\left[\frac{2z(B-2x)}{4z^2+(B-2x)^2}+\operatorname{atan}\left(\frac{B-2x}{2z}\right)\right]\right]\cdot\left[\left[\frac{2z(L+2y)}{4z^2+(L+2y)^2}+\operatorname{atan}\left(\frac{L+2y}{2z}\right)\right]+\left[\frac{2z(L-2y)}{4z^2+(L-2y)^2}+\operatorname{atan}\left(\frac{L-2y}{2z}\right)\right]\right] \tag{5.2}$$

where z, as above, is a vertical coordinate, while x and y are horizontal coordinates, x in the *B*-direction and y in the *L*-direction.

For as strip or a long raft, $L=\infty$, equation 5.2 can be written as:

$$\sigma_v(x,z)=\frac{p}{\pi}\cdot\left[\left[\frac{2z(B+2x)}{4z^2+(B+2x)^2}+\operatorname{atan}\left(\frac{B+2x}{2z}\right)\right]+\left[\frac{2z(B-2x)}{4z^2+(B-2x)^2}+\operatorname{atan}\left(\frac{B-2x}{2z}\right)\right]\right] \tag{5.3}$$

By integrating the vertical stresses divided by the compression modulus, *M(z)* over a soil layer *H*, the settlements can be obtained:

$$s(x)=\int_H\frac{\sigma_v(x,z)}{M(z)}dz \tag{5.4}$$

For a strip, the integral in equation 5.4 can be approximated as below. If the compression modulus, *M*, is constant, the settlements can be calculated as:

$$s_M(x)=\frac{P}{\pi\cdot M}\cdot\left[\ln(H^2+x^2)-\ln(B^2+x^2)-\frac{x^2(H^2-B^2)}{(H^2+x^2)(B^2+x^2)}\right][+s_0] \tag{5.5}$$

and for a compression modulus increasing with depth, $m \cdot z$:

$$s_m(x) = \frac{P}{\pi \cdot m} \cdot \left[\frac{\operatorname{atan}(\frac{H}{x}) - \operatorname{atan}(\frac{B}{x})}{x} + \frac{(H-B)(H \cdot B - x^2)}{(H^2 + x^2)(B^2 + x^2)} \right] [+ s_0] \qquad (5.6)$$

For x=0 the formulas can be simplified to:

$$s_M(0) = \frac{2 \cdot P}{\pi \cdot M} \cdot [\ln(H) - \ln(B)] [+ s_0] \qquad (5.5a)$$

and

$$s_m(0) = \frac{2 \cdot P}{\pi \cdot m} \cdot \frac{H-B}{H \cdot B} [+ s_0] \qquad (5.6a)$$

respectively. Both equations 5.5-5.6 have the restriction $H>B$. The last term, s_0, denotes the local settlements obtained from the soil just below the strip, x<B and z<B. This settlement has to be added if x<B. It can in most cases be approximated as:

$$s_0 \approx 0{,}75 \cdot \frac{P}{M_*} \cdot \frac{B-x}{B} \qquad (5.7)$$

where M_* is the "local" modulus. Finally, for an increasing compression modulus with depth, $M+ m \cdot z$:

$$s_{M,m}(x) = \left[s_M(x)^{-1} + s_m(x)^{-1} \right]^{-1} [+ s_0] \qquad (5.8)$$

where the local settlement, s_0, has to be added separately.

Equation 5.5 can be further approximated as:

$$\begin{aligned} s_{Ma}(x) &= \frac{P}{\pi \cdot M} \cdot \left[\left(\frac{50 \cdot H}{40x + H} \right)^{2/3} - 1 \right] \quad ; \quad x > B/4 \\ s_{Ma}(x) &= \frac{P}{\pi \cdot M} \cdot \left[\left(\frac{50 \cdot H}{10 \cdot B + H} \right)^{2/3} - 1 \right] \quad ; \quad x < B/4 \end{aligned} \qquad (5.9)$$

if x<H. In equation 5.9, local settlements are included. P, in all the equations above, is the total load on a unit length of the strip.

For a quadratic pad the settlements can, for a constant compression modulus, M, be calculated as:

$$s_{PM}(x) = \frac{2 \cdot P}{\pi^2 \cdot M} \cdot \left[\frac{\operatorname{atan}\left(\frac{H}{x}\right) - \operatorname{atan}\left(\frac{B}{x}\right)}{x} + \frac{(H-B)(H \cdot B - x^2)}{(H^2 + x^2)(B^2 + x^2)} \right] + s_0 \qquad (5.10)$$

which for x=0 becomes:

$$s_{PM}(0) = \frac{4 \cdot P}{\pi^2 \cdot M} \cdot \frac{H-B}{H \cdot B} [+ s_0] \qquad (5.10a)$$

Equation 5.10 has the same restriction as equations 5.5 and 5.6. Q is the total load on the pad. The local settlement, s_0, can in this case be expressed as:

$$s_0 \approx 0{,}65 \cdot \frac{P}{M_*} \cdot \sqrt{\frac{B-x}{B}} \qquad (5.11)$$

5.3.3 Piled foundations

The neutral plane

When designing pile foundations, a critical issue is the distribution of the shaft friction. Fellenius et al., (1989) presented the concept of the neutral plane, which is a pragmatic way of determining the shaft friction. The basic principle is presented in Figure 5.2. The idea is to determine the level at which the pile movement is equal to the soil settlements, the neutral plane. Another consequence of the relative movement between the pile and the soil is that the shaft friction changes, from negative to positive, at the neutral plane. The level of the neutral plane is obtained by an equilibrium equation between the load and the reaction. The relation between pile load, bearing capacity and settlements is shown in Figure 5.3. The pile head settlement is calculated as the sum of the pile deformation above the neutral plane and the soil deformation below the neutral plane

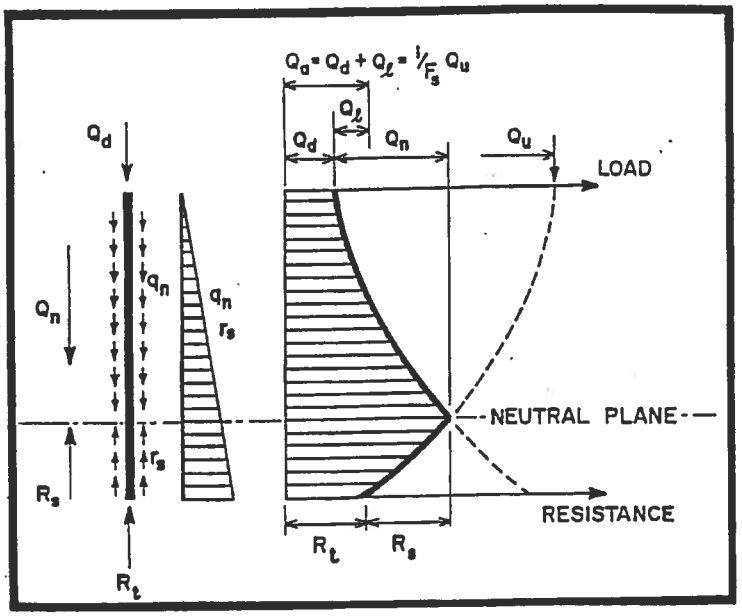

Notations in Figure 5.2 and Figure 5.3

q_n=negative shaft friction
r_s=(unit)shaft resistance
Qd=dead load
Q_n=drag load
Q_a=allowable load
Q_l=live load
Q_u=ultimate load
R_t=toe resistance
R_s=shaft resistance

Figure 5.2 Determination of the neutral plane. From (Fellenius et al., 1989)

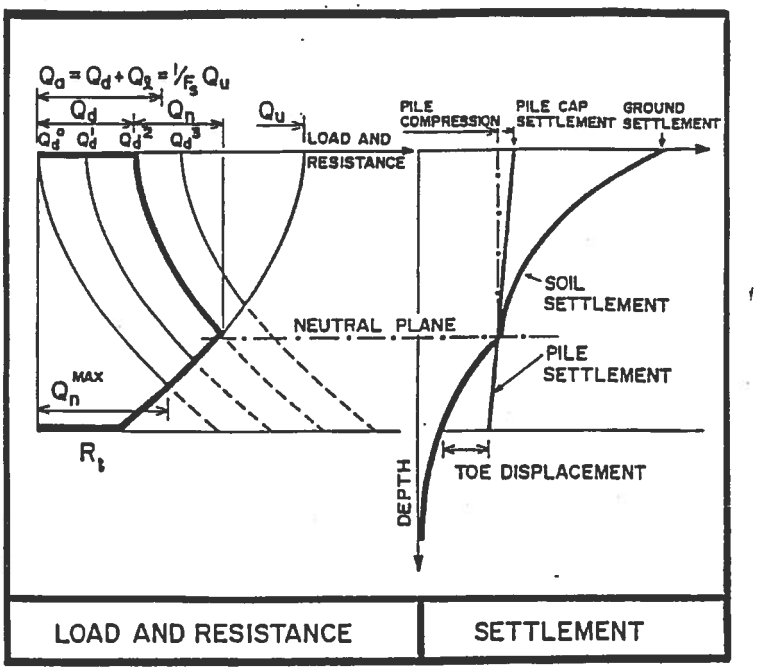

Figure 5.3 Pile load, bearing capacity as well as settlement as a function of the location of the neutral plane. From (Fellenius et al., 1989)

The key assumption in the foregoing reasoning is that settlements always will take place in the upper layers of the soil, caused by pile driving, changes in the water table etc. Even if this is not a proven fact, it can be shown that the neutral plane concept is a way to cal-

culate settlements on the safe side. Assume that a single pile influences a horizontal area of the soil, $A_{soil,,eff}$, and that the compression modulus of the soil is M, the product $M \cdot A_{soil,,eff}$ then describes the soil stiffness. In the same way, the pile stiffness can be described as the product of the cross-section area A_p and the module of elasticity, E_p. Assume further that the pile is stiffer than the soil, i.e. $E_p \cdot A_p > M \cdot A_{soil,,eff}$.[1] If, on the other hand, the soil is stiffer than the pile, the reason for a pile foundation is doubtful. Figure 5.4 shows the principle situation.

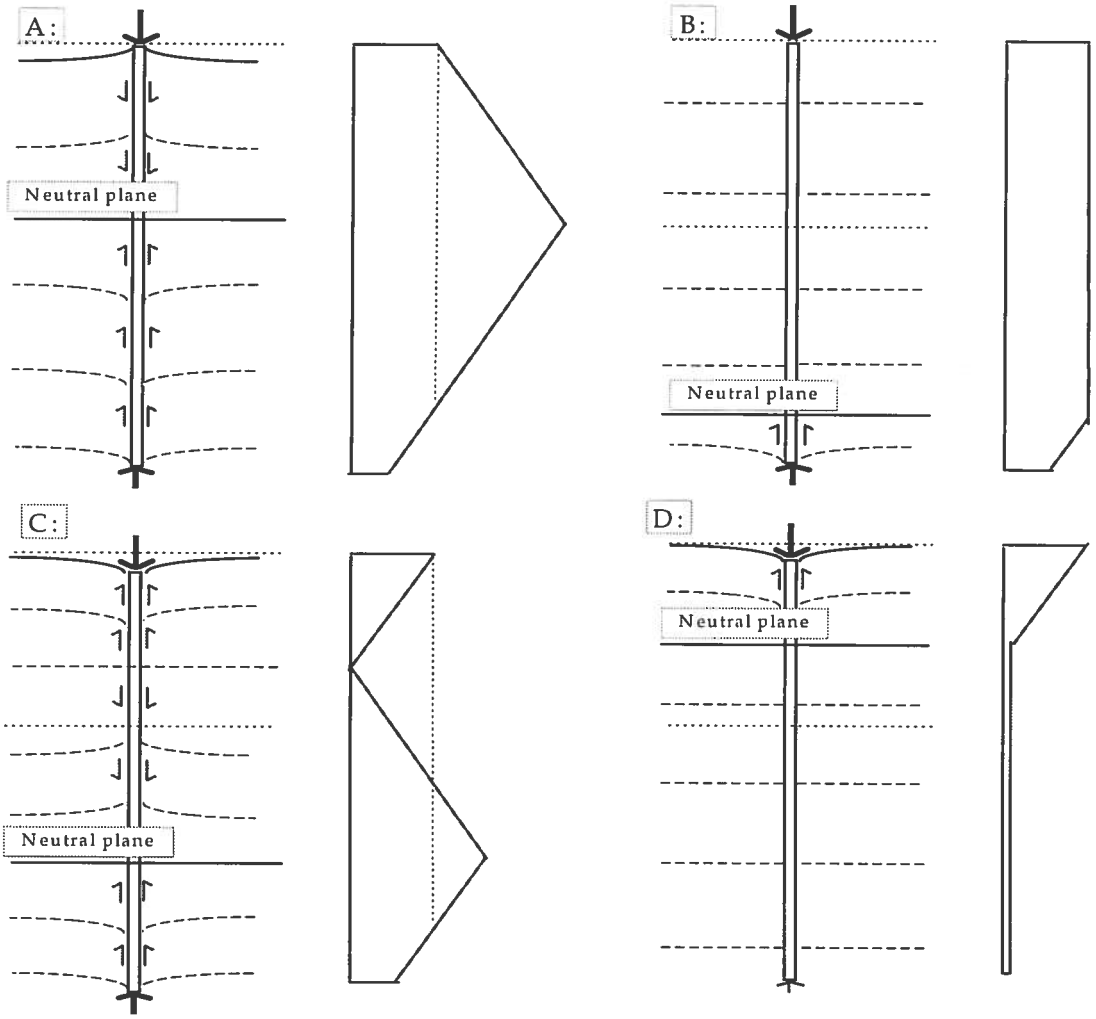

Figure 5.4 Soil movement versus pile and axial force in pile. Principle situations.

[1] Normally $E_p \cdot A_p >> M \cdot A_{soil,,eff}$. Timber piles in overconsolidated clay might for example be an exception.

Case A shows a situation normally assumed when applying the neutral plane concept. Settlement of the soil in the upper layers causes the soil to deform more than the pile. The negative shaft friction increases the axial force in the pile. However, the axial force can never exceed the bearing capacity of the pile in the underlying layers. Hence the location of the neutral plane is fixed. Case B shows the situation when no compression in the upper layers is assumed. The only difference compared to the situation in A, is that the neutral plane moves downwards and the total settlements become smaller[1]. In C is shown a situation in which the load at the pile head for some reason is distributed to the soil in the upper layers. This will cause deformation of the soil, and the lower parts of the pile/soil profile will react similar as the whole profile in A. The situation seems at a first glance to be physically unlikely. However, for example in a case of excavation, the soil will behave very stiffly for reloading up to the pre in situ stresses. This influence will not reach deep down into the soil. Thus a situation similar to the one in C might occur. The case will be captured on the safe side by the principle in A. Finally, in D is shown a situation when the whole soil profile is stiffer than the pile. The upper part of the profile will react similarly to the lower part of the profile in A. Below the neutral plane, the pile will move downwards together with the soil. The force in the pile and the stresses in the soil are proportioned in accordance with the corresponding stiffnesses. In this case the neutral plane will move upwards compared to case A. However, as mentioned before, there is normally not any reason for piling in this case, nevertheless, the situation can occur. Clay for example can behave very stiffly in an early phase of the consolidation.

The solution presented by Fellenius et al., see Figure 5.2 and Figure 5.3, is based upon a rigid/plastic model of the pile and soil. Matyas and Santamarina (1994) have extended the principle into an elastic/plastic model. In Alén (1997) both situations have been captured and expressions for the location of the neutral plane for different assumptions have been derived.

[1] At least if the soil modulus is constant or increasing with depth.

For case A in Figure 5.4 the depth to the neutral plane can be summarised as:

$$z_{Nf} = k \cdot (1-\eta) \cdot L \tag{5.12}$$

for a constant shaft friction f and as:

$$z_{Ng} = \sqrt{k} \cdot \sqrt{1-\eta} \cdot L \tag{5.13}$$

for an increasing shaft friction $f' \cdot z$.

In the above equations k is a constant in the range 0,5-1, with a reasonable average of $k \approx 0{,}7$. The degree of mobilisation, η, for the shaft is computed as:

$$\eta = \frac{S-R}{f \cdot L} \quad \text{and} \quad \eta = \frac{S-R}{f' \cdot \frac{L^2}{2}} \quad \text{respectively} \tag{5.14}$$

where S is the pile load at the head and R is the toe capacity.

Conventional piled foundations

The main reason for using piles for foundation is to transfer the actions from the superstructure down to deep, underlying, stiff layers. The principle of the neutral plane, discussed in the previous section, is then a very useful tool when calculating settlements of the pile head. In Alén (1997) closed forms for the settlements of single piles are derived. Mindlin's equation for a point at some depth of an elastic half sphere (see e.g. Terzaghi 1943) is then simplified as:

$$\sigma(x,z,d) = \frac{2 \cdot P}{\pi^2} \cdot \left[\frac{|z-d| \cdot (z-d)}{\left[(z-d)^2 + x^2\right]^2} + \frac{(z+d)^2}{\left[(z+d)^2 + x^2\right]^2} \right] \tag{5.15}$$

For a single pile, with constant shaft friction, the stress distribution is obtained as:

$$\sigma_P(x,z)=\frac{P}{\pi^2(L-z_N)}\cdot\left[\frac{\left(\begin{array}{l}\operatorname{atan}(\frac{L+z}{x})-\operatorname{atan}(\frac{z_N+z}{x})-\\ -\operatorname{atan}(\frac{|L-z|}{x})+\operatorname{atan}(\frac{|z_N-z|}{x})\end{array}\right)}{x}+\right.$$
$$\left.+\left(\begin{array}{l}\frac{z_N+z}{x^2+(z_N+z)^2}-\frac{L+z}{x^2+(L+z)^2}+\\ +\frac{|L-z|}{x^2+(L-z)^2}-\frac{|z_N-z|}{x^2+(z_N-z)^2}\end{array}\right)\right] \quad (5.16)$$

In application of equation 5.16, stress contributions for $x>2\cdot z$ can be omitted[1]. Similarly as for spread foundations, x is a horizontal coordinate and z is a vertical coordinate. For a single pile, with constant shaft friction, the settlement can be calculated as:

$$s_P(x)=\frac{1}{M}\cdot\int_{\frac{L+z_N}{2}}^{H}\sigma_P(x,z)dz \quad (5.17)$$

In equation 5.17 the settlements are integrated from a depth of $(L+z_N)/2$, which gives almost the same result as if the settlements are integrated from z_N but negative stress contributions are omitted.[2] As the unloading modulus normally is much larger than the loading one, this may be seen as a reasonable principle.

[1] The integral for a part of a plane, the circle with $r=2z$ is:
$2\cdot\pi\cdot\int_0^{2\cdot z}\sigma(x,z,d)\cdot x\,dx\approx P$, i.e. overall equilibrium.

[2] In application of equation 5.17 it is assumed that the same value of the modulus is used for both positive and negative stress contributions.

If equation 5.16 is combined with equation 5.17 a closed form for the settlement is obtained:

$$s_p(x)=\frac{P}{\pi^2 M\cdot(L-z_N)}\cdot\left[\frac{\left(\begin{array}{l}(3z_N+L)\text{atan}(\frac{3z_N+L}{2x})-(3L+z_N)\text{atan}(\frac{3L+z_N}{2x})-\\-2(z_N+H)\text{atan}(\frac{z_N+H}{x})+2(L+H)\text{atan}(\frac{L+H}{x})+\\+2(z_N-H)\text{atan}(\frac{z_N-H}{x})+2(L-z_H)\text{atan}(\frac{L-z_N}{2x})-\\-2(L-H)\text{atan}(\frac{L-H}{x})\end{array}\right)}{2x}+\right.$$
$$\left.+\left(\begin{array}{l}\ln\left[4x^2+(3L+z_N)^2\right]-\ln\left[4x^2+(3z_N+L)^2\right]+\\+2\ln\left[4x^2+(L-z_N)^2\right]-\ln\left[4x^2\right]+\\+\ln\left[x^2+(L-H)^2\right]+\ln\left[x^2+(z_N+H)^2\right]-\\-\ln\left[x^2+(L+H)^2\right]-\ln\left[x^2+(H-z_N)^2\right]\end{array}\right)\right] \qquad (5.17a)$$

with the natural restriction x>½ width of pile element. In accordance with equation 5.16, the equation above can be restricied to $x<2\cdot H$.

Pile groups can be seen as deep, spread foundations, i.e. the piles and the soil in a group are treated as a rigid bloc. The principle of the neutral plane applied on a single pile can then be used to determine the foundation level for the bloc. In analogy with equation 5.17, the level can be approximated as $(L+z_N)/2$.

Piled rafts

In this type of foundations the actions are transferred to the soil partly by the raft and partly by the piles (see e.g. Jendeby, 1986). Thus they can be categorised as a class of piled foundations being somewhere between spread foundations and piled foundations. They are efficient designs in those cases when the soil capacity is sufficient to carry only part of the actions from the superstructure. The most important feature for a successful design is that the piles are long enough to transfer the actions to sufficiently deep layers. This fact can be illustrated by the result from calculations for four case histories of foundations in slightly overconsolidated clay. The data for the calculations are taken from four case studies described

in Jendeby (1986). The four examples are similar in many respects. In all four cases, friction piles are used for the foundation of multi-storey buildings. Excavations were made for the basements. Thus there is a net action effect, which is considerably smaller than the gross action effect. The data for the four buildings are summarised in Table 5.1.

	Olskroken 1	Olskroken 2	Enköping	Uppsala
p_{gross} [kN/m²][1]	66	62	53	56
p_{net} [kN/m²][2]	22	11	21	33
η_{gross}[3]	0,47	1,55	3,57	1,43
η_{net}	0,16	0,28	1,41	0,84
Pile length [m]	28	26	13	25
Soil depth [m]	50	50	18	35
Width of building [m]	14	12	11	14
Area of building [m²/pile]	3,3	9,1	7,7	11,1
Neutral plane [m]	16	13	[< 0]	3
OCR	1,1	1,1	1,1	1,0-1,2
M_0 [kPa][4]	80+240z	80+240z	1500+147z	1000+166z max 2000
M_L [kPa][5]	60+48z	60+48z	500+59z	1000

[1]Total weight, [2]Excl. excavation, [3] 'Degree of mobilisation', total weight and net weight resp.
[4] Below preconsolidation pressure, [5] Above preconsolidation pressure

Table 5.1 Data for four case studies. Based upon (Jendeby, 1986)

As can be seen in Table 5.1, there is a distinct difference among the four cases. For the first building, Olskroken 1, the pile capacity is sufficient to carry the total weight of the building, without respect to the excavation. For the second building, Olskroken 2, the pile capacity is sufficient for the net weight but not for the gross weight. In Enköping, the capacity is too small to carry the net weight. Finally, in the last case, Uppsala, the capacity is just enough to carry the net weight. For all of the buildings, except Olskroken 1, the capacity is too small to carry the gross weight. Thus, the foundations for the last three buildings fulfil the definition of a piled raft.

The efficiency of the piling for the four buildings can be seen in Figure 5.5. In the figure are given the results of settlement calculations without considering the piles. The black, solid lines show the long term settlement. The calculations are based upon equation 5.3 and the data in Table 5.1. For the third case, the effect of a fill on the

side of the building is also included. This is assumed as a surcharge of 40 kN/m². The dotted lines in the figure show the results of long term field observations. These curves are simplified compared to the data presented by Jendeby (1996) but show the basic pattern. Finally the lengths of the piles are also illustrated by thick grey lines.

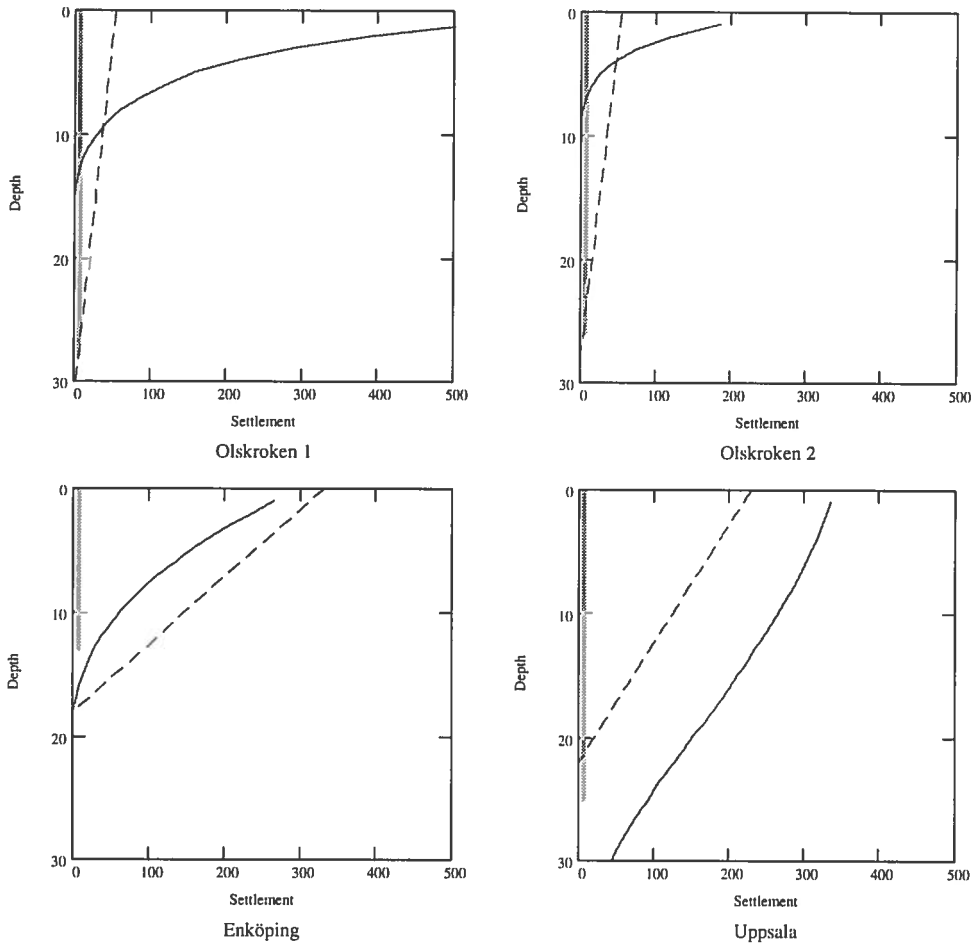

Figure 5.5 Comparison of computed settlements, without respect to the piles (——) and results from long term field observations (- - -). Pile length

As can be concluded from the figures, Olskroken 1&2 can be regarded as successful designs. The piles are long enough to transfer the actions to stiffer layers and the settlements are considerably reduced by the piles. The results of the piling in Enköping and Uppsala are not that efficient. The piles are short and only redistribute the actions into layers, which would be affected by the actions even if no piles were used.

In each case the frame of the buildings forms a stiff superstructure. Thus the whole foundation can be regarded as a pile group. The

principle of the neutral plane can be applied. Two extreme assumptions are investigated. In the first alternative A, the action effects of the net weight are applied at a depth of $(L + z_N) / 2$, cf. page 17. In the second alternative B, the action effects of the gross weight are applied at a depth of $(L + z_N) / 2$, while the unloading caused by the excavation is applied at the raft level, see Figure 5.6.

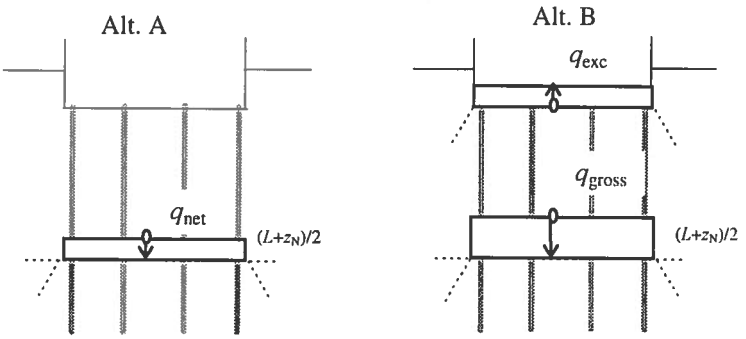

Figure 5.6 Principles of application of load. Alt. A and alt. B respectively.

The result of calculations, using the data in Table 5.1, is presented in table 5.2. In the table are also shown extrapolations of long term field observations.

	Olskroken 1	Olskroken 2	Enköping [1]	Uppsala
Alt. A [mm]	40	20	200[2]	185
Alt B[mm]	90	80	340[2]	245
Observ.[mm][3]	52	53	330	230
[1]Incl. fill, [2] Based upon M_L, [3]Extrapolation of 10-15 year values (Jendeby, 1996)				

table 5.2 Comparison of computed settlements, with respect to the piles and results from long term field observations.

As can be seen in the table, there is a rather good agreement between computed and observed values[1]. In all the four cases the observed values fall between the calculated values. For Olskroken 1 & 2 the conditions are rather indisputable and the application is straightforward. However, Uppsala is not that simple. The preconsolidation situation is not to easy to interpret (see Jendeby, 1986). The results are very sensitive to the chosen value of the compression modulus. The good agreement might be a pure coincidence. For Enköping finally, it can be questioned whether the calculation prin-

[1] The calculated values are based upon a very simple model. Hence they should just be seen as an indication of the effect of piling compared with a no piling alternative, cf. Figure 5.5.

ciples are applicable at all. A conclusion, which might be drawn from the results, is that the two designs of Olskroken 1 & 2 are basically similar. The two major factors governing the design are the length of the piles and the degree of mobilisation for the net weight. The degree of mobilisation for the gross weight seems to be of minor importance.

5.4 Time dependence

5.4.1 General

A special complication when calculating the interaction between the ground and the superstructure is that the soil behaviour is time dependent. This is particularly valid for foundations on clay. Long term settlements are delayed due to the consolidation process in the soil, that is the outflow of pore water and the corresponding compression of the clay. The low permeability of the soil makes this a very slow process. Thus there will be a long time until the elastic/plastic deformation will reach its final value. The clay is also prone to creep, i. e. deformation which develops over time for a constant level of effective stresses[1]. This means that the settlements will not reach any final stage during the life time of a structure. Even structural materials, such as concrete and timber, show time dependent behaviour but of a much lesser significance. For the latter material, the behaviour can often be treated with simple stereotyped assumptions. Hence, structural mechanic methods are rarely developed to handle this sort of problems for soil.

5.4.2 Classical theory of consolidation

Terzaghi derived a differential equation for one-dimensional consolidation in clay (see e.g. Terzaghi, 1943):

$$\frac{\partial u}{\partial t} = \frac{k \cdot M}{\gamma_w} \frac{\partial^2 u}{\partial z^2} \tag{5.18}$$

Creep behaviour of the soil is not accounted for in the equation. Terzaghi and Fröhlich presented solutions of the differential equation using the concept degree of consolidation, *U*. This concept describes the amount of settlements which has occurred after a cer-

[1] This is the strict definition used traditionally in solid mechanics, see e.g. (Hult, 1968). In soil mechanics the term is often defined less strictly.

tain time compared to the final consolidation settlements. The results were presented in graphs for different boundary conditions, see Figure 5.7. The three curves in the figure represents different consolidation pressures, i.e. the excess pore pressures, which will be transmitted to effective stresses during the consolidation process, see Figure 5.8.

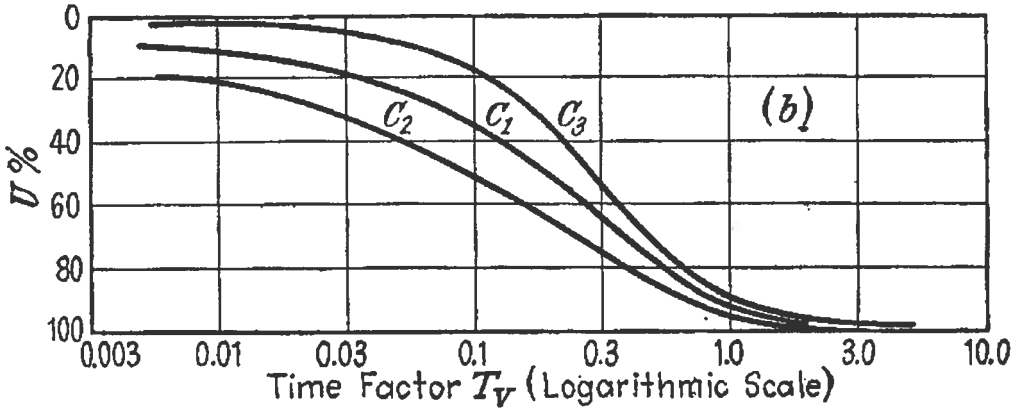

Figure 5.7 Degree of consolidation as a function of time. Time is represented by a dimensionless time factor. From (Terzaghi, 1943).

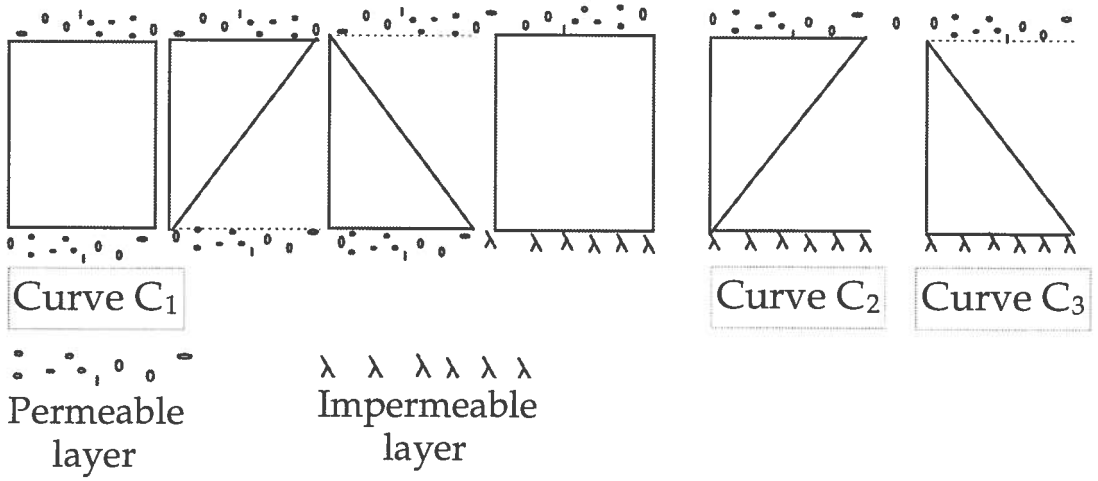

Figure 5.8 Initial and boundary conditions for the three curves in Figure 5.7.

The three curves in Figure 5.7 can be described analytically, with sufficient accuracy, with the following formulas:

$$U_{C1} = \begin{cases} 1{,}15 \cdot \sqrt{T_v} & \text{if } T_v < 0{,}2 \\ 1 - 0{,}8 \cdot e^{-2{,}5T_v} & \text{if } T_v > 0{,}2 \end{cases} \qquad (5.19\text{ a})$$

$$U_{C2} = \begin{cases} 1{,}2 \cdot T_v^{\frac{3}{8}} & \text{if } T_v < 0{,}16 \\ 1 - 0{,}6 \cdot e^{-2{,}6T_v} & \text{if } T_v > 0{,}16 \end{cases} \qquad (5.19\text{ b})$$

$$U_{C3} = \begin{cases} 2 \cdot T_v & \text{if } T_v < 0{,}1 \\ 1 - 1{,}05 \cdot e^{-2{,}6T_v} & \text{if } T_v > 0{,}1 \end{cases} \qquad (5.19\text{ c})$$

$$U_{C3} = \begin{cases} 1{,}2 \cdot T_v^{\frac{3}{8}} & \text{if } T_v < 0{,}16 \\ 1 - 0{,}8 \cdot e^{-2{,}5T_v} & \text{if } T_v > 0{,}16 \end{cases} \qquad (5.19\text{ c})$$

The three equations 5.19 a-c are taken from Alén (1998b). Equation 5.19 is a reformulation of a solution of the form $T_v = f(U)$, given by Terzaghi (1943)

The classic solutions presented in the previous paragraph were derived for soil conditions with constant parameters over depth. However, they are often used in cases with a moderate variation of the soil properties. The soil parameters have, in these cases, to be taken as average values over depth. Janbu (1970) showed that in such cases it is preferable to choose the curve from the pattern of the distribution of final strain. If the compression modulus is constant with depth, the pattern of the consolidation pressure will of course coincide with the pattern of distribution of the final strain.

5.4.3 Creep parameters

Creep deformation develops with a decreasing rate over time. A common observation, reported in the literature, is that the creep deformation can be represented with a straight line in a strain/time graph, if the time is plotted in a logarithmic scale. Hence, the derivative, $\frac{\partial \varepsilon_{cr}}{\partial \ln(t)}$, is constant

Janbu (1969) introduced a creep number, r, such that :

$$\frac{\partial \varepsilon_{cr}}{\partial \ln(t)} = \frac{1}{r} \tag{5.20}$$

Creep effects have since long time been described with a coefficient of secondary consolidation, α_S, such that (see e.g. Hansbo, 1994):

$$\frac{\partial \varepsilon_{cr}}{\partial \log(t)} = \alpha_s \tag{5.21}$$

Equation 5.21 can be rewritten as:

$$\alpha_s = \frac{\partial \varepsilon_{cr}}{\partial \log(t)} = \frac{\partial \varepsilon_{cr}}{\partial \ln(t)} \cdot \frac{\partial \ln(t)}{\partial \log(t)} = \frac{\partial \varepsilon_{cr}}{\partial \ln(t)} \cdot \ln(10) \tag{5.22}$$

Combining equation 5.20 and equation 5.22 gives the following relations between α_s and r:

$$\alpha_s = \frac{\ln(10)}{r} \approx \frac{2{,}3}{r} \quad \text{or} \quad r = \frac{\ln(10)}{\alpha_s} \approx \frac{2{,}3}{\alpha_s} \tag{5.23}$$

Thus the two concepts, creep resistance number and coefficient of secondary consolidation, basically describe the same soil property.

In Christensen (1995) empirical observations of creep parameters are presented. It includes both Norwegian references and data observed from Swedish clays (for the latter see e.g. Larsson, 1986). A plot of the observations is shown in Figure 5.9. The values plotted are the values at the preconsolidation pressure[1]. This is from experience the minimum value interpreted from an oedometer test (Janbu, 1989). From Figure 5.9, solid line, it can be seen that a good estimation of the creep number is:

$$r = \frac{75}{w^{1,5}} \tag{5.24}$$

where w is the natural water content.

[1] As interpreted in e.g. Norway. That is $p'_{c,sup}$ in figure XX, Appendix P.

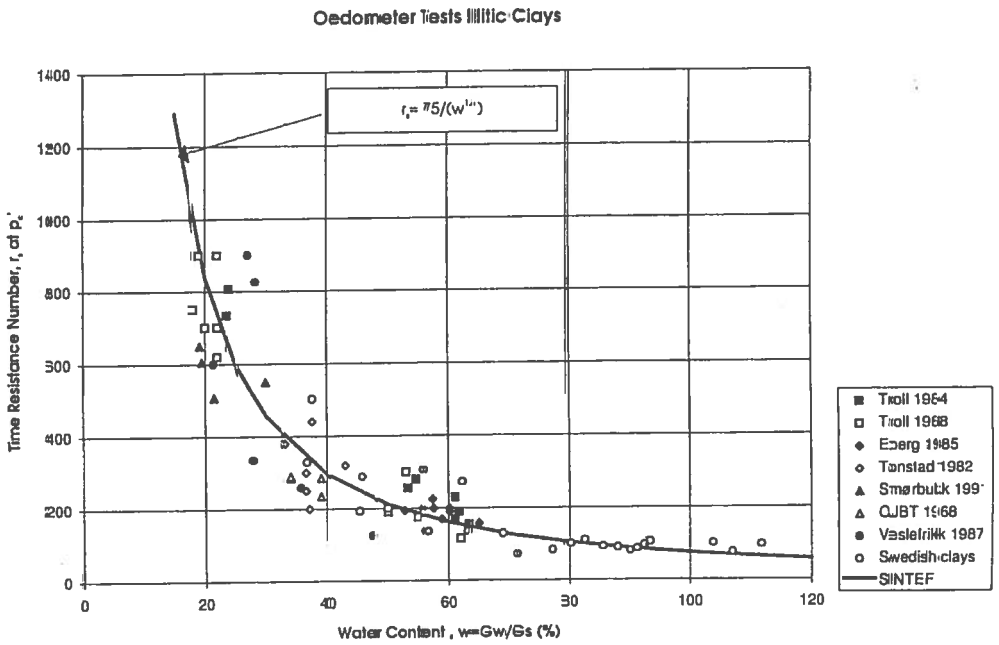

Figure 5.9 Creep number r as a function of the natural water content. From (Christensen, 1995).

5.4.4 A Creep model

In appendix P is presented a calculation model for creep deformation. It is aimed to be a tool in engineering practice, not a detailed scientific presentation. As a starting-point it is assumed that the calculation of the creep deformation is not too complex a problem. It is based on a hypothesis that the time dependent deformation in clay can be described sufficiently by three separate physical phenomena:

- Consolidation - Deformation of the clay due to dissipation of pore water
- Elastic/plastic deformation - Strain, which arises immediately due to a stress increment
- Creep deformation - Strain, which occurs over time at a constant stress level

The interaction of these phenomena is assumed to be described by a rheological model, see Figure 5.10.

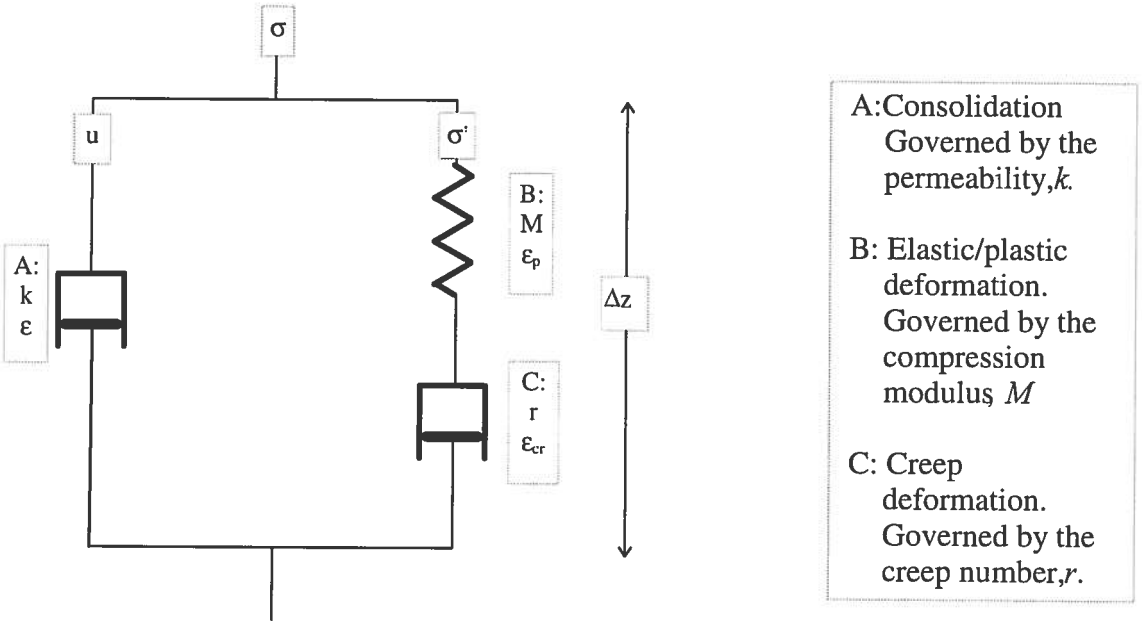

Figure 5.10 Rheological soil model describing long term deformation in clay

The term consolidation is in the model restricted to the strain settled by the outflow of pore water. If both the water and the solids of the soil are considered incompressible, this strain is equal to the total strain for a saturated clay. The definition is in accordance with a general definition of consolidation, see e.g (Terzaghi, 1943). In classical theory, when creep is not considered, the interaction of A and B in Figure 5.10 governs the consolidation, thus such a theory can be called a theory of consolidation. However, in the model described here, it is the interaction of all three phenomena, A, B and C, in Figure 5.10, that governs the consolidation, which means that any separation of A and B compared to C has no relevance. On the other hand, in parallel to what is said above, the theory for the complete model might me called a theory of consolidation. It could also be remarked that the two concepts often used, primary consolidation, "A+B", and secondary consolidation, "A+C", are irrelevant in the proposed model.

By geometrical compatibility, the strain can be seen as a sum of the two sub strains, $\varepsilon = \varepsilon_{pl} + \varepsilon_{cr}$. Hence, a differential equation is established, i.e. the model is based upon an equality of strains. A key factor to solve the model is a separation of the creep strain into constrained and unconstrained strain. With constrained strain is here understood a creep strain, which develops at a reduced strain rate compared to the rate given by the creep number, cf. equation 5.20.

The strain rate is instead governed by the outflow of pore water, i.e $\frac{\partial \varepsilon_{cr}}{\partial t} \leq \frac{\partial \varepsilon}{\partial t}$.

Here two different ways of solving the differential equation describing the rheological model in Figure 5.10 have been used:

- A finite difference scheme, named method A below.
- An explicit analytical solution, " " B " .

Larsson et al. (1994) describe a computer program, EMBANCKO, for prediction of long term settlements in soft soil. It is based on a another computer program, Conmult, originating from Laboratoires des Ponts et Chaussées in Paris (Larsson, 1986). In EMBANCKO finite differences are used to solve the problem. The solution scheme is based on equilibrium of stresses. The change of pore pressure is the sum of two calculations for each time step, first a primary calculation by the classical theory of consolidation, see equation 5.18, then a re-adjustment of the pore pressure due to the creep effects. In Figure 5.11, the results of a comparison between method A & B and EMBANCKO are presented.

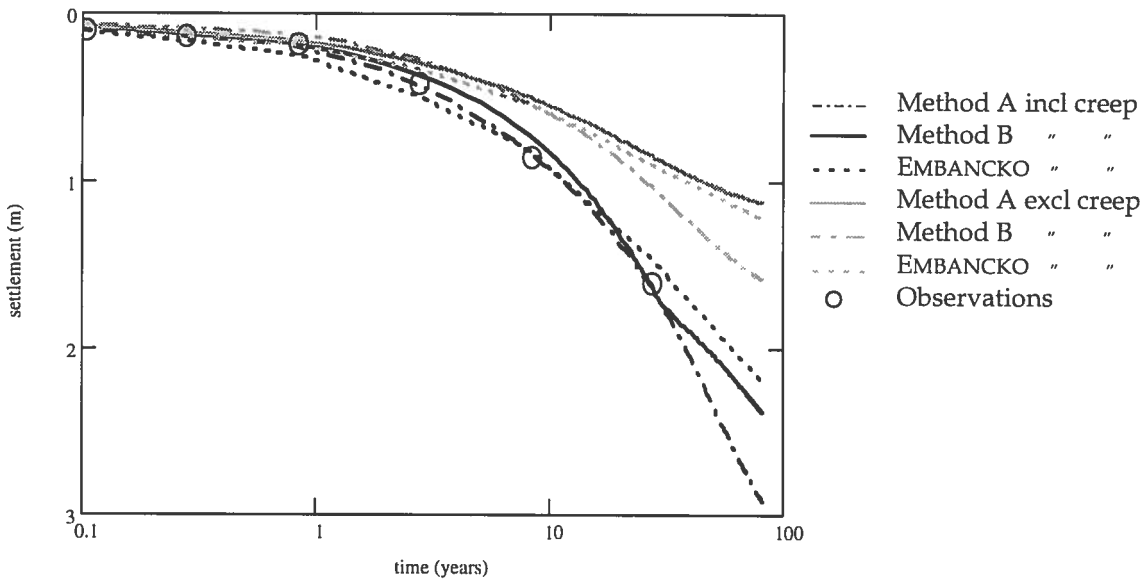

Figure 5.11 Calculated and observed settlements from a test field at Lilla Mellösa. From (Alén, 1998b) and (Larsson, 1986).

The results in Figure 5.11 are based on data from a test field at Lilla Mellösa (Larsson, 1986). In the figure results from calculations both

including creep effects, black lines, and without creep effects, grey lines, are given. The results of the calculations are also compared to field observations. Method A gives somewhat larger settlements after a long time in this case. The explanation of this fact is that settlements below the ground water table, i. e. for a reduced surcharge, are not considered for method A. Apart from this there is a good agreement between the different methods. This is to be expected as they are mainly based upon the same physical assumptions.

In Svanø et al. (1991) a finite element program, KRYKON, is briefly described. It is a finite element program for computation of consolidation and creep. The basic rhelogical assumption is that all strains are creep strain, with a strain rate in accordance with equation 5.20 (Svanø et al., 1988). This assumption may appear to be in contrast with the rheological model described in Figure 5.10. However, elastic/plastic deformation is in that model given a pragmatic definition as strain developing faster than in a reference test (cf. appendix P). Hence elastic/plastic deformation might be seen as creep strain developing faster than a given strain rate (cf. Larsson, 1986). In KRYKON, for each time step, an iterative approach is used to calculate the change in effective stress/pore pressure and, due to the creep effects, an equivalent, softer soil stiffness (Nordal, 1993). Results obtained by KRYKON are compared to calculations with method B, see Figure 5.12.

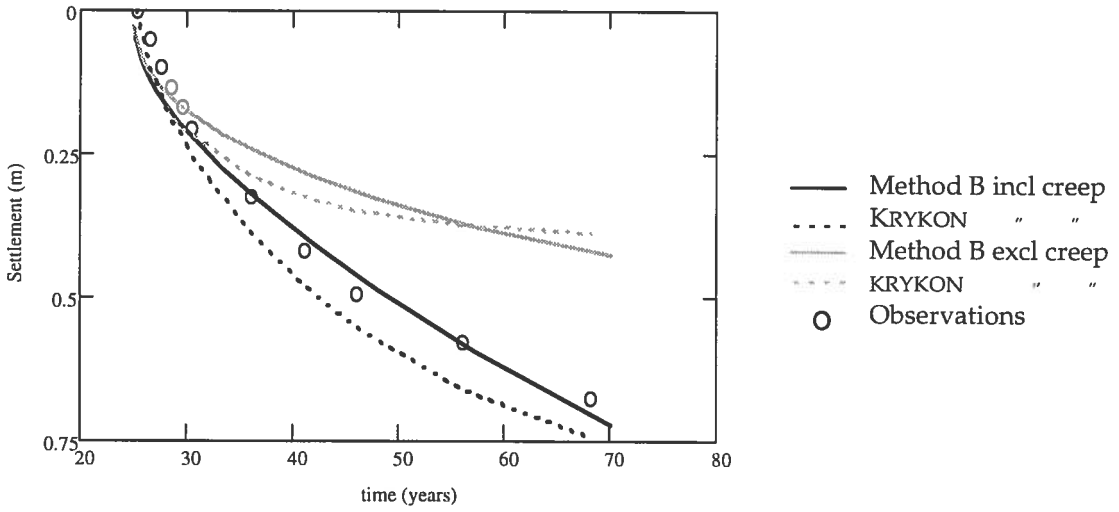

Figure 5.12 Oslo railroad customs building. Calculated and observed settlements. From (Alén, 1998b) and (Svanø et al., 1991).

The calculations, made with method B in this case, are primarily based upon a concise presentation of the case record given by Svanø et al., (1991). However, some additional information from the authors regarding the increase of the compression modulus with depth is accounted for, cf. page 23. There is an overall acceptable agreement between the two methods. The differences might be explained by the lack of detailed information in the application of method B.

The advantage of the calculation model, resulting in method A and B, is the simplicity by which it can be applied to different problems. Both solution alternatives can for example easily be incorporated in a spread sheet program. The analytical alternative, method B, is most simple. However, the result is restricted to the average conditions in a soil profile, i.e. the same level of "resolution" as is obtained with the degree of consolidation in classical theory, see page 22. With the finite difference scheme, method A, more details can be predicted.

5.5 Stiffness of the supports

5.5.1 Spring support

The simplest model for a flexible support is a traditional spring. The stiffness of a spring i is defined by the relation between the reaction R_i and the deformation s_i:

$$R_i = S_i \cdot s_i \tag{5.25}$$

where S_i is the stiffness. In serviceability limit state design, the stiffness can normally be regarded as a constant property. The term constant refers here to a situation where the modulus of the soil is independent of the stress level, which does not prevent the stiffness from being modelled as a random variable.

A complication in foundation in clay arises if the stresses pass the preconsolidation pressure. In Figure 5.13 three different ways of describing the relation between stresses and strains and a corresponding deformation modulus are illustrated.

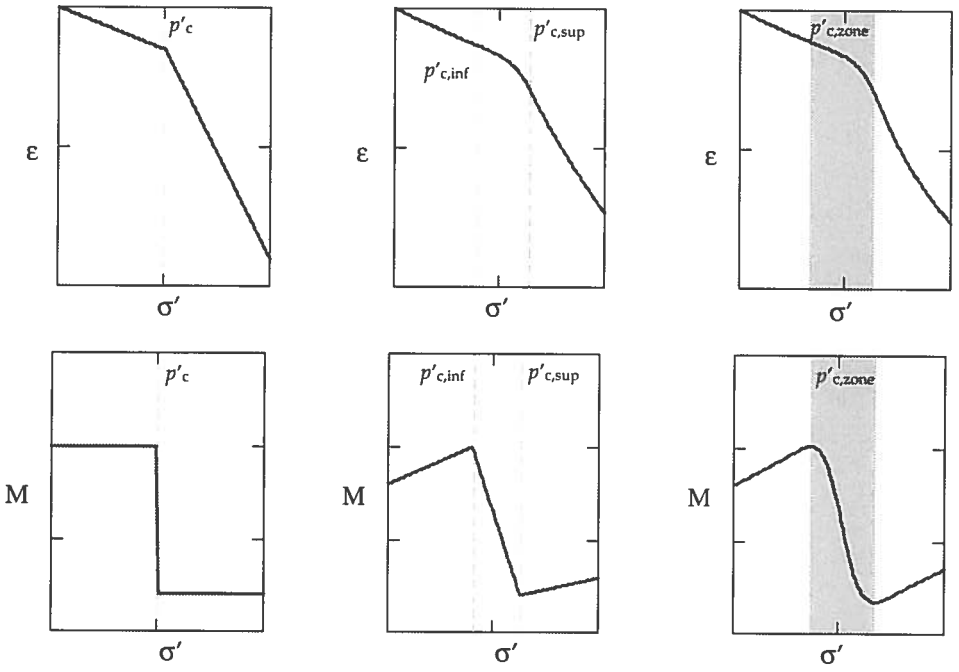

Figure 5.13 Different descriptions of the stress-strain relation and the corresponding compression modulus for clay.

To limit the complexity of the analysis, a description as in the left plot has normally to be chosen in the analysis of interaction between ground and superstructure, i.e. to base the stiffness of a support upon a single value of the soil modulus. However, when choosing an appropriate value of the stiffness, the choice can be based upon a more detailed analysis of the deformation for the stress increment at hand. This implies that the modulus is chosen as a secant modulus $M_s = \Delta\sigma'/\Delta\varepsilon$, see Figure 5.14.

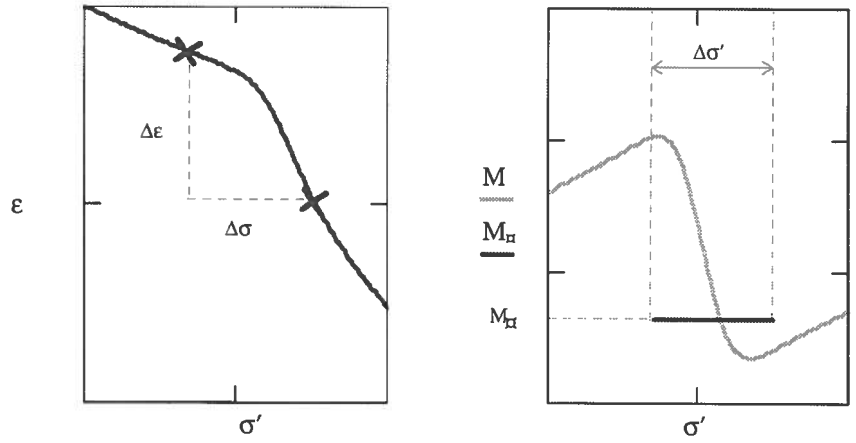

Figure 5.14 Determination of a secant value $M_s = \Delta\sigma'/\Delta\varepsilon$ of the soil stiffness for a given stress increment $\Delta\sigma'$.

5.5.2 Time influence

Another complication in clay foundation is the time dependence of the deformations. This dependence can in 'classical theory' be described with the principle formula for the settlements:

$$s(t) = U(t) \cdot \frac{P}{S} \tag{5.26}$$

where P is action at a support, S is the 'secant' stiffness chosen as above and $U(t)$ is a function describing the time dependence. The interaction analysis can then be undertaken for different points of time by applying a time dependent stiffness:

$$S(t) = \frac{S}{U(t)} \tag{5.27}$$

If the conditions for the consolidation are equal at all supports, this means that the relation between the stiffness of the supports is unchanged by the degree of consolidation. For a case when the superstructure is treated as a rigid body, this means that the reactions, but not the deformations are constant over time. For one dimensional consolidation, $U(t)$ is given by classical consolidation theory, cf. section 5.4.2 and appendix P. For two or three dimensional consolidations the situation becomes more complex. An approximate way to deal with the situation of both vertical and horizontal pore water flow is to use Carillo's formula for the compound degree of consolidation (see e.g. Hansbo, 1994):

$$U = U_v + U_h - U_v \cdot U_h \tag{5.28}$$

where the indices v and u denote pore water flow in the two different directions.

By the model for creep effects given in appendix P, equation 5.26 is altered into:

$$s(t) = U_{cr}(t) \cdot \frac{P}{S} + s_{cr}(t) \tag{5.29}$$

in which the elastic/plastic deformations are given by the first term and the creep deformations by the second term[1]. Hence, the 'degree

[1] Note, this separation is not equal to a separation into primary consolidation and secondary consolidation, cf. appendix P.

of consolidation' $U_{cr}(t)$ is a measure of the time dependence of the elastic/plastic deformations with respect to creep. It can be separated into two factors, $U_{cr} = \eta_{cr} \cdot U_0$, where U_0 is the classical degree of consolidation and η_{cr} is a creep consolidation ratio, which is a measure of the delay of the elastic/plastic deformations of the consolidation due to the creep effects. In appendix P, explicit formulations of the terms in equation 5.29 are given. It is shown how the deformations are governed by three dimensionless factors, the classical time factor T, cf. Figure 5.7, the creep number r, see equation 5.20, and a strain rate factor, $\psi = M/(r \cdot q)$. M is an average value of the compression modulus and q is an average value of the consolidation pressure, i.e. the initial excess pore pressure.

As can be seen from equation 5.29, a time dependent equivalent stiffness, cf. equation 5.27, can not be obtained easily as one part of the deformation is independent of the reaction. In the interaction analysis this effect can be incorporated in the analysis by prescribing an 'initial' deformation at each point of time analysed. For homogeneous soil conditions and equal depth of soil layers, this 'initial' deformation will be the same at all supports. Thus, they will not affect the magnitude of the reactions, i.e. the only influence on the analysis will be on the deformations.

5.5.3 Piled supports

In the context at hand, i.e. the stiffness of piled supports, three types of deformation have to be considered.

- Strains in the piles.
- Displacements at the shaft between the pile and the soil.
- Strains in the soil.

By the concept 'the neutral plane', see section 5.3.3, the displacements between the pile and the soil are eliminated from the analysis.

For end-bearing piles, the neutral plane is situated at the toe level. Hence, in this case, the strains in the soil, surrounding the piles, are eliminated from the analysis. An appropriate stiffness of the support is obtained from equation 5.25, in which the deformation is

summed up as the pile deformations and the deformations in the soil beneath the pile. The latter are often of minor importance. In the same way, time effects can normally be ignored.

For shaft-bearing piles, the neutral plane concept reduces the analysis to a question of an appropriate foundation level, cf. equation 5.17. In this case, the strains in the soil beneath the neutral plane mostly govern the design, while the pile deformations are of minor concern. Time effects can be considered in accordance with the principles outlined in the previous section.

5.6 Random models

5.6.1 General

In section 5.2, the design situation for deterministic modelling of ground/superstructure interaction is outlined. If the interaction is to be calculated in a realistic manner, rather complicated models have to be adopted[1]. This often results in a design solution with a deterministic calculation without considering any interaction between the ground and the superstructure. Only the results are judged from an interaction point of view. The uncertainty in such a design procedure is obvious. One of the purposes of this thesis is to present as simple models as possible, from a ground/superstructure interaction point of view, to facilitate the use of a random modelling technique. However, the problem is indeed complicated and a certain lack of precision in the results should be expected. It might be convenient to quote a standpoint from the British Institution of Structural Engineers: "Any design that relies for its success on precise analysis is a bad design" (Payne, 1995). Below results of calculations for all the three different levels of calculation are presented. They are basically different solutions for the same structural problem, that is the foundation for a building with a cross-section of two spans, see Figure 5.15. The width of the building is assumed to be small compared to the length. Hence, the analysis can be restricted to a 2-D analysis. All values given in coming sections are applicable to a unit length of the building in longitudinal direction.

[1] This is with the exceptions of cases in ultimate limit state when limit design can be applied, see section 2.1.2.

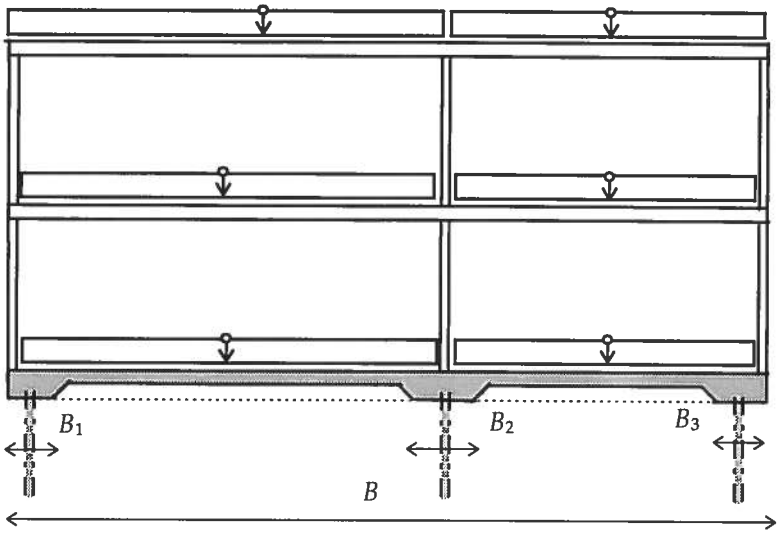

Figure 5.15 Cross-section of analysed building.

The structure of the analysed foundation is deliberately chosen to be very simple. Hence the principles of the different methods of analysis can be illustrated, without the risk that the complexity of the problem will hide the basic ideas. In a general case, the principles can be extended to an arbitrary, elastic structure. For the probability analysis Monte-Carlo simulation is chosen. The interaction problem is as mentioned above a serviceability limit analysis. Hence only moderate values of probability of failure have to be accounted for, a fact that reduces the number of iterations demanded. In the analyses undertaken 1000 iterations are used in each case. Furthermore, in serviceability analysis any distinct failure limits do not exist normally, which means that reliability analysis[1] as outlined in section 2.4.4. is less suitable compared with Monte-Carlo simulation. Finally, PEM-calculation does not offer any specific advantages compared with Monte-Carlo simulation in this case, as the problems are rather easy to programme. However, for more complex structures, in which one wants to take advantage of existing computer soft-ware. PEM might offer the only alternative in a practical case.

[1] This type of analysis is suitable to answer a 'question' with yes or no, i.e. safe or not safe.

5.6.2 Application of a level 1 method

Rigid superstructure - Flexible supports

In section 5.2.1 different levels of complexity of calculation models were discussed. For the simplest level the models were separated into two main groups, rigid supports or rigid superstructure. The first principle is very common in daily practice. However, from a geotechnical point of view it does not offer much challenge[1]. The second alternative combined with flexible supports can be a very useful geotechnical model. Different aspects of such an application are discussed below. The principle apperance of the interaction model is shown in Figure 5.16.[2] In appendix Q formulas for the applied model is given. Three different types of analysis are performed:

- A Spread foundation. Long term settlements without respect to creep.
- B Spread foundation. Time dependent settlements including creep
- C Piled foundation. Long term settlements without respect to creep.

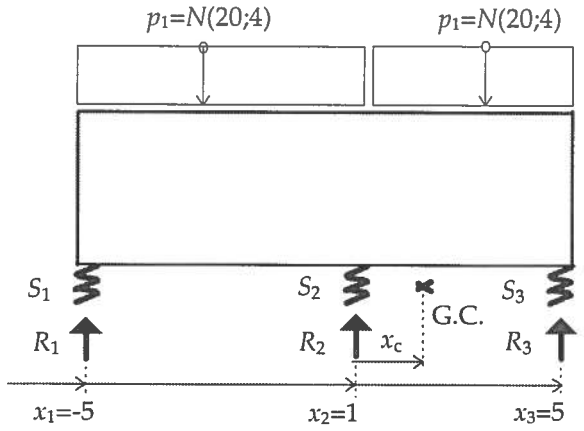

Figure 5.16 Interaction model. Rigid superstructure / Flexible supports.

[1] A complex superstructure might be a challenge for a structural engineer.
[2] All values given are applicable for a unit length of the building in longitudinal direction.

A Long term settlements without respect to creep.

The problem is basically very simple. The only input data needed is the location of the supports, the load on the building and the stiffness of the supports. If only the reactions are of interest the relation between the stiffnesses is sufficient. The stiffness of a support is calculated as:

$$S_i = \frac{P}{s(0)} \tag{5.30}$$

where P is an applied action and $s(0)$ is the corresponding settlement, in this case determined by equation 5.9. In Table 5.3 input data is given.

	H [m]	B_1 [m]	B_2 [m]	B_3 [m]	
Fixed	20	1	1.5	1	
Random	p_1 [kN/m²]	p_2 [kN/m²]	M_1[kN/m²]	M_1[kN/m²]	M_1[kN/m²]
μ	20	20	800	800	800
V [%]	20	20	30	30	30
Type	N	N	LN	LN	LN

Table 5.3 Input data. Case A. Long term reactions and settlements.

The load of the two spans are set to be independent of each other. This may seem to be unjustified as at least the dead load can be assumed to be highly correlated, while it is more natural to regard the variable loads as uncorrelated. However, if the variance of the dead load is negligible, the total load is a sum of a fixed part and a random part of which only the latter, independent part has any influence on the covariance. Hence the correlation can be set to zero. For the stiffness of the supports it is assumed that the coefficient of correlation for the compression modulus is 0,5 between the different supports. Hence the correlation can be summarised as in Table 5.4.

	p_1	p_1	M_1	M_2	M_3
p_1	1	0	0	0	0
p_1	0	1	0	0	0
M_1	0	0	1	0,5	0,5
M_1	0	0	0,5	1	0,5
M_1	0	0	0,5	0,5	1

Table 5.4 Correlation matrix. Case A. Long term reactions and settlements.

The simulation gives the following result for the stiffness of the supports.

	S_1[kN/m]	S_1[kN/m]	S_1[kN/m]
μ	281	317	280
V[%]	22	22	21
	S_1/ S_2	S_1/ S_3	S_2/ S_3
Correlation	0,5	0,5	0,5

Table 5.5 Stiffness of supports. Case A. Long term reactions and settlements.

The result of the Monte-Carlo simulation is summarised in Figure 5.17. The differential settlement, given in the lower left plot, is calculated as:

$$\Delta s = \max\left\{\frac{|s_2 - s_1|}{x_2 - x_1}; \frac{|s_3 - s_2|}{x_3 - x_2}\right\} \tag{5.31}$$

The results in Figure 5.17 are given as plots, with a probability scale for a standard normal distribution on the y-axis. This means that, for linear plots, the numbering of the axis is equal to the reliability index, see equation 2.15. The scale covers the range of probabilities [2%;98%], i.e. β=±2. The sign of the reliability index depends upon whether a large or a small value of the quantity plotted is favourable or unfavourable. In serviceability analysis it is normally large values, i.e. the upper tail of a distribution which governs the problem at hand. Hence the sign of the reliablity index has to be reversed compared to e.g. a plot of the safety margin.

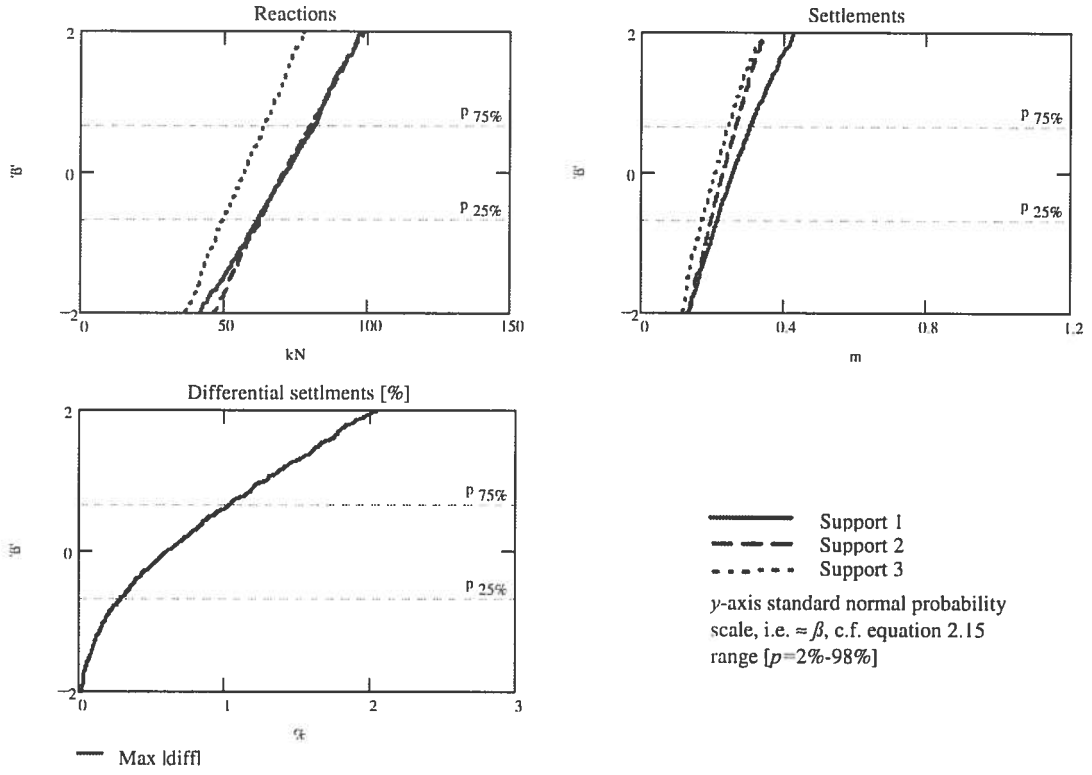

Figure 5.17 Case A. Rigid superstructure. Long term reactions and settlements.

Time dependent settlements including creep

In the example in the previous section, long term settlements were calculated. For intermediate settlements the degree of consolidation has to be determined. Creep effects can be included with the creep model outlined in appendix P. Hence the settlements are determined by equation 5.29, i.e. a sum of elastic/ plastic deformations and creep deformations. Assume that the consolidation can be modelled as one-dimensional consolidation and double-sided drainage. In Figure 5.18 the consolidation pressure for the profile, applied at the whole width of the building, is shown. It is calculated according to equation 5.3. From inspection of the figure it seems appropriate to approximate the consolidation pressure, i.e. the initial excess pore pressure, with a linear distribution over depth. Input demanded for the creep analysis is given in Table 5.6. The three varaibles *M*, *k*, and *r* are assumed to be fully correlated as they can be seen as a result of the pre pressure of the soil.

Random	q [kN/m²]	M [kN/m²]	k[m/s]	r
μ	15	800	0,1	200
V [%]	20	30	30	30
Type	N	N	LN	LN

Table 5.6 Input data. Creep analysis.

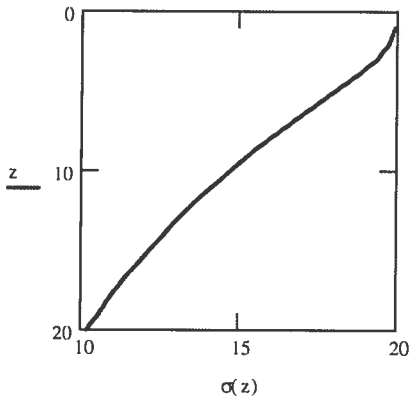

Figure 5.18 Consolidation pressure

A simulation of the 'degree of consolidation' is shown in Figure 5.19. For comparison with the degree of consolidation with respect to creep, the corresponding quantity in classical theory is also shown. The figure shows why the traditional concepts 'primary consolidation' and 'secondary consolidation' are irrelevant in the applied model as the creep effect, i.e. about 'secondary consolidation', delays the 'primary consolidation'.

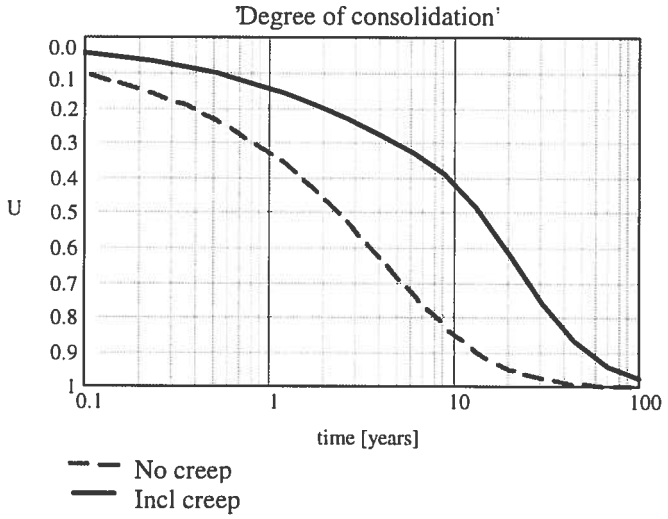

Figure 5.19 Degree of consolidation

The plots in Figure 5.19 are plots of the mean value. In Figure 5.20 'the degree of consolidation' is plotted in a probability plot at three

different times. The plot shows a complex pattern with a type of distribution which changes with time. Figure B.6, appendix B, shows a similar plot of different distributions. A comparison shows that the 5-year-plot is approximately normally distributed, the 20-year plot close to uniform, while the 100-year plot naturally is 'truncated' to 100%. To illustrate the variance by plotting the mean value ± standard deviation causes problems. For example the 100-year value is larger than 100%, i.e. a physically impossible situation. A conclusion, which can be drawn from this, is that PEM is unsuitable for this type of analysis as the impossible value is an input in the analysis.

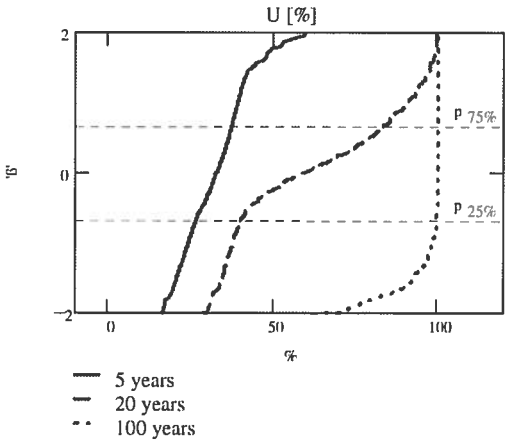

Figure 5.20 Variations of the degree of consolidation

Given the degree of consolidation, the same quantities as in the previous example, alt. A, can be determined. In Table 5.7 the 20-year stiffness of the supports is given, c.f. equation 5.27.

	S_1[kN/m]	S_1[kN/m]	S_1[kN/m]
μ	488	549	489
V[%]	30	31	31
	S_1/ S_2	S_1/ S_3	S_2/ S_3
Correlation	0,7	0,7	0,7

Table 5.7 Stiffness of supports. Case B. 20-year values incl. creep effects.

Reactions and settlements are given in Figure 5.21 and Figure 5.22.

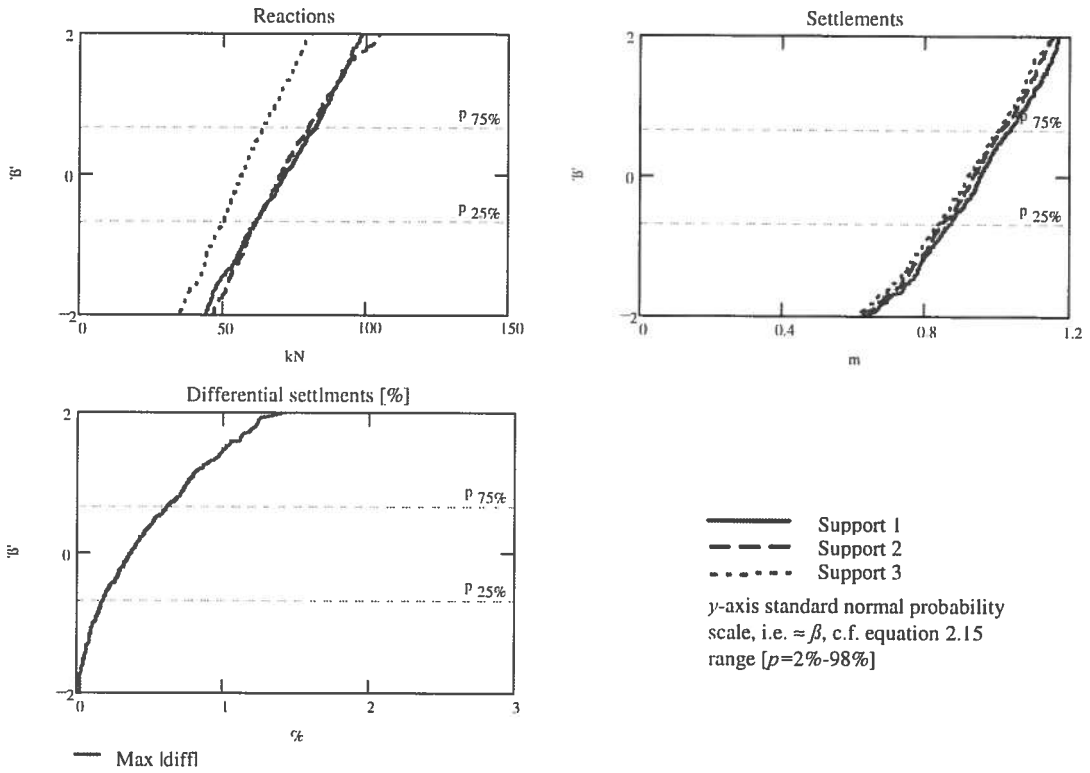

Figure 5.21 Case B. Rigid superstructure. Reactions and settlements incl. creep. 20- year values.

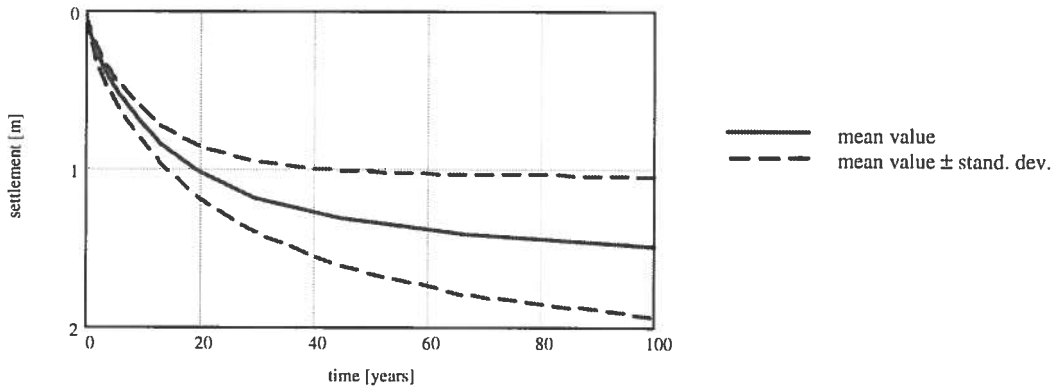

Figure 5.22 Case B. Rigid superstructure. Variations of settlements versus time.

As can be seen in Figure 5.22, the analysis shows incredibly large settlements. The largest proportion is the creep deformations. They exceed by far what one would expect for a foundation as above. One explanation is that the clay is analysed with soil properties as for a young, normally consolidated clay. For an aged clay, which is the general case, a certain amount of overconsolidation must be

accounted for.[1] For the problem at hand, it could be expected that a large proportion of the stress increment falls within the preconsolidation zone, cf. Figure 5.13. Hence adjusted values of the soil properties would be more correct. However, such an analysis isbeyond the scope of this thesis.

Piled foundation. Long term settlements

Assume, regardless of the discussion concluding the previous section, that the results of the foregoing analysis result in a descision to choose a piled foundation. Presume conditions somewhat changed compared to the previous examples. The depth to the bedrock is instead 80 m. This to avoid the alternative with end-bearing piles, which are of less interest in a geotechnical analysis. Furthermore the clay is assumed to be slightly overconsolidated, OCR=1,1. Hence it is possible to drive piles down to layers in which the overconsolidation can be utilised. In Figure 5.23 a plot of an assumed stress state compared to the preconsolidation pressure[2] is given. The figure also shows cumulative strain contributions for stress increments above the preconsolidation pressure[3].

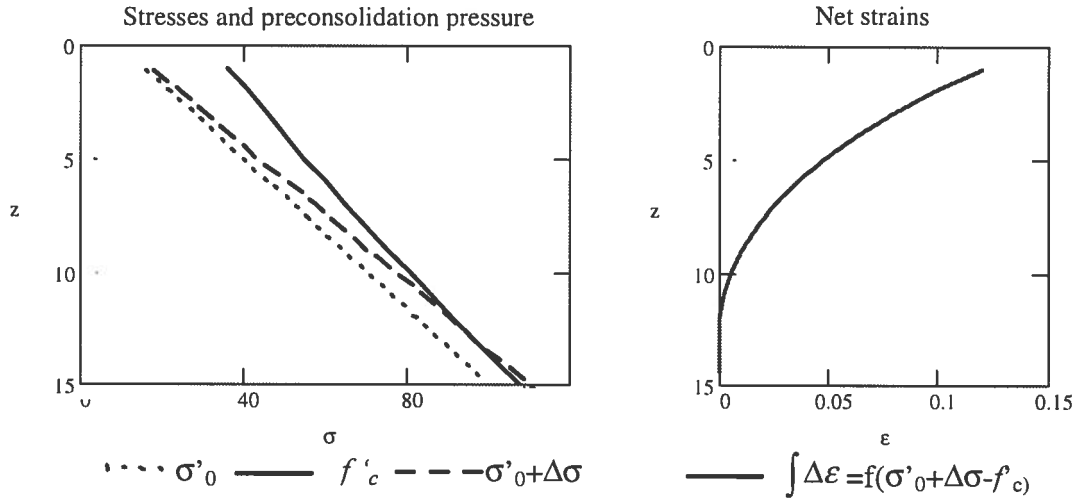

Figure 5.23 Stresses, pre-consolidation pressure and corresponding, cumulative net strains.

[1] If the clay is treated as normally consolidated and creep is not included in the analysis, one make two 'unjustified' assumptions, which might balance each other.

[2] Given as single value at each depth, cf. Figure 5.13.

[3] The in-situ stresses are assumed to be: $\sigma' = 10 + 6 \cdot z$ and the stress increments are calculated according to equation 5.3, cf. Figure 5.18.

From Figure 5.23 can be concluded that the pile should be designed with a neutral plane below a depth of 12 m. In Table 5.8 input data for such a pile design is shown.

Derived values for the neutral plane and the stiffness of the supports are given in Table 5.9. The neutral plane is determined with equation 5.12, k=0,7. The piles are arranged as rows under each of the three foundation strips, cf. Figure 5.15. Hence the analysis can be based upon a 2-D analysis and equation 5.9 can be used for the stiffness analysis.[1]

	H [m]	L[m][1]	P_1-P_3 [kN][2]	B_P [m] [3]	
Fixed	80	25	75		
Random	p_1 [kN/m²]	p_2 [kN/m²]	f_1,f_3[kN/m] [4]	f_2 [kN/m]	M_1-M_3[kN/m²]
μ	20	20	12	16	5000
V [%]	20	20	15	15	30
Type	N	N	LN	LN	LN
[1] Pile length [2] For determination of z_N [3] Pile width [4] Shaft friction					

Table 5.8 Input data. Case C. Piled foundation.

	z_{N1}	z_{N1}	z_{N1}
μ	13.1	14.2	13.1
	S_1[kN/m]	S_1[kN/m]	S_1[kN/m]
μ	1350	1350	1360
V[%]	22	22	21
	S_1/ S_2	S_1/ S_3	S_2/ S_3
Correlation	0,5	0,5	0,5

Table 5.9 Stiffness of supports. Case C. Piled foundation.

The calculated values of the supports are long term values, i.e. after full consolidation and with no creep effects. As the design is based upon stress increments below the preconsolidation pressure, this might be a justified assumption. Similarly as was said in the foregoing example, section Time dependent settlements including creep, a detailed discussion of this issue is beyond the scope of this thesis. The stiffness of the supports is plotted in Figure 5.24.

[1] Equation 5.17a could also be used. However, then stress contribution from all piles in a row must be incorporated in the analysis.

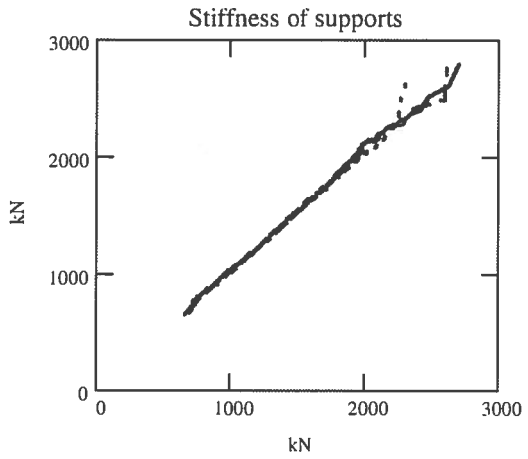

Figure 5.24 Simulated stiffness of the supports. y-axis 'lognormal' scale.

The y-axis in Figure 5.24 has a lognormal probability scale[1], with parameters μ and V from Table 5.9, cf. appendix B. The plot is close to linear. Hence, the stiffness of the supports is lognormal. Results in the form of calculated reactions and settlements are given in Figure 5.25 and Figure 5.26.

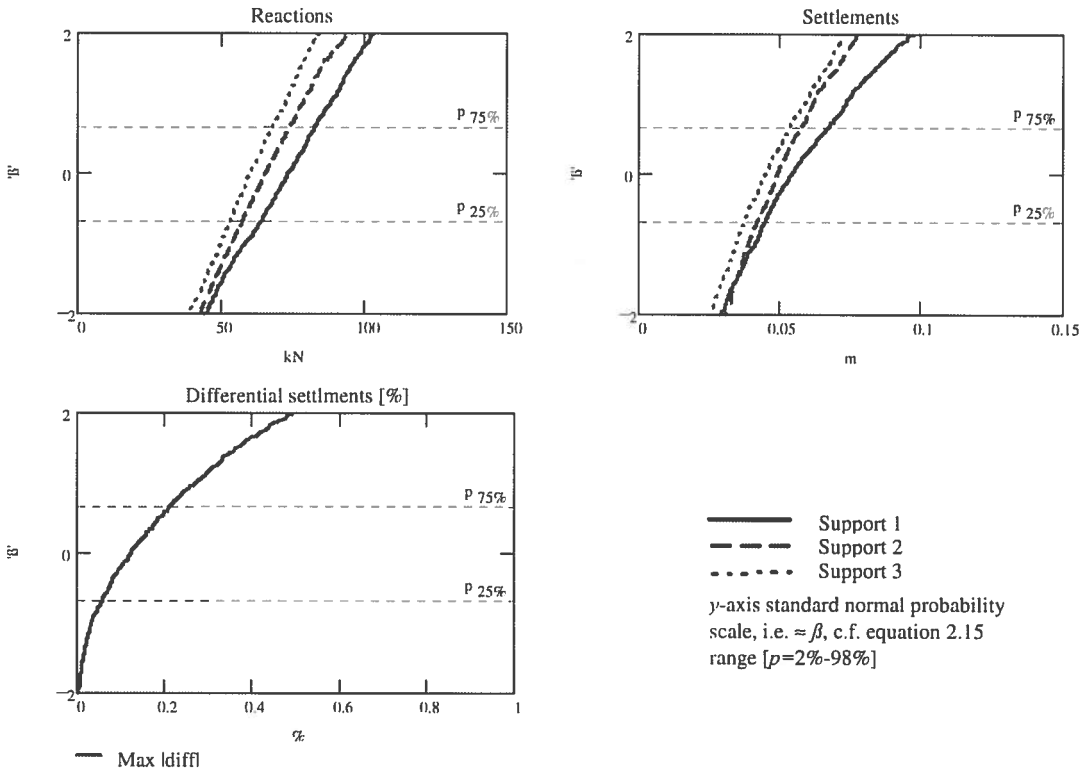

Figure 5.25 Case C. Rigid superstructure. Piled foundation. Reactions and settlements

[1] i.e. a plot of $F^{-1}(p)$ where $F(x)$ is the cumulative distribution for $LN_V(\mu,V)$, cf. appendix B

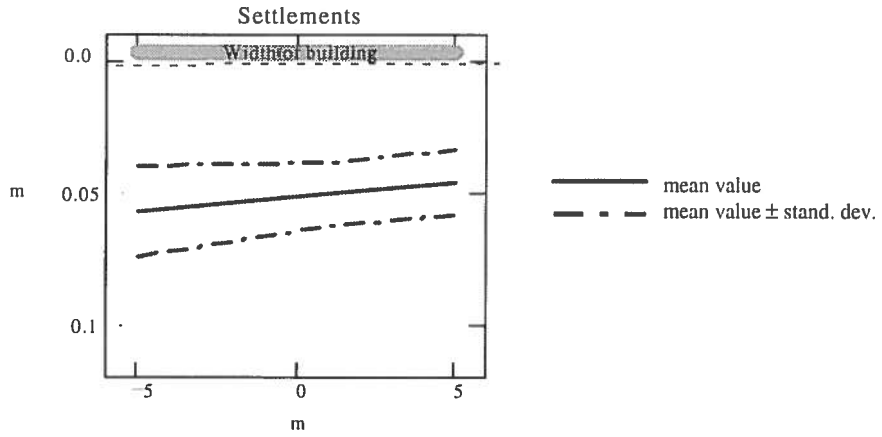

Figure 5.26 Case C. Rigid superstructure. Piled foundation. Settlements.

5.6.3 Application of a level 2 method

Flexible superstructure - Flexible supports

The model used to describe the interaction between the round and the superstructure in the previous section 5.6.2 was a one-sided model. Different aspects of soil deformation could be considered, though only in a simplified manner. The superstructure on the other hand was treated as a rigid body. Thus only the location of the supports and the resulting action were considered for the superstructure. This is in contrast to a conventional structural design in which the flexibility of the superstructure often is a main feature. Below is given an example in which the flexibility of the superstructure is combined with flexible supports in the form of conventional springs. The principle outlook of the interaction model is shown in Figure 5.27.[1] A detailed description of the model is given in appendix R.

[1] All values given are applicable for a unit length of the building in longitudinal direction.

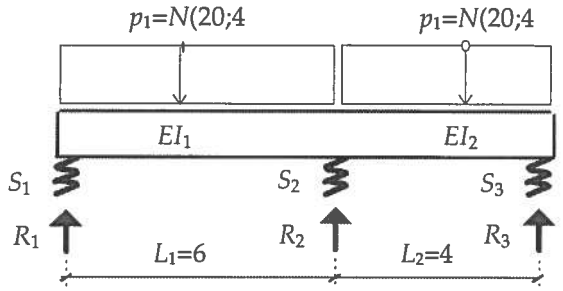

Figure 5.27 Interaction model. Flexible superstructure / Flexible supports.

Piled foundation

The example analysed is in principle the same example as the piled foundation, which was analysed with a level-1 model in the previous section 'Piled foundation. Long term settlements'. The only difference is that the frame of the building is modelled as an elastic beam. Three different alternatives are analysed:

- A 'Weak structure'
- B 'Average structure'
- C 'Stiff structure'

Input data for the different alternatives are given in Table 5.10.

	Alt.A	Alt. B	Alt. C
	EI_1, EI_2[kNm²/m]	EI_1, EI_2[kNm²/m]	EI_1, EI_2[kNm²/m]
μ	$3\ 10^3$	$32\ 10^3$	$75\ 10^3$
V [%]	20	20	15
Type	LN	LN	LN
Correlation	0	0	0

Table 5.10 Input data for the 'frame' of the building.

The details of the internal load bearing system of the building are not analysed. The applied stiffness can be seen as a cumulative stiffness of the structure. Hence, the data given should only be regarded as principle alternatives. However, as a conceptual interpretation of the different alternatives, they could be seen and understood as:

- A 'Unintentional' stiffness[1]. Concrete slab, H=150mm.
- B Foundation beams 700mm · 700mm, spacing 6m.
- C As alternative B + Two prestressed concrete slabs[2].

Obviously, the stiffness of the structural beam can be much larger, e.g. for load-bearing basement walls. However, in such a case the model with a rigid superstructure is an appropriate model.

Alt A-'Weak structure'

Results of the calculations are given in Figure 5.28 - Figure 5.30. Apart from the reactions and settlements, as given in the previous example with a rigid superstructure, the section moment at the middle support is shown. This section moment is defined as positive for tension stresses at the bottom.

Alt B-'Average structure'

Results of the calculations are given in Figure 5.31- Figure 5.33.

Alt C-'Stiff structure'

Results of the calculations are given in Figure 5.34- Figure 5.35..

[1] The load-bearing system is perpendicular to the cross-section.
[2] The stiffness is a result of three different elements. Hence the reduced coefficient of variation.

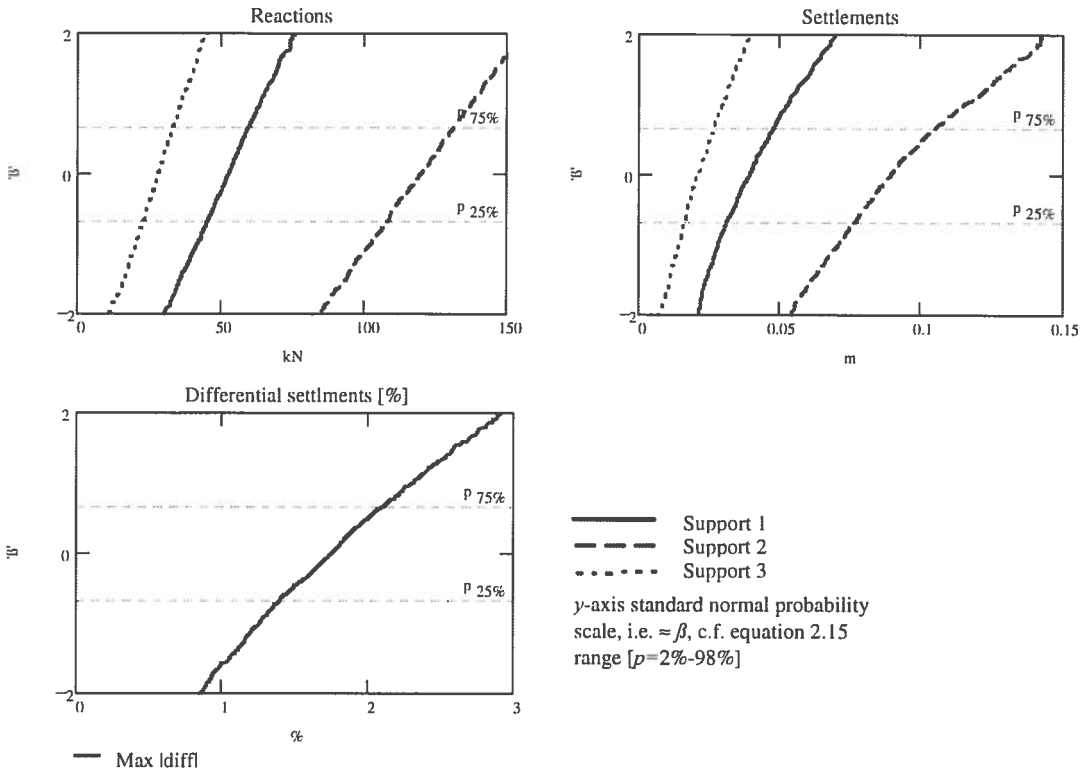

Figure 5.28 Alt. A 'weak' superstructure. Reactions and settlements

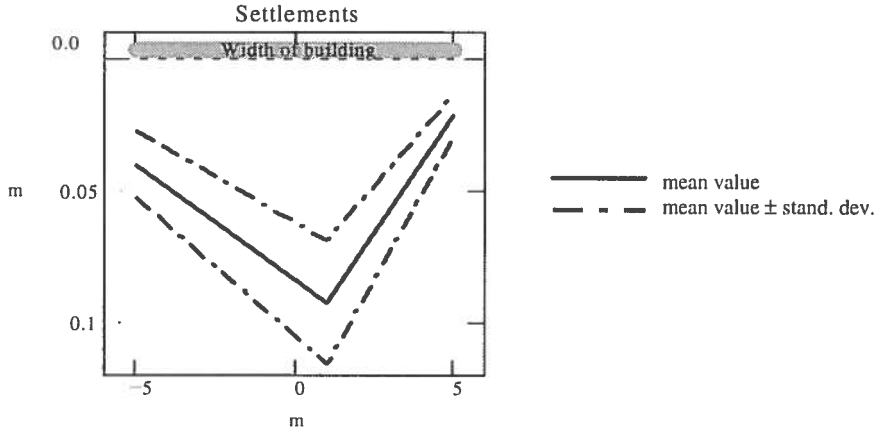

Figure 5.29 Alt. A 'weak' superstructure. Settlements

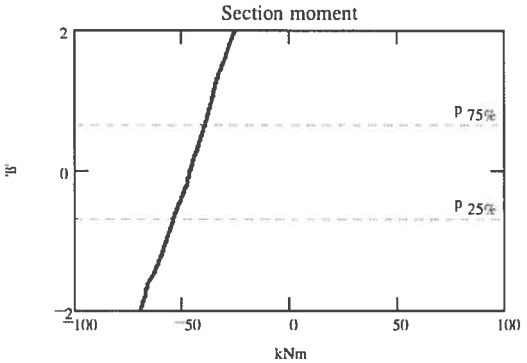

Figure 5.30 Alt. A 'weak' superstructure. Section moment.

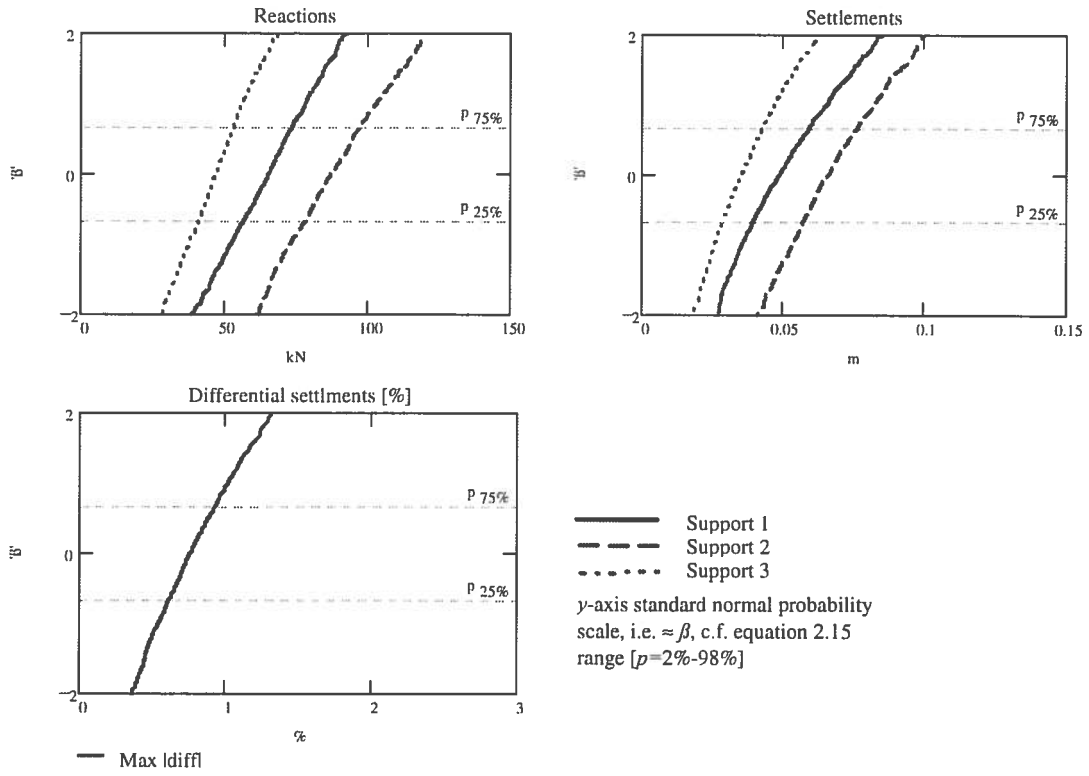

Figure 5.31 Alt. B 'average' superstructure. Reactions and settlements

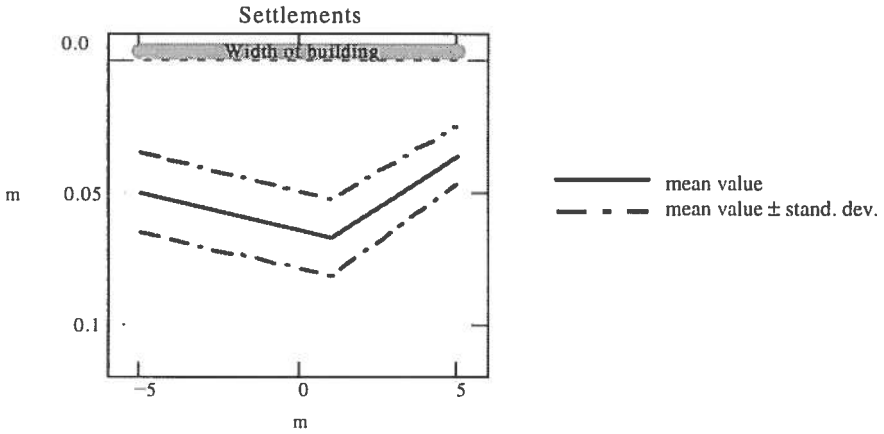

Figure 5.32 Alt. B 'average' superstructure. Settlements

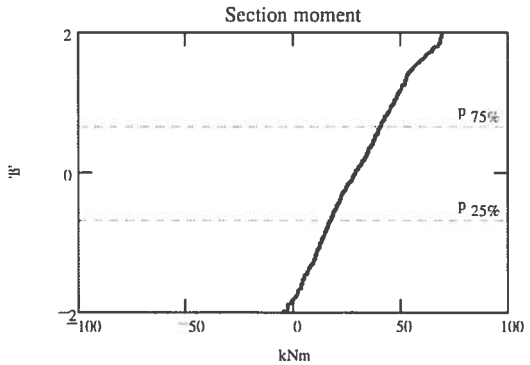

Figure 5.33 Alt. B 'average' superstructure. Section moment.

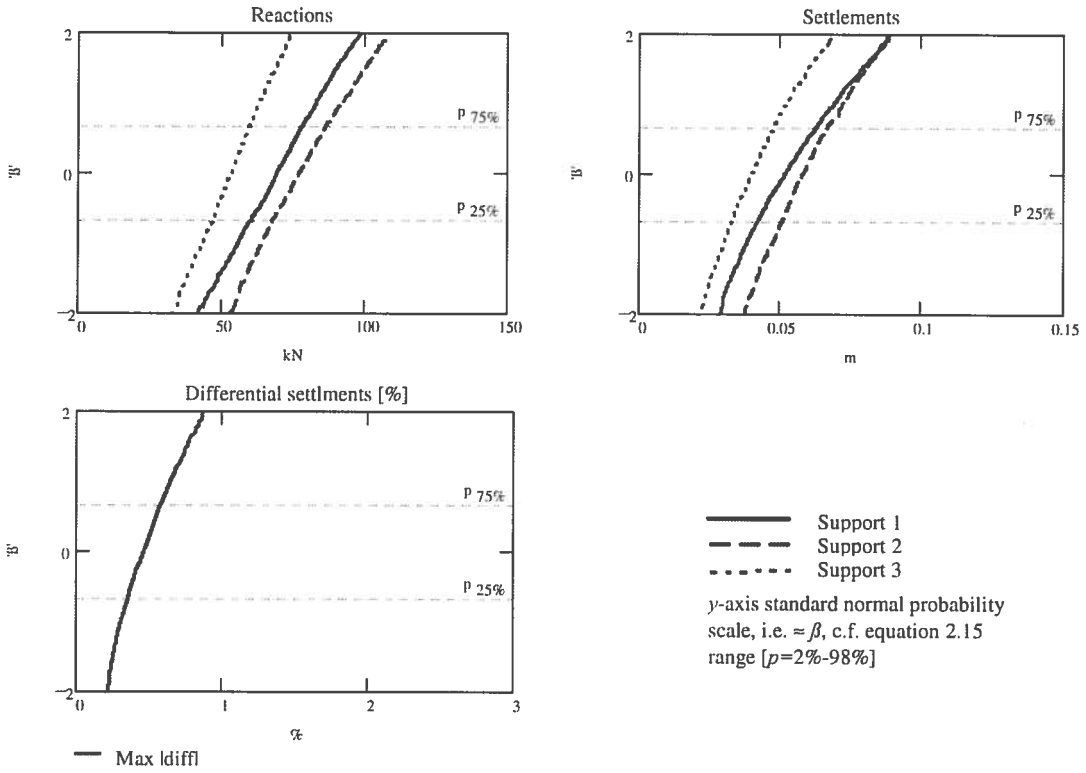

Figure 5.34 Alt. C 'stiff' superstructure. Reactions and settlements

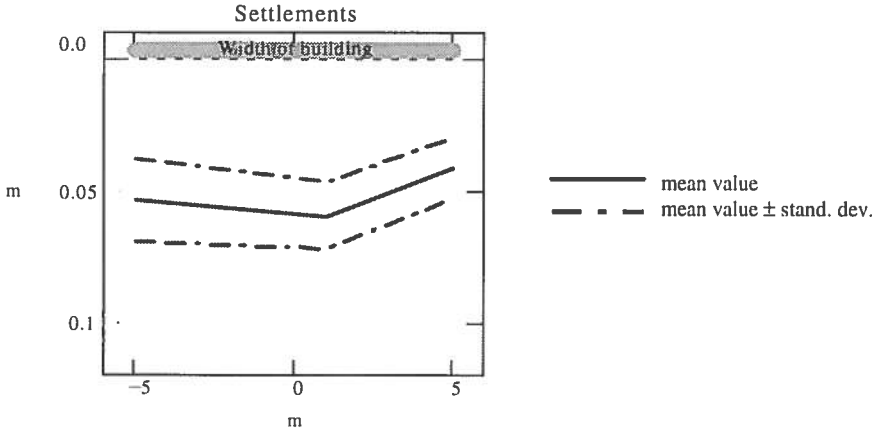

Figure 5.35 Alt. C 'stiff' superstructure. Settlements

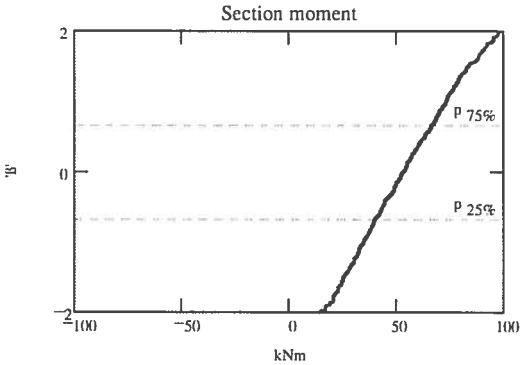

Figure 5.36 Flexible superstructure. Alt. C 'stiff' superstructure. Section moment.

5.6.4 Application of a level 3 method

Introduction

In the previous sections 5.6.2 and 5.6.3, two different degrees of simplification of the analysis have been used. In the first case, level-1, the interaction between ground and superstructure was modelled in combination with flexibility in the ground and interaction within the superstructure. In the second case, level-2, flexibility in the superstructure was added to the model. In a general case, interaction within the ground has to be considered as well. It is reasonable to start from the two calculation models, sophisticated soil model/simple superstructure and simple soil model/sophisticated superstructure, when applying a 'general', random model for ground/superstructure interaction. There ought to be a balance between the accuracy of the soil model and the model for the superstructure. The problem can be summarised as it is to find an 'interface' between the two different calculation models. If the ambition is not to increase the complexity compared to existing models, it seems justified to consider only two-dimensional models.

A soil beam model

Normally, the geometry of the soil can be described in a schematic way. In existing computer programs, the soil is often modelled as a half sphere or a square block, continuous or separated into different layers. The superstructure on the other hand can have an arbitrary geometrical shape. From this point of view it is more simple to describe the soil in such a manner that the description can be integrated into the model of the superstructure. In Figure 5.37 a proposal for such a soil model is given.

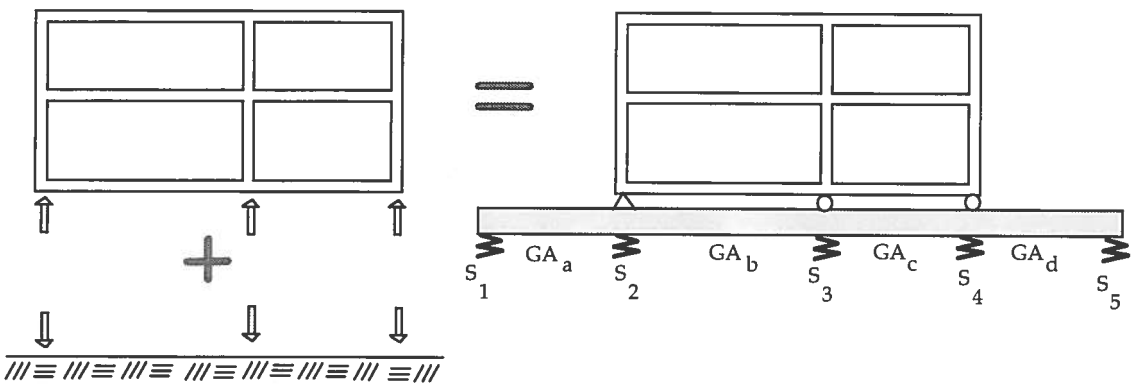

Figure 5.37 A proposal for a model of ground/superstructure interaction. The soil modelled as a discrete element model in the form of a soil beam supported by conventional elastic springs.

The model consists of a fictitious soil beam, in the form of a discrete element model. It is the same type of abstraction as the model of a slope as a frame of shear beams, see section 4.7.2. The proposed calculation model consists of a design in three steps.

- The properties of the soil beam and the spring supports are established.
- An analysis of the beam, combined with the superstructure in a conventional frame program, is performed.
- As a control, the reactions at the supports are applied as actions on the soil.

The soil exists independent of any future superstructure. Hence, as a first step the soil beam can be described with properties of the soil, which are independent of the superstructure. The purpose is to create a beam, which, at the foundation level of the superstructure, corresponds to the soil behaviour. It should be possible to calibrate such a beam against a more sophisticated soil model. The beam properties should be such that the beam together with traditional spring supports, creates relevant reactions and deformations at the supports of the superstructure. The purpose of using a beam model is to simulate the coupling between two nearby supports. To model the influence of the soil surrounding the superstructure, extra supports have to be added outside the superstructure. The fact that the soil is a structural material mainly characterised by its compression and shearing properties, makes it natural to let the soil beam repre-

sent shearing between the supports and the spring compression at the supports. Hence , the soil beam is characterised by its modulus of shearing and its cross-section, i.e. the shearing stiffness *GA*. The spring supports are modelled similarly as in level 1 and level 2, the only difference being that the interaction between the supports is considered, see below. A beam with fixed properties does not have to represent a real, physical beam. The purpose is only to obtain input data for a conventional frame calculation program, aimed at simulating the deformation at the supports of the superstructure. In step two, the beam is integrated in a conventional frame program. As no new types of elements are introduced, existing programs can be fully used[1]. Hence, principles and computer programs for reliability analysis of structural mechanics problems can be utilised.

In the third and last step, which is a control step, the reactions at the supports are applied as actions on the soil. It is then possible to control whether or not the calculated reactions create deformations in the soil, which correspond to the deformations of the supports calculated in step two.

Stiffness properties

To estimate 'correct' stiffness properties of the soil beam is in principle a complex problem. However, the idea with the soil beam model is not to replace more rigorous FEM models but to give a simple alternative as a complement to such models.. Hence the principels of the model should be simple. Below a two step procedure is given by which one can estimate appropriate stiffness properties.

- Stiffness properties are applied to the beam, considering load distribution to adjacent supports.
- The overall stiffness of the model is adjusted.

In Figure 5.38 the principle of the first step is shown. The relation between the stiffness of the supports is estimated, apart from a factor η_1, as a start value S_0. This is the same procedure for applying the stiffness as used in the previous examples in sections 5.6.2 and 5.6.3.

[1] Provided the programme can handle shear deformations.

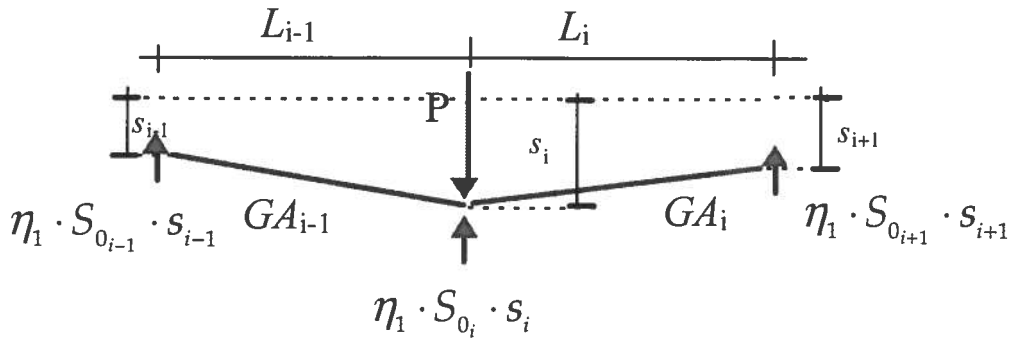

Figure 5.38 Load distribution to adjacent supports

For an applied load at the middle support, the settlements of the adjacent supports are determined as well. This can be done by any appropriate geotechnical model. In section 5.3.2 and 5.3.3 explicit formulas, which can serve this purpose, were presented. The unknown factor can now be determined from vertical equilibrium as:

$$\eta_1 = \frac{P}{\sum_{i-1}^{i+1} S_i \cdot s_i} \tag{5.32}$$

The corresponding shear stiffness can then be estimated as:

$$\begin{aligned} \frac{\eta_1 \cdot S_{i-1} \cdot s_{i-1} \cdot L_{i-1}}{GA_{i-1}} &= s_i - s_{i-1} \quad ; \quad GA_{i-1} = \frac{\eta_1 \cdot S_{i-1} \cdot s_{i-1} \cdot L_{i-1}}{s_i - s_{i-1}} \\ \frac{\eta_1 \cdot S_{i+1} \cdot s_{i+1} \cdot L_i}{GA_i} &= s_i - s_{i+1} \quad ; \quad GA_i = \frac{\eta_1 \cdot S_{i+1} \cdot s_{i+1} \cdot L_i}{s_i - s_{i+1}} \end{aligned} \tag{5.33}$$

The procedure gives a set of correction factors η_1 and shear stiffnesses GA_{i-1} and GA_i for each support. Hence, for the internal supports multiple values are derived for the soil beam quantities. In the analysis these have to be chosen as mean values.

In the previous examples it has been assumed that no redistribution to nearby supports through the soil is considered. This is an assumption on the unsafe side. In Figure 5.39 the principle interaction between nearby supports is shown. The solid line shows the actual deformations for two equal loads. If the stiffness is estimated independent of the nearby support the settlement of a support will be equal to the maximum settlement given by the dashed lines. To

adjust for this overestimation of the support stiffness, the overall stiffness can be multiplied by a factor η_2, which can be derived by an energy relationship. For a unit load applied at each support of the building, the work of the settlements of the supports will be:

$$W_1 = \sum_{i=1}^{n} \left[\sum_{j=0}^{n+1} S_{i,j} \cdot s_{i,j} \right] \tag{5.34}$$

where i,j denotes j^{th} support for a load applied at the i^{th} support and where n is the number of actual supports of the building, i.e. the supports of the soil beam except the first and last. This work can be compared with the corresponding work considered in the first step:

$$W_0 = \sum_{i=1}^{n} \left[\sum_{j=i-1}^{i+1} S_{i,j} \cdot s_{i,j} \right] \tag{5.35}$$

Hence the correction factor η_2 can be written as the ratio:

$$\eta_2 = \frac{W_0}{W_1} \tag{5.36}$$

The stiffness of a support is then applied in the analysis as:

$$S_i = \eta_1 \cdot \eta_2 \cdot S_{0_i} \tag{5.37}$$

It has to be remarked that the correction factor η_2 will result in overall larger settlements compared with the analyses in section 5.6.2 and section 5.6.3. In principle a similar correction of the overall stiffness could be applied in those cases. However, it has to be balanced aginst the fact that current practice often is a model with fixed supports.

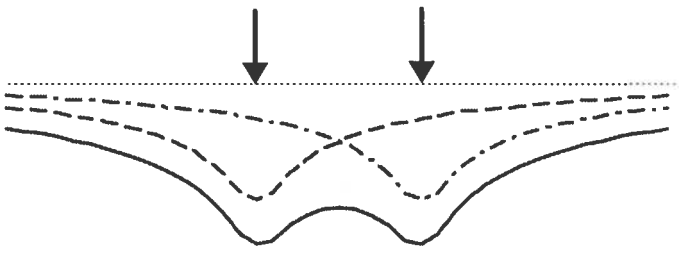

Figure 5.39 Load distribution between adjacent supports

Application on a piled foundation

The soil beam model outlined above is applied on the same example of piled foundation, which was analysed with a level-1 and level-2 model in the previous sections. The interaction model is shown in Figure 5.40.[1]. A detailed description of the model is given in appendix S.

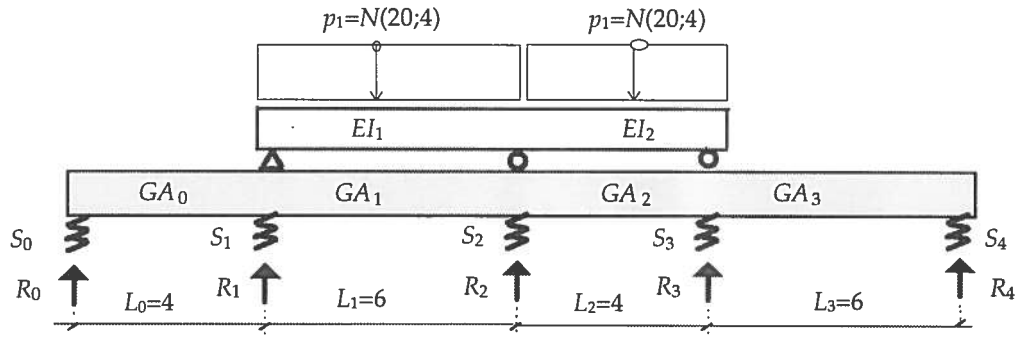

Figure 5.40 Interaction model. flexible superstructure/Soil beam model.

The first and second span of the soil beam are chosen to L_0= 4m and L_4= 6m. The reason for this is that the choice results in three equal sub-systems used in the assignment of stiffness properties, see Figure 5.38. The properties of the soil beam are determined from the principles in the previous section 'Stiffness properties'. Equation 5.9 is in this case used as a 'true' model of the soil behaviour. In Table 5.11 the stiffness properties of the soil beam are given. The results are derived from the same data as the example in section 5.6.2, see Table 5.8. [2]

S_{0i}; i=0-4 [kN/m]	η_1	GA_i; i=0-3 [kN]	η_2
1293	0,59	1963-1994	0,83

Table 5.11 Estimation of stiffness properties of the soil beam.

In the application of the soil beam model, the input data given in Table 5.12 is used. The coefficient of variation for the supports is assigned the same value as in Table 5.9. The soil beam is regarded as

[1] All values given are applicable for a unit length of the building in longitudinal direction.

[2] S_0=1293 is the result of a deterministic analysis, while S=1350 in Table 5.9 is the mean value of a simulation (of a skewed variable). Hence the difference.

one model. Hence the coefficient of correlation for the shear stiffness is 1,0.

	$S_0 - S_4$ [kN/m]	$GA_0 - GA_3$ [kN]
μ	630	1980
V [%]	22	20
Correlation	0,5	1,0

Table 5.12 Assigned stiffness properties of the soil beam.

The superstructure is analysed for the same three different alternatives of bending stiffness as in section 5.6.3.

Alt A-'Weak structure'

Results of the calculations are given in Figure 5.41 -Figure 5.43. As a control of the soil beam model, the calculated reactions are applied as actions in the 'true' soil model, i.e. in this case equation 5.9. The mean value of this control is shown as a thin dashed line, Figure 5.43.

Alt B-'Average structure'

Results of the calculations are given in Figure 5.44- Figure 5.46.

Alt A-'Stiff structure'

Results of the calculations are given in Figure 5.47- Figure 5.49.

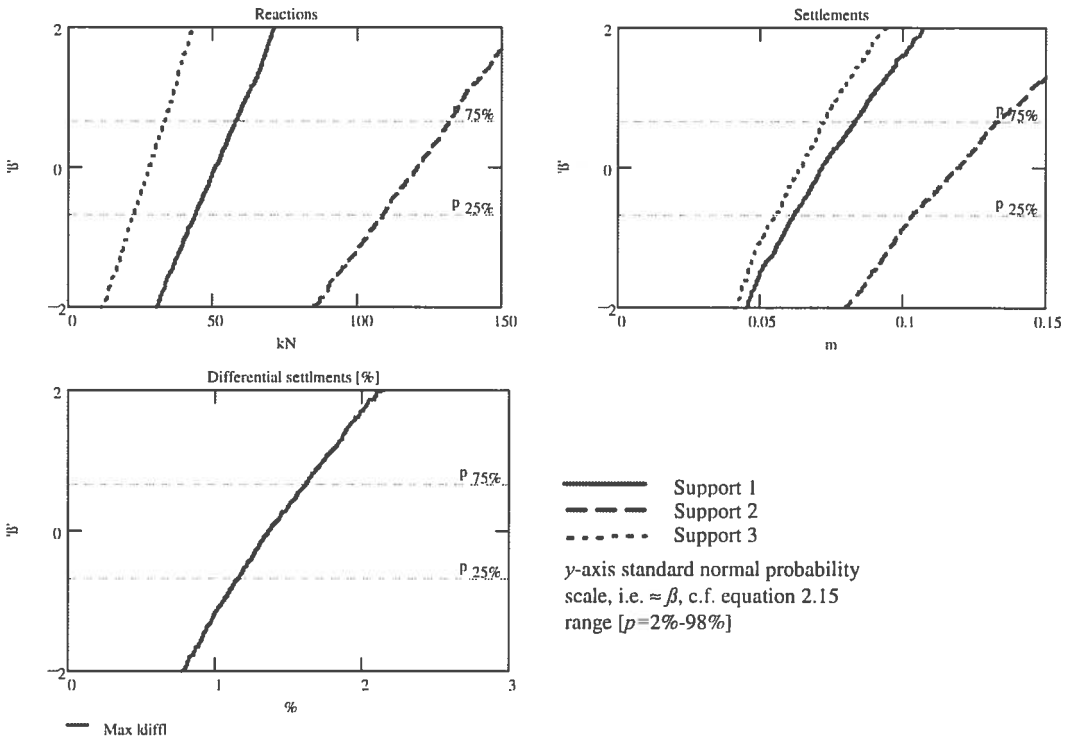

Figure 5.41 Soil beam model. Alt. A 'weak' superstructure. Reactions and settlements

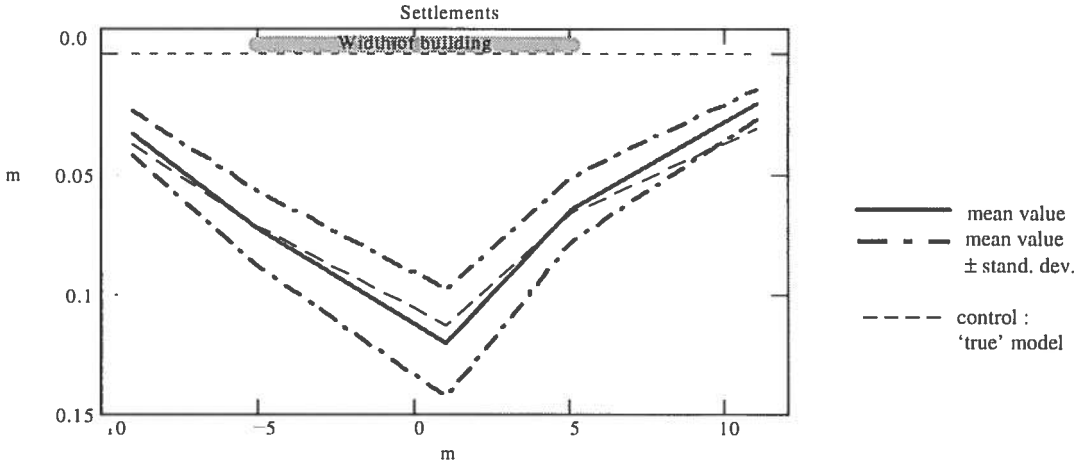

Figure 5.42 Soil beam model. Alt. A 'weak' superstructure. Settlements.

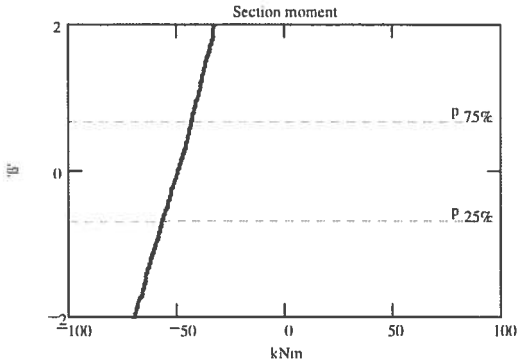

Figure 5.43 Soil beam model. Alt. A 'weak' superstructure. Section moment.

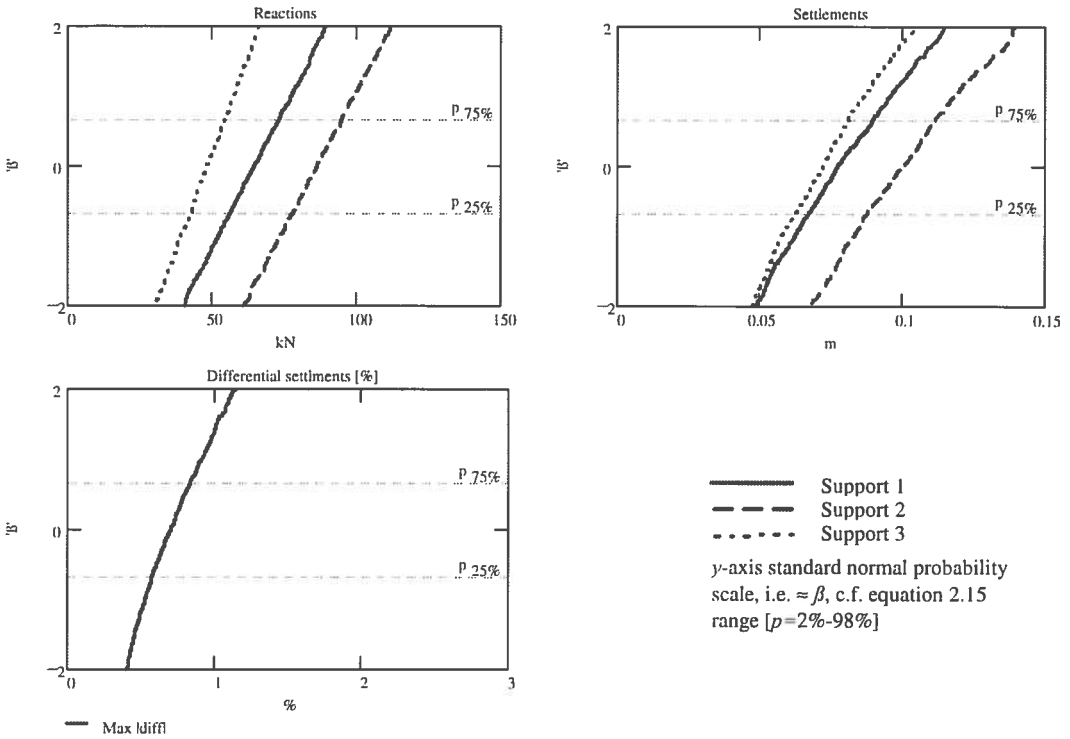

Figure 5.44 Soil beam model. Alt. B 'average' superstructure. Reactions and settlements

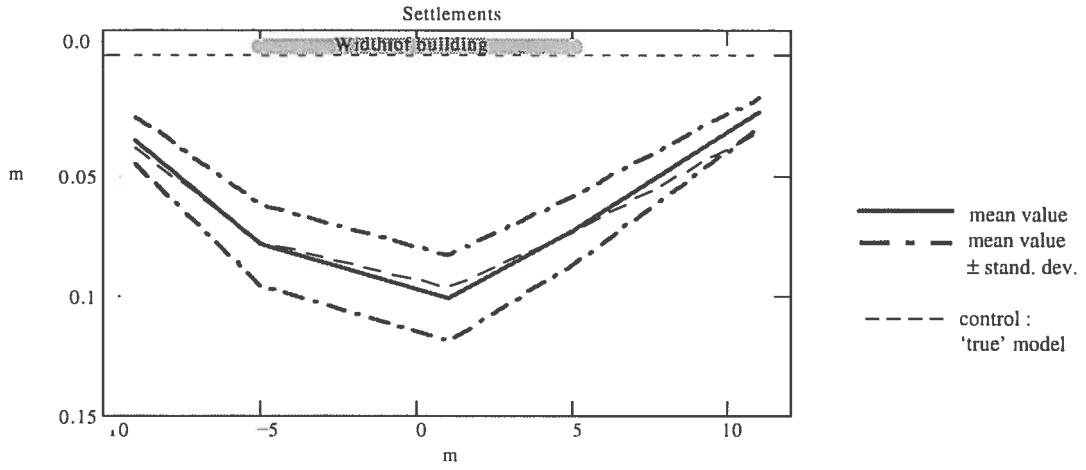

Figure 5.45 Soil beam model. Alt. B 'average' superstructure. Settlements.

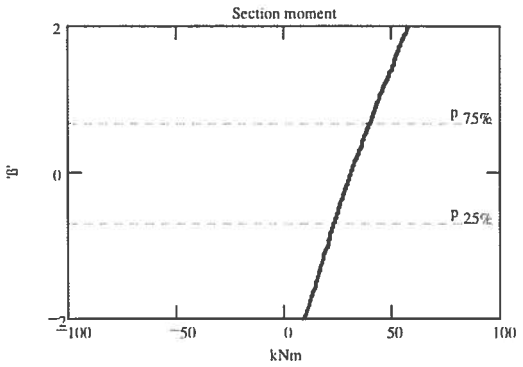

Figure 5.46 Soil beam model. Alt. B 'average' superstructure. Section moment.

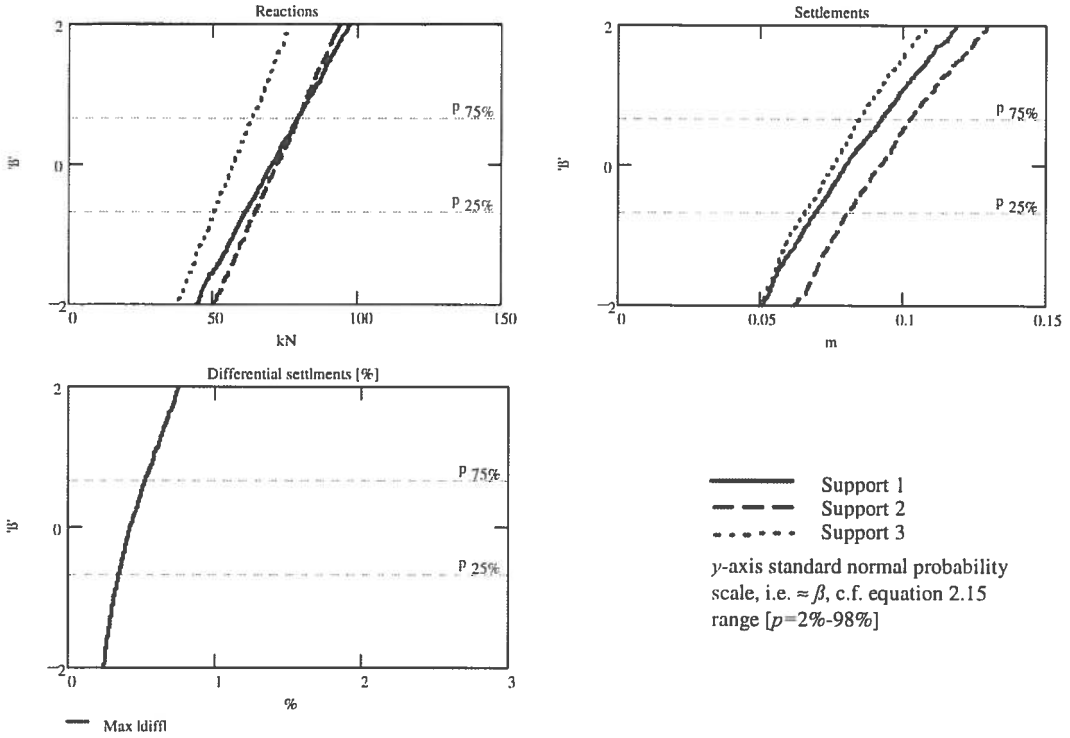

Figure 5.47 Soil beam model. Alt. A 'stiff' superstructure. Reactions and settlements

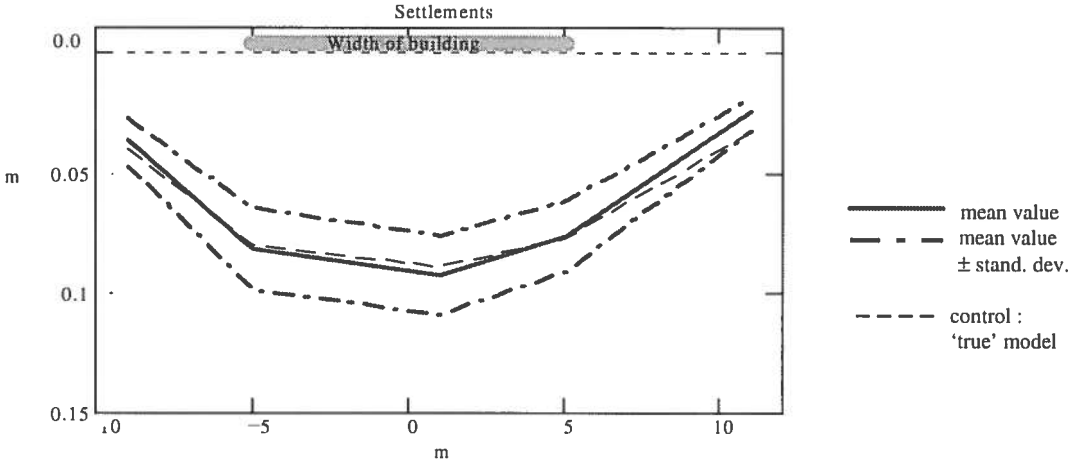

Figure 5.48 Soil beam model. Alt. A 'stiff' superstructure. Settlements

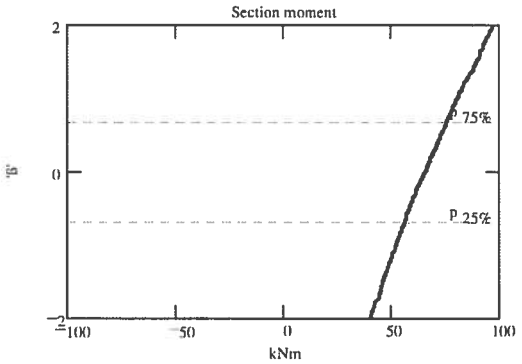

Figure 5.49 Soil beam model. Alt. A 'stiff' superstructure. Section moment.

5.6.5 Fixed supports

In the previous sections the foundation of a building with a two-span cross-section has been analysed with three different ground/superstructure interaction models. For comparison, the result of an analysis of the same building with the common model fixed supports is shown in Figure 5.50 and Figure 5.51.

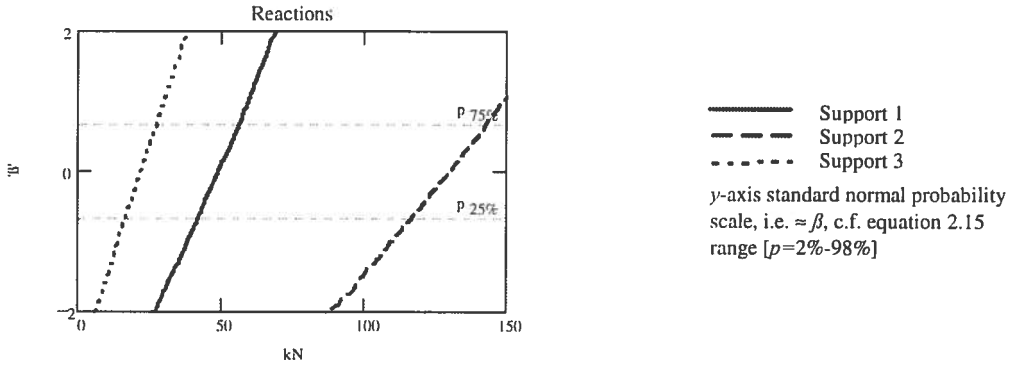

Figure 5.50 Fixed supports. Reactions.

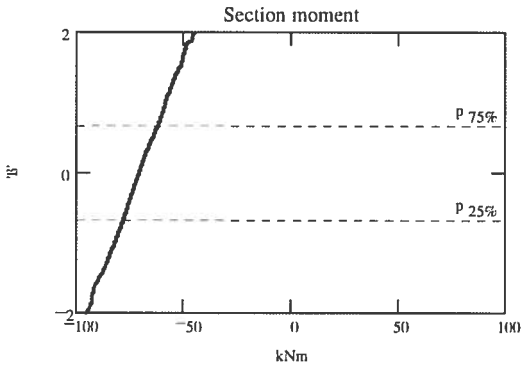

Figure 5.51 Fixed supports. Section moment.

5.6.6 Summary

The results of the Monte-Carlo simulations in sections 5.6.2.-5.6.5 are summarised in Table 5.13. When interpreting the results one should remember that for the soil beam model, the overall stiffness was adjusted due to interaction between the supports through the soil, see section 5.6.4, 'Stiffness properties'. Hence for a fair comparison, the settlements in the level-1 and level-2 analyses should be increased with about 60%.

	R_1 [kN]		R_2 [kN]		R_3 [kN]		s_1 [mm]		s_2 [mm]		s_3 [mm]		Δs[%]		M [kNm]	
	μ	v%	μ	v%	μ	v%	μ	v%	μ	v%	μ	v%	μ	v%	μ	v%
Level - 1	*Rigid superstructure, Flexible supports*															
A	71	20	72	18	57	18	260	27	230	22	210	26	0,7	76	-	-
B	72	20	72	19	57	20	950	14	930	14	910	14	0,4	77	-	-
C	73	20	66	19	61	18	60	30	50	23	50	26	0,2	82	80	28
Level - 2	*Flexible superstructure, Flexible supports*															
A	53	21	120	15	28	29	40	31	90	25	20	36	2	29	-47	23
B	65	20	88	17	47	21	50	29	70	21	40	30	0,8	30	28	60
C	69	20	78	17	53	19	50	28	60	21	40	28	0,5	35	52	37
Level - 3,	*Flexible superstructure, Flexible supports, Soil beam*															
A	51	21	120	15	28	28	70	21	120	18	70	20	1,4	24	-50	19
B	65	20	86	15	48	19	80	21	100	18	70	20	0,7	26	32	38
C	70	19	72	15	57	17	80	21	90	18	80	19	0,4	30	66	22
Fixed	49	22	130	15	22	35	-	-	-	-	-	-	-	-	-70	17

Table 5.13 Summary of Monte-Carlo simulation. Ground/Superstructure interaction

From the results in Table 5.13 a number of conclusions can be drawn.

- For the absolute settlements

  All three models with flexible supports result in settlements of the same magnitude

  The coefficient of variation is reduced with the soil beam model

  With the applied creep model the coefficient of variation is reduced when creep effects are taken into account

- For the differential settlements

  The soil beam model reduces the differential settlements compared to the level-2 model[1]

  Creep effects reduce the differential settlements although the absolute settlements are increased

[1] The model with rigid superstructure is probably a very unjustified model for determining differential settlements unless the superstructure is very stiff.

- For the magnitudes of the reactions

  Both the alternatives with flexible superstructure are good approximations.

  The model with rigid superstructure is a good approximation for the alternative with a stiff superstructure.

  The model with fixed supports is a good approximation only for the alternative with a weak superstructure, i.e. the alternative with the 'unintentional stiffness'. Hence this model is normally not a reasonable model in practical design of a piled foundation with friction piles in soft clay.

  The mean value of a calculation with fixed supports and rigid superstructure respectively might be a reasonable approximation for the reactions in the alternative with a superstructure of average stiffness.

- For the magnitude of the section forces, i.e. here the section moment

  The section moment is difficult to determine. Both the magnitude and the sign of the moment are very sensitive to different assignments of stiffness.

  Both the alternatives with flexible superstructure result in moments of the same magnitude but the coefficient of variation is reduced in the soil beam model.

6 FUTURE RESEARCH

6.1 Introduction

The thesis deals with subjects from tree disciplines. In each discipline there is naturally a need for further research. This section is limited to a number of issues, which are discussed in the thesis. These issues range from problems of a general form, for which the answers go far beyond the scope of the thesis, to detailed issues, for which no ready solutions have been reached in the thesis.

6.2 User's manual

During the last few decades a lot of research has been undertaken to develop different probabilistic procedures, which are applicable to structural and engineering problems. The thesis at hand is just one of of many such studies. At the same time, probabilistic thinking has only marginallyinfluenced engineering practice. The most important part of future research might be to develop a user's manual, i.e. how to apply probabilistic concepts in engineering practice.

6.3 Geostatistics

The mathematics of random field is well developed. Geostatistics have been used for a long time to describe overall characteristics of geological formations. In the thesis two examples of application of undrained shear strength are presented, which gave different results. This raises the question: When is geostatistics applicable in geotechnical design? How does the nature of geotechnical properties meet the requirements of random field theory?

6.4 Slope stability

It is often remarked in the thesis that underlying deterministic model is very important. A key issue in slope stability analysis is: What is the triggering factor for a slide? Back calculation of slides often shows a low safety, low enough to declare that the slope was not stable, but not always explaining why the slide occurred at that particular time.

The 'design chart' method extended to probabilistic analysis is restricted to undrained analysis and slip circles below the toe. To

meet a more general demand, the model should be extended to existing 'design charts' for effective stress analysis and toe circles.

The application of Bishop's simplified method, given in the thesis, is restricted to toe circles and a rough description of the pore pressure. An extension to arbitrary circles and a more general pore pressure description should improve the applicability of the method.

The shear beam model presented is a prototype model. A key issue in application of the model is the stiffness distribution in the slope. The introductory examples showed a strong redistribution of the stiffness, compared to a simple geometry interpretation. The hypothesis that shear creep within a slope governs the stress state needs future research.

6.5 Interaction ground/superstructure

The creep model presented in the thesis is based upon a very simple rheological model and restricted to volumetric creep. Creep deformations form a complex research area. For settlements of buildings and civil works, the behaviour of the clay in the pre-consolidation zone is a research area of great interest. Shear creeping might be a triggering factor for slope failures.

The soil beam model, introduced to describe interaction between the ground and the superstructure, shows a very good aggreement for a simple superstructure and homogeneous soil conditions. Application on more complex problems and long term field observations are of great interest.

7 SUMMING-UP DISCUSSION

"If the engineer is fully aware of the uncertainties involved in the fundamental assumptions of his computations he is able to anticipate the nature and the importance of the differences which may exist between reality and his original concept of the situation." (Terzaghi, 1943)

The thesis deals with uncertainty in calculation modelling. Emphasis is put on the design state. Design is a creative task that includes other demands than purely scientific modelling. The operative methods developed in the thesis are aimed to enable rapid assessments of the main characteristics of a problem in a design situation. With random modelling technique uncertainties can be addressed in the calculations. Naturally, this is restricted to uncertainties for which the existence is known. A probabilistic approach can not replace lack of knowledge.

Uncertainty in geotechnical design compared with structural design

The often stated fact that soil has a larger variation than other structural materials can be discussed. Comparing manufacturing by man and by nature, it is likely that nature do present a manufacturing process with smaller variations compared with the man made process. Alteration of an industry building from the beginning of the century, with no kept records from the initial construction phase, involves uncertainties at least comparable with a geotechnical design. Variations of concrete strength from say 15 Mpa - 80 MPa, are in no way smaller than the variations in the soil, while new concrete produced to a detailed specification shows very small variations. Thus, the variation in the soil is a question of how properly one tests the soil. The difficulties in geotechnical design are not due to larger variations compared with structural design, but in the way the 'manufacturing' process is controlled.

About random models

Random model analysis means that calculation models, with different accuracy, can be used in a comparable way. It does not mean that the randomness of the model can substitute the relevance of a model. As an example, erection of medieval Gothic cathedrals is impossible according to the theory of elasticity, but verified both by

plastic theory and reality, (Heyman, 1964). Hence, the underlying deterministic model is just as important in a probabilistic as in a deterministic analysis.

To use random models means that one wants to measure the influence of variations. Hence it is essential that the model used gives not only an overall 'correct' solution but also relevant information about the influence of different alternatives. This is the reason why just as much effort in the studies are put into developing simple but relevant physical models as into the random application of the models.

Soil properties

Contrary to steel, concrete and timber, for which the specified material to be used at the time of design might be nonexistent, the true state of the soil is given, but hidden to the designer due to insufficient testing. This means that the uncertainties of the soil can always be controlled by additional testing. The probabilistic approach is a way to systematically value such additional testing.

A complication in geotechnics is the pore-pressure, which physical nature can be compared with natural actions, e.g. wind and snow loads. Hence it has to be given as a prognosis of the future.

The relevance of geostatistics,

Geostatistics is a valuable instrument as it makes it possible to eliminate measurement errors. But the application of the theory is not straight-forward. One has to deal with rather complex mathematics. Are the prerequisites for the theory satisfied?. It could be argued that an autocorrelation distance larger than zero is just a proof of an insufficient model.

The necessity of Bayesian statistics

The Bayesian statistics form, in the author's opinion the most abstract part of the thesis. Principal , simple formulas can be derived, but the underlying philosophical concepts are difficult to capture. Nevertheless, the concept is necessary if one wants to incorporate testing statistics in the design. A situation in which experience is not valued in a way equal to testing, will lead to a very rigid design situation.

A dimensionless safety margin

In many parts of the thesis it is underlined that the linear safety margin is to preferable as a safety concept compared to the traditional factor of safety. The dimensionsless safety margin, introduced in the chapter 'Slope stability' satisfies this computational demand as well as it works as a measure of the location of the critical shear surface. Furthermore it is easily incorporated into a partial factor format.

Shear strength in slope stability analysis

The introduction of a 'new' definition of the shear strength can be misunderstood as a provocative proposal. Much of the effort in the thesis is to develop models, which require little computational work and hence are suitable for example in Monte-Carlo simulation. The shear strength concept should be regarded as a step in this work. Nevertheless, the definition is logical and solves some of the problems with a probabilistic approach in slope stability analysis. The application in Bishop's simplified method is straightforward, but the interpretation of the concept for rigorous methods has not been analysed in detail.

About slope geometry

In the applications of slope stability analysis, the geometry of the analysed slopes was described with random variables. It can be argued that the geometry is easily surveyed and hence there is no need to treat the geometry as random. In the author's opinion the uncertainty of the geometry is comparable to the uncertainty of soil parameters. The geometry is deterministic to its nature but like soil parameters unkown in detail to the designer. The reliability analysis gives answer to the question whether it is worth to put more effort in additional surveying.

The shear beam model

Shortcomings in limit equilibrium methods inspired the idea of a new slope stability model in which the slope is described as a framework of shear beams. The shear beam model differs from traditional limit equilibrium methods in that a constant degree of mobilisation is not a prerequisite for the analysis. The stress state, based upon given assumptions, can be determined both at the shear

surface and at the interslice surfaces. This means that the lower bound theorem can be used to determine whether a solution for a given shear surface is on the safe side or not.

The model is not in any sense fully developed, but the first attempts to apply the model on a real slope showed promising results. The concept may fill a gap between traditional limit equilibrium methods and finite element analyses.

Interaction between ground engineers and superstructure engineers

The purpose of a foundation design is to meet the requirements put on the superstructure. For a successful design, it is an imperative that the geotechnical and the structural engineer speak a unified language. Development of refined methods in geotechnical or structural engineering can never, without co-operation, meet this requirement. The models developed in the thesis are aimed to be an 'interface' between the two disciplines. Hence they should be seen as a complement to, and not a replacement of, more sophisicated methods in any of the disciplines.

The creep model and the soil beam model

Both the creep model and the soil beam model presented in the thesis are results of the 'interface' ambition discussed above. Results of analyses show a dual levelling effect for both models, i.e. the physical variations in the form of differential settlements and the statistical variations in the form of calculated variance are decreased when creep effects in the soil or interaction between supports are considered.

Random modelling as a part of the designer's toolbox

The study in the thesis is aimed to simplify application of random models in geotechnical design, that is to provide the designer with improved tools. Engineering simplicity is favoured instead of refined scientific precision.

Probabilistic application is not just a question of applying well defined mathematics but a way of thinking. The benefits of this study depend just as much of the skill of the designer as on the quality of the tools.

Epilogue

A risk is either a hazard or a opportunity. The probabilistic approach is a way to quantify such a risk. The result the analysis is uncontroversial only if the same persons are subject to both the hazard and the opportunity.

REFERENCES

@t Risk, (1994), *Risk analysis and simulation add-in for Microsoft Excel or Lotus 1-2-3*, Palisade Corporation, Newfield, NY

Alén, C. et al (1993a), *NAD-EC7-Geokostruktioner. Beräkningar med bl a ß-metod*, Arb. Rapport 1, SGI Dnr: 1-9308-392, Linköping, (extract in Alén, 1995b).

Alén, C. et al (1993b), *NAD-EC7-Geokostruktioner. Beräkningar med bl a ß-metod*, Arb. Rapport 2, SGI Dnr: 1-9401-010 , Linköping, (extract in Alén, 1995b).

Alén, C. & Lendeby, L., (1993), Design Value of the Bearing Capacity for a Friction Pile at a given Risk level, *Proc. Int. Symposium on Limit State Design 93*, Vol 1/3, Copenhagen

Alén, C. & Sällfors, G.. (1994). Stabilitetsanalys med statistiska metoder. Skredriskanalys för södra Göta älvdalen, Teknikbilaga 8. *The southern Göta River report, part 8*. SGI. Linköping. (in Swedish, published in Alén, 1995b).

Alén, C. (1995). *Att räkna ungefär rätt istället för exakt fel.* Report B, 1993:3. Department of Geotechnical Engineering. Chalmers University of Technology. Göteborg (in Swedish).

Alén, C. (1996). Application of a Probabilistic Approach in Slope Stability Analyses. *Proc. 7th International Symposium on Landslides. Trondheim.*, Vol 2, Balkema, Roterdam

Alén, C. (1996). A shear beam model, A proposal for a new stability. *Proc. 7th International Symposium on Landslides. Trondheim.*, Vol 2, Balkema, Rotterdam

Alén, C., (1997), *Spännings- och sättningsberäkningar vid platt- och pålgrundläggning*, Report B 1997:6, Department of Geotechnical Engineering. Chalmers University of Technology. Göteborg (in Swedish).

Alén, C., (1998a), *Geostatistical analyses of clay properties. Examples from a test site at Nödinge*, Rapport B 1998:1, Department of Geotechnical Engineering, Chalmers University of technology. Göteborg

Alén, C., (1998b), *Long term deformation in clay, Report , Department of Geotechnical Engineering*. Chalmers University of Technology. Göteborg, (Preliminary Draft).

Andersson, S., & Wiklert, P., (1972), Markfysikaliska undersökningar i odlad jord, *Grundförbättring,* Vol. **25**, Uppsala (in Swedish)

Ang, A. H-S.& Tang, W.H, (1975), *Probability Concepts in Engineering Planning and Design*, Vol. 1, Basic Principles, John Wiley & Sons, New York

Beigler, S-E., (1976), *Soil-Structure Interaction under Static Loading, Doctoral thesis*, Dept. of Geotechnical Engineering, Chalmers University of Technology, Göteborg

Benjamin, J. R. & Cornell, C. A., (1970), *Probability, Statistics, and Decision for Civil Engineers*, McGraw-Hill Book Company, New York

Beta, (1990) see Råde & Westergren

Bishop, A. W. (1955), The Use of the Slip Circle in the Stability Analysis of Slopes, *Geotechnique,* **V**, No. 1

Bjerager, P., (1989), Probability computations methods in structural and mechanical reliability, Contr. to the book *Mechanics of probabilistic and reliability analysis*, W.K. Liu & T. Belytschko, Editors, Elme Press Int., Lausanne

BKR 94:1 (1994), *Boverkets konstruktionsregler*, Boverket, Karlskrona, (In Swedish)

Blom, G., (1984a), *Sannolikhetsteori med tillämpningar*, Student-litteratur, Lund, Second edition, (in Swedish)

Blom, G., (1984b), *Statistiksteori med tillämpningar*, Studentlitteratur, Lund, Second edition, (in Swedish)

Calladine, C. R., (1969), *Engineering Plasticity,* Pergamon Press, London

Chang, S. C. (1992). Discrete element method for slope stability analysis. *ASCE J of Geotech. Eng.* **118**, nr 12. 1189-1905.

Christensen, S., (1995), *Long-term processes in Geomaterials, Creep parameters from oedometer tests on illitic clays*, Report STF69 A95025, SINTEF, Trondheim

Christian, C., T., Ladd, C., C. & Baecher, G., B., (1992), Reliability and Probability in Stability Analysis, *Proc. Stability and Performance of Slopes and Embankments,* Vol. II, Publ. No. 31, Geotechnical Engineering Division of American Society of Civil Engineers, .Berkeley

Davis, J.C., (1986), *Statistics and data analysis in Geology*, Second edition, John Wiley & Sons, New York

DeGroot, D. J., Baecher, G. B., (1993), Esimating Autocovariance of In-Situ Soil Properties, *ASCE J of Geotech. Eng.* **119,** No 1.

Ditlevsen, O., (1984). *Probabilistic Thinking: An Imperative in Engineering Modelling*, Report Ser R No 192, Department of Structural Engineering, Technical University of Denmark, Lyngby

Ditlevsen, O. & Madsen, H. O., (1990). *Bærende konstruktioners sikkerhed.* SBI-rapport 211. "the Danish National Building Research Board". Hørsholm. (in Danish).

Ditlevsen, O., (1993). Open debate at *Int. Symposium on Limit State S'Design 93*, Copenhagen

Donald, I. B. Zhao, T. (1994). Default Failure Surfaces for Slope Stability Analysis. *Proc. Int. Conference on Landslides, Slope Stability & the Safety of Infra-Structures.* Kuala Lumpur.

ENV 1991-1. (1994) *Eurocode 1: Basis of design and Actions on Structures.* Part 1: Version sent to CEN/CS Aug 1994. European Committee for Standardization. Bruxelles.

ENV 1997-1. (1994) *Eurocode 7: Geotechnical design - Part 1:General rules* Version sent to CEN/CS Oct 1994. European Committee for Standardization. Bruxelles

Excel for Windows, (1996), *Electronic help Files for Excel*, Microsoft Corp.

Fellenius, B. H., Samson, L. & Tavenas, F., (1989), *Geotechnical Guidelines - Pile design*, Public Works Canada, Marine Works Sector

Hansbo, S. (1990), *Jordmekanik 1, Spänningar av yttre last, sättningar och jordtryck*, Chalmers University of Technology, Göteborg

Hansbo, S., (1994), *Foundation engineering*, Elsevier Science B.V, Amsterdam

Harr, M. E. (1987). *Reliability-Based design in Civil Engineering*. McGraw-Hill Company. New York

Harr, M. E., (1997), *Personal communication*

Hasofer, A. M. Lind, N. C. (1974). An Exact and Invariant First-Order Reliability Format. *Jour of Eng. Mech., ASCE.* vol. 100. 1974.

Heyman, J., (1964), *Beams and Framed Structures*, The Commonwealth and Industrial Library, Pergamon Press, London

Hult, J., (1968), *Hållfasthetslära*, Almqvist & Wiksell, Stockholm (in Swedish)

ISO 2394. (1986). *General principles on reliability for structures*. 2 Edition, October 1986. International Organization of Standardization.

Janbu, N. (1954). *Stability analysis of slopes with dimensionless parameters*. Doctoral Thesis. Cambridge. Massachusetts.

Janbu, N., (1969) The resistance concept applied to deformations of soils, *Proc. 7th ICSMFE*: Vol 1, pp191-196, Mexico City

Janbu, N., (1970), *Grunnlag i geotekknik*, Tapir forlag, (Trondheim, in Norwegian)

Janbu, N. (1989). *Design analyses in Geotechnical Engineering*. Soil as an engineering material and Slope stability analyses , Concept to two chapters in a book with referred title, Lecturer material. Geotechnical Division. Norwegian University of Science and Technology, Trondheim.

Janbu, N., (1996), Slope stability evaluations in engineering practice, *Proc. 7th International Symposium on Landslides. Trondheim.*, Vol 1, Balkema, Roterdam

Jendeby, L., (1986), *Friction piled foundations in soft clay. A study of load transfer and settlements,* PhD Thesis, Department of Geotechnical Engineering, Chalmers University of Technology, Göteborg

Jendeby, L., (1996), *Långtidsuppföljning av fyra byggnader grundlagda med hjälp av kohesionspålar,* Report B 1996:7, Department of Geotechnical Engineering, Chalmers University of Technology, Göteborg (in Swedish)

Kulhawy, F. H., (1992), On the Evaluation of Static Soil Properties, *Proc. Stability and Performance of Slopes and Embankments,* Vol. I, Publ. No. 31, Geotechnical Engineering Division of American Society of Civil Engineers, .Berkeley

Lapin, L:, L:, (1990), *Pobability and statistics for modern engineering,* Second edition, PWS-KENT Publ. Comp., Boston

Larsson, R. & Sällfors, G., (1981), Hypothetical yield envelope at stress rotation. *Proc. 10th Int. Conference on Soil Mechanics and Foundation Engineering,* Vol. 1, Stockholm

Larsson, R., Bergdahl, U. & Eriksson, L., (1984), *Utvärdering av skjuvhållfasthet i kohesionsjord,* Information 3, SGI, Linköping, (In Swedish)

Larsson, R., (1986), *Consolidation of soft soils,* Report 29, Swedish Geotechnical Institute, Linköping

Larsson, R., Bengtsson, P-E., Eriksson, L., (1994), *Sättningsprognoser för bankar på lös finkornig jord,* Information 13, Swedish geotechnical institue, Linköping, (In Swedish)

Li. K. S. & Lumb P. (1987). Probabilistic design of slopes. *Can. Geotech.* J. **24**.

Li, K.S (1992) A unified solution scheme for slope stability analysis. *Proc. 6th International Symposium on Landslides*. Christchurch. 1:481-486.

Madsen, H. O., Krenk, S. & Lind, N., C., (1986), *Methods of structural safety*, Prentice-Hall, Inc., Englewood Cliffs, New Jersey

Mangushev, R., (1994), *General description of laboratory and field study of homogenous fat clay in Nodinge*, Department of geotechnical engineering, Chalmers university of technology.

Mathcad, (1996), *User's Guide. Mathcad 6.0 Mathcad PLUS 6.0*, MathSoft, Inc., Cambridge, Massachusetts

Michalowski, (1995), R., L., Slope stability analysis: a kinematical approach, *Geotechnique*, Vol **XLV**, No 2 June 1995

Morgenstern, N.R. & Price, V.E., (1965), The analysis of the stability of general slip surfaces, *Geotechnique*, **XV**, No 1

Nordal, S., (1993), *Special cases, creep, cyclic effects*, Lecturer material, Design analyses in geotechnical engineering, Lyngby

Olsson, L., (1986), *Användning av ß-metoden i geotekniken*. Doctoral thesis, Division of Soil and Rock Mechanics, Royal Institute of Technology, Sstockholm (in Swedish)

Payne, I., (1995), Aspects of soil structure interaction, *Ground Engineering*, **28**, No 1

Petersson, J., *Tillämpad linjär algebra*, Rex Offsettryck, Hisings-Backa, (in Swedish)

Pettersson, K. & Hultin, S., (1955), The Early History of Circular Sliding Surfaces, *Geotechnique*, **V**, No 5, December 1955

prENV 1997-3, (1996), *Eurocode 7, part 3, Geotechnical design by field testing*, Final draft, European Committee for Standardization. Bruxelles

Rankka, K. ,(1994), *In situ stress conditions across clay slopes*, Doctoral thesis, Dept. of Geotechnical Engineering, Chalmers University of Technology, Göteborg

Rootzén, H., (1995), *Extreme value distributions*, Lecturer notes, Dept, of Mathematical Statistics, Chalmers University of Technology, Göteborg

Rosenblueth, E., (1975), Point estimates for probability moments, *Proc. Nat. Acad. Sci. USA* Vol 72, No 10

Runesson, K., (1978) *On non-linear consolidation of soft clay, Doctoral thesis*, Dept. of Structural Mechanics, Chalmers University of Technology, Göteborg,

Råde, L. & Westergren, B., (1990), *Beta*, Mathematics Handbook, Studentlitteratur, Chartwell-Brtatt Ltd, Lund

Sah, N., Sherorey, P., Upadhaya, R., (1994), Maximum Likelihood Estimation of Slope Stability, *Int. J. Rock. mech. Min. Sci. & Geotech.*, **31**, No 1

Samuelsson, A. & Wiberg, (1988), N-E, *Byggnadsmekanik, Struktur-mekanikens grunder*, Studentlitteratur, Lund

Samuelsson, A. & Wiberg, (1990), N-E, *Byggnadsmekanik, Bärverk*, Studentlitteratur, Lund

Strifors, H., (1991), Elasticitet, *Nationalencyklopedin*, **5**, Bra böcker, Höganäs, 367-368, (In Swedish)

Svensson, C. & Sällfors, G., (1982), *Extremvärdesanalys av 11 grundvattenserier*, Interim report, Geo-hydrological Reserach Group, Chalmers University of Technology, Göteborg, (in Swedish)

Svensson, C. & Sällfors, G., (1988), *Beräkning av dimensionerande grundvattentryck*, Report 87, Geo-hydrological Reserach Group, Chalmers University of Technology, Göteborg, (in Swedish)

Sällfors, G., *Preconsolidation pressure of soft, high-plastic clays*, Doctoral thesis, Dept. of Geotechnical Engineering, Chalmers University of Technology, Göteborg,

Sällfors, G. & Larsson, R. (1984). Beräkning av slänters stabilitet. *Väg- och Vattenbyggaren*. Nr 7-8. 43-46 (in Swedish).

Svanø, G:, Christensen, S. & Nordal, S.,(1991) A soil model for consolidation and creep, *ECSMFE*, Vol. 1, pp 269-272, Firenze

Taylor, D. W., (1937), Stability of earth slopes, *Jour. Boston Soc. Civ. Eng.*, Vol **24**, No 3, Boston

Terzaghi, K., (1943), *Theoretical Soil Mechanics*, John Wiley and Sons, New York,

Terzaghi, K. & Peck, R., (1948), *Soil mechanics in engineering practice*, New York, John Wiley & Sons.. Inc, / London, Chapman & Hall. Inc.

Thoft Christensen, P. & Baker, M.J. (1982). *Structural Reliability and its Applications*. Springer-Verlag. Berlin,Heidelberg, New York.

Tremblay, M., (1995), *Modelling of groundwater conditions in silts and fine sands*, Doctoral thesis, Dept. of Geotechnical Engineering, Chalmers University of Technology, Göteborg

Vanmarcke, E. H. (1977). Probabilistic Modelling of Soil Profiles. *ASCE J of Geotech. Eng.* no 11. 1227-1246.

Wood, D. M., (1990), *Soil Behaviour and Critical State Soil Mechanics*, Cambridge University Press, Cambridge

Öberg. A-L., (1996), Improving engineering practice of slope stability for unsaturated soils, *Proc. 7th International Symposium on Landslides. Trondheim.*, Vol 2, Balkema, Rotterdam

Öberg, A-L., (1997), *Matrix Suction in Silt and Sand Slopes*, Doctoral thesis, Dept. of Geotechnical Engineering, Chalmers University of Technology, Göteborg

Öberg Högsta, A-L., (1997), *Personal communication.*

INDEX

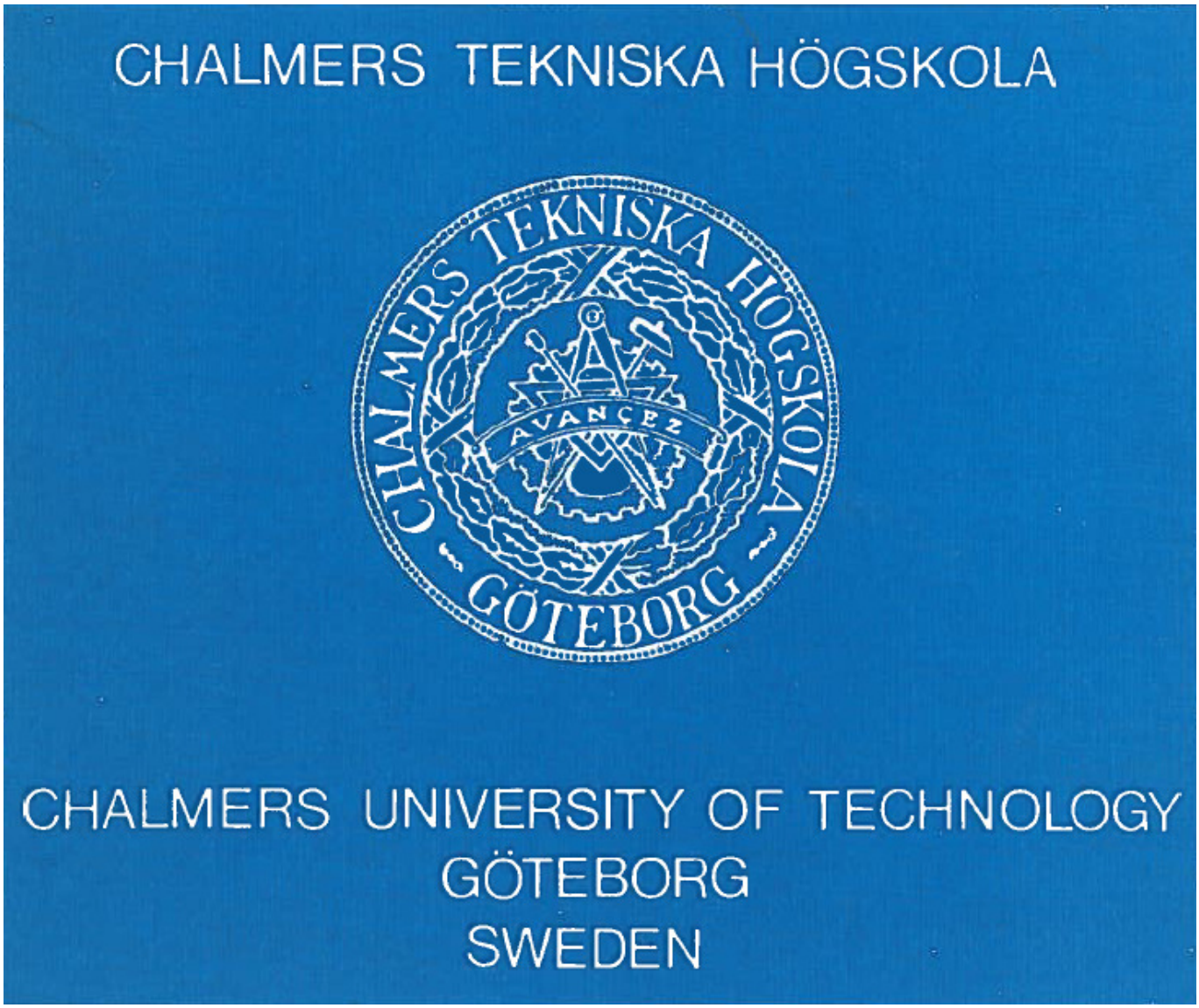

ON PROBABILITY IN GEOTECHNICS

APPENDICES

VOLUME 2

CLAES ALÉN

DEPARTMENT OF GEOTECHNICAL ENGINEERING

1998

ON PROBABILITY IN GEOTECHNICS

Volume 2 - Appendices

Claes Alén

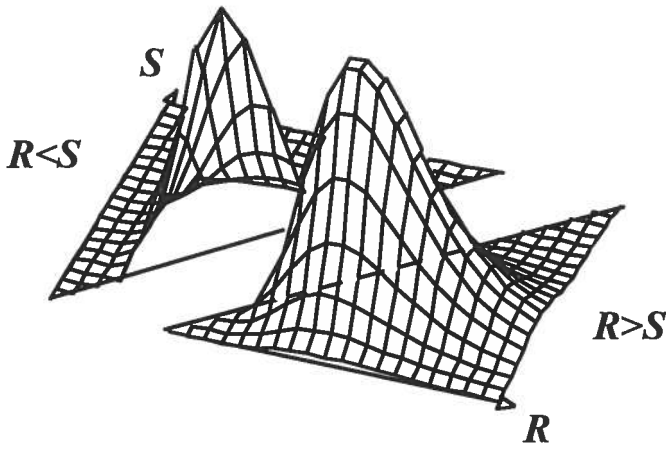

Department of Geotechnical Engineering
Chalmers University of Technology
S-412 96 Göteborg, Sweden

ISBN 91-7197-637-X
ISSN 0346-718X

ON PROBABILITY IN GEOTECHNICS

Claes Alén
Department of Geotechnical Engineering
Chalmers University of Technology
S-412 96 Göteborg, Sweden

ERRATA VOLUME 2

Page	Location[1]	Printed	Corrected
A1	(A.3)	$x+\frac{1}{2\cdot\sqrt{x}}$	$\lvert x\rvert+\frac{1}{2\cdot\sqrt{\lvert x\rvert}}$
A4	(A.16a)	$/b-a$	$/(b-a)$
A6	(A.23)	$\mu_{x_i}=\mu_{x_j}\approx\sigma$	$\mu_{x_i}=\mu_{x_j}=\mu$
A7	(A.27b)	$df(E[X])$	$dg(E[X])$
D1	(D.2)	$f_{\rightarrow}=f(X_+,Y_+)$	$f_{\rightarrow}=f(X_-,Y_+)$
D2	(D.6)	$+\frac{1+\rho}{4}\cdot\left[(\mu_x+\sigma_x)+(\mu_y+\sigma_y)\right]$	$+\frac{1+\rho}{4}\cdot\left[(\mu_x-\sigma_x)+(\mu_y-\sigma_y)\right]$
D21	(D.25)	$\ldots\sigma_R)\cdot s$ (at 4 places)	$\ldots\sigma_R)\cdot Q$
D23	(D.30)	$Var\left[f(R,M_0)\right]$	$Var\left[s(R,M_0)\right]$
D23	8b	'variable'	'variable' R-Q
D27	(D.32)	$\ldots\sigma_M)\cdot Q$ (at 4 places)	$\ldots\sigma_M)\cdot s$
D28	(D.34)	$\mu_R\cdot\mu_M\cdot Q$	$\mu_R\cdot\mu_M\cdot s$
E2	4a	$\mu_x(z)=\mu_x(z+r)=\mu_x(z)$	$\mu_x(z)=\mu_x(z+r)$
F1	3a	report B 1998:x	report B 1998:1
F12	5a	see F.3.3	see Alén (1998a)
F12	11a	cf. figure	cf. figure 3.9
J4	6b	…for $m_d=R_d-S_d\ldots$	…, i.e. $m_d=R_d-S_d=0\ldots$
J4	(J.10)	$\mu\approx\gamma_S\cdot\gamma\cdot\mu_S\cdot\exp(2\cdot\alpha\cdot V)$	$\mu_R\approx\gamma_S\cdot\gamma_R\cdot\mu_S\cdot\exp(2\cdot\alpha\cdot V)$
J4	(J.6a)	$\mu_R-\gamma_S\cdot\gamma_R\cdot\exp(2\cdot\alpha\cdot V)$	$\mu_R-\gamma_S\cdot\gamma_R\cdot\mu_S\cdot\exp(2\cdot\alpha\cdot V)$
K3	(K.11a,b)	$y_0\ldots x_0\ldots\theta_u$	$y_c\ldots xc\ldots\theta_w$
L2	(L.2)	$m_0+\varepsilon_m+\frac{\Delta_R+\Delta_S}{\mu_R}=m_0+\varepsilon_m+\Delta m$	$m_0-\varepsilon_m+\frac{\Delta_R+\Delta_S}{\mu_R}=m_0-\varepsilon_m+\Delta m$
N1	9a	section 1.3.7	section 4.3.7
N3	(N.8)	$\sin(\varsigma_{sup})$	$\cos(\varsigma_{sup})$
N4	7a	H^2	$\gamma\cdot H^3$
N4	(N.11)	$m_S=\frac{M_S}{H^2}$	$m_S=\frac{M_S}{\gamma\cdot H^3}$
N7	(N.25)	$u_{crest}\approx\frac{u_{crest}}{2}$	$u_{neg}\approx\frac{u_{crest}}{2}$
N7	(N.26)	u_{icrest}	u_{crest}

[1] a = from above, b = from below

Page	Location	Printed	Corrected
N8	2a	$S=\int_{inf}^{\varsigma_{sup}}R\,d\varsigma$	$S=\int_{\varsigma_{inf}}^{\varsigma_{sup}}R\,d\varsigma$
O5	9a	reactions	internal forces
O7	(O.9)	$A^T_{i,2i-}=-1$	$A^T_{i,2i-1}=-1$
O7	3b	section 1.1.3	section O.1.3
O8	4a-7a	A more exact… in the node.	-
P2	1a	e.g. a virgin curve	e.g. defined by a virgin curve
P3	(P.3)	$\ldots=-\frac{v}{\Delta z}=-\frac{ki}{\Delta z}=-\frac{k\cdot\frac{\Delta u}{\gamma_w\Delta z}}{\Delta z}=\ldots$	$\ldots=-\frac{\Delta v}{\Delta z}=-\frac{\Delta(ki)}{\Delta z}=-\frac{\Delta\left(k\cdot\frac{\Delta u}{\gamma_w\Delta z}\right)}{\Delta z}=\ldots$
P4	(P.7a)	$(t+t)$	$(t+t_r)$
P6	(P.13)	max	min
P6	(P13a)	max	min
P7	1b	f'c,inf and f'c,sup	p'c,inf and p'c,sup
P8	(P.15)	max	min
P9	foot note	in such a case	otherwise
P12	5a	$(0{,}5-0{,}7\cdot\ln(\frac{M}{r\cdot q})$	$(0{,}5-0{,}7\cdot\ln(\frac{M}{r\cdot q}))$
P13	(P.25)	s_{max}	$s_{max,pl}$
Q1	(Q.3)	$P_\Sigma=$	$M_\Sigma=$
R2	Fig R.2	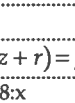	

CONTENTS - APPENDICES

Appendix A Formulas

Appendix B 'Probability paper'

Appendix C Correlation / Two variables

Appendix D PEM / Accuracy

Appendix E Geostatistics / Formulas

Appendix F Geostatistics/Examples

Appendix G On Bayesian statistics

APPENDIX A FORMULAS

A.1 Distributions

A.1.1 Standard normal distribution

Density function: $$\varphi(x) = \frac{1}{\sqrt{2\pi}} e^{-\frac{x^2}{2}} \quad \text{(A.1)}$$

Cumulative distribution: $$\Phi(x) = \int_{-\infty}^{x} \frac{1}{\sqrt{2\pi}} e^{-\frac{z^2}{2}} dz \quad \text{(A.2)}$$

Approximate formulation[1]:

$x < -0{,}65$: $$\Phi_1(x) = \frac{1}{\sqrt{2 \cdot \pi}} \cdot e^{-\frac{x^2}{2}} \cdot \frac{1}{x + \frac{1}{2 \cdot \sqrt{x}}} \quad \text{(A.3)}$$

$-0.65 < x < 0{,}65$: $$\Phi_2(x) = 0{,}5 + \frac{x}{2{,}65} \quad \text{(A.3a)}$$

$0{,}65 < x$: $$\Phi_3(x) = 1 - \Phi_1(-x) \quad \text{(A.3b)}$$

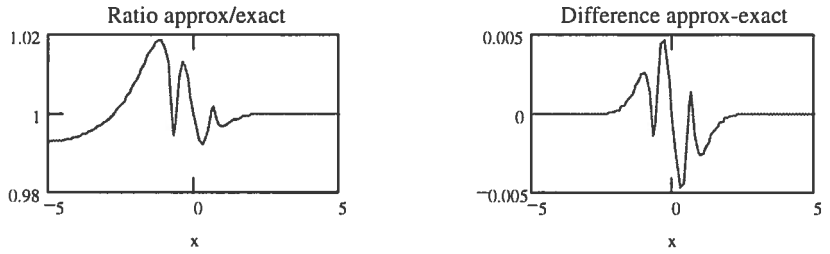

Figure A1 Accuracy of approximate formulation of $\Phi(x)$

Inverse distribution: $$x = \Phi^{-1}(p) \quad \text{(A.4)}$$

Approximate formulation:

$p < 0{,}25$:

$$x = \Phi_1^{-1}(p) = -\sqrt{-\ln(p^2) - 100 \cdot \left\{-\ln(p) - 0{,}05\right\}^{0{,}0115} + 98} \quad \text{(A.5)}$$

$0{,}25 < p < 0{,}75$: $$x = \Phi_2^{-1} = 2{,}65 \cdot (0{,}5 - p) \quad \text{(A.5a)}$$

$0{,}75 < p$: $$x = \Phi_3^{-1}(p) = -\Phi_1^{-1}(1 - p) \quad \text{(A.5b)}$$

[1] intended as a good approximation of the tails

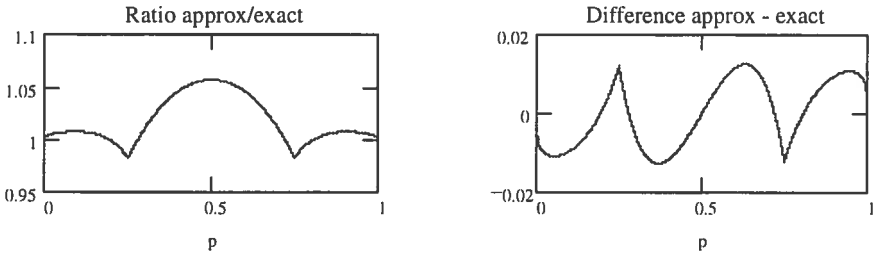

Figure A2 Accuracy of approximate formulation of $\Phi^{-1}(p)$

A.1.2 Lognormal distribution

$$x = LN(\mu,\sigma) \quad \text{and} \quad y = \ln(x) \Rightarrow y = N(\mu_y,\sigma_y) \approx N(\ln(\mu),V) \quad \text{(A.6)}$$

$$\mu_y = \ln(\mu) - \frac{1}{2}\cdot\ln(1+\frac{\sigma^2}{\mu^2}) = \ln(\mu) - \frac{1}{2}\cdot\ln(1+V^2) \approx \ln(\mu) \quad \textit{(A.7)}$$

$$\sigma_y^2 = \ln(1+\frac{\sigma^2}{\mu^2}) = \ln(1+V^2) \approx V^2 \quad \text{(A.8)}$$

$$\mu = \exp(\mu_y + \frac{1}{2}\cdot\sigma_y^2) \approx \exp(\mu_y) \quad \text{(A.9)}$$

$$\sigma^2 = \mu^2\cdot(e^{\sigma_y^2} - 1) = \mu^2\cdot V^2 \quad \text{(A.10)}$$

The approximations given in equations A.6 - A.10 were obtained by a Gaussian approximation, see section A.2.6. For accuracy of the approximation, see Figure A3.

Remark: μ and σ refer here to the basic variable x. In the literature the lognormal distribution is often defined by the parameters for the corresponding normal distribution, i.e. μ_y and σ_y.

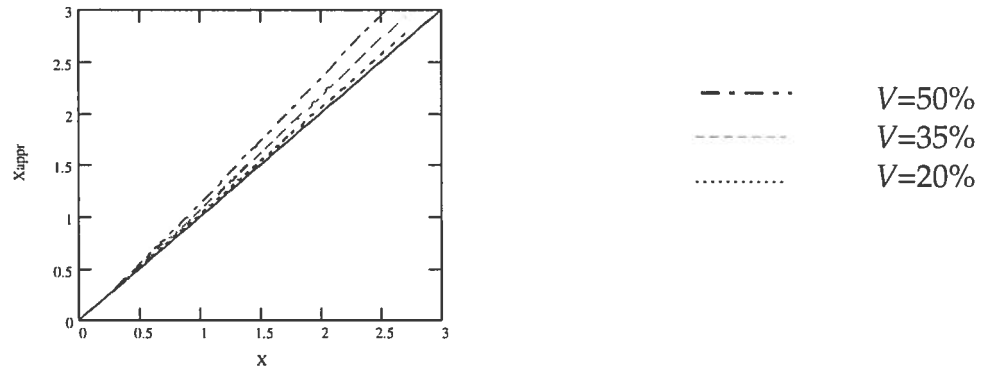

Figure A3 Gaussian approximation of lognormal distributions. μ=1

Skewness and kurtosis (Benjamin & Cornell, 1970):

$$\beta(1) = 3 \cdot V + V^3 \approx 3 \cdot V \qquad \text{(A.11)}$$

$$\beta(2) = 3 + 16 \cdot V^2 + 15 \cdot V^4 + 6 \cdot V^6 + V^8 \approx 3 + 16 \cdot V^2 \qquad \text{(A.12)}$$

A.1.3 Gumbel distribution

Cu1mulative distribution:

$$F(x) = \exp\{-\exp[-\alpha \cdot (x - u)]\} \qquad \text{(A.13)}$$

$\alpha = \dfrac{\pi}{\sigma \cdot \sqrt{6}}$ and $u = \mu - \sigma \cdot \sqrt{6} \cdot \dfrac{\gamma}{\pi} \approx^{2} \mu - \sigma \cdot \dfrac{\sqrt{2}}{\pi}$ gives

$$F(x) = \exp\left\{-\exp\left[-\frac{\pi}{\sigma \cdot \sqrt{6}} \cdot \left(x - \mu + \sigma \cdot \frac{\sqrt{2}}{\pi}\right)\right]\right\} \qquad \text{(A.13a)}$$

Probability density function

$$f(x) = \alpha \cdot \exp\{-\alpha \cdot (x - u) - \exp[-\alpha \cdot (x - u)]\} \qquad \text{(A.14)}$$

$$f(x) = \frac{\pi}{\sigma \cdot \sqrt{6}} \cdot \exp\left\{\frac{\pi}{\sigma \cdot \sqrt{6}} \cdot (\mu - x) - \frac{1}{\sqrt{3}} - \exp\left[\frac{\pi}{\sigma \cdot \sqrt{6}} \cdot (\mu - x) - \frac{1}{\sqrt{3}}\right]\right\} \qquad \text{(A.14a)}$$

Inverse distribution (to equation A.13a):

$$F^{-1}(p) = u - \frac{1}{\alpha} \cdot \{\ln[-\ln(p)]\} \qquad \text{(A.15)}$$

$$F^{-1}(p) = \mu - \frac{\sigma \cdot \sqrt{2}}{\pi} \cdot \{1 + \sqrt{3} \cdot \ln[-\ln(p)]\} \qquad \text{(A.15a)}$$

[2] γ is Euler's constant = 0.5772...

A.1.4 ß-distribution

The probability density function, for a variable defined in the range [0;1], is given by, see e.g. (Beta, 1990):

$$f_{01}(x) = \frac{\Gamma(p+q)}{\Gamma(p)\cdot\Gamma(q)} \cdot x^{p-1} \cdot^{(1-x)} q - 1 \qquad \text{(A.16)}$$

where p and q are two scale parameters. $\Gamma(\,)$ is the gamma function.

Equation A.16 corresponds to, for a variable in the range [a;b]:

$$f_{ab}(x) = f_{01}\left(\frac{x-a}{a-b}\right)\Big/ b-a$$

with the cumulative distribution

$$F_{ab}(x) = F_{01}\left(\frac{x-a}{a-b}\right) \qquad \text{(A.16a-c)}$$

and the inverse

$$F_{ab}^{-1}(p) = F_{01}^{-1}(p)\cdot(b-a)+a$$

The distribution can as an alternative be defined by the four parameters, μ, σ, a and b, see (Harr, 1987). The following relations apply:

$$\frac{p}{p+q} = \frac{\mu-a}{b-a} \quad ; \quad \frac{q}{p+q} = \frac{b-\mu}{b-a}$$

and (A.17a-c)

$$p+q = \frac{(\mu-a)\cdot(b-\mu)-\sigma^2}{\sigma^2}$$

which give:

$$p = \left(\frac{\mu-a}{\sigma}\right)^2 \cdot \frac{b-\mu}{b-a} - \frac{\mu-a}{b-a}$$

and (A.17d,e)

$$q = \left(\frac{b-\mu}{\sigma}\right)^2 \cdot \frac{\mu-a}{b-a} - \frac{b-\mu}{b-a}$$

A.2 Functions of random variables

Formulas are rewritten from (Blom, 1984a)

A.2.1 Sum

$$E[X+Y]=E[X]+E[Y]$$

correlated variables

$$Var[X+Y]=Var[X]+Var[Y]+2Cov[X,Y] \qquad \text{(A.18a-c)}$$

uncorrelated variables

$$Var[X+Y]=Var[X]+Var[Y]$$

A.2.2 Difference

$$E[X-Y]=E[X]-E[Y]$$

correlated variables

$$Var[X-Y]=Var[X]+Var[Y]-2\cdot Cov[X,Y] \qquad \text{(A.19a-c)}$$

uncorrelated variables

$$Var[X-Y]=Var[X]+Var[Y]$$

A.2.3 Linear combination

$$E\left[\sum c_i X_i\right]=\sum c_i E[X_i]$$

$$Var\left[\sum c_i X_i\right]=\sum c_i^2\cdot Var[X_i]+2\sum_{i<j} c_i c_j\cdot Cov\left[X_i X_j\right] \qquad \text{(A.20a,b)}$$

Example

$$E[aX+b]=a\cdot E[X]+b \qquad \text{(A.21a,b)}$$

$$Var[aX+b]=a^2\cdot Var[X]$$

Special case 1: Mean of uncorrelated variables

$$\text{Mean } \overline{X} = \sum_n X_i \Big/ n \quad ; \quad c_i = 1/n$$

$$E[\overline{X}] = \frac{\sum E[X_i]}{n} \qquad \text{(A.22a-c)}$$

$$Var[\overline{X}] = \frac{\sum Var[X_i]}{n^2} \quad \text{(Variance reduction)}$$

Special case 2 $\quad \mu_{X_i} = \mu_{X_j} = \sigma,\ c_i = 1$

$$E[\sum X_i] = n \cdot \mu \qquad \text{(A.23)}$$

Special case 3 $\quad \sigma_{X_i} = \sigma_{X_j} = \sigma,\ c_i = 1$

$$Var[\sum X_i] = n \cdot \sigma^2 + n(n-1) \cdot \rho \cdot \sigma^2 \qquad \text{(A.24)}$$

A.2.4 Product:

Uncorrelated variables

$$E[X \cdot Y] = E[X] \cdot E[Y]$$

$$Var[X \cdot Y] = Var[X] \cdot E^2[Y] + Var[Y] \cdot E^2[X] + Var[X] \cdot Var[Y]$$
$$\approx Var[X] \cdot E^2[Y] + Var[Y] \cdot E^2[X] \qquad \text{(A.25a-c)}$$

$$V^2[X \cdot Y] = V^2[X] + V^2[Y] + V^2[X] \cdot V^2[Y]$$
$$\approx V^2[X] + V^2[Y]$$

The last parts of the two last equations are obtained by a Gaussian approximation, see section A.2.6. In appendix D are given other approximations obtained by the PEM-method, cf. Volume 1, Chapter 2.

A.2.5 Ratio:

Uncorrelated variables

$$E\left[\frac{X}{Y}\right] \approx \frac{E[X]}{E[Y]}$$

$$Var\left[\frac{X}{Y}\right] \approx Var[X]\cdot\frac{1}{E^2[Y]} + Var[Y]\cdot\frac{E^2[X]}{E^4[Y]} + \\ + Var[X]\cdot Var[Y]\cdot\frac{E^2[X]}{E^4[Y]} \approx \qquad \text{(A.26a,b)}$$

$$\approx Var[X]\cdot\frac{1}{E^2[Y]} + Var[Y]\cdot\frac{E^2[X]}{E^4[Y]}$$

$$V^2\left[\frac{X}{Y}\right] \approx V^2[X] + V^2[Y] + V^2[X]\cdot V^2[Y] \approx V^2[X] + V^2[Y]$$

The middle parts of the two last equations are derived as the product X·1/Y, in which parameters for the factor 1/Y are obtained by a Gaussian approximation. The last parts are obtained by a Gaussian approximation for the function $g(X,Y)=X/Y$, see section A.2.6

A.2.6 Gaussian approximation

Taylor expansion around μ, keeping two terms, i.e. linear approximation

One-dimensional random variables

$$E[g(X)] \approx g(E[X])$$

(A.27a,b)

$$Var[g(X)] \approx Var[X]\cdot\left\{\frac{df(E[X])}{dX}\right\}^2$$

Special case 1: $g(X)=\frac{1}{X}$

$$E\left[\frac{1}{X}\right]\approx\frac{1}{E[X]}$$

$$Var\left[\frac{1}{X}\right]\approx Var[X]\cdot\frac{1}{E[X]^4} \qquad \text{(A.28a-c)}$$

$$V\left[\frac{1}{X}\right]=\sqrt{Var\left[\frac{1}{X}\right]}\Big/E\left[\frac{1}{X}\right]\approx\frac{\sqrt{Var[X]}}{E[X]}=V[X]$$

Special case 2: $g(X)=\ln X$

$$E[\ln X]\approx\ln\mu_X$$

$$Var[\ln X]\approx\sigma^2\cdot\left(\frac{1}{\mu_X}\right)^2=V^2 \qquad \text{(A.29a,b)}$$

Random vectors

$$E\left[g(X_1,X_2,\ldots X_n)\right]\approx g\left(E[X_1],E[X_2],\ldots E[X_n]\right)$$

$$Var\left[g(X_1,X_2,\ldots X_n)\right]\approx\sum_{i=1}^{n}Var[X_i]\cdot\left\{\frac{\partial g(E[\mathbf{X}])}{\partial X_i}\right\}^2+$$

$$+2\cdot\sum_{i<j}Cov(X_i,X_j)\cdot\frac{\partial g(E[\mathbf{X}])}{\partial X_i}\cdot\frac{\partial g(E[\mathbf{X}])}{\partial X_j} \qquad \text{(A.30a,b)}$$

with the notation $\frac{\partial g(E[\mathbf{X}])}{\partial X_i}=\frac{\partial g\left(E[X_1],E[X_2],\ldots E[X_n]\right)}{\partial X_i}$

Uncorrelated variables:

$$E[g(X_1, X_2, \ldots X_n)] \approx g(E[X_1], E[X_2], \ldots E[X_n])$$

(A.31a,b)

$$Var[g(X_1, X_2, \ldots X_n)] \approx \sum_{i=1}^{n} Var[X_i] \cdot \left\{ \frac{\partial g}{\partial X_i}(E[\mathbf{X}]) \right\}^2$$

Special case 1: $g(X_1, X_2, \ldots X_n) = \sum c_i \cdot X_i$

Solution exact, see section A.2.3

Special cases 2 and 3: Product and ratio, see sections A.2.4 and A.2.5

A.2.7 Inequalities

$$E\left[\frac{1}{X}\right] > \frac{1}{E[X]} \quad \text{if} \quad \text{all} \quad x > 0$$

$$E[X^2] > E^2[X] \qquad \text{(A.32a-c)}$$

$$Var[X \cdot Y] > Var[X] \cdot Var[Y]$$

A.3 Statistical parameters

A.3.1 Population

Variance:

$$Var[X] = E\left[(X-\mu)^2\right] = E\left[X^2\right] - E^2[X] \qquad \text{(Steiners rule)}$$

Covariance

$$Cov[X,Y] = E\left[(X-\mu_X)\cdot(Y-\mu_Y)\right] = E[X\cdot Y] - E[X]\cdot E[Y]$$

Coefficient of correlation

$$\rho_{X,Y} = \frac{Cov[X,Y]}{D[X]\cdot D[Y]}$$

Coefficient of skewness

$$\beta(1) = \frac{E\left[(X-\mu)^3\right]}{D[X]^3}$$

Coefficient of kurtosis (A.33a-e)

$$\beta(2) = \frac{E\left[(X-\mu)^4\right]}{D[X]^4}$$

A.3.2 Sample

From (Blom, 1984b)

Product sum

$$S_{XY} = \sum\left(X_i - \bar{x}\right)\cdot\left(Y - \bar{y}\right) = \sum x_i y_i - \frac{1}{n}\sum x_i \cdot \sum y_i$$

(A.34a,b)

Quadratic sum

$$S_{XX} = \sum\left(X_i - \bar{x}\right)^2 = \sum x_i^2 - \frac{1}{n}\left(\sum x_i\right)^2$$

Estimation of

mean value:

$$\bar{x} = \frac{\sum x_i}{n}$$

variance:

$$s_X^{\,2} = \frac{S_{XX}}{n-1}$$

covariance:

$$c_{XY} = \frac{S_{XY}}{n-1} \qquad \text{(A.35a-f)}$$

correlation:

$$r = \frac{c_{XY}}{s_X \cdot s_Y}$$

skewness (EXCEL, 1996)

$$\beta(1) = \frac{n}{(n-1)\cdot(n-2)} \sum \left(\frac{x_i - \bar{x}}{s_X} \right)^3$$

kurtosis (EXCEL, 1996)

$$\beta(2) - 3 = \frac{n\cdot(n+1)}{(n-1)\cdot(n-2)\cdot(n-3)} \sum \left(\frac{x_i - \bar{x}}{s_X} \right)^4 - \frac{3\cdot(n-1)^2}{(n-2)\cdot(n-3)}$$

A.3.3 Linear regression

Population

Linear regresion: (Blom, 1984a)

$$Y - \mu_Y = \frac{Cov[X,Y]}{Var[X]} \cdot (X - \mu_X) \qquad \text{(A.36)}$$

Sample

Linear regression

$$Y - \bar{y} = \frac{S_{XY}}{S_{XX}} \cdot \left(X - \bar{x} \right) \qquad \text{(A.37)}$$

A.4 Probability of failure / Reliability index β

A.4.1 Probability of failure as a function of β

$$p = \Phi(-\beta) \tag{A.38}$$

Approximately (cf. section A.1.1):

$$0 < \beta < 0{,}65: \qquad p = 0{,}5 - \frac{\beta}{2{,}65} \tag{A.38a}$$

$$\beta > 0{,}65: \qquad p = \frac{1}{\sqrt{2 \cdot \pi}} \cdot e^{-\frac{\beta^2}{2}} \cdot \frac{1}{\beta + \frac{1}{2 \cdot \sqrt{\beta}}} \tag{A.38b}$$

A.4.2 β as a function of probability of failure

$$\beta = -\Phi^{-1}(p) \tag{A.39}$$

Approximately (c.f. section A.1.1):

$$0{,}25 < p < 0{,}50 \qquad \beta = 2{,}65 \cdot (0{,}5 - p) \tag{A.39a}$$

$$p < 0{,}25 \qquad \beta = \sqrt{-\ln p^2 - 100(-\ln p - 0{,}05)^{0{,}0115} + 98} \tag{A.39b}$$

A.5 Partial factors

Design values on general form:

$$x_d = F^{-1}\{\Phi(-\alpha\beta\} \tag{A.40}$$

where $F(x)$ is the distribution for the random variable at hand.

Partial factors for resistance variables:

$$\gamma_R = R_k / R_d \tag{A.41}$$

Partial factors for action variables:

$$\gamma_S = S_d / S_k \tag{A.42}$$

A.5.1 Actions/action effects

Normal distribution

$S = N(\mu,\sigma), \quad V = \sigma/\mu$

$$S_d = \mu + \alpha \cdot \beta \cdot \sigma \quad \Rightarrow \quad \gamma = (\mu + \alpha \cdot \beta \cdot \sigma) / S_K$$

$$S_K = \mu \quad \Rightarrow \quad \gamma = 1 + \alpha \cdot \beta \cdot V \qquad \text{(A.43a-c)}$$

$$S_K = S_{98\%} \approx \mu + 2 \cdot \sigma \quad \Rightarrow \quad \gamma = \frac{1 + \alpha \cdot \beta \cdot V}{1 + 2 \cdot V}$$

Lognormal distribution

S: $LN(\mu,\sigma), \quad V = \sigma/\mu$

$Y = \ln S$ with

$$\mu_Y = \ln \mu - \frac{1}{2}\ln(1 + \frac{\sigma^2}{\mu^2}) = \ln \mu - \frac{1}{2}\ln(1 + V^2) \approx \ln \mu$$

$$\sigma_Y = \sqrt{\ln(1 + \frac{\sigma^2}{\mu^2})} = \sqrt{\ln(1 + V^2)} \approx \frac{\sigma}{\mu} = V$$

$$S_d = \exp(\mu_Y + \alpha\, \beta\, \sigma_Y) \quad \Rightarrow \quad \gamma = \exp(\mu_Y + \alpha \beta \sigma_Y)/S_k$$

$$S_k = \mu = \exp(\mu_Y + \tfrac{1}{2} \cdot \sigma_Y^2) \quad \Rightarrow \quad \gamma = \exp(\alpha \beta \sigma_Y - \tfrac{1}{2} \cdot \sigma_Y^2) \qquad \text{(A.44a-c)}$$

$$S_k = S_{98\%} \approx \exp(\mu_Y + 2 \cdot \sigma_Y) \quad \Rightarrow \quad \gamma = \exp(\langle \alpha \beta - 2 \rangle\, \sigma_Y)$$

or for small V (<25-30%)

$$S_d = \exp(\mu_Y + a\, \beta\, \sigma_Y) \approx \mu \cdot \exp(\alpha \beta V)$$

$$S_k = \mu \approx S_{50\%} \quad \Rightarrow \quad \gamma = \exp(\alpha \beta V) \qquad \text{(A.45a,b)}$$

$$S_k = S_{98\%} \approx \mu \cdot \exp(2 \cdot V) \quad \Rightarrow \quad \gamma = \exp(\langle \alpha \beta - 2 \rangle V)$$

Gumbel distribution

S: Gu(u,α) with

$$\alpha = \frac{\pi}{\sigma \cdot \sqrt{6}} \quad \text{and} \quad u \approx \mu - \sigma \cdot \frac{\sqrt{2}}{\pi}, \quad V = \sigma/\mu$$

$$S_d = \mu - \frac{\sigma \cdot \sqrt{2}}{\pi} \cdot \left\{1 + \sqrt{3} \cdot \ln\left[-\ln(\Phi\langle -\alpha\beta\rangle)\right]\right\} \quad \Rightarrow \quad \gamma = S_d/S_k$$

$$S_k = \mu \qquad \Rightarrow \quad \gamma = 1 - \frac{V \cdot \sqrt{2}}{\pi} \cdot \left\{1 + \sqrt{3} \cdot \ln\left[-\ln(\Phi\langle -\alpha\beta\rangle)\right]\right\} \tag{A.46a-c}$$

$$S_k = S_{98\%} = \mu - \frac{\sigma \cdot \sqrt{2}}{\pi} \cdot \left\{1 + \sqrt{3} \cdot \ln\left[-\ln(0{,}98)\right]\right\} \approx \mu + 2{,}6 \cdot \sigma \Rightarrow$$

$$\Rightarrow \quad \gamma = \frac{1 - \frac{V \cdot \sqrt{2}}{\pi} \cdot \left\{1 + \sqrt{3} \cdot \ln\left[-\ln(\Phi\langle -\alpha\beta\rangle)\right]\right\}}{1 + 2{,}6 \cdot V}$$

A.5.2 Resistance

Normal distribution
(to be used with caution, cf. Volume 1, Chapter 2, Distributions)

$R =$ $N(\mu,\sigma)$, $V = \sigma/\mu$, $\alpha \le 0$

$$R_d = \mu - |\alpha| \cdot \beta \cdot \sigma \qquad \Rightarrow \qquad \gamma = R_k/(\mu - |\alpha| \cdot \beta \cdot \sigma) \tag{A.47a-c}$$

$$R_K = \mu \qquad \Rightarrow \qquad \gamma = 1/(1 - |\alpha| \cdot \beta \cdot V)$$

$$R_K = R_{5\%} \approx \mu - 1{,}65 \cdot \sigma \qquad \Rightarrow \qquad \gamma = \frac{1 - 1{,}65 \cdot V}{1 - |\alpha| \cdot \beta \cdot V}$$

Lognormal distribition

$LN(\mu,\sigma)$, $V=\sigma/\mu$, $\alpha \le 0$

$Y = \ln R$ with

$$\mu_Y = \ln\mu - \frac{1}{2}\ln(1+\frac{\sigma^2}{\mu^2}) = \ln\mu - \frac{1}{2}\ln(1+V^2) \approx \ln\mu$$

$$\sigma_Y = \sqrt{\ln(1+\frac{\sigma^2}{\mu^2})} = \sqrt{\ln(1+V^2)} \approx \frac{\sigma}{\mu} = V$$

$$R_d = \exp(\mu_Y - |\alpha|\beta\sigma_Y) \quad \Rightarrow \quad \gamma = R_K / \exp(\mu_Y - |\alpha|\beta\sigma_Y)$$

$$R_K = \mu = \exp(\mu_Y + \tfrac{1}{2}\sigma_Y^2) \quad \Rightarrow \quad \gamma = \exp(|\alpha|\beta\sigma_Y + \tfrac{1}{2}\sigma_Y^2) \qquad \text{(A.48a-c)}$$

$$R_K = R_{5\%} = \exp(\mu_Y - 1{,}65\cdot\sigma_Y) \Rightarrow \gamma = \exp(|\alpha|\beta\sigma_Y - 1{,}65\sigma_Y)$$

or for small V (< 25-30%)

$$R_d = \exp(\mu_Y - |\alpha|\beta V) \approx \mu\cdot\exp(-|\alpha|\beta V) \Rightarrow \gamma \approx \frac{R_K}{\mu\cdot\exp(-|\alpha|\beta V)}$$

$$R_K = \mu \quad \Rightarrow \quad \gamma = \exp(|\alpha|\beta V) \qquad \text{(A.49a-c)}$$

$$R_K = R_{5\%} \approx \mu\cdot\exp(-1{,}65V) \quad \Rightarrow \quad \gamma = \exp(|\alpha|\beta V - 1{,}65\cdot V)$$

APPENDIX B 'PROBABILITY PAPER'

Let x be given by a fixed but unknown distribution $F(x)$, see Figure B.1

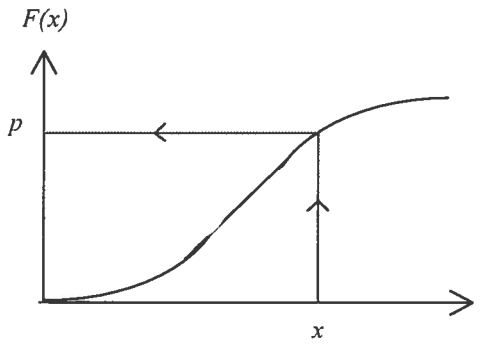

Figure B.1 Distribution $F(x)$

Assume a sorted sample of n elements such that:

$$\boldsymbol{x} = \{x_1 < x_2 < \ldots < x_i < \ldots < x_n\} \tag{B.1}$$

and with corresponding probabilities, cf. Figure B.2:

$$p = \left\{\frac{1-\frac{1}{2}}{n}, \frac{2-\frac{1}{2}}{n}, \ldots, \frac{i-\frac{1}{2}}{n}, \ldots, \frac{n-\frac{1}{2}}{n}\right\} \tag{B.2}$$

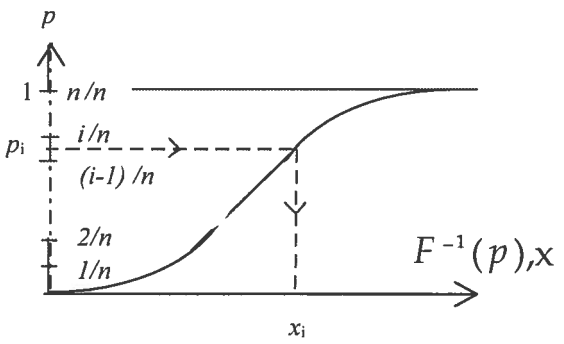

Figure B.2 'Probablities' for a sample of a distribution $F(x)$

The y-axis in Figure B.2 is divided into n equal intervals. The mid value for each interval is equal to $i-\frac{1}{2}/n$. Thus

$$x_i = F^{-1}(p_i) \quad \text{with} \quad p_i = \frac{i-\frac{1}{2}}{n} \tag{B.3}$$

Obviously the plot $\{x_i, F_*^{-1}(p_i)\}$ will give approximately the straight line $y=x$ for a representative sample, if $F_*(x) = F(x)$. If instead $F_*(x)$ is a normed[1] distribution of the "right" type, e.g. $\Phi(x)$ instead of $N(\mu,\sigma)$, the scale and the location of the "line" will change and the plot will give the line $y = (x-\mu)/\sigma$, see Figure B.3.

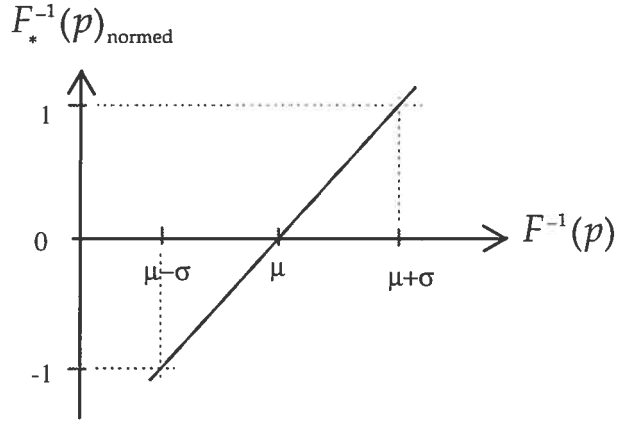

Figure B.3 Location and scale transformation by a "normed" distribution

In the latter procedure, described above, the standard deviation will be given by the slope of the line, $1/\sigma$, and the mean value by the x-intercept. However, the latter procedure has two requirements. Firstly, the obvious one, the 'normed' form of the distribution must exist. This is for example not the case for a lognormal distribution, which is not defined for non-negative values. Secondly, the location and scale transformation must not change the shape of the distribution, i.e. a plot as in Figure B.3 is a straight line[2]. A lognormal distribution for example requires that the coefficient of variation is kept unchanged by the transformation. A more simple way to graph a lognormal distribution is to plot the logarithms of the sample values, or in other words, to plot the values in a logscale, see Figure B.4. Such a plot draws attention to a difficulty with lognormal distributions, i.e. to know the 'true' origo. For a strength variable the choice seems obvious as one normally assumes that zero is a natural lower bound. However, it is possible to choose another bound. For example $x_*=x-x_{inf}$ might be a lognormal distribution. The situation is illustrated in Figure B.5, in which three different sets of values x-a, x and x+a are plotted. The values of x are

[1] $\mu=0$, $\sigma=1$

[2] The location parameter must not be the expected value, μ, and the scale parameter must not be the standard deviation, σ.

lognormal distributed, while a is a constant. The different sets of values can be seen as the same sample, but with different chosen values for origo. Only the middle graph reveals the lognormal character of the variable.

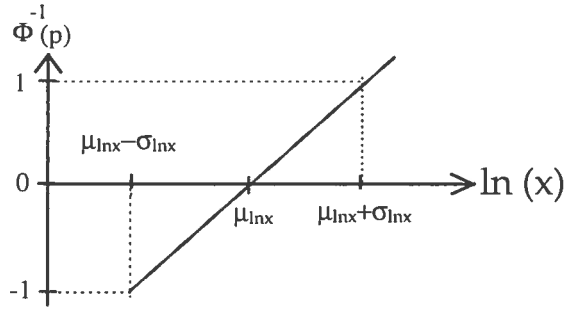

Figure B.4 Graph of lognormal distribution
x-axis logscale, y-axis 'standard normal distribution scale'

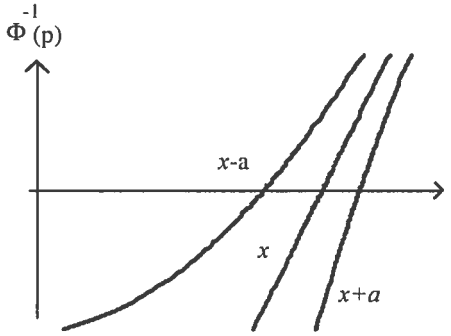

Figure B.5 Graphs of three sets of values obtained from a lognormal distribution x. x-axis logscale, y-axis 'standard normal distribution scale'

In Figure B.6 comparisons of the density curves and the corresponding distributions, plotted in a 'probability scale', are given for five completely different random variables.

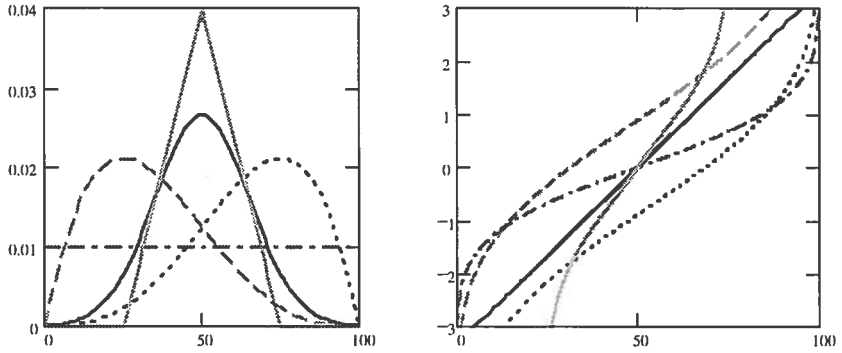

Figure B.6 Examples of density curves and distributions plotted in a 'probability paper'. y-axis 'standard normal distribution scale'

APPENDIX C CORRELATION / TWO VARIABLES

C.1 Introduction

In Chapter 2, "Dependence/Correlation", it was discussed how dependence between random variables often can be described by the concept of correlation. It was conveniently made in a matrix formulation based upon the covariance matrix. Below, the concept will be exemplified for the simple but important case of two correlated variables X and Z. It will also be illustrated how the concept can be utilised in the simulation of two correlated variables.

C.2 Simulation

For two correlated variables X and Z, with the coefficient of correlation ρ, the covariance matrix becomes:

$$\mathbf{Cov} = \begin{bmatrix} \sigma_x^2 & \rho \cdot \sigma_x \cdot \sigma_z \\ \rho \cdot \sigma_x \cdot \sigma_z & \sigma_z^2 \end{bmatrix} \qquad \text{(C.1)}$$

Let $\lambda = [\lambda_1, \lambda_2]$ be the eigenvalues of the covariance matrix and $\mathbf{a}_1$ and $\mathbf{a}_2$ the corresponding orthonormed eigenvectors, i.e. $\mathbf{Cov} \cdot \mathbf{a} = \lambda \cdot \mathbf{a}$. Then a set of uncorrelated variables Y_1 and Y_2 can be obtained by the transformation (see Chapter 2):

$$\mathbf{Y} = \mathbf{A}^T \cdot \mathbf{X} \qquad \text{(C.2)}$$

where $\mathbf{A}$ is formed by the eigenvectors:

$$\mathbf{A} = [\mathbf{a}_1 \quad \mathbf{a}_2] = \begin{bmatrix} a_{11} & a_{12} \\ a_{21} & a_{22} \end{bmatrix} \qquad \text{(C.3)}$$

Equation C.2 can then be rewritten as:

$$\begin{bmatrix} Y_1 \\ Y_2 \end{bmatrix} = \begin{bmatrix} a_{11} & a_{21} \\ a_{12} & a_{22} \end{bmatrix} \cdot \begin{bmatrix} X \\ Z \end{bmatrix} \qquad \text{(C.2a)}$$

The variables Y_1 and Y_2 are linear combinations of X and Z, which gives (see appendix A):

$$\begin{bmatrix} \mu_{y_1} \\ \mu_{y_2} \end{bmatrix} = \begin{bmatrix} a_{11} & a_{21} \\ a_{12} & a_{22} \end{bmatrix} \cdot \begin{bmatrix} \mu_x \\ \mu_z \end{bmatrix} \tag{C.4}$$

The variances of Y_1 and Y_2 can be obtained from the corresponding 'covariance matrix' as (see Chapter 2):

$$\mathbf{Cov}_y = \mathbf{A}^T \cdot \mathbf{Cov} \cdot \mathbf{A} = \begin{bmatrix} \lambda_1 & 0 \\ 0 & \lambda_2 \end{bmatrix} = \begin{bmatrix} \sigma_{Y_1}^2 & 0 \\ 0 & \sigma_{Y_2}^2 \end{bmatrix} \tag{C.5}$$

Thus, from the given correlated variables X and Z, two new uncorrelated variables Y_1 and Y_2, with known mean values and variances, are obtained.

If the variables y_1 and y_2 are assumed to be normal distributed random values can be simulated as (see Chapter 2, "Monte Carlo simulation":

$$y_1 = \Phi^{-1}(p_1) \cdot \sigma_{y_1} + \mu_{y_1} \tag{C.6}$$

$$y_2 = \Phi^{-1}(p_2) \cdot \sigma_{y_2} + \mu_{y_2} \tag{C.7}$$

where p_1 and p_2 are random numbers, 0-1. Solving the equation system C.2a, gives values of X and Z:

$$\begin{bmatrix} x \\ z \end{bmatrix} = \frac{1}{\det(\mathbf{A}^T)} \cdot \begin{bmatrix} a_{22} & -a_{21} \\ -a_{12} & a_{11} \end{bmatrix} \cdot \begin{bmatrix} y_1 \\ y_2 \end{bmatrix} \tag{C.8}$$

The results of three different simulations of the joint density distribution $f_{XZ}(x,z)$ of two correlated normal distributions X=N(10;2) and Z=N(10;3) are illustrated in Figure C.1. Three different simulations were made and the coefficients of correlation were set to 0; 0,7 and -0,7 respectively. The plots to the left in the figure show the simulated pairs of values. In the middle, 3-D graphs of the joint distributions are shown. Finally, the marginal distributions, obtained from the joint distributions, are shown to the right. These return the original distributions X and Z, which is correct for a fair simulation.

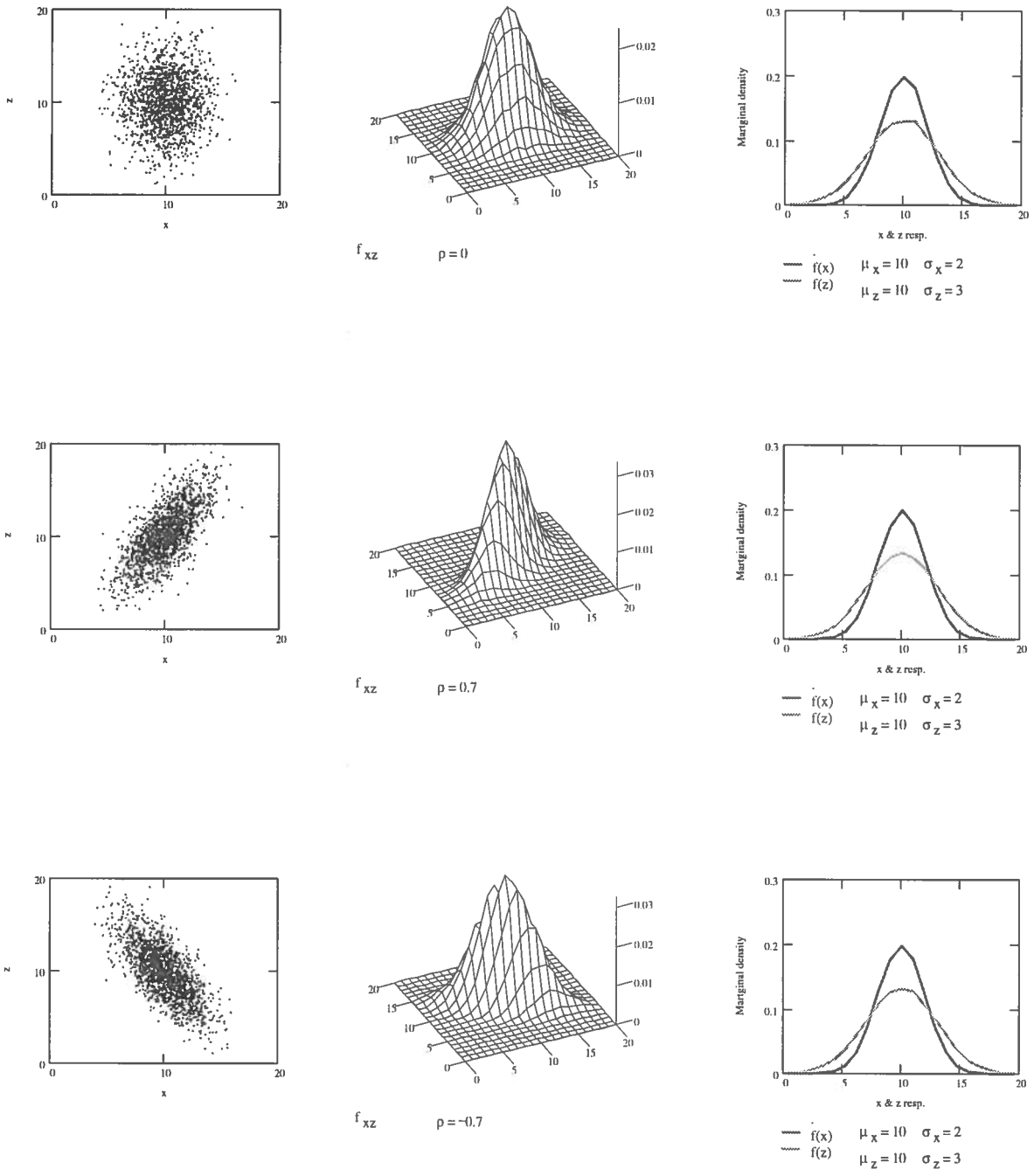

Figure C.1 Simulation of joint distribution $f_{XZ}(x,z)$ and marginal distributions $f_X(x)$ and $f_Z(z)$ of two correlated random variables $X = \mathrm{N}(10;2)$ and $Z = \mathrm{N}(10;3)$ for different values of the coefficient of correlation.

C.3 Non-normal variables

C.3.1 General

In volume 1, section 2.4.4, it was mentioned that dependency between basic variables can be dealt with by a transformation of the variables. This is normally done in a two-step procedure:

- The variables are transformed to independent/uncorrelated variables.
- The independent variables are normalised.

However, the value of the coefficient of correlation is in many cases insensitive to a transformation of the basic variables. Thus in such cases it can be simpler to make the transformation in reverse order, i.e. firstly the variables are normalised by the transformation (cf. volume 1, equation 2.16):

$$u = \Phi^{-1}(F_X(x)) \tag{C.9}$$

and secondly uncorrelated variables are obtained by the procedure described in section C2. Below, this procedure is illustrated for two cases, namely

- Lognormal variables and
- Gumbel distributed variables

C.3.2 Lognormal variables

An important transformation for a lognormal distribution X is to transform it to a normal distribution by taking the logarithms of the values of X. The influence of such a transformation on the correlation, between two variables X and Y, is shown in Figure C.2. Three different situations are considered; X is transformed, Y is transformed and both X and Y are transformed. Thus, the figure shows the results of the following cases.

- $\ln(X)=N(\,),Y=N(\,)$ compared to $X=LN(\,), Y=N(\,)$
- $X=N(\,), \ln(Y)=N(\,)$ compared to $X=N(\,), Y=LN(\,)$
- $\ln(X)=N(\,), \ln(Y)=N(\,)$ compared to $X=LN(\,), Y=LN(\,)$

The coefficient of correlation for the untransformed variables is plotted on the x-axis. The differences of the coefficient of correlation for the transformed pairs of variables and the untransformed variables are shown on the y-axis. As can be seen in the figure, the transformation has little influence on the coefficient of correlation as long as the variances are moderate. This behaviour is more pronounced for positive correlation compared to negative correlation.

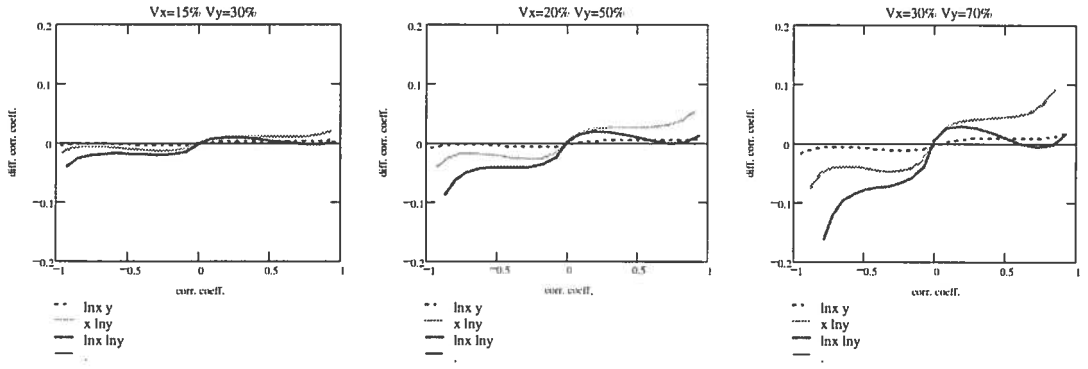

Figure C.2 The influence on the coefficient of correlation by transformation of lognormal distributions to corresponding normal distributions

From the above it can be concluded that the procedure of simulating correlated variables, given in section C2, can often, with good accuracy, be used for lognormal variables. A lognormal variable X in calculations then has to be substituted by e^Y. The variable Y is here the corresponding normal distribution to X.

C.3.3 Gumbel distributed variables

The transformation given by equation C.9 can basically be used to normalise an arbitrary distribution. The results of such a transformation of Gumbel distributions are given in Figure C.3. The figure shows the influence on the correlation between two variables. The results are also compared to the results given by a transformation of lognormal distributions, cf. Figure C.2. As in section C.3.2, three different situations are considered; X is transformed, Y is transformed and both X and Y are transformed.

Thus, the figure shows the results of the following situations.

- $u_X=\Phi(\,),Y=N(\,)$ compared to $X=\mathrm{Gu}(\,), Y=N(\,)$
- $X=N(\,),u_Y=\Phi(\,)$ compared to $X=N(\,), \mathrm{Y=Gu}(\,)$
- $u_X=\Phi(\,), u_Y=\Phi(\,)$ compared to $X=\mathrm{Gu}(\,), Y=\mathrm{Gu}(\,)$

In this case the results are not affected by the variances of the untransformed variables. For comparison one of the simulations of lognormal distributions from the middle plot in Figure C.2 is also shown.

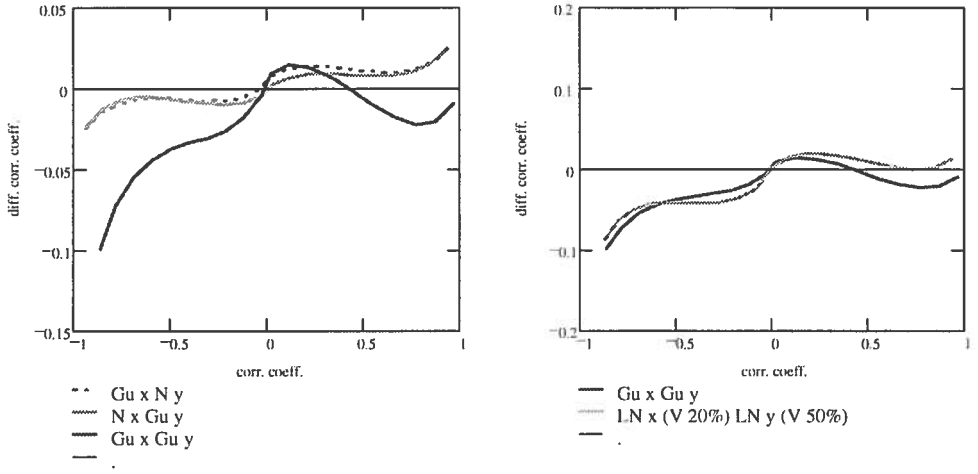

Figure C.3 The influence on the coefficient of correlation by a normalising transformation of Gumbel distributions, left graph. Comparison of transformation of Gumbel distribution and lognormal distributions, right graph.

In the same way as in section C.3.2 it can be concluded, that the procedure of simulating correlated variables, given in section C2, can also be used for Gumbel distributed variables. The substitution of the given variable is not as trivial in this case. It is given by the 'inverse' of equation C.9:

$$X = F_X^{-1}[\Phi(\,)] \quad \text{(C.10)}$$

APPENDIX D PEM / ACCURACY

D.1 Introduction

In Chapter 2, the 'Point Estimate Method (PEM)', a simple method for reliability analysis was discussed. In this appendix the accuracy of the method is investigated for the following functions of random variables:

- The sum of correlated and uncorrelated variables
- The product of correlated and uncorrelated variables
- The ratio of correlated and uncorrelated variables
- A hyperbolic function with two parameters, which are given as random variables.

When possible, the results from the PEM are compared to exact solutions. In those cases when this was not possible, the results are instead compared with Monte-Carlo simulations, as described in Chapter 2, and Gaussian approximation as given in appendix A.

D.2 PEM for two variables

Below, a summary of the PEM method for two variables is given[1]. A random variable X is given by the two-point estimation:

$$X_- = \mu_X - \sigma_X \qquad X_+ = \mu_X + \sigma_X \tag{D.1}$$

Thus the mean value and the standard deviation has to be given (or estimated).

A function of two variables, $f(X,Y)$, is then given as a discrete 4-point distribution[2] :

$$\begin{aligned} f_{++} &= f(X_+, Y_+) \\ f_{+-} &= f(X_+, Y_-) \\ f_{-+} &= f(X_+, Y_+) \\ f_{--} &= f(X_-, Y_-) \end{aligned} \tag{D.2}$$

[1] A complete description of the method is given in (Harr, 1987)

[2] A function of N variables is given as a 2^N-point distribution

with the corresponding probabilities:

$$p_{++} = p_{--} = \frac{1+\rho}{4}$$
$$p_{+-} = p_{-+} = \frac{1-\rho}{4} \qquad \text{(D.3)}$$

where ρ is the coefficient of correlation between the two variables[1].

The expected value then becomes:

$$E[f_{XY}] = p_{++} \cdot f_{++} + p_{+-} \cdot f_{+-} + p_{-+} \cdot f_{-+} + p_{--} \cdot f_{--} \qquad \text{(D.4)}$$

and the variance, (cf. appendix A):

$$Var[f_{XY}] = E[f_{XY}^2] - E^2[f_{XY}] \qquad \text{(D.5)}$$

$$Var[f_{XY}] = p_{++} \cdot f_{++}^2 + p_{+-} \cdot f_{+-}^2 + p_{-+} \cdot f_{-+}^2 + p_{--} \cdot f_{--}^2 - \left(p_{++} \cdot f_{++} + p_{+-} \cdot f_{+-} + p_{-+} \cdot f_{-+} + p_{--} \cdot f_{--}\right)^2 \qquad \text{(D.5a)}$$

In the interpretation of the result, f(*X*,*Y*) is often assumed to be a normal distribution. However, there is no reason to make this a requirement for the application of the method.

D.3 Sum of two variables

The expected value of a sum becomes:

$$\begin{aligned} E[X+Y] = {} & \frac{1+\rho}{4} \cdot \left[\left(\mu_x + \sigma_x\right) + \left(\mu_y + \sigma_y\right)\right] + \\ & + \frac{1-\rho}{4} \cdot \left[\left(\mu_x + \sigma_x\right) + \left(\mu_y - \sigma_y\right)\right] + \\ & + \frac{1-\rho}{4} \cdot \left[\left(\mu_x - \sigma_x\right) + \left(\mu_y + \sigma_y\right)\right] + \\ & + \frac{1+\rho}{4} \cdot \left[\left(\mu_x + \sigma_x\right) + \left(\mu_y + \sigma_y\right)\right] \end{aligned} \qquad \text{(D.6)}$$

which gives:

[1] Hence, for the marginal distributions of *X* and *Y*,
$p_{X+} = p_{X-} = p_{Y+} = p_{Y-} = 1/2$ as $p_{X+} = p_{++} + p_{+-}$ etc.

$$E[X+Y]=\mu_X+\mu_Y=E[X]+E[Y] \tag{D.6a}$$

The variance is:

$$Var[X+Y]=\left[\begin{array}{l}\frac{1+\rho}{4}\cdot\left[(\mu_x+\sigma_x)+(\mu_y+\sigma_y)\right]^2+\\ +\frac{1-\rho}{4}\cdot\left[(\mu_x+\sigma_x)+(\mu_y-\sigma_y)\right]^2+\\ +\frac{1-\rho}{4}\cdot\left[(\mu_x-\sigma_x)+(\mu_y+\sigma_y)\right]^2+\\ +\frac{1+\rho}{4}\cdot\left[(\mu_x-\sigma_x)+(\mu_y-\sigma_y)\right]^2\end{array}\right]-$$
$$-\left[\begin{array}{l}\frac{1+\rho}{4}\cdot\left[(\mu_x+\sigma_x)+(\mu_y+\sigma_y)\right]+\\ +\frac{1-\rho}{4}\cdot\left[(\mu_x+\sigma_x)+(\mu_y-\sigma_y)\right]+\\ +\frac{1-\rho}{4}\cdot\left[(\mu_x-\sigma_x)+(\mu_y+\sigma_y)\right]+\\ +\frac{1+\rho}{4}\cdot\left[(\mu_x-\sigma_x)+(\mu_y-\sigma_y)\right]\end{array}\right]^2 \tag{D.7}$$

or after simplifying:

$$\begin{aligned}Var[X+Y]&=\sigma_x^{\,2}+\sigma_y^{\,2}+2\cdot\rho\cdot\sigma_x\cdot\sigma_y=\\&=Var[x]+Var[Y]+2\cdot Cov[X,Y]\end{aligned} \tag{D.7a}$$

For a difference, since $X-Y=X+(-Y)$ and $Cov[X,-Y]=-Cov[X,Y]$, the corresponding equations become:

$$E[X-Y]=E[X]+E[-Y]=E[X]-E[Y] \tag{D.6b}$$

and

$$\begin{aligned}Var[X-Y]&=Var[x]+Var[-Y]+2\cdot Cov[X,-Y]=\\&=Var[x]+Var[Y]-2\cdot Cov[X,Y]\end{aligned} \tag{D.7b}$$

The results are in agreement with the exact solution for a sum, see appendix A. Thus, PEM is correct for a sum (or difference) of two random variables.

D.4 Products of two variables

D.4.1 Uncorrelated variables

The expected value of a product becomes:

$$\begin{aligned} E[X\cdot Y]=&\frac{1}{4}\cdot\left[(\mu_x+\sigma_x)\cdot(\mu_y+\sigma_y)\right]+\\ &+\frac{1}{4}\cdot\left[(\mu_x+\sigma_x)\cdot(\mu_y-\sigma_y)\right]+\\ &+\frac{1}{4}\cdot\left[(\mu_x-\sigma_x)\cdot(\mu_y+\sigma_y)\right]+\\ &+\frac{1}{4}\cdot\left[(\mu_x-\sigma_x)\cdot(\mu_y-\sigma_y)\right] \end{aligned} \tag{D.8}$$

which gives:

$$E[X\cdot Y]=\mu_X\cdot\mu_Y=E[X]\cdot E[Y] \tag{D.8a}$$

The variance is:

$$\begin{aligned} Var[X\cdot Y]=&\left[\begin{array}{l} \frac{1}{4}\cdot\left[(\mu_x+\sigma_x)\cdot(\mu_y+\sigma_y)\right]^2+\\ +\frac{1}{4}\cdot\left[(\mu_x+\sigma_x)\cdot(\mu_y-\sigma_y)\right]^2+\\ +\frac{1}{4}\cdot\left[(\mu_x-\sigma_x)\cdot(\mu_y+\sigma_y)\right]^2+\\ +\frac{1}{4}\cdot\left[(\mu_x-\sigma_x)\cdot(\mu_y-\sigma_y)\right]^2 \end{array}\right]-\\ &-\left[\begin{array}{l} \frac{1}{4}\cdot\left[(\mu_x+\sigma_x)\cdot(\mu_y+\sigma_y)\right]+\\ +\frac{1}{4}\cdot\left[(\mu_x+\sigma_x)\cdot(\mu_y-\sigma_y)\right]+\\ +\frac{1}{4}\cdot\left[(\mu_x-\sigma_x)\cdot(\mu_y+\sigma_y)\right]+\\ +\frac{1}{4}\cdot\left[(\mu_x-\sigma_x)\cdot(\mu_y-\sigma_y)\right] \end{array}\right]^2 \end{aligned} \tag{D.9}$$

or after simplifying:

$$\begin{aligned} Var[X \cdot Y] &= \sigma_x^{\,2} \cdot \mu_y^2 + \sigma_y^{\,2} \cdot \mu_x^2 + \sigma_x^2 \cdot \sigma_y^2 = \\ &= VarX \cdot E[Y]^2 + Var[Y] \cdot E[X]^2 + Var[X] \cdot Var[Y] \end{aligned} \qquad \text{(D.9a)}$$

The results are in agreement with the exact solution for a product, see appendix A. Thus, PEM is correct for a product of two uncorrelated random variables.

D.4.2 Correlated variables

The expected value of a product becomes:

$$\begin{aligned} E[X \cdot Y] = &\frac{1+\rho}{4} \cdot \left[(\mu_x + \sigma_x) + (\mu_y + \sigma_y) \right] + \\ &+ \frac{1-\rho}{4} \cdot \left[(\mu_x + \sigma_x) + (\mu_y - \sigma_y) \right] + \\ &+ \frac{1-\rho}{4} \cdot \left[(\mu_x - \sigma_x) + (\mu_y + \sigma_y) \right] + \\ &+ \frac{1+\rho}{4} \cdot \left[(\mu_x - \sigma_x) + (\mu_y - \sigma_y) \right] \end{aligned} \qquad \text{(D.10)}$$

which gives:

$$\begin{aligned} E[X \cdot Y] &= \mu_X \cdot \mu_Y + \rho \cdot \sigma_x \cdot \sigma_y = \\ &= E[X] \cdot E[Y] + Cov[X, Y] \end{aligned} \qquad \text{(D.10a)}$$

The variance is:

$$Var[X\cdot Y]=\left[\begin{array}{l}\frac{1+\rho}{4}\cdot\left[(\mu_x+\sigma_x)\cdot(\mu_y+\sigma_y)\right]^2+\\+\frac{1-\rho}{4}\cdot\left[(\mu_x+\sigma_x)\cdot(\mu_y-\sigma_y)\right]^2+\\+\frac{1-\rho}{4}\cdot\left[(\mu_x-\sigma_x)\cdot(\mu_y+\sigma_y)\right]^2+\\+\frac{1+\rho}{4}\cdot\left[(\mu_x-\sigma_x)\cdot(\mu_y-\sigma_y)\right]^2\end{array}\right]-$$
$$-\left[\begin{array}{l}\frac{1+\rho}{4}\cdot\left[(\mu_x+\sigma_x)\cdot(\mu_y+\sigma_y)\right]+\\+\frac{1-\rho}{4}\cdot\left[(\mu_x+\sigma_x)\cdot(\mu_y-\sigma_y)\right]+\\+\frac{1-\rho}{4}\cdot\left[(\mu_x-\sigma_x)\cdot(\mu_y+\sigma_y)\right]+\\+\frac{1+\rho}{4}\cdot\left[(\mu_x-\sigma_x)\cdot(\mu_y-\sigma_y)\right]\end{array}\right]^2 \qquad \text{(D.11)}$$

or after simplifying:

$$\begin{aligned}Var[X\cdot Y]=&\sigma_x{}^2\cdot\mu_y^2+\sigma_y{}^2\cdot\mu_x^2+\sigma_x^2\cdot\sigma_y^2+\\&+2\cdot\rho\cdot\sigma_x\cdot\sigma_y\cdot\mu_x\cdot\mu_y-\rho^2\cdot\sigma_x^2\cdot\sigma_y^2\end{aligned} \qquad \text{(D.11a)}$$

With Gaussian approximation, see appendix A, one obtains for the mean value the trivial equation:

$$E[X\cdot Y]=\mu_x\cdot\mu_y \qquad \text{(D.12)}$$

and for the variance

$$Var[X\cdot Y]=\sigma_x{}^2\cdot\mu_y^2+\sigma_y{}^2\cdot\mu_x^2+2\cdot\rho\cdot\sigma_x\cdot\sigma_y\cdot\mu_x\cdot\mu_y \qquad \text{(D.13)}$$

Thus, the difference between PEM and Gaussian approximation is for the mean value:

$$\Delta E[X\cdot Y]=\rho\cdot\sigma_x\cdot\sigma_y=Cov[X,Y] \qquad \text{(D.14)}$$

and for the variance:

$$\Delta Var[X \cdot Y] = \sigma_x^{\,2} \cdot \sigma_y^2 \cdot (1 - \rho^2) \qquad \text{(D.15)}$$

In Figure D.1 the result of a PEM calculation is compared with the results of simulations. The random variables X and Y are assumed to be described with probability distributions, X=*PD*(*1:0,2*) and Y=*PD*(1;0,5). Two different simulations are performed. In the first simulation both X and Y are assumed to be lognormal distributions and in the second simulation they are assumed to be normal distributions. The influence of correlation is determined for values of the coefficient of correlation in the range, ρ= -1 -- +1. The values μ and σ marked in the figure are the true values for lognormal distributions and ρ=0. As can be seen in the figure there is an extremely good agreement between the different calculation methods for the mean value. For the standard deviation there is an overall good agreement, but the influence of correlation for lognormal distributions is not quite captured by the PEM calculations.

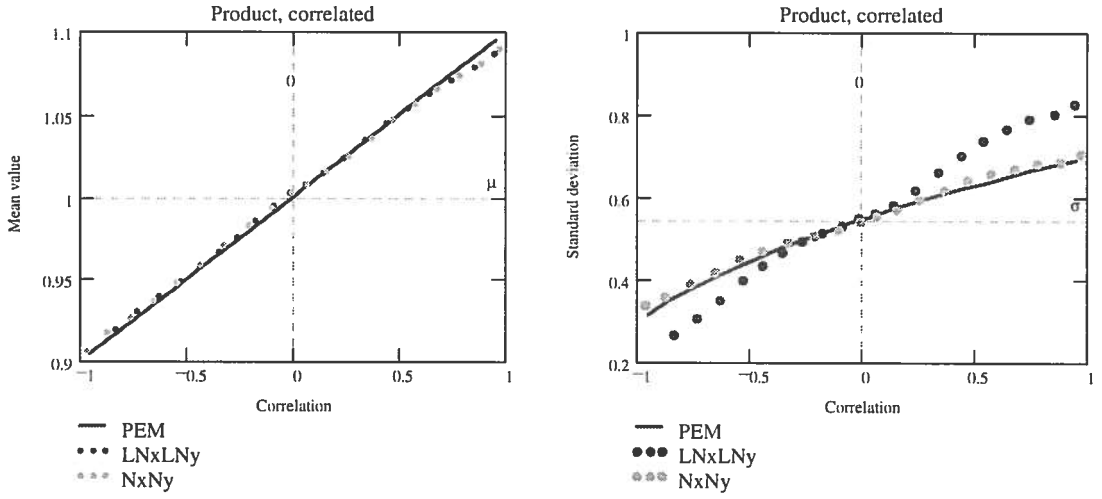

Figure D.1 Product of two correlated, random variables. Comparison between PEM and Monte Carlo simulations. μ_x=μ_y=1; σ_x =0,2; σ_y =0,5.

In Figure D.2 the PEM calculations are compared with the results obtained by Gaussian approximation for the same conditions as described above. The Gaussian approximation does not capture the influence of correlation on the mean value, cf. equation D.14. One might say that the approximation formula is too trivial. However, it has to be remarked that the Gaussian approximation for the mean

value probably can be regarded as a systematic formulation of traditional engineering practice by deterministic analysis, i.e. calculations with 'mean values'. The calculated differences for the standard deviation are extremely small, cf. equation D.15.

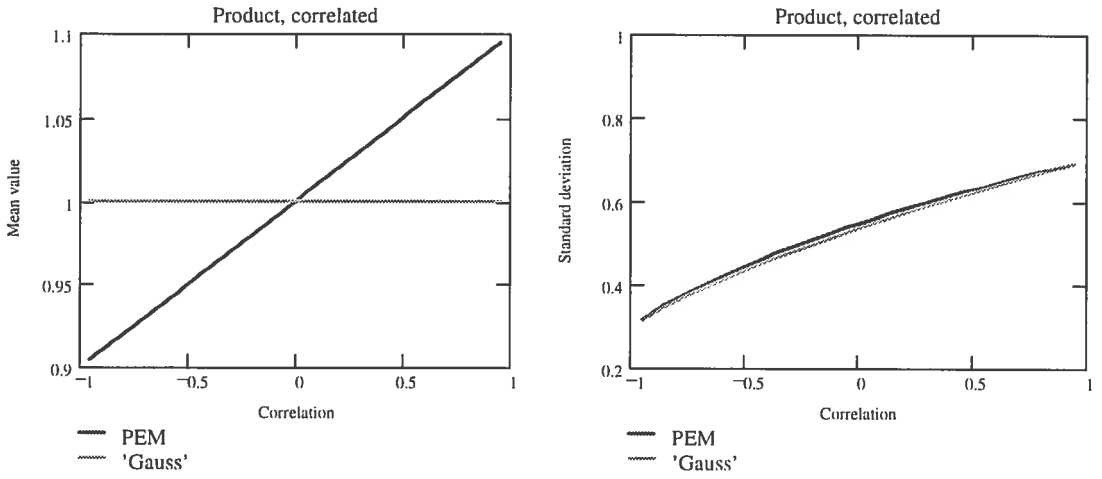

Figure D.2 Product of two correlated, random variables. Comparison between PEM and Gaussian approximation. $\mu_x=\mu_y=1$; $\sigma_x=0{,}2$; $\sigma_y=0{,}5$.

D.5 Ratio

D.5.1 Uncorrelated variables

The expected value of a ratio becomes:

$$E\left[\frac{X}{Y}\right]=\frac{1}{4}\cdot\left[\left(\mu_x+\sigma_x\right)/\left(\mu_y+\sigma_y\right)\right]+ +\frac{1}{4}\cdot\left[\left(\mu_x+\sigma_x\right)/\left(\mu_y-\sigma_y\right)\right]+ +\frac{1}{4}\cdot\left[\left(\mu_x-\sigma_x\right)/\left(\mu_y+\sigma_y\right)\right]+ +\frac{1}{4}\cdot\left[\left(\mu_x-\sigma_x\right)/\left(\mu_y-\sigma_y\right)\right] \tag{D.16}$$

which gives:

$$E\left[\frac{X}{Y}\right]=\frac{\mu_X\cdot\mu_Y}{\left(\mu_Y+\sigma_y\right)\cdot\left(\mu_Y-\sigma_y\right)} \tag{D.16a}$$

The variance is:

$$Var\left[\frac{X}{Y}\right]=\left[\begin{array}{l}\frac{1}{4}\cdot\left[(\mu_x+\sigma_x)/(\mu_y+\sigma_y)\right]^2+\\+\frac{1}{4}\cdot\left[(\mu_x+\sigma_x)/(\mu_y-\sigma_y)\right]^2+\\+\frac{1}{4}\cdot\left[(\mu_x-\sigma_x)/(\mu_y+\sigma_y)\right]^2+\\+\frac{1}{4}\cdot\left[(\mu_x-\sigma_x)/(\mu_y-\sigma_y)\right]^2\end{array}\right]-$$

$$-\left[\begin{array}{l}\frac{1}{4}\cdot\left[(\mu_x+\sigma_x)/(\mu_y+\sigma_y)\right]+\\+\frac{1}{4}\cdot\left[(\mu_x+\sigma_x)/(\mu_y-\sigma_y)\right]+\\+\frac{1}{4}\cdot\left[(\mu_x-\sigma_x)/(\mu_y+\sigma_y)\right]+\\+\frac{1}{4}\cdot\left[(\mu_x-\sigma_x)/(\mu_y-\sigma_y)\right]\end{array}\right]^2 \qquad \text{(D.17)}$$

or after simplifying:

$$Var\left[\frac{X}{Y}\right]=\frac{\sigma_x^{\,2}\cdot\mu_y^2+\sigma_y^{\,2}\cdot\mu_x^2+\sigma_x^2\cdot\sigma_y^2}{(\mu_y+\sigma_y)^2\cdot(\mu_y-\sigma_y)^2} \qquad \text{(D.17a)}$$

With Gaussian approximation, see appendix A, one obtains for the mean value the equation:

$$E\left[\frac{X}{Y}\right]=\frac{\mu_x}{\mu_y} \qquad \text{(D.18)}$$

and for the variance

$$Var\left[\frac{X}{Y}\right]=\frac{\sigma_x^{\,2}}{\mu_y^2}+\frac{\sigma_y^{\,2}\cdot\mu_x^2}{\mu_y^4}=\frac{\sigma_x^{\,2}\cdot\mu_y^2+\sigma_y^{\,2}\cdot\mu_x^2}{\mu_y^4} \qquad \text{(D.19)}$$

In Figure D.3 and Figure D.4 the result of a PEM calculation is compared with the results of Gaussian approximation and Monte Carlo simulations. The ratio X/Y is assumed to be described by probability distributions, $X=PD(1;\sigma_x= 0{,}1 - 0{,}3)$ and $Y=PD(1;\sigma_y= 0{,}3 - 0{,}7)$.

The analyses are divided into two groups, where σ_x is varied and σ_y is varied:

- X=*PD*(1; 0,1 – 0,3) and Y=*PD*(1; 0,5). Results in Figure D.3
- X=*PD*(1; 0,2) and Y=*PD*(1; 0,2 -- 0,7). Results in Figure D.4

For each calculation group two different simulations were performed. In the first simulation both X and Y were assumed to be lognormal distributions and in the second simulation they were assumed to be normal distributions. The values $\mu_{\square}$ and $\sigma_{\square}$, marked to the right in the figures, are the true values for lognormal distributions, σ_x=0,2 and σ_y=0,5[1].

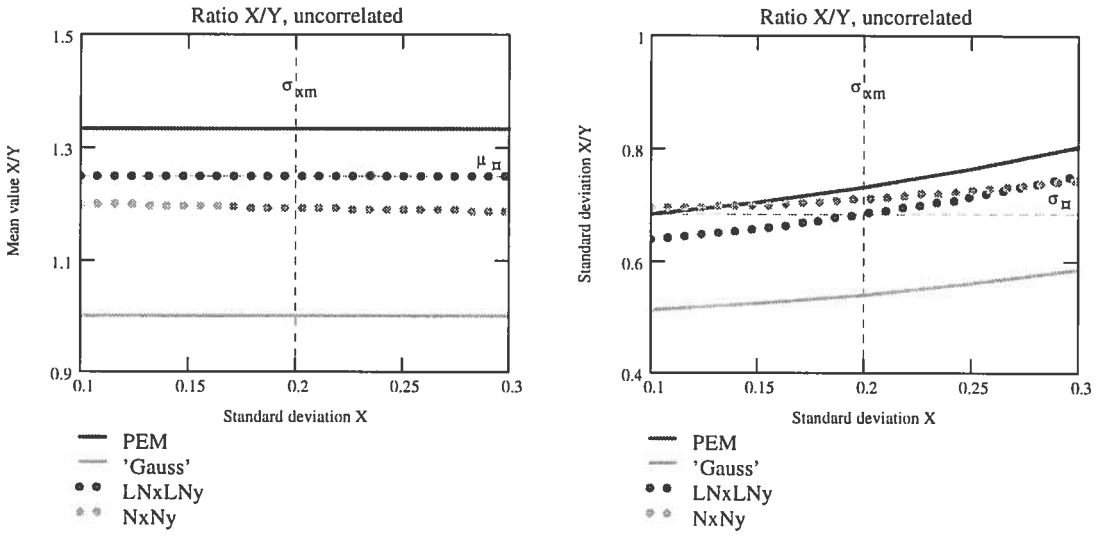

Figure D.3 Ratio X/Y of two uncorrelated random variables. Comparison between PEM, Gaussian approximation and Monte Carlo simulations. NxNy truncated (0,03-0,97). μ_x=μ_y=1; σ_x =0,1 – 0,3; σ_y =0,5.

[1] Naturally, they coincide with the simulation of the ratio of the two uncorrelated variables *LN*(1;0,2) and *LN*(1;0,5).

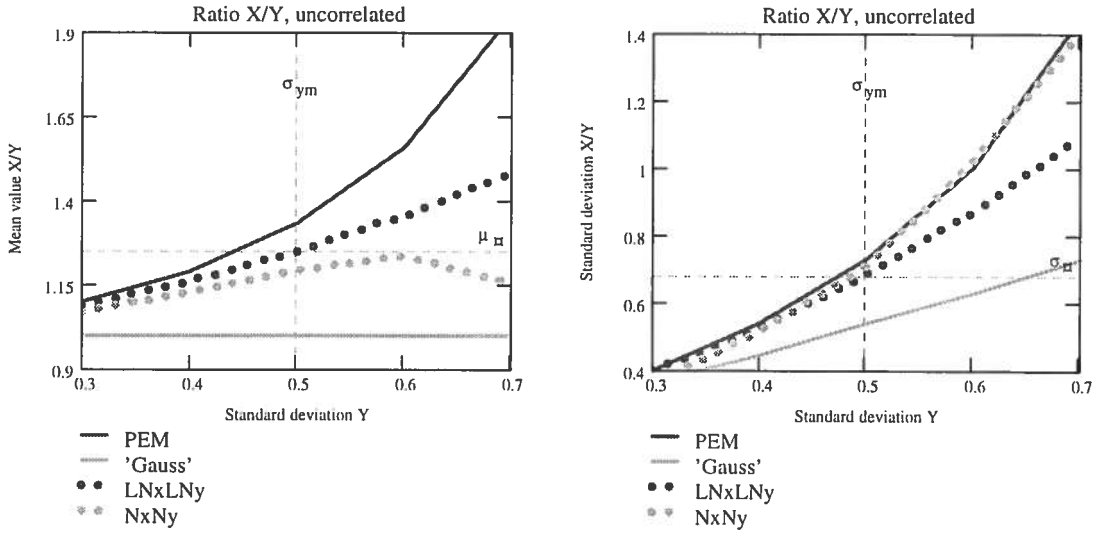

Figure D.4 Ratio *X/Y* of two uncorrelated random variables. Comparison between PEM, Gaussian approximation and Monte Carlo simulations. NxNy truncated (0,03-0,97). $\mu_x=\mu_y=1$; $\sigma_x = 0{,}2$; $\sigma_y = 0{,}3 - 0{,}7$.

The results shown in Figure D.3 and Figure D.4 are truncations of the simulations of normal distributions. The values displayed are the mid 94% values, i.e. 3% of each tail is truncated. The reason for the truncation is that the simulations of the ratio for normal distributions are extremely sensitive to large variations of the variables, especially of the denominator *Y*. This is due to the fact that a normal distribution can take negative values and values close to zero. This makes the result of a simulation quite unpredictable. This is clearly demonstrated in Figure D.5 and Figure D.6 in which the results of two different simulations are shown

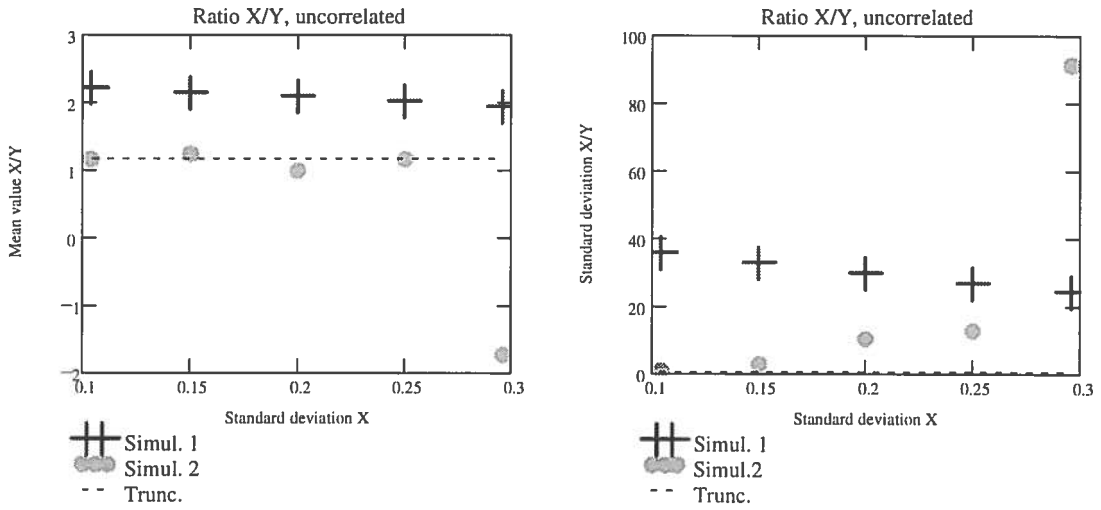

Figure D.5 Ratio *X/Y* of two uncorrelated, normal distributions. Comparison between two Monte Carlo simulations. Dotted line = truncation of simulation 1 = NxNy in Figure D.3. $\mu_x=\mu_y=1$; σ_x =0,1 – 0,3; σ_y =0,5.

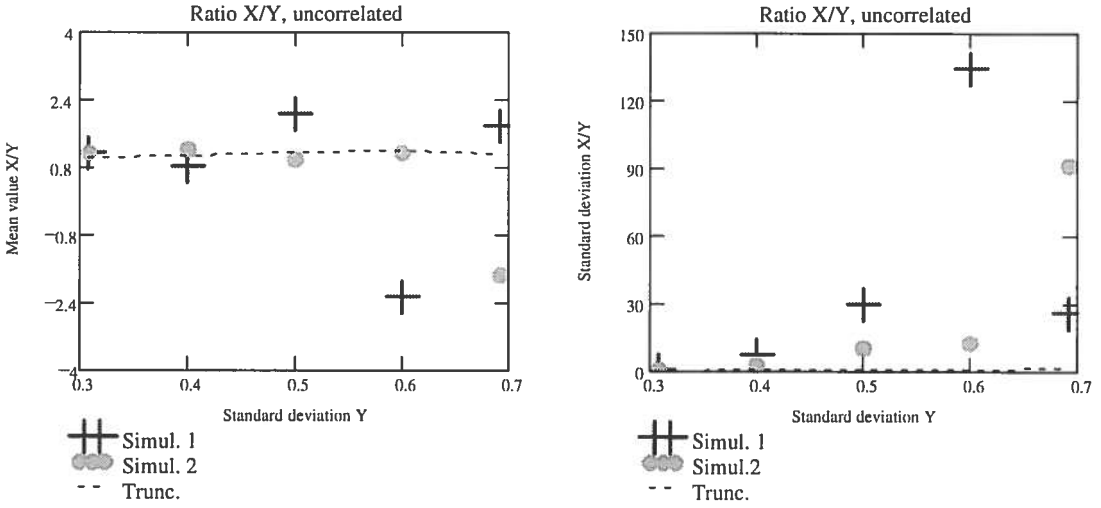

Figure D.6 Ratio *X/Y* of two uncorrelated, normal distributions. Comparison between two Monte Carlo simulations. Dotted line = truncation of simulation 1 = NxNy in Figure D.4. $\mu_x=\mu_y=1$; σ_x = 0,2; σ_y =0,3 – 0,7.

The PEM method captures the overall behaviour of the analysed ratio, which can be seen in Figure D.3 and Figure D.4, and which is fairly accurate for a moderate magnitude of the variance of *Y*, σ_y <0,5. There is a better agreement for the standard deviation than for the mean value. The Gaussian approximation underestimates both the mean value and the standard deviation considerably. From reasons mentioned above the results of the simulations of normal distributions are not too reliable.

Above, the behaviour of a ratio in which the denominator has a rather large variation was investigated. Below is the case when the numerator has the largest variation analysed instead. Hence, for the same conditions as above the ratio *Y/X* is analysed:

- $Y=PD(1; 0{,}2 \text{ -- } 0{,}7)$ and $X=PD(1; 0{,}2)$. Results in Figure D.7.
- $Y=PD(1; 0{,}5)$ and $X=PD(1; 0{,}1 - 0{,}3)$. Results in Figure D.8.

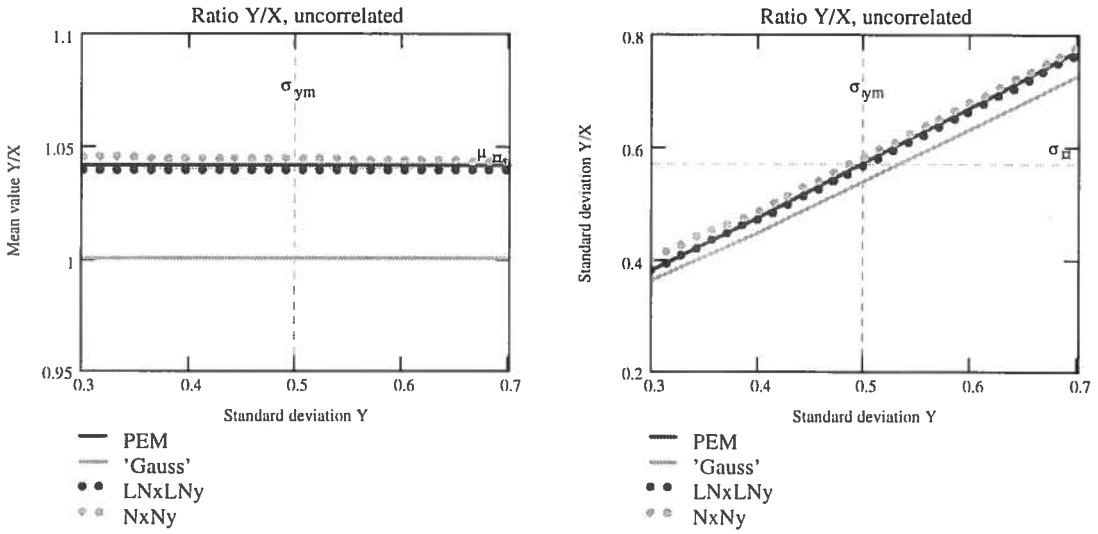

Figure D.7 Ratio *Y/X* of two uncorrelated random variables. Comparison between PEM, Gaussian approximation and Monte Carlo simulations. $\mu_x=\mu_y=1$; $\sigma_y=0{,}3 - 0{,}7$;$\sigma_x = 0{,}2$.

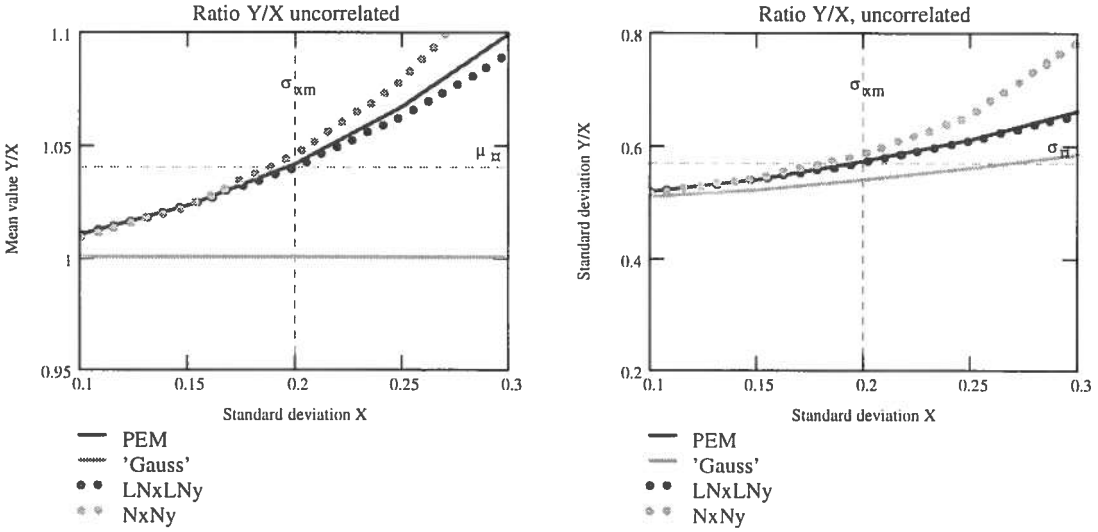

Figure D.8 Ratio *Y/X* of two uncorrelated random variables. Comparison between PEM, Gaussian approximation and Monte Carlo simulations. $\mu_x=\mu_y=1$; $\sigma_y=0{,}5$; $\sigma_x=0{,}1 - 0{,}3$.

In the cases described in Figure D.7 and Figure D.8 the agreement between the different methods is very good. In this case the underestimation by the Gaussian approximation is more marginal than in the case described previously. However, the Gaussian approximation does not capture the influence of variation in the numerator. The simulations of normal distributions are not truncated in Figure D.7 and Figure D.8. The influence of truncation and comparison by different simulations are shown in Figure D.9 and Figure D.10. Note the change of scale of the vertical axis compared to Figure D.5 and Figure D.6.

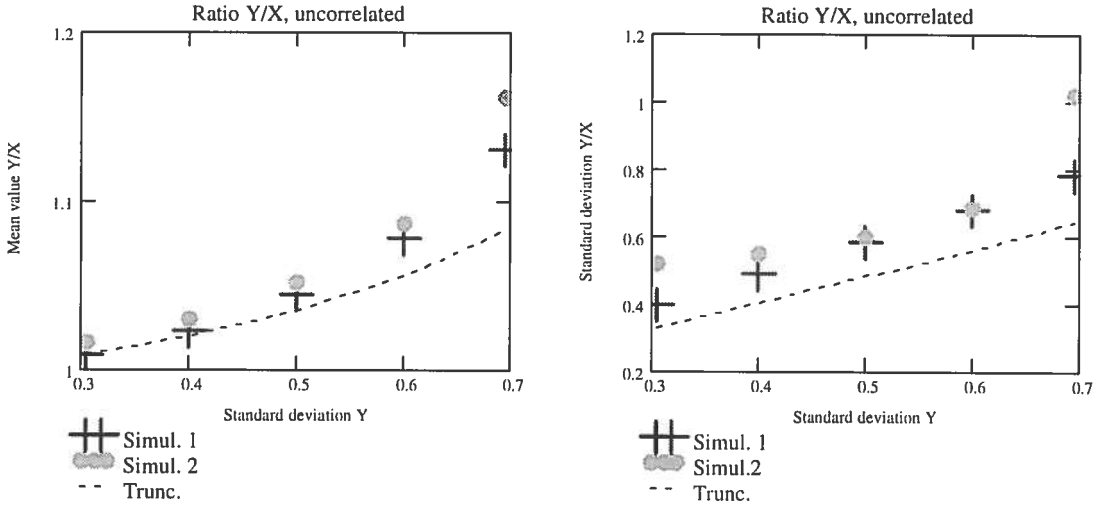

Figure D.9 Ratio *Y/X* of two uncorrelated, normal distributions. Comparison between two Monte Carlo simulations. Dotted line = truncation of simulation 1. $\mu_x=\mu_y=1$; $\sigma_y=0{,}3-0{,}7$;$\sigma_x=0{,}2$.

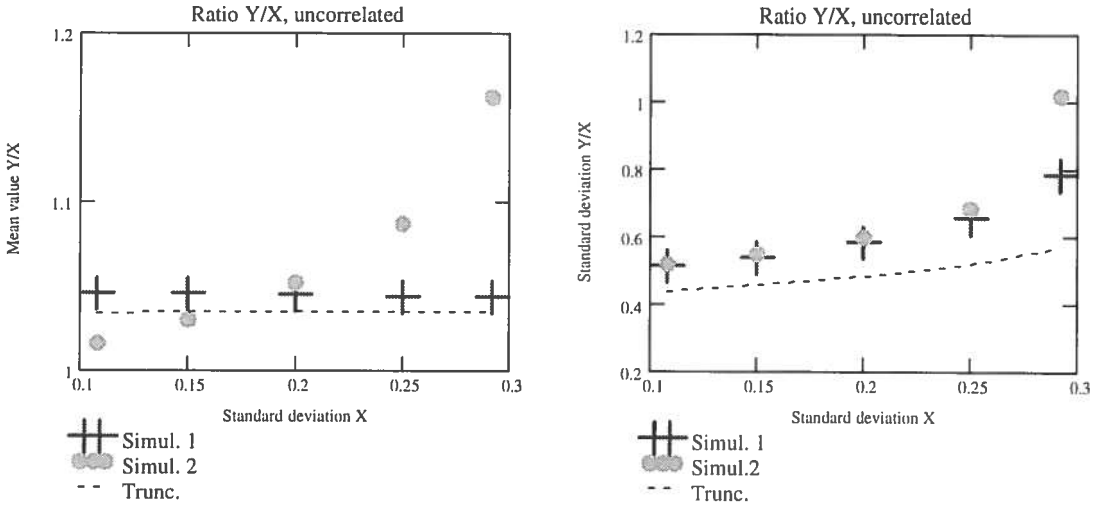

Figure D.10Ratio *Y/X* of two uncorrelated, normal distributions. Comparison between two Monte Carlo simulations. Dotted line = truncation of simulation 1. $\mu_x=\mu_y=1$; $\sigma_y=0{,}5$; $\sigma_x=0{,}1-0{,}3$.

D.5.2 Correlated variables

The expected value of a ratio becomes:

$$\begin{aligned} E\left[\frac{X}{Y}\right] = \frac{1+\rho}{4}\cdot\left[\left(\mu_x+\sigma_x\right)/\left(\mu_y+\sigma_y\right)\right]+ \\ +\frac{1-\rho}{4}\cdot\left[\left(\mu_x+\sigma_x\right)/\left(\mu_y-\sigma_y\right)\right]+ \\ +\frac{1-\rho}{4}\cdot\left[\left(\mu_x-\sigma_x\right)/\left(\mu_y+\sigma_y\right)\right]+ \\ +\frac{1+\rho}{4}\cdot\left[\left(\mu_x-\sigma_x\right)/\left(\mu_y-\sigma_y\right)\right] \end{aligned} \qquad \text{(D.20)}$$

which gives:

$$E\left[\frac{X}{Y}\right] = \frac{\mu_X\cdot\mu_Y-\rho\cdot\sigma_x\cdot\sigma_y}{\left(\mu_Y+\sigma_y\right)\cdot\left(\mu_Y-\sigma_y\right)} \qquad \text{(D.20a)}$$

The variance is:

$$Var\left[\frac{X}{Y}\right]=\left[\begin{array}{l}\frac{1+\rho}{4}\cdot\left[\left(\mu_x+\sigma_x\right)/\left(\mu_y+\sigma_y\right)\right]^2+\\+\frac{1-\rho}{4}\cdot\left[\left(\mu_x+\sigma_x\right)/\left(\mu_y-\sigma_y\right)\right]^2+\\+\frac{1-\rho}{4}\cdot\left[\left(\mu_x-\sigma_x\right)/\left(\mu_y+\sigma_y\right)\right]^2+\\+\frac{1+\rho}{4}\cdot\left[\left(\mu_x-\sigma_x\right)/\left(\mu_y-\sigma_y\right)\right]^2\end{array}\right]-$$
$$-\left[\begin{array}{l}\frac{1+\rho}{4}\cdot\left[\left(\mu_x+\sigma_x\right)/\left(\mu_y+\sigma_y\right)\right]+\\+\frac{1-\rho}{4}\cdot\left[\left(\mu_x+\sigma_x\right)/\left(\mu_y-\sigma_y\right)\right]+\\+\frac{1-\rho}{4}\cdot\left[\left(\mu_x-\sigma_x\right)/\left(\mu_y+\sigma_y\right)\right]+\\+\frac{1+\rho}{4}\cdot\left[\left(\mu_x-\sigma_x\right)/\left(\mu_y-\sigma_y\right)\right]\end{array}\right]^2 \qquad \text{(D.21)}$$

or after simplifying:

$$Var\left[\frac{X}{Y}\right]=\frac{\left[\begin{array}{l}\sigma_x{}^2\cdot\mu_y^2+\sigma_y{}^2\cdot\mu_x^2+\sigma_x^2\cdot\sigma_y^2-\\-\left(2\cdot\rho\cdot\sigma_x\cdot\sigma_y\cdot\mu_x\cdot\mu_y+\rho^2\cdot\sigma_x^2\cdot\sigma_y^2\right)\end{array}\right]}{\left(\mu_y+\sigma_y\right)^2\cdot\left(\mu_y-\sigma_y\right)^2} \qquad \text{(D.21a)}$$

With Gaussian approximation, see appendix A, one obtains for the mean value the equation:

$$E\left[\frac{X}{Y}\right]=\frac{\mu_x}{\mu_y} \qquad \text{(D.22)}$$

and for the variance

$$Var\left[\frac{X}{Y}\right]=\frac{\sigma_x{}^2\cdot\mu_y^2+\sigma_y{}^2\cdot\mu_x^2-2\cdot\rho\cdot\sigma_x\cdot\sigma_y\cdot\mu_x\cdot\mu_y}{\mu_y^4} \qquad \text{(D.23)}$$

In the same manner as for a product of correlated variables, section D.4.2, and a ratio of uncorrelated variables, section D.5.1, the results of a PEM calculation are compared to the results of Monte Carlo

simulations. The random variables X and Y are assumed to be equal to the ones used for the analysis of a product, i.e. $X=PD(1:0,2)$ and $Y=PD(1;0,5)$. Both the ratio X/Y and Y/X were analysed. Two different simulations were performed for each ratio. In the first simulation both X and Y were assumed to be lognormal distributions and in the second simulation they were assumed to be normal distributions. The influence of the correlation was determined for values of the coefficient of correlation in the range, ρ= -1 -- +1. The results for the ratio X/Y are shown in Figure D.11, while the results of Y/X are shown in Figure D.13. Corresponding results for PEM and Gaussian approximation are for X/Y shown in Figure D.12 and for Y/X in Figure D.14. The values μ and σ marked in the figure are the true values for lognormal distributions and ρ=0, cf. section 5.1. Similarly as for the ratio of uncorrelated variables, for the ratio X/Y, the result of the simulation of normal distributions are truncated, 3%-97%.

Generally speaking, the results are comparable to those obtained for the ratio of uncorrelated variables. There is a good agreement for the ratio Y/X, i.e. a denominator with small variance. For the ratio X/Y, i.e. a denominator with large variance, PEM and Monte Carlo simulations give similar results, even if the mean value is somewhat overestimated by the PEM. The result of the Gaussian approximation is a considerable underestimation, especially for the mean value. Nor is the influence of the correlation calculated by the Gaussian approximation.

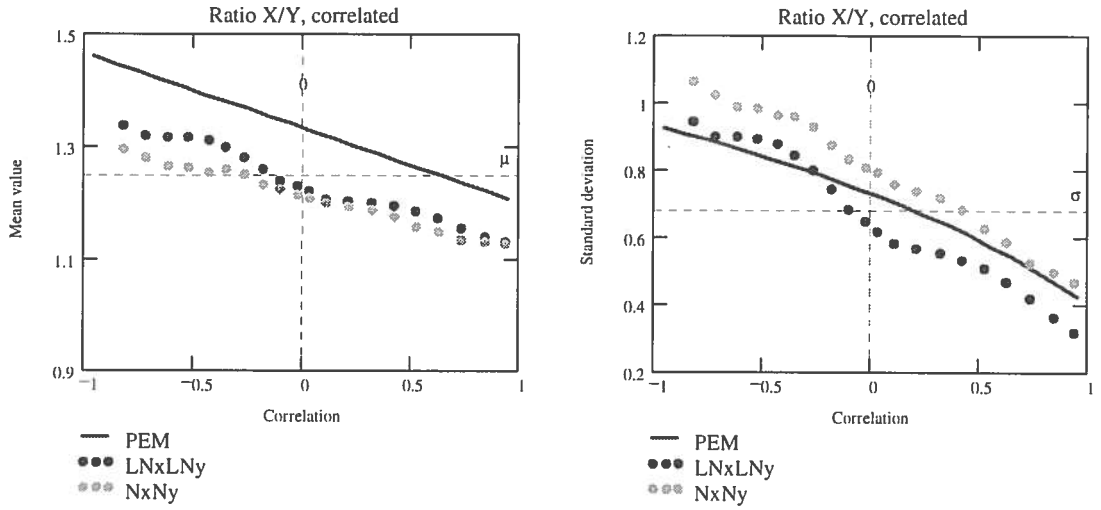

Figure D.11Ratio *X/Y* of two correlated, random variables. Comparison between PEM and Monte Carlo simulations. NxNy truncated (0,03-0,97). $\mu_x=\mu_y=1$; $\sigma_x=0{,}2$; $\sigma_y=0{,}5$.

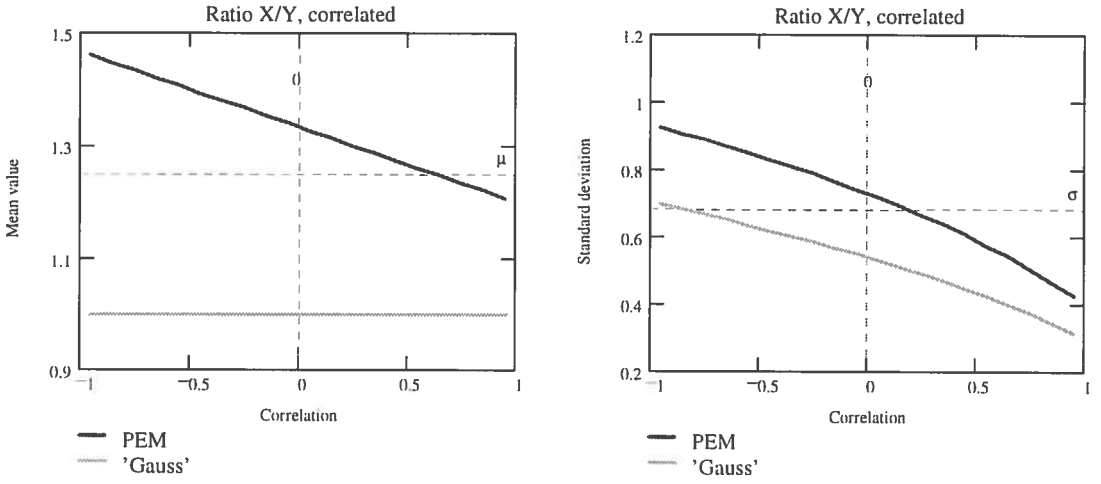

Figure D.12Ratio *X/Y* of two correlated, random variables. Comparison between PEM and Gaussian approximation.
$\mu_x=\mu_y=1$; $\sigma_x=0{,}2$; $\sigma_y=0{,}5$.

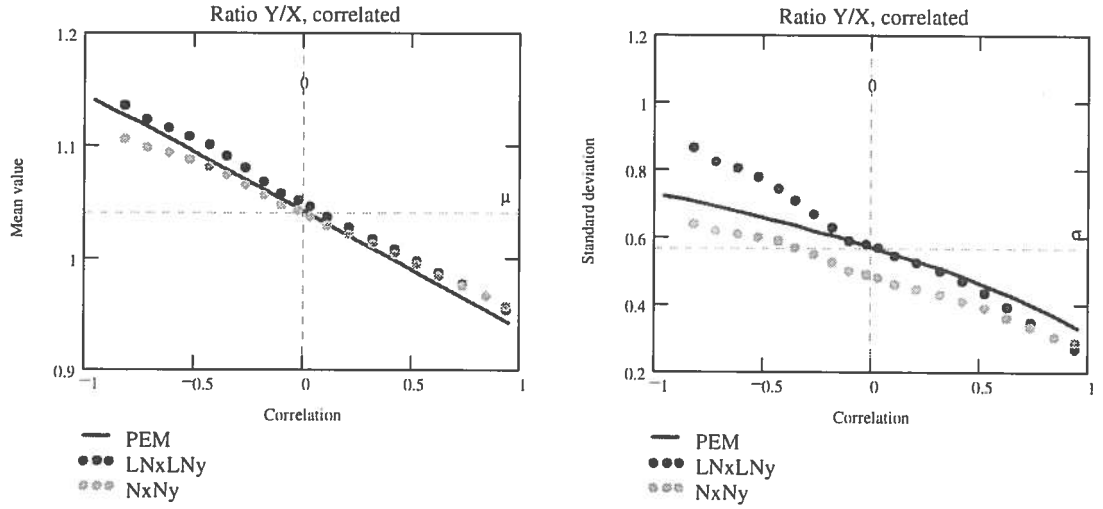

Figure D.13Ratio *Y/X* of two correlated, random variables. Comparison between PEM and Monte Carlo simulations.
$\mu_x=\mu_y=1$; $\sigma_y=0{,}5$; $\sigma_x=0{,}2$.

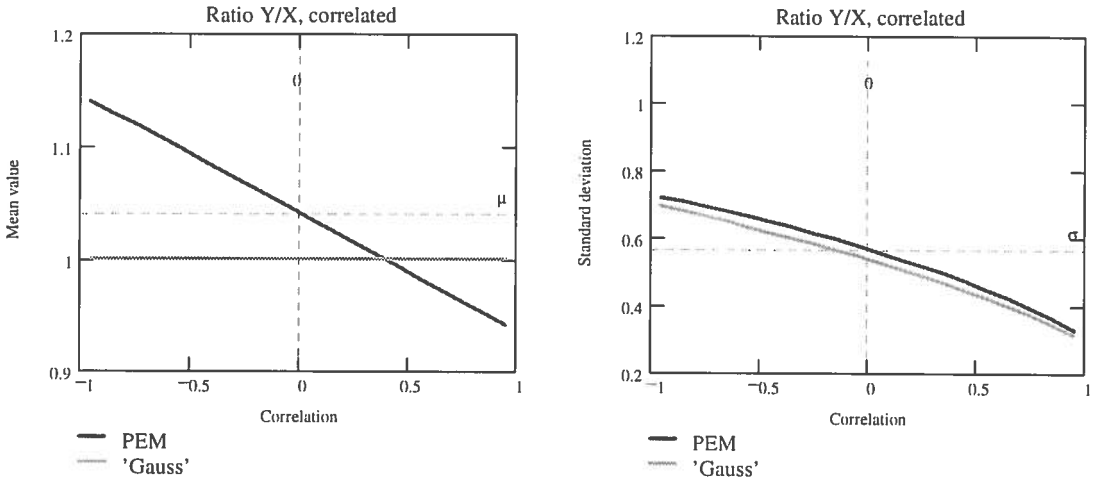

Figure D.14Ratio *Y/X* of two correlated, random variables. Comparison between PEM and Gaussian approximation.
$\mu_x=\mu_y=1$; $\sigma_y=0{,}5$; $\sigma_x=0{,}2$.

D.6 Load/deformation - Hyperbola

D.6.1 Deformation as a function of the load

As an example of a more complex function, the result of a hyperbolic function is analysed. The deformation, s, as a function of the load is often described with the equation:

$$s(R,M_0)=\frac{R}{M_0\cdot(R-Q)}\cdot Q \qquad \text{(D.24)}$$

In the interpretation of the equation, Q is the load, R is asymptotic maximum value, i.e. the bearing capacity, and M_0 is the slope of the tangent in the origo, i.e. the modulus for small deformations given as force/length. In Figure D.15, the relation is plotted for R=100 and M_0=1000.

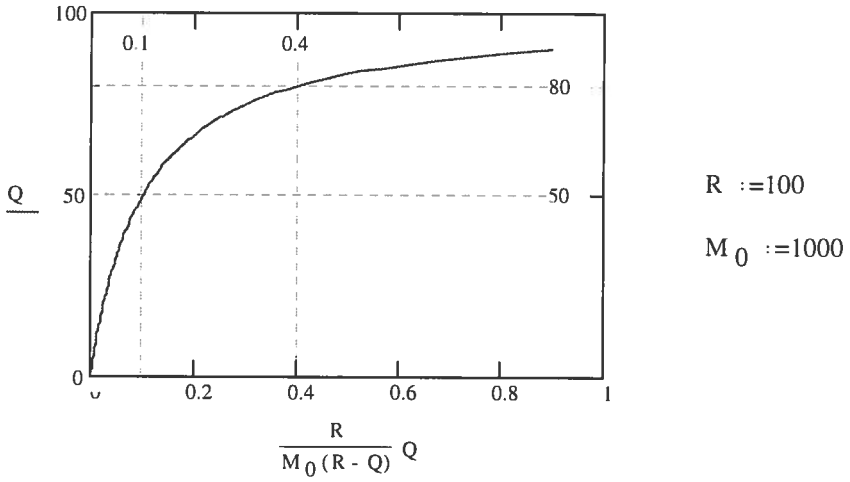

Figure D.15Example of a load/deformation curve described as a hyperbola,

If the load Q is assumed to be deterministic and the parameters R and M_0 are assumed to be given as distributions, $PD(\mu_R,\sigma_R)$ and $PD(\mu_M,\sigma_M)$ respectively, the deformation for a deterministic load can be calculated by PEM in a similar manner as in the previous sections. It has to be remarked that the assumption of a deterministic load should not be interpreted as that the load is less uncertain than the material parameters. In this case it is just a matter of simplification of the calculations. In the real world the load is often, but far from always, given by a national code. This implies that a considerable safety margin is included in the design values of the load.

PEM gives for the mean value:

$$E[s(R,M_0)]=\frac{1+\rho}{4}\cdot\left[\frac{(\mu_R+\sigma_R)\cdot s}{(\mu_M+\sigma_M)\cdot(\mu_R+\sigma_R-Q)}\right]+ \\ +\frac{1-\rho}{4}\cdot\left[\frac{(\mu_R+\sigma_R)\cdot s}{(\mu_M-\sigma_M)\cdot(\mu_R+\sigma_R-Q)}\right]+ \\ +\frac{1-\rho}{4}\cdot\left[\frac{(\mu_R-\sigma_R)\cdot s}{(\mu_M+\sigma_M)\cdot(\mu_R-\sigma_R-Q)}\right]+ \\ +\frac{1+\rho}{4}\cdot\left[\frac{(\mu_R-\sigma_R)\cdot s}{(\mu_M-\sigma_M)\cdot(\mu_R-\sigma_R-Q)}\right] \qquad \text{(D.25)}$$

or after some effort:

$$E[s(R,M_0)]=\frac{(\mu_R+\sigma_R)\cdot(\mu_R-\sigma_R)\cdot\mu_M-(\mu_R\cdot\mu_M-\rho\cdot\sigma_R\cdot\sigma_M)\cdot Q}{(\mu_R+\sigma_R-Q)\cdot(\mu_R-\sigma_R-Q)\cdot(\mu_M+\sigma_M)\cdot(\mu_M-\sigma_M)}\cdot Q \qquad \text{(D.26)}$$

The variance is:

$$Var[s(R,M_0)] = \frac{1+\rho}{4}\cdot\left[\frac{(\mu_R+\sigma_R)\cdot Q}{(\mu_M+\sigma_M)\cdot(\mu_R+\sigma_R-Q)}\right]^2 + \\ + \frac{1-\rho}{4}\cdot\left[\frac{(\mu_R+\sigma_R)\cdot Q}{(\mu_M-\sigma_M)\cdot(\mu_R+\sigma_R-Q)}\right]^2 + \\ + \frac{1-\rho}{4}\cdot\left[\frac{(\mu_R-\sigma_R)\cdot Q}{(\mu_M+\sigma_M)\cdot(\mu_R-\sigma_R-Q)}\right]^2 + \\ + \frac{1+\rho}{4}\cdot\left[\frac{(\mu_R-\sigma_R)\cdot Q}{(\mu_M-\sigma_M)\cdot(\mu_R-\sigma_R-Q)}\right]^2 - \\ - \left[\begin{array}{l} \frac{1+\rho}{4}\cdot\left[\frac{(\mu_R+\sigma_R)\cdot Q}{(\mu_M+\sigma_M)\cdot(\mu_R+\sigma_R-Q)}\right] + \\ + \frac{1-\rho}{4}\cdot\left[\frac{(\mu_R+\sigma_R)\cdot Q}{(\mu_M-\sigma_M)\cdot(\mu_R+\sigma_R-Q)}\right] + \\ + \frac{1-\rho}{4}\cdot\left[\frac{(\mu_R-\sigma_R)\cdot Q}{(\mu_M+\sigma_M)\cdot(\mu_R-\sigma_R-Q)}\right] + \\ + \frac{1+\rho}{4}\cdot\left[\frac{(\mu_R-\sigma_R)\cdot Q}{(\mu_M-\sigma_M)\cdot(\mu_R-\sigma_R-Q)}\right] \end{array}\right]^2 \quad \text{(D.27)}$$

or after much effort:

$$Var[s(R,M_0)] = \frac{\left[\begin{array}{l} \sigma_M^2\cdot\left[\mu_R^2\cdot(\mu_R-Q)^2+\sigma_R^4+\sigma_R^2\cdot\left(2\cdot\mu_R\cdot Q+Q^2-2\cdot\mu_R{}^2\right)\right]+ \\ +\sigma_R^2\cdot\mu_M^2\cdot Q^2 \\ +\rho\cdot\sigma_R\cdot\sigma_M\left[2\cdot\mu_M\cdot\left[\mu_R\cdot(\mu_R-Q)\right]-\rho\cdot\sigma_R\cdot\sigma_M\cdot Q\right]\cdot Q \end{array}\right]}{(\mu_R+\sigma_R-Q)^2\cdot(\mu_R-\sigma_R-Q)^2\cdot(\mu_M+\sigma_M)^2\cdot(\mu_M-\sigma_M)^2}Q^2$$

(D.28)

With Gaussian approximation, see appendix A, one obtains for the mean value the equation:

$$E[s(R,M_0)] = \frac{\mu_R\cdot Q}{\mu_M\cdot(\mu_R-Q)} \quad \text{(D.29)}$$

and for the variance with $\frac{\partial s(\mu_R,\mu_M)}{\partial R} = -\frac{Q^2}{\mu_M \cdot (\mu_R - Q)^2}$

and $\frac{\partial s(\mu_R,\mu_M)}{\partial M_0} = \frac{-\mu_R \cdot Q}{\mu_M{}^2 \cdot (\mu_R - Q)}$:

$$Var[f(R,M_0)] = \sigma_R^2 \cdot \frac{Q^4}{\mu_M^2 \cdot (\mu_R - Q)^4} + \sigma_M^2 \cdot \frac{\mu_R^2 \cdot Q^2}{\mu_M^4 \cdot (\mu_R - Q)^2} + 2\rho \cdot \sigma_R \cdot \sigma_M \cdot \frac{\mu_R \cdot Q^3}{\mu_M^3 \cdot (\mu_R - Q)^3}$$

(D.30)

In accordance with the analyses of products and ratios in the previous sections, the result of a PEM calculation is compared with the results of Monte Carlo simulations and a Gaussian approximation. The load Q is given a fixed value 80, cf. Figure D.15. The random parameters R and M_0 are assumed to be described as the probability distributions, $R=PD(100:16)$ and $M_0=PD(1000;270)$. Two different simulations were performed. In the first simulation both R and M were assumed to be lognormal distributions and in the second simulation they were assumed to be normal distributions. The influence of correlation was determined for positive correlations, i.e. values of the coefficient of correlation in the range, $\rho = 0$ -- +1. The results of the analyses are presented in Figure D.16 and Figure D.17. The values of μ and σ displayed in the figures are based on the approximation that the 'variable' can be seen as a lognormal distribution. Thus, for $\rho=0$, values of μ and σ can be calculated 'exactly', as $s(R,M)$ is a product/ratio of three lognormal distributions. The assumption of R-Q as a lognormal is just to simplify the calculations. A normal distribution is a better approximation, as the 'variable' is the sum of a lognormal distribution with V=16%, i.e. close to a normal distribution, and a deterministic value.

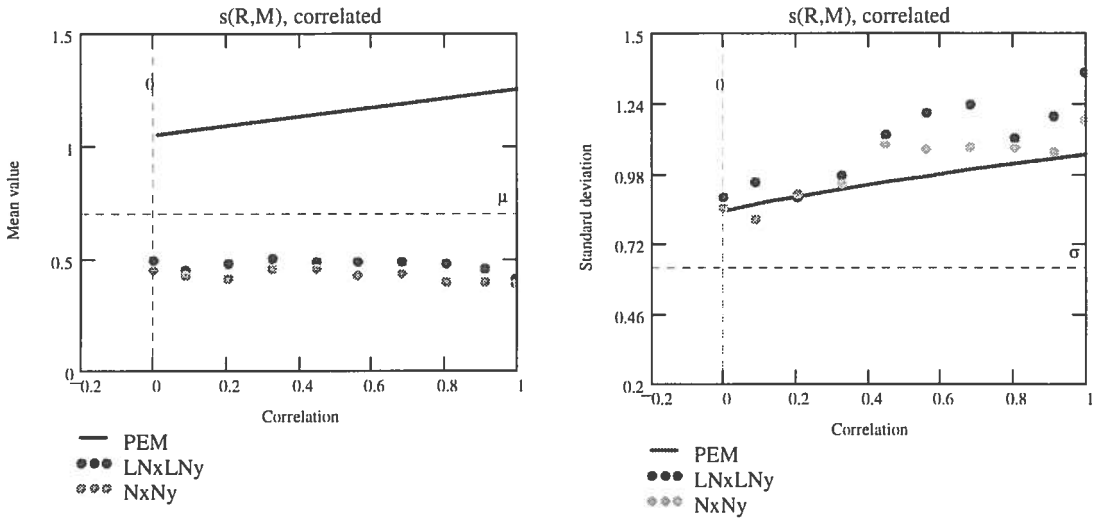

Figure D.16Hyperbolic function to calculate the deformation for a given load Q=80. Comparison between PEM and Monte Carlo simulations. Simulations truncated (0,02-0,98).

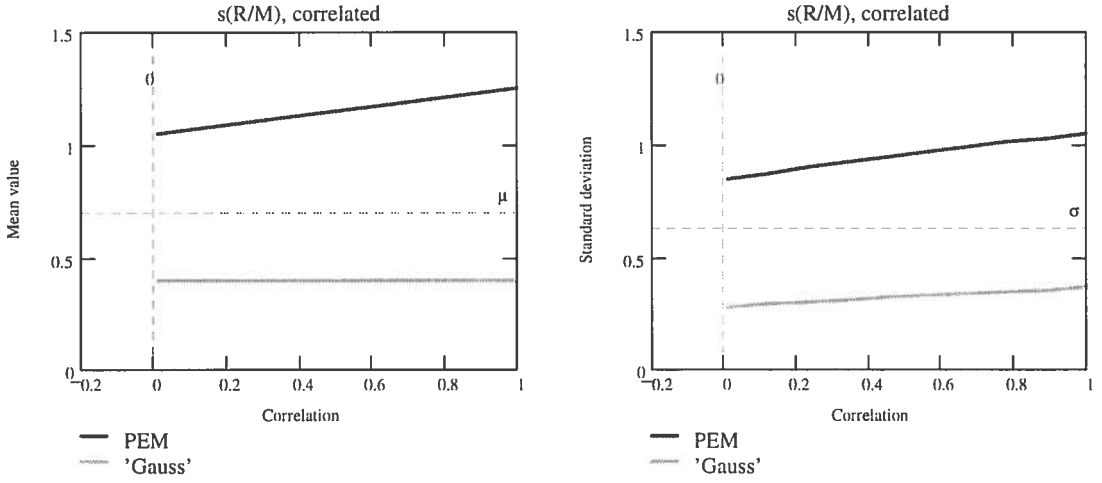

Figure D.17Hyperbolic function to calculate the deformation for a given load Q=80. Comparison between PEM and Gaussian approximation.

The results in Figure D.16 and Figure D.17 indicate that the PEM overestimates the settlements in this case. However, the comments about simulations of normal distributions in section D.5.1 are extremely appropriate in this case. For the results shown in Figure D.16, both R and M are truncated to the mid 96%, i.e. truncated 2% in both ends. In Figure D.18 the corresponding results for nontruncated distributions are given. The mean values are of the same magnitude, while the variance has become unpredictable. The result of the PEM coincides almost with the x-axis.

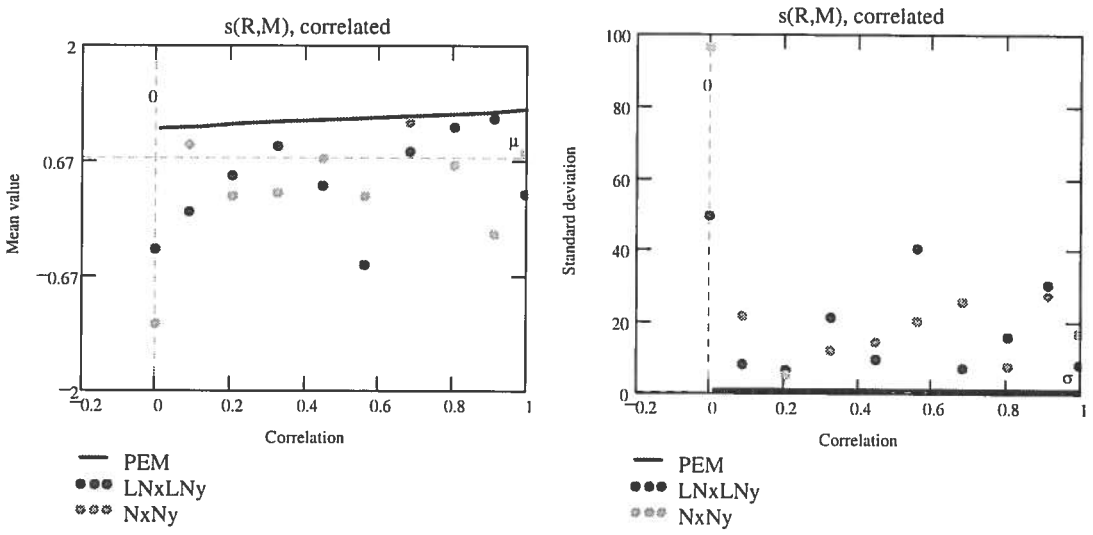

Figure D.18Hyperbolic function to calculate the deformation for a given load Q=80. Comparison between PEM and Monte Carlo simulations. Simulations not truncated.

In this case, the truncation can not be justified by the fact that it is extremely unlikely that the denominator can be negative or close to zero. If the structure is loaded beyond its capacity, i.e. $Q>R$, this will happen. Thus it is difficult to interpret the results. Seen from good engineering practice, it might be stated that the case described above is a pure academic question. Figure D.19 shows two 'extreme' cases, i.e. the results of the '++' and '-- --' calculation in PEM, are given.

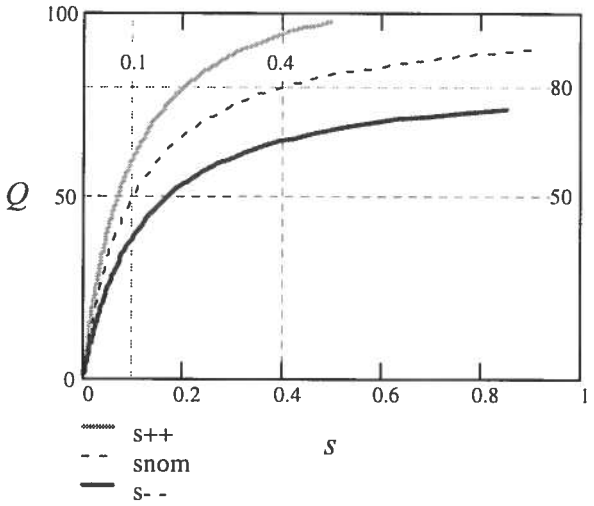

Figure D.19Three different calculations of the hyperbolic load/deformation curve. s_{++} = PEM_{++}; $s_{-\ -}$ = $PEM_{-\ -}$; s_{nom}= Gaussian approximation

From Figure D.19 it is easily seen that a load Q = 80 is quite hazardous compared to the 's- -' calculation. The result of a more sound design situation, Q= 50, is displayed in Figure D.20 and Figure D.21.

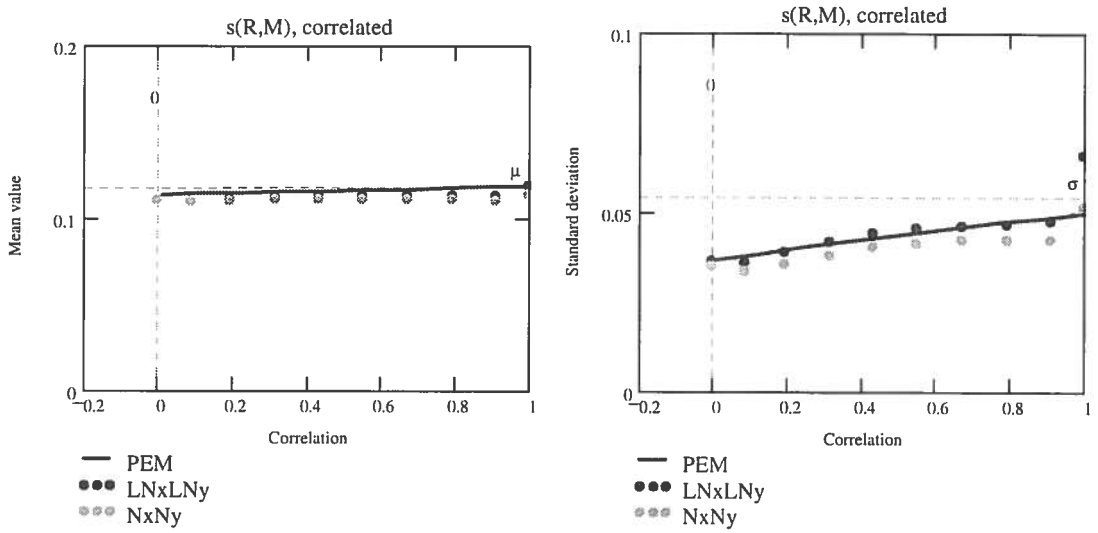

Figure D.20Hyperbolic function to calculate the deformation for a given load Q=50. Comparison between PEM and Monte Carlo simulations. Simulations arenot truncated.

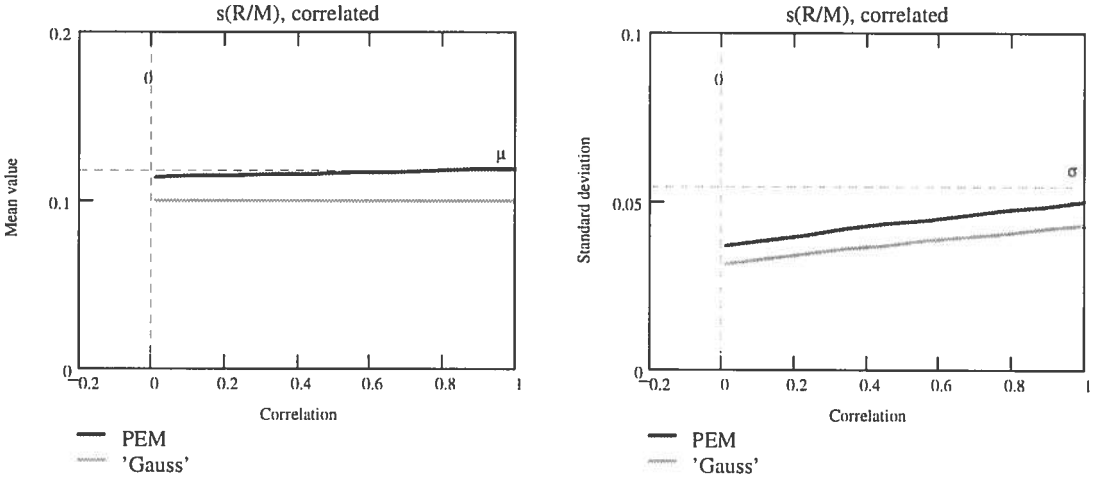

Figure D.21Hyperbolic function to calculate the deformation for a given load Q=50. Comparison between PEM and Gaussian approximation.

For a 'realistic' load of 50 there is a very good agreement between PEM and Monte Carlo simulations. The Gaussian approximation gives a somewhat smaller value than PEM but of the same order of magnitude.

It can be noted that a comparison of the two load cases shows that the latter case results in deformations of just 20% of the first case, despite the fact that the load is only reduced to 60% compared to the first case.

D.6.2 Load as a function of deformation

In theprevious section it was stated that there is a large uncertainty about the magnitude of the deformation for loads close to the ultimate capacity. If the problem is reversed, i.e. which load corresponds to a given deformation, the load/deformation relation becomes much more stable. The inverse of equation D.24 becomes:

$$Q(R,M_0)=\frac{R\cdot M_0}{R+s\cdot M_0}\cdot s \tag{D.31}$$

The PEM-parameters can be obtained in a similar manner as in the previous section. PEM gives for the mean value:

$$\begin{aligned}E[Q(R,M_0)]=&\frac{1+\rho}{4}\cdot\left[\frac{(\mu_R+\sigma_R)\cdot(\mu_M+\sigma_M)\cdot Q}{(\mu_R+\sigma_R)+s\cdot(\mu_M+\sigma_M)}\right]+\\&+\frac{1-\rho}{4}\cdot\left[\frac{(\mu_R+\sigma_R)\cdot(\mu_M-\sigma_M)\cdot Q}{(\mu_R+\sigma_R)+s\cdot(\mu_M-\sigma_M)}\right]+\\&+\frac{1-\rho}{4}\cdot\left[\frac{(\mu_R-\sigma_R)\cdot(\mu_M+\sigma_M)\cdot Q}{(\mu_R-\sigma_R)+s\cdot(\mu_M+\sigma_M)}\right]+\\&+\frac{1+\rho}{4}\cdot\left[\frac{(\mu_R-\sigma_R)\cdot(\mu_M-\sigma_M)\cdot Q}{(\mu_R-\sigma_R)+s\cdot(\mu_M-\sigma_M)}\right]\end{aligned} \tag{D.32}$$

An expression, which is not easily simplified to any great extent.

The general expression for the variance:

$$
\begin{aligned}
Var[Q(R,M_0)] = & \frac{1+\rho}{4}\cdot[Q(\mu_R+\sigma_R,\mu_M+\sigma_M)]^2 + \\
& + \frac{1-\rho}{4}\cdot[Q(\mu_R+\sigma_R,\mu_M-\sigma_M)]^2 + \\
& + \frac{1-\rho}{4}\cdot[Q(\mu_R-\sigma_R,\mu_M+\sigma_M)]^2 + \\
& + \frac{1+\rho}{4}\cdot[Q(\mu_R-\sigma_R,\mu_M-\sigma_M)]^2 - \\
& - \left[\begin{array}{l}
\frac{1+\rho}{4}\cdot[Q(\mu_R+\sigma_R,\mu_M+\sigma_M)] + \\
+\frac{1-\rho}{4}\cdot[Q(\mu_R+\sigma_R,\mu_M-\sigma_M)] + \\
+\frac{1-\rho}{4}\cdot[Q(\mu_R-\sigma_R,\mu_M+\sigma_M)] + \\
+\frac{1+\rho}{4}\cdot[Q(\mu_R-\sigma_R,\mu_M-\sigma_M)]
\end{array}\right]^2
\end{aligned}
\qquad (D.33)
$$

becomes even more complicated. The Gaussian approximations become more simple. The mean value is:

$$
E[Q(R,M_0)] = \frac{\mu_R\cdot\mu_M\cdot Q}{\mu_R + s\cdot\mu_M} \qquad (D.34)
$$

and the variance:

$$
Var[Q(R,M_0)] = \frac{\sigma_R^2\cdot\mu_M^4\cdot s^4 + \sigma_M^2\cdot\mu_R^4\cdot s^2 + 2\rho\cdot\sigma_R\cdot\sigma_M\cdot\mu_M^2\cdot\mu_R^2\cdot s^3}{(\mu_R + s\cdot\mu_M)^4} \qquad (D.35)
$$

In accordance with the analyses of the unknown deformation in previous section, the result of a PEM calculation is compared to the results of Monte Carlo simulations and a Gaussian approximation The deformation s is given a fixed value 0,4, c.f. Figure D.15. The random parameters R and M_0 are assumed to be described as previously, $R=PD(100:16)$ and $M_0=PD(1000;270)$. Even in this case, two different simulations were performed. One in which both R and M were assumed to be lognormal distributions and a second simulation with normal distributions. The influence of the

correlation was determined for a positive correlation. The results of the analyses are presented in Figure D.22 and Figure D.23.

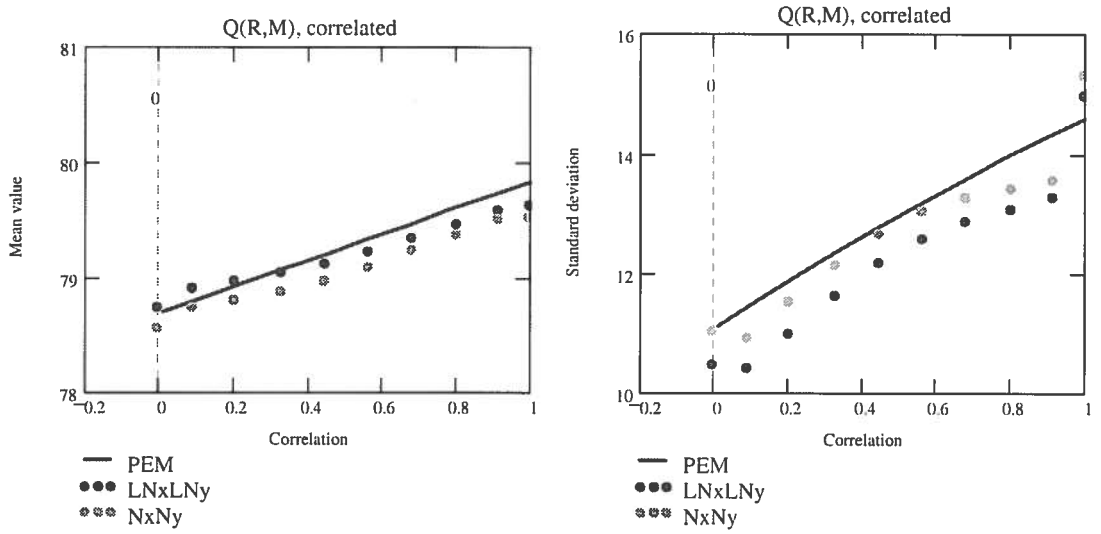

Figure D.22Hyperbolic function to calculate the load for a given deformation s=0,4. Comparison between PEM and Monte Carlo simulations.

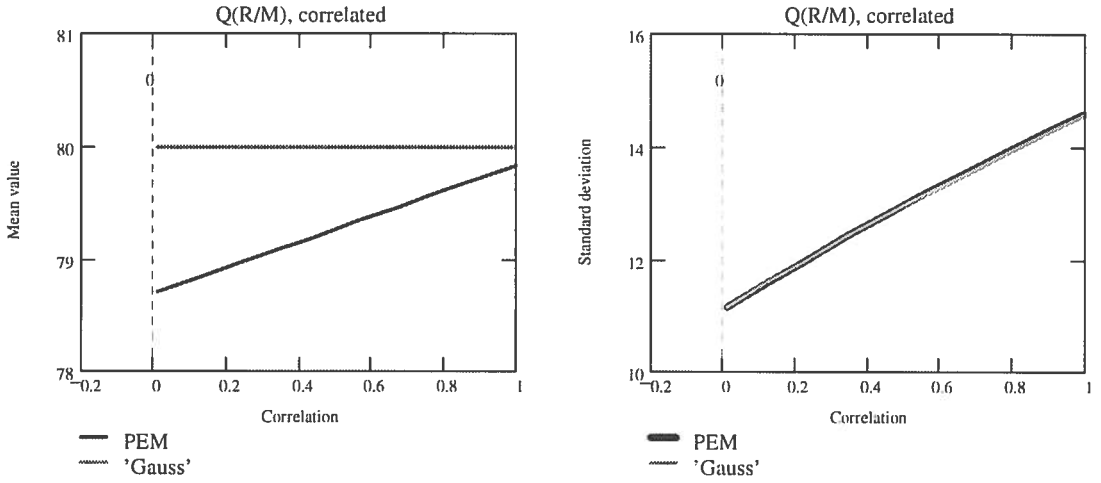

Figure D.23Hyperbolic function to calculate the load for a given deformation s=0,4. Comparison between PEM and Gaussian approximation.

There is a very good agreement between PEM and the simulations. As before, the Gaussian approximation does not take the correlation into account for the mean value. However, in this case the influence of correlation is very small. For the variance there is an extremely good agreement between PEM and Gaussian approximation, the 'PEM-line' being hidden behind the 'Gaussian line'. As mentioned in the beginning of this section, the solutions become very stable when the load is regarded as the unknown variable. None of the

difficulties of predicting a 'correct' solution, which were at hand in the previous section, exist this time.

D.7 Summary

In this appendix, the 'Point Estimate Method', PEM, is compared with alternative methods. The results show that the method predicts the basic behaviour of not too complicated functions of random variables. In calculations with random variables as denominators, the accuracy is reduced for resulting large variances of the denominator, i.e. dominating denominators. From the results given in this appendix the PEM can be said to be a somewhat more accurate approximate method than Gaussian approximation. However, this fact has to be balanced against the simple formulas of Gaussian approximation.

APPENDIX E GEOSTATISTICS / FORMULAS

Below derivations and formulas in geostatistics are given. It is a compilation of the subject reported in (Christian et al., 1992), (Davis, 1986), (DeGroot & Baecher, 1993) and (He, 1994).

E.1 Autocovariance / autocorrelation

E.1.1 General

The covariance for two variables X and Y is, see appendix A:

$$Cov[X,Y] = E\left[(X-\mu_X)\cdot(Y-\mu_Y)\right] \tag{E.1}$$

with the estimator:

$$\hat{C}ov_{XY} = \frac{1}{n-1}\cdot\sum_n (x_i-\bar{x})\cdot(y_i-\bar{y}) \tag{E.2}$$

Hence, for two 'variables' with a distance r apart, $x(z)$ and $x(z+r)$, from a stochastic process yields the autocovariance:

$$C[x(z),x(z+r)] = E\left[(x(z)-\mu_x(z))\cdot(x(z+r)-\mu_x(z+r))\right] \tag{E.3}$$

or after simplifying:

$$C[x(z),x(z+r)] = E\left[x(z)\cdot x(z+r)\right] - \mu_x(z)\cdot\mu_x(z+r) \tag{E.3a}$$

The first term in equation E.3a is in the following denoted:

$$R[x(z),x(z+r)] = E\left[x(z)\cdot x(z+r)\right] \tag{E.4}$$

r=0 gives the variance in a point z, cf. .appendix A:

$$Var\left[x(z)\right] = C[x(z),x(z)] = E\left[x(z)^2\right] - \mu_x(z)^2 \tag{E.5}$$

The autocorrelation coefficient is defined as:

$$\rho_x(z,z+r) = \frac{C[x(z),x(z+r)]}{\sigma_x(z)\cdot\sigma_x(z+r)} \tag{E.6}$$

The estimation corresponding to equation E.2 is:

$$\hat{C}_x(z,z+r)=\frac{1}{n-1}\cdot\sum_n(x(z)-\bar{x}(z))\cdot(x(z+r)-\bar{x}(z+r)) \quad \text{(E.7)}$$

E.1.2 Stationary process

If the process is stationary it is independent of z, i.e. $E[x(z)]=E[x(z+r)]$ and $\mu_x(z)=\mu_x(z+r)=\mu_x(z)$. In this case equation E.3a becomes:

$$C_x[r]=E[x(z)\cdot x(z+r)]-\mu_x{}^2=R_x[r]-\mu_x{}^2 \quad \text{(E.8)}$$

Similarly, for equation E.5 and equation E.6 respectively:

$$Var[x]=\sigma_x^2=C_x[0]=R_x[0]-\mu_x(z)^2 \quad \text{(E.9)}$$

and

$$\rho_x(r)=\frac{C_x[r]}{\sigma_x^2} \quad \text{(E.10)}$$

The estimator of the autocovariance becomes[1]:

$$\hat{C}_x(r)=\frac{1}{n-1}\cdot\sum_n(x(z)-\bar{x}(z))\cdot(x(z+r)-\bar{x}(z)) \quad \text{(E.11)}$$

and for the variance at a point:

$$\hat{C}_x(0)=\frac{1}{n-1}\cdot\sum_n(x(z)-\bar{x}(z))^2 \quad \text{(E.12)}$$

E.1.3 Stationary process. μ_x= 0

If there is no systematic divergence in the process, e.g. no systematic errors in a test series, the autocovariance becomes equal with the first term in equation E.3a, i.e. $R[x(z),x(z+r)]=R[r]$, since the autocovariance is independent of z. Hence, in this case, which is

[1] To use n-1 as a denominator is not indisputable. It is common to let the denominator be the number of data pairs separated by r, e.g. if r is a multiple of a unit length, the denominator becomes n-r. In the context at hand, i.e. one is interested in small separating distances, the different alternatives are of secondary importance.

commonly applied on geotechnical investigations, the autocovariance is:

$$C_x[r] = E[x(z) \cdot x(z+r)] = R_x[r] \tag{E.13}$$

The variance becomes:

$$Var[x] = \sigma_x^2 = C_x[0] = R_x[0] \tag{E.14}$$

Finally the coefficient of autocorrelation is:

$$\rho_x(r) = \frac{C_x[r]}{\sigma_x^2} = \frac{R_x[r]}{R_x[0]} \tag{E.15}$$

E.2 Semi-variance

E.2.1 General

The semivariance is defined by the equation:

$$\gamma[x(z), x(z+r)] = \frac{1}{2} \cdot E\left[\left(x(z) - x(z+r)\right)^2\right] \tag{E.16}$$

which can be expanded to:

$$\gamma[x(z), x(z+r)] = \frac{1}{2} \cdot E\left[x(z)^2 + x(z+r)^2 - 2 \cdot x(z) \cdot x(z+r)\right] \tag{E.16a}$$

For a stationary process is then obtained:

$$\gamma_x[r] = E\left[x(z)^2\right] - E[\cdot\, x(z) \cdot x(z+r)] \tag{E.17}$$

which can be rewritten as:

$$\gamma_x[r] = \left(E\left[x(z)^2\right] - \mu_x^2\right) - \left(E[\cdot\, x(z) \cdot x(z+r)] - \mu_x^2\right) \tag{E.17a}$$

Hence, according to equation E.8 and E.9:

$$\gamma_x[r] = \sigma_x^2 - C_x(r) \tag{E.17b}$$

The special case μ_x=0 does not add any further contribution.

E.2.2 Estimation

For a stationary process the semi-variance can, by introducingting equations E.12 and E.11 into E.17b, be estimated as:

$$\hat{\gamma}_x(r) = \frac{1}{n-1} \cdot \sum_n \left(x(z) - \bar{x}(z)\right)^2 - \left(x(z) - \bar{x}(z)\right) \cdot \left(x(z+r) - \bar{x}(z)\right) \tag{E.18}$$

Rewriting of the equation:

$$\hat{\gamma}_x(r) = \frac{1}{n-1} \cdot \sum_n \left(x(z)\right)^2 - x(z) \cdot x(z+r) + \frac{\bar{x}(z)}{n-1} \cdot \sum_n x(z+r) - x(r) \tag{E.18a}$$

Assuming $\sum_n x(z+r) - x(r) = 0$ by the stationarity, the second term disappears:

$$\hat{\gamma}_x(r) = \frac{1}{2 \cdot (n-1)} \cdot \sum_n 2 \cdot \left(x(z)\right)^2 - 2 \cdot x(z) \cdot x(z+r) \tag{E.18b}$$

Further assumption by stationarity, $\sum_n x(z)^2 = \sum_n x(z+r)^2$,

i.e $\sum_n 2 \cdot x(z)^2 = \sum_n x(z)^2 + x(z+r)^2$, gives:

$$\hat{\gamma}_x(r) = \frac{1}{2 \cdot (n-1)} \cdot \sum_n \left(x(z) - x(z+r)\right)^2 \tag{E.18c}$$

APPENDIX F GEOSTATISTICS / EXAMPLES

This appendix is an extract from the report: Geostatistical analyses of clay properties, Claes Alén, 1998, report B 1998:X, Department of Geotechnical Engineering, Chalmers University of Technology

Example 1 is example 1 in the referenced report
" 2 " " 4 " " " "
" 3 " " 8 " " " "

The examples based on data from a test site at Nödinge, (Mangushev, 1994)

F.1--Undrained shear strength. Vertical autocovariance and semi-variance

F.1.1---Model given as a linear trend

Example 1 - Field vane tests - Bore hole A1

Input data in the matrix A_1. First column, index 0, depth. Second column, index 1, shear strength. Undrained shear strength adjusted according to recommendation by SGI (Larsson et al., 1984).

$i := 0..8 \qquad j := 9..17 \qquad k := 18..26$

$A1_{i,0}$	$A1_{i,1}$
2	7.2
2.5	7
3	6.81
3.5	6.91
4	7.78
4.5	7.76
5	8.52
5.5	8.64
6	9.55

$A1_{j,0}$	$A1_{j,1}$
6.5	9.55
7	10.34
7.5	11.17
8	10.41
8.5	11.32
9	12.26
9.5	11.32
10	12.8
10.5	13.55

$A1_{k,0}$	$A1_{k,1}$
11	12.71
11.5	14.03
12	15.29
12.5	15.45
13	17.17
13.5	17.43
14	18.5
14.5	19.2
15	19.9

Consider the shear strength as a trend, i.e. linear regression of the shear strength versus depth:

Observations: $X := (A1)^{<1>}$ Depth: $z := (A1)^{<0>}$

$a := slope(z, X)$ $a = 0.99$

$b := intercept(z, X)$ $b = 3.52$

$trend := a \cdot z + b$

Residuals: $x := X - trend$

Correlation: $\rho := corr(z, X)$ $\rho = 0.98$

Number of observations, N+1: $N := last(x)$ $N + 1 = 27$

Observation distances: $r := 0, 0.5 .. \frac{N}{2}$

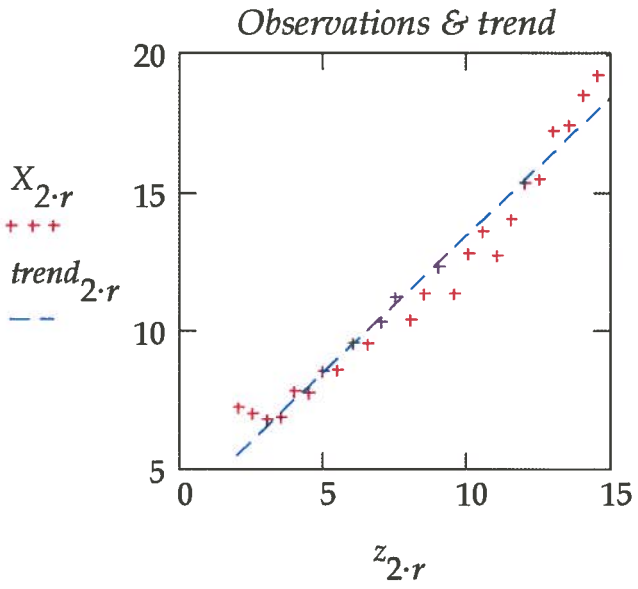

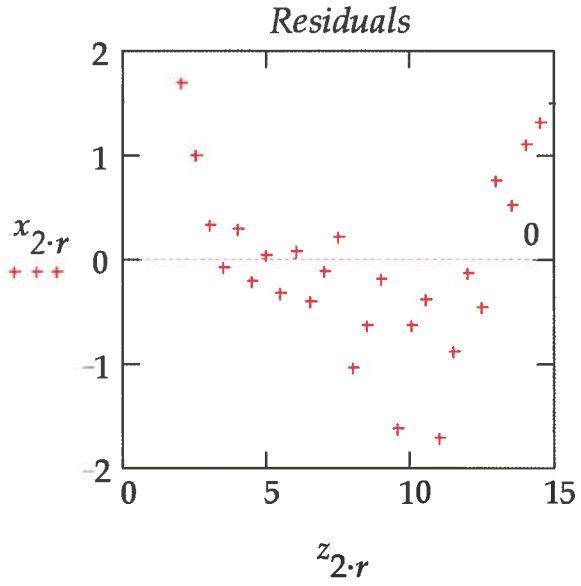

Note:
By inspection, there is a systematic error in the model. X is underestimated at shallow and deep depths. X is overestimated at intermediate depths

Variance:

$$Var := \frac{1}{N-1} \cdot \sum_{n=0}^{N} (x_n)^2 \qquad Var = 0.77$$

$$\sigma_x := \sqrt{Var} \qquad \sigma_x = 0.88$$

$$V_{min} := \frac{\sigma_x}{trend_N} \qquad V_{min} = 0.05$$

$$V_{max} := \frac{\sigma_x}{trend_0} \qquad V_{max} = 0.16$$

Autocovariance:

$$r := 0, 0.5 .. \frac{N-1}{2}$$

$$C_x(r) := \frac{1}{(N-2\cdot r)} \cdot \sum_{n=0}^{N-2\cdot r} x_n \cdot x_{n+2\cdot r} \qquad C_x(0) = 0.74$$

Autocorrelation functions:

Exponential: $C_{xexp}(\sigma_c, r, r_0) := \sigma_c^2 \cdot e^{-\frac{r}{r_0}}$

Spherical: $C_{xsphere}(\sigma_c, r, r_0) := \sigma_c^2 \cdot if\left(r \le r_0, 1 - \frac{3\cdot r}{2\cdot r_0} + \frac{r^3}{2\cdot {r_0}^3}, 0\right)$

Assign: $\sigma_c := \sigma_x \qquad r_{0exp} := 0.9 \qquad r_{0sphere} := 2.5$

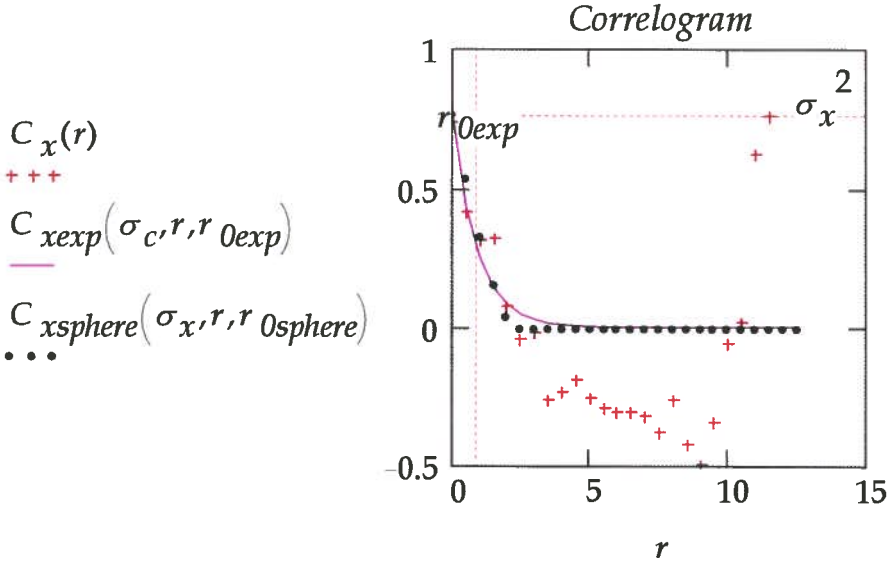

Note:
The correlogram has a distinct dependence on r. There is no tendency of 'zero correlation' for large distances , cf. the systematic error in the observations & trend figure.

Semi-variance

$$\gamma_x(r) := \frac{1}{2\cdot((N - 2\cdot r))} \cdot \sum_{n=0}^{N-2\cdot r} \left(x_n - x_{n+2\cdot r}\right)^2 \qquad \gamma_x(0) = 0$$

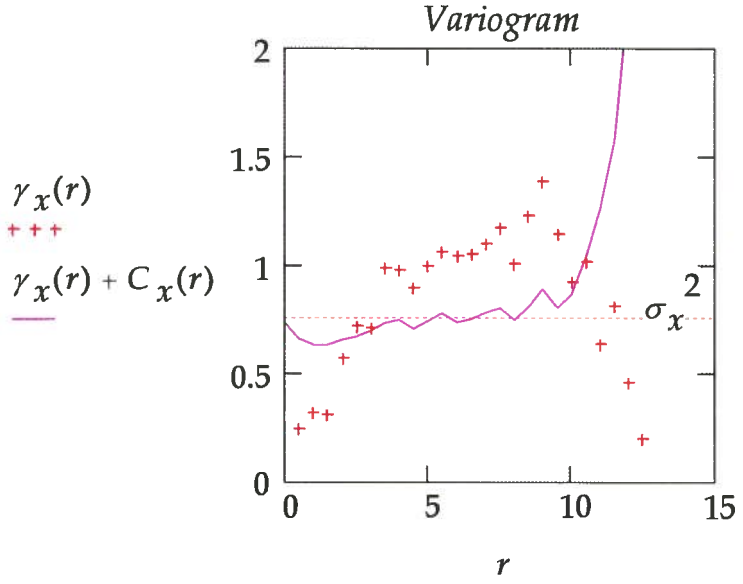

Note:
There is a good agreement between the variogram and the correlogram. The sum of the autocovariance and the semi-variance is close to the variance (for $r < 10$). There is a corresponding dependence on r as in the correlogram.

F.1.2---Model given as a bi-linear trend

Example 2 - Field vane tests - Bore hole A1

Input data in the matrix A_2. First column, index 0, depth. Second column, index 1, shear strength. Undrained shear strength adjusted according to recommendation by SGI (Larsson et al., 1984).

$i := 0..8 \qquad j := 9..17 \qquad k := 18..26$

$A2_{i,0}$	$A2_{i,1}$
2	7.2
2.5	7
3	6.81
3.5	6.91
4	7.78
4.5	7.76
5	8.52
5.5	8.64
6	9.55

$A2_{j,0}$	$A2_{j,1}$
6.5	9.55
7	10.34
7.5	11.17
8	10.41
8.5	11.32
9	12.26
9.5	11.32
10	12.8
10.5	13.55

$A2_{k,0}$	$A2_{k,1}$
11	12.71
11.5	14.03
12	15.29
12.5	15.45
13	17.17
13.5	17.43
14	18.5
14.5	19.2
15	19.9

Consider the clay as separated into two layers, 2-10m and 10.5-15m, and the shear strength as a trend in each layer, i.e. a bi-linear regression of the shear strength versus depth:

Observations: $X := (A_2)^{<1>}$ Depth: $z := (A_2)^{<0>}$

Layer 1 (2-10m)

$i := 0..16 \qquad X1_i := X_i \qquad z1_i := z_i$

$a_1 := slope(z1, X1) \qquad a_1 = 0.76$

$b_1 := intercept(z1, X1) \qquad b_1 = 4.81$

$trend := a_1 \cdot z1 + b_1$

Residuals: $x := X_1 - trend$

Correlation: $\rho_1 := corr(z_1, X_1)$ $\rho_1 = 0.97$

Layer 2 (10.5-15m)

$i := 17..26$ $X2_{i-17} := X_i$ $z2_{i-17} := z_i$

$a_2 := slope(z_2, X_2)$ $a_2 = 1.61$

$b_2 := intercept(z_2, X_2)$ $b_2 = -4.24$

$trend_i := a_2 \cdot z2_{i-17} + b_2$

Residuals: $x_i := X2_{i-17} - trend_i$

Correlation: $\rho_2 := corr(z_2, X_2)$ $\rho_2 = 0.98$

Number of observations, N+1: $N := last(x)$ $N + 1 = 27$

Observation distances: $r := 0, 0.5 .. \frac{N}{2}$

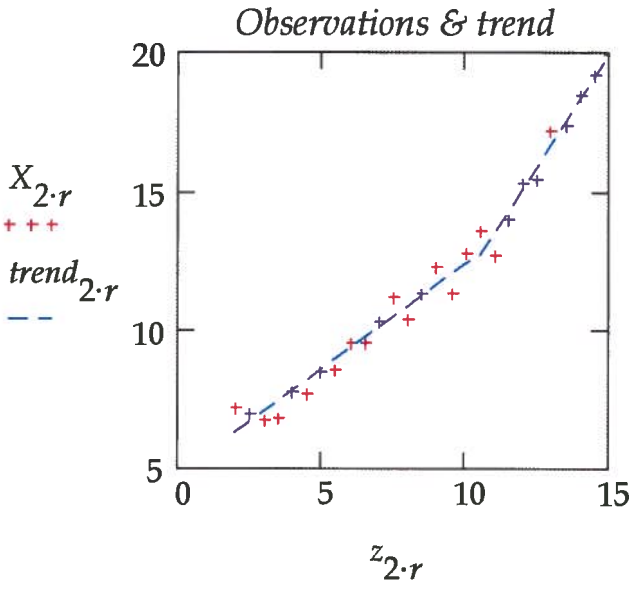

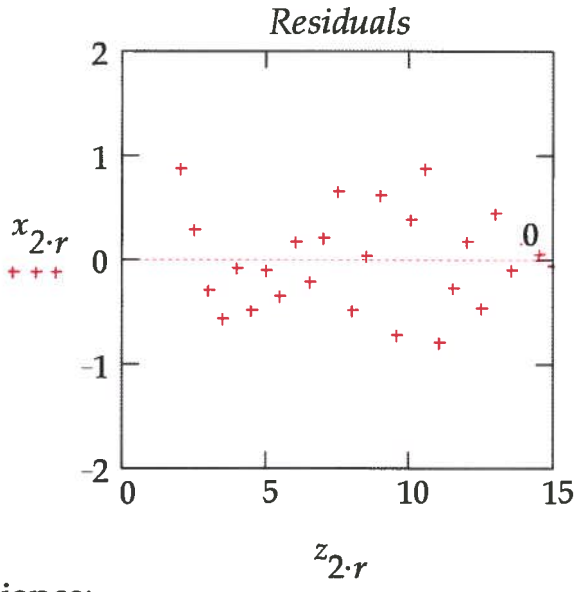

Note:
The figures show the same soil profile as in example 1. By inspection, there is no obvious systematic error in the model as in example 1.

Variance:

$$Var := \frac{1}{N-1} \cdot \sum_{n=0}^{N} (x_n)^2 \qquad Var = 0.21$$

$$\sigma_x := \sqrt{Var} \qquad \sigma_x = 0.46$$

$$V_{min} := \frac{\sigma_x}{trend_N} \qquad V_{min} = 0.02$$

$$V_{max} := \frac{\sigma_x}{trend_0} \qquad V_{max} = 0.07$$

Autocovariance:

$$r := 0, 0.5 .. \frac{N-1}{2}$$

$$C_x(r) := \frac{1}{(N-2\cdot r)} \cdot \sum_{n=0}^{N-2\cdot r} x_n \cdot x_{n+2\cdot r} \qquad C_x(0) = 0.2$$

Autocorrelation functions:

Exponential: $C_{xexp}(\sigma_c, r, r_0) := \sigma_c^2 \cdot e^{-\frac{r}{r_0}}$

Spherical: $C_{xsphere}(\sigma_c, r, r_0) := \sigma_c^2 \cdot if\left(r \le r_0, 1 - \frac{3\cdot r}{2\cdot r_0} + \frac{r^3}{2\cdot r_0^3}, 0\right)$

Assign: $\sigma_c := \sigma_x$ $\qquad r_{0exp} := 0.05$ $\qquad r_{0sphere} := 0.7$

$C_x(r)$

$C_{xexp}(\sigma_c, r, r_{0exp})$

$C_{xsphere}(\sigma_x, r, r_{0sphere})$

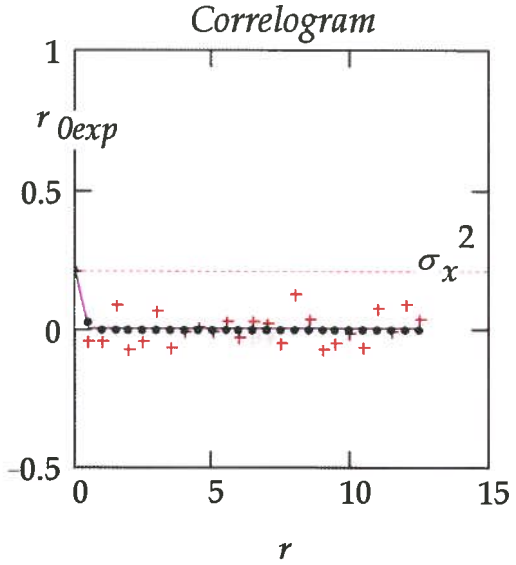

Note:

The correlogram shows the same soil profile as in example 1. The pattern of the correlogram has changed with the new soil model, the bi-linear regression model. The variance is reduced and autocorrelation distances are 'zero'.

Semi-variance

$$\gamma_x(r) := \frac{1}{2\cdot((N - 2\cdot r))} \cdot \sum_{n=0}^{N-2\cdot r} \left(x_n - x_{n+2\cdot r}\right)^2 \qquad \gamma_x(0) = 0$$

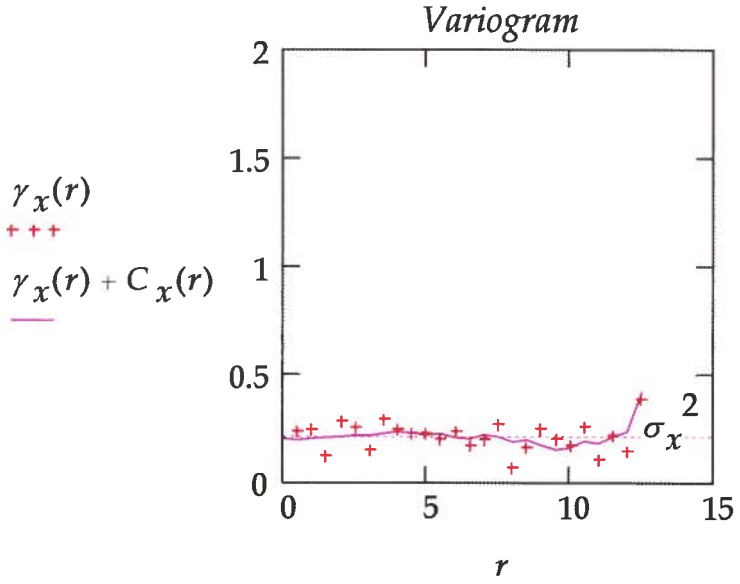

Note:
There is a good agreement between the variogram and the correlogram. The sum of the autocovariance and the semi-variance is close to the variance.

F.2--Undrained shear strength. Horizontal autocovariance and semi-variance

F.2.1---Model given as a bi-linear trend

Example 3 - Field vane tests - 8 no of bore holes/ A1 - F.

Input data in the matrix Y_1, see F.3.3. First column, index 0, depth. Other columns, index 1-8, shear strength. Undrained shear strength adjusted according to recommendation by SGI (Larsson et al., 1984). Values calculated for each level separately.

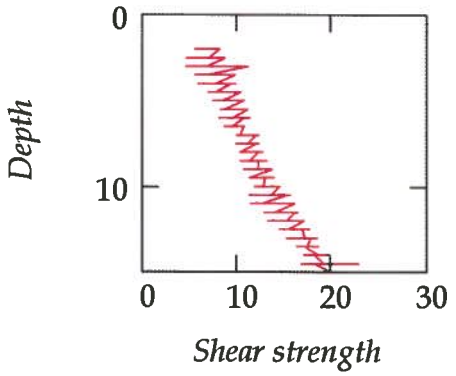

Distances between bore holes in matrix S_1, cf. figure in Chapter 3.

$$S_1 = \begin{pmatrix} 0 & 0 & 54 & 99 & 114 & 114 & 121.5 & 151.5 \\ 0 & 1 & 0 & 0 & 0 & 1 & 0 & 0 \end{pmatrix}$$

Bi-linear trend for all bore holes

No of bore holes:

$$N_1 := last\left[\left(Y_1^T\right)^{<0>}\right]$$

$N_1 = 8$

No of observations / bore hole:

$$N_2 := last\left(Y_1^{<0>}\right) + 1$$

$N_2 = 27$

i index columns $\quad i := 0..N_1 - 1$

j index rows

Upper layers

$j := 0..12$

$z1_{i\cdot 13+j} := \left(Y1^{\langle 0\rangle}\right)_j \qquad X1_{i\cdot 13+j} := \left(Y1^{\langle i+1\rangle}\right)_j$

$trend1_j := slope(z1, X1)\cdot z1_j + intercept(z1, X1)$

Lower layers

$j := 0..13$

$z2_{i\cdot 14+j} := \left(Y1^{\langle 0\rangle}\right)_{j+13} \qquad X2_{i\cdot 14+j} := \left(Y1^{\langle i+1\rangle}\right)_{j+13}$

$trend2_j := slope(z2, X2)\cdot z2_j + intercept(z2, X2)$

All layers

$j := 0..N2 - 1$

$trend_j := if(j<13, trend1_j, trend2_{j-13})$

$z_{i\cdot N2+j} := \left(Y1^{\langle 0\rangle}\right)_j \qquad X_{i\cdot N2+j} := \left(Y1^{\langle i+1\rangle}\right)_j$

Correlation

$\rho := corr(z, X) \qquad \rho = 0.95$

Residuals

$l := 0..N1$

$x_{j,l} := if(l\neq 0, Y1_{j,l} - trend_j, Y1_{j,l}) \qquad x1_{i\cdot N2+j} := \left(x^{\langle i+1\rangle}\right)_j$

$k := 0..last(z)$

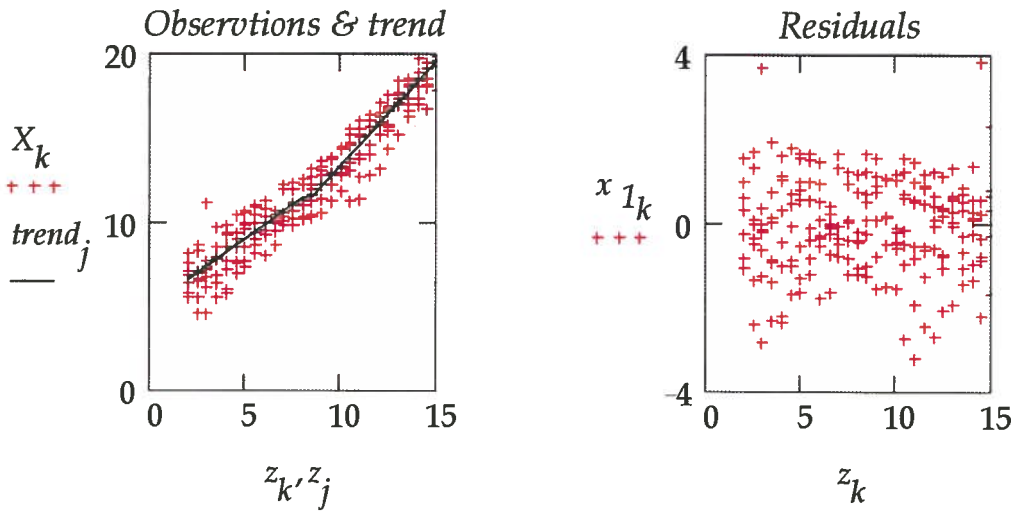

Note:
By inspection, there is no obvious systematic error in the model.

Variance:

$$Var := \frac{1}{N_1 \cdot N_2 - 1} \cdot \sum_{n=1}^{N_1 - 1} \sum_{m=0}^{N_2 - 1} \left(x_{m,n}\right)^2 \qquad Var = 1.02$$

$$\sigma_x := \sqrt{Var} \qquad \sigma_x = 1.01$$

$$V_{min} := \frac{\sigma_x}{trend_{N_2 - 1}} \qquad V_{min} = 0.05$$

$$V_{max} := \frac{\sigma_x}{trend_0} \qquad V_{max} = 0.15$$

Separating distances, from S_1:

i index columns

$i := 0 .. N_1 - 2$

k index difference columns

$k := 1 .. N_1 - 1$

$$r_{i,k-1} := if\left[k \le N_1 - 1 - i, \sqrt{\left(S1_{0,i} - S1_{0,i+k}\right)^2 + \left(S1_{1,i} - S1_{1,i+k}\right)^2}, 0\right]$$

Autocovariance:

$$C_{i,k-1} := \text{if}\left[k \le N_1 - 1 - i, \frac{1}{N_2 - 1} \cdot \left[\sum_{j=0}^{N_2 - 1} \left(x_{j,i+1} \cdot x_{j,i+k+1}\right)\right], \sigma_x^2\right]$$

Semi-variance:

$$\gamma_{i,k-1} := \text{if}\left[k \le N_1 - 1 - i, \frac{1}{2 \cdot \left(N_2 - 1\right)} \cdot \sum_{j=0}^{N_2 - 1} \left(x_{j,i+1} - x_{j,i+k+1}\right)^2, 0\right]$$

The values 0, σ_x^2 and 0 assigned to the variables in the foregoing formulas are 'dummy' values, used to simplify the forth-coming calculations, i.e. values in the matrices at hand, which are not used any further in the calculations, are given simple, arbitrary values.

Arrange the separating distances with corresponding values of the autocovariance and the semi-variance in column vectors.

$i := 0..N_1 - 2 \quad j := 0..N_1 - 2$

$r_{x_{i \cdot}\left(N_1 - 1\right) + j} := \left(r^{\langle i \rangle}\right)_j$

$C_{x_{i \cdot}\left(N_1 - 1\right) + j} := \left(C^{\langle i \rangle}\right)_j \qquad \gamma_{x_{i \cdot}\left(N_1 - 1\right) + j} := \left(\gamma^{\langle i \rangle}\right)_j$

Place r_x, C_x and γ_x in a matrix V

$i := 0..last\left(r_x\right)$

$V_{i,0} := r_{x_i} \qquad V_{i,1} := C_{x_i} \qquad V_{i,2} := \gamma_{x_i}$

Sort the matrix V by the magnitude of r_x

$V := csort(V, 0)$

Replace r_x, C_x and γ_x from the matrix V

$r_{x_i} := V_{i,0} \qquad C_{x_i} := V_{i,1} \qquad \gamma_{x_i} := V_{i,2}$

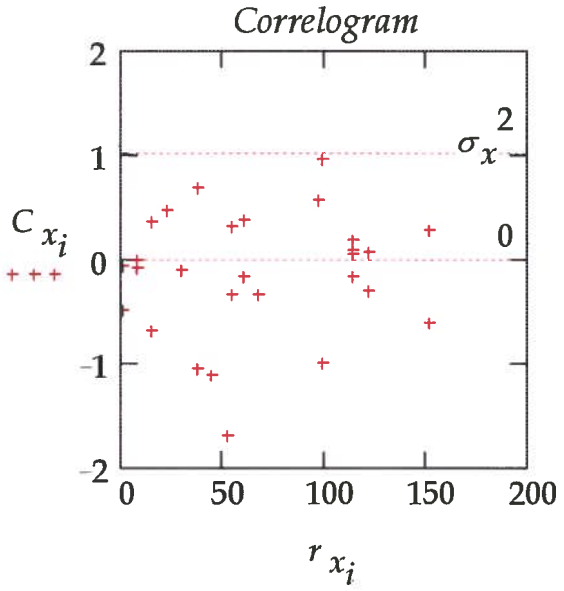

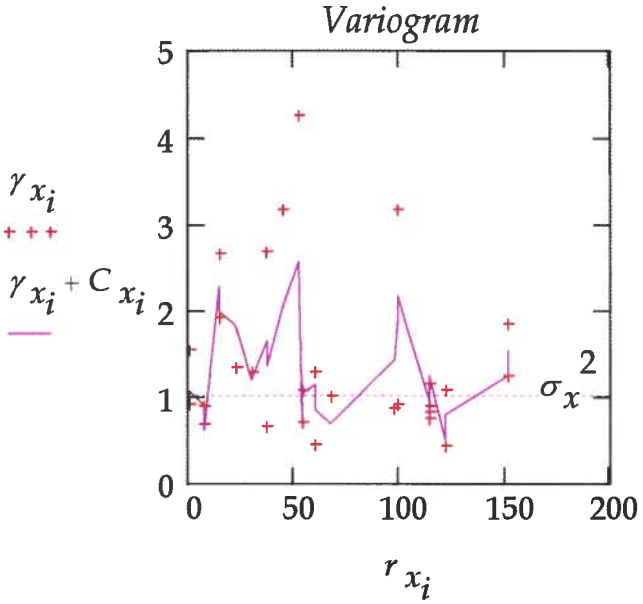

Note:
Both the correlogram and the variogram show a 'noise scatter'. Any interpretation of the autocorrelation distance will be less than 1m, the minimum separating distance.

APPENDIX G ON BAYESIAN STATISTICS

G.1 General

In volume 1, section 3.3.2 , Bayesian updating of a random variable was discussed. Bayes' theorem was introduced:

$$\begin{pmatrix}\text{Posterior prob.}\\ \text{of the true state } \theta\\ \text{given the sample}\end{pmatrix} = \begin{pmatrix}\text{Norma -}\\ \text{lising}\\ \text{constant}\end{pmatrix} \cdot \begin{pmatrix}\text{Sample likelihood}\\ \text{given}\\ \text{the true state } \theta\end{pmatrix} \begin{pmatrix}\text{Prior prob.}\\ \text{of the true}\\ \text{state } \theta\end{pmatrix} \qquad \text{(G.1)}$$

or with a more compound formulation for a basic, continuous variable X, with the density function $f_x(x,\theta)$:

$$f_\theta''(\theta) = k \cdot L(\theta) \cdot f_\theta'(\theta) \qquad \text{(G.1a)}$$

where θ was an unknown parameter of the distribution and k a normalising constant. The sample likelihood, $L(\theta)$, was defined as:

$$L(\theta) = \prod_n f_x(x_i|\theta) \qquad \text{(G.2)}$$

Thus the information of the unknown parameter, given by the prior distribution, could be updated by information from a sample, into a posterior distribution. The information of the parameter distribution, prior or posterior, could be incorporated into an estimation of the underlying distribution of the basic variable as a Bayesian distribution:

$$\hat{f}_x(x) = \int_{-\infty}^{\infty} f_x(x|\theta) \cdot f_\theta(\theta) d\theta \qquad \text{(G.3)}$$

If the prior and the posterior distributions are of the same type, the basic and the prior distributions form a pair of conjugate distributions. Below Bayesian statistics for two simple but important cases of conjugate distributions are analysed

- Normal distributions, known standard deviation
- Lognormal distributions, known coefficient of variation

G.2 Notations in this appendix

$f_N(x;\mu;\sigma)$	Density function $f(x)$ for a normal distribution given by μ and σ, i.e. $N(\mu;\sigma)$
$f_L(x;\mu;V)$	Density function $f(x)$ for a lognormal distribution given by μ and V, *i.e.* $LN(\mu;\mu \cdot V)$

G.3 Conjugate pairs of normal distributions

This case is to a large extent thoroughly discussed by both Benjamin & Cornell (1979) and Ang & Tang (1975).

G.3.1 Basic variable X - normal distribution. Parameter $\theta=\mu_x$. The standard deviation σ known.

Basic variable X

Assume that a basic variable X can be described with a normal distribution $N(\mu_x;\sigma)$. The variable can be seen as a property observed by testing. Thus the scatter, given by σ, has to include both testing errors and natural spatial variations. Consider the case when the mean value is unknown, while the standard deviation is known. The density function of X can then be written as:

$$f_x(x;\theta)=f_x(x;\mu_x)=f_N(x;\mu_x;\sigma) \qquad \text{(G.4)}$$

where $f_N(x;\mu_x;\sigma)$ is a normal density function, see section G.2

Likelihood function - Probability of a sample

From equation G.2 and equation G.4 the likelihood function can be determined:

$$L(\mu_x)=\prod_n f_x(x_i|\mu_x)=\prod_n f_N(x_i;\mu_x;\sigma) \qquad \text{(G.5)}$$

A product of n normal density functions is also a normal density function, see (Ang & Tang, 1975):

$$\prod_n f_N(x;\mu_i;\sigma_i)=f_N(x;\mu_*;\sigma_*) \qquad \text{(G.6)}$$

$$\text{with } \mu_*=\frac{\sum_n \mu_i/\sigma_i^2}{\sum_n 1/\sigma_i^2} \text{ and } \sigma_*^2=\frac{1}{\sum_n 1/\sigma_i^2}$$

Then for the case $\sigma_i=\sigma$:

$$\prod_n f_N(x;\mu_i;\sigma)=f_N(x;\bar{\mu};\sigma/\sqrt{n}) \qquad \text{(G.6a)}$$

$$\text{as } \mu_* = \frac{\sum_n \mu_i/\sigma^2}{\sum_n 1/\sigma^2} = \frac{\sum_n \mu_i}{n} = \bar{\mu} \text{ and } \sigma_*^2 = \frac{1}{\sum_n 1/\sigma^2} = \frac{\sigma^2}{n}$$

Recalling that $f_N(x;\mu;\sigma)=\frac{1}{\sigma}\cdot\varphi\left(\frac{x-\mu}{\sigma}\right)=\frac{1}{\sigma}\cdot\varphi\left(\frac{\mu-x}{\sigma}\right)=f_N(\mu;x;\sigma)$,
cf. appendix A, the likelihood function can now be simplified as:

$$L(\mu_x)=\prod_n f_N(x_i;\mu_x;\sigma)=\prod_n f_N(\mu_x;x_i;\sigma)=f_N(\mu_x;\bar{x};\sigma/\sqrt{n}) \qquad \text{(G.5a)}$$

G.3.2 Prior and posterior distributions - normal distributions

The prior and the posterior distributions describe the uncertainty of the mean value, before and after sampling. If the prior distribution for μ_x is a normal distribution $N(\mu';\sigma')$, according to Bayes theorem, equation G.1a gives the posterior distribution:

$$f''(\mu_x)=k\cdot f_N(\mu_x;\bar{x};\sigma/\sqrt{n})\cdot f_N(\mu_x;\mu';\sigma') \qquad \text{(G.7)}$$

i.e. a product of two normal density functions. According to equation G.6 the posterior distribution can be rewritten as:

$$f''(\mu_x)=f_N(\mu_x;\mu'';\sigma'') \qquad \text{(G.7a)}$$

$$\text{with } \mu''=\frac{n\cdot\bar{x}/\sigma^2+\mu'/\sigma'^2}{n/\sigma^2+1/\sigma'^2} \text{ and } \sigma''^2=\frac{1}{n/\sigma^2+1/\sigma'^2}$$

The normalising constant has to be equal to unity to make the posterior a proper distribution.

G.3.3 Prior information compared to sample information

Case A: m+n tests

Assume that testing is done in two stages. This means that a sample **x** of $m+n$ tests can be divided into two subsamples $\mathbf{x}_1$ and $\mathbf{x}_2$ of m and n tests respectively. Each such subsample can be seen as a combination of a

diffuse prior and a sample. The diffuse prior has to be given as a constant, which can then be included in the normalising constant. Thus according to equation G.7 the density functions for the samples can be written as[1]:

$$f(\mu_{x1}) = f_N(\mu_{x1}; \bar{x}_1; \sigma/\sqrt{m}) \quad \text{and} \tag{G.8}$$

$$f(\mu_{x2}) = f_N(\mu_{x2}; \bar{x}_2; \sigma/\sqrt{n})$$

or equivalent:

$$\mu_{x1} = N(\bar{x}_1, \sigma/\sqrt{m}) \text{ and } \mu_{x2} = N(\bar{x}_2; \sigma/\sqrt{n}) \tag{G.8a}$$

This means that if the first subsample is seen as the prior information to the second sample, then the combined information of the sample is determined as the posterior information[2] by equation G.7a :

$$f(\mu_x) = f_N(\mu_x; \mu_A; \sigma_A) \text{ or } \mu_x = N(\mu_A; \sigma_A) \tag{G.8b}$$

$$\text{with } \mu_A = \frac{m \cdot \bar{x}_1 + n \cdot \bar{x}_2}{m+n} \text{ and } \sigma_A^2 = \frac{\sigma^2}{m+n}$$

Case B: Prior + n tests

Assume that the first subsample is substituted by the information given by the prior information. Hence equation G.7a implies:

$$\mu_x = N(\mu_B; \sigma_B) \tag{G.9}$$

$$\text{with } \mu_B = \frac{n \cdot \bar{x}/\sigma^2 + \mu'/\sigma'^2}{n/\sigma^2 + 1/\sigma'^2} \text{ and } \sigma_B{}^2 = \frac{1}{n/\sigma^2 + 1/\sigma'^2}$$

Comparison case A and case B

The pre-knowledge, i.e. the information given by the prior distribution, can be see as the results of prior testing. This means that if case A and case B are seen as equivalent, the pre-knowledge can be interpreted as a

[1] A diffuse prior and a sample are basically the concept of analysis with confidence intervals. Hence, such an analysis will give the same result.

[2] Appendix A, the mean value of a linear combination of random variables, gives the same result.

sample of m tests. Both the equalities $\mu_A = \mu_B$ and $\sigma_A^{\,2} = \sigma_B^{\,2}$ give for the number of tests:

$$m = \frac{\sigma^2}{\sigma'^2} \tag{G.10}$$

In the interpretation of the first equality it has to be assumed that the pre-knowledge gives the same mean value as the subsample $\mathbf{x}_1$, i.e. $\mu' = \bar{x}_1$. The variance of prior distribution, σ'^2, describes the uncertainty of the mean value and not the observed variable in itself. Thus testing errors have to be excluded from σ'^2. This means that in the normal case m>1.

G.3.4 Bayesian distribution

The Bayesian distribution, i.e. the estimation of the basic variable, can be determined for both the cases:

- prior information given as a sample $\mathbf{x}_1$ of m tests or a equivalent distribution $N(\mu';\sigma')$
- posterior information given by the prior information and a sample $\mathbf{x}_2$ of n tests

For the first case, equation G.3 and equation G.8 give:

$$\begin{aligned} \hat{f}_x(x) &= \int_{-\infty}^{\infty} f_x(x|\mu) \cdot f_\mu(\mu) d\mu = \\ &= \int_{-\infty}^{\infty} f_N(x;\mu;\sigma) \cdot f_N(\mu;\bar{x}_1;\sigma/\sqrt{m}) d\mu \end{aligned} \tag{G.11}$$

which yields (Ang & Tang, 1975):

$$\hat{f}_x(x) = f_N\left(x;\bar{x}_1;\sqrt{\sigma^2 + \sigma^2/m}\right) = f_N\left(x;\bar{x}_1;\sigma\sqrt{(m+1)/m}\right) \tag{G.11a}$$

or with $\mu' = \bar{x}_1$ and $\sigma'^2 = \sigma^2/m$

$$\hat{f}_x(x) = f_N\left(x;\mu';\sqrt{\sigma^2 + \sigma'^2}\right) \tag{G.11b}$$

Similarly for the second case, i.e. by added information from n tests, introducing equation G.8b in equation G.3:

$$\hat{f}_x(x) = \int_{-\infty}^{\infty} f_x(x|\mu) \cdot f_\mu(\mu) d\mu =$$
$$= \int_{-\infty}^{\infty} f_N(x;\mu;\sigma) \cdot f_N\left(\mu; \frac{m \cdot \overline{x_1} + n \cdot \overline{x_2}}{m+n}; \sigma/\sqrt{m+n}\right) d\mu \qquad \text{(G.12)}$$

which yields, cf. equation G.11a:

$$\hat{f}_x(x) = f_N\left(x; \frac{m \cdot \overline{x_1} + n \cdot \overline{x_2}}{m+n}; \sigma \cdot \sqrt{\frac{m+n+1}{m+n}}\right) \qquad \text{(G.12a)}$$

or with $\mu' = \overline{x}_1$ and $m = \sigma^2/\sigma'^2$

$$\hat{f}_x(x) = f_N\left(x; \frac{\mu' \cdot \sigma^2 + n \cdot \overline{x_2} \cdot \sigma'^2}{\sigma^2 + n \cdot \sigma'^2}; \sigma \sqrt{\frac{\sigma^2 + (n+1) \cdot \sigma'^2}{\sigma^2 + n \cdot \sigma'^2}}\right) \qquad \text{(G.12b)}$$

G.3.5 Summary - known standard deviation σ

Information about the mean value of a property can be up-dated by information given by a sample $\mathbf{x}_2$ of n tests. The pre-knowledge of the property can then be interpreted as an equivalent sample $\mathbf{x}_1$ of m tests such that:

- For the equivalent sample:

$$\overline{x_1} = \mu' \text{ and } m = \frac{\sigma^2}{\sigma'^2} \qquad \text{(G.10a)}$$

- For the posterior distribution - the uncertainty of the mean value:

$$\mu'' = \frac{m \cdot \overline{x_1} + n \cdot \overline{x_2}}{m+n} \text{ and } \sigma'' = \sigma/\sqrt{m+n} \qquad \text{(G.8c)}$$

- For the Bayesian distribution - the uncertainty of the basic variable:

$$\mu_x = \mu'' \text{and } \sigma_x = \sigma \cdot \sqrt{\frac{m+n+1}{m+n}} \qquad \text{(G.12c)}$$

In the formulas above it was assumed that both the basic variable and the mean value of the basic variable could be modelled as normal distributions.

G.4 Conjugate pairs of lognormal distributions

This case is an extension of the case discussed previously in section G.3

G.4.1 Basic variable *X* - lognormal distribution. Parameter $\theta=\mu_{\ln x}$. The coefficient of variation *V* known.

Basic variable X

In section G.3, the basic variable was given by a normal distribution. An assumption of the prior distribution also being normal, resulted in the convenient result of normal distributions for both the posterior distribution and the Bayesian distribution. However, for reasons discussed in volume 1, section 2.3.2, a lognormal distribution is often a better choice, for example a resistance property of the soil. What does this entail in Bayesian statistics? From a mathematical point of view, analysis of lognormal distributions can always be transformed into analyses of normal distributions by the substitution $x=e^y$, which implies that the analysis is undertaken for the variable $y=\ln x$ instead of x. For the case that the coefficient of variation is of moderate magnitude, $V<25\%$-30%, the procedure becomes especially easy as the lognormal distribution $LN(\mu;\sigma)=LN(\mu;V\mu)$ corresponds approximately to the normal distribution $N(\ln\mu;V)$, see appendix A. Hence the analysis can be undertaken exactly as in section G.3 but with the substitutions $\ln x$ instead of x, $\ln\mu$ instead of μ and V instead of σ. For such an analysis to be meaningful, it is implied that it is restricted to cases when the uncertainty of the variable[1] could be modelled with a constant coefficient of variation.

The density function of $\ln(X)$ can then be written as:

$$f_{\ln x}(\ln x;\theta)=f_{\ln x}(\ln x;\mu_{\ln x})=f_N(\ln x;\mu_{\ln x};V) \qquad \text{(G.13)}$$

Likelihood function - Probability of a sample

The likelihood function becomes the density function:

$$L(\mu_{\ln x})=f_N(\mu_{\ln x};\overline{\ln x};V/\sqrt{n}) \qquad \text{(G.14)}$$

[1] That is including both testing errors and natural variation, cf. section G.3.1

G.4.2 Prior and posterior distributions

The prior and the posterior distributions can be given as normal distributions for $\ln\mu_x$:

$$f'(\mu_{\ln x}) = f_N(\mu_{\ln x}; \ln\mu'; V') \qquad \text{(G.15)}$$

and

$$f''(\mu_{\ln x}) = f_N(\mu_{\ln x}; \ln\mu''; V'') \qquad \text{(G.16)}$$

with $\ln\mu'' = \dfrac{n\cdot\overline{\ln x}/V^2 + \ln\mu'/V'^2}{n/V^2 + 1/V'^2}$ and $V'' = \sqrt{\dfrac{1}{n/V^2 + 1/V'^2}}$.

Alternatively the prior and posterior distributions can be expressed as lognormal distributions for μ_X:

$$f'(\mu_x) = f_L(\mu_x; \mu'; V') \qquad \text{(G.15a)}$$

and

$$f''(\mu_x) = f_L(\mu_x; \mu''; V'') \qquad \text{(G.16a)}$$

G.4.3 Prior information compared to sample information

Case A: m+n tests

Assume that the testing is done as two subsamples $\mathbf{x}_1$ and $\mathbf{x}_2$ of m and n tests respectively. This gives:

$$\mu_{\ln x1} = N(\overline{\ln x_1}, V/\sqrt{m}) \text{ and } \mu_{\ln x2} = N(\overline{\ln x_2}; V/\sqrt{n}) \qquad \text{(G.17)}$$

or combined:

$$\mu_{\ln x} = N(\mu_{\ln A}; V_A) \qquad \text{(G.18)}$$

with $\mu_{\ln A} = \dfrac{m\cdot\overline{\ln x_1} + n\cdot\overline{\ln x_2}}{m+n}$ and $V_A = \dfrac{V}{\sqrt{m+n}}$

Case B: Prior + n tests

Assume that the first subsample is substituted by the information given by prior information, i.e.

$$\mu_{\ln_x} = N(\mu_{\ln B}; V_B) \tag{G.19}$$

$$\text{with } \mu_{\ln B} = \frac{n \cdot \overline{\ln x}/V^2 + \ln \mu'/V'^2}{n/V^2 + 1/V'^2} \text{ and } V_B = \frac{1}{\sqrt{n/V^2 + 1/V'^2}}$$

Comparison case A and case B

The pre-knowledge can be interpreted as a sample of m tests.

$$m = \frac{V^2}{V'^2} \qquad \text{if } \ln \mu' = \overline{\ln x_1} \tag{G.20}$$

G.4.4 Bayesian distribution

The Baysian distribution, i.e. the estimation of the basic variable, can be determined for both the cases

- prior information given as a sample $\mathbf{x}_1$ of m tests or equivalent a lognormal distribution $LN(\mu'; V'\mu)$
- posterior information given by the prior information and a sample $\mathbf{x}_2$ of n tests

The first case gives for the sample case:

$$\hat{f}_{\ln x}(\ln x) = f_N\left(\ln x; \overline{\ln x_1}; V\sqrt{(m+1)/m}\right) \tag{G.21}$$

or equivalent

$$\hat{f}_x(x) = f_L\left(x; \exp\left(\overline{\ln x_1}\right); V\sqrt{(m+1)/m}\right) \tag{G.21a}$$

or in the prior information case:

$$\hat{f}_x(\ln x) = f_N\left(\ln x; \ln \mu'; \sqrt{V^2 + V'^2}\right) \tag{G.21b}$$

or equivalent

$$\hat{f}_x(x) = f_L\left(x; \mu'; \sqrt{V^2 + V'^2}\right) \tag{G.21c}$$

Similarly for the second case, i.e. by added information from n tests:

$$\hat{f}_{\ln x}(\ln x) = f_N\left(\ln x; \frac{m \cdot \overline{\ln x_1} + n \cdot \overline{\ln x_2}}{m+n}; V \cdot \sqrt{\frac{m+n+1}{m+n}}\right) \quad \text{(G.22)}$$

or equivalent

$$\hat{f}_x(x) = f_L\left(x; \exp\left(\frac{m \cdot \overline{\ln x_1} + n \cdot \overline{\ln x_2}}{m+n}\right); V \cdot \sqrt{\frac{m+n+1}{m+n}}\right) \quad \text{(G.22a)}$$

or with $\ln \mu' = \overline{\ln x}_1$ and $m = V^2/V'^2$

$$\hat{f}_{\ln x}(\ln x) = f_N\left(\ln x; \frac{\ln \mu' \cdot V^2 + n \cdot \overline{\ln x_2} \cdot V'^2}{V^2 + n \cdot V'^2}; V\sqrt{\frac{V^2 + (n+1) \cdot V'^2}{V^2 + n \cdot V'^2}}\right)$$

or equivalent (G.22b)

$$\hat{f}_x(x) = f_L\left(x; \exp\left(\frac{\ln \mu' \cdot V^2 + n \cdot \overline{\ln x_2} \cdot V'^2}{V^2 + n \cdot V'^2}\right); V\sqrt{\frac{V^2 + (n+1) \cdot V'^2}{V^2 + n \cdot V'^2}}\right)$$

(G.22c)

G.4.5 Summary - known coefficient of variation V

Information about the mean value of a property can be up-dated by information given by a sample $\mathbf{x}_2$ of n tests. The pre-knowledge of the property can then be interpreted as an equivalent sample $\mathbf{x}_1$ of m tests such that:

- For the equivalent sample:

$$\overline{\ln x_1} = \ln \mu' \text{ and } m = \frac{V^2}{V'^2} \qquad \text{(G.20a)}$$

- For the posterior distribution - the uncertainty of the mean value:

$$\mu'' = \exp\left(\frac{m \cdot \overline{\ln x_1} + n \cdot \overline{\ln x_2}}{m+n}\right) \text{ and } V'' = V/\sqrt{m+n} \qquad \text{(G.16b)}$$

- For the Bayesian distribution - the uncertainty of the basic variable:

$$\mu_x = \mu'' \text{ and } V_x = V \cdot \sqrt{\frac{m+n+1}{m+n}} \qquad \text{(G.22d)}$$

In the formulas above it was assumed that both the basic variable and the mean value of the basic variable could be modelled as lognormal distributions. Further, the known coefficient of variation had to be of moderate magnitude, $V<25\%$-30%.

APPENDIX H 'CHARACTERISTIC SHEAR STRENGTH' - AN EXAMPLE.

The example below was produced to illustrate a proposal of how to determine the characteristic value of a soil property. It formed a part of a Swedish interim report to a CEN-meeting in Prague, June 1995.

Background

The proposed method for selection of characteristic values, in the Swedish NAD, means that one has to 'estimate' an interval which contains the mean value of the parameter in question. The position and the size of the interval are determined from

- previous knowledge,
- systematic errors in the test method,
- scatter in the test results,
- the number of tests.

The upper and lower interval limits are used as the characteristic value, depending on whether a high or low value governs the problem. In statistical terms, the method means that a mean value is determined for the population, not for the sample. The outlined procedure is illustrated in an example below.

Example

The task is to define the undrained shear strength at a test site in the Göta River valley. The site, Nödinge, is located approximately 30 km north of Göteborg. The soil consists of a deep layer of soft, high-plasticity clay. The geotechnical investigation includes field vane tests from 8 test holes, see Figure H.1 The profile is very typical for the river valley, with an undrained shear strength 5 - 10 kPa near the surface and with an increase with depth of around 1 kPa/m.

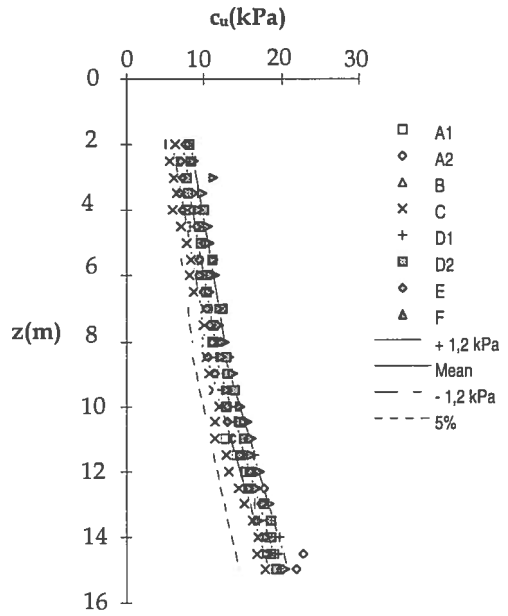

Figure H.1 Measured values of undrained shear strength. The values are reduced with regard to the liquid limit.

If we assume that the shear strength increases linearly with depth, the shear strength can normally be characterised by a line. This line is regarded as a random "object", i.e. the line varies between different test holes. In the project in question, we have two lines, as the clay consists of two different layers, a post glacial layer down to a depth of 8 m and an underlying glacial layer. From each test hole a pair of regression lines are determined, see Figure H.2. These pairs of lines can be seen as a sample from the whole population of the clay. The intercepts and the slopes of the lines can be regarded as random variables. In this way, the problem is reduced to determine the parameters of these variables.

The interval of the mean values of the pairs of lines is established with a simple formula:

$$X_{inf} = \overline{X}\left(1 - \frac{V}{\sqrt{n}}\right) \qquad \text{(H.1)}$$

X_{inf} is the lower limit
$\overline{X}$ is the arithmetic mean of the sample
V is a prescribed coefficient of variation (=15%)
n is the number of test holes
The upper limit, X_{sup}, is determined in the same way but with a plus sign in the formula.

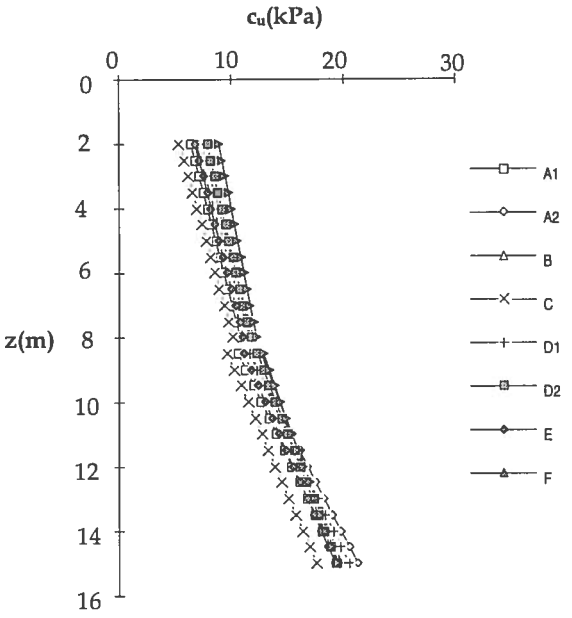

Figure H.2 Regression lines for the various test holes

Varying extents of the geotechnical investigation are simulated. Analyses are made for different numbers of test holes. In Figure H.3 the results of such an analysis, with the test holes taken in a random order, are presented.

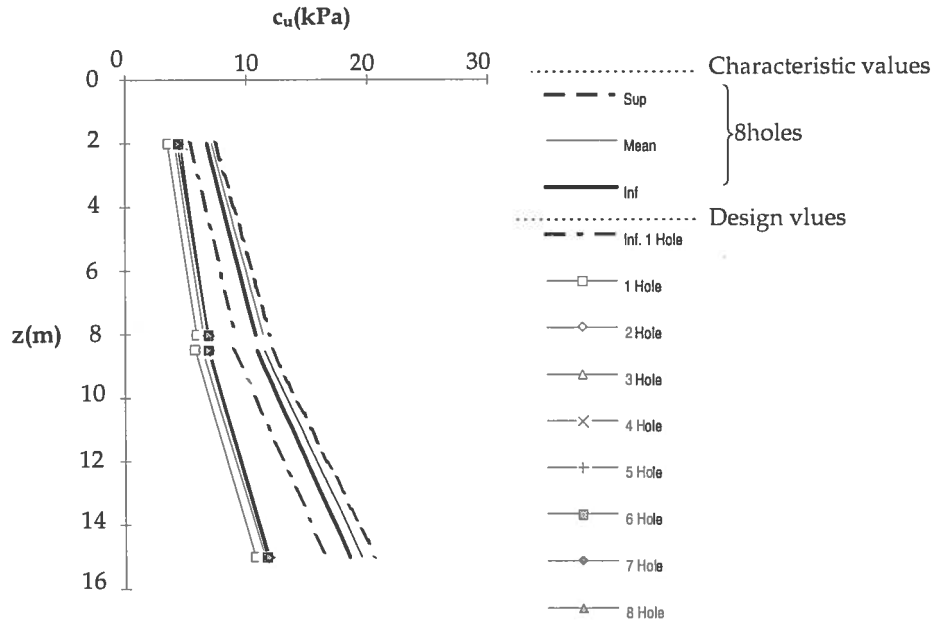

Figure H.3 Characteristic values compared to design values.

The characteristic lines presented are valid when all the eight holes are taken into account. For comparison, the lower characteristic limit, when only test hole A1 is considered, is also shown. The figure also shows the corresponding design values for different extents of the investigation, with a partial factor γ_m equal to 1,55.

The coefficient of variation has to be prescribed in the proposed method. A calculation on "the safe side" demands a conservative value. In this example it is chosen equal to 15%. The appropriateness of the choice is investigated. If the determined mean value is regarded as the true value, the outcome of a test hole can be simulated in a Monte Carlo-simulation, with different assumptions of the spatial variation of the soil. In Figure H.4 the result of such a simulation is presented. The shear strength is assumed to have a log-normal distribution with a standard deviation of 1,2 kPa. This corresponds to a coefficient of variation between 6% and 16%, see Figure H.5. The simulation shows a good agreement with the measured values, compare Figure H.1.

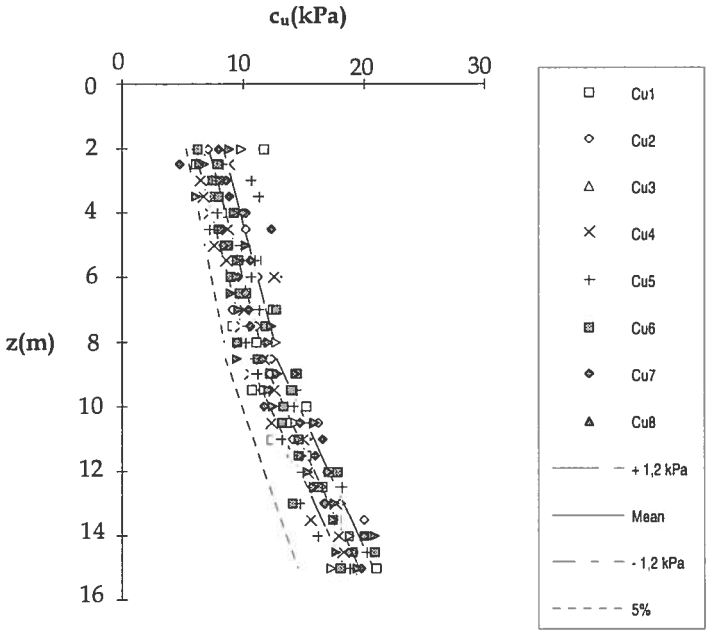

Figure H.4 Simulation of field vane tests. Log-normal distribution of the undrained shear strength. Standard deviation 1,2 kPa

Comments

The example presented illustrates how the characteristic values can be determined in a way consistent with statistical methods. The formulas used for determination of the upper and lower bounds are a compromise

between extensive analyses and the simplicity demanded in daily practice. An experienced geotechnical engineer can probably find the 'path', from the measured values in Figure H.1 to the design values in Figure H.3, without all the calculations undertaken in this example.

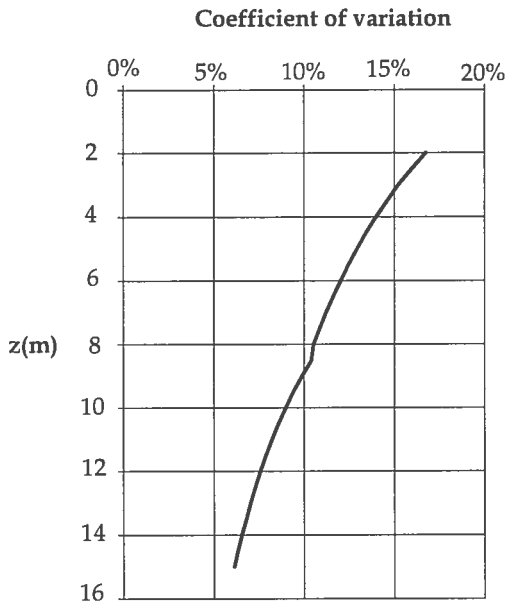

Figure H.5 The coefficient of variation as a function of depth.

APPENDIX J DIMENSIONLESS SAFETY MARGIN

J.1 Idea

Consider a safety margin, $M = R - S$ where R is the bearing capacity and S is the action effect. By making the safety margin dimensionless, it can serve as a measurement of safety, i.e. the influence on the safety margin of the magnitude of R or S is of secondary importance compared with the influence of the difference between R and S

J.2 Alternative formulations of the safety margin

The scaling of the safety margin in order to make it dimensionless can be done in a number of different ways. Below five different formulations are suggested. The dimensionless safety margin is denoted m. F is the factor of safety $F = R/S$ and f is the degree of mobilisation $f = 1/F = S/R$. In each alternative, the ranges given are for a safe state, i.e. m>0.

- Scaled with bearing capacity

$$m_1 = \frac{R-S}{R} = 1 - f \qquad \text{with range 0-1} \qquad \text{(J.1)}$$

- Scaled with action effect

$$m_2 = \frac{R-S}{S} = F - 1 \qquad \text{with the range 0-}\infty \qquad \text{(J.2)}$$

- Scaled with arithmetic mean value of bearing capacity and action effect

$$m_3 = \frac{R-S}{\left(\frac{R+S}{2}\right)} = 2 \cdot \frac{F-1}{1+F} \qquad \text{with the range 0-2} \qquad \text{(J.3)}$$

- Scaled with geometric mean value of bearing capacity and action effect

$$m_4 = \frac{R-S}{\sqrt{R \cdot S}} = \frac{F-1}{\sqrt{F}} \qquad \text{with the range 0-}\infty \qquad \text{(J.4)}$$

- Scaled with harmonic mean value of bearing capacity and action effect

$$m_5 = \frac{R-S}{\left[\frac{1}{2} \cdot \left(\frac{1}{R} + \frac{1}{S}\right)\right]^{-1}} = \frac{R^2 - S^2}{2 \cdot R \cdot S} \qquad \text{with the range 0-}\infty \qquad \text{(J.5)}$$

Note: Alternative 5 is the mean value of alternatives 1 and 2

$$\frac{m_1 + m_2}{2} = \frac{\dfrac{R-S}{R} + \dfrac{R-S}{S}}{2} = \frac{R^2 - S^{"}}{2 \cdot R \cdot S} = m_5 \qquad \text{(J.5a)}$$

Comparison of safety margin m with the safety factor F and the degree of mobilisation f respectively

In Figure J.1 the different formulations of the safety margin m are plotted against corresponding values of the safety factor F, left plot, and the degree of mobilastion f, right plot.

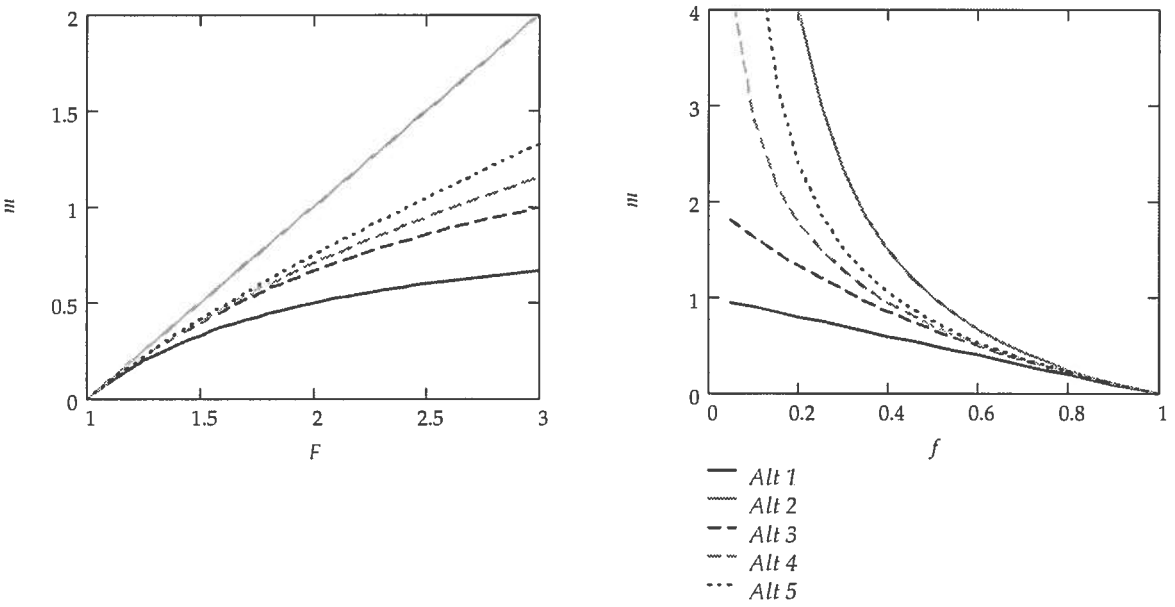

Figure J.1 Comparison of alternative formulation of m compared with F and f.

The plots shown in Figure J.1 are based upon the assumption that values of R and S are the same in the definitions of m, F and f. Traditionally, the factor of safety, defined as the ratio R/S, is regarded as the *true* values of R and S, cf. volume 1, section 2.2.3. In the partial factor format these values 'correspond' to the characteristic values. Thus the safety margin shown in the figure might be called a 'characteristic safety margin', m_k. However, in partial factor design the safety margin is defined as the difference between the design values of R and S, i.e. a design safety margin. By replacing R with R_d and S with S_d, i.e R/γ_R and $\gamma_s \cdot S$ resp., in the expression for m given previously, 'design values' of m are obtained. Thus:

$$m_{1d} = \frac{R/\gamma_R - \gamma_S \cdot S}{R/\gamma_R} = 1 - \gamma_S \cdot \gamma_R \cdot f \qquad \text{(J.6)}$$

$$m_{2d} = \frac{F}{\gamma_R \cdot \gamma_S} - 1 \text{ etc.} \qquad \text{(J.7)}$$

This means that the design values are obtained by replacing f with $\gamma_s \cdot \gamma_R \cdot f$ or F with $F/\gamma_s \cdot \gamma_R$ in the foregoing expressions. In Figure J.2 , the design value based formulations for the two 'extreme' alternatives 1 and 2, are compared with the formulations based upon characteristic values. The partial factors are set to $\gamma_R = 1{,}5$ and $\gamma_S = 1{,}25$.

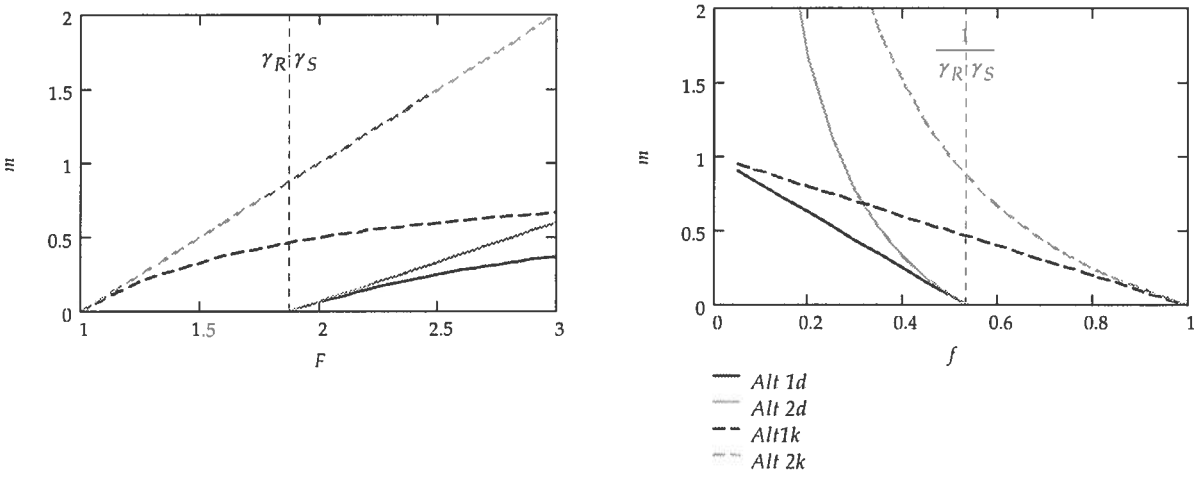

Figure J.2 Comparison of dimensionless safety margins given as design values or characteristic values resp. $\gamma_R = 1{,}5$ and $\gamma_S = 1{,}25\gamma$

Of the different formulations given, the first alternative has the convenient quality that its range is 0-100%. It also has a very simple formulation, 1-f , and it is hard to see any obvious disadvantages compared with the other formulations.

Comparison with reliability index β

A disadvantage with the idea to use the safety margin as a safety concept is that the uncertainty of the variables at hand is not expressed explicitly[1] . Below a simple example is given to illustrate this circumstance.

Assume that R and S are independent random variables, $R=LN_V(\mu_R;V)$ and $S=LN_V(\mu_S;\alpha V)$. This means approximately that the reliability index $ß$ is, see appendix A:

$$ß \approx \frac{\ln(\mu_R) - \ln(\mu_S)}{\sqrt{1+\alpha^2}\cdot V} \qquad \text{(J.8)}$$

Assume further that the characteristic value of R is the mean value and the characteristic value of S is the 98-percentile. This means:

$$R_k = \mu_R$$

$$R_d = \mu_R/\gamma_R$$

$$S_k \approx \mu_S \cdot \exp(2\cdot\alpha\cdot V) \qquad \text{(J.9a-d)}$$

$$S_d \approx \gamma_S \cdot \mu_S \cdot \exp(2\cdot\alpha\cdot V)$$

Failure for $m_d = R_d - S_d$ gives:

$$\mu_d \approx \gamma_S \cdot \gamma \cdot \mu_S \cdot \exp(2\cdot\alpha\cdot V) \qquad \text{(J.10)}$$

and by substitution into equation J.8:

$$ß \approx \frac{\ln(\gamma_S\cdot\gamma_R) + 2\cdot\alpha\cdot V}{\sqrt{1+\alpha^2}\cdot V} \qquad \text{(J.8a)}$$

and for the safety margin according to equation J.6:

$$m_{1d} \approx \frac{\mu_R - \gamma_S\cdot\gamma_R\cdot\exp(2\cdot\alpha\cdot V)}{\mu_R} \qquad \text{(J.6a)}$$

[1] This is a disadvantage also with the alternatives, the factor of safety and the degree of mobilisation.

In Figure J.3 the relation between the reliability index and the safety margin are given. Plots are given for the following six alternatives:

- $\mu_R/\mu_S = 3$; $V_S = 100\%$, 50% and 10% of V_R;
- $\mu_R/\mu_S = 4.5$; $V_S = 100\%$, 50% and 10% of V_R;

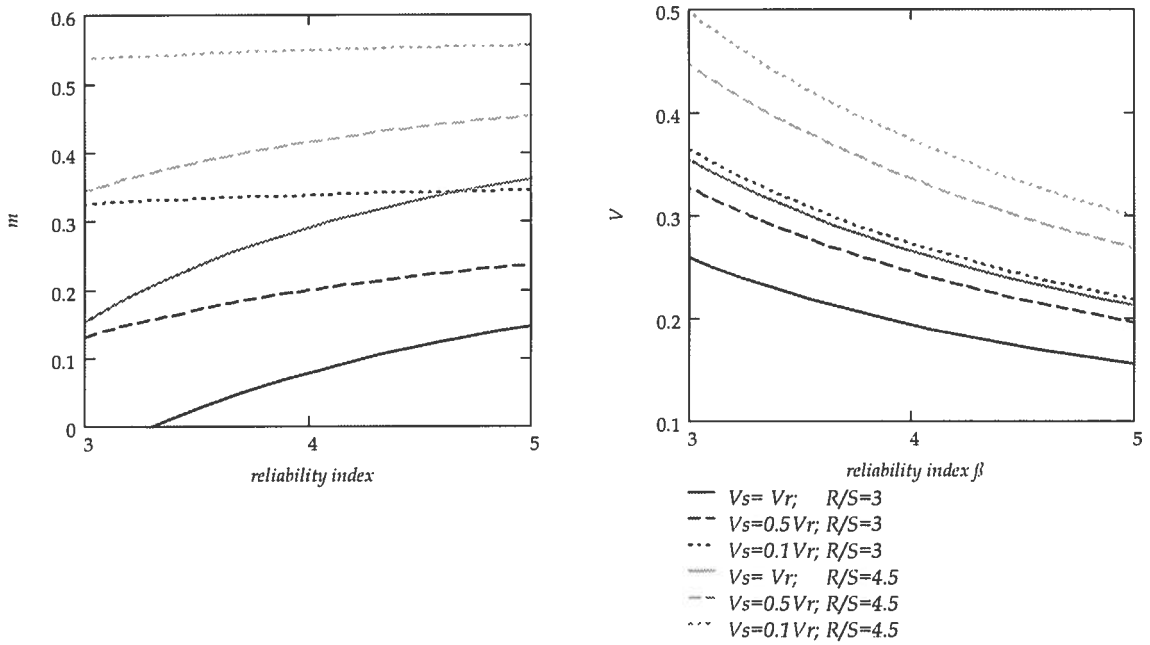

Figure J.3 Comparison of reliability index $ß$ and safety margin m_{1d}. R and S indicated in the legend are the mean values.

As can be seen from the left plot in Figure J.3, there is only a weak increase in m for increasing $ß$. This is due to the fact that the uncertainty, in this example given by the coefficient of variation V, is of secondary importance for the magnitude of m, compared with the influence on $ß$. Thus the suggested dimensionless safety margin does not serve as any indicator of the probability of failure, i.e. it does not in any sense replace the reliability index $ß$. The same is valid for the safety margin, defined by characteristic values and the traditional concept, the factor of safety. In Figure J.4 these two properties are compared with the reliability index $ß$, for the same alternatives of mean values and coefficient of variation as in Figure J.3. As can be seen in the figure, also for the 'characteristic' safety margin and the factor of safety, there is only a weak increase of these concepts for an increase of $ß$.

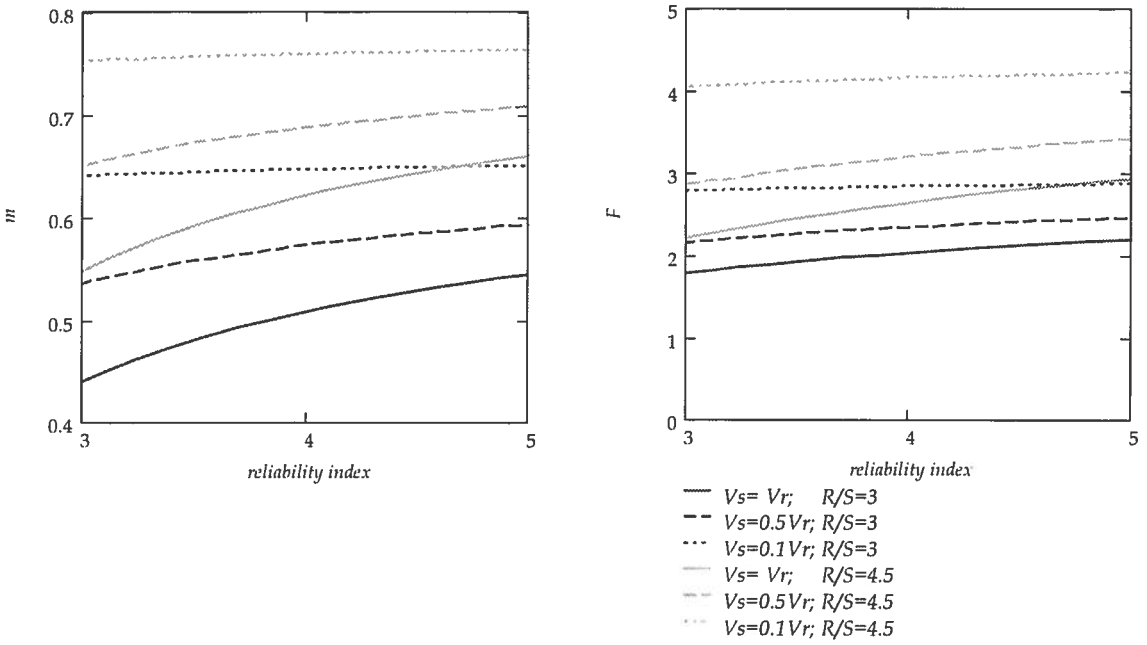

Figure J.4 Comparison of reliability index β with safety margin $m_{1k.}$ and factor of safety F, defined by the characteristic values. R and S indicated in the legend are the mean values.

Summary

In this appendix alternative formulations of a dimensionless safety margin have been investigated. There are two main reasons for replacing the traditional factor of safety with the safety margin:

- To use the (global) factor of safety in conjunction with partial factors is, if not impossible, at least very confusing.
- In a probabilistic approach, the safety margin, is preferable for computational reasons , cf. volume 1, section 2.4.2 and section 2.4.4.

By using one of the suggested formulations of a dimensionless safety margin, a unique relation with the factor of safety is obtained. Thus the emperi in using the factor of safety can be inherited in the new concept. The first alternative has the convenient quality that its range is from 0-100%.

In a probabilistic calculation the safety margin is a random variable, defined by the two random variables R and S. The purpose of the denominator is to use it as a scaling factor. Hence in a probabilistic

approach, when R and S are random variables, the denominator does not need to be a random variable. In the formulation:

$$m = \frac{R - S}{R_{fixed}} \tag{J.11}$$

m is a linear combination of R and S. In this latter case the range, for a safe state, is altered to $\left[0 - R_{\sup} / R_{fixed}\right]$.

APPENDIX K
ON SHEAR STRENGTH IN SLOPE STABILITY.

K.1 General

The drained shear strength in slope stability is normally assumed according to Mohr-Coulomb's failure criterion, i.e. as a function of the stresses:

$$c_{c,\phi} = c' + (\sigma_N - u) \cdot \tan(\phi) \qquad \text{(K.1)}$$

Traditionally the stresses are assumed to be the stresses at hand in the slope. As an alternative the shear strength can be seen as a function of the stresses at failure. The difference between these two alternatives is discussed below. Slope stability analysis is frequently performed with slice methods, see volume 1, Chapter 4. A common assumption is then that the shear strength between the slices is disregarded, e.g. in the procedure known as Bishop's simplified, (Bishop, 1955). The description below is restricted to this simple but common case in slope stability analysis.

K.2 Formulation of shear strength

K.2.1 Traditional alternative

The shear strength is based upon the actual (assumed) stresses. The factor of safety format gives:

$$\tau = \frac{c' + (\sigma_N - u) \cdot \tan(\phi)}{F} \qquad \text{(K.2)}$$

Vertical equilibrium for a slice, see Figure K.1 gives:

$$p \cdot \Delta x = \sigma_N \cdot \frac{\Delta x}{\cos(\alpha)} \cdot \cos(\alpha) + \tau \cdot \frac{\Delta x}{\cos(\alpha)} \cdot \sin(\alpha) \qquad \text{(K.3)}$$

Substituting equation K.2 into equation K.3 and solving for the normal stress gives:

$$\sigma_N = \frac{p \cdot F - \tan(\alpha) \cdot c' + \tan(\alpha) \cdot \tan(\phi) \cdot u}{F + \tan(\phi) \cdot \tan(\alpha)} \qquad \text{(K.4)}$$

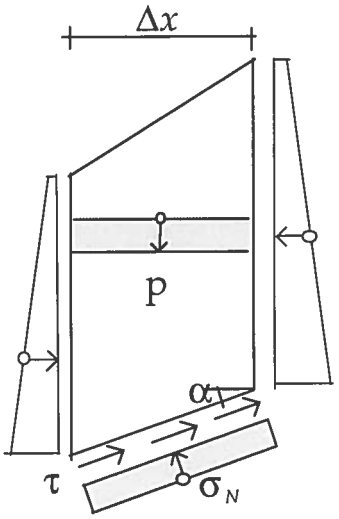

Figure K.1 Slice of a slope. Shear strength between slices disregarded.

Thus equation K.1 becomes:

$$c_{c,\phi} = c' + (\sigma_N - u)\cdot\tan(\phi) = \frac{c' + (p-u)\cdot\tan(\phi)}{1 + \frac{\tan(\alpha)\cdot\tan(\phi)}{F}} \qquad \text{(K.1a)}$$

and the combined shear strength:

$$c_{comb} = \min\left\{\frac{c' + (p-u)\cdot\tan(\phi)}{1 + \frac{\tan(\alpha)\cdot\tan(\phi)}{F}}; c_u\right\} \qquad \text{(K.5)}$$

K.2.2 Alternative formulation

The shear stress equal to the shear stress at failure, index *ult*, is:

$$c_{c,\phi} = \tau_{ult} = c' + \left(\sigma_{N_{ult}} - u\right)\cdot\tan(\phi) \qquad \text{(K.6)}$$

Vertical equilibrium for a slice at failure:

$$p\cdot\Delta x = \sigma_{N_{ult}}\cdot\frac{\Delta x}{\cos(\alpha)}\cdot\cos(\alpha) + \tau_{ult}\cdot\frac{\Delta x}{\cos(\alpha)}\cdot\sin(\alpha) \qquad \text{(K.7)}$$

Substituting equation K.6 into equation K.7 and solving for the normal stress at failure gives:

$$\sigma_{N_{ult}} = \frac{p - \tan(\alpha)\cdot c' + \tan(\alpha)\cdot\tan(\phi)\cdot u}{1 + \tan(\phi)\cdot\tan(\alpha)} \qquad \text{(K.8)}$$

Thus equation K.6 becomes:

$$c_{c,\phi} = c' + (\sigma_{N_{ult}} - u)\cdot\tan(\phi) = \frac{c' + (p-u)\cdot\tan(\phi)}{1 + \tan(\alpha)\cdot\tan(\phi)} \qquad \text{(K.6a)}$$

and the combined shear strength:

$$c_{comb} = \min\left\{\frac{c' + (p-u)\cdot\tan(\phi)}{1 + \tan(\alpha)\cdot\tan(\phi)}; c_u\right\} \qquad \text{(K.9)}$$

Note: This alternative is from a computational point of view equal to the first iteration in a traditional analysis, with an assumed factor of safety F=1.

K.3 Numerical example

Assume a toe circle, see Figure K.2, with the following data:

Geometry: H=5m, θ=26,5^0, θ_w=0,5θ,

Soil parameters: c'=5 kPa, ϕ=30^0, c_u=16 kPa

Density: Soil γ=16 kN/m^3, Water γ_w=10 kN/m^3

The weight of an infinitesimal slice Δx is:

$$p\cdot\Delta x = \left[R\cdot\cos(\alpha) - y_0 + \left(R\cdot\sin(\alpha) + x_0\right)\cdot\tan(\theta)\right]\cdot\gamma\cdot\Delta x$$

below the crest:

$$p\cdot\Delta x = \left[R\cdot\cos(\alpha) - y_0 + H\right]\cdot\gamma\cdot\Delta x \qquad \text{(K.10a,b)}$$

and above the crest.

The corresponding values of the pore pressure are:

$$u = \left[R\cdot\cos(\alpha) - y_0 + \left(R\cdot\sin(\alpha) + x_0\right)\cdot\tan(\theta_u)\right]\cdot\gamma_w \quad \text{and}$$

$$u = \left[R\cdot\cos(\alpha) - y_0 + H\cdot\frac{\tan(\theta_u)}{\tan(\theta)}\right]\cdot\gamma_w \text{ resp.} \qquad \text{(K.11a,b)}$$

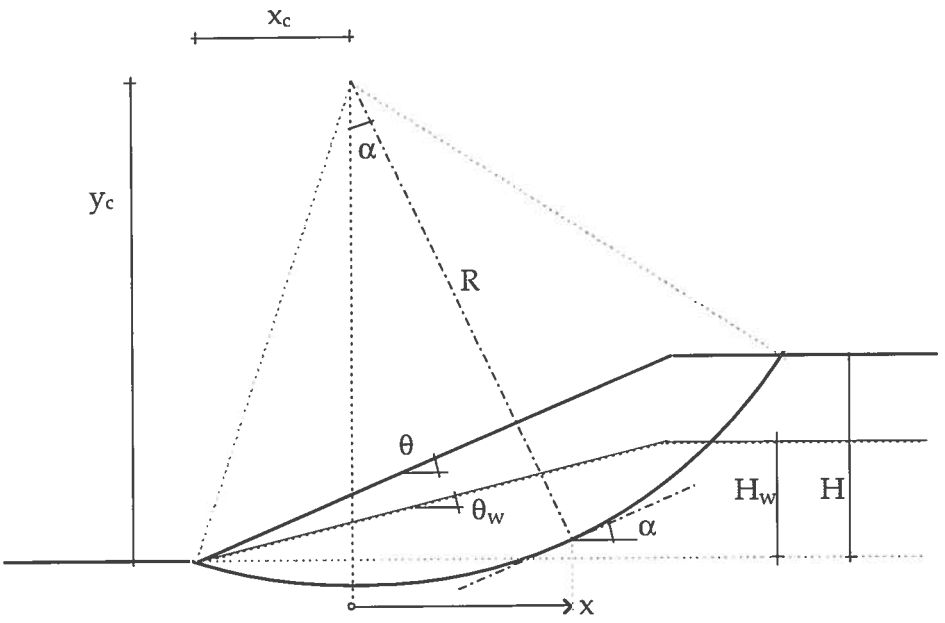

Figure K.2 Geometry of assumed slip circle

The average shear stress along the slip circle is:

$$\bar{\tau} = \frac{\int_{R\sin\alpha_0}^{R\sin\alpha_1} p \cdot x \cdot R \cdot \cos(\alpha)\mathrm{d}x}{(\alpha_1 - \alpha_0)\cdot R^2} = \frac{\int_{\alpha_0}^{\alpha_1} p \cdot \sin(\alpha)\cdot\cos(\alpha)\mathrm{d}\alpha}{(\alpha_1 - \alpha_0)} \quad \text{(K.12)}$$

with $\alpha_0 = \mathrm{atan}(-x_c/y_c)$ and $\alpha_1 = \mathrm{acos}\left((y_c - H)/R\right)$, while the average shear strength becomes:

$$\overline{c(F)} = \frac{1}{\alpha_1 - \alpha_0}\cdot\int c(F)\mathrm{d}\alpha \quad \text{(K.13)}$$

where $c(F)$ is the 'local' shear strength given by one of the equations K.1a, K.5, K.6a or K.9 respectively, i.e. F=1 in the latter two equations. In Figure K.3 the results of a numerical calculation of the shear strength for the different alternatives, with x_c=3m and y_c=9m, are given. The traditional alternative is based upon an assumption of F=2, which is an overestimation for the given slip circle. The ratio between the average shear strength for the alternative formulation and the traditional formulation becomes in this case for the drained analysis 0,90 and for the combined analysis 0,98.

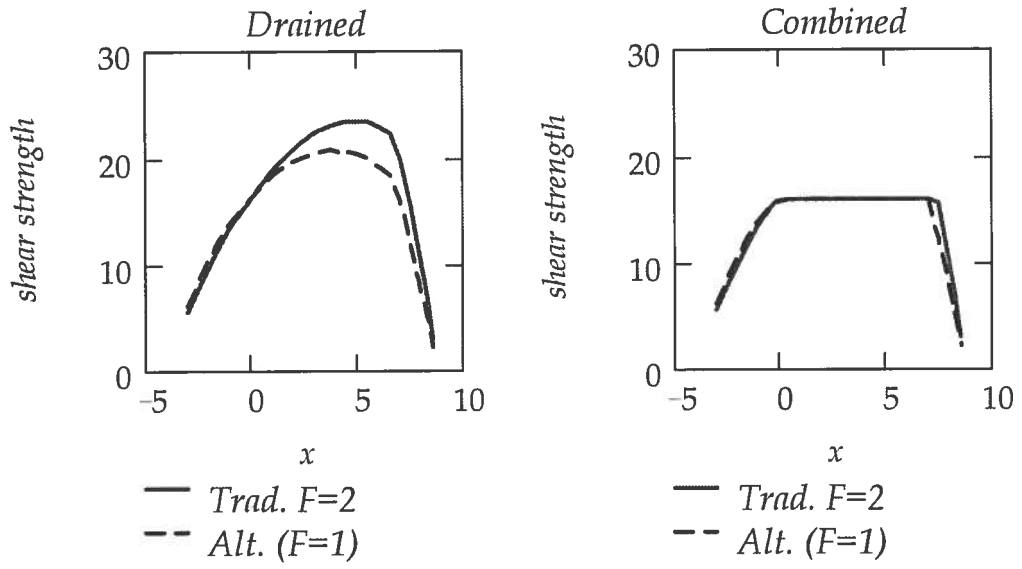

Figure K.3 Comparison of the shear strength for the two alternative formulations. x_c=3m, y_c=9m

The global factor of safety can, in traditional analysis, be calculated according to equation K.12 and equation K.13 by iteration as:

$$F_{i+1} = \frac{\overline{c(F_i)}}{\bar{\tau}} \tag{K.14}$$

while the alternative formulation gives:

$$F = \frac{\overline{c(1)}}{\bar{\tau}} \tag{K.15}$$

The corresponding dimensionless safety margin, see appendix J, becomes with the substitution $F = 1/(1-m)$:

$$m_{i+1} = 1 - \frac{\bar{\tau}}{\overline{c(m_i)}} \tag{K.14a}$$

and

$$m = 1 - \frac{\bar{\tau}}{\overline{c(0)}} \tag{K.15a}$$

In Table K.1 the results of a calculation of drained analysis for the critical slip circle are given and in Table K.2 The corresponding results of combined analysis are presented. In the tables are given

both the dimensionless safety margin, the factor of safety and the corresponding critical slip circle.

	m	F	x_c [m]	y_c [m]
Traditional	0,40	1,67	3,2	8,2
Alternative	0,35	1,54	2,9	8,3

Table K.1 Safety concepts and critical circle for drained analysis

	m	F	x_c [m]	y_c [m]
Traditional	0,16	1,19	5,5	7,9
Alternative	0,16	1,19	5,5	7,5

Table K.2 Safety concepts and critical circle for combined analysis

APPENDIX L ON IMPROVEMENT OF SLOPE STABILITY

L.1 Existing situation

Consider two almost identical slopes, i.e. two slopes with the same geometry and the same soil parameters. The only difference is that one slope, named A, has existed for a very long time, while the other slope, named B, is new, e.g. the result of a fill or a cut. The safety of the slopes is described with a probabilistic formulation of a safety margin, cf. appendix J:

$$m = \frac{R - S}{\mu_R} \tag{L.1}$$

where R and S are random variables and μ_R is the mean value of R. The equation can be rewritten as:

$$m = \frac{(\mu_R - \varepsilon_R) - (\mu_S + \varepsilon_S)}{\mu_R} = \frac{\mu_R - \mu_S}{\mu_R} - \frac{\varepsilon_R + \varepsilon_S}{\mu_R} = m_0 - \varepsilon_m \tag{L.1a}$$

where m_0 is the deterministic safety margin while ε_m is a random disturbance of the safety margin, formed by random disturbances of the stabilising and destabilising influences, ε_r and ε_S respectively. For the two different cases the following can be assumed:

- *The natural slope A.* The slope has proved to be stable, i.e. the safety margin $m_A > 0 \Rightarrow m_0 - \varepsilon_{m_A} > 0 \Rightarrow \varepsilon_{m_A} < m_0$. Thus in a stability analysis, ε_m can be truncated with $\varepsilon_{m,sup}=m_0$.
- *The constructed slope.* No observational knowledge exists about the slope stability. Hence ε_m must be left untruncated.

L.2 Improvement of the slope

The safety of the slope is considered insufficient, thus an improvement is undertaken. By the safety margin concept, one does not have to determine whether the improvement is an increase of the stabilising influences, ε_R, or a decrease of the destabilising influences, ε_S, as the improved safety margin can be written:

$$m = \frac{(\mu_R - \varepsilon_R + \Delta_R) - (\mu_S + \varepsilon_S - \Delta_S)}{\mu_R} = \\ = m_0 + \varepsilon_m + \frac{\Delta_R + \Delta_S}{\mu_R} = m_0 + \varepsilon_m + \Delta m \qquad \text{(L.2)}$$

where Δm is the improvement of the safety margin[1].

The different terms in equation L.2 can be determined in the following way. If the safety margin for the original slope is described with a distribution $PD(m_0;\sigma_0)$ the random part of the safety margin ε_m has the distribution $PD(0;\sigma_0)$. In the case with the natural slope, it has an upper bound $\varepsilon_{mA,sup}=m_0$. In the same way, if the safety margin for the improved slope is described with the distribution $PD(m_1;\sigma_1)$, the improvement of the safety margin Δm has the distribution $PD(m_1\text{-}m_0;\ \sigma_{\Delta m})$ with $\sigma_{\Delta m} = \sqrt{\sigma_1^2 - \sigma_0^2}$ [2]. If the distributions at hand are assumed to be normal distributions, the probability corresponding to the upper bound in case A becomes:

$$p_{sup} = \Phi(m_0/\sigma_0) \qquad \text{(L.3)}$$

i.e. the probability of the untruncated distribution corresponding to the upper bound of ε_m. Hence, values of the improved safety margin, in case A, can be simulated as a sum of one fixed and two random properties:

$$m_{A_{i,j}} = m_0 - \varepsilon_{mA_i} + \Delta m_j = \\ = m_0 - \Phi^{-1}(p_i \cdot p_{sup}) \cdot \sigma_0 + m_1 - m_0 + \Phi^{-1}(p_j) \cdot \sigma_{\Delta m} = \qquad \text{(L.4)} \\ = m_1 - \Phi^{-1}(p_i \cdot p_{sup}) \cdot \sigma_0 + \Phi^{-1}(p_j) \cdot \sigma_{\Delta m}$$

where the second term follows from equation 3.9,[3] volume 1, and p_i and p_j are two independent, random probabilities.

[1] In a traditional, deterministic calculation with the factor of safety, the improvement can be obtained as $\Delta m = m_1 - m_0 = (1 - 1/F_1) - (1 - 1/F_0) = 1/F_1 - 1/F_0$

[2] If the improvement of the safety margin is considered independent of the original safety margin.

[3] IN equation 3.9 p_{inf}=0.

A value of the reliability index can be obtained as:

$$\beta_A = \frac{\mu_{m_A}}{\sigma_{m_A}} \tag{L.5}$$

In case B, the reliability index can be obtained directly as:

$$\beta_B = \frac{m_1}{\sigma_1} \tag{L.6}$$

As an example of the considerations given above, the result of a Monte Carlo simulation for an improved natural slope is compared with a corresponding new slope, see Figure L.1. The left plot shows the random parts of the safety margin according to equation L.2, while the right part shows plots of the simulated safety margins. There is a good agreement between the Monte Carlo simulation and the calculated values of the reliability indices, β_A and β_B respectively.

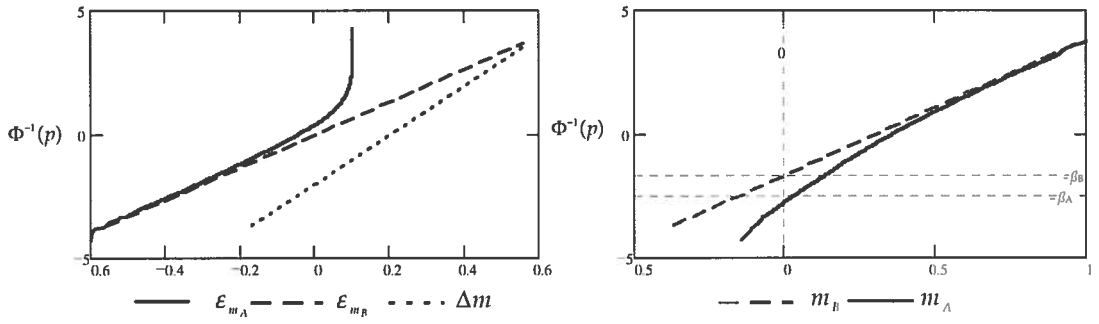

Figure L.1 Monte Carlo simulation of the safety margin. m_0=0,1; σ_0=0,1; m_1=0,3; σ_1=0,18; i.e. $\sigma_{\Delta m}$=0,1

APPENDIX M SLOPE STABILITY -'DESIGN CHARTS'

M.1 Transformation to a simple slope geometry - equivalent triangle

M.1.1 Idea

The slope stability analysis becomes easy for a simple slope geometry, i.e. here understood as a linear slope with a horizontal level at the toe and the crest. Below, an approximate transformation of the geometry of an arbitrary slope into a simple slope geometry is given.

M.1.2 Transformation

Assume that the geometry of the slope can be defined by a polygon $(x_0,y_0),(x_1,y_1)\ldots(x_n,y_n)$, see Figure M.1

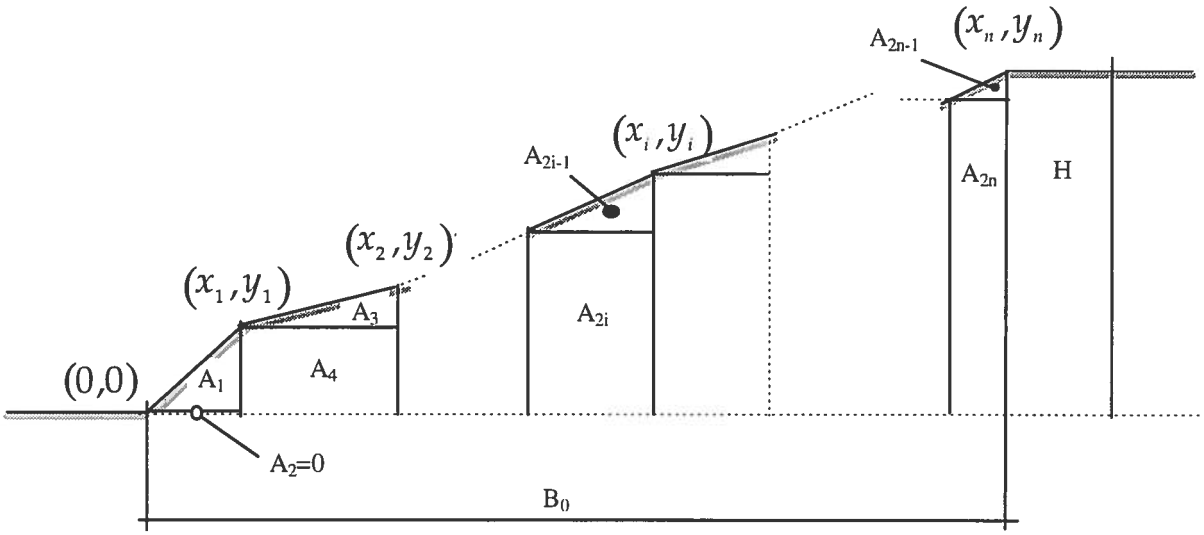

Figure M.1 Slope geometry

Set for simplicity the co-ordinates for the toe as $(x_0=0,y_0=0)$. The height of the slope is then $H=y_n$ and the initial length $B_0=x_n$. The geometry of the slope is built up of a number of triangles and rectangles. The area of a triangle 2*i*-1 is:

$$A_{2i-1}=\tfrac{1}{2}\cdot(y_i-y_{i-1})\cdot(x_i-x_{i-1}) \qquad \text{(M.1)}$$

and the location of the centre of gravity centre from the toe:

$$a_{2i-1} = (x_{i-1} + 2 \cdot x_i)/3 \tag{M.2}$$

The area of a rectangle $2i$ is:

$$A_{2i} = y_{i-1} \cdot (x_i - x_{i-1}) \tag{M.3}$$

and the centre of gravity:

$$a_{2i} = (x_i + x_{i-1})/2 \tag{M.4}$$

Assume that the slope can be approximated by a simple slope with the same cross sectional area, the same height and the same centre of gravity, see Figure M.2. For comparison of the original and approximate slope, the area marked with A_{add} in the figure has to be added to the areas $A_1 - A_{2n}$ computed above.

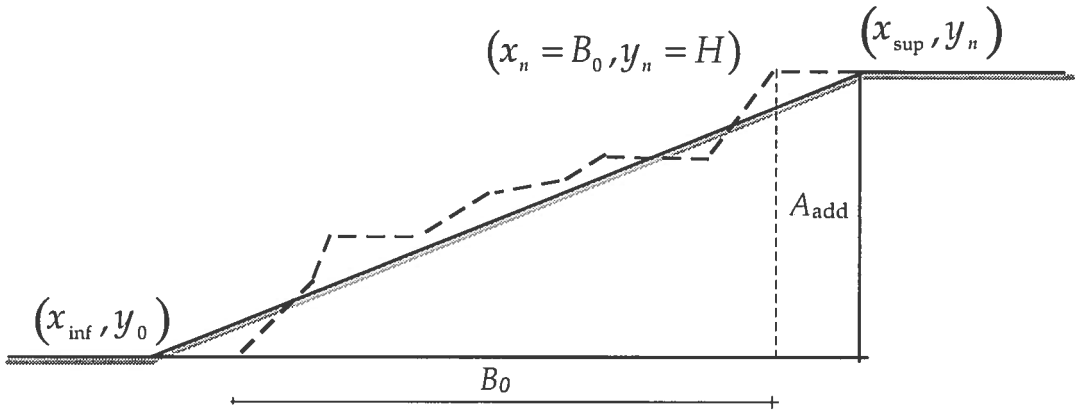

Figure M.2 Geometry of equivalent slope

Let the toe and the crest of the equivalent slope be defined by the co-ordinates $(x_{inf}, y_0 = 0)$ and $(x_{sup}, y_n = H)$. The centre of gravity can, based upon the geometry of the original slope, be calculated as:

$$x_c = \frac{Aa_\Sigma + H \cdot (x_{sup} - x_n) \cdot \frac{1}{2} \cdot (x_{sup} + x_n)}{A_\Sigma + H \cdot (x_{sup} - x_n)} \tag{M.5}$$

and from geometry of the equivalent slope:

$$x_c = x_{sup} - \frac{1}{3} \cdot \frac{Area_{total}}{H/2} = x_{sup} - \frac{2}{3} \cdot \frac{A_\Sigma + H \cdot (x_{sup} - x_n)}{H} \tag{M.6}$$

where $Aa_\Sigma = \sum_{j=1}^{2n} A_j \cdot a_j$ and $A_\Sigma = \sum_{j=1}^{2n} A_j$

Equation M.5 and equation M.6 give:

$$x_{sup} = \frac{Aa_\Sigma + H \cdot \left(x_{sup} - x_n\right) \cdot \frac{1}{2} \cdot \left(x_{sup} + x_n\right)}{A_\Sigma + H \cdot \left(x_{sup} - x_n\right)} + \frac{2}{3} \cdot \frac{A_\Sigma + H \cdot \left(x_{sup} - x_n\right)}{H} \tag{M.7}$$

Solving x_{sup} from equation M.7 and using the equality of areas:

$$(x_{sup} - x_{inf}) \cdot H / 2 = A_\Sigma + H \cdot \left(x_{sup} - x_n\right) \tag{M.8}$$

gives the expressions for x_{inf} and x_{sup}:

$$x_{inf} = B_0 - \frac{A_\Sigma + \sqrt{3} \cdot \sqrt{2 \cdot A_\Sigma \cdot H \cdot B_0 - 2 \cdot Aa_\Sigma \cdot H - A_\Sigma{}^2}}{H} + x_0 \tag{M.9}$$

and

$$x_{sup} = B_0 - \frac{A_\Sigma - \sqrt{3} \cdot \sqrt{2 \cdot A_\Sigma \cdot H \cdot B_0 - 2 \cdot Aa_\Sigma \cdot H - A_\Sigma{}^2}}{H} + x_0 \tag{M.10}$$

respectively, with $B_0 = x_n - x_0$. The restriction x_0=0 is here eliminated, provided that equation M.2 and equation M.4 are changed into

$$a_{2i-1} = (x_{i-1} + 2 \cdot x_i)/3 - x_o \,. \tag{M.2a}$$

and

$$a_{2i} = (x_i + x_{i-1})/2 - x_0 \tag{M.4a}$$

respectively.

M.2 Stability number and critical slip circle - Explicit formulas

M.2.1 General

Design charts for slope stability have been published by Taylor and reproduced by Terzaghi (1943). Janbu (1954) developed these charts further. Thus simple slopes have for a long time been possible to analyse with the general formula:

$$F = \frac{N \cdot \bar{c}}{\gamma \cdot H} \qquad \text{(M.11)}$$

where N is a dimensionless stability number and $\bar{c}$ is the average shear strength. The density of the soil is γ and H is the height of the slope. The charts are intended for total stress analysis and give the co-ordinates for the critical circle, i.e. the rotation centre, and the corresponding minimum stability number. In principle their use is not restricted to total stress analysis, though their usefulness is limited in effective stress, partly as the problem to obtain the correct average shear stress is not accounted for, partly as the charts might not give the correct critical slip circle.[1]

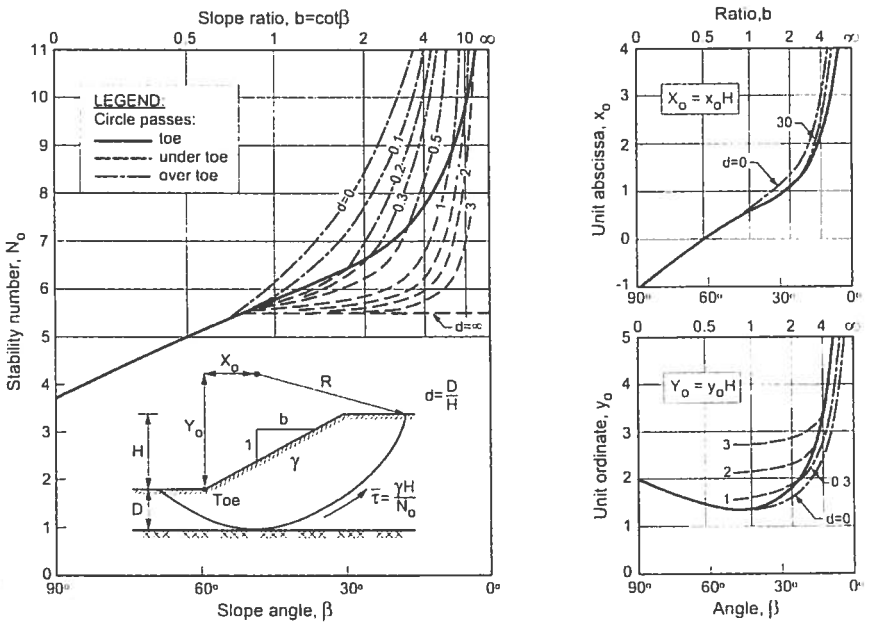

Figure M.3 Stability charts for slope stability analysis. From (Janbu, 1996)

[1] Janbu has presented design charts also for effective stress analysis, see e.g. Janbu,1996)

The charts were developed at a time, when slide-rules were the optional calculators in design practice. In application of random models, and with today's access to desk-top computers it is desirable to use explicit formulas in the calculations. Below, approximate, explicit formulations of some of the equations 'behind' the plots in Figure M.3 are given. The equations are mostly derived by curve-fitting procedures. Thus they should not be interpreted in a scientific way but just be seen as a means to simplify the calculation procedure.

M.2.2 Location of critical slip circle. Slip circle passes under toe. *x*-direction

Arbitrary slope

Assume a slope with geometry as in Figure M.4.

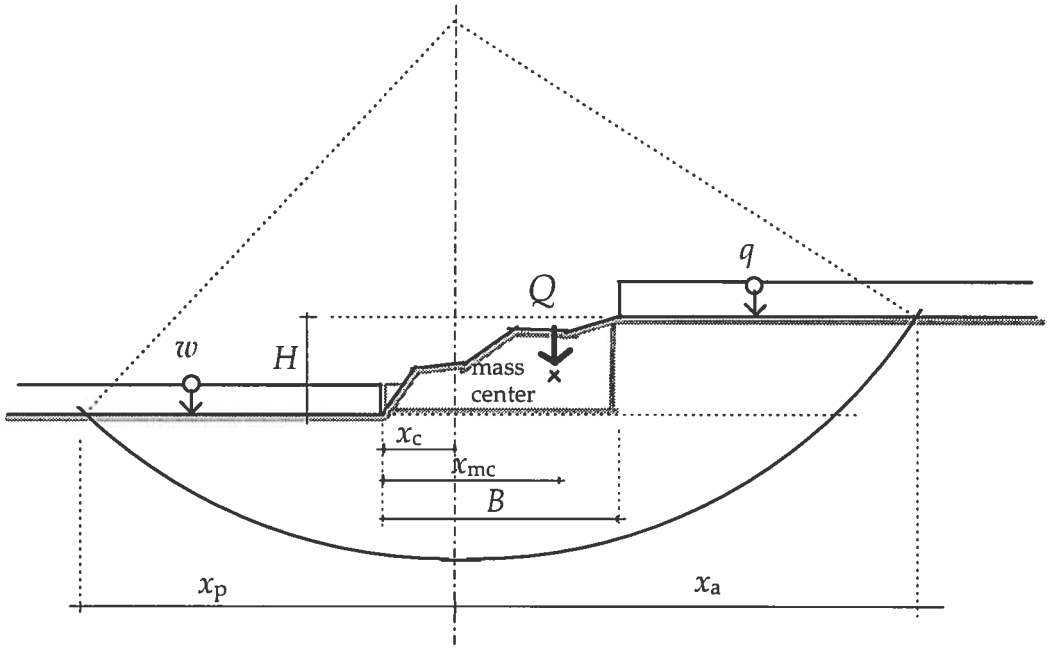

Figure M.4 Geometry of a slip circle for an 'arbitrary' slope

The slope is defined by the level of the toe and the crest. The section area marked in the figure has the weight Q and the density of the soil is γ. The slope is loaded above the crest with a surcharge q and below the toe with a 'surcharge' w, of which the latter might be e.g. an external water pressure. Any external loads or water pressure between the toe and the crest has to be incorporated in the determination of Q. Consider the special but common assumption that there is no horizontal variation of

the shear strength, i.e. in a deterministic analysis[1]. This means that the resisting moment is independent of a horizontal translation of the slip circle. Thus the location of the critical circle is governed by the maximum disturbing moment, which can be calculated by a moment equilibrium equation for the soil and the loads above the toe level:

$$M_S = (q+\gamma\cdot H)\cdot[x_a-(B-x_c)]\cdot\left[\frac{x_a-(B-x_c)}{2}+(B-x_c)\right]+ \\ +Q\cdot(x_{mc}-x_c)-w\cdot(x_p-x_c)\cdot\left(\frac{x_p-x_c}{2}+x_c\right) \qquad \text{(M.12)}$$

with the notations defined in Figure M.4. Searching the maximum moment gives:

$$\frac{dM_S}{dx_c} = (\gamma\cdot H+q)\cdot B-Q-x_c\cdot(\gamma\cdot H+q-w)=0$$

$$\text{i.e. } x_c = \frac{(\gamma\cdot H+q)\cdot B-Q}{\gamma\cdot H+q-w} \qquad \text{(M.13)}$$

$$\frac{d^2M_S}{d(\Delta x)^2} = -\cdot(\gamma\cdot H+q-w)<0 \quad ;\gamma\cdot H+q>w$$

Hence, the x-coordinate for the rotation centre of the critical slip circle is obtained as[2]:

$$x_c = \frac{(\gamma\cdot H+q)\cdot B-Q}{\gamma\cdot H+q-w} \qquad \text{(M.13a)}$$

with the natural restriction $\gamma\cdot H+q>w$

[1] A corresponding probabilistic analysis might incorporate a random, horizontal variation.

[2] In the derivation of equation M.13a-e it has been assumed that the density of the soil is constant throughout the slope. Cases when this assumption cannot be justified, at least as a good approximation, go beyond the scope of the description of slope stability analyses given in this appendix.

Special case - Linear slope

If the inclination of the slope is defined by a single line, the weight is $Q = \gamma \cdot H \cdot B/2$. Thus, equation M.13a gives:

$$x_c = \frac{(\gamma \cdot H + q) \cdot B - \gamma \cdot H \cdot B/2}{\gamma \cdot H + q - w} = \frac{B}{2} \cdot \frac{\gamma \cdot H + 2 \cdot q}{\gamma \cdot H + q - w} \qquad \text{(M.13b)}$$

The important case, a natural slope without any surcharges or external water pressure gives:

$$x_c = \frac{B}{2} \qquad \text{(M.13c)}$$

Special case - Vertical cut

A vertical cut can be defined into two ways, based upon the geometry given in Figure M.4. First with cut at the toe, i.e. $Q = \gamma \cdot H \cdot B$. With q=0 equation M.13 gives:

$$x_c = \frac{\gamma \cdot H \cdot B - \gamma \cdot H \cdot B}{\gamma \cdot H + q - w} = 0 \qquad \text{(M.13d)}$$

Or, second, with a cut at the crest, i.e. Q=0. With w=0 in this case, equation M.13 becomes:

$$x_c = \frac{(\gamma \cdot H + q) \cdot B}{\gamma \cdot H + q} = B \qquad \text{(M.13e)}$$

Combined the two cases implies that the rotation centre is located vertically above the cut as long as any surcharges or external water pressure 'reaches' the cut.

M.2.3 Location of critical slip circle. General

In the previous section, the location in the x-direction for slip circles, which pass under the toe, was derived by simple formulas. For a linear slope without any external loads equation M.13c gave the trivial result $x_c = B/2$. If instead the location is given as a function of the height of the slope and the slope inclination 1:b, the location is obtained as:

$$x_c = \frac{b}{2} \cdot H \qquad \text{(M.13f)}$$

or if the inclination is defined by the angle θ, i.e. $\tan(\theta) = H/B$ or $b = 1/\tan(\theta)$, the location becomes:

$$x_c = \frac{H}{2 \cdot \tan(\theta)} \qquad \text{(M.13g)}$$

However, for steep slopes a toe circle often 'loses' a large proportion of the resistance surface and thus becomes critical, see Figure M.5.

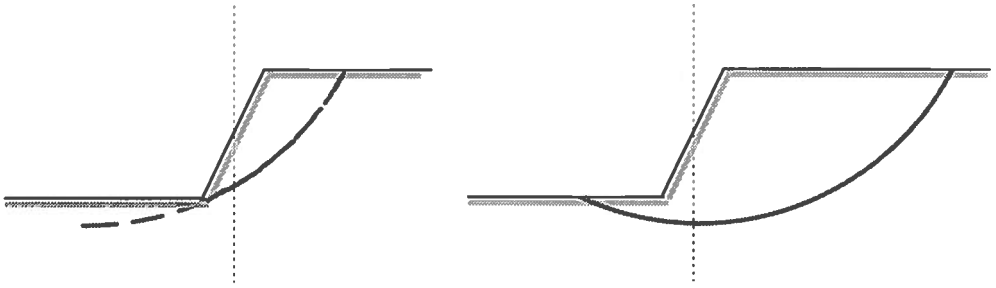

Figure M.5 Principle locations for critical toe and base circles

For the critical toe circle it is not that easy to derive a simple formula like equation M.13f—g. However for practical purposes an explicit formulation can be obtained by curve-fitting of the plot in Figure M.3. The location of the x-coordinate for the critical circle can be approximated as:

$$x_c(\theta) \approx \begin{cases} \dfrac{H}{2 \cdot \tan(\theta)} & \text{if} \quad \theta < \dfrac{\pi}{4} \quad \text{or} \\ \dfrac{1{,}4 \cdot \mathrm{H}}{\tan(1{,}3 \cdot \theta + 0{,}2)} & \text{otherwise} \end{cases} \qquad \text{(M.14)}$$

or alternatively:

$$x_c(b) \approx \begin{cases} \dfrac{b}{2} \cdot H & \text{if} \quad b > 1 \quad \text{or} \\ \dfrac{1{,}4 \cdot \mathrm{H}}{\tan(1{,}3 \cdot \mathrm{a}\tan(1/b) + 0{,}2)} & \text{otherwise} \end{cases} \qquad \text{(M.14a)}$$

In a similar way an approximate formula can be derived for the vertical location, the y-coordinate:

$$y_c \approx \left\{\left[(d+1{,}36)^{-2{,}2}+0{,}04\right]\cdot\left(\left|b(\theta)-0{,}75\right|\right)^{1{,}7}+0{,}38\cdot d^{1{,}3}+1{,}25\right\}\cdot H \qquad \text{(M.15)}$$

where d is the relative depth below the toe for the slip circle, $d = D/H$, see Figure M.3.

M.2.4 Stability number

Expressions for the stability number, given in Figure M.3, are obtained by a curve-fitting procedure similar to those for the location of the critical slip circle given in the previous sections. For a base circle the stability number N can be approximated as:

$$N_{base} \approx \frac{\left[\operatorname{acos}\left(\frac{y_c-1}{y_c+d}\right)+\operatorname{acos}\left(\frac{y_c}{y_c+d}\right)\right]\cdot\left(y_c+d\right)^2}{y_c\cdot d+\frac{1}{2}\cdot d^2-\frac{1}{24}\cdot b^2+\frac{1}{2}\cdot y_c-\frac{1}{6}} \quad ; \quad 0{,}1<d<10 \qquad \text{(M.16)}$$

where y_c is given by equation M.15. For the toe circle the stability number can be calculated as:

$$N_{toe} \approx 5{,}5\cdot\theta^{-0{,}22}-0{,}45\cdot\theta^{2{,}5}+0{,}25 \qquad \text{(M.17)}$$

A combination of equation M.16 and equation M.17 gives:

$$N \approx \begin{cases} N_{base} & \text{if } \left\{N_{base}<N_{toe} \text{ and } d>0{,}1\right\} \\ N_{toe} & \text{otherwise} \end{cases} \quad \text{for } d<10 \qquad \text{(M.18)}$$

It has to be remarked that no approximations have been made for the stability numbers for slope circles, cf. Figure M.3.

M.2.5 Summary

Results obtained by equation M.14 to equation M.18 are plotted in Figure M.6. The purpose is to give an overall comparison between the approximate formulas, given in previous sections, and the original design charts, see Figure M.3. The agreement between the design charts for the stability number and the horizontal location of rotation centre is very good. The agreement between the charts for the vertical location is close, if not as good as for the other two plots. However, the stability

analysis is rather insensitive to the vertical location why the small discrepancy is of secondary importance for the stability analysis. For example, for the values of the stability number, for which the vertical location is an input variable in equation M.16, the agreement is as stated above, very good.

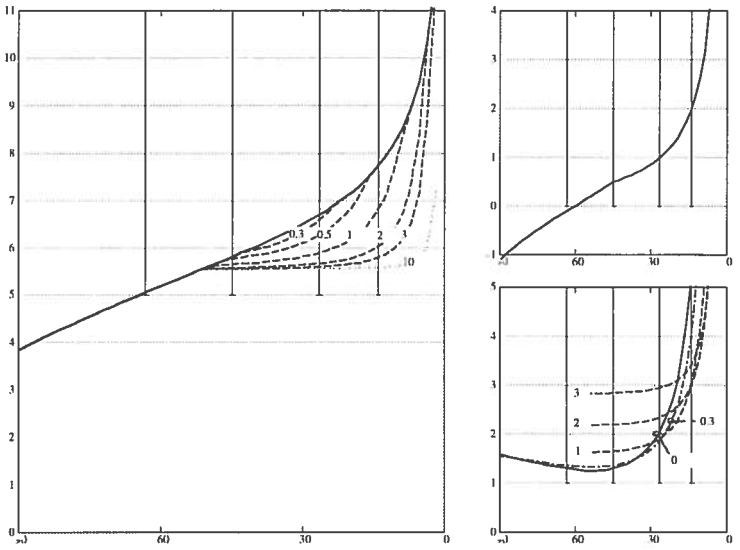

Figure M.6 Design charts derived from equations M.14 t- M.18. Units on axes are the same as in Figure M.3.

APPENDIX N ON BISHOP'S SIMPLIFIED METHOD

N.1 Background

In volume 1, section 4.3.2 'Drained analysis / Effective stresses', different approximations of slope stability analysis are discussed. A simple method, which has been proved very useful and which has become very popular, is the limit equilibrium method known as 'Bishop's simplified' (Bishop, 1955). It is a method for slip circle analysis in which the shear strength between the slices is neglected, i.e. an assumption on the safe side, c.f. section 1.3.7 'Calculations on the safe or unsafe side' in volume 1. Below is given a description of the method suitable for random analysis.

N.2 Application for a toe circle

N.2.1 Principles

For a slope with an arbitrary geometry and in-homogeneous soil conditions, the application of the method may be done with commercial computer software. However, a random analysis approach is difficult to perform in such a case. In principle, the only of the algorithms discussed in Chapter 2, volume 1, which is suitable for a random analysis is the PEM-method. To be able to extend the possible methods of analysis it is desirable to give an analytical formulation of the method. Furthermore, to take advantage of the versatility of the probabilistic approach, the uncertainty of the calculation has to be described with a limited number of basic variables. If for example one wants to distinguish the uncertainty of slope geometry in the results of the analysis, the geometry cannot be described with 'unlimited' number of co-ordinates. For this reason, and for simplicity, the slope is described as a regular linear slope, which means that the geometry of the slope can be described with just two variables, e.g. the height and the inclination. In appendix M a method by which an arbitrary slope, in a systematic, way can be transformed into such a regular slope is given.

For similar reasons as above, the shear strength of the slope is limited to constant soil parameters, with the important exception that the undrained shear strength might increase with depth.

N.2.2 Geometry

In Figure N.1 the layout and the soil parameters of the slope are given.

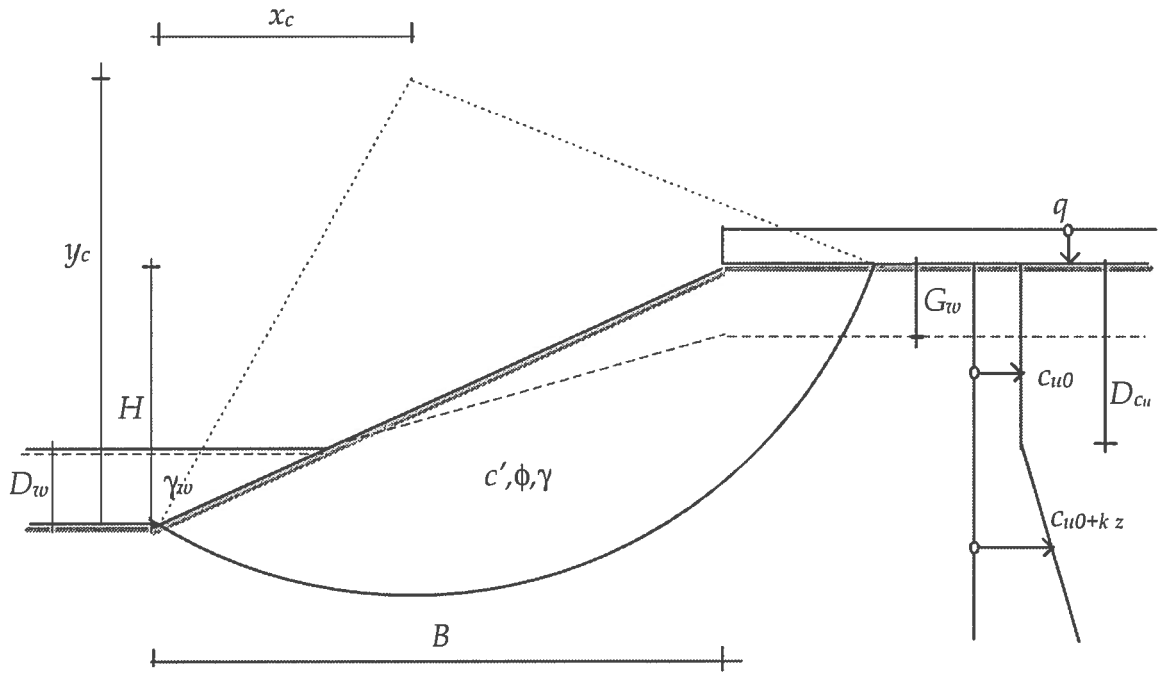

Figure N.1 Layout and input parameters of a slope analysed with Bishop's simplified method

Notations, which are used in the analysis, are, apart from those already defined in Figure N.1, given in Figure N.2.

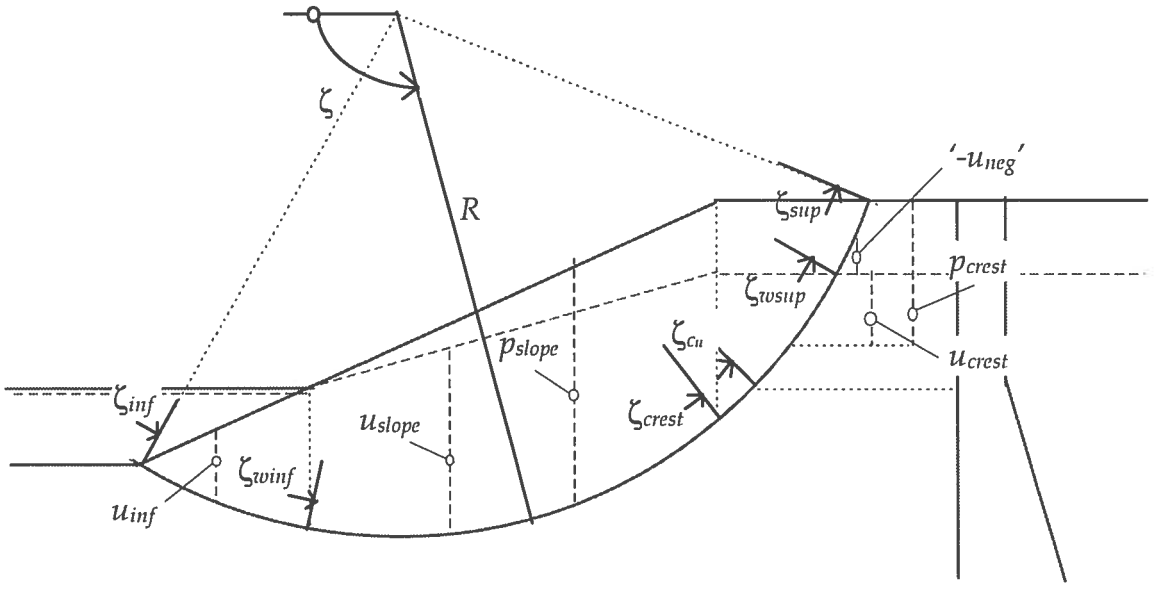

Figure N.2 Notations.

The angles, which are marked in Figure N.2 can be calculated as:[1]

$$\varsigma_{\inf} = \frac{\pi}{2} - \operatorname{atan}\left(\frac{x_c}{y_c}\right) \tag{N.1}$$

$$\varsigma_{\sup} = \frac{\pi}{2} + \operatorname{acos}\left(\frac{y_c - H}{R}\right) \tag{N.2}$$

$$\varsigma_{crest} = \frac{\pi}{2} + \operatorname{asin}\left(\frac{B - x_c}{R}\right) \tag{N.3}$$

$$\varsigma_{w\inf} = \frac{\pi}{2} - \operatorname{asin}\left(\frac{x_c - D_w \cdot B/H}{R}\right) \tag{N.4}$$

$$\varsigma_{w\sup} = \frac{\pi}{2} + \operatorname{acos}\left(\frac{y_c - H + G_w}{R}\right) \tag{N.5}$$

$$\varsigma_{Cu} = \frac{\pi}{2} + \operatorname{acos}\left(\frac{y_c - H + D_{Cu}}{R}\right) \tag{N.6}$$

in which $R = \sqrt{x_c^{\,2} + y_c^{\,2}}$

N.2.3 Overturning moment

Soil

The overturning moment for 'unity weight of the slope', i.e. $\gamma \cdot H = 1$, can be derived as:

$$M_{S0} = \frac{H}{2} \cdot \left(y_c - \frac{H}{3}\right) + \frac{B}{2} \cdot \left(x_c - \frac{B}{3}\right) \tag{N.7}$$

External load at crest

Unity load at the crest, i.e. q=1 adds to the overturning moment:

$$M_q = \frac{\left[R \cdot \sin(\varsigma_{\sup}) - (B - x_c)\right] \cdot \left[R \cdot \sin(\varsigma_{\sup}) + (B - x_c)\right]}{2} \tag{N.8}$$

[1] The formulations given are restricted to slopes for which $\varsigma_{w\sup} > \varsigma_{crest}$ and for which the slip circle reach the crest.

External water

Unity load of water, i.e. $\gamma_w \cdot D_w = 1$, subtract the overturning moment:

$$M_w = \frac{D_w}{2} \cdot \left(y_c - \frac{D_w}{3} \right) + \frac{D_w}{H} \cdot \frac{B}{2} \cdot \left(x_c - \frac{D_w}{H} \cdot \frac{B}{3} \right) \qquad \text{(N.9)}$$

Geometric driving

The total overturning moment, with actual loads, is:

$$M_S = \gamma \cdot H \cdot M_{S0} + q \cdot M_q - \gamma_w \cdot D_w \cdot M_w \qquad \text{(N.10)}$$

By dividing by H^2, a dimensionless overturning moment is obtained:

$$m_S = \frac{M_S}{H^2} \qquad \text{(N.11)}$$

which is a measure of the influence of the geometry on the overturning moment, hence might be called the geometric driving. It can be separated as:

$$\begin{aligned} & m_S = m_{S0} + m_q - m_w \\ & \text{where} \\ & m_{s0} = M_{S0}/H^2 \quad ; \quad m_q = \left(q/\gamma H\right) \cdot \left(M_q/H^2\right) \quad \text{and} \\ & m_w = \left(\gamma_w D_w/\gamma H\right) \cdot \left(M_w/H^2\right) \end{aligned} \qquad \text{(N.11a)}$$

N.2.4 Stabilising moment

The resistance moment, for unity of the shear strength, i.e. c=1, can be derived as:

$$M_{R0} = \left(\varsigma_{\text{sup}} - \varsigma_{\text{inf}}\right) \cdot R^2 \qquad \text{(N.12)}$$

i.e. the actual resistance moment $M_R = \bar{c} \cdot M_{R0}$, where $\bar{c}$ is the average shear strength along the slip circle. Similar as for the driving moment, a dimensionless driving resistance, a geometric resistance, is obtained as:

$$m_R = \frac{M_{R0}}{H^2} \qquad \text{(N.13)}$$

N.2.5 Safety concepts

The dimensionless safety margin m, see appendix J, becomes:

$$m = \frac{M_R/H^2 - M_S/H^2}{M_R/H^2} = \frac{m_R \cdot \bar{c} - m_S \cdot \gamma \cdot H}{m_R \cdot \bar{c}} \qquad \text{(N.14)}$$

The traditional factor of safety F is:

$$F = \frac{M_R}{M_S} = \frac{m_R \cdot \bar{c} \cdot H^2}{m_S \cdot \gamma \cdot H^3} = \frac{m_R}{m_S} \cdot \frac{\bar{c}}{\gamma \cdot H} \qquad \text{(N.15)}$$

Hence, the well-known stability number N is equal to the ratio m_R/m_S. Equation N.15 is often written as (see e.g. Janbu, 1996):

$$F = N \cdot \frac{\bar{c}}{P_d} \qquad \text{(N.15a)}$$

with the denominator P_d denoted the unbalanced stress at the toe plane, i.e. in principle $P_d = \gamma \cdot H + q - \gamma_w \cdot D_w$ and where N is obtained from a design chart, cf. appendix M. The design chart value corresponds to the value obtained from the slope geometry, i.e. $N = m_R/m_{S0}$. Hence one obtains the equality $m_S \cdot \gamma \cdot H = m_{S0} \cdot P_d$, which results in:

$$P_d = \gamma \cdot H + q \cdot \frac{M_q}{M_{S0}} - \gamma_w \cdot D_w \cdot \frac{M_w}{M_{S0}} \qquad \text{(N.16)}$$

Equation N.16 results in a slightly different unbalanced stress compared with the principle formulation above[1].

N.2.6 Average stresses

The average shear stress can be obtained by a moment equilibrium equation, i.e. the numerator in equation N.14 equal to zero:

$$m_R \cdot \bar{\tau} = m_S \cdot \gamma \cdot H \quad ; \quad \bar{\tau} = \frac{m_S}{m_R} \cdot \gamma \cdot H \qquad \text{(N.17)}$$

The average normal stress can easily be obtained by a horizontal equilibrium equation:

[1] By dividing with correction factors the principle formulation is often adjuste'.

$$\int_{\varsigma_{inf}}^{\varsigma_{sup}} \bar{\tau} \cdot \cos\left(\varsigma - \frac{\pi}{2}\right) \cdot R\mathrm{d}\varsigma - \int_{\varsigma_{inf}}^{\varsigma_{sup}} \overline{\sigma_N} \cdot \sin\left(\varsigma - \frac{\pi}{2}\right) \cdot R\mathrm{d}\varsigma + \gamma_w \cdot \frac{D_w^{\,2}}{2} = 0 \qquad \text{(N.18)}$$

with the solution:

$$\bar{\sigma}_N = \frac{\bar{\tau} \cdot R \cdot \left[\cos(\varsigma_{sup}) - \cos(\varsigma_{inf})\right] - \gamma_w \cdot \frac{D_w^{\,2}}{2}}{R \cdot \left[\sin(\varsigma_{sup}) - \sin(\varsigma_{inf})\right]} \qquad \text{(N.18a)}$$

For the special case no external horizontal load, i.e. in this case no external water, the solution can be simplified to:

$$\bar{\sigma}_N = \tan\left(\pi - \frac{\varsigma_{sup} + \varsigma_{inf}}{2}\right) \cdot \bar{\tau} = \tan\left(\pi - \frac{\varsigma_{sup} + \varsigma_{inf}}{2}\right) \cdot \frac{m_S}{m_R} \cdot \gamma \cdot H \qquad \text{(N.18b)}$$

N.2.7 Average shear strength

Infinitesimal slice

The weight intensity p of an infinitesimal slice, with unity density of the soil, can be separated in one formulation below the crest:

$$p_{slope} = R \cdot \sin(\varsigma) - y_c + \frac{x_c - R \cdot \cos(\varsigma)}{B} \cdot H \qquad \text{(N.19)}$$

and another above the crest:

$$p_{crest} = R \cdot \sin(\varsigma) - y_c + H \qquad \text{(N.20)}$$

Combining equation N.19 and equation N.20 gives:

$$p(\varsigma) = \begin{cases} p_{slope} & \text{if} \quad \varsigma < \varsigma_{crest} \\ p_{crest} & \text{otherwise} \end{cases} \qquad \text{(N.21)}$$

In a similar way the pore pressure[1] can be given different expressions in different parts along the slip surface

For unit density of the water the pore pressure becomes:

[1] This is with the exclusion of shear induced pore pressure, cf. section 3.4.3, volume 1

$$u_{\inf} = p_{slope}{}^{1} \tag{N.22}$$

$$u_{slope} = R \cdot \sin(\varsigma) - (y_c - D_w) + \frac{x_c - D_w \cdot B/H - R \cdot \cos(\varsigma)}{B - D_w \cdot B/H} \cdot (H - G_w - D_w) \tag{N.23}$$

$$u_{crest} = R \cdot \sin(\varsigma) - y_c + H - G_w \tag{N.24}$$

and as an approximation of the negative pore pressure:

$$u_{crest} \approx \frac{u_{crest}}{2} \tag{N.25}$$

Combining equation N.22 - equation N.25 gives:

$$u(\varsigma) = \begin{vmatrix} u_{\inf} & \text{if} & \varsigma < \varsigma_{\text{winf}} \\ u_{slope} & \text{if} & \varsigma_{w\inf} < \varsigma < \varsigma_{\text{crest}} \\ u_{icrest} & \text{if} & \varsigma_{crest} < \varsigma_{\text{wsup}} \\ u_{neg} & \text{if} & \varsigma > \varsigma_{\text{sup}} \end{vmatrix} \tag{N.26}$$

Drained shear strength

In appendix K, the shear strength in slope stability is discussed. Two alternatives were discussed

- The shear strength is based upon the actual stresses
- The shear strength is based upon the stresses at failure

If the shear strength between slices is omitted, the two alternatives can be summarised as:

$$c_{c,\phi}(\varsigma) = \frac{c' + \left[\gamma \cdot p(\varsigma) - \gamma_w \cdot u(\varsigma)\right] \cdot \tan(\phi)}{1 + \tan(\phi) \cdot \tan(\varsigma - \pi/2) \cdot (1 - m)} \tag{N.27}$$

with m=0 in the second alternative.

The average drained shear strength is then obtained as:

[1] The water pressure of external water must not be incorporated in the expression for u if it is not included in p.

$$\bar{c}_{c,\phi} = \frac{1}{S}\int_{\varsigma_{inf}}^{\varsigma_{sup}} c_{c,\phi}(\varsigma)\cdot R\,\mathrm{d}\varsigma \qquad \text{(N.28)}$$

where $S = \int_{inf}^{\varsigma_{sup}} R\,\mathrm{d}\varsigma$ is the length of the slip circle.

Undrained shear strength

The undrained shear strength becomes:

$$c_u(\varsigma) = \begin{cases} c_{u0} + k\cdot\left[R\cdot\sin(\varsigma) - (y_c - H) - D_{Cu}\right] & \text{if} \quad \varsigma < \varsigma_{Cu} \\ c_{u0} \quad \text{otherwise} \end{cases} \qquad \text{(N.29)}$$

and the average shear strength:

$$\bar{c}_{Cu} = \frac{1}{S}\int_{\varsigma_{inf}}^{\varsigma_{sup}} c_{Cu}(\varsigma)\cdot R\,\mathrm{d}\varsigma \qquad \text{(N.30)}$$

Combined shear strength

The combined shear strength becomes:

$$c_{comb}(\varsigma) = \begin{cases} c_{c,\phi}(\varsigma) & \text{if} \quad c_{c,\phi}(\varsigma) < c_u(\varsigma) \\ c_u(\varsigma) & \text{otherwise} \end{cases} \qquad \text{(N.31)}$$

and the average shear strength:

$$\bar{c}_{comb} = \frac{1}{S}\int_{\varsigma_{inf}}^{\varsigma_{sup}} c_{comb}(\varsigma)\cdot R\,\mathrm{d}\varsigma \qquad \text{(N.32)}$$

N.2.8 Calculation of safety margin

The safety margin is given by equation N.14, with the average shear strength from equation N.28, N.30 or N.32, depending on the sort of analysis. For the undrained analysis and for the drained or combined analysis, given the second alternative interpretation of the shear strength, the calculation becomes particularly simple as the average shear strength in these cases is independent of the safety margin. Given the first shear strength alternative the calculation is not that trivial. The safety margin is obtained as the root of the rewriting of equation N.14:

$$m = \frac{m_R \cdot \bar{c}(m) - m_S \cdot \gamma \cdot H}{m_R \cdot \bar{c}(m)} \qquad \text{(N.14a)}$$

which normally is solved by iteration as:

$$m_{i+1} = \frac{m_R \cdot \bar{c}(m_i) - m_S \cdot \gamma \cdot H}{m_R \cdot \bar{c}(m_i)} \qquad \text{(N.14b)}$$

In a probabilistic approach the calculations are simplified if the denominator is given a deterministic value, cf. appendix J, and the strength interpretation with m=0 is used:

$$m = \frac{m_R \cdot \bar{c}(0) - m_S \cdot \gamma \cdot H}{\mu_{m_R} \cdot \mu_c} \qquad \text{(N.14c)}$$

where $\mu_{m_R} = E[m_R]$ and $\mu_c = E[\bar{c}(o)]$

APPENDIX O SLOPE STABILITY. A SHEAR BEAM MODEL

O.1 Calculation model

O.1.1 Frame model

In section 4.7.1, volume 1, the general principles of a shear beam model for slope stability analysis are discussed. In this appendix an example of such a model is presented. The description is given for a toe circle, see Figure O.1. However, in principle there are no restrictions on the slip surface for which the shear beam model can be applied. The slope in Figure O.1 is the same type of slope that was analysed with Bishop's simplified method in appendix N.

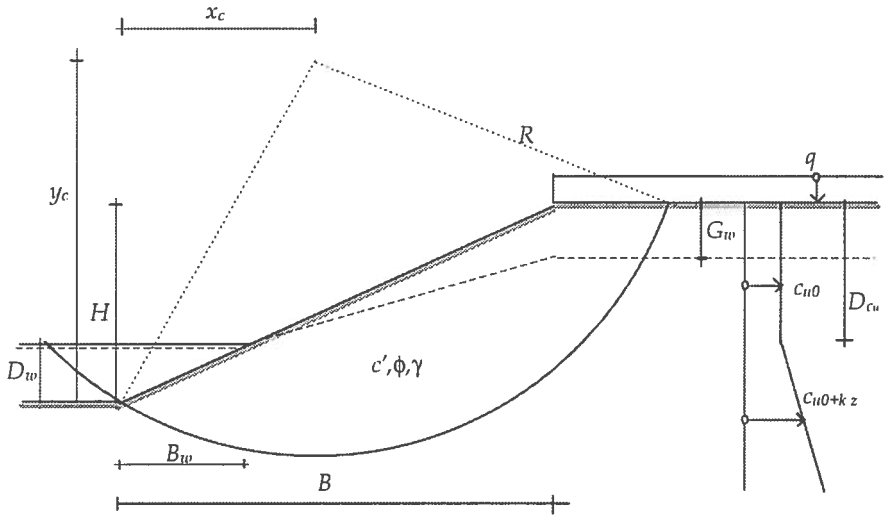

Figure O.1 Geometry and properties of the analysed slope.

The principal actions and reactions of the slope divided into slices are shown in Figure O.2. The dotted line in the figure shows the assumed line of thrust.

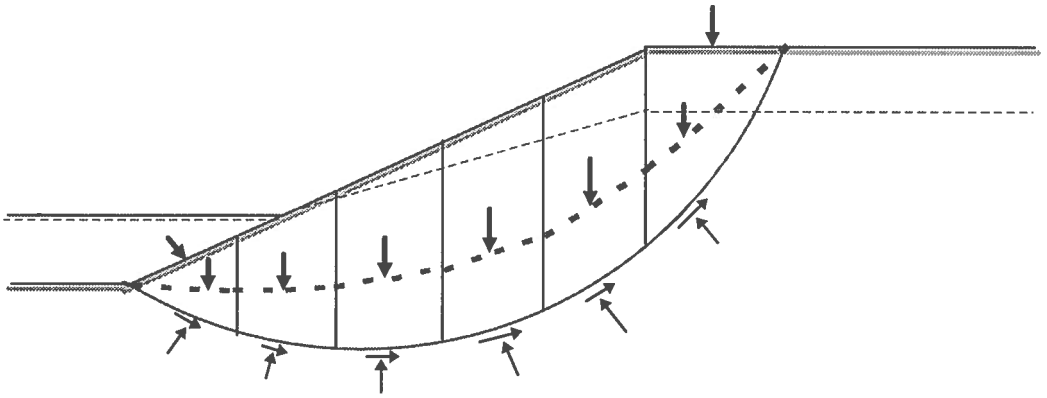

Figure O.2 Actions and reactions in the slope

Inspired by Janbu's general procedure of slices, GPS, (see e.g. Janbu, 1996), the shear beams can be arranged in such a way that a 'line of thrust' is prescribed. This will give a shear beam model as in Figure O.3. The frame model consists of 'shear legs' perpendicular to the slip surface, i.e. the deformations along the slip surface are assumed to be mainly shearing, which can be modelled with a prescribed shear stiffness GA_i in a shear leg. Similarly, the elements along the line of thrust are 'compression struts', i.e. the deformations along the line of thrust are assumed to be pure compression. Hence the deformation properties of a compression strut are prescribed with a compression stiffness MA_j.. By putting hinges in the nodes between the legs and the struts the line of thrust is fixed. The stability of the frame model is achieved by assuming fixed end of the shear legs at the shear surface. The compression stiffness of a shear leg and the shear stiffness of a compression strut is assumed to be equal to infinity.

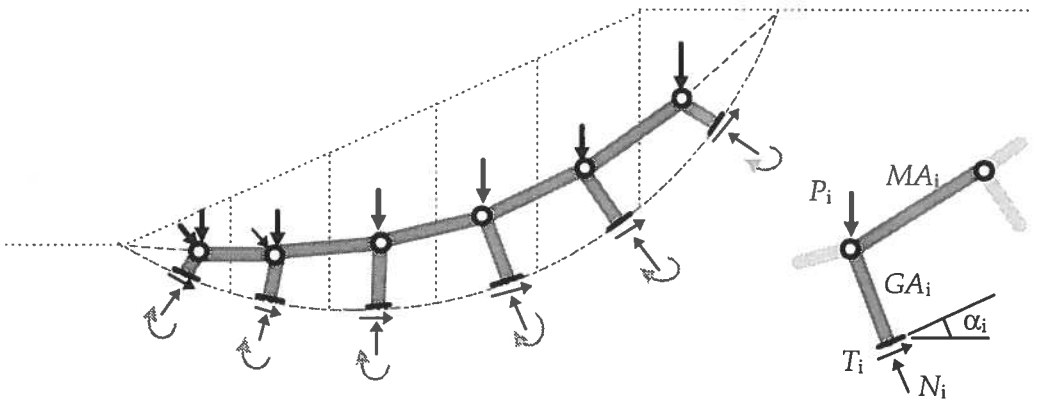

Figure O.3 The shear beam model

O.1.2 Actions

The actions in the shear beam model consists of the weight of the soil, external loads and water pressure. The weight of a slice has in principle to be applied at the mass centre, i.e. approximately in the middle of a slice with the exception of the first and last 'triangular' slices. Hence the nodes are located at the corresponding points of a slice, or in other words, a 'slice' is defined by the location of a node. By the same principle, external actions are replaced by concentrated actions , which are in equilibrium with the external actions. In Figure O.4 this is illustrated for the water pressure at the toe.

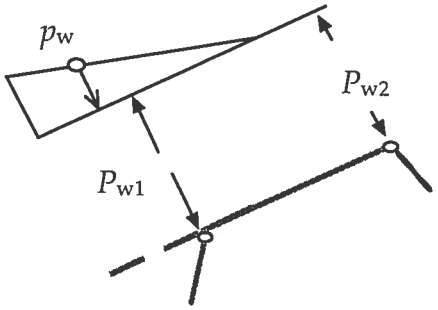

Figure O.4 Principle of modelling external water pressure at the toe of a slope.

O.1.3 Separation of actions

The assumption of a compression stiffness for a shear leg $MA_i=\infty$, simplifies the analysis. A shear leg will carry an axial load in a shear leg completely, i.e. it can be treated statically determined, while a

transversal load will be distributed in accordance with the deformation properties of the frame model. Hence the nodal loads can be separated into axial and transversal loads, of which only the latter have to be incorporated into the structural analytical model. This principle is illustrated in Figure O.5.

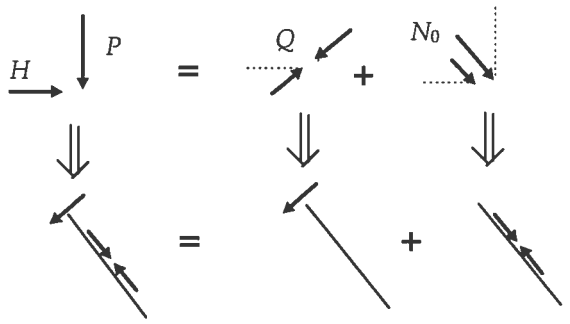

Figure O.5 Separating of nodal loads P and H in transversal loads Q and axial loads N_0.

For a node i, the transversal load can be written as:

$$Q_i = P_i \cdot \sin(\alpha_i) - H_i \cdot \cos(\alpha_i) \qquad \text{(O.1)}$$

while the axial load becomes:

$$N_{0i} = P_i \cdot \cos(\alpha_i) + H_i \cdot \sin(\alpha_i) \qquad \text{(O.2)}$$

O.1.4 Structural algorithm

General

To be able to calculate the stability of the slope, the reactions at the supports must be determined. These can be obtained by standard methods in structural mechanics. In the scheme below, the deformations of the slope structure and the corresponding reaction are obtained by a displacement method, see e.g. Samuelsson & Wiberg, (1988):

$$\begin{array}{ccc} \mathbf{R} & \xrightarrow{\mathbf{A}^T} & \mathbf{Q} \\ \mathbf{E}_n \uparrow & & \uparrow \mathbf{S} = \mathbf{A}^T \cdot \mathbf{E}_n \cdot \mathbf{A} \\ \mathbf{r} & \xleftarrow[\mathbf{A}]{} & \mathbf{q} \end{array} \qquad \text{(O.3)}$$

Q is a column vector of the nodal loads as defined in the previous section, while **R** is the corresponding vector for the internal forces of the structure. Hence $\mathbf{Q}=\mathbf{A}^T\cdot\mathbf{R}$ is a matrix equation for equilibrium in the nodes. The deformations corresponding to **Q** and **R** are denoted **q** and **r**

respectively. The relation between **q** and **r** can be obtained by the transpose of $\mathbf{A}^T$, i.e. **A**, as **r**=**A**·**q**. This follows from a theorem in structural mechanichs sometimes named Clebsch's theorem. $\mathbf{E}_n$ is a matrix, which describes the stiffness of the elements. The matrix operation $\mathbf{A}^T \cdot \mathbf{E}_n \cdot \mathbf{A}$ forms the structural stiffness **S**. From the scheme O.3 the nodal displacements are obtained by the inverse of the structural stiffness **S** as:

$$\mathbf{q} = \mathbf{S}^{-1} \cdot \mathbf{Q} \qquad \text{(O.4)}$$

and the reactions as:

$$\mathbf{R} = \mathbf{E}_n \cdot \mathbf{A} \cdot \mathbf{q} \,. \qquad \text{(O.5)}$$

Stiffness of the elements

Notations used in the analysis are given in Figure O.6.

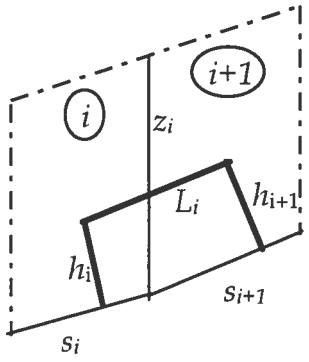

Figure O.6 Notations of elements.

As a first assumption, the shear stiffness of a shear leg can be modelled as GA/h, where G is an assumed shear modulus, A_i is the section 'area' of the leg, e.g. the sub-length s_i of the slip surface for the slice at hand and h_i is the length of the shear leg, i.e. the perpendicular distance from the line of thrust to the slip surface. In the same way, the compression stiffness of the struts can be modelled as Mz/L, where M is a compression modulus, z_i is the section 'area', e.g. the height of the slice, and L_i is the length of a strut. In Figure O.7 a systematic numbering of the nodes and the elements is given.

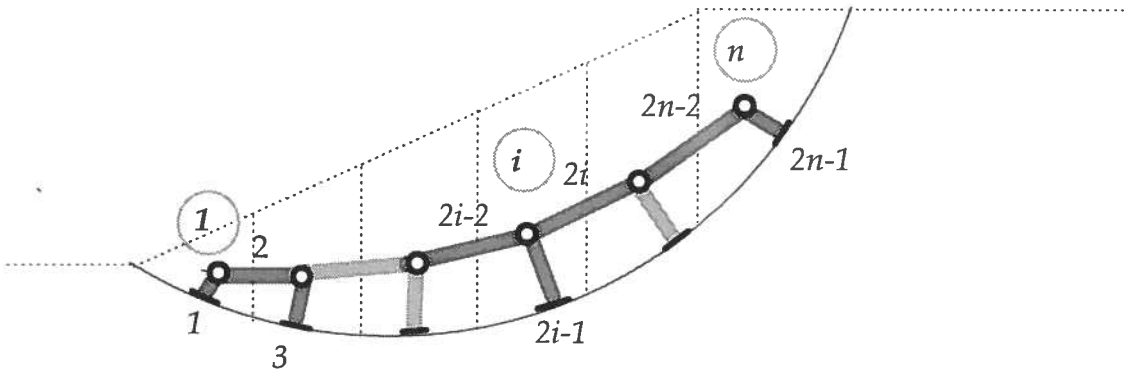

Figure O.7 Numbering of the nodes and the elements.

The element stiffness matrix $\mathbf{E}_n$ becomes, for a slope divided in n 'slices', a $\{2n-1\}\times\{2n-1\}$ diagonal matrix with the elements:

$$E_{n_{2i-1,2i-1}} = \frac{G \cdot s_i}{h_i} \quad ; \quad i = 1...n \tag{O.6}$$

for the shear legs and :

$$E_{n_{2i,2i}} = \frac{M \cdot z_i}{L_i} \quad ; \quad i = 1...n-1 \tag{O.7}$$

for the compression struts.

Nodal equilibrium

The matrix $\mathbf{A}^T$ is obtained from equilibrium in the nodes. It is a $\{n\}\times\{2n-1\}$ matrix, which, apart from the first and last row, has three elements in each row along the diagonal:

$$\mathbf{A}^T = \begin{bmatrix} A_{1,1}^T & A_{1,2}^T & 0 & 0 & 0 & \cdots & & & & & \\ 0 & A_{2,2}^T & A_{2,3}^T & A_{2,4}^T & 0 & \cdots & & & & & \\ 0 & & & & & & & & & & \\ \vdots & & & \cdots & 0 & A_{i,2i-2}^T & A_{i,2i-1}^T & A_{1,2i}^T & 0 & \cdots & \\ & & & & & & & & & & 0 \\ & & & & & \cdots & 0 & A_{n-1,2n-4}^T & A_{n-1,2n-3}^T & A_{n-1,2n-2}^T & 0 \\ & & & & & \cdots & 0 & 0 & 0 & A_{n,2n-2}^T & A_{n,2n-1}^T \end{bmatrix} \tag{O.8}$$

With the notations in Figure O.8 the elements in the matrix become:

$$\begin{aligned} A_{i,2i-2}^T &= \cos(\alpha_i - \varsigma_{i-1}) \\ A_{i,2i-1}^T &= -1 \\ A_{i,2i}^T &= -\cos(\varsigma_i - \alpha_i) \end{aligned} \tag{O.9}$$

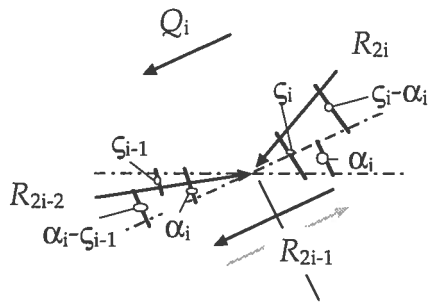

Figure O.8 Definitions of nodal forces and node geometry for a node *i*.

Reactions

The shear reactions at the slip surface are identified as:

$$T_i = -R_{2i-1} \tag{O.10}$$

The normal reactions of the loads **Q** are obtained from an equilibrium equation in the shear leg direction. Hence, together with the reactions N_0, see section 2.1.3, the normal reaction at slice *i* is:

$$N_i = N_{0_i} - R_{2i-2} \cdot \sin(\varsigma_{i-1} - \alpha_i) + R_{2i} \cdot \sin(\varsigma_i - \alpha_i) \tag{O.11}$$

Note that for *i*=1, $R_{2i-2} = R_0 = 0$ and similarly $R_{2n} = 0$.

The pore pressure 'forces' U_i can be estimated as[1]:

$$U = u \cdot s \tag{O.12}$$

where the pore pressure u_i can be taken as the pore pressure at a point on the slip surface, vertically below the nodes[2]. A more exact 'location' of the pore pressure can be obtained by determining the intersection between the slip surface and the direction of the resultant of T_i and N_i applied in the node. The 'effective' normal reaction can then be calculated as:

$$N' = N - U \tag{O.13}$$

Shear strength

In the same way as for the pore pressure in the previous section, an undrained shear resistance can be established:

$$C_{u_i} = c_{u_i} \cdot s_i \tag{O.14}$$

The drained shear resistance is:

$$C_{c,\phi_i} = c' \cdot s_i + N'_i \cdot \tan(\phi) \tag{O.15}$$

Finally, the combined shear resistance naturally becomes:

$$C_{comb_i} = \min\left\{C_{u_i}; C_{c,\phi_i}\right\} \tag{O.16}$$

Safety margin

Each slice will have a local safety margin:

$$m_i = \frac{C_i - T_i}{C_i} \tag{O.17}$$

where C_i denotes the shear resistance of the type of analysis of interest. A global safety margin is obtained as, cf. section 4.7.1 'Safety concept,' volume 1:

---

[1] For a, in principle, more correct estimation the pore pressure 'force' can be obtained by integration along the slip surface, cf. appendix N.

$$m = \frac{C_\Sigma \cdot \cos(|\alpha_C - \alpha_T|) - T_\Sigma}{C_\Sigma \cdot \cos(|\alpha_C - \alpha_T|)} \qquad \text{(O.18)}$$

where C_Σ is the magnitude of the total shear resistance vector, T_Σ is the magnitude of the shear force vector and $|\alpha_C - \alpha_T|$ denotes the angle between these two vectors.

O.2 Example - Deterministic calculation

The application of the proposed shear beam model is illustrated with an example taken from (Janbu 1989). It is an example of deterministic, drained analysis for a slope with simple geometry and homogenous soil conditions, see Figure O.9. The analysed slope is an example of deterministic, drained analysis.

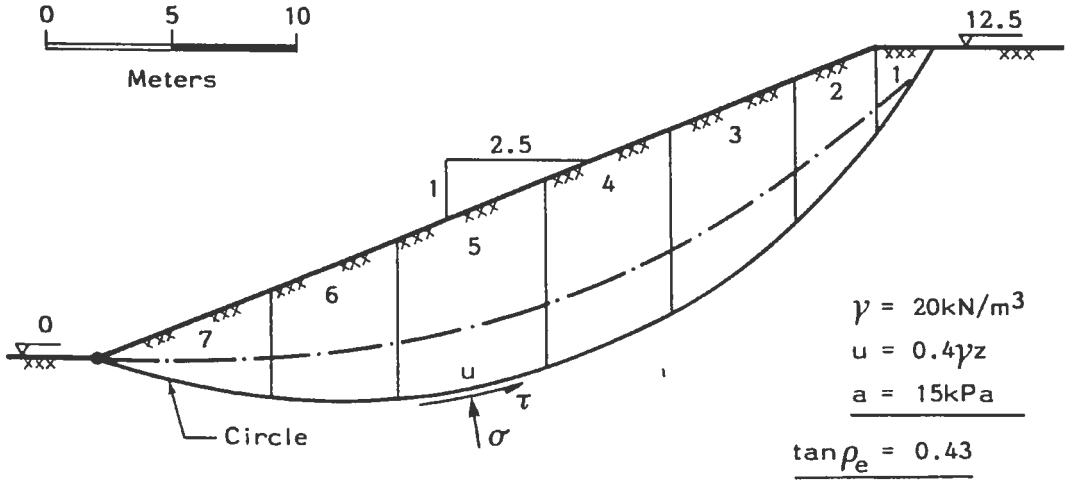

Figure O.9 Analysed slope. From Janbu, (1989).

[2] A more exact 'location' of the pore pressure can be obtained by determining the intersection between the slip surface and the direction of the resultant of T_i and N_i applied in the node.

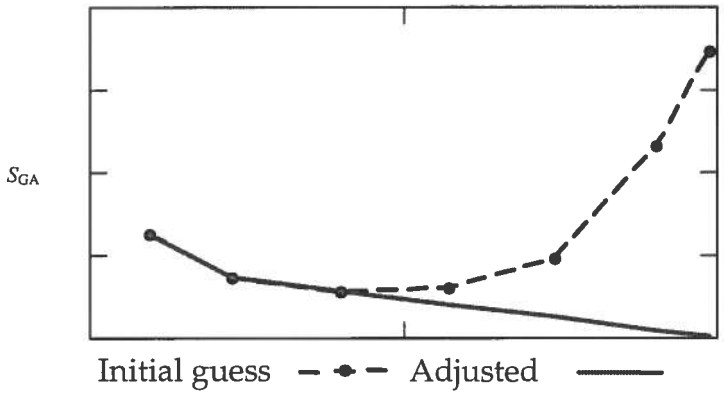

Figure O.10 Distribution of shear stiffness.

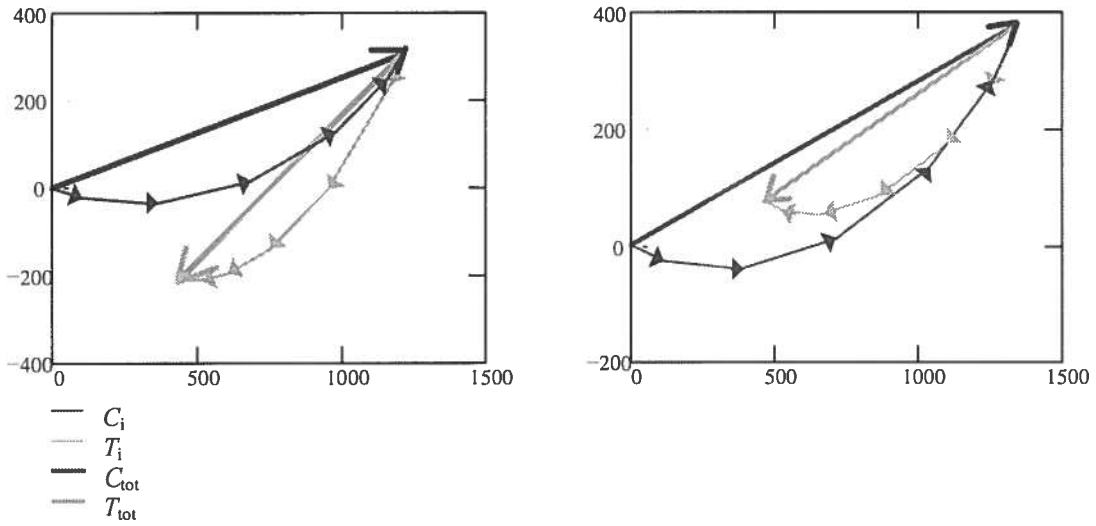

Figure O.11 Shear resistance and shear action. Left plot 'Initial shear stiffness'. Right plot 'Adjusted shear stiffness'.

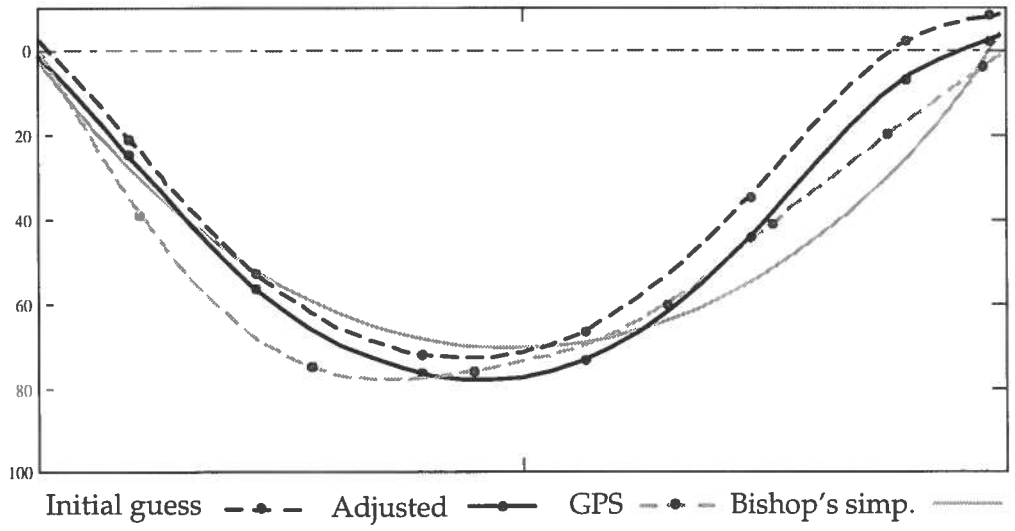

Figure O.12 Effective normal stress distribution

APPENDIX P CREEP DEFORMATION

P.1 General

In (Alén, 1998b) is described a soil model for calculation of deformation in clay. The purpose of this model is to obtain an analytical, i.e. a differentiable, calculation model, suitable for incorporation in, for example, a random calculation model. This appendix is an abstract of those parts of the report, which describe how to calculate creep deformation in clay. The model, as described below, is restricted to one-dimensional consolidation. Furthermore unloading is omitted.

P.2 Rheological model

The time dependent deformation of the soil is assumed to be characterised by three different phenomena:

A: Consolidation. Dissipation of pore water and simultaneous equalising of excessive pore pressure. Darcy's law:

$$v = k \cdot i \tag{P.1}$$

is assumed to be sufficient to describe the process. The term consolidation is in the model restricted to the strain settled by the outflow of pore water. If both the water and the solids of the soil are considered incompressible, this strain is equal to the total strain for a saturated clay. The definition is in accordance with a general definition of consolidation, see e.g. (Terzaghi, 1943).

B: Elastic/plastic deformation, which is caused by an increase of the effective stress. The deformation is here restricted to deformation, which occurs immediately at an increase of the stress. (For practical purposes 'immediately' can be defined as faster than the development of the deformation in a reference test, e.g. an oedometer test.). Elastic deformation is defined as deformation, which disappears immediately at unloading. If the analysis is restricted to loading, there is no need to make any distinction between elastic and plastic deformation. The deformation can be described with a compression modulus M,

given as a function of the effective stress, e.g. a virgin curve obtained from an oedometer test.

C: Creep deformation, defined as time dependent deformation, which develops under constant effective stress (see e.g. Hult, 1968). In the described calculation model only creep deformation caused by compression is considered.[1] The magnitude of the deformation is assumed to be described with a creep number r such that (cf. Janbu, 1969):

$$r = \frac{\partial \ln(t)}{\partial \varepsilon_{cr}} \qquad \text{(P.2)}$$

The three different phenomena A, B and C as above, are assumed to take place simultaneously. In this way, any of the phenomena are strongly interrelated and affects the 'environment' in which the other two phenomena take place. Apart from this time dependent interference, the phenomena are assumed to be independent of each other. The relation can be described by the rheological model given in Figure P.1.

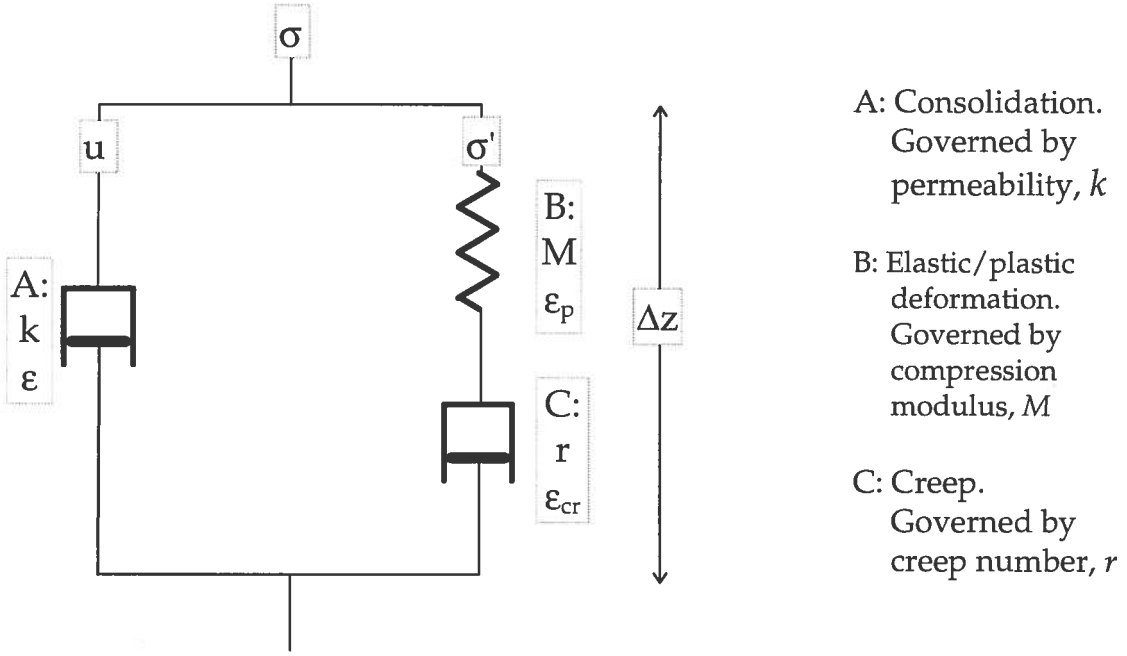

Figure P.1 Rheological soil model describing long term deformation in clay

[1] This means that shear strains, apart from those incorporated in the compression modulus, are not considered

P.3 Derivation of differential equation

From the model in Figure P.1, a differential equation describing the problem can be derived[1]:

Rheology:

A The strain rate is equal to the relative change in height of a volume, during a time increment and is governed by Darcy's law:

$$\frac{\partial \varepsilon}{\partial t} = -\frac{v}{\Delta z} = -\frac{ki}{\Delta z} = -\frac{k \cdot \frac{\Delta u}{\gamma_w \Delta z}}{\Delta z} = -\frac{\partial}{\partial z}\left(\frac{k}{\gamma_w}\frac{\partial u}{\partial z}\right) \qquad \text{(P.3)}$$

The minus sign is a notional convention. Seepage is seen as going in a negative direction.

B: Assuming constant total stress, the change in effective stress equals the change in pore pressure:

$$\Delta \varepsilon_p = \frac{\Delta \sigma'}{M} = -\frac{\Delta u}{M} \qquad \text{(P.4)}$$

Or for a time increment

$$\frac{\partial \varepsilon_p}{\partial t} = -\frac{1}{M} \cdot \frac{\partial u}{\partial t} \qquad \text{(P.4a)}$$

C: Equation P.2 is equivalent to

$$\frac{\partial \varepsilon_{cr}}{\partial t} = \frac{\partial \varepsilon_{cr}}{\partial \ln(t)} \cdot \frac{\partial \ln(t)}{\partial t} = \frac{1}{r \cdot t} \qquad \text{(P.5)}$$

As can be seen from equation P.5 the creep strain rate is dependent of the 'magnitude' of time. Thus, to keep the linear behaviour in a logarithmic time scale[2], the time has to be adjusted by introducing a reference time, t_r, for a starting point with a known strain rate:

[1] The scheme follows a general scheme for rheological models, see Hult, (1968)

[2] $\frac{\partial \varepsilon_{cr}}{\partial \ln(t)} = 1/r \rightarrow \varepsilon_{cr} = \ln(t)/r + C = \ln(t+t_r)/r$

$$\frac{\partial \varepsilon_{cr}}{\partial t} = \frac{1}{r \cdot (t + t_r)} \qquad \text{(P.5a)}$$

From a pragmatic point of view, t can be seen as the time elapsed from the start of a 'project', t_r as the reference time for that point and $t+t_r$ as a 'total' time. The 'total' time at the starting point then 'becomes t_r.

Geometrical compatibility:

The total strain must equal the sum of elastic/plastic strain and creep strain

$$\varepsilon = \varepsilon_p + \varepsilon_{cr} \qquad \text{(P.6)}$$

Or for a time increment

$$-\frac{\partial \varepsilon_p}{\partial t} = -\frac{\partial \varepsilon}{\partial t} + \frac{\partial \varepsilon_{cr}}{\partial t} \qquad \text{(P.6a)}$$

Hence:

$$\frac{1}{M}\frac{\partial u}{\partial t} = \frac{\partial}{\partial z}\left(\frac{k}{\gamma_w}\frac{\partial u}{\partial z}\right) + \frac{1}{r \cdot (t + t_r)} \qquad \text{(P.7)}$$

If k and γ_w are constant with depth equation P.7 becomes:

$$\frac{1}{M}\frac{\partial u}{\partial t} = \frac{k}{\gamma_w}\frac{\partial^2 u}{\partial z^2} + \frac{1}{r \cdot (t + t\ )} \qquad \text{(P.7a)}$$

If the last term, which describes the creep part of the process, is omitted, the equation coincides with Terzaghi's solution for one-dimensional consolidation, (Terzaghi, 1943).

P.4 Constrained/unconstrained creep

If equation P.7 is applied to a problem without any further considerations, there is a risk that one will obtain a solution with increasing pore pressure over time, despite no additional loading. This, in turn, means that the effective stress is reduced. The phenomenon will happen if the calculated creep strain rate exceeds the total strain rate, $\partial \varepsilon_{cr}/\partial t > \partial \varepsilon/\partial t$. Since the creep process is

caused by the effective stress, this describes a physically impossible situation. Hence a further condition has to be introduced in the rheological model. In Figure P.2 the creep part of the rheological model is modelled as a Bingham body, i.e. an absorber in parallel with a slider. Runesson (1978) introduced a similar model for creep in clay, even if his model as a whole is far more complex than the model described here.

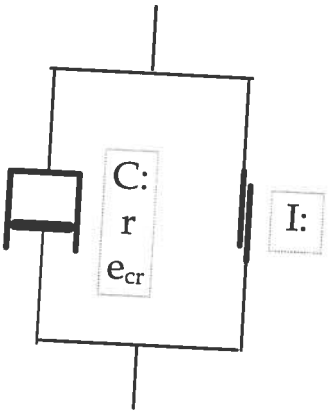

Figure P.2 Creep modelled as a Bingham body. *I* describes a condition for which the slider becomes active.

By the extended model in Figure P.2, the creep strain can be controlled by a condition, I, for which the slider becomes active, i.e. $I=(\partial\varepsilon_{cr}/\partial t \le \partial\varepsilon/\partial t)$. This means that the creep strain rate, according to equation P.3 and equation P.5a can be written as:

$$\frac{\partial\varepsilon_{cr}}{\partial t} = \min\begin{cases} \dfrac{1}{r\cdot(t+t_r)} \\ -\dfrac{\partial}{\partial z}\left(\dfrac{k}{\gamma_w}\dfrac{\partial u}{\partial z}\right) \end{cases} \qquad \text{(P.8)}$$

A complication in this case is that the creep strain rate no longer can be described by equation P.5a. This because the 'time origo', t_r, will change all the time depending upon whether creep takes place with a 'reduced' strain rate or not. This complication can be overcome by the use of the concept time resistance, *R*, defined as (Janbu, 1969):

$$R = \frac{\partial t}{\partial\varepsilon_{cr}} \qquad \text{(P.9)}$$

Substituting this into equation P.5a leads to

$$\frac{\partial \varepsilon_{cr}}{\partial t} = \frac{1}{r \cdot (t + t_r)} = \frac{1}{R} \tag{P.10}$$

Unconstrained creep strain can, in accordance with equation P.5, be calculated as:

$$\varepsilon_{cr} = \int_{t_r}^{t+t_r} \frac{1}{r \cdot x} dx = \frac{1}{r} \cdot \ln\left(\frac{t + t_r}{t_r}\right) \tag{P.11}$$

Combining equation P.10 and equation P.11 gives:

$$\varepsilon_{cr} = \frac{1}{r} \cdot \ln\left(\frac{t + t_r}{t_r}\right) = \frac{1}{r} \cdot \ln\left(\frac{r \cdot (t + t_r)}{r \cdot t_r}\right) = \frac{1}{r} \cdot \ln\left(\frac{R}{R_r}\right) \tag{P.12}$$

In this way creep strain can be calculated independently of time and equation P.8 be rewritten as:

$$\frac{\partial \varepsilon_{cr}}{\partial t} = \min\begin{cases} \dfrac{1}{R} \\ -\dfrac{\partial}{\partial z}\left(\dfrac{k}{\gamma_w}\dfrac{\partial u}{\partial z}\right) \end{cases} \tag{P.8a}$$

Hence, equation P.7 can, since $\partial u/\partial t \leq 0$, be rewritten as:

$$\frac{1}{M}\frac{\partial u}{\partial t} = \max\begin{cases} 0 \\ \dfrac{\partial}{\partial z}\left(\dfrac{k}{\gamma_w}\dfrac{\partial u}{\partial z}\right) + \dfrac{1}{R} \end{cases} \tag{P.13}$$

or if k and γ_w are constant with depth:

$$\frac{1}{M}\frac{\partial u}{\partial t} = \max\begin{cases} 0 \\ \dfrac{k}{\gamma_w} \cdot \dfrac{\partial^2 u}{\partial z^2} + \dfrac{1}{R} \end{cases} \tag{P.13a}$$

In Figure P.3 the strain is shown as a function of the effective stress. The upper curve in part A of the figure shows a typical curve obtained in an oedometer test. Part B shows the corresponding compression modulus.

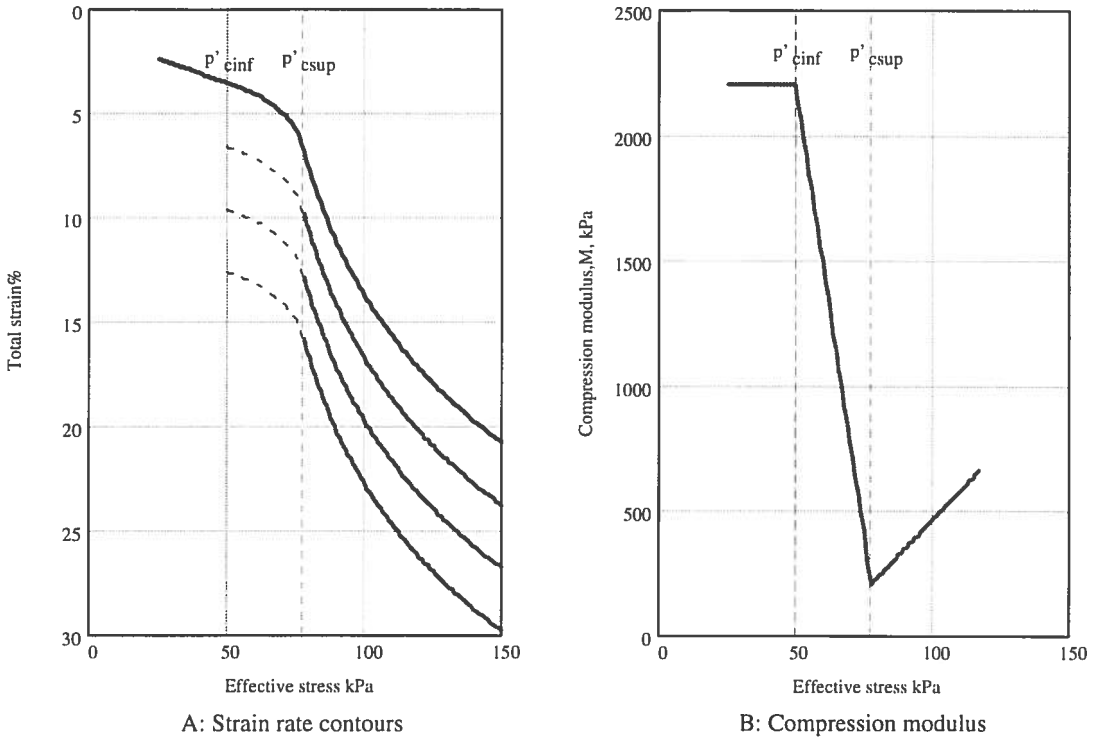

Figure P.3 Principle graph of strain versus stress.

As can be seen from equation P.12, the creep strain is independent of the stress level (if r is assumed to be a constant). If the oedometer curve is taken as the reference curve, points in the σ–ε graph with equal strain rate (or time resistance) can be defined by adding, in accordance with equation P.12, a strain increment to the reference curve. Thus, each contour in part A of Figure P.3 corresponds to a defined time resistance R. Equation P.12 gives:

$$R = R_r \cdot e^{r \cdot \varepsilon_{cr}} = r \cdot t_r \cdot e^{r \cdot \varepsilon_{cr}} \qquad \text{(P.14)}$$

For practical purposes, the curve obtained from an oedometer test can be treated as the curve defining immediate elastic/plastic strain. Theoretically, the curve involves both elastic/plastic strain and creep strain developed during the oedometer test period. However, by defining an appropriate reference time and a corresponding creep number, the curve is only used as a reference curve with a defined strain rate (or time resistance) together with a given creep number. Hence, there is no need to distinguish between elastic/plastic strain and creep strain for the reference curve. Furthermore, any of the contours in Figure P.3 could be used as a reference curve. In the figure $f'_{c,inf}$ and $f'_{c,sup}$ mark a zone of

decreasing modulus for the material (cf. Sällfors, 1975). This applies not only to the modulus, but also to material properties in general, see Figure P.4 (Janbu, 1989).

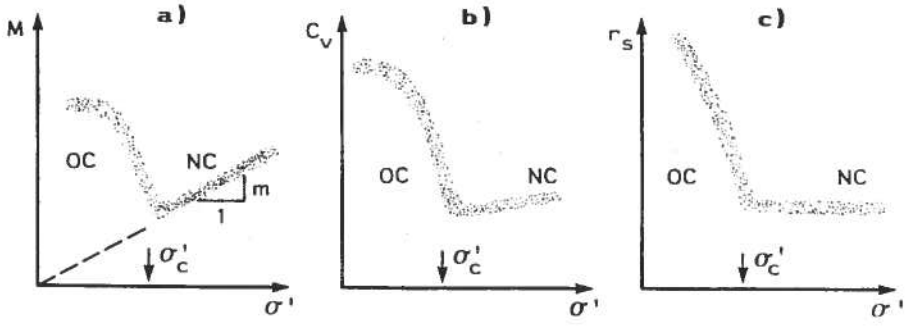

Figure P.4 Examples of material properties as a function of effective stress. a) compression modulus, M, b) coefficient of consolidation, c_v (classical theory) and c) creep number, r. (From Janbu,1989)

The stress range of declining material properties defines a zone, which, as an extension of the concept of preconsolidation pressure, could be named the preconsolidation zone.[1] The creep number, r, decreases rapidly in this zone. This means that any assumption of a constant value of r is a too crude approximation even for practical applications. Hence, the contours for equal time resistance are dotted in the preconsolidation zone. Any further discussion of the magnitude of r, in the zone, is omitted in this thesis, but is further discussed in (Alén, 1998b).

P.5 Finite difference model

For practical applications, the differential equation can easily be solved with the help of finite differences. The equation can, if k and γ_w are constant, be rewritten as

$$u_{i+1} - u_i = \max\begin{cases} 0 \\ \dfrac{k \cdot M}{\gamma_w}\dfrac{\Delta t}{\Delta z^2}\left(u_{j+1} - 2u_j + u_{j-1}\right) + \dfrac{M \cdot \Delta t}{R} \end{cases} \quad \text{(P.15)}$$

The index i here denotes time, while the index j denotes depth. This is a form suitable for incorporation in a spread sheet program. As the pore pressure at a certain level is calculated solely from values at

[1] Or more precisely, the transition zone at the preconsolidation pressure.

an earlier time step, the solving scheme will be straightforward, with no iterations involved. In the same manner as for the pore pressure, the strain can be given in a finite difference form by rewriting of equation P.3:

$$\varepsilon_{i+1} - \varepsilon_i = \frac{-k}{\gamma_w}\frac{\Delta t}{\Delta z^2}\left(u_{j+1} - 2u_j + u_{j-1}\right) \qquad \text{(P.16)}$$

in which the pore pressure, u, first has to be calculated for each time step by equation P.15.

By equations P.15 and P.16 the pore pressure as well as the strain can be calculated for any soil level and at any time. For simple applications, e.g. in a spread sheet program, it is advisable to restrict the variations of k, M and r to variations with the depth[1] (and not as variation with the stress or the strain).

P.6 Analytical model

P.6.1 General

The total strain equals the sum of elastic/plastic strain and creep strain. In classical theory, the degree of consolidation, U_o, can be used to describe the development of settlements, without respect to creep, i.e. the elastic/plastic settlements:

$$s(t) = U_0(t) \cdot s_{\max} \qquad \text{(P.17)}$$

where s_{max} is the final settlement at full consolidation. With full consolidation is here understood when the consolidation pressure, i.e. the excess pore pressure, is fully transmitted into effective stress. The degree of consolidation describes the rate of this process. It could be defined from a stress concept (cf. Terzaghi, 1943):

$$U_\sigma(t) = \frac{\overline{\Delta\sigma}(t)}{\overline{\Delta\sigma}(\infty)} \qquad \text{(P.18)}$$

or from a strain concept (Janbu, 1970):

$$U_\varepsilon(t) = \frac{\overline{\Delta\varepsilon}(t)}{\overline{\Delta\varepsilon}(\infty)} \qquad \text{(P.19)}$$

[1] The solving scheme has in such a case to be based upon eq P.13 and not eq P.13a.

that is the ratio between the average stress or strain and the final corresponding quantity. If the compression modulus is constant, the two definitions are equal. The same principle can be used to calculate the elastic/plastic part of the settlements, when creep is considered. However, the latter definition has then to be altered to:

$$U_\varepsilon(t) = \frac{\overline{\Delta\varepsilon_{pl}}(t)}{\overline{\Delta\varepsilon_{pl}}(\infty)} \qquad \text{(P.19a)}$$

To the elastic/plastic settlement one has to add the settlement due to the creep strain.

P.6.2 'Degree of consolidation'

The finite difference model, presented in section P5, can be used to calculate the stress and strain in a soil profile. By integrating the results over the profile, the 'degree of consolidation', as defined in the previous section, can be obtained. This will be denoted U_{cr}, when creep strain is considered and U_0, without respect to creep. The term 'degree of consolidation' is somewhat inappropriate for the first term as it refers only to the elastic/plastic part of the strain. From the reasoning in section P.4 it can be concluded that the time resistance is positive, $R \geq 0$. Thus the creep process delays the equalisation of the pore pressure. In Figure P.5 is shown the principal appearance of the ratio U_{cr}/U_0, (Alén, 1998b).

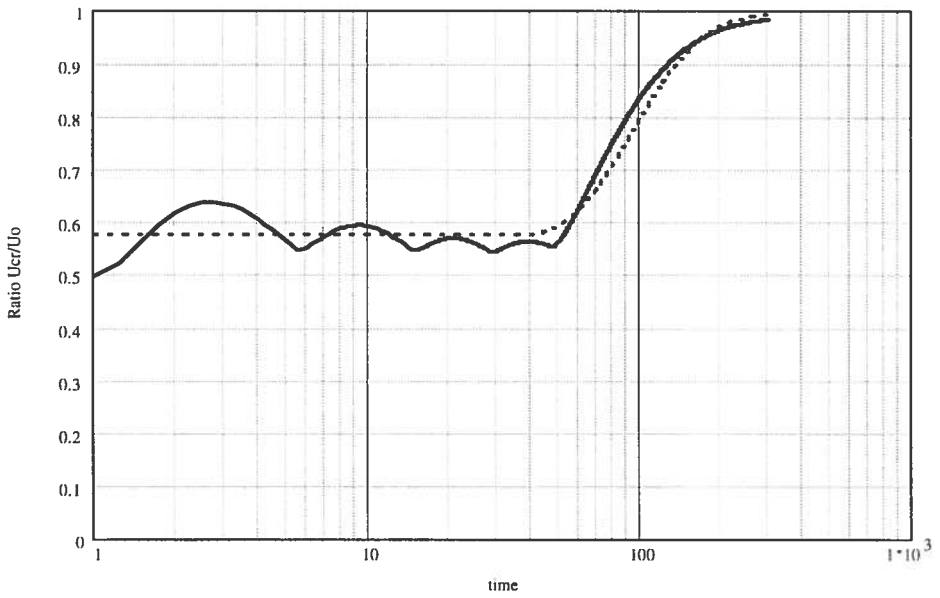

Figure P.5 Ratio U_{cr}/U_0

The solid line in Figure P.5 shows the result of a calculation with the finite difference model. The jagged shape of the line is a consequence of the fact that the soil profile is divided, in the illustrated case, only into 5 layers. As can be seen in the figure there is a distinct rise of the curve after a certain time, t_{lim}. This represents physically the time after which the creep becomes unconstrained throughout the whole soil profile The dotted line shows an approximation of the ratio U_{cr}/U_0. It is of the form:

$$\frac{U_{cr}}{U_0} = \begin{cases} K_0 \text{ if } t < 0{,}9 \cdot t_{lim} \\ 1 - \cdot \dfrac{2 \cdot (1 - K_0)}{e^{f(t)} + e^{-f(t)}} \text{ if } t > 0{,}9 \cdot t_{lim} \end{cases} \qquad \text{(P.20)}$$

This ratio U_{cr}/U_0, can with reasonably good accuracy be defined by two dimensionless parameters, one being the time factor:

$$T = \frac{k \cdot M}{\gamma_w \cdot L^2} \cdot t \qquad \text{(P.21)}$$

where L is the length of a characteristic drainage path, i.e. normally the height of the soil profile for one-sided drainage and half the height for two-sided drainage. The second parameter is a strain rate factor:

$$\Psi = \frac{M}{r \cdot q} \left[= \frac{\partial \varepsilon_{cr}}{\partial \ln(t)} \cdot \frac{1}{\varepsilon_{pl}} \right] \qquad \text{(P.22)}$$

where q is the consolidation pressure. The first parameter, the time factor, T, is a dimensionless time parameter describing the consolidation process (see e.g. Terzaghi, 1943). The second parameter, the strain rate factor, Ψ, describes the creep strain rate compared to the elastic/plastic deformation. The variables M, k, r and q have to be taken as average values[1].

By an extensive number of quantitative evaluations of equation P.20, with the finite difference method, the unknown quantities in the equation, have been determined in an approximate way. It shows that, whether the degree of consolidation is defined by

[1] Whether these are best given as arithmetic mean values, geometric mean values or harmonic mean values is a question for further research.

equation P.18 or equation P.19 is of minor importance for the ratio. The following result is obtained (Alén, 1998b):

$$K_0 = 0{,}25 - \ln(\frac{M}{r \cdot q}) = 0{,}25 - \ln(\Psi) \leq 1$$

$$t_{\lim} = \frac{4 \cdot \gamma_w \cdot L^2}{q \cdot r \cdot k} \quad or \quad T_{\lim} = 4\Psi$$

$$f(t) = \frac{k \cdot M}{\gamma_w \cdot L^2} \cdot (t - 0{,}9 \cdot t_{\lim}) \cdot (0{,}5 - 0{,}7 \cdot \ln(\frac{M}{r \cdot q}) \quad or$$

$$F(T) = (T - 3{,}6 \cdot \Psi) \cdot (0{,}5 - 0{,}7 \cdot \ln(\Psi))$$

This makes equation P.20, in a dimensionless form:

$$\frac{U_{cr}}{U_0} = \begin{cases} 0.25 - \dfrac{\ln(\Psi)}{7} & \text{if } T < 3.6 \cdot \Psi \\ 1 - \dfrac{\left(1{,}5 + \dfrac{\ln(\Psi)}{3{,}5}\right)}{\exp[F(T)] + \exp[-F(T)]} & \text{if } T > 3.6 \cdot \Psi \end{cases}$$

with the restriction $\Psi > \frac{1}{190}$ to keep $U_{cr}>0$ (P.20a)

The 'degree of consolidation', with respect to creep, can then be calculated as:

$$U_{cr} = \frac{U_{cr}}{U_0} \cdot U_0 = \eta_{cr} \cdot U_0 \qquad (P.23)$$

where η_{cr} is a consolidation ratio given by equation P.20 and U_0, the degree of consolidation obtained by classical theory. In contrast to what is said previously about the consolidation ratio, it is often of vital importance whether U_0 is defined from a stress or a strain concept.

P.6.3 Deformation

The elastic/plastic settlements can be calculated as:

$$s_{pl}(t) = U_{cr}(t) \cdot s_{\max,pl} \qquad (P.24)$$

where $s_{max,pl}$ is the final elastic/plastic settlement at full consolidation. To obtain the total settlements one must add the

creep settlements. However, one must distinguish between constrained and unconstrained creep strain, see section P4. If the creep strain becomes unconstrained in the whole profile, H, at the time, t_{lim}, the creep strain is constrained in approximately $\alpha \cdot H$ of the profile at the time $\alpha \cdot t_{lim}$, $0<\alpha<1$. A simple assumption is then that the average elastic/plastic strain, in the constrained phase, is:

$$\varepsilon_{pl} = U_{cr}(\alpha \cdot t_{\lim}) \cdot \frac{s_{\max}}{H} \tag{P.25}$$

and that the average creep strain is

$$\varepsilon_{cr} = (U_0(\alpha \cdot t_{\lim}) - U_{cr}(\alpha \cdot t_{\lim})) \cdot \frac{s_{\max}}{H} \tag{P.26}$$

Thus, equation P.14 can be rewritten as:

$$R(\alpha) = r \cdot t_r \cdot e^{r \cdot (U_0(\alpha \cdot t_{\lim}) - U_{cr}(\alpha \cdot t_{\lim})) \cdot \frac{s_{\max}}{H}} \tag{P.27}$$

and the settlements at a specified time calculated as:

$$\begin{aligned} s(t) &= s_{pl}(t) + s_{cr,unconstr}(t) + s_{cr,constr}(t) \\ s(t) &= \int_0^H \varepsilon_{pl} dz + \int_0^H \varepsilon_{cr,unconstr} dz + \int_0^H \varepsilon_{cr,constr} dz \end{aligned} \tag{P.28}$$

with

$$s_{pl}(t) = \begin{cases} \int_0^{\frac{t}{t_{\lim}}} (U_{cr}(t) \cdot s_{\max}) d\alpha + \int_{\frac{t}{t_{\lim}}}^1 (U_0(t) \cdot s_{\max}) d\alpha & if\ t < t_{\lim} \\ \int_0^1 (U_{cr}(t) \cdot s_{\max}) d\alpha & if\ t > t_{\lim} \end{cases}$$

$$s_{cr,unconstr}(t) = \begin{cases} \int_0^{\frac{t}{t_{\lim}}} \frac{H}{r} \ln\left(\frac{r \cdot (t - \alpha \cdot t_{\lim}) + R(\alpha)}{R(\alpha)}\right) d\alpha & if\ t < t_{\lim} \\ \int_0^1 \frac{H}{r} \ln\left(\frac{r \cdot (t - \alpha \cdot t_{\lim}) + R(\alpha)}{R(\alpha)}\right) d\alpha & if\ t > t_{\lim} \end{cases}$$

and

$$s_{cr,constr}(t) = \begin{cases} \int_0^{\frac{t}{t_{\lim}}} (U_0(\alpha \cdot t_{\lim}) - U_{cr}(\alpha \cdot t_{\lim})) \cdot s_{\max}) d\alpha & if\ t < t_{\lim} \\ \int_0^1 (U_0(\alpha \cdot t_{\lim}) - U_{cr}(\alpha \cdot t_{\lim})) \cdot s_{\max}) d\alpha & if\ t > t_{\lim} \end{cases}$$

By equation P.28, settlements, when considering creep, can be calculated in the same manner as settlements without respect to creep (equation P.24). However, the formulation demands numerical integration and is, for example, not easily incorporated in a spread sheet program, or demands at least long calculation time. In (Alén, 1998b) the integrals involved in equation P.28 are thoroughly evaluated. By introducing a number of simplifications, it has been able to express approximate, closed forms as an alternative to equation P.28:

$$s_{pl}(t) = U_{cr}(t) \cdot s_{\max} \qquad \text{(P.29)}$$

$$s_{cr}(t) = \begin{cases} \frac{t}{t_{\lim}} \cdot \left\{ \frac{H}{r} \cdot \left[\ln(\frac{t_{\lim}}{t_r}) - 1 \right] \right\} + \left[U_0(t) - U_{cr}(t) \right] \cdot \left(1 - \frac{t}{t_{\lim}} \right) \cdot s_{\max} & \\ & if\ t < t_{\lim} \\ \frac{H}{r} \cdot \left[\left(1 - \frac{t}{t_{\lim}} \right) \cdot \ln(\frac{t - t_{\lim}}{t_r}) + \frac{t}{t_{\lim}} \cdot \ln(\frac{t}{t_r}) - 1 \right] \cdot s_{\max} & if\ t > t_{\lim} \end{cases}$$

(P.30)

Or in a dimensionless form

$$\varepsilon_{pl}(T) = U_{cr}(T) \cdot \frac{1}{\Psi \cdot r} \qquad \text{(P.29a)}$$

$$\varepsilon_{cr}(T) = \begin{cases} \frac{T}{4\Psi} \cdot \left\{ \frac{1}{r} \cdot \left[\ln(\frac{4\Psi}{T_r}) - 1 \right] \right\} + \left[U_0(T) - U_{cr}(T) \right] \cdot \left(1 - \frac{T}{4 \cdot \Psi} \right) & \\ & if\ T < 4\Psi \\ \frac{1}{r} \cdot \left[\left(1 - \frac{T}{4\Psi} \right) \cdot \ln(\frac{T - 4\Psi}{T_r}) + \frac{T}{4\Psi} \cdot \ln(\frac{T}{4\Psi}) - 1 \right] & if\ T > 4\Psi \end{cases}$$

(P.30a)

The analytical model described above can be used to determine the pore pressure, as well as the long term settlements, with respect to creep. However, in contrast to the finite difference scheme, described in P5, only the average values over depth are accounted for. In this respect the model is on the same level of simplification as the classical way of solving consolidation problems with the help of the degree of consolidation, (see e.g. Terzaghi, 1943, cf. equation P.24).

APPENDIX Q RIGID SUPERSTRUCTURE

In this appendix formulas applicable for the case when a superstructure is modelled as a rigid body and the foundation as elastic springs are given. Notations used are given in Figure Q.1. The figure shows three supports, but the formulas given are applicable for any number of supports.

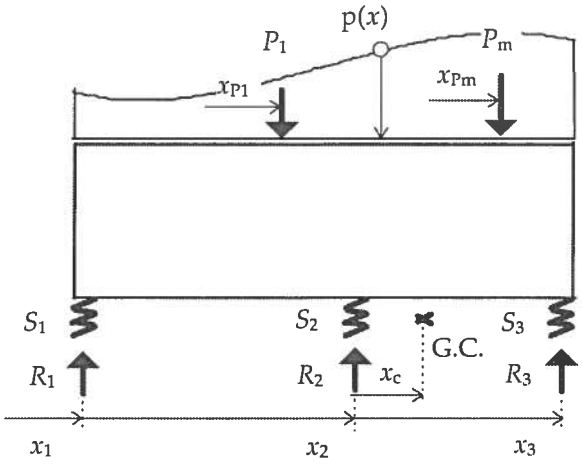

Figure Q.1 Rigid superstructure - Elastic supports

The 'gravity' centre of the supports, with respect to their stiffness can be calculated as:

$$x_c = \frac{\sum_n S_i \cdot x_i}{\sum_n S_i} \qquad \text{(Q.1)}$$

where n is the number of supports, S_i the stiffness of a support and x_i a horizontal co-ordinate for the support.

The actions can be transformed to a vertical action P_Σ and an action moment M_Σ applied at the centre of gravity:

$$P_\Sigma = \int_{x_1}^{x_n} p(x)\,dx + \sum_m P_i \qquad \text{(Q.2)}$$

$$P_\Sigma = \int_{x_1}^{x_n} p(x)\cdot(x - x_c)\,dx + \sum_m P_i \cdot (x_i - x_c) \qquad \text{(Q.3)}$$

where $p(x)$ is the distributed load and m the number of concentrated loads P.

The reactions at a support i can then be determined:

$$R_i = \frac{P_\Sigma \cdot S_i}{\sum_m S_i} + \frac{M_\Sigma \cdot S_i \cdot (x_i - x_c)}{I_S} \qquad \text{(Q.4)}$$

I_S is the moment of inertia for the supports with respect to their stiffnesses:

$$I_S = \sum_n S_i \cdot (x_i - x_c)^2 \qquad \text{(Q.5)}$$

The corresponding deformations become:

$$r_i = \frac{R_i}{S_i} \qquad \text{(Q.6)}$$

APPENDIX R FLEXIBLE SUPERSTRUCTURE

R.1 Introduction

The simplest model, in which both the superstructure and the ground are given flexible properties, is when the superstructure is modelled as an elastic beam supported by springs. In this appendix an algorithm for the analysis of such a case is given. The description is a summary of a general procedure used in structural mechanics, see e.g. Samuelsson & Wiberg, (1988). It is restricted to three supports, but applicable to any number of supports. Furthermore, in a general case, the superstructure can be modelled as an arbitrary, elastic frame. Such an application alters the description given below, but not the principles.

R.2 Algorithm

In Figure R.1 the analysed case is outlined. It is basically the same case as is described in appendix Q, but with the difference that the superstructure is an elastic beam instead of a rigid body.

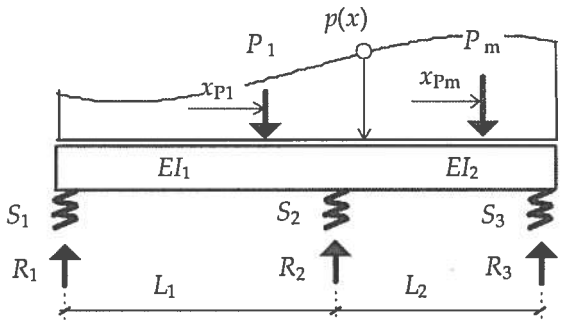

Figure R.1 Elastic superstructure - Elastic supports

In appendix O, a scheme was given, equation O.3, in which the structural stiffness was obtained by a matrix operation for the element stiffnesses and the nodal equilibrium relations. The scheme, which is general, can be used in this case too. As a first step, the actions have to be transformed to nodal actions. This is achieved by a partial solution in which the nodes are treated as fixed. The partial solution, with fixed nodes, is complemented with a solution from actions in the nodes. The nodal actions are the reactions in the nodes for the partial solution, but with the opposite sign, see Figure R.2. This second complementary solution gives the reactions and the corresponding deformations in the

nodes, i.e. the quantities, which are of interest from a geotechnical point of view. The 'structural' solution is obtained as the sum of the partial and the complementary solution.

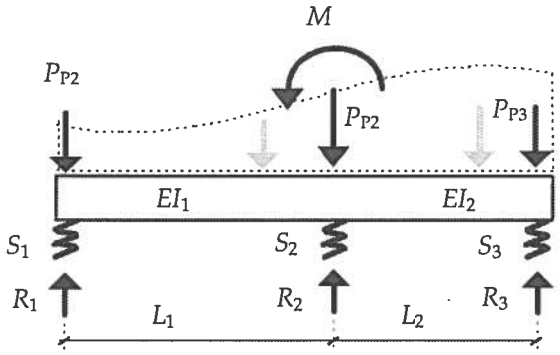

Figure R.2 Complementary case. Nodal actions

For the trivial but common case of uniformly distributed loads in each span, the nodal actions become:

$$\mathbf{P}_P = \begin{bmatrix} P_{P1} \\ P_{P2} \\ P_{p3} \\ M \end{bmatrix} = \begin{bmatrix} \frac{3}{8} \cdot p_1 \cdot L_1 \\ \frac{5}{8} \cdot \left(p_1 \cdot L_1 + p_2 \cdot L_2 \right) \\ \frac{3}{8} \cdot p_2 \cdot L_2 \\ \frac{1}{8} \cdot \left(p_1 \cdot L_1^{\,2} - p_2 \cdot L_2^{\,2} \right) \end{bmatrix} \qquad \text{(R.1)}$$

with the relation between the actions $\mathbf{P}_p$ and the displacements $\mathbf{p}_p$:

$$\mathbf{P}_P = \mathbf{S} \cdot \mathbf{p}_P \qquad \text{(R.2)}$$

The structural stiffness $\mathbf{S}$ is in this case is $\{4x4\}$-matrix. For the simple case outlined, it can be arranged directly by considering equilibrium for each nodal displacement separately, see Figure R.3.

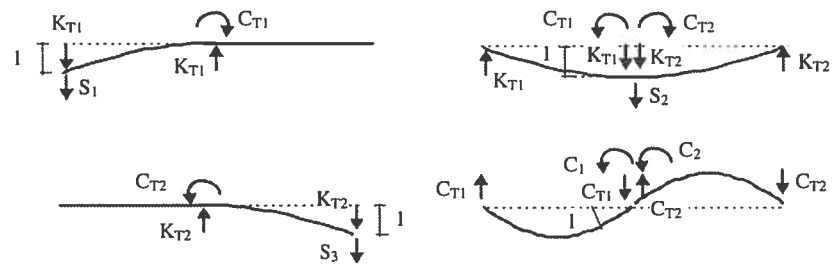

Figure R.3 Equilibrium for nodal displacement

The structural stiffness matrix **S** becomes:

$$\mathbf{S} = \begin{bmatrix} K_{T1} + S_1 & -K_{T1} & 0 & -C_{T1} \\ -K_{T1} & K_{T1} + S_2 + K_{T2} & -K_{T2} & C_{T1} - C_{T2} \\ 0 & -K_{T2} & S_3 + K_{T2} & C_{T2} \\ -C_{T1} & C_{T1} - C_{T2} & C_{T2} & C_1 + C_2 \end{bmatrix} \quad \text{(R.3)}$$

with the stiffness properties of the elements:

$$K_{Ti} = \frac{3 \cdot EI_i}{L_i^3} \quad ; \quad C_{Ti} = \frac{3 \cdot EI_i}{L_i^2} \quad ; \quad C_i = \frac{3 \cdot EI_i}{L_i} \quad \text{(R.4)}$$

S_i is the stiffness of the supports respectively.

The deformations at the supports are obtained from:

$$\mathbf{p}_P = \mathbf{S}^{-1} \cdot \mathbf{P}_P \quad \text{(R.2a)}$$

and the corresponding reactions as:

$$R_i = S_i \cdot p_{P_i} \quad , \quad i = 1...3 \quad \text{(R.5)}$$

The section forces and deformations in the superstructure, in this case the beam, can be analysed from the deformation pattern. In Figure R.4 the deformation of the left beam element is given.

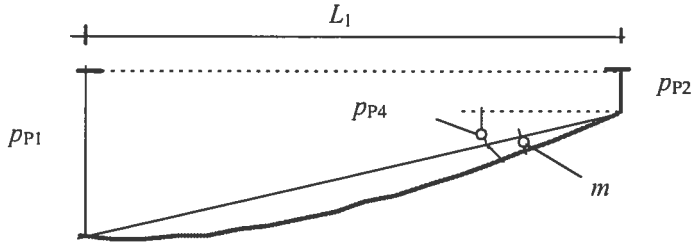

Figure R.4 Deformation of beam element 1.

The rotation m of the right end compared to the chord is identified as[1]:

$$m = p_{P4} - \frac{p_{P1} - p_{P2}}{L_1} \quad \text{(R.6)}$$

[1] The rotation in the partial solution was set equal to zero.

Hence the section moment in the beam cab be derived as[1]:

$$m = \frac{M \cdot L_1}{3 \cdot EI_1} + \frac{p_1(x) \cdot L_1^{\,3}}{24 \cdot EI_1} \quad \Rightarrow \quad M = \left(m - \frac{p_1(x) \cdot L_1^{\,3}}{24 \cdot EI_1} \right) \cdot \frac{3 \cdot EI_1}{L_1} \qquad \text{(R.7)}$$

for a uniformly distributed load $p_1(x)$.

[1] In this simple case the section moment is more easily derived as $M = R_1 \cdot L_1 - \frac{p_1 \cdot L_1^{\,2}}{2}$

APPENDIX S A SOIL BEAM MODEL

S.1 Introduction

In the appendices P and R, procedures for analysing interaction between the superstructure and the ground are described. Both appendices are based upon a model in which the flexibility of the ground is modelled as springs at the supports. Hence interaction between the supports through the ground is not accounted for. In this appendix a model, in which such interaction can be considered, is outlined. The ground is modelled as a soil beam supported by springs. The description given is restricted to cases of foundation in which the supports are separated by some distance away, i.e. not any continuously supported foundations.

S.2 The soil beam

The soil beam is a conventional beam, where deformations are restricted to shearing. Hence it is formed by a number of elements, characterised by the shearing stiffness GA. To model the soil outside the superstructure, the beam is extended one span at each end, see Figure S.1. The description is for simplicity given for a two-span superstructure, which results in a four-span soil beam.

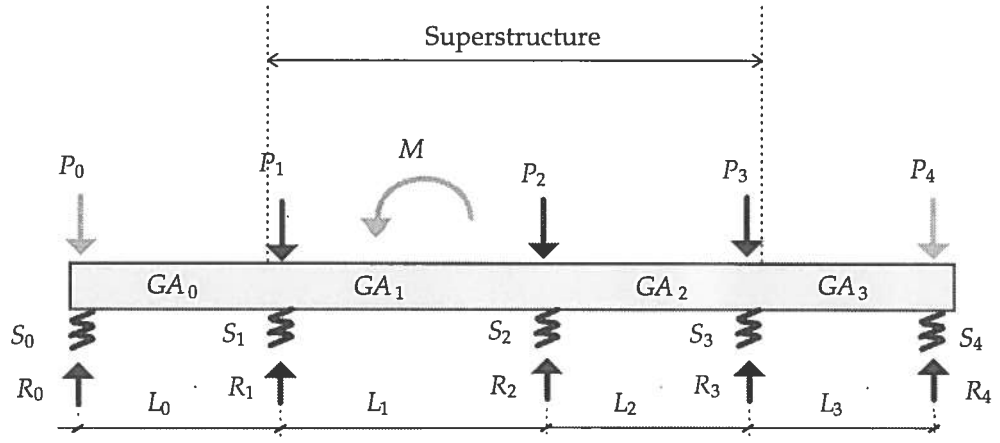

Figure S.1 The soil beam.

In appendix R a structural algorithm for a flexible beam on a number of spring supports is described. The soil beam forms, in principle, the same sort of structure. The fact that the beam described in appendix R represents the superstructure, while the soil beam represents the ground, does not change the basic

principles of the structural algorithm. However, compared with the 'superstructure case', three differences exist:

- No actions between the supports need to be considered.
- The properties of the beam elements are given by their shearing stiffness instead of their bending stiffness.
- The rotation of the soil beam is equal in all sections[1]. Hence the location of any applied moment does not need to be considered.

The relation between the actions **P** and the displacements **p** can be written:

$$\mathbf{P} = \mathbf{S}_G \cdot \mathbf{p} \tag{S.1}$$

The applied actions are given by

$$\begin{aligned} \mathbf{P}^T &= \begin{pmatrix} P_0 & P_1 & P_2 & P_3 & P_4 & M \end{pmatrix} = \\ &= \begin{pmatrix} 0 & P_1 & P_2 & P_3 & 0 & 0 \end{pmatrix} \end{aligned} \tag{S.2}$$

where P_1-P_3 are the reactions between the superstructure and the ground. The zero elements, P_0, P_4 and M, do not correspond to zero displacement. Hence they must be incorporated into the analysis, even though they are set to zero. The structural stiffness **S** is in this case a{6x6}-matrix. Similarly, as in appendix R, it can be assessed directly by considering equilibrium for each nodal displacement separately, see Figure S.2. The structural stiffness becomes

$$\mathbf{S}_G = \begin{bmatrix} K_{T0}+S_0 & -K_{T0} & 0 & 0 & 0 & -C_{T0} \\ -K_{T0} & K_{T0}+S_1+K_{T1} & -K_{T1} & 0 & 0 & C_{T0}-C_{T1} \\ 0 & -K_{T1} & K_{T1}+S_2+K_{T2} & -K_{T2} & 0 & C_{T1}-C_{T2} \\ 0 & 0 & -K_{T2} & K_{T2}+S_3+K_{T3} & -K_{T3} & C_{T2}-C_{T3} \\ 0 & 0 & 0 & -K_{T3} & K_{T3}+S_4 & C_{T3} \\ -C_{T0} & C_{T0}-C_{T1} & C_{T1}-C_{T2} & C_{T2}-C_{T3} & C_{T3} & \sum_{i=0}^{4} C_i \end{bmatrix} \tag{S.3}$$

[1] This is due to the assumption of a bending stiffness $EI=\infty$.

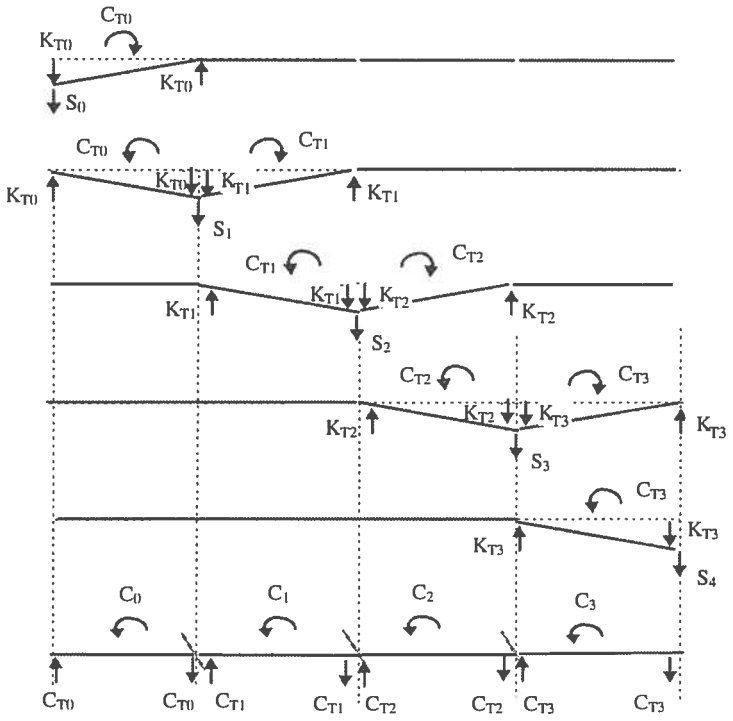

Figure S.2 Equilibrium for displacements (=1) in the nodes.

The stiffness properties of the elements in equation S.3 are:

$$K_{Ti} = \frac{GA_i}{L_i} \quad ; \quad C_{Ti} = GA_i \quad ; \quad C_i = GA_i \cdot L_i \tag{S.4}$$

For a case with given reactions, i.e. a statically determined superstructure, the deformations of the ground are obtained from equation S.1:

$$\mathbf{p} = \mathbf{S}_G^{-1} \cdot \mathbf{P} \tag{S.1a}$$

and the corresponding 'reactions' as:

$$R_i = S_{Gi} \cdot p_{P_i} \quad , \quad i = 0 \ldots 4 \tag{S.5}$$

Note that these reactions are fictitious reactions in the ground. The reactions on the superstructure are equal to the statically determined actions, but with opposite signs.

S.3 Interaction

The model of the superstructure, cf. appendix R, and the soil beam can easily be combined, see Figure S.3.

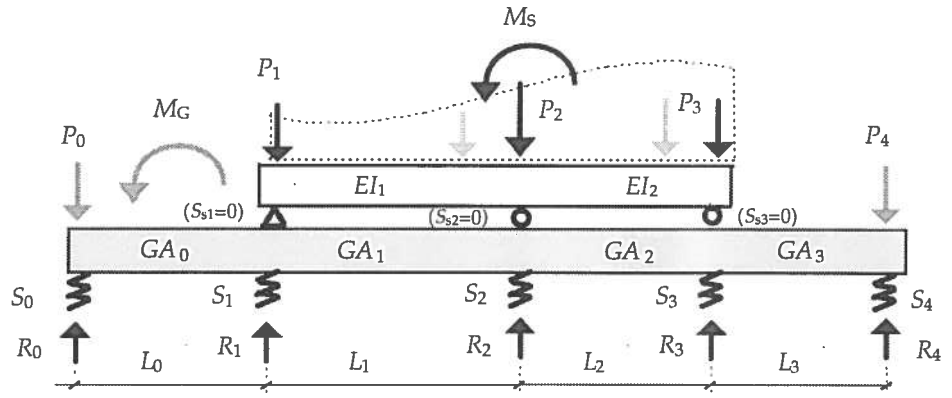

Figure S.3 Interaction model between the superstructure and the soil beam.

The relation between the actions **P** and the displacements **p** can be written:

$$\mathbf{P} = \mathbf{S} \cdot \mathbf{p} \tag{S.6}$$

with the applied actions given by:

$$\begin{aligned} \mathbf{P}^T &= \begin{pmatrix} P_0 & P_1 & P_2 & P_3 & P_4 & M_S & M_G \end{pmatrix} = \\ &= \begin{pmatrix} 0 & P_1 & P_2 & P_3 & 0 & M_S & 0 \end{pmatrix} \end{aligned} \tag{S.7}$$

The structure stiffness can then be combined from the elements in equation R.3 and equation S.3. If the elements in the structure stiffness are indexed S, the combined stiffness can be written:

$$\mathbf{S} = \begin{bmatrix} S_{G11} & S_{G12} & 0 & 0 & 0 & 0 & S_{G16} \\ S_{G21} & \underline{S_{S11}} + S_{G22} & \underline{S_{S12}} + S_{G23} & 0 & 0 & \underline{S_{S14}} & S_{G26} \\ 0 & \underline{S_{S21}} + S_{G32} & \underline{S_{S22}} + S_{G33} & \underline{S_{S23}} + S_{G34} & 0 & \underline{S_{S24}} & S_{G36} \\ 0 & 0 & \underline{S_{S32}} + S_{G43} & \underline{S_{S33}} + S_{G44} & S_{G45} & \underline{S_{S34}} & S_{G46} \\ 0 & 0 & 0 & S_{G54} & S_{G55} & 0 & S_{G56} \\ 0 & \underline{S_{S41}} & \underline{S_{S42}} & \underline{S_{S43}} & 0 & \underline{S_{S44}} & 0 \\ S_{G61} & S_{G62} & S_{G63} & S_{G64} & S_{G65} & 0 & S_{G66} \end{bmatrix} \tag{S.8}$$

The underlining of the elements S_S is only a typographic distinction. The stiffness of the supports for the superstructure, i.e. S_i in an element S_{Sii}, has to be given as S_i=0, as the stiffness of the supports already are included in the elements for the soil beam S_{Gii}.

The deformations at the supports are obtained as previously:

$$\mathbf{p}_P = \mathbf{S}^{-1} \cdot \mathbf{P}_P \tag{S.9}$$

and the corresponding 'reactions' as:

$$R = S \cdot p_i \quad , \quad i = 0...4 \tag{S.10}$$

As mentioned in section S.2 these reactions are only fictitious. In this case, the actual reactions at foundation level are structural section forces. They can be obtained from an analysis of the deformation pattern, see Figure S.4

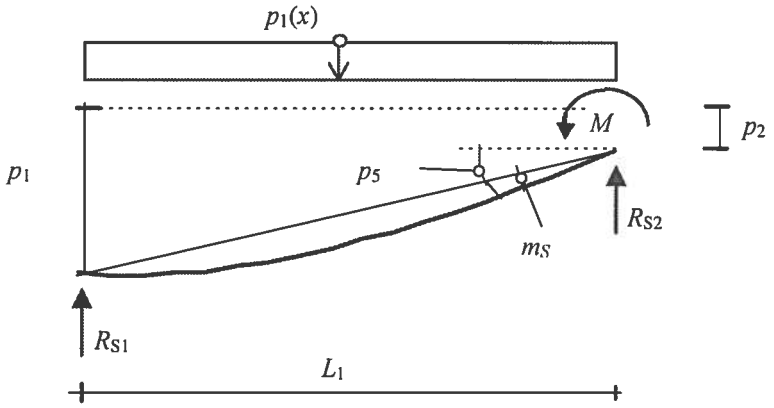

Figure S.4 Deformations and actions on the structural beam element no. 1

The bending moment is, cf. appendix R:

$$M = \left(m_S - \frac{p_1(x) \cdot L_1^{\,3}}{24 \cdot EI_1} \right) \cdot \frac{3 \cdot EI_1}{L_1}$$
$$\text{with} \quad m_S = p_5 - \frac{p_1 - p_2}{L_1} \tag{S.11}$$

The reactions are obtained from equilibrium analysis:

$$R_1 = p_1(x) \cdot L_1/2 + M/L_1$$
$$R_2 = p_1(x) \cdot L_1/2 + p_2(x) \cdot L_2/2 - M \cdot \left(1/L_1 + 1/L_1\right) \tag{S.12}$$
$$R_3 = p_2(x) \cdot L_2/2 + M/L_2$$